STRUCTURES IN FIRE PROCEEDINGS OF THE SECOND INTERNATIONAL WORKSHOP

Editor
Peter Moss

University of Canterbury, Christchurch, New Zealand

18 to 19 of March of 2002

Session 1:
Steel joints and composite structures

NUMERICAL DETERMINATION OF 3D TEMPERATURE FIELDS IN STEEL JOINTS

Jean-Marc FRANSSEN, Luc BRAUWERS
Univ. of Liege, 1, Chemin des Chevreuils, 4000, Liège 1, Belgium
jm.franssen@ulg.ac.be

ABSTRACT

A numerical study was undertaken to investigate the temperature field in steel joints and to compare the temperatures in the joints to the temperatures of the adjacent steel members in the hypothesis that the thermal protection is the same on the joint and in the members.

Very brief information is given on the numerical model, supplemented with parametric studies made in order to determine the required level of discretisation in the time and in the space domain. A simplified assumption for representing the thermal insulation is also discussed and validated.

Different numerical analyses are performed, with a variation of the following parameters:

- Type of joints, from very simple to more complex configurations, with welds and/or bolts, all of them representing joints between elements located in the same plane.
- Unprotected joints or protected by one sprayed material.
- ISO, Hydrocarbon or one natural fire scenario.

The fact that the thermal attack from the fire might be less severe because the joints are usually located in the corner of the compartment is not taken into account.

KEYWORDS: *temperature, steel, joints, numerical analysis, 3D*

INTRODUCTION

It is usually assumed that the joints in steel construction don't require any special verification as far as their thermal insulation is at least equal to the insulation applied on the adjacent members.

For example, in the most recent draft of Eurocode 3 [1], it is written concerning connections:

The resistance of category A and B connections may be assumed to be sufficient provided that the two following conditions are met :

1) the thermal resistance $(d_f / \lambda_f)_c$ of the fire protection of the connection is not less than the minimum value of the thermal resistance $(d_f / \lambda_f)_m$ of the fire protection of any of the steel members joined by that connection, where:

d_f is the thickness of the fire protection material — take $d_f = 0$ for unprotected members;

λ_f is the effective thermal conductivity of the fire protection material.

2) the utilisation $E_{d,fi} / R_d$ of the connection is not higher than the maximum value of the utilisation of any of the steel members joined by that connection.

Also, concerning members verification, it is written in [1]:

Net-section failure at fastener holes need not be considered, provided that there is a fastener in each hole, because the steel temperature is lower at connections due to the presence of additional material.

The assumption behind these rules is clearly that the temperature in the joint will be lower than the temperature in the members because there is a higher mass concentration in the joint. In fact, the local massivity, i.e. the ratio between the mass and the exposed surface, is the leading parameter and not only the mass. A numerical study was thus undertaken to see whether the assumption of lower temperature in the joints is systematically valid.

SCOPE

Only steel connections are considered, i.e. no concrete slab is present. Three fire scenario are considered, namely the ISO 834 fire curve, the hydrocarbon fire curve and one natural fire curve taken from Eurocode 1 [2] with a heating phase duration of 31 minutes and a maximum temperature of 773°C. Each joint is analysed as unprotected, then as thermally protected.

HYPOTHESES

The thermal properties of steel are taken from Eurocode 3 [3]. The boundary conditions are taken from Eurocode 1 [2], i.e. $h = 25$ W/mK for convection and $\varepsilon^* = 0.50$ for radiation. Thermal contact is assumed to be perfect between any 2 adjacent objects; there is no thermal resistance produced by an eventual imperfect contact.
The temperature field is determined with the software SAFIR [4], using linear finite elements and an Euler-Backward implicit time integration scheme ($\theta = 0.90$).

PRELIMINARY STUDY ON THE DISCRETISATION

It is important to know what is the required level of refinement in the discretisation, both in the time as well as in the space domain; the precision must not be excessively deteriorated by a too crude approximation, but the calculation time has to be maintained within reasonable limits. Figure 1, for example, shows the isotherms after 30 minutes of ISO fire in a bolt passing through a 40 mm steel plate (the head and the screw are hexagonal, and the extremity of the cylindrical shank has also be approximated as hexagonal, which allows discretising only a 30° sector). Figure 2 shows that a very similar temperature pattern can be obtained with a cruder discretisation in which each extremity of the bolt is represented by a single finite element. On the other hand, if the bolt is not represented at all and only the steel plate is represented, the hot spot that appears near the bolt on Figure 1 and Figure 2 will not appear and this cannot be accepted.
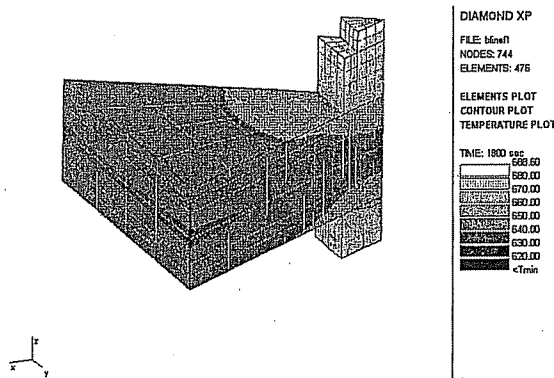

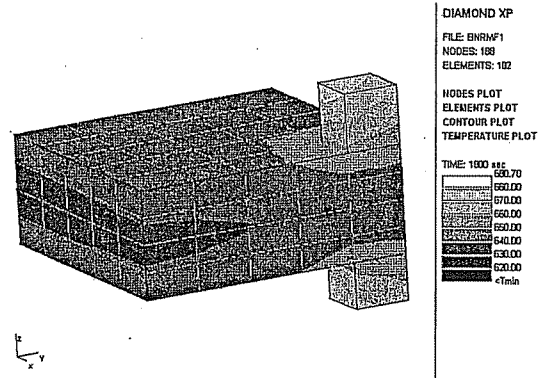**Figure 1 : fine discretisation for a bolt**

Figure 2 : discretisation used for a bolt

A simplified modelling is also proposed for the protection, that allows a significant reduction in the time for calculation, but above all in the time required for discretising. This simplification is explained here in a 2D situation for simplicity reasons.

The most general way to take the thermal insulation into account is to represent it explicitly by some layers of finite elements, see Figure 3. Of course, this requires a large number of additional finite elements and this has severe consequences on the time required for calculation but even more on the time required for building the model. In fact, if the thermal protection is provided by a lightweight material with a negligible specific heat, the thermal resistance R provided by the layer of insulating material can be evaluated, in the uniaxial situation that prevails for most parts of the steel sections, by the following equation:

$$R = \frac{1}{\alpha_p} + \frac{t_p}{\lambda_p} \tag{1}$$

where t_p thickness of the protection layer,

λ_p thermal conductivity of the protection material,

α_p coefficient of heat exchange at the surface of the protection, see equation 2.

$$\alpha_p = h_p + \varepsilon_p^* \sigma_0 \left(T_g^3 + T_g^2 T_p + T_g T_p^2 + T_p^3 \right) \tag{2}$$

3

where h_p coefficient of convection,

ε_p^* relative emissivity,

σ_0 Stefan-Boltzman constant,

T_g temperature of the gas,

T_p temperature at the surface of the protection.

In fact, it can be shown that in most commonly used thermal protections, the surface resistance is negligible in equation 1 when compared to the resistance to conduction provided by the thermal protection. Equation 3 is therefore a good approximation of equation 1; replacing equation 1 by equation 3 amounts to assume that the temperature at the surface of the insulation is equal to the temperature of the gas.
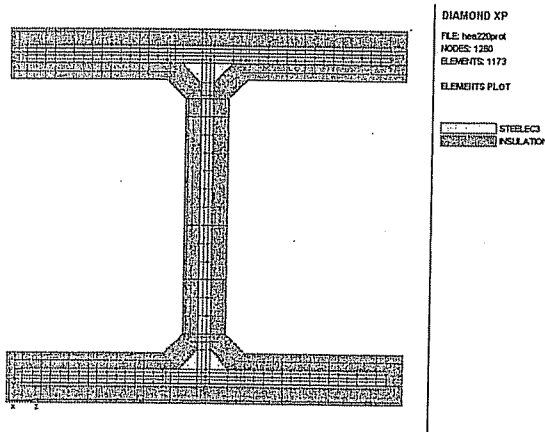
$$R = \frac{t_p}{\lambda_p} \tag{3}$$

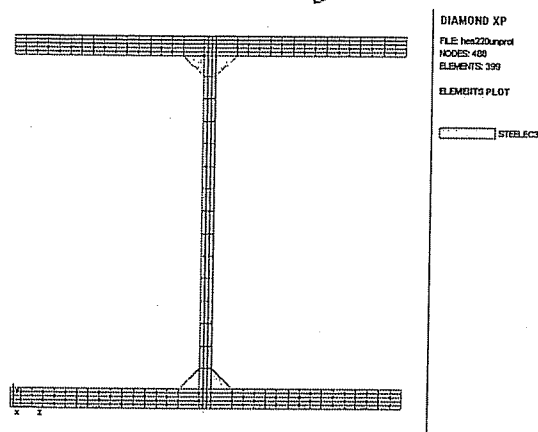**Figure 3 : protection represented**

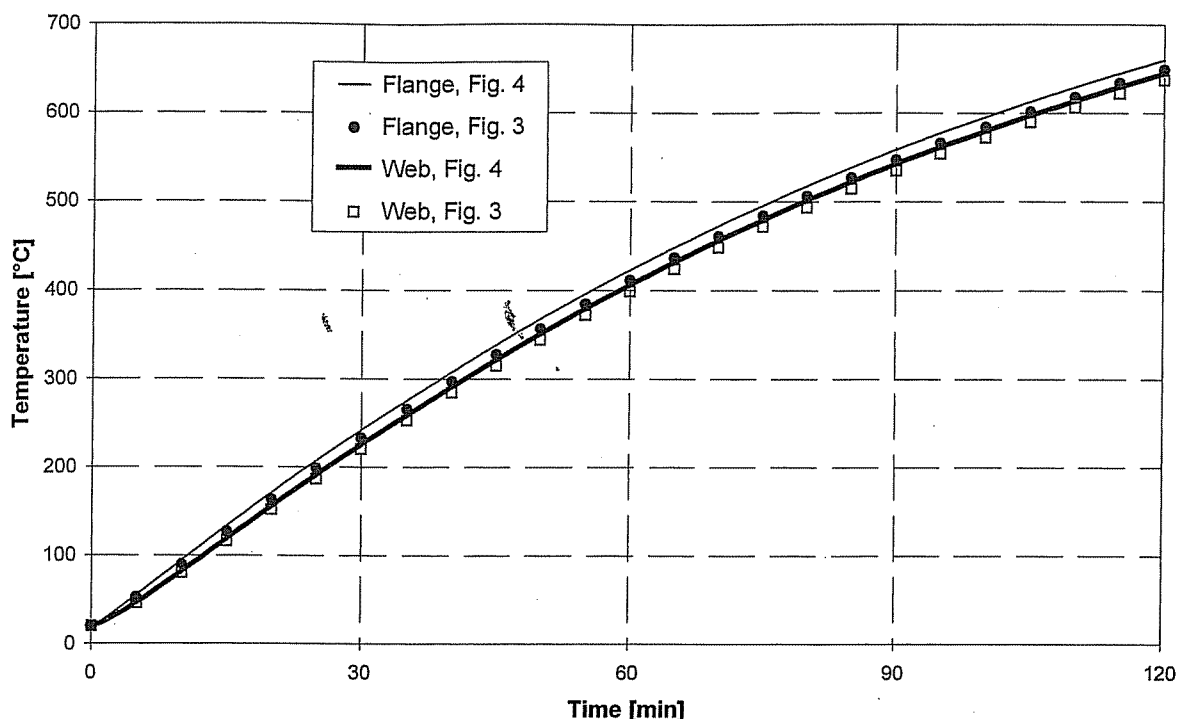

Figure 4 : equivalent protection

In an unprotected section, the surface resistance on the steel plate $1/\alpha_s$ is the only thermal resistance with α_s given by equation 4.

$$\alpha_s = h_s + \varepsilon_s^* \sigma_0 \left(T_g^3 + T_g^2 T_s + T_g T_s^2 + T_s^3 \right) \tag{4}$$

It is therefore possible consider the effect of the insulation and yet to represent only a non-insulated section, see Figure 4, provided that the surface properties of steel are adapted accordingly. The simplest solution is given by equation 5.

$$\varepsilon_s^* = 0$$

$$\frac{1}{h_s} = \frac{t_p}{\lambda_p} \tag{5}$$

For example, in order to model a 10 mm layer of insulation with a thermal conductivity $\lambda_p = 0.04$ W/mK, it is possible to use an unprotected section with an emissivity equal to 0 and a convection factor equal to 4 W/m²K. This has been done for the HEA220 represented on Figure 3 and Figure 4 and the comparison in the obtained temperatures is given in Figure 5.

4

Figure 5 : comparison between represented protection and equivalent protection

As far as the time step is concerned, it was shown by comparisons with a very small time step that the relative error on the temperature does not exceed 0.5% with a rather large time step of 60 seconds in a protected joint and 12 seconds in an unprotected joint. The relative temperature difference between two different locations in a joint is not influenced by the time step.

FIN EFFECT FROM THE BOLT

A fin effect is produced when an object having a low mass but a high surface is in contact with a massif object. It is sometimes referred to as the "extended surface" effect. This effect is particularly used in the heat exchanger technology where a large number of thin plates are welded to the body that has to exchange heat as efficiently as possible with the environment; because of the high surface of the plates and because of the low contact thermal resistance between the plates and the object, the heat exchange is increased by the plates.

In a joint submitted to the action of the fire, the bolts might play the role of fins for the plates that they are connecting. This effect is in fact visible on Figure 1 and Figure 2. Under which conditions will this appear and how significant is this effect?

This effect has been analysed in different geometrical configurations, different fire scenarios and different protection configurations. Figure 6 and Figure 7, for example, refer to the situation after 20 minutes of ISO fire in an unprotected joint with an M27 bolt connecting 2 steel plates of 20 mm (Figure 6) and 8 mm (Figure 7). In each case, the length of the screw extending beyond the nut is 10 mm.
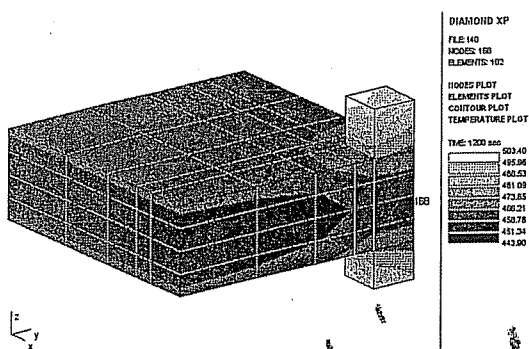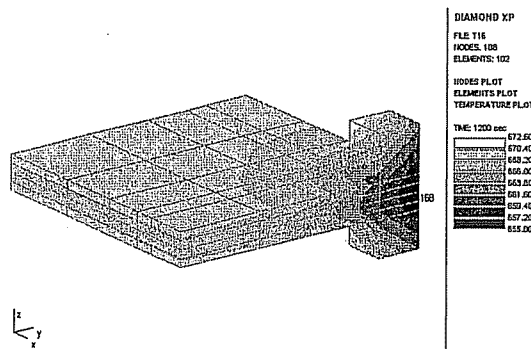
Figure 6 : M27 bolt on 2 x 20mm plates   **Figure 7 : M27 bolt on 2 x 8mm plates**

One temperature that is significant for the strength of the connection is the temperature in the shear plane in the bolt (node 168). This temperature of the bolt can be compared to the temperature in the plate as calculated away from the bolt, i.e. neglecting the influence of the bolt. It can be observed that the bolt on thick plates makes the temperature in the bolt higher than the temperature of the plate, see Figure 6, whereas the same bolt on thin plates makes the temperature in the bolt lower than the temperature in the plate, see Figure 7. What was a fin for a massive object becomes a protection for the thin object.

From all the analyses performed, it appears that the significant parameter is the ratio $d/2\ t$ between the diameter of the screw and the total thickness of plates that is significant; for $d/2\ t < 1$, the bolt is a hot spot whereas, for $d/2\ t > 1$, the bolt is a cold spot.

Although the second situation might not be the most common one, it can be immediately accepted in this case to neglect the effect of the bolt when evaluating the temperature, because this is on the safe side.

For the first situation, must the local effect of the bolt absolutely be taken into? In fact, it appears that the local increase of temperature caused by the presence of the bolt is quantitatively very limited. This is shown on Figure 8 that represents the evolution of the temperature in the centre of the bolt (node 168, see Figure 6) and of the temperature in the centre of the plate far away from the bolt. This figure has been drawn for the case in which the highest differences can be observed, namely in an unprotected joint, with the very fast hydrocarbon fire curve and with a excessively long screw extending 40 mm beyond the nut. The amount by which the temperature is underestimated if calculated with the massivity of the 2 plates is very limited, with a peak value for ΔT of 36°C after 18 minutes. For any other time within the fire or any other configuration, the difference would be less than 36°C. By configuration, we refer here to the combination fire-protection-geometry.

The effects of the configuration on the fin effects are:

- The faster the fire, the more pronounced the fin effect; with slower fires, time has a tendency to render the temperature field more homogeneous. This is why the effect is more pronounced with a hydrocarbon fire than with the ISO fire.

- The effect is reversed during the cooling down phase of a natural fire; if the fin effect is increasing the heat exchange with the environment, it will accelerate the heating as well as the cooling and, hence, a hot spot during heating will turn in a cold spot during the cooling.

- Thermal protection, because it slows down the temperature elevation, has also a tendency to render the situation more homogeneous.

- An excessively long screw will emphasize the fin effect on massive onbjects and the protection effect of thin objects.
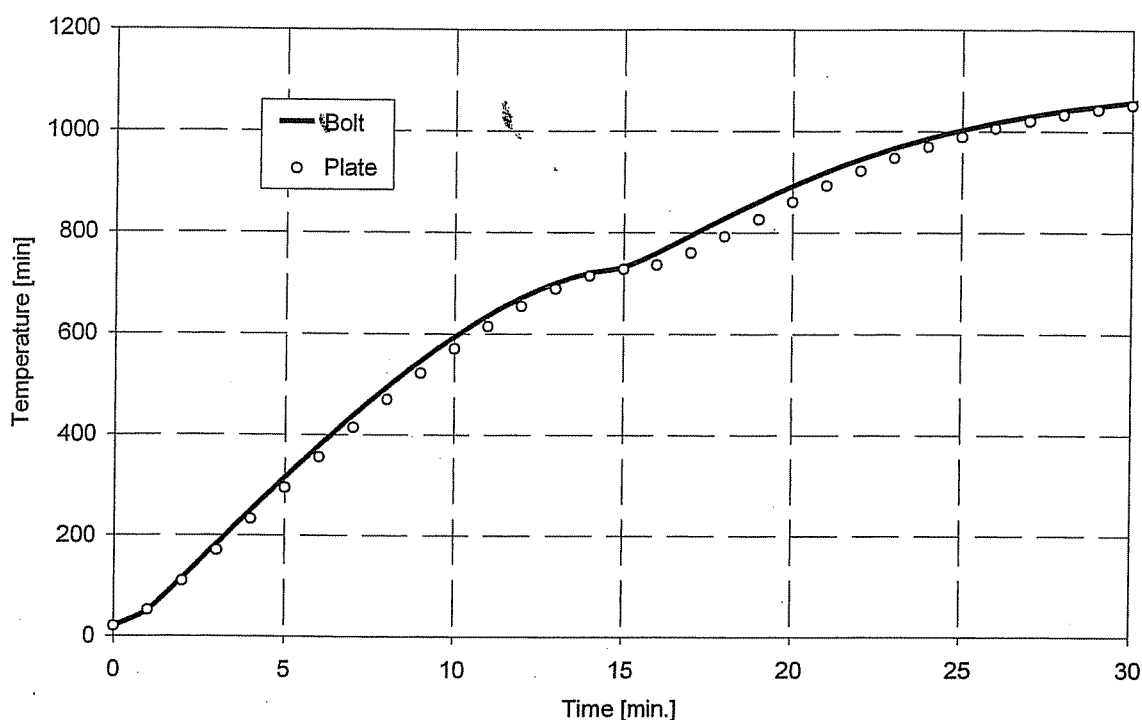
Figure 8 : M27 on 2x20 plates - hydrocarbon fire

According to the above considerations, it appears that the local effect of the bolts can really be neglected when evaluating the temperature distribution in a joint.

EFFECT OF THE WELDS

A geometry commonly encountered in joints is when a stiffener is made of a thin plate welded on a thicker plate. The weld in this case has several different effects: a) it decreases locally the area of the surface that is exchanging heat with the environment, b) it increases locally the mass of material to be heated, c) it increases the surface available for the heat to pass by conduction from the thin plate to the thick plate.

The influence of the weld can also be analysed in a 2D model, see Figure 9, Figure 10 and Figure 11. They refer to a 20 mm thick plate (half thickness represented here for symmetry reason) welded on a 40 mm plate with a 5 mm weld. The fire is the hydrocarbon fire and the section is not thermally protected. The figures seem to indicate that a very fine discretisation is not really required, but that the weld absolutely has to be taken into account. In fact, the difference in temperatures between Figure 10 and Figure 11 are not quantitatively so important and a discretisation without the weld could represent an acceptable approximation.
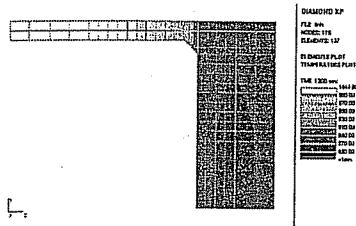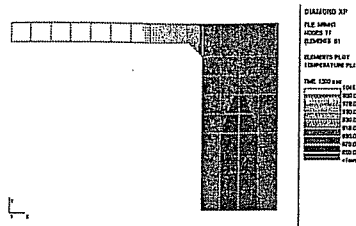
Figure 9 : fine discretisation
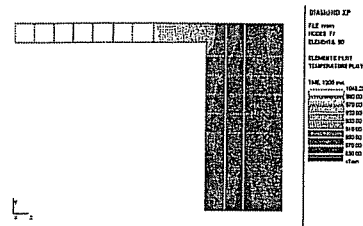

Figure 10 : normal discretisation

Figure 11 : weld not represented

TEMPERATURE OF THE WELD

Figure 12 refers to the same geometry as seen in Figure 9, but now for an ISO fire. The upper curve shows the temperature evolution as calculated by SAFIR in the thin plate far away from the connection. It can be observed that the curve corresponds exactly to the curve that is calculated with the simple equation of Eurocode 3 in the hypotheses of a uniform temperature in this plate. The same holds for the lower curve that depicts the evolution in the thick plate. The central curve corresponds to the temperature in the weld. It is closer to the temperature of the thick plate than to the temperature of the thin plate. It would be very uneconomical to design the weld based on the temperature of the thin plate, yet unsafe to design on the bases of the temperature in the thick plate.
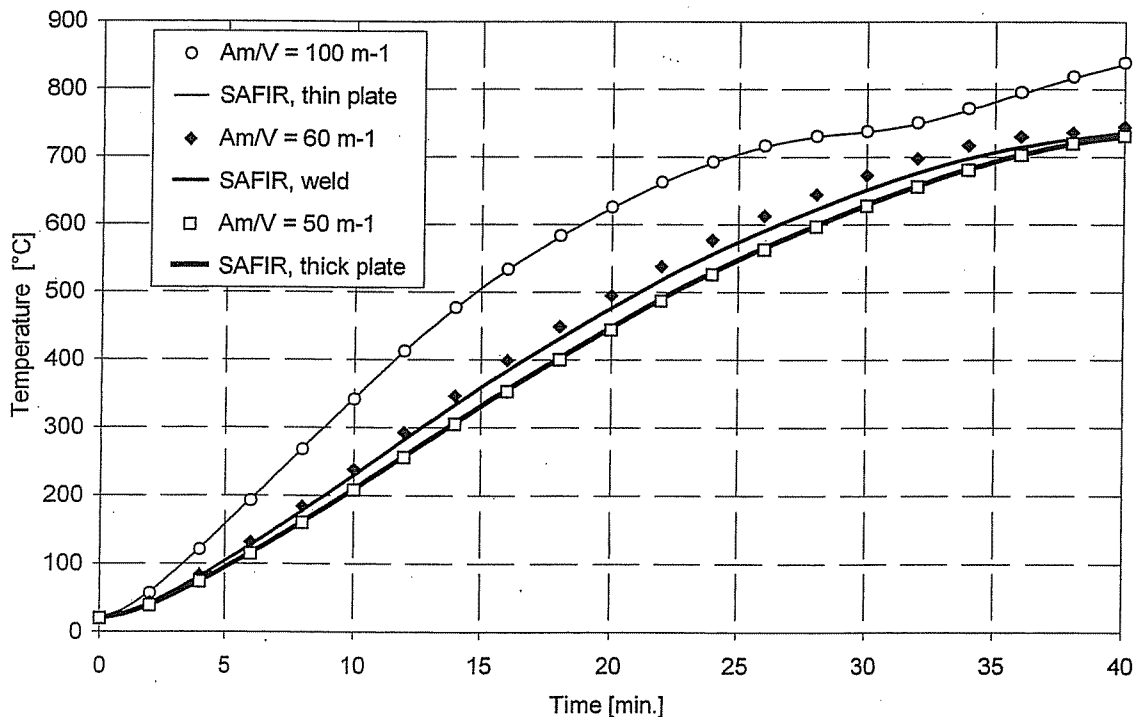

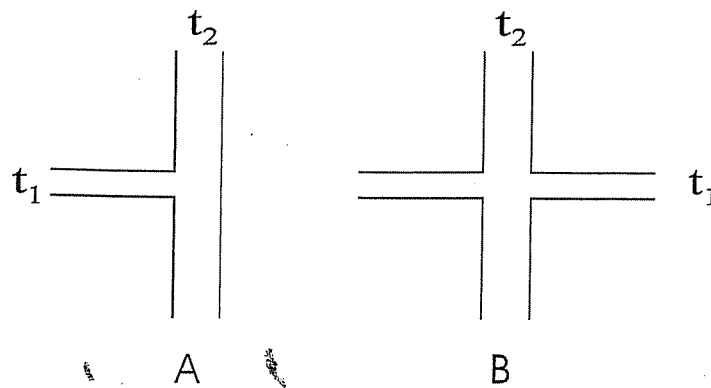Figure 12 : evolution of the temperature under ISO fire

Figure 13 : two different configurations

A good and safe approximation is obtained if one considers the thermal massivity in this region as the one being calculated in the hypothesis of Figure 13-A where a unit length is considered in each direction from the weld. The massivity is then calculated according to equation 7.

$$\frac{A_m}{V} = \frac{6}{t_1 + 2 t_2} \tag{7}$$

In this particular case, equation 7 yields $A_m/V = 6 / (0.02 + 2 \times 0.04) = 60$ m^{-1} and it can be observed on Figure 12 that the temperature calculated on the base of this thermal massivity is an acceptable approximation of the numerical solution.

In the geometrical configuration depicted by Figure 13-B, the temperature in the weld is somewhat higher. It can be safely estimated on the base of the thermal massivity evaluated by equation 8.

$$\frac{A_m}{V} = \frac{8}{2 t_1 + 2 t_2} = \frac{4}{t_1 + t_2} \tag{8}$$

In this case, it yields $A_m/V = 4 / (0.02 + 0.04) = 67$ m^{-1}

In fact, a more precise equation could be written instead of equation 7. Changing the coefficient applied to t_2 in this equation from 2 to 9/4 yields as a consequence that the temperature of the weld is the same as the temperature of the thick plate if $t_1 = 0.75\ t_2$ as observed in the numerical calculations. In this case, this would lead to $A_m/V = 55$ m^{-1} for the weld and the temperature calculated by the simple method would be somewhat colder, in fact nearly exactly the same as the temperature calculated by SAFIR. The expression of equation 7 has been kept for simplicity reasons.

3D ANALYSES

Bar in tension – one cover plate

Figure 14 shows the isotherms in an <u>unprotected</u> tension joint with one single cover plate after 30 minutes of ISO fire. The bars to join have a 12 x 150 mm² section and the 12 mm thick cover sheet is 352 mm long. One quarter of the joint only has been analysed for symmetry reasons; in fact, a total of eight bolts is used in the joint.

DIAMOND XP

FILE: platf1
NODES: 892
ELEMENTS: 520

ELEMENTS PLOT
TEMPERATURE PLOT

TIME: 1800 sec

809.50
806.00
789.00
772.00
755.00
738.00
734.40
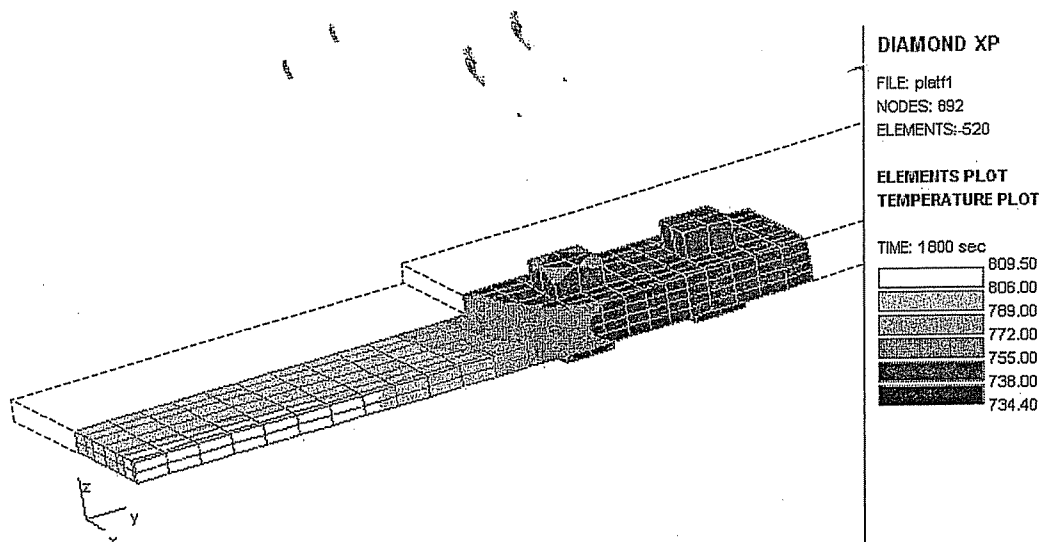
Figure 14 : bars in tension – one cover plate - unprotected

In this case, the ratio between the diameter of the bolt and the thickness of the plate is equal to 20 / 24 and, as it is smaller than 1, the bolts create a hot spot in the joint.

The temperature after 30 minutes calculated by the simple method using the thermal massivity of the tension plates $A_m/V = 2 \ (0.012 + 0.150) / (0.012 \times 0.150) = 180 \text{ m}^{-1}$ is equal to 806°C, whereas the temperature calculated with the thermal massivity of the joint (neglecting the effect of the bolts) $A_m/V = 2 \ (0.150 \times 0.352 + 0.024 \times 0.352 + 0.150 \times 0.012) / (0.024 \times 0.150 \times 0.352) = 100 \text{ m}^{-1}$ is 738°C. These two significant temperatures are represented on the temperature scale on the right in Figure 14. It can be observed in this unprotected connection that:

1. The joint is definitively colder than the tension plates.
2. The colder zone in the tension plates near the joint has a limited extension.
3. Nearly the whole joint has a temperature that is by 20°C in excess of the temperature that is calculated by the simple method using the massivity of the joint.

Figure 15 refers to the same joint, now <u>thermally protected</u>. The temperatures calculated by the simple method after 90 minutes of exposure are 523°C in the tension bars away from the joint and 367°C in the joint. From the isotherms on the figure, it can be observed that:

1. The joint is still colder than the tension plates.
2. The colder zone in the tension plates near the joint has extends to a longer distance.
3. The temperature at any point in the joint is at least 410°C. The temperature in the bolt that is closest to the bars is 425°C. This means that the temperature in the joint is 40 to

60°C higher than temperature that is calculated by the simple method using the massivity of the joint.
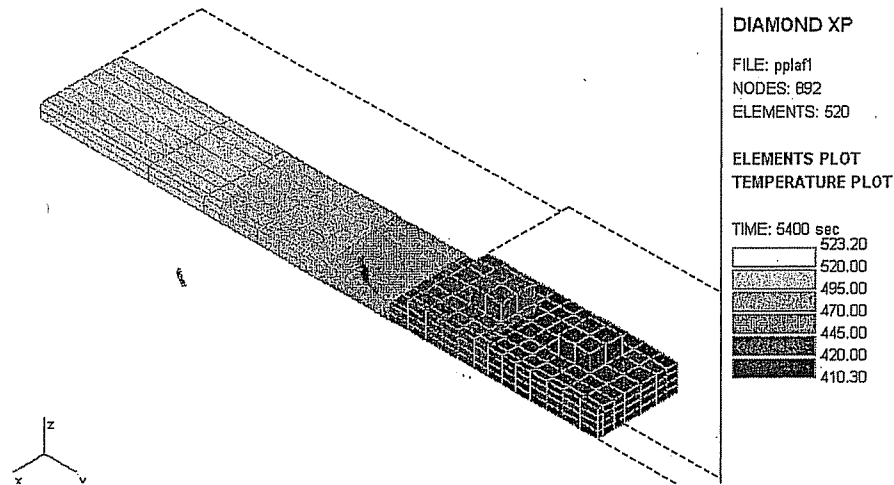
Figure 15 : bar in tension - one cover plate - thermally protected

The observations that have been made here in the simplest case of a joint with 2 different thickness, and the difference between the insulated or non insulated joint, will in fact generally be observed in all the more complex geometries that can be analysed. This is illustrated in the next sections.

Bars in tension – two cover plates

Figure 16 is a joint for the same bars as presented in Figure 14, i.e. non protected, but now with two symmetrically located cover plates with a thickness of 6 mm each. The same observations can be made here, namely; a cold zone of limited extension in the bar close to the joint; a joint that is significantly colder than the bar; the temperature in the joint somewhat higher than the temperature of 738°C than can be calculated by the simple method on the base of the massivity of the joint.
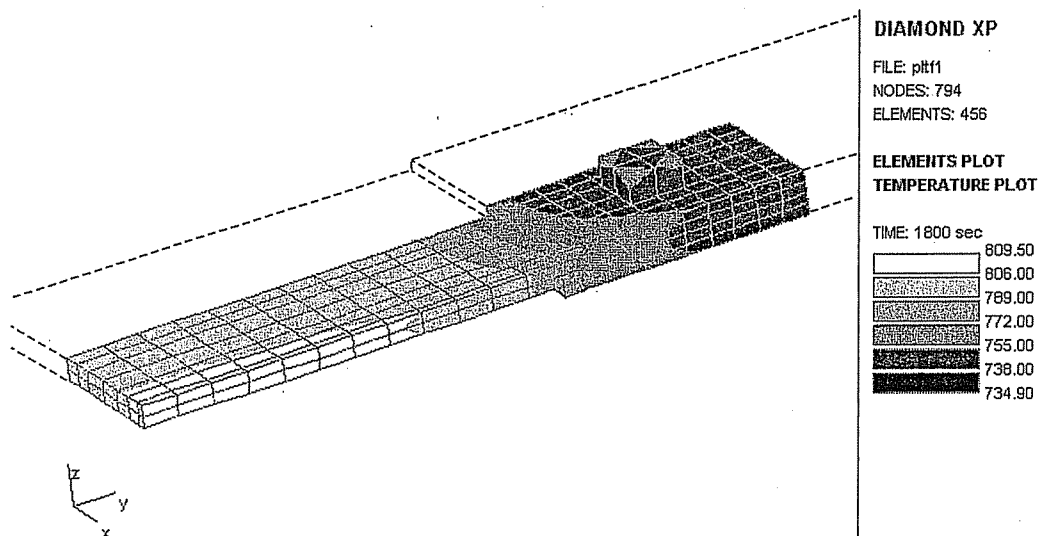
Figure 16 : bars in tension - two cover plates - unprotected

11

Bars in tension – net or whole section

It is written in Eurocode 3 [1] that net-section failure at fasteners holes need not be considered because of the presence of additional material.

Figure 17 shows the evolution of the temperature in the thermally protected joint depicted in Figure 16 at the level of the bolt, first as calculated by SAFIR, then as calculated on the base of the local massivity in the joint, 97 m^{-1}, and it is seen that this is unsafe, and finally on the base of the massivity of the connected bars, 180 m^{-1}, and it is seen that this is safe.
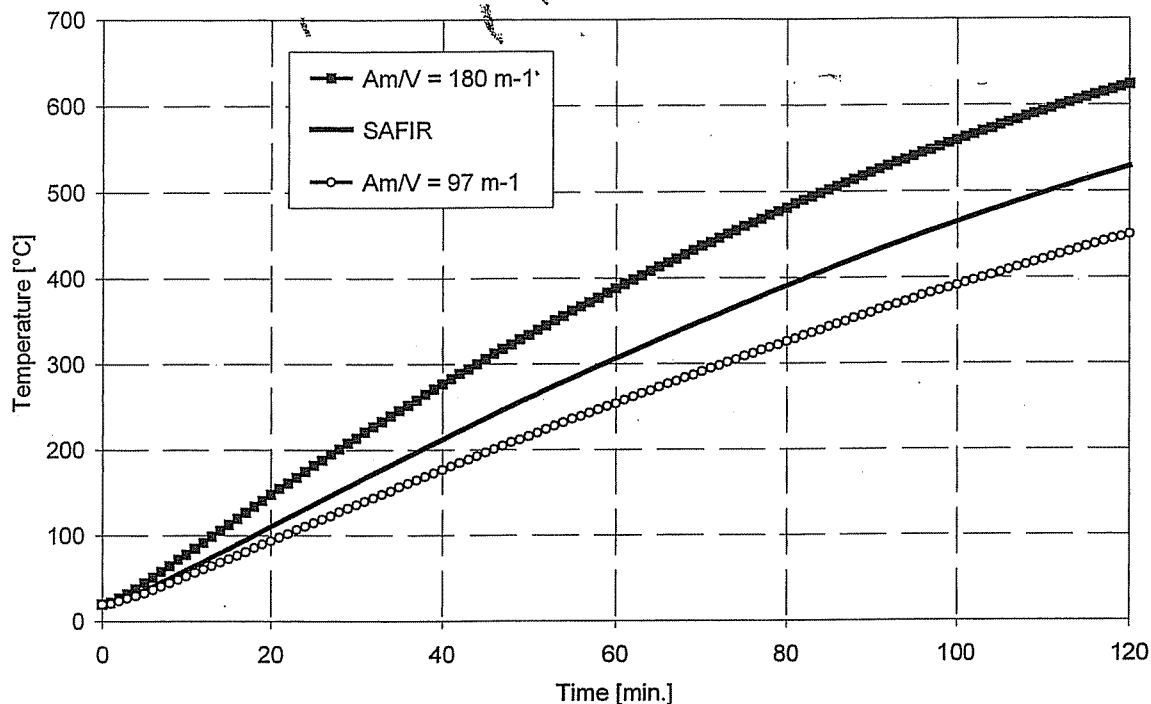
Figure 17 : evolution of the temperature in the protected joint

Figure 18 shows the evolution of the tension strength in the bar, first according to the temperature computed by SAFIR and considering the net section of 12 x 110 = 1320 mm², then calculated on the base of the simple temperature in the bar and on the gross section of 12 x 150 = 1800 mm².

It can be observed that the procedure recommended by Eurocode to neglect the reduction in section of the bars at the locations of the fasteners is not safe when the temperature simply calculated is not sufficiently lower than the '*true*' temperature, i.e. namely during the first moments of the fire (90 minutes for the case of Figure 18) and also for longer durations when the temperatures in the whole structure tend to level off to a same uniform level because of the tendency of nominal fire curves to end up in a quasi steady state constant temperature (not seen on Figure 18).
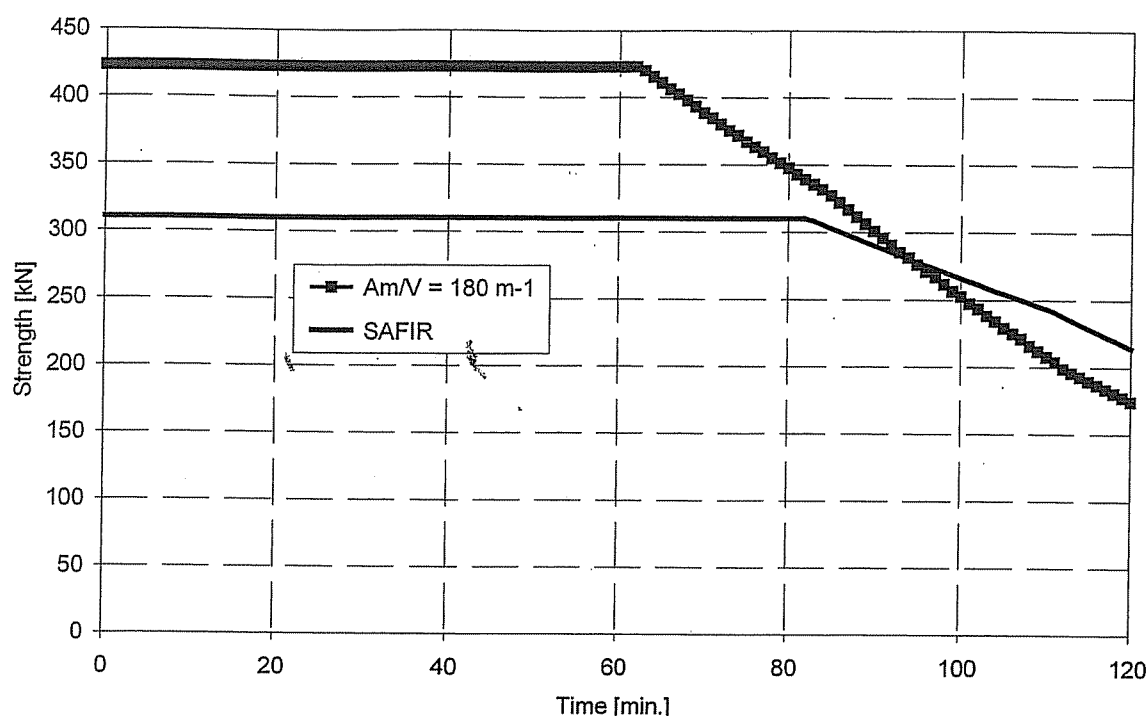
Figure 18 : evolution of the strength in the protected joint

Beam in bending – cover plates

Figure 19 shows 1/8 of a thermally protected joint in an IPE 330 steel beam submitted to bending and to shear. The joint is made of 20 mm bolts and 6 mm thick steel plates.

If calculated by the simple method based on the local massivity, the temperatures after 90 minutes of ISO fire are;

- 552°C in the steel beam ($A_m/V = 200$ m^{-1})
- 400°C in the cover plate on the flanges ($A_m/V = 114$ m^{-1})
- 373°C in the cover plates on the web ($A_m/V = 103$ m^{-1})

As in the joint of Figure 15 that was geometrical simpler, the temperature in this joint is in fact colder than the temperature calculated in the element by the simple method, but the temperature in the different parts of the joint is significantly higher than the temperature calculated on the base of the local massivity. It can even be observed that the temperature on the plate covering the web is higher than the temperature covering the flange, whereas the local massivity should indicate the contrary; this is of course because of the influence of the thin web that is surrounding this part of the joint.

13

DIAMOND XP

FILE: ppouf1
NODES: 1539
ELEMENTS: 743

NODES PLOT
ELEMENTS PLOT
TEMPERATURE PLOT

TIME: 5400 sec
575.50
550.00
535.00
520.00
505.00
490.00
486.50
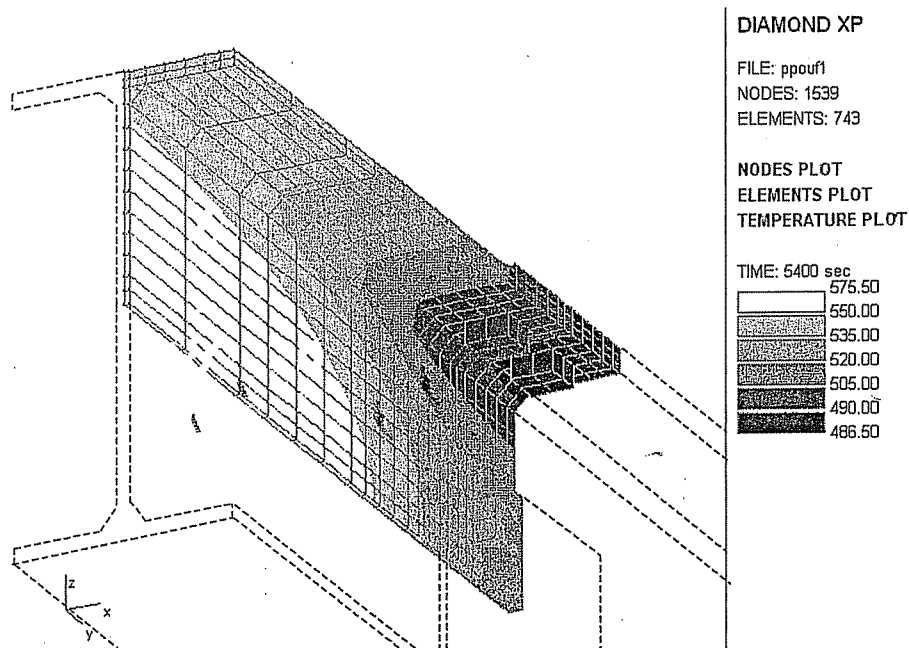
Figure 19 : beam with cover plates - protected

The same holds for the unprotected beam, see Figure 20; the temperatures in the joint are higher than the temperature calculated on the base of the local massivity, namely 633°C in the plate on the web and 654°C in the plate on the flange.

DIAMOND XP

FILE: pouf1
NODES: 1539
ELEMENTS: 743

NODES PLOT
ELEMENTS PLOT
TEMPERATURE PLOT

TIME: 1200 sec
734.10
730.00
720.00
710.00
700.00
690.00
680.00
672.50
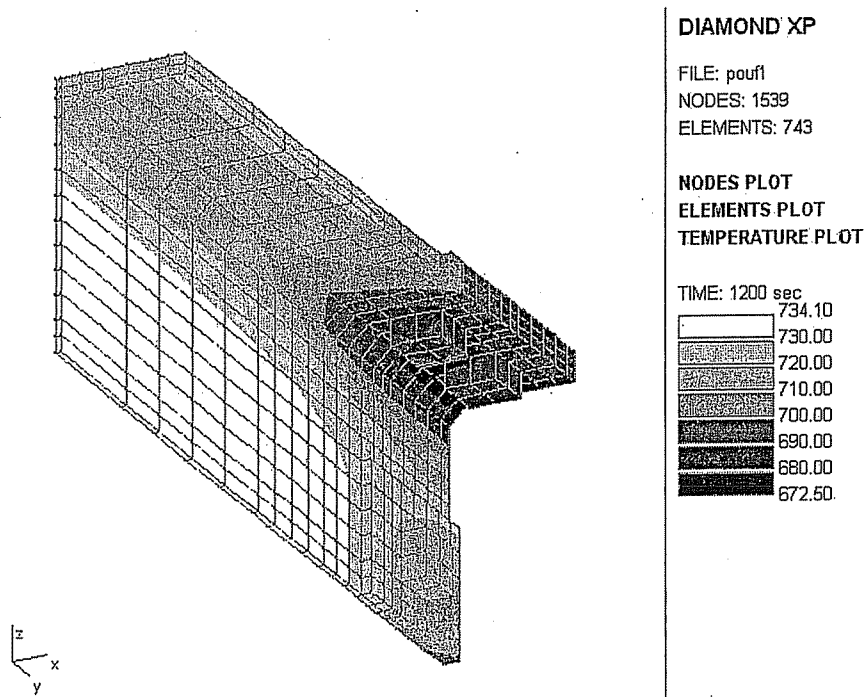
Figure 20 : beam with cover plates - unprotected

Beam in bending – flush end plates

DIAMOND XP

FILE: pop11
NODES: 1288
ELEMENTS: 702

NODES PLOT
ELEMENTS PLOT
TEMPERATURE PLOT

TIME 1200 sec

732.40
730.00
690.00
650.00
610.00
570.00
530.00
529.70
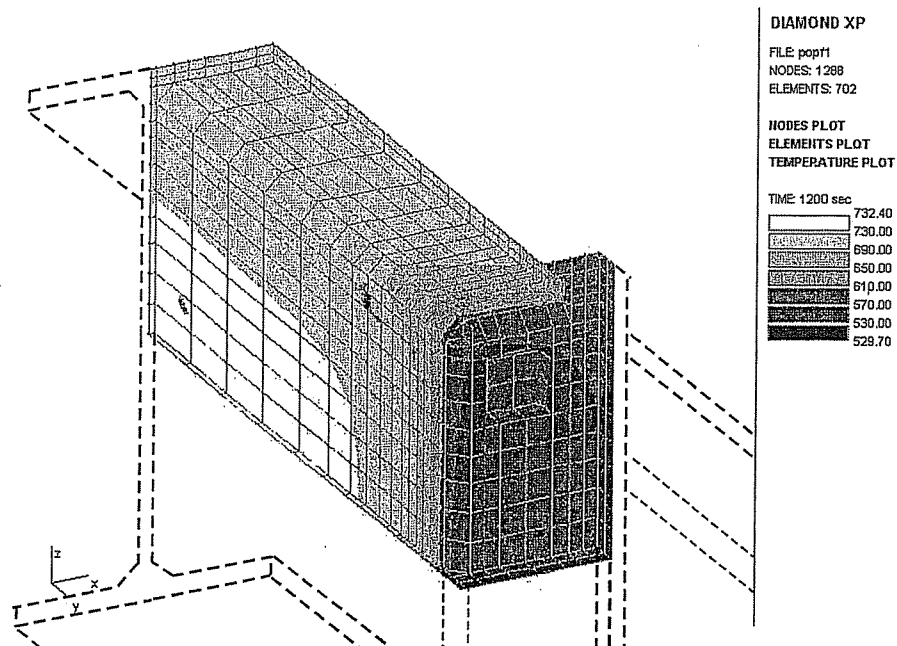
Figure 21 : unprotected flush end plate

Figure 21 is about two IPE360 beams with welded flush end plates connected by 24 mm bolts. The steel plates are 20 mm thick and 20 mm wider in each transverse dimension than the beam section.

Calculated according to the simple method based on the local massivity, the temperatures after 20 minutes of ISO fire are;

719°C in the beam ($A_m/V = 186 \text{ m}^{-1}$)

445°C in the plates ($A_m/V = 50 \text{ m}^{-1}$)

Here also, the temperature in the connection is lower than the simple temperature in the elements, but significantly higher than the temperature calculated by the simple method based on the local massivity.

Beam to column joint – flush end plates

Two IPE360 beams are connected by flush end plates to a HEA240 column. The joint is a moment resisting joint but no stiffener is provided. The end plates are 20 mm thick and 20 mm wider in each transverse dimension than the beam. 20 mm bolts are used to connect the end plates to the flanges of the column.

Figure 22 shows the isotherms after 120 minutes of ISO fire in 1/8 of the protected joint. Simply calculated temperatures are:

634°C in the beam ($A_m/V = 186$ m^{-1})
621°C in the column ($A_m/V = 178$ m^{-1})
389°C in the plates ($A_m/V = 77$ m^{-1})

It has to be noted that the local massivity calculated simply on the base of the cumulated thickness of the plate and of the flange of the column would yield $A_m/V = 2$ / $0.032 = 63$ m^{-1} and a temperature of 340°C. Here, the local massivity has been evaluated on the base of a horizontal section through these 2 pates, taking into account the additional lateral surfaces.

Here again, the temperature in the joint is lower than the temperature simply calculated in both connected members, but the temperature is higher than the temperature calculated on the base of the local massivity.

Beam to column joint – angles

Figure 23 represents the isotherms after 20 minutes of ISO fire in an unprotected joint connecting the IPE360 beams to the HEA240 column. The bolts are M20 bolts. The angles or cleats are 14 mm thick, 240 mm wide and 140/65 mm long.
Simply calculated temperatures are:
719°C in the beam ($A_m/V = 186$ m^{-1})
716°C in the column ($A_m/V = 178$ m^{-1})
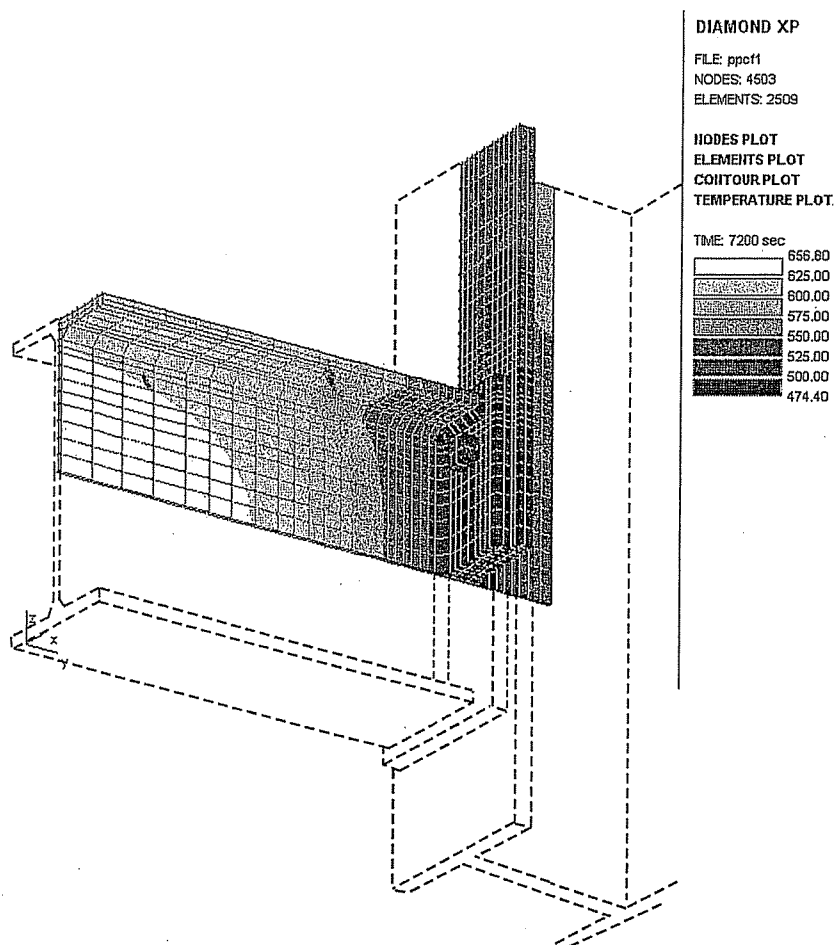
Figure 22 : protected flush end plate
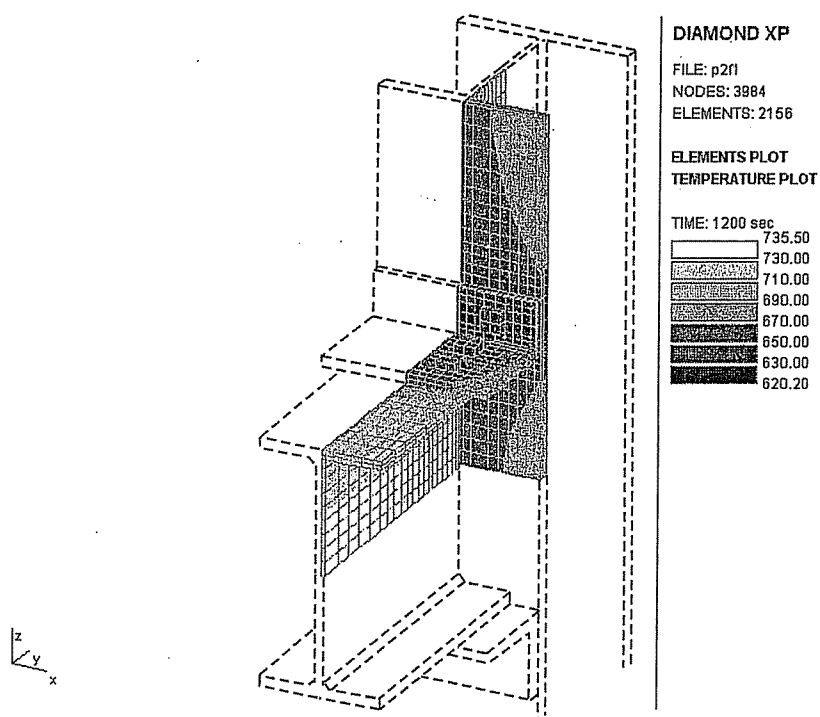
Figure 23 : unprotected joint with angles

Beam to column joint – flush end plate and stiffener

Figure 24 refers to a protected joint connecting the IPE360 beam with the HEA240 column with 24 mm thick flush end plates and 12.7 mm thick stiffeners between the flanges of the column.

Temperatures calculated by the simple method after 90 minutes of ISO fire in 1/8 of the protected joint are are:

532°C in the beam (A_m/V = 186 m^{-1})
520°C in the column (A_m/V = 178 m^{-1})
269°C in the end plates (A_m/V = 64 m^{-1})
485°C in the stiffeners (A_m/V = 157 m^{-1})

In this case, it is found that the temperature in the end plates is higher than the simply calculated temperature, but the temperature in the stiffener is lower than the simply calculated temperature.

DIAMOND XP

FILE: pp3f1
NODES: 4921
ELEMENTS: 2718

NODES PLOT
ELEMENTS PLOT
CONTOUR PLOT
TEMPERATURE PLOT

TIME: 5400 sec
557.00
500.00
480.00
460.00
440.00
420.00
400.00
396.50

Figure 24 : protected joint with flush end plate and stiffeners

Beam to column joint – angles and stiffener

Figure 25 is a joint between the IPE360 beams and HEA240 column made of bolted cleats and involving stiffeners between the flanges of the column. The thickness of the stiffener is 12.7 mm. The thickness of the cleats is 14 mm for the connection to the flanges of the beams and 10 mm for the connection to the web of the beams.

The figure shows the isotherms after 30 minutes of ISO fire in this joint without thermal protection. They have to be compared with:

809°C in the beam ($A_m/V = 186$ m^{-1})
805°C in the column ($A_m/V = 178$ m^{-1})
732°C in the cleats on the flanges of the beam ($A_m/V = 87$ m^{-1})
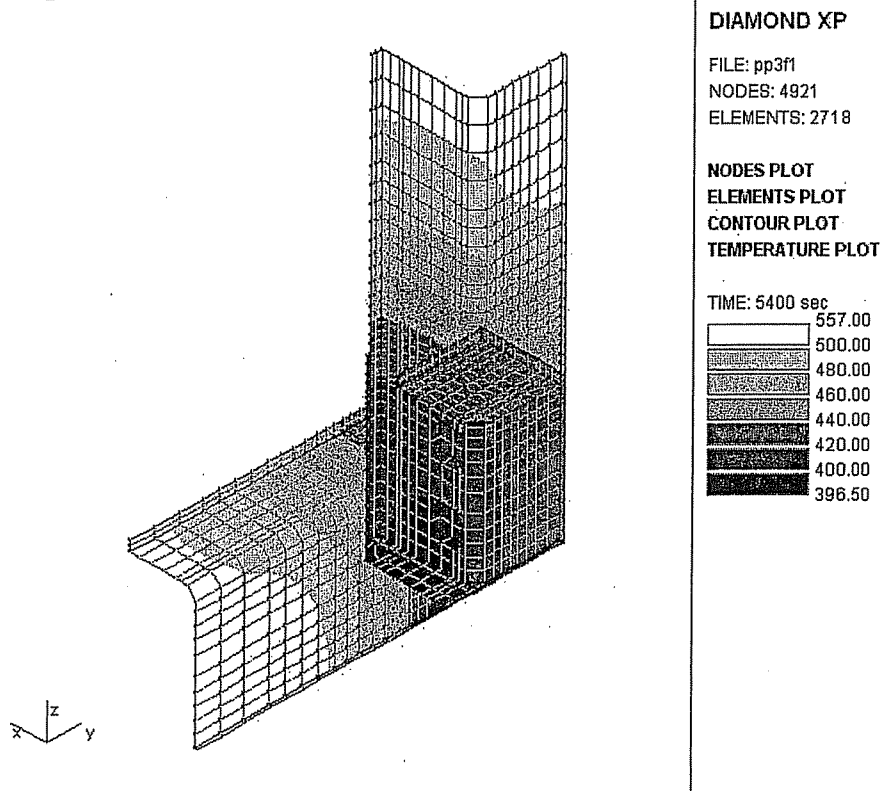792°C in the stiffeners ($A_m/V = 157$ m^{-1})
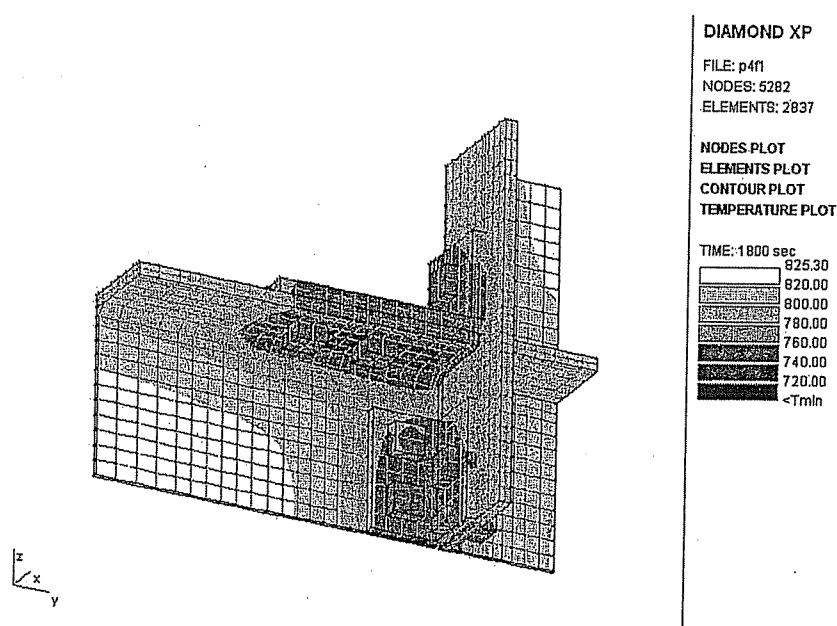
Figure 25 : unprotected joint with cleats and stiffener

It has to be noted that the results of the simulation made on the two joints of Figure 24 and Figure 25 have been compared with experimental results obtained by Kruppa [5]. The agreement was generally quite good, with a tendency for the experimental temperatures to be somewhat lower than the numerically calculated values in the joints, owing to a corner effect in the testing compartment. These comparisons can not be shown here because of the limited amount of allocated space for each paper.

CONCLUSIONS

From all the examples that have been calculated, there has been no single occurrence where the temperature in the joint would have been higher than the temperature of the connected elements. This result was obtained although the favourable effect of colder temperatures in the corners of the compartment which can play a role in most of the cases has not been taken into account. It is therefore indeed safe to design the connection on the base of the temperature calculated in the connected elements.

The recommendation of Eurocode 3 [1] that net-section failure at fasteners holes need not be considered cannot be supported because, after an important duration of exposure to a fire curve that has a tendency to reach a nearly steady state condition – such as the nominal fire curves – there is a tendency for the temperature to become more and more uniform and, hence, the effect of additional material near the hole is very much diluted. Furthermore, this local effect of the fastener can be negative in some cases, namely when the diameter of the bolt is smaller that the total thickness of the plates that the bolt connects.

The recommendation that the temperature of a connection may be assessed using the local massivity value of the components comprising the connection can also not be supported. In nearly all calculated examples, the temperature in the components was higher than what the local massivity would have indicated. This is probably because the dimensions of the components are of an order of magnitude smaller than the dimensions of the connected members and the influence of these members is felt in the components.

REFERENCES

[1]   Draft prEN 1993-1-2, *Eurocode 3: Design of steel structures - Part 1-2: General rules - Structural fire design*, Third preliminary draft, May 2001.

[2]   ENV 1991-1-2, *Eurocode 1- Basis of design and actions on structures – Part 2-2: Actions on structures – Actions on structures exposed to fire*, [3]   ENV   1993-1-2, *Eurocode 3: Design of steel structures - Part 1-2: General rules - Structural fire design*, CEN, Brussels, May 1995.

[3]   ENV 1993-1-2, *Eurocode 3: Design of steel structures - Part 1-2: General rules - Structural fire design*, CEN, Brussels, May 1995.

[4]   Franssen J.-M., Kodur V. K. R. & Mason J., *User's Manual for SAFIR (Version NZ). A Computer Program for Analysis of Structures Submitted to the Fire*, Univ. of Liege, Ponts et Charpentes, Rapport interne SPEC/2000_03, 2000

[5]   J. Kruppa, *Résistance au feu des assemblages par boulons haute résistance*, C.T.I.C.M., Puteaux, France, June 1976.

EXPERIMENTAL AND ANALYTICAL STUDIES OF STEEL JOINT COMPONENTS AT ELEVATED TEMPERATURES

Spyros SPYROU[1], Buick DAVISON[1] Ian BURGESS[1] Roger PLANK[2]

[1] *Department of Civil and Structural Engineering, University of Sheffield, Sheffield S1 3JD, UK*
[2] *School of Architectural Studies, University of Sheffield, Sheffield S10 2TN, UK*

ABSTRACT

This paper reports on experimental furnace testing and development of simple analytical models intended to initiate the development of a Component Method for modelling of steel beam-to-column connections in fire conditions. The basic theme of the Component Method is to consider any joint as an assembly of individual simple components. Each of these components is simply a non-linear spring, possessing its own level of strength and stiffness in tension, compression or shear, and these will degrade as its temperature rises.

The main objective of this study was to investigate experimentally and analytically the behaviour of tension and compression zones of end-plate connections at elevated temperatures. A series of experiments has been carried out, and these are described in the paper. Simplified analytical models of the component behaviour have been developed, and these have been validated against the tests and against detailed finite element simulations. The simplified models have been shown to be very reliable for this very common type of joint, although similar equations will need to be developed for other configurations. The component models developed have been shown to produce moment-rotation curves which correlate well with the results of previous furnace tests on complete connection behaviour in fire. The principles of the Component Method can be used directly in either simplified or finite element modelling, without attempting to predict of the overall joint behaviour in fire. This will enable semi-rigid behaviour to be taken into account in the analytical fire engineering design of steel-framed buildings, for which it is inadequate simply to consider the degradation of the ambient-temperature moment-rotation characteristics of a joint without taking account of the high axial forces which also occur.

KEYWORDS: *fire engineering, joints, component method, steel structures, furnace testing, simplified modelling, FE modelling.*

INTRODUCTION

Structural steel frames usually consist of universal beams and columns assembled together by means of connections. In conventional analysis and design of steel and composite frames, beam-to-column joints are assumed to behave either as "pinned" or as fully "rigid". Although the pinned or fixed assumption significantly simplifies analysis and design procedures for the engineer, real joint behaviour exhibits characteristics over a wide spectrum between these two extremes.

To date, data on the real response of joints at elevated temperatures has been gathered from full-scale furnace tests [1-3] on cruciform arrangements, which have concentrated exclusively on moment-rotation behaviour in the absence of axial thrusts. However, when steel-framed structures are subjected to fire, the behaviour of the joints within the overall frame response is greatly affected by the high axial forces, which are created by restraint to the thermal expansion of unprotected beams. If moment-rotation-thrust surfaces were to be generated at different temperatures this process would require prohibitive numbers of complex and expensive furnace tests for each joint configuration. The alternative, and more practical, method is to extend the principles of the "Component Method" of joint analysis and design to the elevated-temperature situation.

The basis of the Component Method is to consider any joint as an assembly of individual simple components as shown in Fig. 1. A steel joint under the action of a member end-moment is divided into the three principal zones shown: the tension, compression and shear zones.
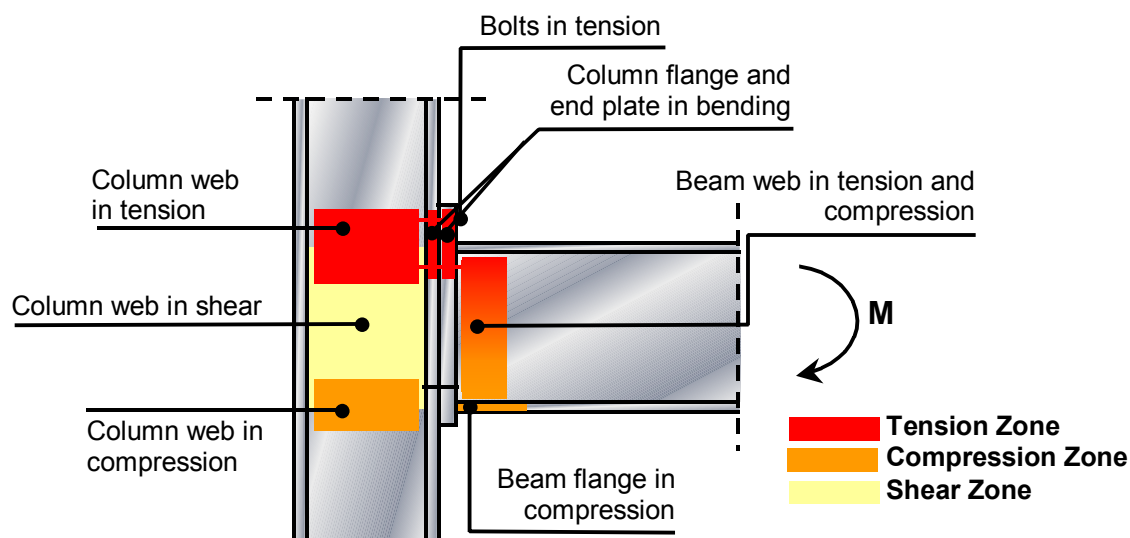
FIGURE 1: The three zones and their components within an end-plate steel joint.

Each of these components is simply a non-linear spring, possessing its own level of strength and stiffness in tension, compression or shear, and these will degrade as its temperature rises. The main objective of the study reported here was to investigate experimentally and analytically the behaviour of tension and compression zones of end-plate connections at elevated temperatures. A series of experiments has been carried out, and these are described in the paper. A simplified analytical model has been developed, and this has been validated against the tests and against detailed finite element simulations. The simplified model is shown to be very reliable for this very common type of joint, although similar methods will

need to be developed for other configurations. The principles of the Component Method can be used directly in either simplified or finite element modelling, without attempting to predict the overall joint behaviour in fire, to enable semi-rigid behaviour to be taken into account in the analytical fire engineering design of steel-framed and composite buildings.

APPARATUS FOR ELEVATED TEMPERATURE TESTING

Testing at high temperatures poses a major problem, mainly because the conventional types of displacement-measurement devices could not be applied. The usual method of using silica rods as extensions to transducers mounted outside the furnace is highly unreliable; the rods are very fragile, undergo some extension over their heated lengths, and often lose contact with the specimen. Inclinometers are usually used to measure rotations in the furnace, but need to be continuously cooled throughout a test and their wiring is very vulnerable to being burnt-through. An efficient and robust form of measurement of deflections was required for the large number of high-temperature component tests. For this reason a novel image acquisition and processing technique [4,5] was developed to measure deflections during high-temperature tests.

Video cameras were mounted outside a $1m^3$ capacity electric furnace capable of reaching 1100^0C and equipped with viewports at the top and on the side perpendicular to the loading direction. In total three video cameras were used to view the critical zone of the component under test. The testing procedure was to take the specimen up to a pre-determined temperature and then apply a sequence of load steps using a 500kN horizontal actuator (Fig. 2). Images were captured at different load steps in constant-temperature tests, and these were processed using image processing software, producing a load-displacement plot.
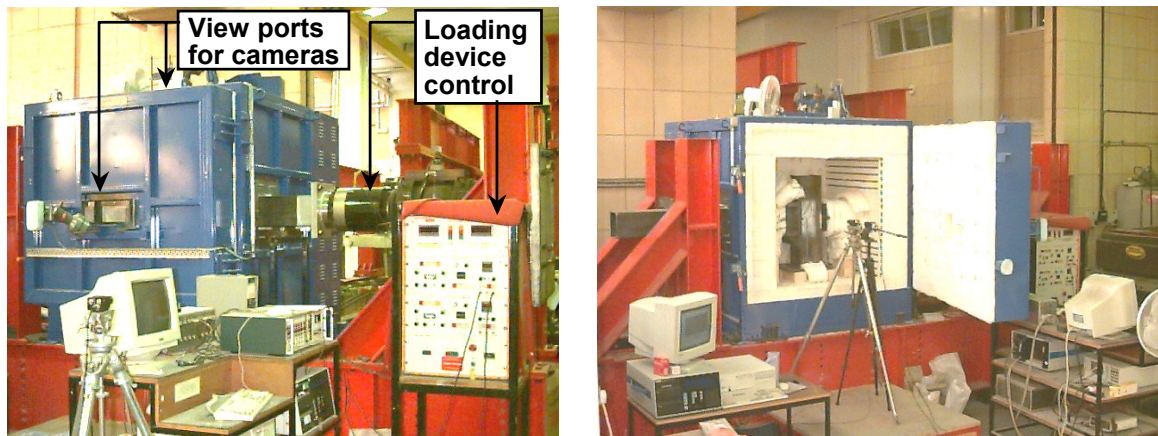
FIGURE 2: The experimental set-up: electric furnace and loading gear.

TENSION ZONE TESTS

The first elevated temperature tests were performed on components of the tension zone of a steel beam-to-column end-plate joint. The tension zone plays a fundamental role in the behaviour of a joint at ambient and elevated temperatures. The three major components within the tension zone are:

- The end-plate in bending,
- The column flange in bending,

Bolts in tension.All these components are modelled using an equivalent T-stub, which consists of two T-elements connected as shown in Fig. 3 through the flanges by means of one or more bolt rows.
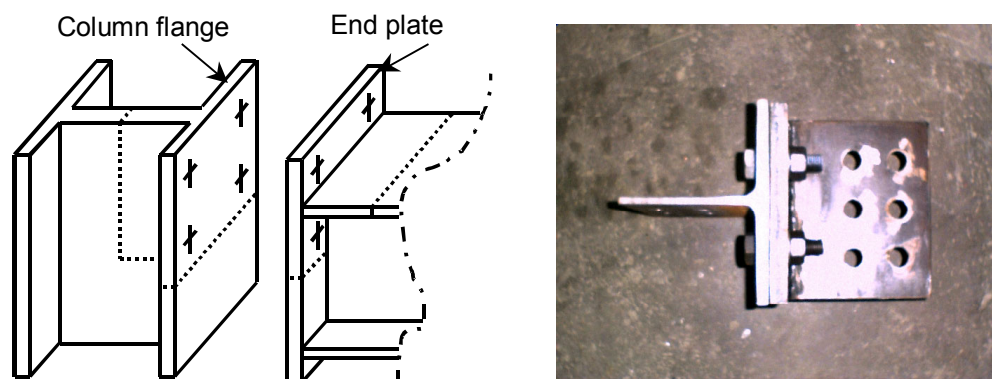
FIGURE 3: T-stub identification and orientation for extended end-plate joint.

The deformation of each equivalent T-stub assembly is a combination of the elastic and plastic flexure of the column flange and end plate, and the elastic and plastic elongations of the bolts. It is well known that these T-stub assemblies can fail according to the three possible failure modes shown in Fig. 4.

1. Yielding in the T-stub flange, followed by yielding and fracture of the bolts,

2. A complete yield mechanism in the T-stub flange,

3. The T-stub flange remains elastic until fracture of the bolts.
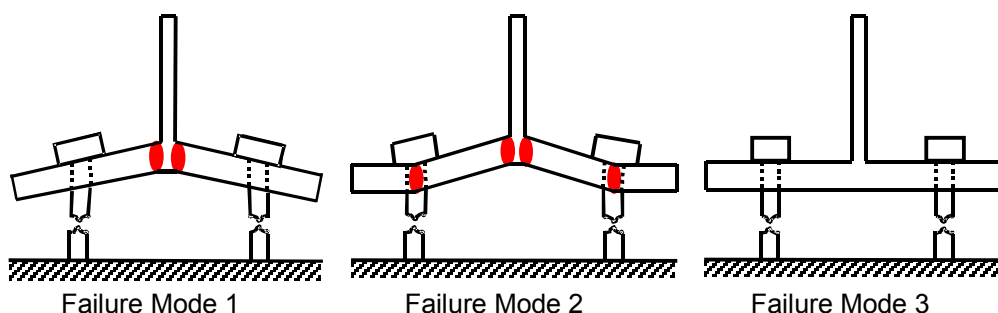
FIGURE 4: Failure modes for the T-stub flange.

A simplified model was developed using plastic theory and classical elastic structural mechanics [6,7]. The model was then extended to predict the three failure modes of the T-stub specimens from their geometrical and mechanical properties at ambient and elevated temperatures. Tests were performed at elevated temperatures on specimens with different geometrical properties to investigate these three failure modes. In total 45 specimens were tested at temperatures ranging from 20°C to 800°C, these temperatures being measured using thermocouples at different positions on the flange and bolts. The last 25 T-stub specimens were connected as shown in Fig. 5, representing the real tension zone of an extended-end-plate joint. The use of Grade 8.8 bolts and nuts resulted in a nut-stripping failure, so instead High Strength Friction Grip nuts were used for subsequent tests. From the first tests at elevated temperatures it was obvious that bolt flexibility was a key parameter in the behaviour of the T-stub tension zone specimens.

The load-deformation comparisons between the simplified model and the actual elevated-temperature test results were in good agreement for all the failure modes, as shown in Figs. 5-7, especially so considering the complexity of the problem of interacting flange and bolt forces and the stress-strain curves at elevated temperatures.
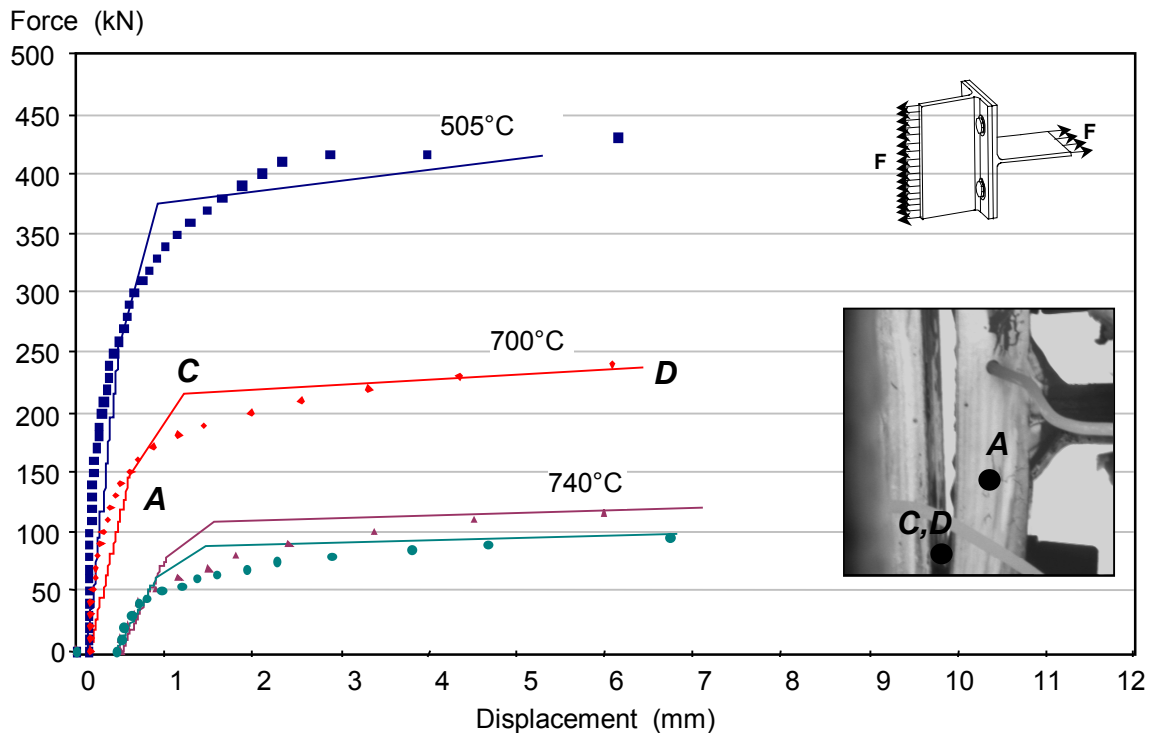
FIGURE 5: Typical force-deflection curves for end plate T-stub in Failure Mode 1.
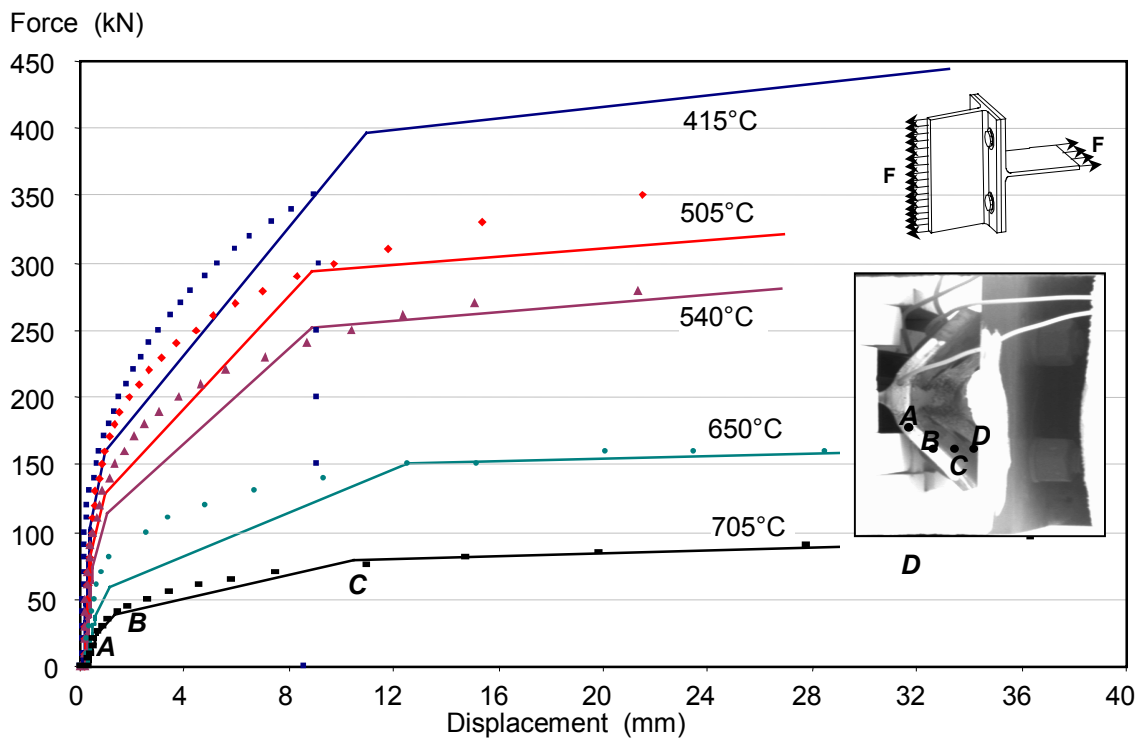
FIGURE 6: Typical force-deflection curves for end plate T-stub in Failure Mode 2.

25
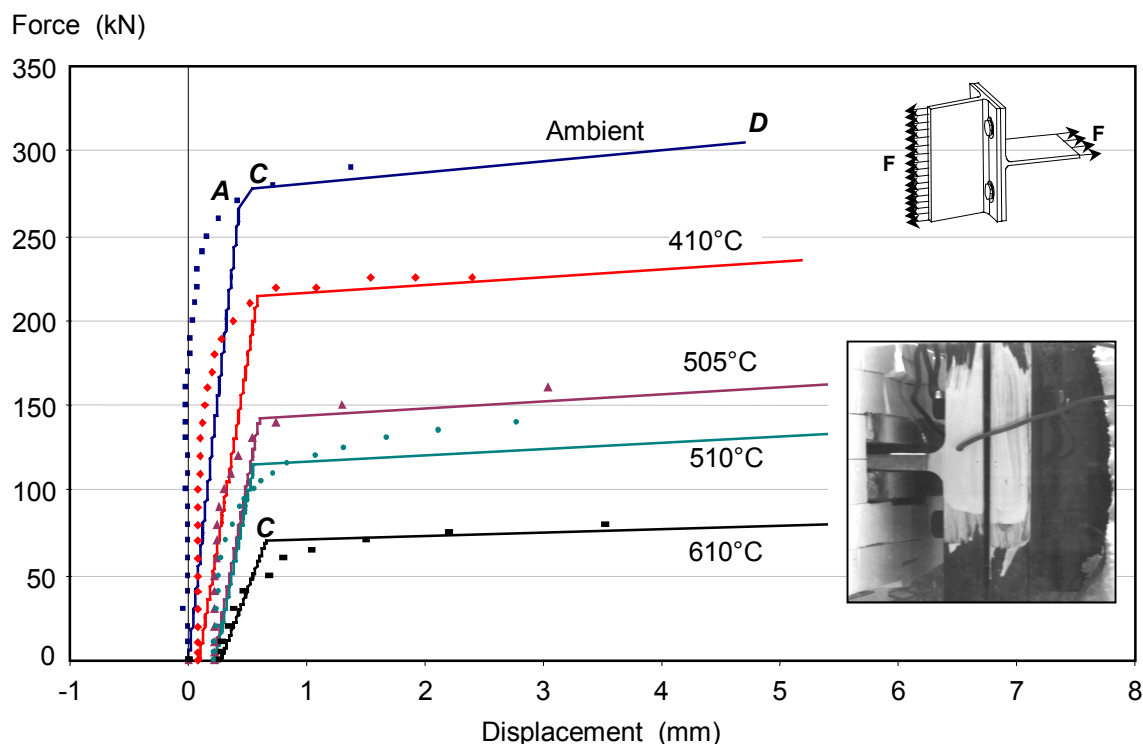
FIGURE 7: Typical force-deflection curves for end plate T-stub in Failure Mode 3.

In contrast 2-D finite element analysis using ANSYS did not generate particularly good comparisons with the test results. This concurs with the findings of the COST C1 Workgroup WG6, which performed studies using 2-D and 3-D modelling, and concluded [8] that 2-D modelling is not satisfactory. Factors affecting the accuracy of FE modelling include the meshing of the model (the optimum mesh size), simulation of bolts (to model the bolt as a flexural element is not an easy task), choice of elements, material behaviour, and most importantly the modelling of contact and gap elements.

COMPRESSION ZONE

At ambient temperatures researchers [9-11] have focused on producing simplified models in order to predict the ultimate capacity of a column web subjected to transverse compressive forces (Fig. 8) and thereby assist engineers to design steel joints efficiently. Another reason for producing these models was to eliminate the use of column web stiffeners, which are expensive to install and interfere with the minor-axis framing of beams into the column.
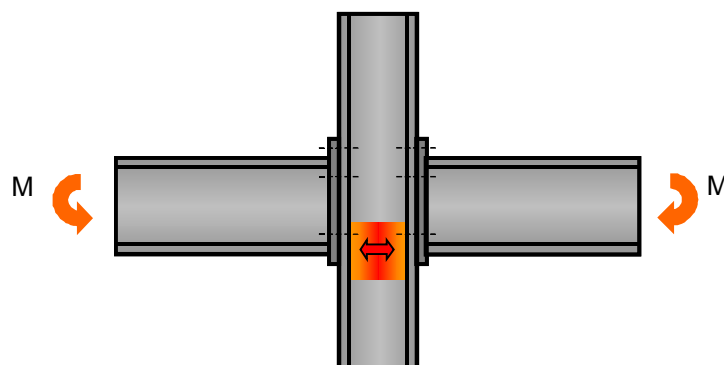
FIGURE 8: Extended end-plate joint showing the column web component (shaded).

Resistance to concentrated forces is a complex problem to which it is difficult to derive closed-form theoretical solutions. Therefore, studies aimed at predicting the ultimate resistance of column webs to concentrated forces tend towards empirical solutions. In this project, a parametric study was performed initially to verify the accuracy of the formulae described in BS5950 [12] and EC3:Annex J [13] at ambient temperatures. It was apparent from a wide range of sources [14] that both current design codes gave very conservative results for the ultimate capacity of column webs under transverse compressive force when compared with test results. The problem acquires a further degree of complexity when another variable, such as temperature, is introduced. A new empirical model was investigated, with the aim of providing not only the ultimate capacity of the column web at elevated temperatures but also its stiffness in the elastic and plastic regions. An experimental investigation was carried out first and then, based on the test observations and results, a simplified empirical model was developed.

The experimental set-up is illustrated in Fig. 9. Compressive forces were applied directly across the column section, and in order to prevent the column specimen from rotating freely in space finger-tight bolts were placed below the compression force contact point. In total 29 compression zone tests were performed, at ambient and elevated temperatures, covering a broad range of web slenderness (*depth between fillets/web thickness* between 12.7 and 22.3). From the early stages of this investigation it was realised that the ultimate load capacity of the column web was determined essentially by the strength characteristics of the specimen.
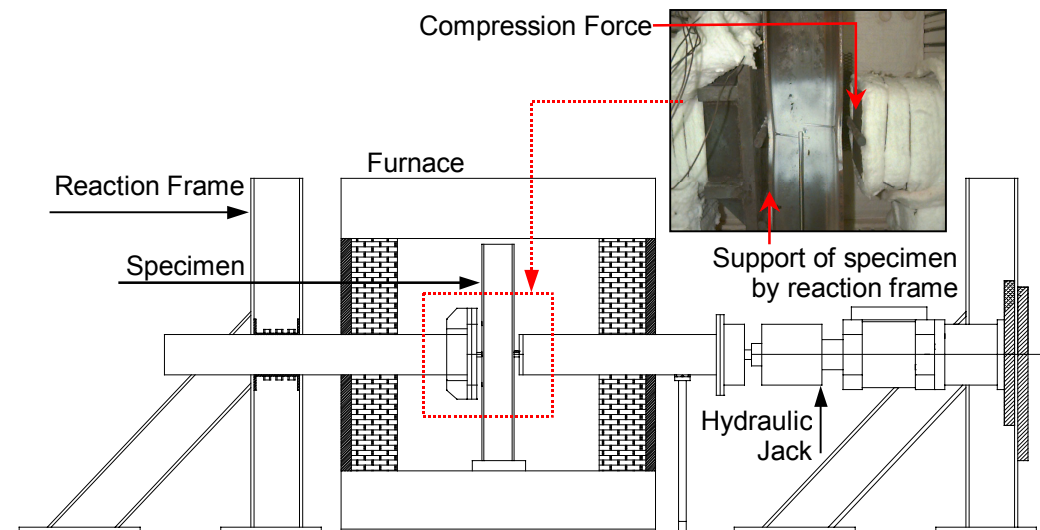
FIGURE 9: Arrangement for compression zone tests.

Literature searches for empirical formulas for calculating the ultimate load capacity of column webs at ambient temperature were unsuccessful, as these did not include the effects of the stiffness of the column flanges, but studies of plate girders subjected to patch loading [15] proved useful. One formula by Drdacky [16], for rather thick plate girder webs, had given good correlation with ambient-temperature tests [15].

$$P_u = 0.55t_{wc}^2\sqrt{E_{wc}\sigma_{wc}}\sqrt{\frac{t_{fb}}{t_{wc}}}\left[0.9+\left(\frac{1.5c}{d_{wc}}\right)\right] \qquad (1)$$

Where E_{wc} and σ_{wc} are the Young's Modulus and yield strength respectively of the column web, t_{wc} is the thickness of the web, t_{fb} is the flange thickness, d_{wc} is the depth between fillets, and c is the patch load length.

Markovic *et al* [15] suggest that the mean value for the ratio of predicted to experimental capacity should be 0.72. This means that, instead of using a coefficient of 0.55 in equation (1), a new value of 0.76 could be used. This formula, altered to take into account the degradation of material properties at elevated temperature, gave good correlation with the test results from the current study, but when compared with finite element studies performed to investigate the significance of the *c* value (the uniformly distributed patch length in Fig. 10) on the behaviour of the column web it was found to give unconservative values for the ultimate capacity of the column web. For this reason a new empirical formula was derived, based on the Drdacky formula:

$$P_u = t_{wc}^2 \sqrt{E_{wc}\sigma_{wc}} \sqrt{\frac{t_{fb}}{t_{wc}}} \left\{ 0.65 + \left[\left(\frac{1.6c}{d_{wc}} \right) \left(\frac{2\beta}{2\beta + c} \right) \right] \right\} \tag{2}$$
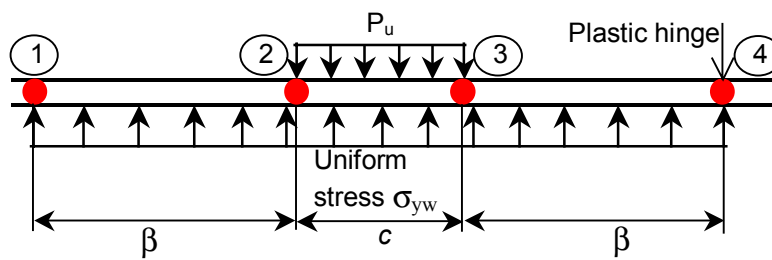
where β is defined in Fig. 10.

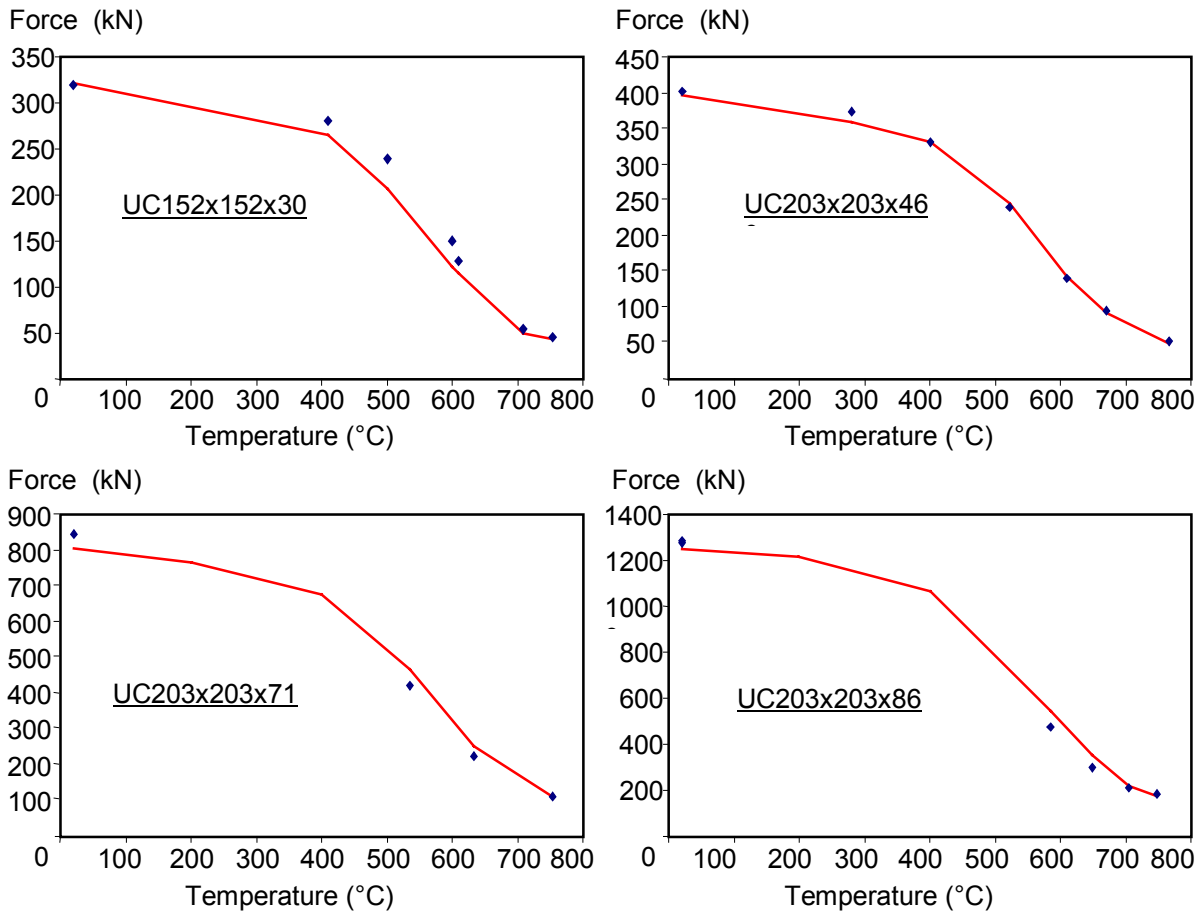**FIGURE 10: Assumed mechanism of web yielding.**

FIGURE 11: Test and Equation (2) results for strength of various column webs.

The comparison of column web strength with experimental results at elevated temperatures is shown in Fig. 11, in which the continuous lines plot the simplified equation (2) and the individual points show the experimental results.

For the stiffness parameters of a column web under transverse compressive loading, an empirical model has been derived based on experimental observations, together with 2-D and 3-D finite element analyses [17]. The results from these finite element analyses and the simplified model compared very well with the test results, and a typical case is shown in Fig. 12. It is only beyond the peak load, when there is some fall-off of load capacity, that 3-D finite element modelling (rather than 2-D web modeling only) is necessary to find the falling path. The clear logic of the comparison is that the load capacity is essentially controlled by the development of plasticity in the web-plate, and that buckling is essentially a secondary effect. This was repeated across the whole range of web slenderness tested, as well as for some more slender webs analysed using ANSYS [17].
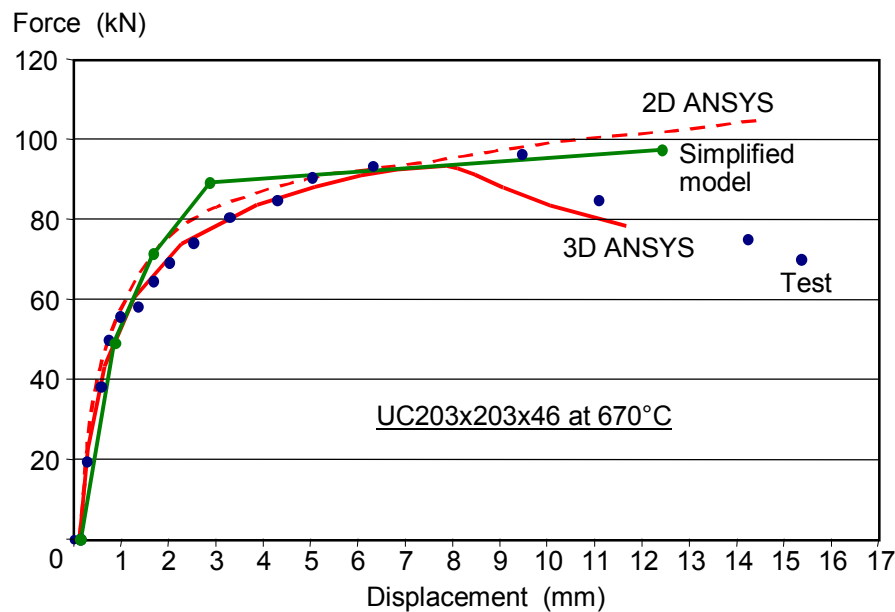
FIGURE 12: Comparison of test results, ANSYS 2-D, and 3-D modelling and the simplified model.

JOINT MODELLING AND FRAME RESPONSE

In early studies of steel frame response at ambient temperature the most appropriate means of including the effects of semi-rigid joint action relied on representations of moment-rotation test data. Whilst this is an effective way of representing the joint response, and in early studies that resulted in a better understanding of the role of the steel joints within a steel frame, there are several limitations associated with the use of experimentally derived joint characteristics. These are the expense associated with testing, the wide range of steel joint types commonly adopted and the effects of their detailed parameters, and the limited availability of carefully documented existing test data. At elevated temperatures there is the added complexity caused by high compressive and tensile axial thrusts on the joint which act simultaneously with the rotational effects.

As a result there was a real need to consider ways in which joint characteristics might be generated analytically. The form of expression used must represent the joint response in terms of the main parameters, such as initial stiffness and moment resistance, and should

have the capability of representing the entire non-linear moment-rotation response. Having investigated experimentally and analytically the main components within the tension and compression zones, the principles of the component approach were developed to predict the moment-rotation behaviour of joints at ambient and elevated temperatures. The response of a joint as a whole may be obtained by modeling it as an assembly of individual components in the compression and tension zones, as shown in Fig. 13. This assumes that the interaction between connected components has a negligible effect on the response of individual components.

The moment-rotation results given by assembling joints from their individual component models have been compared against ten elevated-temperature cruciform tests on flush end-plate joints conducted by Leston-Jones [2] and Al-Jabri [3]. The correlations were excellent, as illustrated in Fig. 14, and show that the analytical component models may be combined very effectively to represent the overall rotational response of a joint.
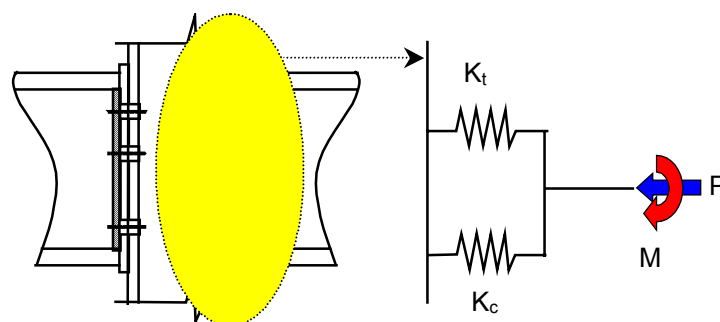
FIGURE 13: Component modelling of a joint under axial force and moment.
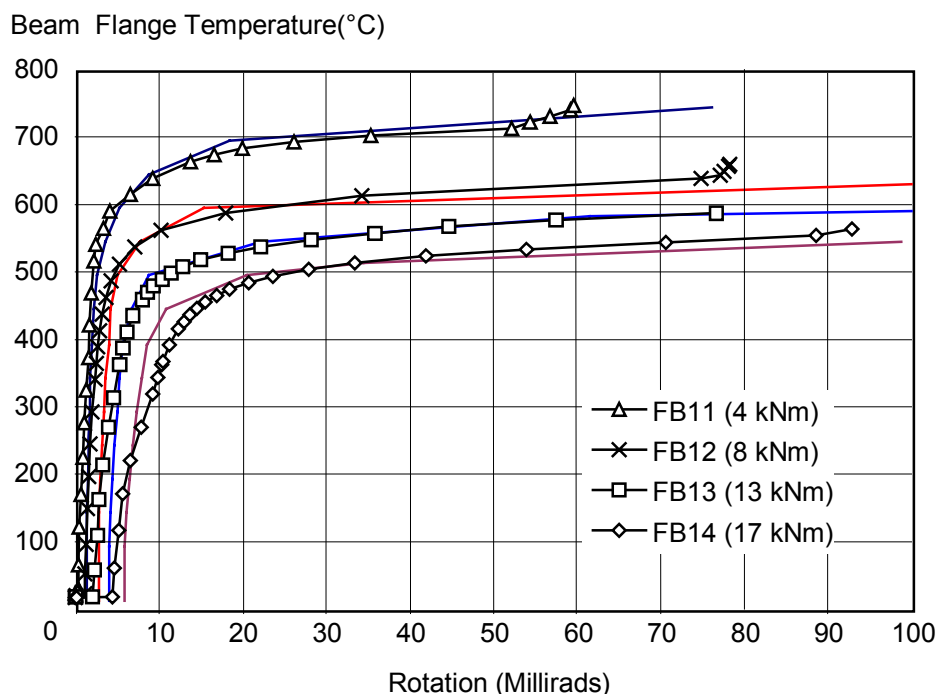
FIGURE 14: Comparison of Al-Jabri fire tests and component-based model on flush end-plate joints.

The main advantage of using the component approach to analyse a steel joint at elevated temperatures is that it becomes unnecessary to predict full high-temperature moment-rotation

characteristics. Instead it is possible to incorporate the tension and compression components *directly* as springs into the frame analysis, and hence the moment-rotation-temperature response is generated within the analysis and does not need to be input as data. The advantage of this approach is clear when it becomes necessary to account for the effect of large axial forces generated in the beams during a fire. It is important to consider these tensile or compressive axial forces as they may completely change the rotational characteristics of the joints. High axial compressive forces can be developed in the initial stages of a fire, but in the later stages the net thrust is usually tensile. With the conventional approach to frame analysis, moment-rotation-temperature-thrust-displacement relationships would be required, making the problem three degrees more difficult than an ambient-temperature semi-rigid frame problem. Clearly these would be extremely cumbersome to predict and to input into frame analysis programs. Using the temperature-thrust-deflection relationships for the individual component zones (Fig. 15) directly in the analysis would remove this complication and allow different temperatures to be used for different zones or components.
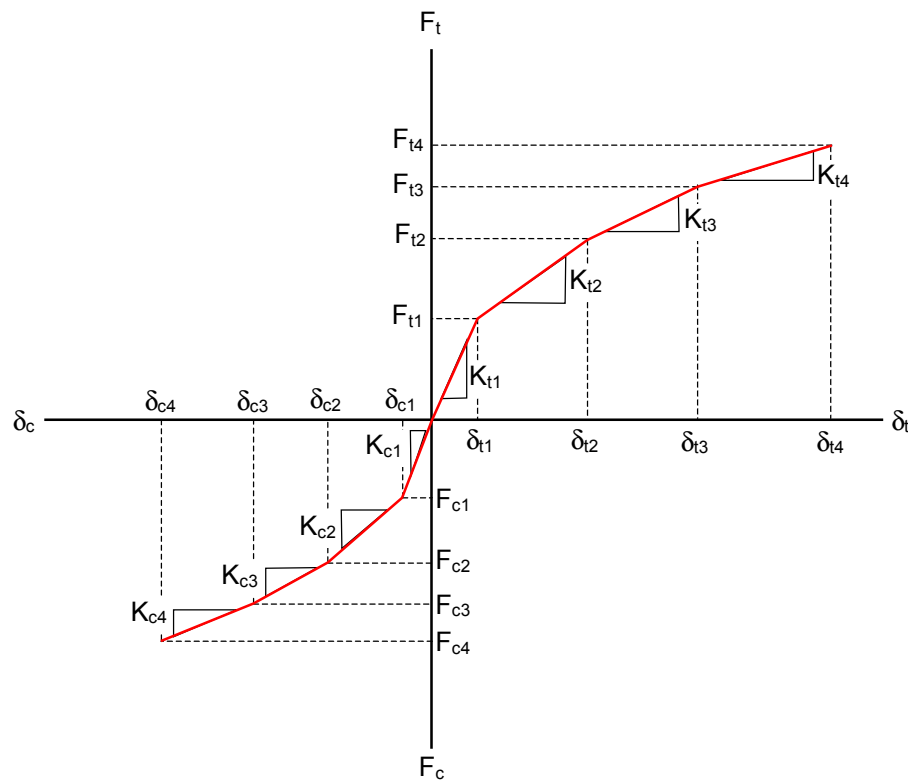
FIGURE 15: Load-deformation characteristics of the tension and compression zones.

The methodology would permit the effect of critical ductile components on overall frame behaviour to be studied, assisting designers to identify these critical locations and to assess how best to protect them in order to avoid premature failure of the steel joints at elevated temperatures.

CONCLUSIONS

This study has been a first step in demonstrating the potential for incorporating component-based models in the modeling of steel joint behaviour at elevated temperatures. Having the advantage of being able to predict the behaviour of any joint arrangement under fire

conditions from geometrical and mechanical properties minimises the need to carry out costly, time consuming and complex tests at elevated temperatures.

The major components within a steel flush end-plate joint, in the tension and compression zones, have been furnace-tested and investigated analytically, and load-deformation characteristics for individual components at elevated temperatures have been collected for the first time. The influence of compressive axial force on joint response is very important, especially because this force can result in local inelastic buckling of the column web or beam bottom flange. This was observed in the Cardington fire tests in several cases. This local inelastic buckling of the lower flange of the beam needs to be further investigated experimentally and analytically, although the indication from the compression zone studies is that inelastic buckling only affects the post-peak loss of stiffness of the component

The research has been limited to a single, though very common, type of beam-to-column joint, so other types of component need to be investigated experimentally and acceptable analytical models developed in order to generalise the applicability of the method. However, the very good correlation between the component tests and modelling, and the subsequent use of the simple models to reproduce high-temperature moment-rotation characteristics, show that the component method is potentially the best way to include semi-rigid connection behaviour in full-frame analysis.

REFERENCES

[1] Lawson, R.M., "Behaviour of Steel Beam-to-Column Connections in Fire", *The Structural Engineer*, **68** (14), (1990) pp263-271.

[2] Leston-Jones, L.C., *"The Influence of Semi-Rigid Connections on the Performance of Steel Framed Structures in Fire"*, Ph.D. Thesis, Department of Civil and Structural Engineering, University of Sheffield, 1997.

[3] Al-Jabri, K.S., *"The Behaviour of Steel and Composite Beam-to-Column Connections in Fire"*, Ph.D. Thesis, Department of Civil and Structural Engineering, University of Sheffield, 1999.

[4] Spyrou, S., Davison, J.B., and Burgess, I.W., *"Experimental and Analytical Studies of Steel T-stubs at Elevated Temperatures"*, Abnormal Loading on Structures: Experimental and Numerical Modelling, Ed. Virdi, K.S., Matthews, R.S., Clarke, J.L., and Garas, F.K., E&FN Spon, London, 2000.

[5] Spyrou, S., and Davison, J.B., *"Displacement Measurements in Studies of Steel T-stub Connections"*, J. Construct. Steel Research, **57** (6), (2001) pp647-659.

[6] Gere J.M., and Timoshenko, S.P., *"Mechanics of Materials"*, Second SI Edition, PWS Engineering, Wadsworth International, 1985.

[7] Shi, Y.J., Chan, S.L., and Wong, Y.L., "Modelling for Moment-Rotation Characteristics for End-Plate Connections", *ASCE J. Structural Engineering*, **122** (11), (1996) pp1300-1306.

[8] *"Control of the Semi-Rigid Behaviour of Civil Engineering Structural Connections"*, Final COST Action C1 Report, EUR 19244, 1999.

[9] Bose, S.K., McNeice, G.M., and Sherbourne, A.N., "Column webs in steel beam to column connections Parts I and II", *Computers and Structures*, **2**, (1972) pp253-279, 281-301.

[10]   Hendrick, A., and Murray, T., "Column web compression strength at end plate connections", *AISC Engineering Journal*, 3rd Quarter, (1984) pp161-169.

[11]   Bose, B., "Design resistance of unstiffened column web subject to transverse compression in beam to column joints", *J. Construct. Steel Research*, **45** (1), (1988) pp1-15.

[12]   *"BS 5950 Structural Use of Steelwork in Building: Part 1: Code of Practice for Design in Simple and Continuous Construction"*, British Standards Institution, London, 1985.

[13]   *"EC3:Design of Steel Structures, Part 1.1:Revised Annex J Joints and Building Frames"*, (Draft), Document CEN/TC250/SC3 N419E, European Committee for Standardization, 1994.

[14]   Bailey, C. G., and Moore, D. B., *"The influence of local and global forces on column design"*, Final report for DETR, Partners in Technology Contract No. CC1494, September 1999.

[15]   Markovic, N., and Hajdin, N., "A contribution to the analysis of the behaviour of plate girders subject to patch loading", *J. Construct. Steel Research*, **21**, (1992) pp163-173.

[16]   Drdacky, M., and Novotny, R., "Partial Edge Loading-Carrying Capacity Tests of Thick Plate Girder Webs", *Acta Technika CSAV*, **5**, (1977) pp614-20.

[17]   Block, F., *"2D and 3D Finite Element Analysis of a Column Web under Transverse Compressive Forces at Elevated Temperatures"*, Internal Report, University of Sheffield, 2001.

A UNIFIED APPROACH FOR FIRE RESISTANCE PREDICTION OF STEEL COLUMNS AND FRAMES

Chu Yang TANG

Nanyang Technological University, School of Civil and Environmental Engineering,N1-B4-04, Singapore

p141449244@ntu.edu.sg

Kang Hai TAN

Nanyang Technological University, School of Civil and Environmental Engineering,N1-1c-97, Singapore

ckhtan@ntu.edu.sg

ABSTRACT

For a long time, the Rankine method has been applied successfully to steel columns and frames subjected to increasing loads but maintained at constant ambient temperature. This paper extends the Rankine formula to steel columns and frames under fire conditions. The authors present a simple expression for buckling coefficient that can be used for both columns and frames under fire conditions, taking the deterioration of steel properties at elevated temperature into consideration. The Rankine predictions are compared to test results of 34 axially-loaded columns, 12 sway-frames and 6 non-sway frames. It is found that the predictions agree very well with the test results. For the 34 steel columns, the mean of agreement of ratios of collapse temperatures $T^{test}/T^{Rankine}$ is 0.98 with a coefficient of variation (COV) of 5.4%. As for the 18 steel frames, the mean is equal to 0.99 with a COV of 9.2%.

KEYWORDS: *fire resistance, frame, column, steel, fire test*

INTRODUCTION

The Rankine formula was originated by Prof Rankine [1] of Glassgow University in the latter part of the 19th century. It was later modified in the mid 20th century [2] and was adopted in various design codes since then. The formula basically involved a linear interaction between two terms, the elastic buckling load factor λ_e and the plastic collapse load factor λ_p as follows:

$$\frac{1}{P_R} = \frac{1}{P_p} + \frac{1}{P_e} \tag{1}$$

with P_R Rankine load
        P_p plastic collapse load
        P_e elastic critical load

The formula, when used for frames loaded to failure at ambient temperature, yields very good agreement with test results. The ratio of the actual failure load factor λ_c to the Rankine load factor λ_R is around 1.00 to 1.20 [3]. In their recent paper, Tang et al. [4] provided the theoretical derivation of the Rankine formula and they further applied the Rankine formula to steel columns and frames under fire conditions [4, 5]. The current paper is to show that the Rankine formula is a unified approach for steel columns, sway and non-sway steel frames.

RANKINE FORMULA IN FIRE CONDITIONS

In fire conditions, the Rankine formula takes the following form:

$$\frac{1}{P_R(T)} = \frac{1}{P_p(T)} + \frac{1}{P_e(T)} \tag{2}$$

with T steel member temperature; T = 20 for ambient conditions.

By adopting the material reduction factors for the respective yield strength (k_y) and elastic modulus (k_e) at elevated temperatures, the Rankine formula can expressed as:

$$\frac{1}{P_R(20)} = \frac{1}{k_y(T)P_p(20)} + \frac{1}{k_e(T)P_e(20)} \tag{3}$$

Clearly, the Rankine formula provides a linear interaction relationship between the plastic squashing load P_p and the elastic buckling load factor P_e. The actual behaviour of a column or a frame is dependent on its normalized slenderness ratio [4, 5, 6]:

$$\Lambda(20) = \sqrt{P_p(20)/P_e(20)} \tag{4}$$

For steel columns, the normalized slenderness ratio $\Lambda(20)$ depends on the member slenderness and end conditions by the following relationship [4]:

$$\Lambda(20) = \frac{\lambda}{\lambda_E(20)} \tag{5}$$

with λ slenderness ratio;
         λ_E transition slenderness ratio.

Here,

$$\lambda_E(20) = \pi\sqrt{E(20)/f_y(20)} \tag{6}$$

with E elastic modulus of steel;
         f_y yield strength of steel.

For frames, the term Λ not only depends on the member slenderness and boundary conditions, but also on the loading patterns. Generally, non-sway frames have smaller normalized slenderness ratio than sway frames; sway frames without lateral loading have smaller normalized slenderness ratio than those with lateral loading. The normalized slenderness ratio is a very important parameter for both steel columns and frames. It determines the relative importance of the plastic collapse load and elastic critical load. From Equation (2), it can be seen that, for $\Lambda << 1$ (very stocky columns or frames), the load capacity is determined by the plastic collapse load. On the other hand, for $\Lambda >> 1$ (very slender columns or frames), the load capacity is determined by the elastic critical load. For Λ in the intermediate range, both the plastic collapse load and the elastic critical load are important for determining the failure load of the structure.

By substituting Equation (4) into Equation (3), one obtains

$$\frac{P_p(20)}{P_R(T)} = \frac{1}{k_y(T)} + \frac{[\Lambda(20)]^2}{k_e(T)}$$

At failure, $P_R(T)$ is equal to the applied load P. Thus,

$$N(20) = \frac{k_y(T)}{1 + \frac{k_y(T)}{k_e(T)} \cdot [\Lambda(20)]^2} \tag{7}$$

where N is the buckling coefficient, given by:

$$N(20) = \frac{P}{P_p(20)} \tag{8}$$

Firgure 1 shows the buckling curves for both steel columns and frames at elevated temperatures based on Equation (7). Here, Eurocode 3 [7] is adopted for the material reduction factors $k_y(T)$ and $k_E(T)$.
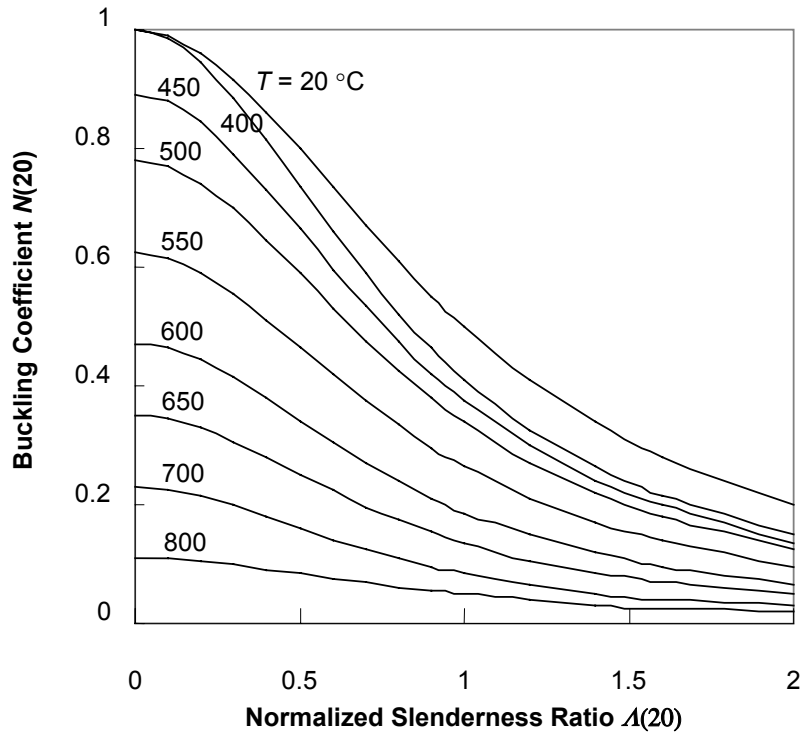
FIGURE 1 : Buckling coefficient for steel columns and frames at elevated temperatures

Figure 1 provides a simple and unified way to determine the fire resistance of both steel columns and frames. By performing the necessary analysis at *ambient temperature* in order to determine the normalized slenderness ratio for the structures under concern, one can then read from Figure 1 to determine the structural fire resistance.

CASE STUDIES

Case studies comprising axially loaded columns, sway-frames, and non-sway frames, tested under standard fire ISO 834 [8] are analysed to verify the Rankine formula. The first case study comprises 34 axially loaded steel column, which are summarized in Table 1. The comparisons of the Rankine predictions with test results for the 34 steel columns are shown in Figure 2. For comparison purpose, the $N(T)$ - $\Lambda(T)$ curve is plotted, where

$$N(T) = \frac{P}{P_p(T)} \tag{9}$$

$$\Lambda(T) = \sqrt{P_p(T) / P_e(T)} \tag{10}$$

Items	Descriptions
(1)	(2)
Laboratories	Borehamhood, Braunschweig, CTICM, Gent, LABEIN, Rennes, & Stuttgart. [9, 10, 11]
Steel grade	S 235 & S 355.
End conditions	Pinned-pinned, pinned-fixed & fixed-fixed.
Slenderness ratios λ	Vary from 14 to 230.
Mean Temperatures	Vary from 160 to 863 °C.
Load factors	Vary from 1 % to 72 % with respect to yield load at ambient temperature.
Loading eccentricities	Vary from 0 to 650 mm.

Table 1 : test conditions of the four case studies

Thus, from Equation (2), the Rankine formula can be expressed by

$$N(T) = \frac{1}{1 + [\Lambda(T)]^2} \tag{11}$$

The normalized squashing load $N_l(T) = 1$ and normalized Euler buckling load $N_l(T) = 1/\Lambda_l(T)^2$ are also shown in the figure for comparison purpose.
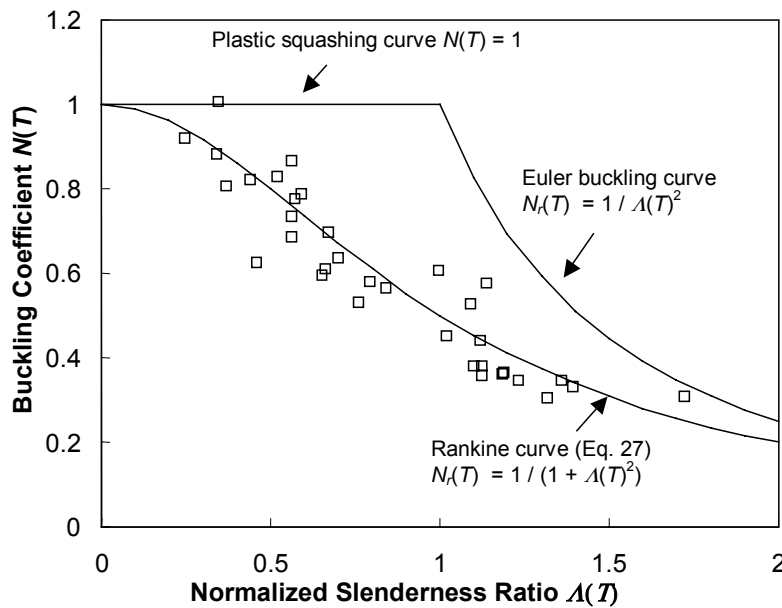
FIGURE 2 : Comparison of predictions and test results for axially-loaded steel columns

The test results agree well with the Rankine predictions for the 34 columns, with a mean of agreement of $T^{test}/T^{Rankine}$ of 0.98 and a COV of 5.4%.

The second case study comprises 6 non-sway frames (including the two EHR frames), and 12 sway-frames (including the single-storey one-bay EGR frames and single-storey two-bay ZSR frames) [6], as shown in Figure 3.
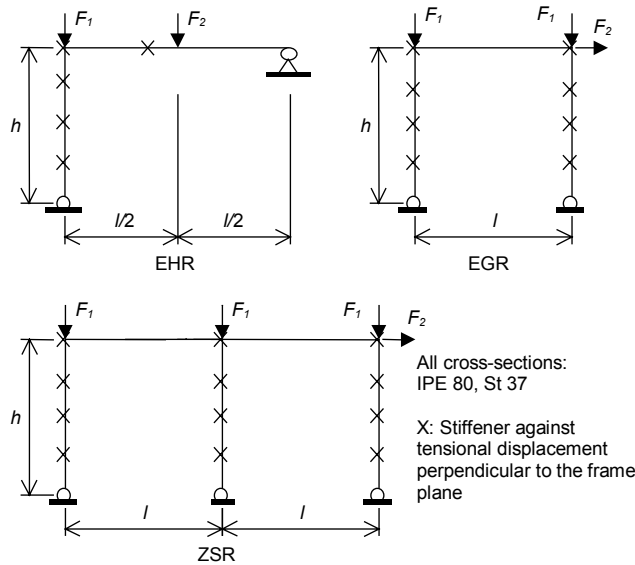
FIGURE 3 : Types of frames [12]

Figure 4 shows the test results of the 18 steel frames. The mean value of $T_c^{Rankine}/T_c^{test}$ is 1.01 with a coefficient of variation of 9.2%. This accuracy of predictions for steel frames under fire conditions is almost as good as the finite element results [4].
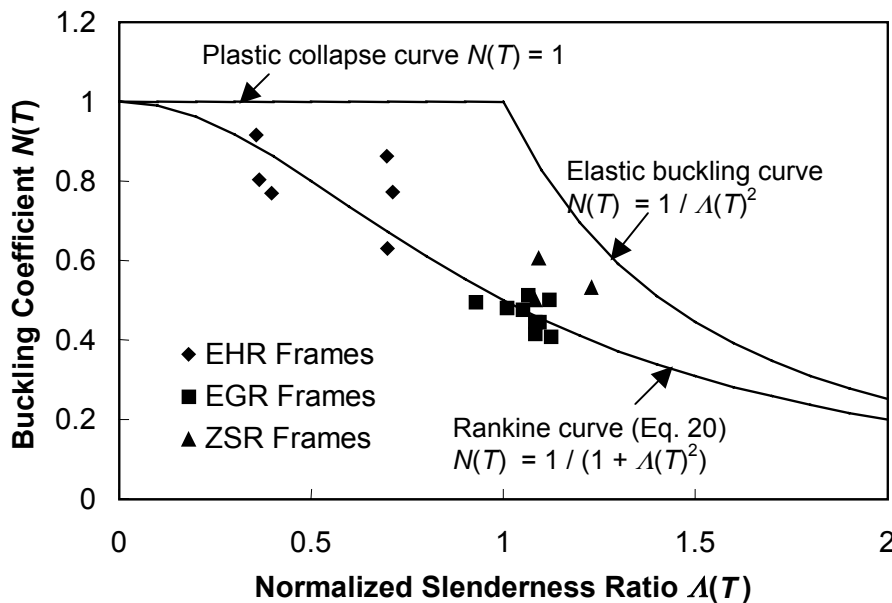
FIGURE 4 : Comparison of predictions and test results for sway and non-sway frames

CONCLUSIONS

The Rankine formula provides a simple and unified approach to fire resistance calculation of steel columns and frames under fire conditions. The authors presents a simple expression for buckling coefficient that can be used for both columns and frames under fire conditions, taking the deterioration of steel properties at elevated temperature into consideration. Good agreement with test results is obtained for the Rankine predictions.

REFERENCES

[1] Rankine, W. J. M., *Useful Rules and Tables*, London: C. Griffin & Co., Limited, 1908.

[2] Merchant, W., *The Failure Loads of Rigid Jointed Frameworks as Influenced by Stability*, The Structural Engineer, 32, pp185-190, 1954.

[3] Horne, M. R. & Merchant, W, *The Stability of Frames*, Oxford: Pergamon Press Ltd, 1965.

[4] Tang, C. Y., Tan, K. H. and Ting, S. K., *Basis and Application of a Simple Interaction Formula for Steel Columns under Fire Conditions*, J. Struct. Engrg., ASCE, October, Vol. 127, No. 10, pp 1206-1213, 2001.

[5] Tang, C. Y. and Tan, K. H., *Basis and Application of a Simple Interaction Formula for Steel Frames under Fire Conditions*, J. Struct. Engrg., ASCE, October, Vol. 127, No. 10, pp 1214-1220, 2001.

[6] Rubert, A., and Schaumann, P., *Structural Steel and Plane Frame Assemblies under Fire Action*, Fire Safety J., 10, 173-184, 1986.

[7] CEN, *Eurocode 3: Design of Steel Structures. Part 1.2: General Rules – Structural Fire Design*, ENV 1993-1-1, European Committee for Standardization, 1995.

[8] ISO 834, *Fire Resistance Teats-Elements of Building Construction*, International Standards Organisation, 1975.

[9] Janss, J., *Statistical Analysis of Fire Tests on Steel Beams and Columns to Eurocode 3, Part 1.2*, J. Constr. Steel Res., 33, pp 39 – 50, 1995.

[10] Talamona, D., *Buckling Curves in Case of Fire – ECSC 7210 SA 316/515/931/618: Fire Resistance of Steel Columns with Eccentric Load*, CTICM, Report No. INC-96/450-DT/VG Part 1, Saint-Remy-les-Chevreuse, Paris, 1995.

[11] Schleich, J. B. & Cajot, L. G., *Buckling Curves in Case of Fire: Draft Final Report, Part I (Main Text)*, CEC Agreement 7210-SA 316/515/618/931, ProfilARBED-Recherches, Luxembourg, 1996.

FIRE RESISTANCE OF REINFORCED CONCRETE FILLED STEEL COLUMNS

Kang Hai TAN

Nanyang Technological University, School of Civil and Environmental Engineering,N1-1c-97, Singapore

ckhtan@ntu.edu.sg

Chu Yang TANG

Nanyang Technological University, School of Civil and Environmental Engineering,N1-B4-04, Singapore

p141449244@ntu.edu.sg

ABSTRACT

A simple calculation method, the Rankine method, is applied to determine fire resistance of reinforced concrete filled steel (RCFS) columns. The same method has been applied to steel and reinforced concrete columns successfully.

RCFS columns in fire can fail under two modes: plastic squashing for stocky columns and buckling for slender columns. For columns in the intermediate range, these two modes will interact to each other, causing a reduction in the load capacity of real columns. The Rankine approach assumes a linear interactive relationship between the two failure modes, which has been shown to be a lower bound approach. The formulation is presented for both axially- and eccentrically-loaded columns. The Rankine predictions are compared to four case studies comprising 61 tested RCFS columns. Good agreement is observed.

KEYWORDS: *fire resistance, concrete, column, reinforced concrete, steel, fire test*

INTRODUCTION

Fire resistance of reinforced concrete filled steel (RCFS) columns, which is traditionally determined by expensive furnace tests, presents a formidable problem to structural engineers.

1. Steel tube of RCFS columns softens quickly at elevated temperatures and the load is transferred to the cooler concrete core, which is reinforced by steel reinforcement. Therefore, the concrete core largely determines the load capacity of RCFS columns, with only small contribution from the steel tube.

2. The moment capacity of steel tube is also greatly reduced. This phenomenon is particularly detrimental to columns with steel tubes filled with plain concrete, as the concrete section cannot resist bending moment by itself. At ambient temperature, such a column can resist large bending moment by the steel tube. However, when subjected to elevated temperatures, the moment capacity of the column diminishes quickly as the steel tube softens. This will likely lead to a loss of ductility and thus a premature failure, as observed by Lie and Stringer [1]. As a general comment, only design plain concrete filled steel (PCFS) columns to carry axial loads in fire conditions. Where load eccentricity is anticipated, reinforced concrete filled steel (RCFS) columns should always be used.

3. The confinement effect to the concrete core will also diminish as a result of the softening of steel tube.

This paper outlines a simple analytical method, the Rankine method, to determine the fire resistance of reinforced concrete filled steel (RCFS) columns. The same method has been applied to steel columns, steel frames, and reinforced concrete columns successfully [2 - 4]. The Rankine predictions are compared to four case studies comprising of 61 tested RCFS columns and good agreement is observed.

RANKINE FORMULA

The Rankine formula for columns under fire conditions has the following form:

$$\frac{1}{P_R(t)} = \frac{1}{u_{pr}P_p(t)} + \frac{1}{P_e(t)} \tag{1}$$

with P_R predicted failure load by the Rankine formula;
        u_{pr} reduction factor of the plastic squashing load due to load eccentricity;
        P_p plastic squashing load;
        $u_{pr}P_p$ short column capacity;
        P_e elastic buckling load;
        t fire exposure time; t = 0 for ambient conditions.

The theoretical basis of the above formula has been discussed by Tang et al [2]. RCFS columns in fire can fail under two modes: plastic squashing for stocky columns and buckling for slender columns. For columns in the intermediate range, these two modes will interact with each other,

causing a reduction in the load capacity of real columns. Clearly, the Rankine formula provides a linear interaction relationship between the plastic squashing load P_p and the elastic buckling load P_e. The Rankine load has been shown to be a lower bound approach [2, 3].

FIRE RESISTANCE OF RCFS COLUMNS

Due to the softening of the steel tube at elevated temperatures, the confinement effect to the concrete core from steel tube diminishes in fire conditions. Furthermore, separation of the concrete core from the steel tube can also be frequently observed in fire conditions [1], which suggests a loss of bond at the interface between the concrete core and steel tube. As a result, the load capacity P of axially-loaded RCFS columns can be simply taken as the sum of the capacity of concrete core P^{core} and that of the steel tube P^{tube}:

$$P(t) = P^{core}(t) + P^{tube}(t) \tag{2}$$

where the superscripts "core" and "tube" indicate the contribution from the concrete core and steel tube, respectively. Both P^{core} and P^{tube} can be determined by the Rankine formula.

CONCRETE CORE CAPACITY

For the concrete core at elevated temperatures:

$$\frac{1}{P^{core}(t)} = \frac{1}{u_{pr}{}^{core} P_p{}^{core}(t)} + \frac{1}{P_e{}^{core}(t)} \tag{3}$$

In Equation (3), the plastic squashing load of the concrete core can be determined from

$$P_p{}^{core}(t) = \beta_c(t)\, f_c'(0)\, A_c + \beta_{yr}(t)\, f_{yr}(0)\, A_{sr} \tag{4}$$

with f_c' concrete cylinder strength;
       f_{yr} yield strength of steel reinforcement;
       A_c area of concrete;
       A_{sr} area of steel reinforcement.

The terms $\beta_c(t)$ and $\beta_{yr}(t)$ are the respective strength reduction factors accounting for the deterioration of concrete and steel reinforcement under fire conditions.

$$\beta_c(t) = \frac{\int f_c'(t) dA_c}{f_c'(0) A_c} \tag{5}$$

$$\beta_{yr}(t) = \frac{\sum f_{yr}(t) A_{sr}}{f_{yr}(0) A_{sr}} \tag{6}$$

Similarly, the elastic buckling load of the concrete core can be determined from:

$$P_e^{core}(t) = \frac{\pi^2 [\beta_{Ec}(t) \cdot 0.2 E_c(0) I_c + \beta_{Esr}(t) \cdot E_{sr}(0) I_{sr}]}{L_e^2} \tag{7}$$

with E_c elastic modulus for concrete;
I_c second moment of area of concrete;
E_{sr} elastic modulus of steel reinforcement;
I_{sr} second moment of area of steel reinforcement;
L_e column effective length taking note of different support conditions

The terms $\beta_{Ec}(t)$ and $\beta_{Esr}(t)$ are the respective stability reduction factors accounting for the deterioration of concrete and steel reinforcement under fire conditions.

$$\beta_{Ec}(t) = \frac{\int E_c(t) dI_c}{E_c(0) I_c} \tag{8}$$

$$\beta_{yr}(t) = \frac{\sum E_{sr}(t) I_{sr}}{E_{yr}(0) I_{sr}} \tag{9}$$

The material reduction factors $\beta_c(t)$, $\beta_{yr}(t)$, $\beta_{Ec}(t)$ and $\beta_{Esr}(t)$ can be determined either experimentally or by finite element analysis. Based on their previous study of RC columns in fire conditions [4], the authors proposed to adopt the following material models. They are modified from Dotreppe et al. [5]:

$$\beta_c(t) = \frac{\gamma(t_e)}{\sqrt{1 + (0.3 A_c^{-0.5} t_e)^{A_c^{-0.25}}}} \tag{10a}$$

$$\beta_{yr}(t) = \gamma(t_e) \cdot (1 - \frac{0.9 t_e}{0.046 c + 0.11}) \geq 0 \tag{10b}$$

$$\beta_{Ec}(t) = (1.1 A_c^{0.15})^{t_e} \cdot \beta_c(t) \tag{10c}$$

$$\beta_{Esr}(t) = 0.8 \beta_{yr}^2(t) + 0.2 \beta_{yr}(t) \tag{10d}$$

with c concrete cover;

$\gamma(t_e)$ an empirical factor to account for the effect of concrete spalling; $\gamma(t_e) = 1.0$ for
RCFS columns as they are protected from spalling by the steel tube;

Here, the equivalent time t_e in terms of fire severity can be estimated by

$$t_e = \alpha_{agg}\alpha_{ISO}t \tag{13}$$

where
α_{agg} = 1.0 for siliceous aggregate and α_{agg} = 0.9 for carbonate aggregate;
α_{ISO} = 1.0 for ISO 834 fire and α_{ISO} = 0.85 for ASTM-E119 fire.

STEEL TUBE CAPACITY

The steel tube capacity can be determined from:

$$\frac{1}{P^{tube}(t)} = \frac{1}{u_{pr}^{tube} P_p^{tube}(t)} + \frac{1}{P_e^{tube}(t)}$$

where

$$P_p^{tube}(t) = k_y(t) \cdot f_y(0) A_s \tag{14}$$

$$P_e^{tube}(t) = k_E(t) \cdot \frac{\pi^2 E_s(0) I_s}{L_e^2} \tag{15}$$

with f_y yield strength of the steel tube;

A_s area of the steel tube;
E_s elastic modulus for steel tube;
I_s second moment of area of steel tube.

The factors $k_y(t)$ and $k_E(t)$ are the respective material reduction factors to yield strength and elastic modulus of structural steel at elevated temperatures. Table 1 shows the values of $k_y(t)$ and $k_E(t)$ at different fire temperatures for ISO 834 [6] and ASTM E119 [7] fires obtained from the finite element program SAFIR [8], by adopting the Eurocode 3 structural steel material model [9].

Time t (hour)	Reduction factor $k_y(t)$		Reduction factor $k_E(t)$	
	ISO 834	ASTM E119	ISO 834	ASTM E119
0	1.000	1.000	1.000	1.000
0.5	0.371	0.362	0.242	0.235
1.0	0.065	0.073	0.073	0.077
1.5	0.050	0.055	0.051	0.057
2.0	0.034	0.042	0.039	0.047
2.5	0.027	0.037	0.030	0.041
3.0	0.020	0.032	0.023	0.036
3.5	0.015	0.028	0.017	0.031
4.0	0.011	0.023	0.012	0.026

Table 1 : strength reduction factors $k_y(t)$ and $k_E(t)$ of steel tube

EFFECT OF LOAD ECCENTRICITY

The effect of load eccentricity e on concrete core is to lower the short column capacity $u_{pr}^{core} P_p^{core}$. For axially-loaded columns, u_{pr}^{core} is unity. The magnitude of u_{pr}^{core} for eccentrically-loaded columns can be determined from the conventional axial-load-bending-moment interaction diagram, as shown in Figure 1 [10]. From computing the short column capacity $u_{pr}^{core} P_p^{core}$, the value to u_{pr}^{core} can be readily determined.
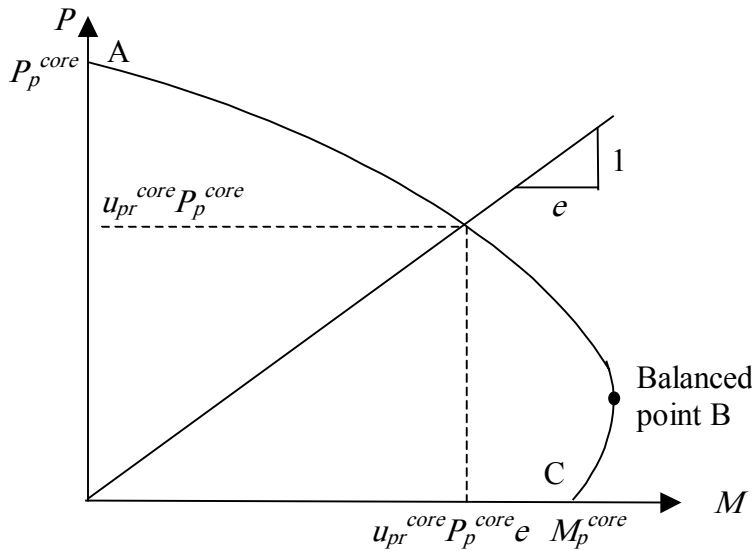
FIGURE 1 : Determination of u_{pr}^{core}

For steel tubes, the term u_{pr}^{tube} can be readily determined from [2]:

$$u_{pr}^{tube} = \frac{1}{1 + eA_s / S_s} \qquad (16)$$

with S_s plastic modulus of the steel tube.

CASE STUDIES

Four case studies comprising a total of 61 RCFS columns tested under standard fire ISO 34 and ASTM E119 are analysed to verify the Rankine formula. The test conditions of these case studies are summarized in Table 1.

Case Study	Ref	No	Section	Size (mm)	Length (m)	End support	Eccentricity (mm)	Fire curve	Aggregate Type
1	[11], UTI/CTICM	22	Square	200×200; 225×225; 260×260; 300×300	3.6	pinned-fixed; fixed-fixed	0 to 100;	ISO 834	Siliceous aggregate
2	[11], CSTB	10	square; circular	140×140; 160×160; 225×225; ∅219.1	3.6	fixed-fixed	0	ISO 834	Siliceous aggregate
3	[12, 13], Technical University of Braunschweig	21	square; circular	200×200; 260×260; 300×300; ∅273	3.7, 4.2, or 5.2	pinned-fixed	0 or 100	ISO 834	Siliceous aggregate
4	[14], CNRC	8	square; circular	203.2×203.2; 254×254; 304.8×304.8; ∅273.1	3.81	fixed-fixed	0	ASTM E119	Carbonate aggregate

Table 2 : test conditions of the four case studies

The comparisons of the Rankine prediction with the test results for the four case studies are shown in Figure 2.
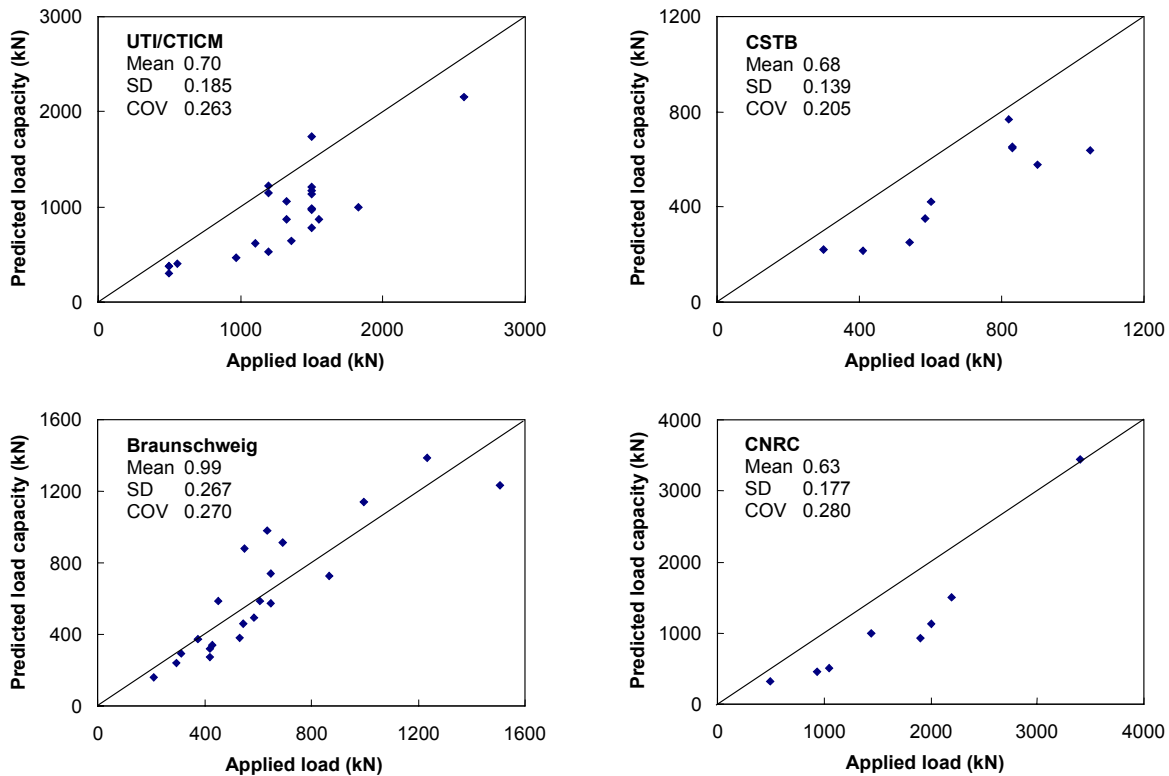
FIGURE 2 : Comparison with test results

For all the four case studies, the Rankine predictions give consistent predictions with coefficient of variations around 25%, which are reasonably good for RCFS columns under fire conditions. Furthermore, for most of the columns, the Rankine predictions are on the conservative side, since the method ignores the confinement effect of steel tube on concrete core.

CONCLUSIONS

The Rankine approach for RCFS columns in fire conditions is presented in the current paper. A theoretical model is derived for both axially- and eccentrically-loaded columns. Four case studies including 61 RCFS columns are analyzed to verify the approach. The experimental results show that the Rankine approach is not only accurate and consistent, but also conservative.

REFERENCES

[1] Lie, T. T. and Stringer, D. C., *Calculation of the Fire Resistance of Steel Hollow Structural Section Columns Filled with Plain Concrete*, Can. J. Civ. Eng., 21, 382-385, 1994.

[2] Tang, C. Y., Tan, K. H. and Ting, S. K., *Basis and Application of a Simple Interaction Formula for Steel Columns under Fire Conditions*, J. Struct. Engrg., ASCE, October, Vol. 127, No. 10, pp 1206-1213, 2001.

[3] Tang, C. Y. and Tan, K. H., *Basis and Application of a Simple Interaction Formula for Steel Frames under Fire Conditions*, J. Struct. Engrg., ASCE, October, Vol. 127, No. 10, pp 1214-1220, 2001.

[4] Tang, C. Y., *An Interactive Formula for Fire Resistance of Columns*, M.Eng. Thesis, School of Civil and Environmental Engineering, Nanyang Technological University, Singapore, 2002.

[5] Dotreppe, J.C., Franssen, J.M., Vanderzeypen, Y., *Calculation Method for Design of Reinforced Concrete Columns under Fire Conditions*, ACI Structural Journal, V. 96, No. 1, 9-18, 1999.

[6] ISO 834, *Fire Resistance Teats-Elements of Building Construction*, International Standards Organisation, 1975.

[7] ASTM-E119, *Standard Methods of Fire Tests of Building Construction and Materials*, American Society for Testing and Materials, Philadelphia, PA, USA, 1995,

[8] Franssen, J.M., Cooke, G.M.E., and Latham, D.J., *Numerical Simulation of a Full Scale Fire Test on a Loaded Steel Framework*, J. of Constructional Steel Research, 35: 377-408, 1995.

[9] Eurocode 3, *Design of Steel Structure. Part 1.2: General Rules – Structural Fire Design, ENV 1993-1-2*, European Committee for Standardization, 1995.

[10] Nilson, A.H. and Winter, G., *Design of Concrete Structures*, 11th Ed., New York: McGraw-Hill, 1991, 1991.

[11] Grandjean, G., Grimault, J.P., and Petit, L., *Determination de la durée au feu des profils creux remplis de béton*, Rapport Final. Commission des Communautés Européennes, Recherche Technique acier. Luxembourg (in French), 1981.

[12] Kordina, K., and Klingsch, W., *Fire Resistance of Composite Columns of Concrete Filled Hollow Sections* – Research report, CIDECT 15 C1/C2-83/27 (part of C.E.C. 7210-SA/108, Studiengesellschaft P. 35, 1983.

[13] Hass, R., *Practical Rules for the Design of Reinforced Concrete and Composite Columns Submitted to Fire*, Technical Report No. 69, Institute für Baustoffe, Massivbau und Brandschutz der Technischen Universitä Braunschweig (in German), 1986 ().

[14] Chabot, M. and Lie, T.T., *Experimental Studies on the Fire Resistance of Hollow Steel columns Filled with Bar-Reinforced Concrete*, Internal report No. 628, National Research Council Canada, 1992.

A SIMPLE AND RATIONAL APPROACH FOR FIRE RESISTANCE PREDICTION OF RC COLUMNS

Kang Hai TAN

Nanyang Technological University, School of Civil and Environmental Engineering,N1-1c-97, Singapore

ckhtan@ntu.edu.sg

Chu Yang TANG

Nanyang Technological University, School of Civil and Environmental Engineering,N1-B4-04, Singapore

p141449244@ntu.edu.sg

ABSTRACT

Fire resistance of reinforced concrete (RC) columns, which is traditionally determined by expensive furnace tests, presents a formidable problem to structural engineers. There is a need for simple calculation methods that are based on sound engineering principles instead of solely relying on tabulated test data.

In this paper, the Rankine approach is presented. The premise is that RC columns in fire can fail under two modes: crushing for stocky columns and buckling for slender columns. For columns in the intermediate range, these two modes will interact with each other, causing a reduction in the load capacity of real columns. The Rankine approach assumes a linear interactive relationship between the two failure modes. The method can also be applied to steel and composite columns. The formulation is presented for both axially- and eccentrically-loaded columns. Four case studies comprising 76 tested RC columns are compiled and compared with Rankine predictions. Satisfactory agreement is obtained.

KEYWORDS: *fire resistance, concrete, column, reinforced concrete, fire test*

INTRODUCTION

There are many papers on the simplified analysis of steel columns in fire conditions, but not as many for RC columns. This is mainly due to the non-uniform temperature distribution in column cross-section when exposed to the fire conditions. Furthermore, spalling of concrete, which is random in nature, may expose steel reinforcement to fire and significantly alter the temperature distribution in concrete [1]. Consequently, the fire resistance of RC columns is also affected.

The authors proposed an interaction formula for fire resistance of RC columns – the Rankine approach. The same method has been applied to steel columns and frames, and also composite columns. Good agreement is observed with test results [2, 3]. Four case studies including a total of 76 RC columns were used to verify the approach.

RANKINE FORMULA

The Rankine formula for RC columns under fire conditions takes the following form:

$$\frac{1}{P_R(t)} = \frac{1}{u_{pr}P_p(t)} + \frac{1}{P_e(t)} \tag{1}$$

with
- P_R predicted failure load by the Rankine formula;
- u_{pr} reduction factor of the plastic squashing load due to load eccentricity;
- P_p plastic squashing load;
- $u_{pr}P_p$ short column capacity;
- P_e elastic buckling load;
- t fire exposure time; $t = 0$ for ambient conditions.

The theoretical basis of the above formula has been discussed by Tang et al [2]. Clearly, the Rankine formula provides a linear interaction relationship between the plastic squashing load P_p and the elastic buckling load factor P_e. The actual behaviour of a column is dependent on its slenderness ratio [4]:

$$\Lambda = \sqrt{P_p / P_e} \tag{2}$$

The term Λ provides a simple and direct indication of the column slenderness. For example, stocky columns dominated by plastic behaviour have Λ less than unity. On the other hand, slender columns are those with Λ greater than unity and are governed by stability. Columns with Λ close to unity are in the intermediate range, where both strength and stability are important factors controlling the ultimate failure load.

In Equation (1), the plastic collapse load $P_p(t)$ can be determined by:

$$P_p(t) = \beta_c(t) \, f_c'(0) \, A_c + \beta_{yr}(t) \, f_{yr}(0) \, A_{sr} \qquad (3)$$

with f_c' concrete cylinder strength;
        f_{yr} yield strength of steel reinforcement;
        A_c area of concrete;
        A_{sr} area of steel reinforcement.

The terms $\beta_c(t)$ and $\beta_{yr}(t)$ are the respective strength reduction factors accounting for the deterioration of concrete and steel reinforcement under fire conditions.

$$\beta_c(t) = \frac{\int f_c'(t) \, dA_c}{f_c'(0) \, A_c} \qquad (4)$$

$$\beta_{yr}(t) = \frac{\sum f_{yr}(t) \, A_{sr}}{f_{yr}(0) \, A_{sr}} \qquad (5)$$

Similarly, the elastic buckling load can be determined by:

$$P_e(t) = \frac{\pi^2 [\beta_{Ec}(t) \cdot 0.2 \, E_c(0) \, I_c + \beta_{Esr}(t) \cdot E_{sr}(0) \, I_{sr}]}{L_e^{\,2}} \qquad (6)$$

with E_c elastic modulus for concrete;
        I_c second moment of area of concrete;
        E_{sr} elastic modulus of steel reinforcement;
        I_{sr} second moment of area of steel reinforcement;
        L_e column effective length taking account of different support conditions

The terms $\beta_{Ec}(t)$ and $\beta_{Esr}(t)$ are the respective stability reduction factors accounting for the deterioration of concrete and steel reinforcement under fire conditions.

$$\beta_{Ec}(t) = \frac{\int E_c(t) \, dI_c}{E_c(0) \, I_c} \qquad (7)$$

$$\beta_{yr}(t) = \frac{\sum E_{sr}(t) \, I_{sr}}{E_{yr}(0) \, I_{sr}} \qquad (8)$$

MATERIAL REDUCTION FACTORS UNDER STANDARD FIRES

The material reduction factors β_c(t), β_{yr}(t), β_{Ec}(t) and β_{Esr}(t) can be determined either experimentally or by finite element analysis. Dotreppe et al. [5] performed thermal analysis for RC columns under ISO 834 fire [6] using a finite element program named SAFIR [7], which is developed at the University of Liège. They proposed the following expressions for β_c(t) and β_{yr}(t):

$$\beta_c(t) = \frac{\gamma(t)}{\sqrt{1 + (0.3 A_c^{-0.5} t)^{A_c^{-0.25}}}} \tag{9a}$$

$$\beta_{yr}(t) = \gamma(t) \cdot (1 - \frac{0.9t}{0.046c + 0.11}) \geq 0 \tag{9b}$$

with c concrete cover;

In Equation (9a) and (9b), the term $\gamma(t)$ is an empirical factor to account for possible spalling of concrete,

$$\gamma(t) = 1 - 0.3t \tag{10}$$

It should be noted that the material reduction factors proposed by Dotreppe et al. [5] are only applicable to RC columns that satisfy the following conditions:

1. with siliceous concrete;

2. subjected to ISO 834 fire;

These restrictions can be removed with the following modifications proposed by the authors:

1. A modification factor α_{agg} is introduced to account for the aggregate types, either siliceous or carbonate. Lie and Woollerton [8] and Lie and Kodur [9] studied the effect of aggregate types. They show that the fire resistance of carbonate aggregate concrete columns is about 10% greater than that of siliceous aggregate concrete columns, due to a greater heat capacity of carbonate aggregate concrete.

2. A modification factor α_{ISO} is applied to the fire exposure time t to account for other standard fire curves, such as the ASTM-E119 fire [10].

From the simulations by the finite element program SAFIR, the authors proposed the following equations:

$$\beta_c(t) = \frac{\gamma(t_e)}{\sqrt{1 + (0.3 A_c^{-0.5} t_e)^{A_c^{-0.25}}}} \tag{11a}$$

$$\beta_{yr}(t) = \gamma(t_e) \cdot (1 - \frac{0.9t_e}{0.046c + 0.11}) \geq 0 \qquad (11b)$$

where

$$\gamma(t_e) = 1 - 0.3t_e \geq 0.85 \qquad (12)$$

Here, the equivalent time t_e in terms of fire severity can be estimated by

$$t_e = \alpha_{agg} \alpha_{ISO} t \qquad (13)$$

where
$\alpha_{agg} = 1.0$ for siliceous aggregate and $\alpha_{agg} = 0.9$ for carbonate aggregate;
$\alpha_{ISO} = 1.0$ for ISO 834 fire and $\alpha_{ISO} = 0.85$ for ASTM-E119 fire.

The authors further propose the following equations for $\beta_{Ec}(t)$ and $\beta_{Esr}(t)$, respectively:

$$\beta_{Ec}(t) = (1.1A_c^{0.15})^{t_e} \cdot \beta_c(t) \qquad (11c)$$

$$\beta_{Esr}(t) = 0.8\beta_{yr}^2(t) + 0.2\beta_{yr}(t) \qquad (11d)$$

EFFECT OF LOAD ECCENTRICITY

The effect of load eccentricity on RC columns is to lower the short column capacity $u_{pr}P_p$. For axially loaded columns, u_{pr} is unity. The magnitude of u_{pr} for eccentrically loaded columns can be determined by the conventional axial-load-bending-moment interaction diagram, as shown in Figure 1 [11]. By calculating the short column capacity $u_{pr}P_p$, the value of u_{pr} can be readily determined.
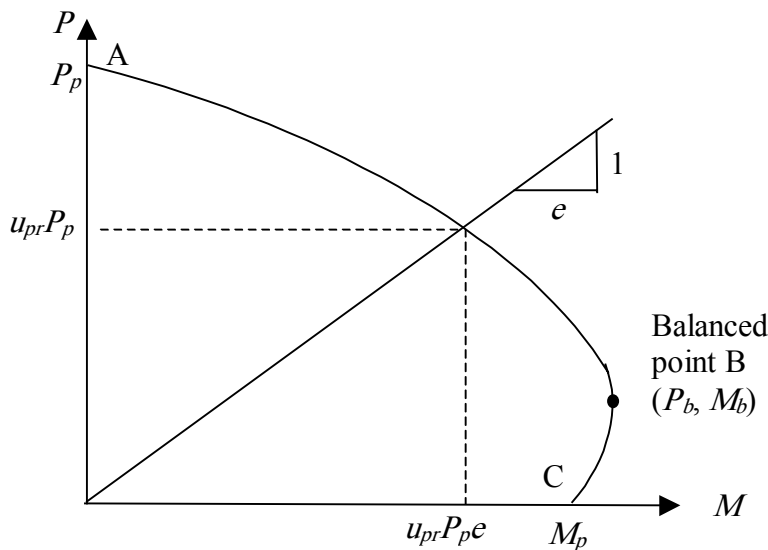

FIGURE 1 : Determination of u_{pr}

57

For columns under bi-axial bending with eccentricities e_x and e_y about the respective major and minor bending axis, the plastic reduction factor u_{pr} can be determined from the Bresler's reciprocal load equation [11]:

$$\frac{1}{u_{pr} P_p} = \frac{1}{u_{prx} P_p} + \frac{1}{u_{pry} P_p} - \frac{1}{P_p}$$

with u_{prx} plastic reduction factor when only eccentricity e_x is present ($e_y = 0$);

           u_{pry} plastic reduction factor when only eccentricity e_y is present ($e_x = 0$).

Thus,

$$\frac{1}{u_{pr}} = \frac{1}{u_{prx}} + \frac{1}{u_{pry}} - 1 \tag{14}$$
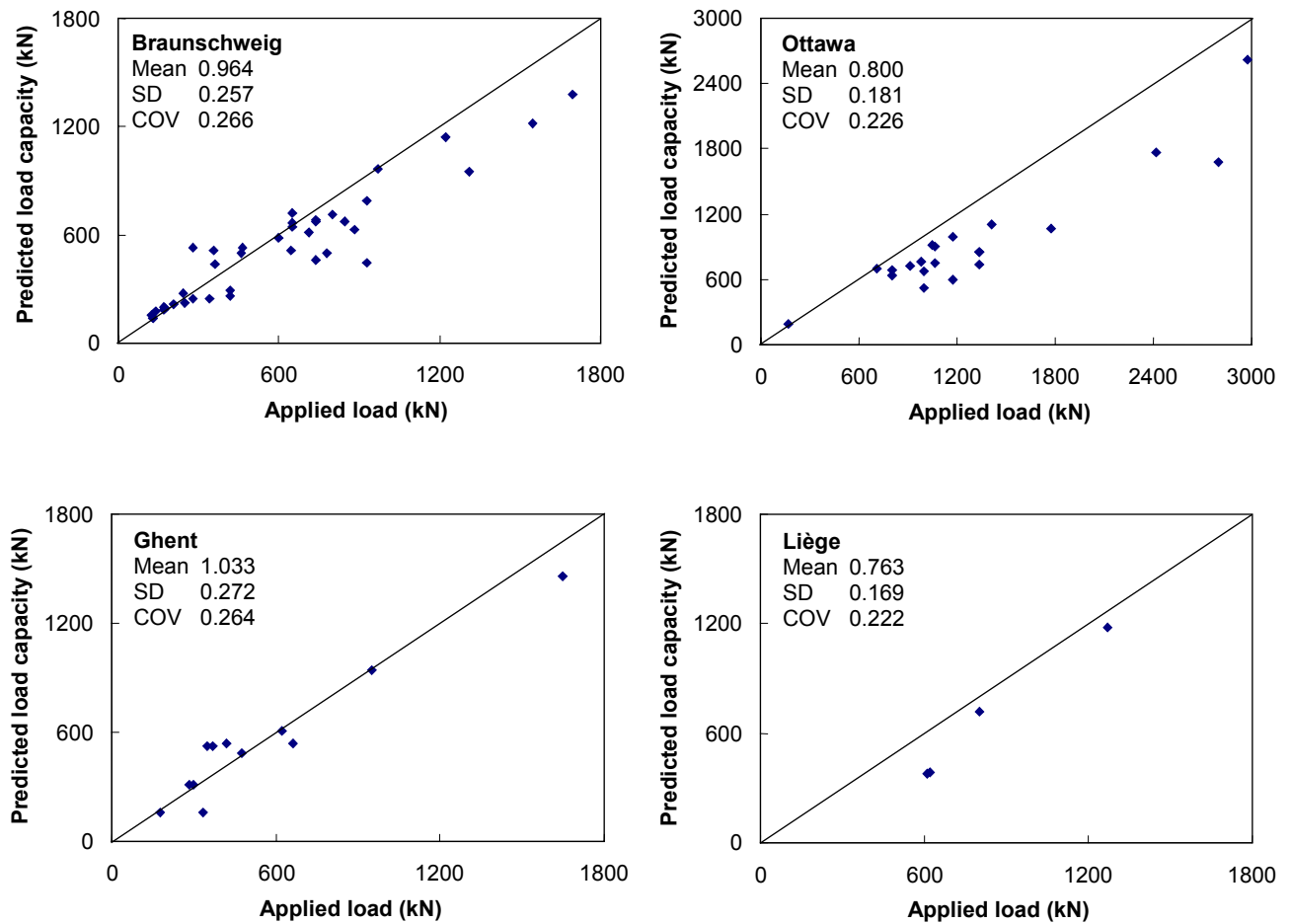
CASE STUDIES

Four case studies comprising of 76 RC columns tested under standard fire ISO 34 and ASTM E119 were analysed to verify the Rankine formula. The test conditions of these case studies are summarized in Table 1.

Case Study	Ref	No	Shape	Size (mm)	Length (m)	End support	Eccentricity (mm)	Fire curve	Aggregate Type
1	[12, 13], University of Braunschweig	39	square	200×200; 300×300	3.76 to 5.76	pinned-pinned; pinned-fixed	0 to 150; some under opposite eccentricity	ISO 834	Silicate aggregate
2	[8], National Research Council, Ottawa	21	square; rectangular	203×203; 305×305; 406×406; 305×457	3.81	pinned-fixed; fixed-fixed	0 or 25	ASTM E119	Carbonate aggregate
3	[14], University of Ghent	12	square; rectangular	300×300; 400×400; 200×300	3.9	pinned-pinned	0 or 20	ISO 834	Silicate aggregate
4	[14], University of Liège	4	square; rectangular	300×300; 200×300	2.1	pinned-pinned	0	ISO 834	Silicate aggregate

Table 1 : test conditions of the four case studies

The comparisons of the Rankine prediction with the test results for the four case studies are shown in Figure 2:

FIGURE 2 : Comparison of predictions with test results

For all the four case studies, the Rankine predictions give consistent predictions with coefficient of variations around 25%, which are reasonably good for RC columns under fire conditions. Furthermore, for most of the columns, the Rankine predictions are on the conservative side due to its interactive nature (Tang et al., 2001).

CONCLUSIONS

The Rankine approach for RC columns in fire conditions is presented in the current chapter. A theoretical model is derived for both axially- and eccentrically loaded columns. Four case studies including 76 RC columns are analysed to verify the approach. The experimental results show that the Rankine approach is not only accurate and consistent, but also slightly conservative

REFERENCES

[1]   Sidibé, K., Duprat, F., Pinglot, M., and Bourret, B., *Fire Safety of Reinforced Concrete Columns*, ACI Structural Journal, V.97, No. 4, pp 642-647, 2000.

[2]   Tang, C. Y., Tan, K. H. and Ting, S. K., *Basis and Application of a Simple Interaction Formula for Steel Columns under Fire Conditions*, J. Struct. Engrg., ASCE, October, Vol. 127, No. 10, pp 1206-1213, 2001.

[3]   Tang, C. Y. and Tan, K. H., *Basis and Application of a Simple Interaction Formula for Steel Frames under Fire Conditions*, J. Struct. Engrg., ASCE, October, Vol. 127, No. 10, pp 1214-1220, 2001.

[4]   Rubert, A., and Schaumann, P., *Structural Steel and Plane Frame Assemblies under Fire Action*, Fire Safety J., 10, 173-184, 1986.

[5]   Dotreppe, J.C., Franssen, J.M., Vanderzeypen, Y., *Calculation Method for Design of Reinforced Concrete Columns under Fire Conditions*, ACI Structural Journal, V. 96, No. 1, 9-18, 1999.

[6]   ISO 834, *Fire Resistance Teats-Elements of Building Construction*, International Standards Organisation, 1975.

[7]   Franssen, J.M., Cooke, G.M.E., and Latham, D.J., *Numerical Simulation of a Full Scale Fire Test on a Loaded Steel Framework*, J. of Constructional Steel Research, 35: 377-408, 1995.

[8]   Lie, T.T. and Woollerton, J.L., *Fire resistance of Reinforced Concrete Columns: Test Results*, Internal Report No. 569, National Research Council Canada, 1988.

[9]   Lie, T.T. and Kodur, V.K.R., *Fire Resistance of Steel Columns Filled with Bar-reinforced Concrete*, J. of Struct. Engrg., ASCE, 122(1), 30 –36, 1996.

[10]   ASTM-E119, *Standard Methods of Fire Tests of Building Construction and Materials*, American Society for Testing and Materials, Philadelphia, PA, USA, 1995.

[11]   Nilson, A.H. and Winter, G., *Design of Concrete Structures*, 11th Ed., New York: McGraw-Hill, 1991.

[12]   Hass, R., *Practical Rules for the Design of Reinforced Concrete and Composite Columns Submitted to Fire*, Technical Report No. 69, Institute für Baustoffe, Massivbau und Brandschutz der Technischen Universitä Braunschweig. (in German), 1986.

[13]   Grandjean, G., Grimault, J.P., and Petit, L., *Determination de la durée au feu des profils creux remplis de béton*, Rapport Final. Commission des Communautés Européennes, Recherche Technique acier. Luxembourg (in French), 1981.

[14]   Dotreppe, J.C., Franssen, J.M., Bruls, A., Vandevelde, P., Minne, R., Van Nieuwenburg, D., and Lambotte, H., *Experimental Research on the Determination of the Main Parameters Affecting the Behavior of Reinforced Concrete Columns under fire Conditions*, Magazine of Concrete Research, V. 49, No. 179, 117-127, 1997.

Session 2:
Concrete slabs

RESTRAINT OF FIRE-EXPOSED CONCRETE FLOOR SYSTEMS

Linus LIM, Andrew H. BUCHANAN, Peter J. MOSS
University of Canterbury, Private Bag 4800, Christchurch, New Zealand

ABSTRACT

This paper describes the numerical analyses of restrained concrete floor slabs exposed to fire. The analyses of the slabs were carried out with the SAFIR finite element program considering a 200mm thick slab, spanning 5 metres between two end supports. The slabs were exposed to the ISO standard fire for up to four hours and were analysed with pinned and rotationally restrained supports. Different heights of the line of thrust at the supports and different levels of axial restraint were also investigated. The analyses show that fully restrained pin-supported slabs can survive the four hour ISO fire without collapse if the position of the line of thrust is located near the soffit of the slab. If the position of the line of thrust is located much above the soffit of the slab, the slabs will rapidly undergo large deformations and sag into a catenary, imposing axial tensile forces at the supports. The analyses have shown that even if the line of thrust is located close to the soffit, the slab can still deform into a catenary if there is insufficient horizontal axial restraint. In this study, rotationally restrained slabs experience much smaller vertical deflections than pin-supported slabs when exposed to fires. Rotationally restrained slabs with low levels of horizontal restraint do not collapse, due to the beneficial effects of moment redistribution. However, high levels of horizontal restraint can be detrimental, causing slabs to collapse at advanced stages of the fire.

KEYWORDS: *fire resistance, restraint, reinforced concrete, flat slabs, SAFIR*

1. Introduction

The fire resistance of floor systems is most often determined by generic ratings which specify the minimum slab thicknesses and concrete cover to the reinforcing steel, such as those specified in the New Zealand Concrete Structures Standard (SNZ, 1995). These generic ratings do not account for the effects of axial restraint at the slab supports.

A first step to quantify the effects of restraint was made by Selvaggio et al (1963) which led to the establishment of restrained and unrestrained fire resistance ratings of proprietary concrete and composite steel-concrete floor systems such as those listed in the Fire Resistance Directory (Underwriters Laboratories, 1999) in the USA. The definition of restraint in these ratings is not well defined and there is no established basis for quantifying the restraint other

than qualitative descriptions such as those in the ASTM E119 testing standard (ASTM, 1999). Restrained ratings of floor systems are generally higher than unrestrained ratings because tests have shown that compressive restraint from the surrounding structure will generally improve the fire resistance of the floor system (Buchanan, 2001).

This paper describes the numerical analysis of single span one-way concrete floor slabs exposed to fire, with varying levels of axial restraint at the supports. Two-way slabs are beyond the scope of this paper.

2. Restraint of concrete floor systems exposed to fire
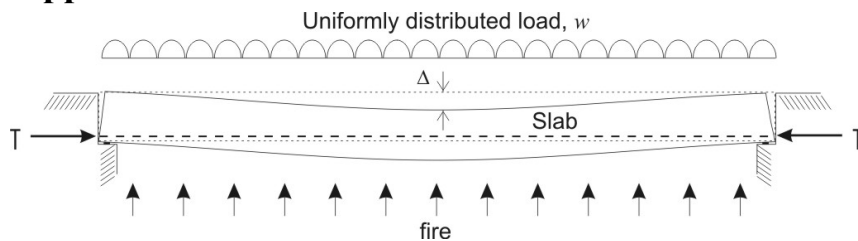
2.1. Pin supported slabs

Figure 1: A restrained simply supported slab exposed to a fire from below

When a simply supported slab is exposed to a fire from below, it will expand and deflect downwards. The vertical deflection is mainly due to thermal bowing of the slab resulting from the non-linear temperature gradient. Additional deflections will occur during the fire due to the loss of flexural stiffness in the structure at elevated temperatures. If the horizontal movement from thermal expansion is restrained by a rigid surrounding structure (Figure 1), compressive axial forces will develop in the slab, generally enhancing the strength and reducing the deflections.
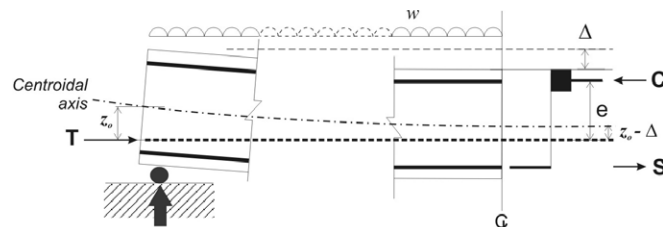

Figure 2: Free body diagram of a restrained simply supported slab

Figure 2 shows the free body diagram of half of a restrained reinforced concrete slab exposed to a fire on the underside. The equilibrium of the forces require the compression stress block to have a force, C, equal to the sum of the tensile forces in the reinforcing steel, S, and the external thrust force, T, i.e.: C = S + T (Buchanan, 2001). The equilibrium between the applied and resisting moments at failure is:

$$R^+_{fire} = wL^2/8 - T(z_o - \Delta) \quad \text{.. Equation 1}$$

Where R^+_{fire} = Positive flexural capacity of the slab at elevated temperatures

z_o = Distance between the position of thrust force and the centroidal axis of slab

Δ = Midspan vertical deflection
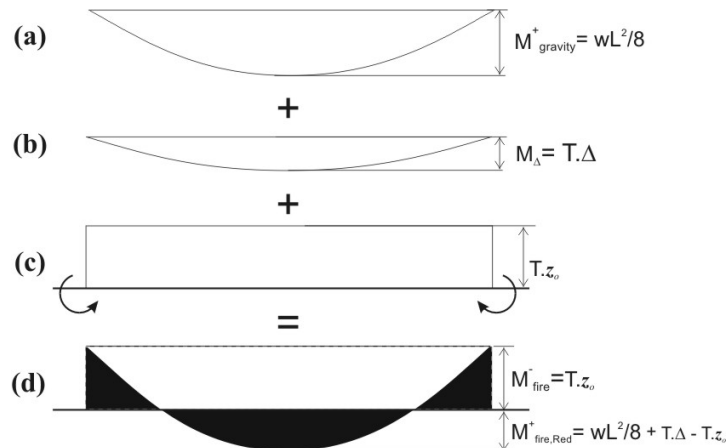
w = Uniformly distributed load

L = Length of slab

Figure 3: Components of moments in a restrained slab with its line of thrust at the slab soffit

The effectiveness of the restraint is dependent on the distance of the thrust force to the centroidal axis of the slab at the end supports, z_o (refer to Figure 2). Figure 3 shows the moments that act on a restrained slab when the line of thrust is located close to the soffit of the slab. Figure 3a shows the bending moment diagram due to the gravity loads. Figure 3b shows the moments due to the downward deflection of the slab, coupled with the restraint force, T, and Figure 3c shows a uniform negative moment due to the restraint force, T, acting at a distance, z_o, below the centroidal axis at the supports of the slab. The combined bending moment diagram due to the external thrust and the gravity load is shown in Figure 3d. The moment due to the gravity loads, $M^+_{gravity}$, remains constant during the fire but the moments due to M_Δ and $T.z_o$ can change during the course of the fire, which will also change the shape of the combined bending moment diagram.
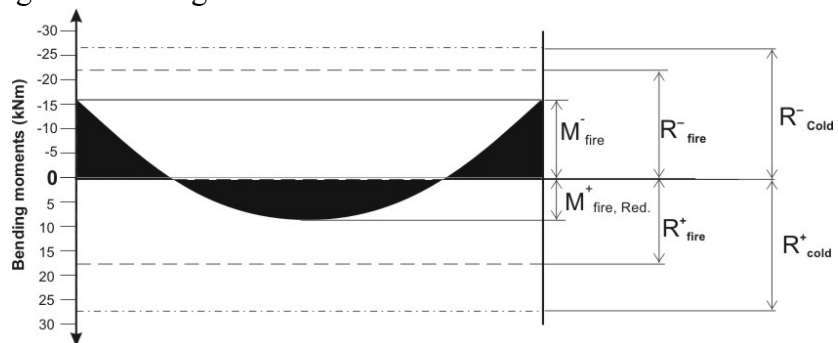

Figure 4: Applied and resisting moments of a restrained slab

Figure 4 shows the same bending moment diagram from Figure 3d, with typical positive (R^+_{cold}) and negative flexural capacities (R^-_{cold}) added. As the temperatures increase during the fire, the flexural capacities will steadily reduce, shown by the lines marked R^+_{fire} and R^-_{fire}. The shape of the bending moment diagram can only change within the limits of the reduced positive and negative flexural capacities. If the reduced positive flexural capacity, R^+_{fire}, falls below the applied bending moment, $M^+_{fire,Red}$, a plastic hinge will form and the slab will collapse. However, the negative moment, M^-_{fire}, which is due to the thrust force acting below the centroidal axis will reduce the positive moments, which will require the positive flexural capacity to be further reduced before it is exceeded by the positive moments, thus allowing the slab to be exposed to the fire for a longer time. If the negative moment is sufficiently large, it can reduce the positive moments at midspan to zero. In this case, the positive flexural capacity can drop to zero without collapse of the slab. However, the negative moments at the slab supports can increase only up to the limit of the negative flexural capacity, R^-_{fire}, which depends on the compressive strength of the bottom reinforcing bars at the end of the span. The

negative moments cannot be further increased if the bottom reinforcing bars yield in compression.

Even with the reduction of the positive moments by the $T.z_o$ moment, a plastic hinge can still form at midspan, causing failure, if the positive moment, $M^+_{fire, Red}$, increases sufficiently and exceeds the slab's positive flexural resistance, R^+_{fire}. This increase of the positive moment during the fire is attributed to the M_Δ moment, which is the product of the deflections and the thrust force. If the slab deflects downwards excessively until the midspan deflections, Δ, equal z_o, the terms $T.\Delta$ and $T.z_o$ in Equation 1 will cancel out and become zero. Thus, the flexural enhancement due to restraint will be lost and only the flexural capacity of the slab can be relied on to resist any additional positive moments.

The thrust force from the rigid supports can increase the flexural stiffness of the slab, to prevent large downward deflections. Paradoxically, the rigid supports will cause large compressive forces in the slab, which will also increase the M_Δ moments, even for small deflections. Therefore, the flexural resistance at midspan can also be exceeded for a rigidly restrained slab with small vertical deflections. This will result in a sudden collapse due to compressive failure of the concrete compression block, causing a plastic hinge at midspan.

2.2. Rotationally restrained slabs

Slabs which are continuous over several supports are subjected to some level of horizontal restraint when exposed to fires and are only unrestrained on rare occasions (Harmathy, 1993). For this reason, the effect of horizontal restraint on slabs with rotational restraint at the supports, such as continuous slabs, is also included in this study. Continuous slabs have better structural fire resistance than pin supported slabs due to their higher level of redundancy against failure. Their better performance in fires is due to moment redistribution which allows the loads to be resisted by alternative means after the first plastic hinge forms.
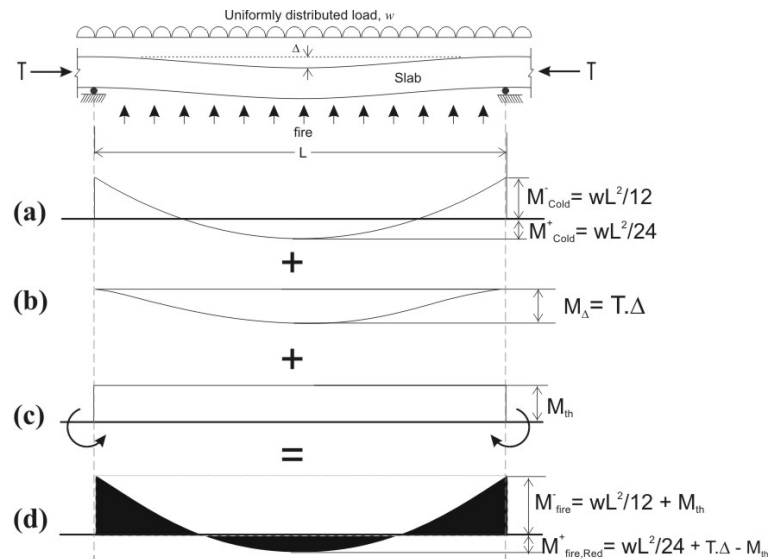

Figure 5: Components of moments in a restrained continuous slab

Figure 5 shows the bending moments of an interior span of a continuous slab, subjected to a fire from the underside. The heated span is assumed to be uniformly loaded and horizontally restrained. The bending moment diagram due to the gravity loads is shown in Figure 5a. The vertical deflections and thermal thrust also produce a moment, M_Δ (Figure 5b). A uniform

hogging moment (Figure 5c) along the length of slab is formed, due to the rotational restraint against the curvature induced by the thermal gradient. This hogging moment increases the negative moments at the supports and reduces the positive moments along the span. The combined bending moment diagram due to the gravity loads and the thermal effects is shown in Figure 5d. The shape of the bending moment diagram will change during the fire, due to the M_{th} and M_{Δ} moments, but only within the limits of the reduced positive and negative flexural capacities, as in the case of the pin supported slab in section 2.1. Unlike the pin supported slab, the continuous slab will not fail until the flexural capacity is exceeded at three plastic hinge locations.

2.3.   Position of line of thrust at the supports

Axial restraint can be detrimental to the structural behaviour of floor slabs if the line of the thermal thrust is not located near the bottom of the cross section. An example of such an application would be in double-tee slabs which have their webs cut out (refer to Figure 6a). In this case, the line of thrust will be too close to the centroidal axis to produce any enhancement. If the thrust force acts above the centroidal axis of the slab, it can produce a sagging moment, which will accelerate the development of the applied positive moments, and reduce the time to forming a plastic hinge, and failure.
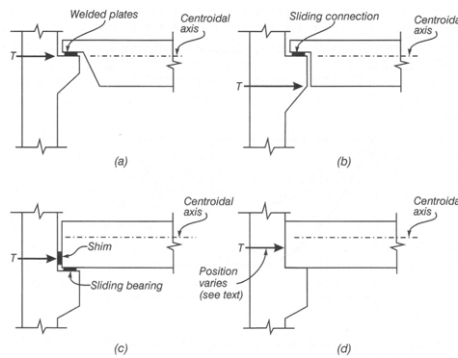

Figure 6: Location of point of action for different support conditions (Carlson et al, 1965)

The height of the line of thrust can only be located accurately for specific support conditions where the line of thrust is well defined due to the method of construction. An example of such an application would be in precast construction where metal shims are placed between the vertical faces of the ends of slabs and the restraining structure (Figure 6b and c).

For cast in-situ or continuous slabs (Figure 6d), the height of the line of thrust at the supports changes during the course of the fire. Fire tests of restrained floor slabs at the PCA furnace (Issen et al, 1970 and Lin et al, 1983) have shown that the line of thrust moves from below the depth of the slab and towards the centroidal axis during the course of the fire.

In a continuous slab, the position of the line of thrust at the supports can be determined from the bending moments at the supports. Figure 5 shows that M^{-}_{fire} consists of the moments imposed due to the gravity loads, $wL^2/12$, and the moments due to restraint against thermal curvature, M_{th}. By definition, the bending moment at the supports is defined as the couple of the axial force in the slab, T, and the eccentricity, e (refer to Equation 2). This eccentricity is the position where the axial force is acting across the depth of the slab at the supports, relative to the centroidal axis of the slab.

$$M^{-}_{fire} = T.e \quad \text{..} \textbf{Equation 2}$$

where T = Axial forces in the slab
e = eccentricity of the point of the action of the axial forces

Therefore, solving for the eccentricity in Equation 2 gives:

$$e = \frac{M^-_{fire}}{T}$$ .... **Equation 3**

2.4.   Catenary action

Large deflections can occur in one-way slabs after significant periods of fire exposure. For simply supported slabs, rapidly increasing deflection indicates the onset of failure. If the slabs have the capacity for horizontal tensile restraint at the supports, the large deflections can result in the loads being carried by catenary action, with tensile forces in the slabs. This requires the supports to have sufficient anchorage and tensile capacity to resist these forces.

3.   Past research

The investigation of the effects of restraint on fire exposed concrete floor systems exposed to fire was pioneered by the Portland Cement Association (PCA) (Selvaggio et al, 1963). The tested specimens consisted mainly of double-tee floor systems. The specimens were fire tested with different amounts of allowable expansion and were subjected to the ASTM E119 standard fire. Issen et al (1970) showed that almost any amount of restraint greatly enhanced the fire resistance of the slabs as they were able to support their loads considerably longer than for the simply supported condition. Based on these results, a step-by-step method incorporating several nomograms was developed by the Prestressed Concrete Institute, PCI (Gustaferro et al, 1988) to determine the amount of thrust required to prevent collapse of the floor system, and the required stiffness of the surrounding structure to provide that level of restraint.

Gustafson (1980) has provided a step-by-step procedure for analysing structures exposed to fires. This procedure is directed to beams, slabs and joist systems. The analysis of the structure is based on the PCI method, or the "thick walled" cylinder analysis, if the floor system forms part of an interior bay. Gustafson (1980) also provides recommendations for evaluating the position of the line of thrust at the slab supports. However, Harmathy (1993) questioned the general applicability of these nomograms, formulas and tables.

Lin et al (1983) have also conducted a large number of fire tests on restrained concrete floor slabs exposed to the ASTM E119 fire. Their test results showed that the performance of the floor slabs is not greatly affected by the degree of restraint, except near the 0% and 100% restraint conditions. Under zero restraint, the slab will behave as a simply supported member and will result in a lower fire resistance. At full restraint (100%), the high restraining forces could result in a compressive failure.

Anderberg et al (1982) developed a non-linear finite element program, CONFIRE, to investigate the structural behaviour and fire resistance of concrete members exposed to fire. Their analysis was on simply supported concrete slabs with different amounts of allowable horizontal expansion of the slabs. Their analyses showed that the fire resistance of the floor slabs does not increase with increasing axial restraint and that the PCI method cannot be universally applied to all types of floor systems. They also argued that the maximum thrust that formed in the slabs analysed cannot be used to determine its fire resistance based on the

PCI method and concluded that the PCI method over-predicts the thermal strains, particularly at strains in excess of 0.15%.

Cooke (1993) has conducted a series of fire tests on restrained concrete flat slabs. The tests showed that when the line of thrust at the supports is located at the exposed face of the slab, the fire resistance of the slabs is significantly better than slabs with their line of thrust located at mid-depth. The tests also showed that an axial load applied at mid-depth of the slab end supports produced significantly shorter times to failure than a slab with no axial restraint.

4. Analysis of slabs

4.1. Introduction

The following section covers the structural analysis of a single span, one-way spanning concrete flat slab exposed to the ISO standard fire. The slab spans 5 metres, and has a depth of 200mm, with different types of support conditions imposed on the end supports. The maximum duration of fire exposure is 4 hours.

4.2. Method of analysis

The analysis of the floor slabs was carried out using a non-linear finite element program, SAFIR, developed at the University of Liege, Belgium (Franssen et al, 2000). SAFIR analysis consists of two components, which are the thermal and structural analysis. The analysis of a structure exposed to fire is simulated as a function of time, using the temperature distributions evaluated with the thermal analysis program built into SAFIR. The structural analysis in SAFIR can account for large displacements and the variation of the thermal and mechanical properties of the materials with temperature. The mechanical properties of the materials (steel and concrete) follow the properties of the Eurocode (EC2, 1995 and EC3, 1995). Although SAFIR can perform 3D analysis, only the 2D structural analysis is utilised in this study.

4.3. Support conditions

The two basic support conditions that are modelled for the single span slab are:
1. Pin supports, where the slabs are free to rotate at the supports; and
2. Rotationally restrained, where the slabs are fully restrained against rotation at the supports.

The support conditions are shown in further detail in Figure 7 and Figure 8.

1)   Pin supports

a) Unrestrained against horizontal movement (pin-roller)

b) Fully restrained against horizontal movement (pin-pin)

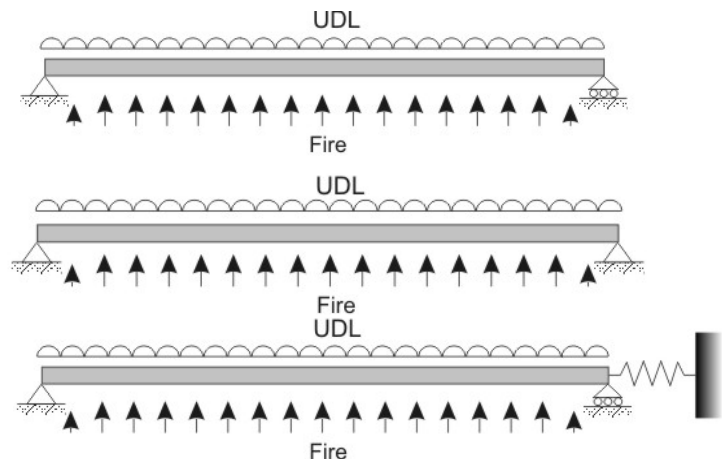c) Horizontally restrained by a spring

Figure 7: SAFIR models of pin supported slabs

2)   Rotationally restrained

a) Unrestrained against horizontal movement (fix-slide)

b) Fully fixed on both supports (fix-fix)

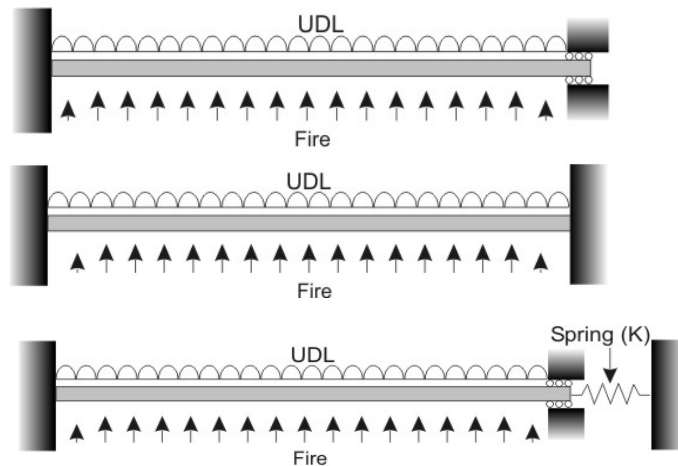c) Rotationally and vertically fixed on both supports, horizontally restrained by a spring

Figure 8: SAFIR models of rotationally restrained slabs

In both Figure 7 and Figure 8, cases (a) represent slabs with no horizontal restraint and are free to translate horizontally. Cases (b) represent slabs with full horizontal restraint and cases (c) represent slabs with some horizontal restraint, modelled by an axial spring. The level of stiffness of the spring varies, depending on the stiffness of the support conditions, from being very soft as shown in case (a), to full horizontal restraint, as in cases (b).

4.4.   Scope of analysis

The different support conditions analysed are shown in Table 1 below.

Case	Support condition	Position of line of thrust	Spring stiffness, k	See Section
(i)	Pin supports	$-25\text{mm} \leq x_o \leq 125\text{mm}$	Full restraint	5.1
(ii)	Pin supports	$x_o = 50\text{mm}$	$0 \leq k \leq$ full restraint	5.2
(iii)	Full rotational restraint	-	$0 \leq k \leq$ full restraint	5.3

Table 1: Cases analysed

Position of line of thrust

The line of thrust can be determined and defined in the program by incorporating vertical rigid elements at the ends of the slab to introduce the eccentricity relative to the centroidal axis of the slab. This assumes that the line of thrust is fixed throughout the course of the fire. For the purposes of discussion, the position of the line of the thrust is measured as a distance, x_o, with reference to the fire-exposed face (soffit) of the slab, as shown in Figure 9. For the analysis of the pin supported slab, the position of the line of thrust at the supports will be varied from -25mm below the soffit of the slab, to 125mm above the soffit of the slab (refer to Figure 9).
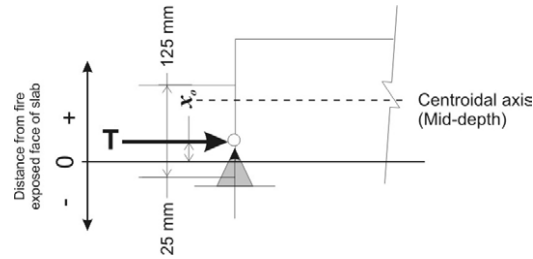
Figure 9: Range of different positions of line of thrust considered for pin supported slabs

Spring stiffness

The spring stiffness ranges from zero to fully restrained. The percentages of the spring stiffness are measured relative to the axial stiffness of the slab, such that 100% stiffness is equivalent to an identical additional slab at one end support.

4.5. Properties of the slab

The slab that is analysed is shown in Figure 10. For the purposes of discussion, a metre width of the slab is considered but in the computer analyses, only a 125mm wide strip with a single reinforcing bar at the top and bottom is modelled. This is to reduce the computational effort of the analysis.
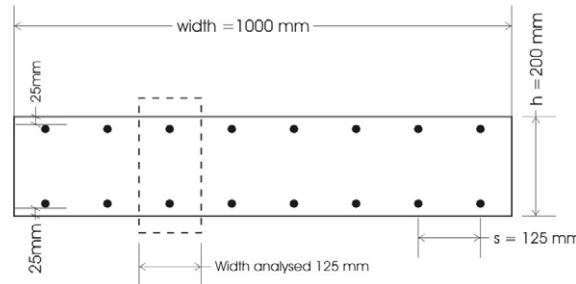

Figure 10: Cross section of the slab modelled with SAFIR.

The properties of the slab that is modelled are as follows:

Slab geometry

Length, *l*	5000mm
Depth, *h*	200mm
Width	1000mm
Aspect ratio, *l/h*	25

Concrete properties

Compressive strength (ambient temperature) f'$_c$:	30 MPa
Elastic modulus (ambient temperature), E$_{c,o}$:	18 GPa
Tensile strength, f'$_t$:	Zero
Concrete model (thermal and mechanical):	Siliceous aggregate (EC2, 1995)
Concrete cover, c$_c$	25mm

Reinforcing steel properties

Yield strength (ambient temperature), *f$_{y,o}$*:	430 MPa
Elastic modulus (ambient temperature), E$_{s,o}$:	210 GPa
Steel model (thermal and mechanical):	Eurocode 2, EC2 (1995)
Bar diameter, d$_b$:	16mm
Bar spacing, s:	125mm (top and bottom)
Bar lengths	Continuous (top and bottom)

Loads

Self weight + Superimposed dead load, G	5.30 kPa
Live load, Q	4.0 kPa
Ultimate load, 1.2G + 1.6Q	12.8 kPa
Fire load, 1.0G + 0.4Q	6.9 kPa
Fire exposure	ISO 834 standard fire (4 hour duration)

4.6.   Thermal analysis

Figure 11 (a) shows the finite element discretisation of the cross section of the slab. It shows a 125mm wide section of the slab. The thermal gradient of the slab, when exposed to the ISO standard fire from below, is shown in Figure 11 (b). Figure 11 (c) shows the evolution of the temperatures at the exposed, mid-depth and unexposed faces.

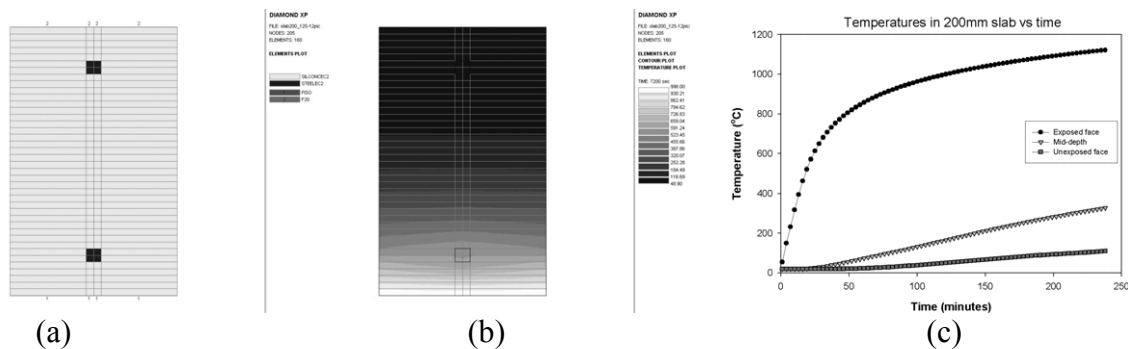|		
(a)	(b)	(c)

Figure 11: Thermal analysis of 125mm wide strip: (a) SAFIR discretisation of the slab, (b) Temperature distribution after a 2 hour exposure to the ISO fire, and (c) Temperature variation with time at the exposed face, centre and unexposed face of the slab.

4.7.   Structural analysis

The structural analysis of the slabs is performed in two-dimensions (plane frame) to model the slabs as one-way spanning slabs. The slab is modelled as a beam, using 20 2D beam finite elements (Figure 12). The beam has the cross section shown in Figure 11 and is loaded with its tributary uniform load. Rigid vertical elements are used at the supports to model the different positions of the line of thrust, relative to the centroidal axis of the slab finite elements. The axial springs are modelled with truss elements with elastic material properties and are not exposed to the fire.
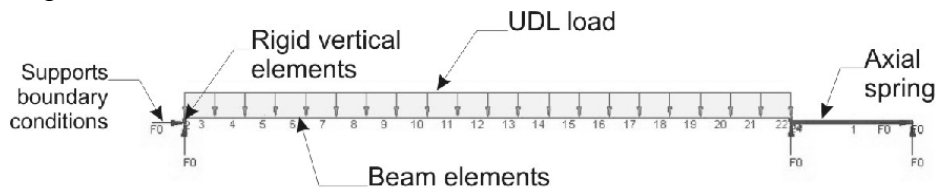

Figure 12: Discretisation of the slab with SAFIR for structural analysis.

4.8.   Assumptions

The assumptions made during the analyses of the slabs are:

*   The slabs behave as one-way slabs. Two-way action in the slabs is ignored.
*   Spalling of concrete does not occur.
*   The fire exposure along the length of the slab is uniform.
*   Shear failure of the slab is ignored in the analysis.
*   The material properties of the slab are homogenous and uniform.

5.   Results of analysis

5.1.   Pin supported; fully restrained

This section investigates the behaviour of pin supported slabs with full horizontal restraint at the supports. The effect of the different positions of the line of thrust on the behaviour of a slab is investigated. Separate analyses were conducted for different positions of line of thrust at the end supports, ranging from -25mm (25mm below the exposed face) to 125mm into the depth of the slab (Figure 9). The position of the line of thrust is fixed for each analysis and does not change during the fire. The behaviour of a simply supported slab with no horizontal restraint, designated "*Pin-roller*" will be compared with the fully restrained slabs.
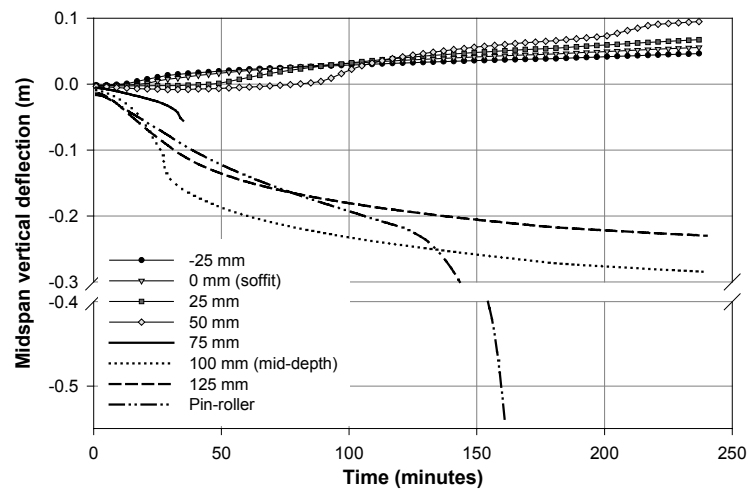
5.1.1.   Midspan deflections and axial forces

Figure 13: Midspan vertical deflection vs. time (Pin supports and full horizontal restraint)
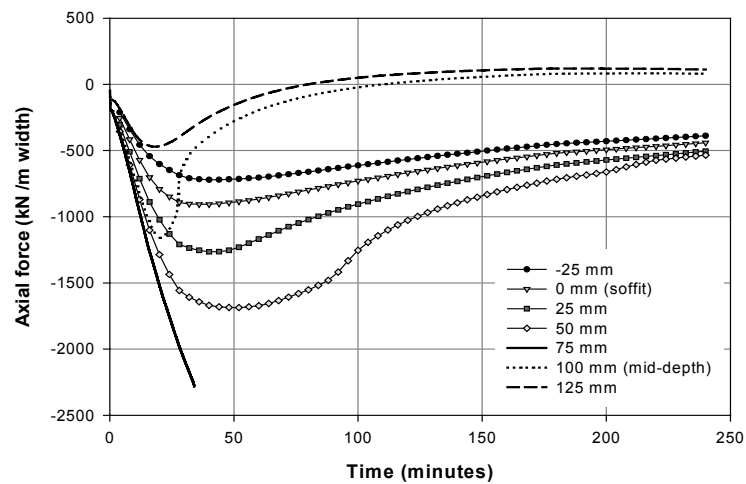

**Figure 14: Axial force in slabs vs. time (Pin supports and full horizontal restraint)
(Note: Compression forces are negative)**

Figure 13 compares the variation of the midspan deflection of the slabs when exposed to the ISO standard fire. Negative deflection is downwards. Figure 14 shows the variation of the axial forces in the slabs. The discussion of the slabs' behaviour is divided into different sections for the different types of behaviour.

Pin-roller slab

Figure 13 shows that a simply supported slab with pin-roller supports gradually deflects downwards during the initial stages of the fire, and reaches a deflection equal to its depth ($\Delta_{midspan}$ = 200mm = L/25) at 105 minutes. At approximately 120 minutes, the deflection rate increases leading to runaway failure of the slab. The initial deflection is due to thermal bowing of the slab while the runaway deflection is due to the inability of the slab to resist the loads due to the loss of strength and stiffness. There are no axial forces in a *pin-roller* slab because there is no horizontal end reaction.

Position of line of thrust, -25mm$\leq x_o \leq$ 50mm

When x_o is located anywhere between -25mm (outside the section of the slab) and 50mm above the soffit, the slab shows very small sagging deflections during the initial stages of the fire. As the fire progresses, the sagging deflection of the slab changes to a hogging deflection when the slab 'pops-up', shown by the upward deflection at midspan (Figure 13). These slabs remain in hogging until the end of the fire without collapse.

Position of line of thrust, 75mm$\leq x_o \leq$ 125mm

When x_o is located between 75mm and 125mm, the slabs exhibit a different behaviour to the other slabs discussed above. Figure 13 shows that these slabs sag downwards into large vertical deflections during the fire. The analysis of a slab with x_o at 75mm stops prematurely at 32 minutes. This is believed to be a numerical problem in the program when the slab snaps-through and goes into catenary mode. When x_o is at 100mm (mid-depth of the slab) and 125mm (25mm above mid-depth), the behaviour of the slabs during the initial stages resemble the simply supported slab where the deflection is caused by thermal bowing. Unlike the *pin-roller* slab, these two slabs do not exhibit a runaway failure and survive the fire for the entire duration of four hours. The slab with x_o at 100mm shows a sudden increase in the deflection rate after approximately 28 minutes due to "snap-through" of the slab. This occurs when the midspan deflection of the slab reaches 100mm and is accompanied by a sudden drop in the axial force (see Figure 14). These slabs subsequently go into axial tension. If they could not resist tensile forces at the supports, the slabs would collapse when they changed into a catenary mode. Referring to Figure 14, the slabs with x_o at 100mm and 125mm would have failed at 110 minutes and 80 minutes, respectively when tensile forces formed in the slab.

When the position of the line of thrust at the supports is located further away from the exposed face, the thrust force cannot sufficiently increase the flexural strength and stiffness of the slabs. This is shown by the relatively small compression forces in the slabs with x_o at 100mm and 125 mm (Figure 14), which increase slightly during the initial stages but trail off into axial tension at the later stages of the fire. The tension forces are due to the slabs deforming into large deflections, forming a catenary.

When x_o is at 75mm, the slab's behaviour lies in a bifurcation region where it could either pop-up and form a hogging deflected shape, or snap-through forming large sagging deflections. However, the deflection trend of this slab shows that it would snap-through. The computer program had difficulty attaining a converged solution when the large compressive

axial forces in the slab decreased very suddenly when the slab snapped through. Consequently, the program could not iterate further and the analysis stopped.
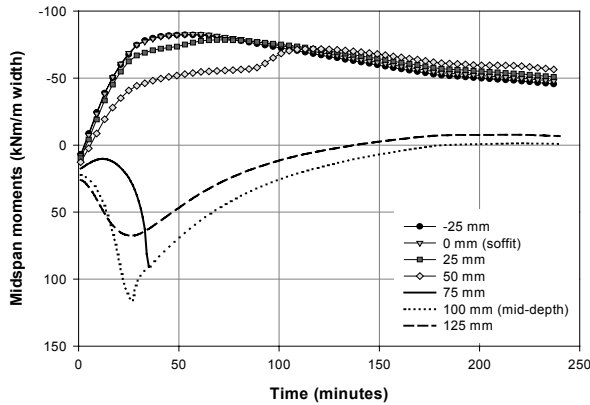
5.1.2.   Bending moments

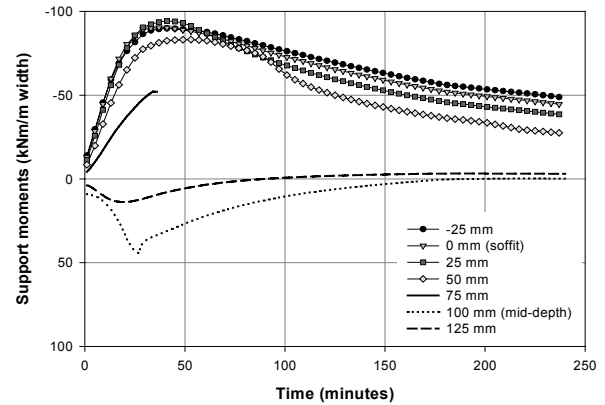**Figure 15: Midspan bending moments vs. time (Pin supports and full horizontal restraint)**

Figure 16: Support bending moments vs. time (Pin supports and full horizontal restraint)

Position of line of thrust, -25mm≤ x_o≤ 50mm

Figures 15 and 16 show the variation of the bending moments in the slabs. In the graphs, the hogging moments have a negative sign convention while the sagging moments are positive. When x_o lies between -25mm and 50mm, the negative moments in the slab rise rapidly during the initial stages when large axial forces act below the centroidal axis of the slab. The negative moments at the supports reach a peak after about 40 minutes, followed by a gradual decrease. The peak is due to the negative moments at the supports reaching the limit of the negative flexural capacity, which depends on the compressive strength of the bottom steel at the supports. The decrease of the moments that follows the peak is due to the reduction of the compressive strength of the steel and concrete at the exposed face due to the elevated temperatures.
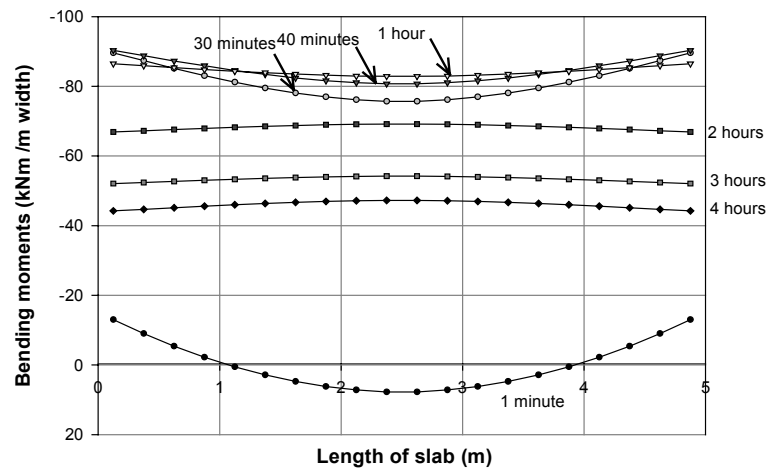

Figure 17: Bending moment diagram at different times (Line of thrust, x_o=0mm and full horizontal restraint)

Figure 17 shows the bending moment diagram of the slab at various times during the fire for the case where the line of thrust is located at the soffit of the slab, i.e.: x_o = 0. Soon after the start of the fire, the positive moments due to the gravity loads are reduced by the negative moments, T.z_o. After two hours, larger negative moments are formed at midspan than the

support due to the M_Δ moments, caused by the hogging deflection of the slab coupled with the external thrust force. The moments along the entire length of the slab remain negative until the end of the fire and the positive flexural strength at midspan is not utilised to resist the loads.

Position of line of thrust, 75mm ≤ x_o ≤ 125mm

When x_o is located at 100mm (mid-depth), Figure 15 shows that the positive moment at midspan increases very rapidly during the initial stage and reach a sharp peak. The positive moments then decrease gradually, reaching zero at the later stage of the fire. This peak occurs when a positive plastic hinge forms at midspan, subsequently causing the loads to be resisted by tensile action, rather than by bending. Although the theoretical flexural strength of the slab is 60kNm/m, the computed peak moment at midspan at the time a plastic hinge forms is in excess of 100 kNm /m. The increase of the positive flexural strength of the slab is due to the strength enhancement by the compressive axial forces in the slab. When x_o is at 75mm, a positive plastic hinge forms at midspan due to the large applied positive moments at midspan. The positive plastic hinge forms in spite of the presence of substantial negative moments at the supports (Figure 16) which would have reduced the positive moments. However, the large positive moments form in the slab due to the high compressive forces (refer to Figure 14) coupled with the deflections. When the positive moments exceed the positive flexural capacity at midspan, a plastic hinge forms and the slab collapses. The large compressive forces form in the slab because the slab is rigidly restrained against thermal bowing and expansion of the slab. If the slab was free to bow or expand, it would prevent the build-up of the compressive forces.

5.2.   Pin supports; partial axial restraint

This section investigates the behaviour of a pin supported slab with different levels of horizontal restraint. The position of the line of thrust at the supports, x_o, is kept constant, at 50mm from the exposed face of the slab. The stiffness of the springs is varied from 1% to full horizontal restraint. A *pin-roller* slab is plotted for comparison.
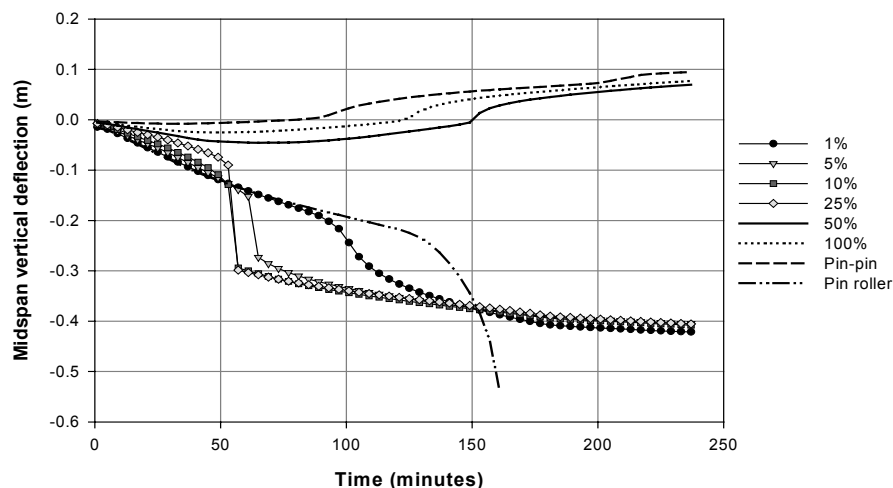
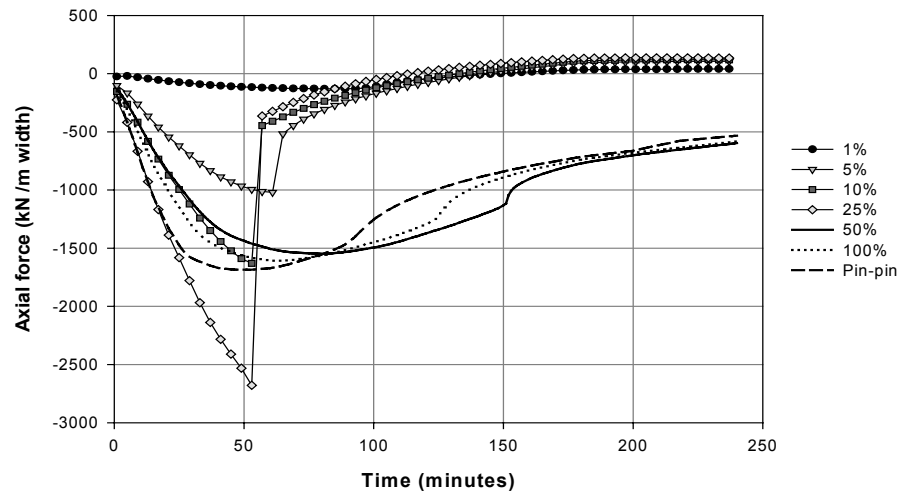**Figure 18: Midspan vertical deflection vs. time (Line of thrust, x_o=50mm and different spring stiffness)**

Figure 19: Axial force in slabs vs. time (Line of thrust, x_o=50mm and different spring stiffness)

Figure 18 shows the behaviour of the pin supported slab with different levels of spring stiffness. The behaviour of the slabs with different levels of restraint can be classified into two groups: k ≤ 25% and k > 25%.

Spring stiffness, 1% ≤ k≤ 25%
Figure 18 shows that when the stiffness (k) of the spring is 1%, its initial deflection trend is very similar to the *pin-roller* slab. After 90 minutes, the deflection rate shows a slight increase due to a minor snap through of the slab. Figure 18 and Figure 19 show that as the spring stiffness is increased from 1% to 25%, the snap-through of the slabs becomes increasingly sudden and the time to snap-through reduces significantly. During the initial stage of the fire, the rate of rise of the compressive axial forces increases significantly as the spring stiffness is increased from 1% to 25%. This rapid increase results in very large compressive axial forces forming in the slabs. When snap-through of the slabs occur, the slabs undergo large deflections which relieves the compressive restraint forces, shown by the marked decrease of the compressive forces in Figure 19. The slabs subsequently deform into a catenary which lead to tensile forces forming in the slabs. This can cause the slabs to collapse if the supports are unable to resist the tensile forces.

Spring stiffness, 50% ≤ k≤ fully restrained
When the stiffness of the spring is increased above 50%, the slabs exhibit a different nature, where they show an initial downward deflection during the first hour. After this, the sagging deflections decrease and the slab eventually pops upwards. None of the slabs collapsed and, all remain in hogging deflection until the end of the simulation. A bifurcation region exists when the spring stiffness lies between 25% and 50%. This represents a transition of behaviour where the slab would form large vertical deflections when the stiffness is less than 25% or upward hogging deflections when the stiffness is greater than 50%.

5.3.   Rotationally restrained slabs, partial axial restraint
This section investigates the behaviour of a single span slab with full rotational restraint at its supports and horizontally restrained by an axial spring (refer to Figure 8c). The behaviour of the slab with different levels of horizontal axial restraint will be investigated. The spring stiffness ranges from zero horizontal restraint (designated *fix-slide*, Figure 8a) to full

horizontal restraint (designated *fix-fix*, Figure 8b). The top and bottom reinforcing bars are assumed to be connected to the end supports.
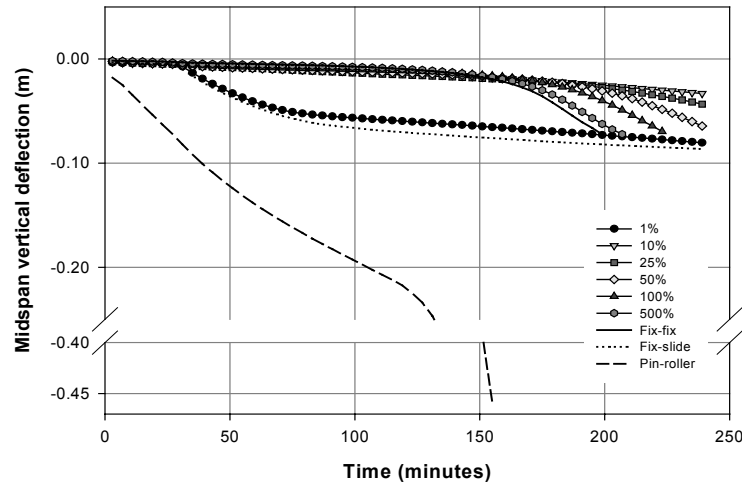
Figure 20: Midspan vertical deflection vs. time (Full rotational restraint and different spring stiffness)
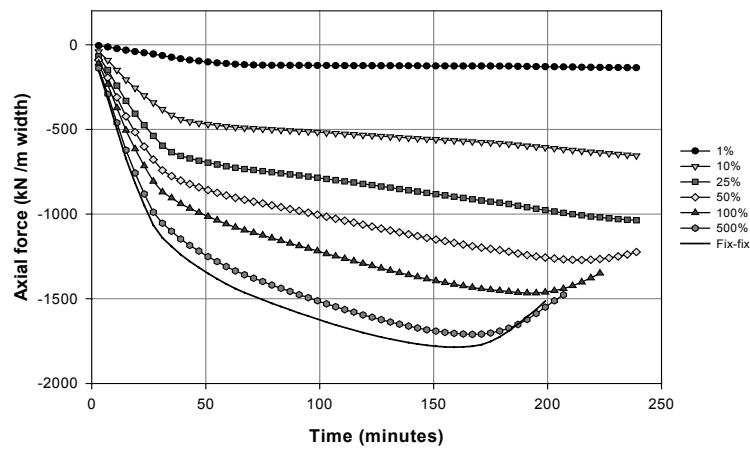

Figure 21: Axial force in slabs vs. time (Full rotational restraint and different spring stiffness)
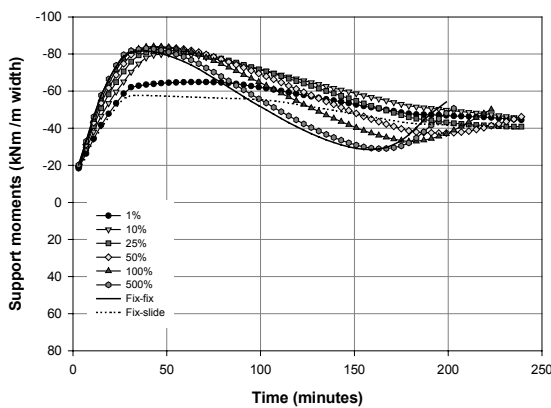

Figure 22: Support bending moments vs. time (Full rotational restraint and different spring stiffness)
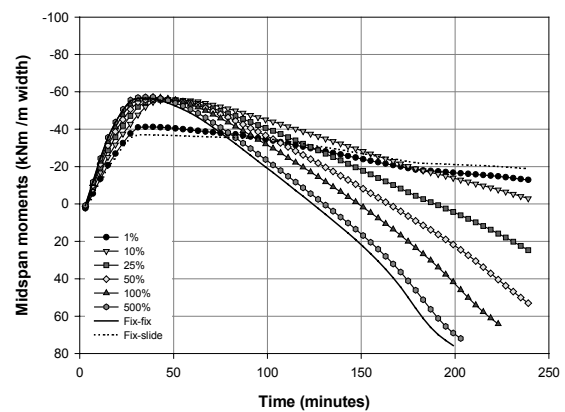

Figure 23: Midspan bending moments vs. time (Full rotational restraint and different spring stiffness)

76

5.3.1. Midspan vertical deflections

Figure 20 shows the midspan vertical deflections of the slabs with rigid rotational restraints at the supports with various levels of horizontal restraint. Also plotted on the same graph is the vertical deflection of a *pin-roller* slab.

Spring stiffness, k= 0% (fix-slide) and 1%

Figure 20 shows that slabs with low axial restraint initially show very small midspan deflections until about 30 minutes when the deflection trend shows a sudden increase. After this, the slab continues to deflect downwards at a linear rate until the end of the fire, where the maximum midspan deflection reaches approximately -90mm. Neither of these two slabs collapsed during the exposure to the four hour ISO fire.

Spring stiffness, 10% ≤ k≤ full horizontal restraint (fix-fix)

Figure 20 shows that when the spring stiffness ranges from 10% to full horizontal restraint, the slabs show very small deflections during the early stage of the fire until 165 minutes, when the deflection rates of the slabs start to increase. When the spring stiffness ranges from 10% to 50%, the slabs do not collapse during the 4 hour fire. However, when the spring stiffness is increased beyond 50%, structural failure of the slabs occurs. The time to collapse of the slab decreases with increasing spring stiffness. The discussion of the failure mechanism is presented in section 5.3.4.

5.3.2. Axial forces

Figure 21 shows the evolution of the axial forces in the slabs. The slabs are in compression throughout the entire duration of the fire exposure. The compressive axial forces in all the slabs show a bilinear increase with time. The slabs with spring stiffnesses above 50% show a decrease at the later stage of the fire, but still remain in the compression region. The decrease corresponds to the sudden increase in deflections, which relieves the compressive forces in the slabs.

5.3.3. Bending moments

Figure 22 and Figure 23 show the variation of the bending moments at the supports and midspan of the slab.

Spring stiffness, k = 0% (fix-slide) and 1%

The graphs show that during the initial stages of the fire, the bending moments at the supports and midspan increase very rapidly in a linear trend until they reach a peak. Then, the moments level off and slowly decrease.

Spring stiffness, 10% ≤ k≤ fully restrained

For these slabs with spring stiffness ranging from 10% to full restraint, the negative moments at the supports and midspan initially increase rapidly until they reach a peak and then drop off. The peak occurs as a result of compressive yielding of the bottom steel at the supports, which prevents further increase of the negative moments. The support moments of the slabs with stiffnesses greater than 50% increase again at the later stage of the fire (after 150 minutes) but the midspan moments continue to decrease. The increase of the negative moments at the supports at this late stage corresponds to the sudden increase in the deflection rates which is due to the reduction of the flexural rigidity of the slab. The reduction of the flexural rigidity increases the curvature in the slab and causes the negative moments at the

supports to increase due to moment redistribution. The increase of the deflections, coupled with the compressive axial forces, increase the M_Δ moments and cause the positive moments to increase.

5.3.4. Reinforcing steel stresses

This section describes the variation of the reinforcing steel stresses in the rotationally restrained slabs. The discussion will be focussed on the slabs horizontally restrained with 1% spring stiffness and the fully fixed slab. In the graphs, the tension stresses are positive and compression stresses are negative. The stresses of the top (unexposed face) and bottom (exposed face) reinforcing steel at the supports and midspan of the slab are plotted, along with their respective proportional (f_p) and yield (f_y) limits. These limits change with time and temperature according to the material properties of the Eurocode (EC2, 1995). The limits for the top and bottom steel are plotted separately because they decrease at different rates during the fire due to the faster heating of the steel strength at the exposed face.
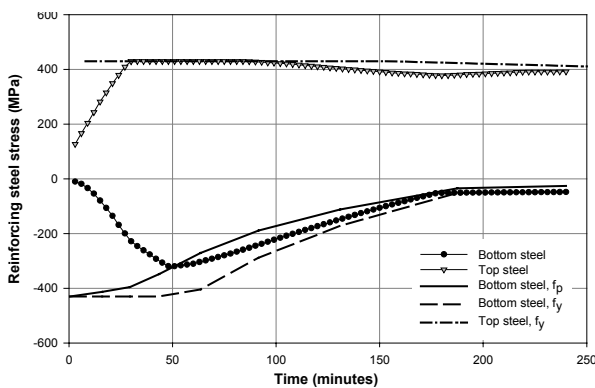
Spring stiffness, k=1%

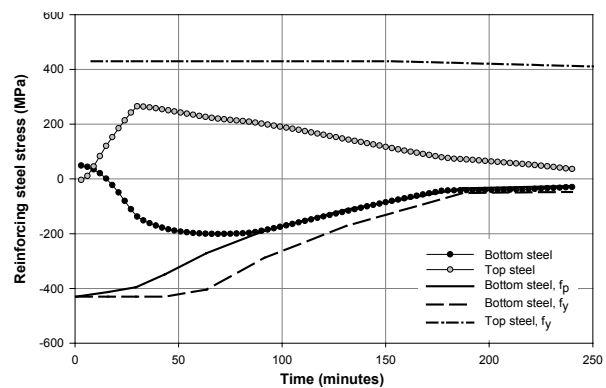| Figure 24: Stresses of reinforcing bars at supports | Figure 25: Stresses of reinforcing bars at midspan |

Figures 24 and 25 show the variation of the steel stresses in the slab with 1% spring stiffness. During the initial stage of the fire, the top steel stresses at the supports and midspan increase rapidly in a linear trend until the steel at the supports yield in tension. At the same time, the compressive stresses at the bottom of the slab also start to increase. The increase of the tensile stresses of the top steel and the compressive stresses of the bottom steel is due to the negative moments induced by restraint against thermal bowing. When the top steel at the supports yield, this causes plastic hinges to form at the supports and the slab loses its rotational restraint. This allows the slabs to bow freely, indicated by the sudden increase in the deflection trend at 30 minutes (Figure 20). At 50 and 80 minutes, the bottom steel at the supports and midspan reach their compression proportional limits, respectively. The positive moments are fully redistributed, preventing a plastic hinge from forming at midspan and subsequent collapse due to a mechanism in the slab.
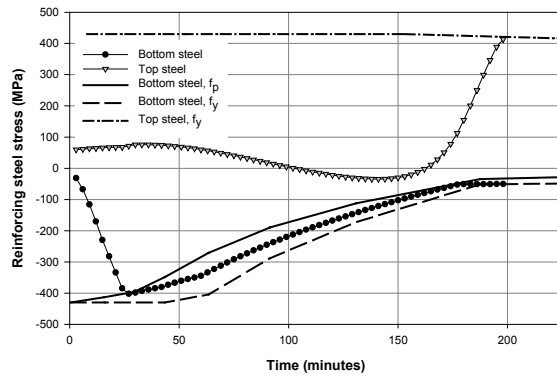
78

Full horizontal restraint

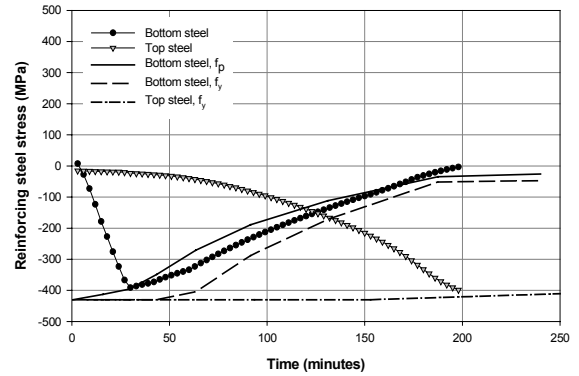**Figure 26: Stresses of reinforcing bars at supports**

Figure 27: Stresses of reinforcing bars at midspan

Figures 26 and 27 show the variation of the stresses in the reinforcing steel for the slabs that are fully fixed at both end supports. The compressive stresses of the bottom steel at both the supports and midspan increase very rapidly during the initial stages of the fire, reaching their compressive proportional limits at 27 minutes and 30 minutes, respectively. This causes the negative moments in the slabs to reach a peak, shown in Figures 22 and 23. In contrast to the lightly restrained slab (k=1%), the top steel stresses of this slab remain relatively low during the initial stages of the fire, with the steel at midspan being in compression and the steel at the supports being in tension. The reason for the tensile stresses remaining low throughout most of the fire is because of the high compressive forces imposed by the rigid horizontal restraint.

Figure 20 shows that the slab deflections start to increase at 165 minutes. The increased deflections coupled with the compressive thrust force cause the positive midspan moments to increase (refer to Figure 23). However, the positive flexural capacity of the slab which is needed to resist the increasing positive moments has been severely depleted. A plastic hinge forms at midspan when the positive moment exceeds the flexural capacity at midspan. The plastic hinge at midspan causes redistribution of the moments to the supports, shown by increase of the negative moments at the supports (Figure 22), which also cause the tensile stresses of the top steel at the supports to increase very suddenly (Figure 26). When the tensile stresses of the top steel at the supports reach their yield limit, a plastic hinge forms at each support, resulting in a mechanism and collapse of the slab.

5.3.5. Variation of the line of thrust at the supports

This section will determine the variation of the height of the line of thrust across the depth of the slab at the supports of a rotationally restrained slab when it is exposed to a fire.
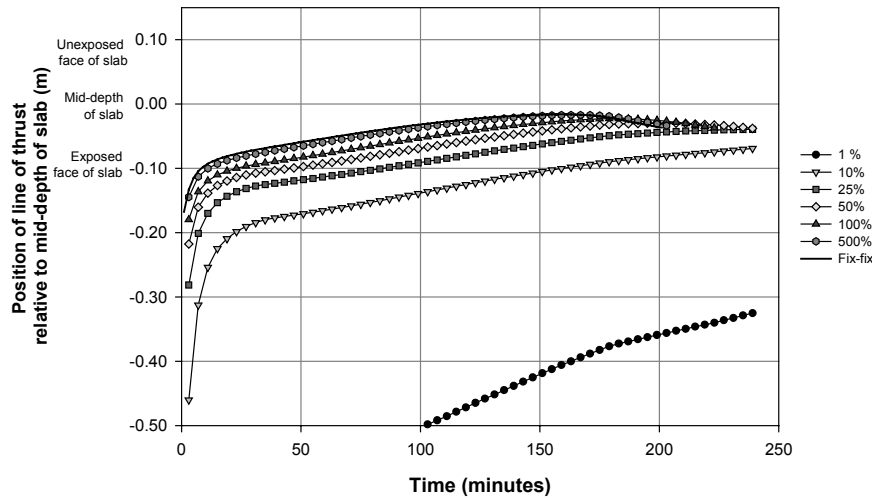
Figure 28: Variation of the position of the line of thrust at end supports (Full rotational restraint, different spring stiffness)

Figure 28 shows the variation of the position of the line of thrust at the supports. The position of the line of thrust, which is an eccentricity measured relative to the centroidal axis of the slab, is calculated from Equation 3. Figure 28 shows that at the start of the fire, the thrust force lies outside the depth of the slab. During the initial stage of the fire, the position of the thrust force rapidly rises. After this initial stage, thrust force gradually rises into the depth of the slab in a linear trend. Towards the end of the fire, the line of thrust drops of slightly for some cases. The graph shows that the line of thrust enters the depth of the slab faster as the stiffness of the spring increases. The rise of the line of thrust during the course of the fire is attributed to the thermal gradient which progressively depletes the strength of the slab from the bottom of the slab.

6.   Conclusions

An analytical study has been carried out into the structural behaviour of reinforced concrete floor systems exposed to fire on the underside, with various levels of axial and flexural restraint at the supports. The main findings are as follows:

- The behaviour of the restrained pin-supported slabs is very sensitive to the location of the line of thrust at the supports and the level of horizontal restraint.
- Computer modelling of restrained reinforced concrete floor systems is difficult because of poor information about the actual boundary conditions in real construction, especially the likely height of the axial restraint force, which may change in location during fire exposure. Another difficulty in modelling restrained floor slabs is numerical problems caused by the high compressive stresses.

For slabs with pinned end conditions and full horizontal restraint:
- For the slabs analysed in this study, axial restraint is beneficial to the slab if the line of thrust is within the bottom 50mm of the slab. The deflections of these slabs are small and upwards during the fire exposure.

- If the axial restraint force is located high up in the slab (greater than 50mm from the bottom of the slab), the deflections are large (L/20) and downwards during fire exposure, with axial tensile forces generated late in the fire.
- If axial tensile forces cannot be resisted at the supports, the slabs fail earlier than a simply supported slab.

For slabs with pinned end conditions and partial horizontal restraint:
- The axial restraint force generated during the fire is strongly dependent on the axial stiffness of the support system. High stiffness produces high axial forces.
- For the slabs analysed in this study with its line of thrust located 50mm from the bottom of the exposed face, a relative axial stiffness of at least 50 percent is required by the supports to enhance the flexural resistance of the slab.
- If the supports' axial stiffness is lower than 50 percent, the slabs will deform into a catenary, resulting in axial tensile forces being generated.

For slabs with rotationally fixed end conditions:
- Slabs with rotationally fixed supports have better fire resistance than simply supported slabs (*pin-roller*) and have smaller deflections than the equivalent pinned supported slabs.
- With axial stiffness greater than 10 percent, the deflections are less than for the fixed-slide condition, where the deflections were about L/60.
- If the supports have an axial stiffness greater than 10 percent, the slabs will eventually fail by first forming a plastic hinge at midspan, followed by two plastic hinges at the supports. The times to failure of these slabs decrease with increasing axial stiffness of the supports.
- If the axial stiffness of the supports is less than 10 percent, the slabs form two plastic hinges at the end supports early in fire, resulting in larger deflections due to thermal bowing. However, these slabs do not collapse in the fire because the third plastic hinge at midspan does not form.
- The calculated height of the axial restraint force at the supports moves up and down during fire exposure.

6.1. Recommendations for design and construction
- For slabs with pin end conditions, some of the bottom reinforcing should be anchored into the supports to prevent catastrophic collapse should the slabs go into catenary mode.
- For continuous slabs, the top reinforcement bars at the supports should not be severely curtailed to allow redistribution of the moments to increase the fire resistance of the slabs.
- The curtailment of the top reinforcement bars at the supports should be determined from the negative moments calculated from the SAFIR analysis.
- The designer should also consider the effect of the restraint forces from the heated elements onto the surrounding structure.

6.2. Recommendations for future research
The following areas should be investigated in future research projects:
- The effect of various arrangements of curtailment of the reinforcing bars (top and bottom steel) on fire resistance, considering the likely amount of moment-redistribution during fire exposure.
- The behaviour of the slabs under realistic support conditions and unsymmetrical loads.
- The behaviour of the slabs subjected to realistic fires.

7.   References

Anderberg, Y. and Forsen, N.E. (1982) Fire Resistance of Concrete Structures, Division of Structural Mechanics and Concrete Construction, Lund Institute of Technology, Lund, Sweden.

ASTM (1999) *Standard test methods for fire tests of building construction and materials, E119-98.* American Society for Testing and Materials.

Buchanan, A.H. (2001) *Structural Design for Fire Safety.* John Wiley & Sons, U.K.

Carlson, C.C., Selvaggio,S.L. and Gustaferro, A.H. (1965) A review of studies of the effects of restraint on the fire resistance of prestressed concrete. *Proc. Symposium on Fire Resistance of Prestressed Concrete, Braunschweig, Germany.* International Federation for Prestressing (F.I.P.) Bauverlag GmbH, Wiesbaden, Germany. Reprinted as PCA Research Department Bulletin 206.

Cooke G.M.E. (1993) *Results of tests on end-restrained reinforced concrete floor strips exposed to standard fires. Report prepared for the Construction Directorate of the Department of the Environment.* Fire Research Station, Hertfordshire, U.K.

EC2, (1995). Eurocode 2: *Design of concrete structures. ENV 1992: Part1-2: General rules-Structural fire design*, European Committee for Standardization, Brussels.

EC3, (1995). Eurocode 3: *Design of steel structures. ENV 1993 Part1-2: General rules-Structural fire design*, European Committee for Standardization, Brussels.

Franssen, J.-M., Kodur, V.K.R. and Mason J. (2000) *User's manual for SAFIR2001: A computer program for analysis of structures at elevated temperature conditions.* University of Liege, Department Structures de Genie Civil, Service Ponts et Charpentes, Belgium.

Gustaferro, A. and Martin, L.D. (1988) *Design for Fire Resistance of Precast Prestressed Concrete, Second Edition.* Prestressed Concrete Institute, Illinois, USA.

Gustafson J.A. (Ed) (1980) *Reinforced Concrete Fire Resistance*, Concrete Reinforcing Steel Institute, Chicago, IL

Harmathy, T.Z. (1993) *Fire Safety Design & Concrete*, Concrete Design and Construction Series, Longman Group Limited, U.K.

Issen, L.A., Gustaferro, A.H. and Carlson, C.C. (1970) Fire tests of concrete members; An improved method for estimating thermal restraint forces. *Fire Test Performance, ASTM, STP 464,* American Society for Testing and Materials, pp. 153-185.

Lin, T.D. and Abrams, M.S. (1983) Simulation of realistic thermal restraint during fire tests of floors and roofs. In: *Fire Safety of Concrete Structures.* Publication SP-80. American Concrete Institute, Detroit.

Selvaggio, S.L. and Carlson, C.C. (1963) Effect of restraint on fire resistance of prestressed concrete, American Society for Testing and Materials, STP 344, pp. 1-25. Reprinted as PCA Research Department Bulletin 164.

SNZ (1995) NZS 3101: Part1: 1995. *The Design of Concrete Structures*, Standards New Zealand, Wellington.

UL (1999). Fire Resistance Directory, Underwriters Laboratories Inc., USA.

COMPARISON OF BRE SIMPLE DESIGN METHOD FOR COMPOSITE FLOOR SLABS IN FIRE WITH NON-LINEAR FE MODELLING

Zhaohui HUANG[1], Ian BURGESS[1], Roger PLANK[2] and Colin BAILEY[3]

[1] *Department of Civil and Structural Engineering, University of Sheffield, Sheffield S1 3JD, UK*
[2] *School of Architectural Studies, University of Sheffield, Sheffield S10 2TN, UK*
[3] *Building Research Establishment, Bucknall's Lane, Watford WD2 7JR, UK*

ABSTRACT

On the basis of test evidence a new design method has been recently developed by one of the authors, for calculating the performance of composite flooring systems subject to fire. The method models simply the influence of tensile membrane action in the composite floor slabs. The objective of this paper is to show some detailed comparisons between the simple design method and finite element modelling using the computer program *Vulcan*, which has been developed at the University of Sheffield, in order to check the applicability and inherent conservatism of the method. Initially a 9m x 9m square ribbed concrete slab, for which all four edges are vertically supported, is analysed. Different temperature distribution patterns across the thickness of the slab are used to investigate the influence of thermal curvature on the structural behaviour. The effect of changing the edge support conditions is also analysed.

As part of this study a large generic composite flooring system with a footprint of 36m x 36m has been designed. The frame is based on a regular 9m x 9m column grid. A series of analyses has been performed, based on different patterns of fire protection to the downstand steel beams. The influence of the proportion of steel reinforcement on the structural behaviour has been investigated, and it is evident that the presence or absence of tensile membrane action in the concrete slabs is a major influence on the ultimate integrity of the flooring system at high distortions. The ability of the slab reinforcement to sustain the tensile stresses caused at high temperatures and deflections is clearly a key factor in ensuring that fracture of slabs does not occur. From both the *Vulcan* modelling and the simplified design method it is shown that tensile membrane action can be important in carrying the loads applied to the slabs at high temperatures and deflections. However it is apparent that the simple design method predicts a greater contribution to load-carrying capacity due to tensile membrane action than does the *Vulcan* modelling, especially for high reinforcement ratios, and that further work needs to be done to resolve this discrepancy.

KEYWORDS: *fire resistance, composite floor slabs, tensile membrane action, FE modelling.*

INTRODUCTION

The six large fire tests carried out in 1995-96 on the full-scale composite building at the BRE Fire Research Laboratory at Cardington [1] demonstrated conclusively that unprotected composite slab systems have significantly greater fire resistance within real multi-storey buildings than when they are tested as one-way-spanning isolated members. This appears to be due to interaction between the heated members within the fire compartment, the concrete floor slabs and the adjacent elements of the steel frame structure. The most significant general observation from the fire tests was that in none of the six was there any indication of run-away failure, which happens in all isolated member tests if temperatures are progressively increased. This is particularly remarkable since in some cases the unprotected steel beams reached well over 1000°C, at which temperature the steel strength is reduced by over 95%; deflections always exceeded *span/30* and in some cases exceeded the usual testing limit of *span/20*.

It seemed probable that tensile membrane action in the concrete floor slabs could have played an important role in preventing run-away failure of the structure during the fire tests, especially when deflections had become very large. Based on this theory and on the test evidence, a new design method was developed at BRE [2, 3], which calculates the enhanced load capacity due to membrane action of composite flooring systems subject to fire. The method models simply the influence of tensile membrane action in the composite floor slabs. Space does not permit a complete re-statement of this method here. Briefly, however, it calculates an enhancement to the slab's normal yield-line bending strength, which is based on the undeflected configuration, on the assumption that deflection continues to take place using the original yield-lines as hinges. It is assumed that the slab yields simultaneously in ultimate tension across the whole of its shorter centre-line, and that fracture finally takes place according to a limiting average-strain criterion. The method has been incorporated into a fire-safe design guide [4] published by SCI for multi-storey steel-framed buildings.

In this paper some detailed comparisons are made between the simple design method and the computer program *Vulcan* [5-9], which has been developed at the University of Sheffield to model the behaviour of composite buildings in fire, in order to check the applicability and inherent conservatism of the method. Initially a 9m x 9m square ribbed concrete slab is analysed, whose four edges are vertically supported. Different temperature distributions are used across the thickness of the slab to investigate the influence of thermal curvature on structural behaviour. The effect of edge support conditions is also analysed.

As part of this study a large generic composite flooring system with footprint 36m x 36m has been designed. The frame is 4 bays wide and 4 bays deep, each bay having dimensions 9m x 9m. The load ratio on all internal secondary beams at the fire limit state is 0.42, resulting in a total floor loading of 6.1 kN/m^2. A series of analyses has been performed, based on different patterns of fire protection to the downstand steel beams. The influence of the steel reinforcement on the structural behaviour has been investigated, and it is evident that the presence or absence of tensile membrane action in the concrete slabs is a major influence on the ultimate integrity of the flooring system at high distortions.

THEORETICAL BASIS OF THE PROGRAM

In the 3-dimensional non-linear finite element procedure which is the theoretical basis of *Vulcan*, a composite steel-framed building is modelled as an assembly of finite beam-column, spring, shear connector and slab elements. It is assumed that the nodes of these different types of element are defined in a common reference plane, which is normally

assumed to coincide with the mid-surface of the concrete slab element. Its location is fixed throughout the analysis. The beams and columns are represented by 2-noded line elements. The cross-section of each element is divided into a number of segments to allow two-dimensional variation of the distributions of temperature, stress and strain through the cross-section. Both geometric and material non-linearities are included. To represent the characteristics of steel-to-steel connections in a frame, a 2-noded spring element of zero length, with the same nodal degrees of freedom as a beam-column element, is used [5, 6].

The interaction of steel beams and concrete slabs within composite steel-framed buildings is represented using a linking shear-connector element, which is two-noded and has zero length; it employs three translational and two rotational degrees of freedom at each node. The shear-connector element permits the modelling of full, partial and zero interaction at the interface between the concrete slab and the steel beam [8]. In order to model the composite slabs including their ribbed lower portion, a modified layered orthotropic slab element has been developed. This element is based on the previously developed formulation [7], in which the slab elements are modelled using a layered plate element based on Mindlin/Reissner theory and each layer can have different temperature and material properties, which may be associated with thermal degradation. An effective-stiffness model has been incorporated into the layered procedure to take account of the orthotropic properties of composite slabs, for which a maximum-strain failure criterion has been adopted. A smeared model has been used in calculating element properties after cracking or crushing has been identified at any Gauss point. After the initiation of cracking in a single direction, concrete is treated as an orthotropic material with principal axes parallel and perpendicular to the cracking direction. Upon further loading of singly cracked concrete, if the tensile mechanical strain in the direction parallel to the first set of smeared cracks is greater than the maximum tensile strain then a second set of cracks forms. After crushing, concrete is assumed to lose all stiffness. The uniaxial properties specified in EC4 [10] for concrete and reinforcing steel at elevated temperatures were adopted in this model. Full details of the modified layered procedure used are given in reference 9.

The layered procedure mentioned above has been further extended to include geometric non-linearity in the modelling of reinforced concrete slabs in fire [11]. A quadrilateral 9-noded higher-order isoparametric element developed by Bathe [12] is used in place of the previous 4-noded geometrically linear element, and a Total Lagrangian approach is adopted. In this geometrically non-linear layered procedure all previous developments in the modelling of material non-linearity are retained, including the effective stiffness modelling of ribbed composite slabs.

ANALYSIS OF SQUARE RIBBED CONCRETE SLAB AT ELEVATED TEMPERATURES

Before attempting the modelling of composite floor systems isolated uniformly loaded (6.1kN/m^2) 9m x 9m ribbed reinforced concrete slabs with different edge support conditions were modelled at elevated temperatures using both *Vulcan* and the simple design method. The slab comprised ribbed concrete of 130mm total depth including 65mm deep ribs and an A393 anti-cracking mesh placed at the bottom of the upper continuous part, which means that in a composite decking slab it would have been resting on the corrugated deck before the slab was cast. The effective stiffness factors parallel and perpendicular to the ribs were then 0.72 and 0.34 according to reference 9. The geometry of the slab and the finite element mesh used are shown in Figure 1. Only one quarter of the plate has been modelled, because using the symmetry of the plate and its loading reduces the computational effort. The

compressive strength of the concrete and the yield strength of the reinforcing mesh have been assumed to be 35 MPa and 460 MPa, respectively.
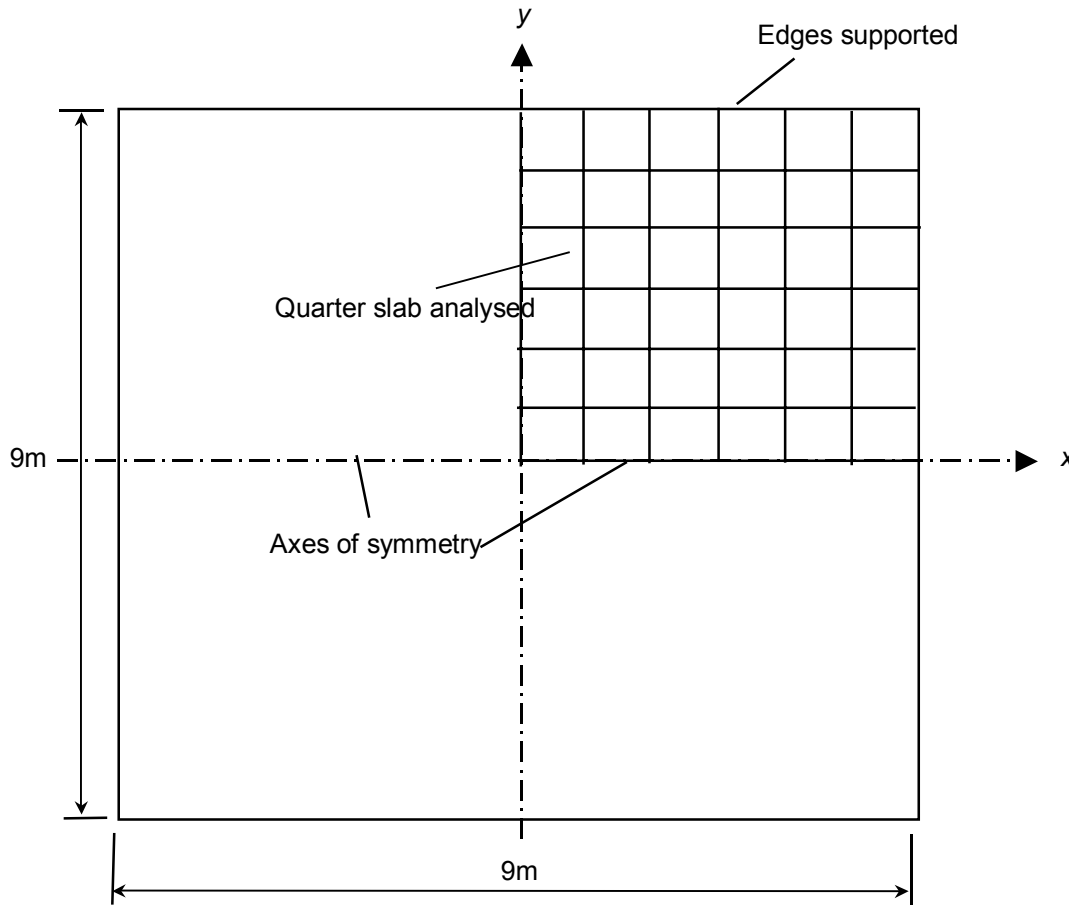

FIGURE 1: Representation of the ribbed reinforced concrete slab subject to uniform loading at elevated temperature, using the symmetry of the case.

In order to make more precise comparisons with the simple design method a linear temperature distribution across the thickness of the slab was adopted. This is one of the assumptions of the simple design method. The temperature of the top surface of the slab is assumed to be 15% of the bottom surface temperature. In this comparison the temperature of the steel reinforcement is used as reference parameter. Two *Vulcan* analyses have been performed, assuming simple (pull-in allowed) and hinge-supported pull-in prohibited) edge conditions. The central deflections of the slab are plotted in Figure 2 against the reinforcing steel temperature for these two cases, together with the limiting cases calculated using the simple design method.

It is evident that the central deflections predicted using *Vulcan* with simply supported edge conditions are greater than those calculated using the simple design method, both at ambient and elevated temperatures. It should be noted that the simple design method always assumes simply supported edge condition. It is interesting that the central deflections predicted by *Vulcan* using hinge-supported edge condition are in good agreement with the simple design method's calculations. In order to investigate the extent to which the deflection of the slab at elevated temperatures is caused by thermal curvature a case with uniform temperature distribution across the thickness of the slab was also analysed using *Vulcan* for simply supported edge conditions.

Reinforcing Steel Temperature (°C)
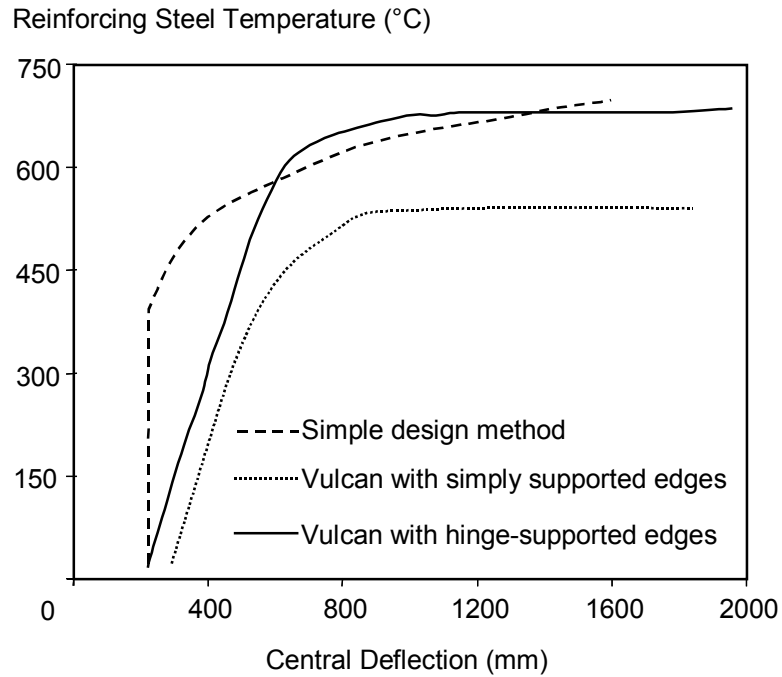
FIGURE 2: Comparison of predicted central deflections using the simple design method and *Vulcan* with different support conditions.

Reinforcing Steel Temperature (°C)
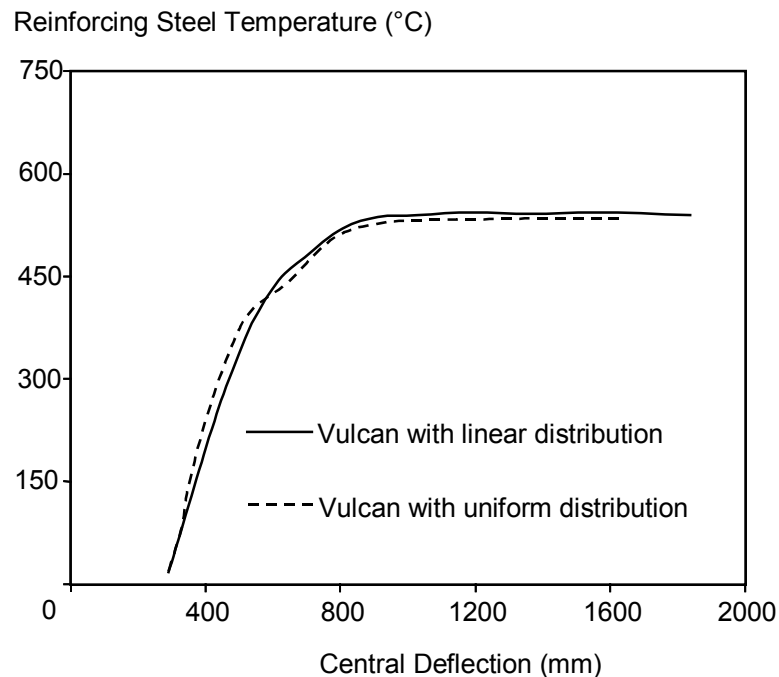
FIGURE 3: Comparison of predicted central deflections using *Vulcan* with different temperature distribution patterns across the thickness of the slab.

Figure 3 shows the comparison between the cases of linear and uniform temperature distribution for simple support conditions. It can be seen that the difference between the two cases is marginal. The ambient-temperature deflection of the slab was high (300mm) in this case, and hence the contribution of thermal curvature of the slab generated by temperature distribution through its thickness was relatively small.

ANALYSIS OF COMPOSITE FLOORS IN FIRE

This study was based on a composite 36m x 36m floor structure comprising 4 bays 9m x 9m in each direction (Figure 4), subject to a whole-storey fire. All primary and secondary beams were standardised as 533x210x92UB and 356x127x39UB sections respectively. A ribbed lightweight concrete slab of 130mm total depth was used, acting compositely with PMF CF70 profiled metal decking. The characteristic dead and imposed loads were assumed to be 4.08kN/m^2 and 2.5kN/m^2 respectively. From BS 5950: Part 8 [13], the partial safety factors in fire are 1.0 for dead loads and 0.8 for non-permanent imposed loads, giving a total design load of 6.1kN/m^2 at the fire limit state. This loading is used throughout the paper, and represents load ratios of 0.42 for secondary beams and 0.41 for primary composite beams if S275 steel and C35 concrete are assumed.

In order to investigate the extent to which fire protection of the steel beams may be reduced as a result of the beneficial influence of the slab, two different protection regimes were considered:

- **Protection Regime I.** All beams on the main gridlines were protected but other secondary beams were unprotected (Figure 4).

- **Protection Regime II.** Similar to I, but secondary beams on Gridlines 2 and 4 were also left unprotected.
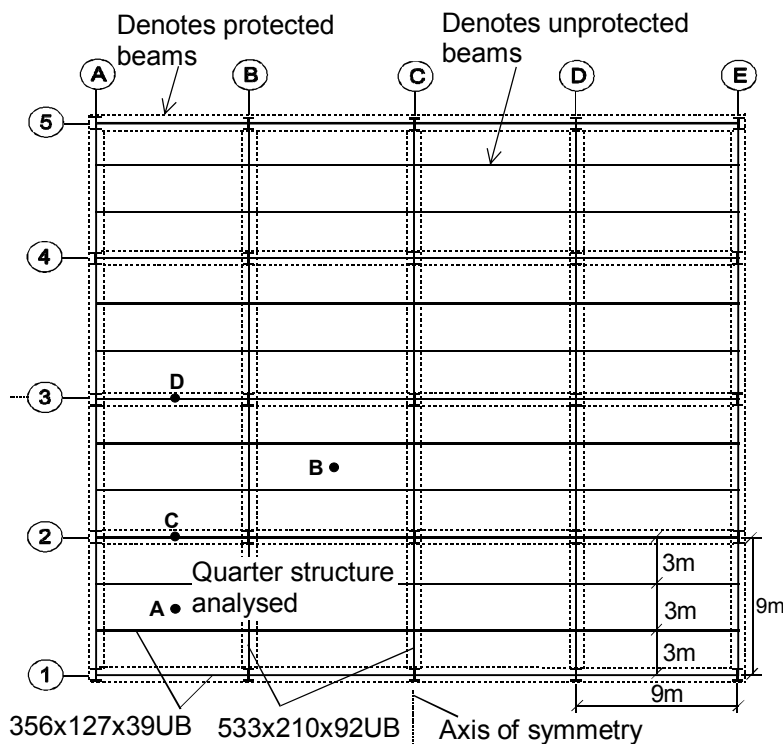
FIGURE 4: Composite floor layout assumed for Protection Regime I

The temperature distributions in the unprotected beams were assumed to follow the patterns indicated in the Cardington tests [14]. These were represented by considering the cross-section as three zones - bottom flange, web and top flange - of the steel beams, the temperature of each being taken from the Cardington test data. The temperatures in the protected beams were assumed to be 50% of those of the unprotected beams. A linear temperature distribution pattern was used across the thickness of the concrete slabs, in which

the temperature of top surface of the slab was assumed as 15% of the bottom surface. All beams were assumed to be hinge-connected. To save computing time, advantage was taken of symmetry of the floor layout (see Figure 4), so that only a quarter of the floor system needed to be analysed. In order to demonstrate the effect of the slab reinforcement on the structural behaviour two different meshes, A142 and A393, were considered. In the following text the temperature of the bottom flange of the unprotected beams is used as the key temperature, against which results are quoted in all figures.
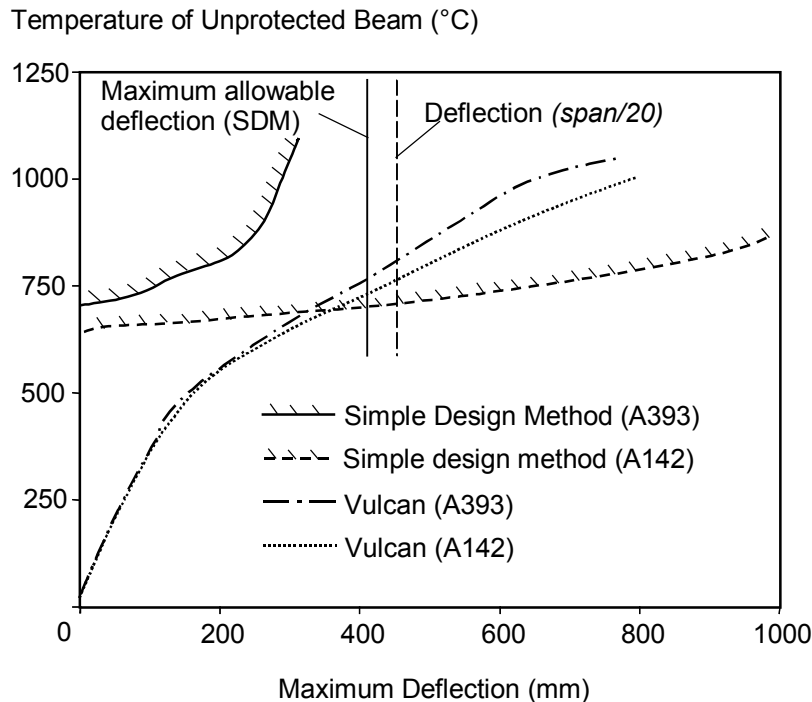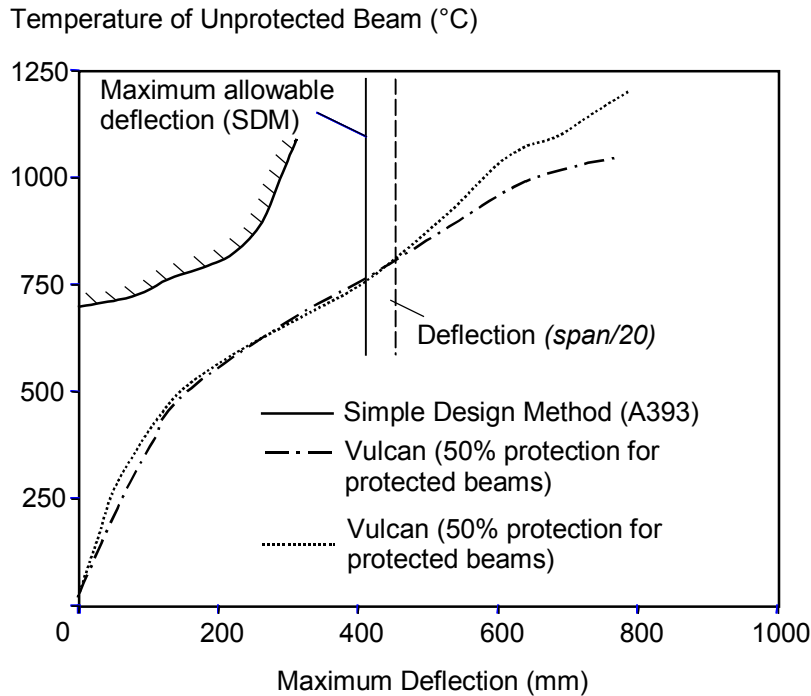

FIGURE 5: Protection Regime I: Predicted deflections using *Vulcan* and simple design method with different slab reinforcement.

For Protection Regime I, Figure 5 compares the maximum vertical deflections predicted by *Vulcan* and the simple design method for the two reinforcing meshes. It can be seen that for the numerical modelling the influence of reinforcement is negligible up to about 600°C, but that beyond this point it becomes increasingly significant. At these higher temperatures the steel beams have lost most of their original strength and stiffness, and support of the loads becomes increasingly the role of the concrete slab, with tensile membrane action being a key factor. When using the simple design method for calculation, the ultimate load-carrying capacity of the concrete slabs appears to be significantly increased for A393 mesh compared with A142. The discrepancy seems less significant when comparing the *Vulcan* modelling for two meshes, and it is evident that the effect of tensile membrane action predicted by the simple design method for mesh A393 is significantly greater than in the numerical modelling.

One of the assumptions of the simple design method is that all edges of the slab are vertically supported, whereas in this example the protected beams which form the slab supports do deflect as their temperatures rise. To investigate the influence of this edge deflection on the slab deflection, the A393 case was re-run in *Vulcan* with 100% protection to the protected beams, so that their temperature was kept at 20°C throughout. The results are shown in Figure 6, together with the simple design method's limit predictions. It is evident that it becomes progressively more important to maintain the vertical edge support

provided by the protected beams in order to continue to mobilise tensile membrane action at high temperatures.

FIGURE 6: Protection Regime I: Predicted deflections using *Vulcan* with different degrees of protection for protected beams (mesh A393).
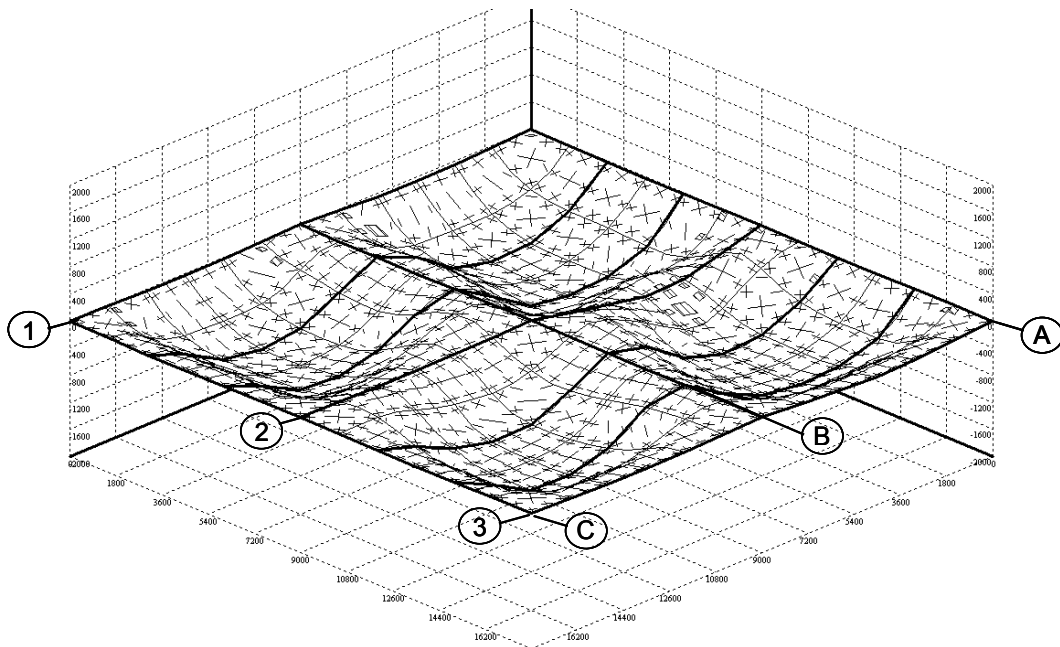
FIGURE 7: Protection Regime I: Deflection profiles at 1200°C, with cracking patterns of top layer of floor slab.

Figure 7 shows the deflection profiles at 1200°C for the case with 100% protected beams and A393 mesh reinforcement. Because the protected beams are now strong enough to vertically support the slab edges the slab is forced to deform in double curvature, which generates significant membrane action to carry the loads.
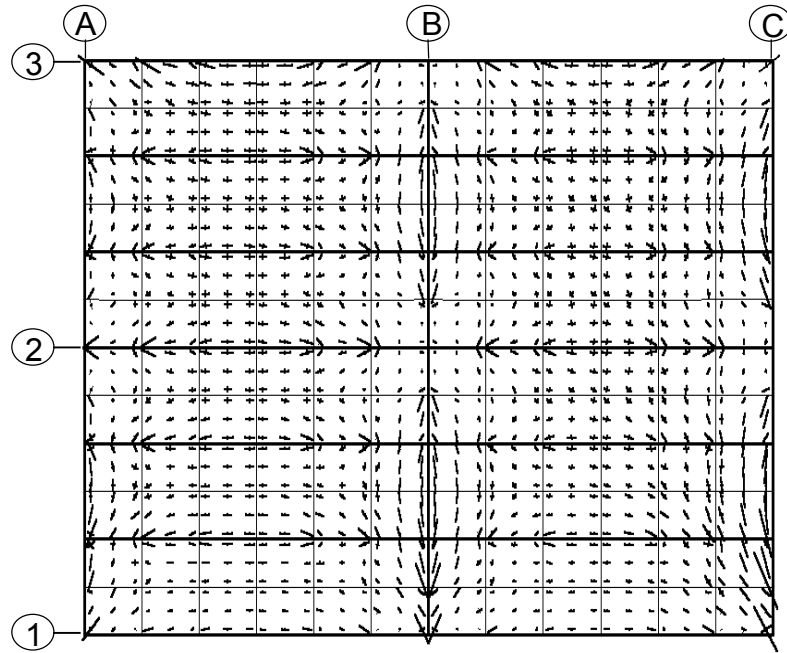
FIGURE 8: Protection Regime I: Principal membrane tractions at 20°C.

Figure 8 shows a vector plot of the distribution of principal membrane tractions (forces per unit width) at the Gauss points of the slab elements at ambient temperature. In this plot the lengths of the vectors are proportional to their magnitudes; thin vector lines denote tension and thick lines compression. The slabs above the secondary and primary beams act according to the normal engineering assumption for the flanges of composite beams, being in compression parallel to the beam. This reduces in the areas mid-way between adjacent beams due to shear lag. In contrast, the membrane tractions within the slab at 1200°C, plotted in Figure 9, clearly show the tensions in the mid-zone of each square panel together with the peripheral compression "rings" which are characteristic of tensile membrane action.
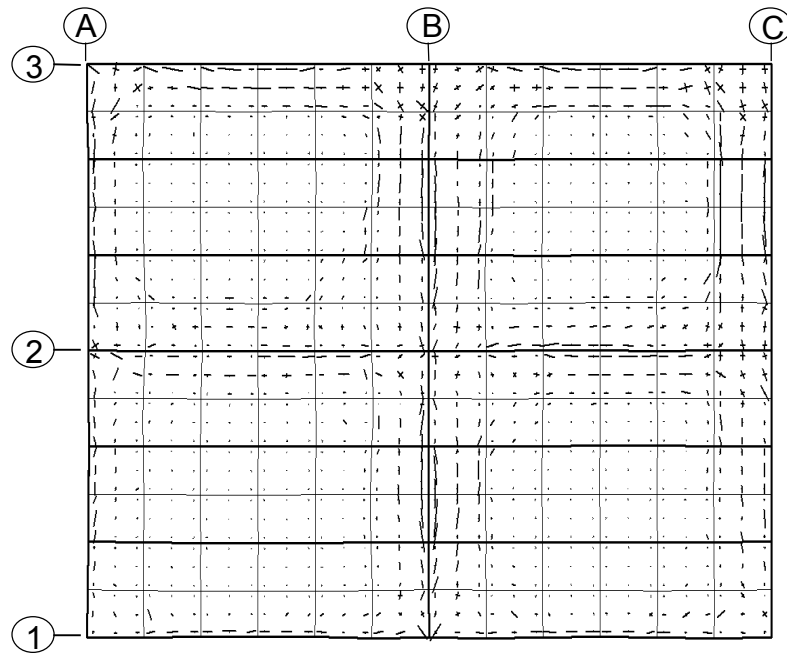
FIGURE 9: Protection Regime I: Principal membrane tractions at 1200°C.

It is clear that Protection Regime I effectively optimises the potential for tensile membrane action in the concrete slab by providing, in its pattern of protected beams, edge-supported bays which are square in plan.

Protection Regime II shows the considerable difference in tensile membrane action which is engendered when the protected beams support non-square slab bays. For this regime the maximum deflections were found in the *Vulcan* modelling to occur at position C, the mid-point of the 9m x 18m unprotected slab. Figure 10 compares the vertical deflections at position C predicted by *Vulcan* and the limits given by the simple design method for two reinforcing meshes. In these analyses the protected beams were assumed to heat at 50% of the rate of the unprotected beams. It can be seen that for temperatures up to about 650°C the slab reinforcement makes very little difference. Between 650°C and 850°C some enhancement of capacity is generated by the slab reinforcement, but this is associated principally with catenary action, rather than with tensile membrane action. This is because the pattern of vertical support provided by the protected beams results in rectangular rather than square bays, and the slab hangs essentially in single curvature between its protected edges. At high temperatures the strength of the protected beam on gridline 3 begins to reduce significantly, and this further compromises the ability of the slab to develop any membrane action. It is also clearly shown that the simple design method indicates very little enhancement of capacity due to tensile membrane action.
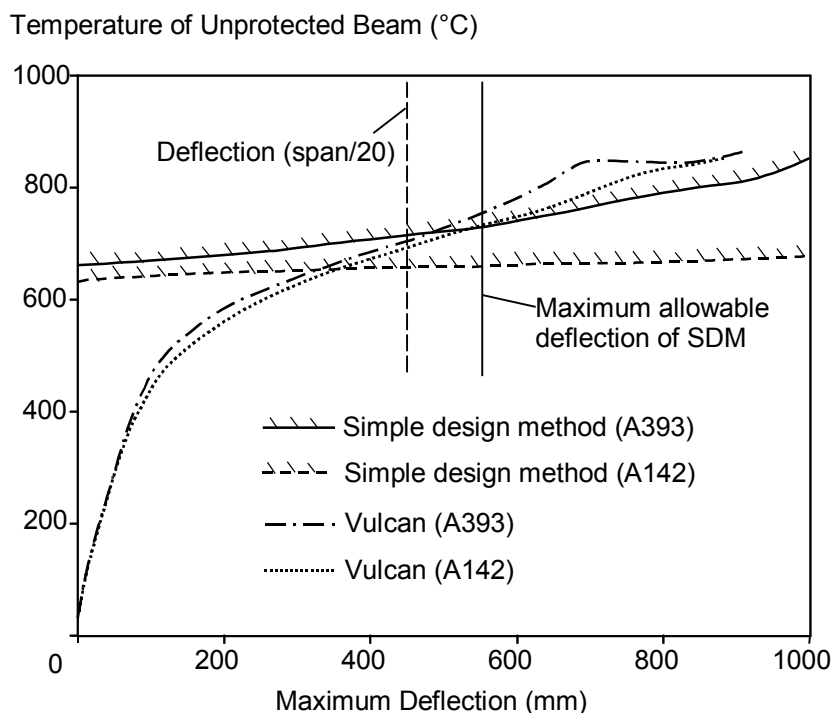
FIGURE 10: Protection Regime II: Predicted deflections using *Vulcan* and simple design method with different reinforcement.

CONCLUSIONS

The main objective of this paper has been to make some detailed comparisons between the simple design method and numerical modelling using the computer program *Vulcan*. From this study some conclusions can be drawn as follows:

- It is evident from both the *Vulcan* modelling and the simplified design method that the presence or absence of tensile membrane action in the concrete slabs can be a major influence on the ultimate integrity of the composite flooring system at high distortions. The ability of the slab reinforcement to sustain the tensile stresses caused at high temperatures and deflections is clearly a key factor in ensuring that tensile membrane action can legitimately be used in structural fire engineering design.

- The extent of tensile membrane action occurs depends very largely on the aspect ratios of the slabs between protected or otherwise supported edges. This is usually a product of the pattern of fire protection adopted for the steel downstand beams. In order to optimise the mobilisation of tensile membrane action it is important to make sure that the concrete slab is forced to deform in double curvature, and that it is incapable of producing folding mechanisms which do not involve membrane straining. Square slabs will always be most effective in producing the effect. For high aspect ratios catenary action of slabs may occur, in which tension which is essentially uniaxial may be resisted by in-plane restraint from adjacent bays, beams and columns. However, this mechanism is much more likely ultimately to lead to run-away structural failures than is tensile membrane action.

- Comparing *Vulcan* solutions with the simple design method it is clear that the simple design method may predict a greater enhancement of capacity due to tensile membrane action than is apparent from *Vulcan* analysis. That means the simple design method may predict greater fire resistance due to tensile membrane action than *Vulcan* modelling does. This is particularly the case for highly reinforced square slabs, for which the simple method predicts very large enhancement. Cases with reinforcement which is typical of anti-crack mesh, as well as the less square slabs, show less enhancement, and the disparity is less apparent.

Tensile membrane action clearly has the potential to become a useful tool as a part of a performance-based fire engineering design approach, but it is clear that work remains to be done in resolving the discrepancies between results which have been shown in this paper.

REFERENCES

[1] *The Behaviour of Multi-Storey Steel-Framed Buildings in Fire: A European Joint Research Programme*, Swinden Technology Centre, British Steel plc, Rotherham, UK, (1999).

[2] Bailey C.G. and Moore D.B., The structural behaviour of steel frames with composite floor slabs subject to fire: Part 1: Theory, *The Structural Engineer*, **78**(11), (2000) pp9-26.

[3] Bailey C.G. and Moore D.B., The structural behaviour of steel frames with composite floor slabs subject to fire: Part 2: Design, *The Structural Engineer*, **78**(11), (2000) pp28-33.

[4] Newman G.M., Robinson J.T. and Bailey C.G., *Fire Safe Design: A New Approach to Multi-Storey Steel-Framed Buildings*, The Steel Construction Institute, Berkshire, UK (2000).

[5] Najjar S.R. and Burgess I.W., A non-linear analysis for three-dimensional steel frames in fire conditions, *Engineering Structures*, **18**(1), (1996) pp77-89.

[6] Bailey C.G., *Simulation of the Structural Behaviour of Steel-Framed Buildings in Fire*, PhD Thesis, University of Sheffield (1995).

[7] Huang Z., Burgess I.W. and Plank R.J., Non-linear analysis of reinforced concrete slabs subjected to fire, *ACI Structural Journal*, **96**(1), (1999) pp127-135.

[8] Huang Z., Burgess I.W. and Plank R.J., Influence of shear connectors on the behaviour of composite steel-framed buildings in fire, *J. Construct. Steel Research*, **51**(3), (1999) pp219-237.

[9] Huang Z., Burgess I.W. and Plank R.J., Effective stiffness modelling of composite concrete slabs in fire, *Engineering Structures*, **22**(9), (2000) pp1133-1144.

[10] European Committee for Standardisation, *Eurocode 4, Design of Composite Steel and Concrete Structures, Part 1.2: Structural Fire Design (Draft)*, Commission of the European Communities, Brussels, (1992).

[11] Huang Z., Burgess I.W. and Plank R.J., Modelling Membrane Action of Concrete Slabs in Composite Buildings in Fire. Part I: Theoretical Development, Research Report DCSE/00/F/4, Department of Civil and Structural Engineering, The University of Sheffield (2000).

[12] Bathe K.J., *Finite Element Procedures*, Prentice-Hall Inc., New Jersey, (1996).

[13] British Standards Institution, *BS5950: Structural Use of Steelwork in Buildings: Part 8: Code of Practice for Fire Resistant Design*, BSI, London, (1990).

[14] Bann M.S., Bentley P.K., Shaw D. and Tomlinson L., *ECSC Project: Behaviour of a Multi-Storey Steel Framed Building Subjected to Natural Fires. Test 3: Corner Compartment, Data Files: Temperature Measurements*, Report S423/1/Part T1, Swinden Technology Centre, British Steel plc, Rotherham, UK, (1995).

BENDING AND MEMBRANE ACTION IN CONCRETE SLABS

Martin GILLIE, Asif USMANI and Michael ROTTER

The University of Edinburgh, School of Civil and Environmental Engineering, Crew Building, King's Buildings, West Mains Road, University of Edinburgh, EH9 3JN, UK

ABSTRACT

It has become apparent from the series of fire tests carried out at Cardington, UK that the response of steel-concrete composite structures in fire conditions is largely governed by the behaviour of the reinforced concrete floor slabs. This paper obtains a detailed understanding of the strength of heated concrete floor slabs when subject to the combined bending and membrane forces that typically result from restrained thermal expansion. To analyse such slabs the computer program FEAST is used. Initially the behaviour of the floor slab in the Cardington frame under pure bending and pure membrane forces is described and explained. The paper then explores the effect that interaction between bending and membrane behaviour has on the strength of the slab when it is uniformly heated, heated with a linear thermal gradient and heated with the non-linear thermal gradient observed during the Cardington tests. Finally, the effects of varying the area and location of the reinforcement in the slab are analysed.

Notation

A	area	**Subscript**	
E	Young's modulus	l	of layer
f_y	yield stress	r	of reference surface
f_p	stress at the proportional limit	θ	at a given temperature
M	moment		
P	force		
z	distance for reference surface		
δ	deflection		
ε	strain		
σ	stress		

INTRODUCTION

A series of fire tests were carried out on an eight storey, steel-concrete composite structure at Cardington, UK in 1995[1]. The tests enabled various numerical and theoretical models of the structure in fire conditions to be developed [2-18]. As a result of these models it has been possible to obtain a good understanding of the mechanical behaviour of highly redundant structures in extreme fires. It was found that the concrete floor slabs in structures such as the Cardington frame dominated the behaviour of the structure when it was heated and that the behaviour of the slabs was complex and difficult to model numerically. The reasons for these modelling difficulties arose from a number of factors such as the material behaviour of concrete being highly non-linear; local instabilities caused by restrained thermal expansion; large deformations causing geometric effects to be important and complex moment-membrane interactions in the heated slab. This paper concentrates on gaining a better understanding of the last of these phenomena by exploring the strength of the Cardington floor slab when subject to various heating regimes.

For design purposes floor slabs are generally assumed to act in one of two ways. Either they are considered to span between beams and to resist loads primarily in bending or they are considered to be part of a beam-slab composite system and to resist loads primarily in membrane compression and tension [19]. The effects of combined membrane and bending forces on the strength of slabs are rarely considered. At ambient temperatures this approach produces safe and serviceable designs and is a reasonable approximation to the true load carrying mechanism. However, when a compartment of a redundant structure is heated, the heated area will thermally expand and bow. This thermal expansion and bowing may be restrained by surrounding areas of the structure that are still cool and large membrane forces can result [2,8,20,21]. In buildings such as the Cardington structure this may produce a range of responses in the floor slab from high membrane compression to membrane tension and bending [22]. These responses will be complicated by P-Δ effects produced by large deflections. These facts mean that before a complete understanding of the behaviour of floor slabs in fire conditions can be obtained, their behaviour under a number of loading conditions not normally considered must be established. The situation is further complicated by the degradation of material properties as slabs are heated.

The purpose of this paper is to obtain a detailed understanding of the strength of concrete floor slabs in fire conditions. To do this the specifically developed computer program, FEAST [7] will be used. The behaviour of the Cardington slab will be presented in two ways. Firstly, the slab will be analysed under conditions of pure membrane strain and of pure bending. Subsequently, the force-moment interaction diagrams of the slab will be presented. Initially these diagrams will be used to describe the behaviour of the slab at ambient temperature. The paper will then explore the effects of heating the slab uniformly, heating it with a linear thermal gradient and heating it with the non-linear thermal gradients observed during the Cardington tests. Finally, the implications of the results for structures designed to resist fire will be considered.

BACKGROUND TO THE ANALYSIS
The Cardington Slab

The design of the concrete floor slab studied in this research was the same as that of the slab used in the Cardington experiments [1,23] and is typical of floor slabs used in composite construction. The slab consisted of a layer of concrete 70mm deep attached to which were concrete ribs, 65mm deep, running in one direction. Fifteen millimetres above the ribs there was a layer of anti-cracking reinforcement mesh that consisted of 6mm diameter bars at

300mm spacing. Steel decking, 0.9mm thick, covered the bottom surface of the ribs and was bonded to the concrete by means of small protrusions. A cross-section of the slab is shown in Fig. 1.

Material Behaviour
The effects of temperature on material behaviour can be broadly divided into loss of material properties (reduced modulus and yield point) and thermal expansion. The two most commonly used materials in steel-framed composite structures are concrete and steel which are often combined to form reinforced concrete. The behaviour of these materials at elevated temperatures is more complex than at ambient temperature and a knowledge of this behaviour is crucial to an understanding of structures in fire conditions.

As concrete is heated, the ultimate compressive strength decreases and the ultimate strain increases [24-26]. Only a limited amount of high temperature stress-strain test data has been published but that shown in Fig. 2 [26] is typical. Data on the tensile behaviour of concrete at high temperature is also hard to obtain. Schneider [26] states that the ultimate tensile strains are generally one tenth of compressive ultimate strains with the initial Young's modulus being approximately equal in tension and compression. For the purposes of this study it was decided to use the mathematical description of concrete behaviour given in the Eurocode 2 [27] and reproduced in Figs 3 and 4. This model includes a full description of concrete's stress-strain behaviour up to its ultimate-stress and implicitly accounts for creep of concrete at elevated temperatures

Steel at ambient temperature is generally considered to have a relatively simple material behaviour in that it is ductile and can be assumed to have the same stress-strain curve in tension and compression. Although these aspects of the behaviour remain, the material properties of steel at high temperatures are very different to those at room temperature. Above approximately 200°C there is no clear yield point and the stress-strain curve becomes increasingly non-linear at higher temperatures. Figure 5 shows the behaviour as defined algebraically by Eurocode 3 Part 1.2 [28] which has been adopted for the analyses presented in this paper. This definition is governed by the parameters E_θ, $f_{(y)\theta}$ and $f_{(p)\theta}$ and includes strain hardening at temperatures below 400ºC.

The FEAST Program
The analyses of the floor slab were performed using a module of the specifically developed FEAST program, a complete description of which has been given elsewhere [7,29]. FEAST is able to model the behaviour of concrete slabs with a high degree of accuracy as it can model slabs of arbitrary geometry and with any number of non-linear materials. There are however a number of assumptions that were made during the analyses. Material behaviour is assumed to be uniaxial although the concrete in the slab was subject to a complex stress state. Biaxial compressive stressing of concrete can lead to strength enhancements of up to 20% and typically of 10% over uniaxial peak values. Ignoring this behaviour was, in effect, equivalent to using a slightly weaker concrete in the model than was used in the Cardington slab. It was felt that this small inaccuracy was justified on pragmatic grounds. To some extent this assumption is offset by also assuming that the design thickness of the floor slab was the actual thickness. In reality the floor slab was somewhat thicker due to the effects of ponding when the concrete was poured [30,31].

PURE BENDING AND MEMBRANE FORCES

Initially the Cardington slab was analysed with pure bending or pure membrane forces. Thermal gradients taken from the Cardington test data [23] were used throughout these analyses and are shown in Figs 6 and 7. The behaviour of the Cardington slab parallel to the ribs in terms of its strain-curvature-temperature behaviour is shown in Figs. 8 to 12. As expected, given the material properties of the slab, it is seen from Fig. 8 that there is a decrease in membrane strength and an increase in ductility as temperature increases. The large amount of ductility in the tensile region can be attributed to the contribution of the steel reinforcement and decking. A detail of the tensile region is shown in Fig. 9. This shows that the concrete fails in tension at very small strains and that the resulting loss of force is not recovered until the reinforcing steel reaches much higher strains.

Moment-curvature behaviour is shown in Fig. 10, and again ductility can be seen to increase and the strength decrease with rising temperature. It is noticeable that for positive curvatures the initial bending stiffness of the section remains roughly constant with increasing temperature but for negative curvatures it decreases. This is explained by noting that positive bending is largely resisted by the concrete in the top of the slab and even for high reference surface temperatures the top part of the slab remains cool and so its stiffness stays almost constant. Negative bending is resisted by the concrete in the lower portion of the slab and it is this region that becomes hot, and so less stiff, at higher reference surface temperatures.

Moment against strain is plotted in Fig. 11 and the coupling between curvature and strain is clearly visible. For positive strains the moments arise largely from the tensile capacity of the steel. This is because the concrete loses almost all its strength (due to cracking) at low strains and so has very little effect on the slab behaviour. All the steel is below the reference surface and therefore gives rise to positive (sagging) moments. The form of the curves produced can be seen to resemble closely the stress-strain relationship of steel. Peak moments in the compressive region are shown to increase under increasing temperature. This is a slightly counter-intuitive result and, as with the moment-curvature behaviour, it can be explained by remembering that the bottom of the slab is heated more quickly than the top. At ambient temperatures moments due to compressive strains result largely from the different areas of concrete providing resistance above and below the reference surface. If the slab were heated uniformly then this moment would decrease since the areas would remain the same but the forces acting would reduce because of loss of material properties. Whilst this effect no doubt exists in the Cardington slab, it is swamped by the temperature gradient causing the concrete in the bottom half of the slab to lose strength much more rapidly than that in the top half, thus increasing the couple about the reference surface and hence the moment over the section. It is seen that at low temperatures with low compressive strains, moments are influenced by the steel behaviour. At ambient temperature this effect is sufficient for the hogging moments to be present until after the steel yields.

The membrane forces produced by applied curvatures are shown in Fig. 12. Both positive and negative bending produce compressive forces, as would be expected given concrete's asymmetric material behaviour. The forces produced by sagging bending are greater than those that result from hogging bending because there is a greater area of concrete above the reference surface than below it.

COMBINED BENDING AND MEMBRANE FORCES

It is normal practice in column design to take account of the effects of combined axial and bending loads. This is commonly done by using moment-force interaction diagrams in the form of a design chart. A sketch of a typical design chart is shown in Fig. 13. Design charts often include only positive moments and compressive forces because it is assumed columns are symmetrical and that the applied axial forces are always compressive. However, the complete interaction diagrams for columns include moments and forces of both signs and, if a column is not symmetrical, this produces two asymmetric diagrams, one for each axis of bending. Interaction diagrams that represent the behaviour of plates, such as the Cardington floor slab, can also be produced. Instead of plotting total moments against total forces, stress-resultants are plotted giving the strength of the plate per unit width. Orthotropic plates require two interaction diagrams to describe their behaviour. It is necessary when producing interaction diagrams to decide on a reference surface about which quantities such as moments are to be measured. For symmetrical columns this is normally assumed to coincide with the column centroid so that the interaction diagrams produced are valid for positive and negative moments. In the case of columns or plates that have asymmetric cross-sections there is no obvious position to place the reference surface and so the most convenient position for the problem in hand must be selected. In the analyses presented here the reference surface was taken to lie 70mm above the lower surface of the ribs.

In the remainder of this paper the effects of combined axial and bending forces on the Cardington slab will be presented making use of interaction diagrams.

The Cardington Slab at Ambient Temperature

The behaviour of the slab at ambient temperature parallel to the ribs is shown in Fig. 14. As expected, the slab is much weaker in tension than in compression as a result of concrete's low tensile strength. Also, the slab is noticeably stronger in sagging (positive) bending than in hogging bending. This is because of the larger area of concrete above the reference surface than below it. It is also clear that the full moment capacity of the slab is only reached when the slab is subject to compressive membrane forces approaching half the slab's pure membrane capacity. This also results from concrete's low tensile capacity and is an effect that is often used to advantage in pre-stressed concrete design. There is a region near the centre of plot where there are very few points plotted. In this region the slab is behaving elastically and so a small change in strain or curvature results in a large change in the actions sustained. The tensile membrane capacity of the slab can be seen to increase with increasing sagging moments until it reaches a distinct peak. In a symmetrical slab this peak would occur on the y-axis but, due to the ribs making the slab stronger in sagging than hogging, it has moved into the sagging region. There is a similar compressive peak that is shifted into the sagging region for the same reason.

When considering column design charts it is common to refer to balanced failure of a section, this occurs when the loads applied to the column result in the concrete failing in compression simultaneously with the steel failing in tension. In column design the tensile capacity of concrete is normally neglected whereas in the present analysis it was included, so the idea of a balanced section is not quite so clear. The inclusion of post-ultimate material behaviour also results in a more complex response. Despite this, it is can be seen from Fig. 14 that there are transitions from primarily tensile governed behaviour to primarily compression governed behaviour for both positive and negative bending. This transition occurs at the peak moment capacity in each case.

The behaviour of the slab in the perpendicular direction is shown in Fig. 15. Many of the same trends are apparent although the diagram is distinctly distorted into the sagging region. The distortion occurs as a result of placing the reference axis in a location that produces a roughly symmetrical interaction diagram in the direction of the ribs. When the perpendicular direction is considered almost all the material in the slab cross section is located above the reference surface and so there is very little resistance to pure negative bending.

Uniform Heating
The simplest form of thermal load that can be applied to a slab is uniform heating. This load case is unlikely to occur in all but extraordinarily severe fires but is worth studying as it highlights some effects that are present in more complex load cases but obscured by other phenomena. The effect of uniformly heating the Cardington slab on its strength parallel to the ribs is shown in Fig. 16. This figure shows only the outline of the interaction diagrams for each case which allows the shapes and sizes of each diagram to be compared easily.

It is clear that heating the slab reduces the size of the interaction diagrams. The reduction is fairly small up to a temperature of 400°C, large at 600°C and at 800°C the slab has lost almost all its strength. The reduction in strength in the early stages of the fire is concentrated in the compressive region. This is to be expected when Figs 3 and 5 are examined. It can be seen that concrete has lost around 25% of its strength by 400°C but that steel has not lost any of its strength at this temperature, although it has become slightly more ductile at low strains. Since the majority of the slab tensile strength comes from the steel it is able to maintain its tensile strength until this point.

The large reduction in strength at higher temperatures is because the material properties of both concrete and steel degrade rapidly above 400°C. The shape and proportions of the interaction diagrams do not change greatly as the slab temperature increases.

Heating With a Linear Gradient
The next load case to be studied was that of a linear gradient through the slab. In most fires floor slabs are heated primarily from below and, because of the high thermal capacity of concrete, a thermal gradient is produced through the slab. The form of this gradient is typically non-linear with a small thickness of the lower part of the slab being heated rapidly while the upper part remains cool [32]. This section will assume however that the gradient is linear and the results will later be contrasted with those from the following section where non-linear gradients are considered. The findings will be useful for developing numerical models because many analysis programs only allow linear temperature gradients to be specified. The Cardington slab was analysed with a reference surface temperature of 400°C together with gradients 0°C/mm, 1°C/mm , 3°C/mm and 5°C/mm and the results are shown in Fig. 17.

The figures show that the hogging (negative) bending capacity of the slab reduces noticeably as the gradient is increased while the sagging capacity remains almost constant. This is because sagging is resisted largely by the cool and therefore stiff concrete above the reference surface whilst hogging is resisted by the hotter, lower portion of the section that rapidly loses strength at higher temperatures. The maximum membrane compressive strength occurs at progressively larger sagging moments as higher gradients are applied. Again this results from the weak lower portion of the slab, to take maximum advantage of the stiff upper portion in compression it is necessary to apply large sagging moments. The

100

overall effect of linear gradients is to exaggerate the already relatively large capacity the slab has in sagging bending as a result of its geometry.

The presence of a linear gradient also gives rise to the peculiar result of the sagging capacity in both tension and compression rising with increasing gradient. The anomaly arises because the effect of an linear gradient is to reduce the temperature of the upper portion of the slab and thereby increase its strength. As sagging bending is resisted by this part of the cross-section, the increased capacity is predicted. This effect demonstrates one shortcoming of assuming a linear temperature gradient through the slab in an a analysis.

Heating With a Non-linear Gradient

As mentioned, slabs in real fires tend to have non-linear gradients. This was true of the Cardington fire tests and the thermal profiles from a typical area of slab in the first of the Cardington tests were shown in Fig. 6. FEAST requires that non-linear gradients be approximated by polynomial relationships and the curves shown in the figure are fourth order curves fitted to the experimental data. Analyses of the Cardington slab with these temperature profiles were performed at reference surface temperatures of 100ºC, 200ºC, 300ºC and 400ºC and the results are shown in Fig. 18.

The figure reveals that the effect of a non-linear gradient results in a combination of the effects seen for uniform heating and linear gradients heating. Overall the slab loses strength as the temperature increases. Initially, however, this loss of strength is concentrated in the compressive region for the same reasons as uniform heating. As the reference-surface temperature rises, the gradient increases and so the slabs becomes proportionally weaker in hogging bending than sagging bending. Although this effect was seen with a linear gradient it is much more marked with non-linear gradients due the large loss of strength in the hot, lower portion of the cross-section.

Comparing the results for a linear gradient and non-linear gradients at 400ºC it is clear the match is close when a linear gradient of 5ºC/mm is chosen.

The Effects of Reinforcement

A number of studies have suggested that tensile membrane action in the reinforcement mesh of floor slabs may be an important loading carrying factor in extreme fires [9.10.33]. It is argued that the large deflections caused by fire conditions result in the floor slabs of structures ceasing to act in the conventional sense and instead behaving as a "net". Since the tensile strength of concrete cannot be relied upon, the load carrying mechanism is assumed to consist solely of the reinforcement mesh. It has been suggested that to ensure structural integrity in fires, more than the minimum quantity of reinforcement necessary to control cracking be placed in floor slabs. The effect of increasing the area of reinforcement steel from an initial area, A, on the strength of the Cardington slab with a reference surface temperature of 300ºC is shown in Fig. 19.

The strength of the slab in tension can be seen to increase almost in proportion to area of steel present. The strength in the compressive region also increases as a direct result of the increased area. In strain states that are close to pure moment, the effect of increasing the area of reinforcement is small because the reinforcement mesh is placed close to the reference surface.

It has also been suggested that varying the depth at which reinforcement is placed in a slab may have some bearing on its strength at high temperatures [9]. Placing the reinforcement high in the slab would result in greater strength due to the lower temperatures in this region. However, the cooler the reinforcement, the less ductility it possesses and the lower its thermal strain and so the more likely it is to rupture at large deflections. The effect of placing the reinforcement throughout the range of practical depths in the Cardington slab with a reference surface temperature of 300ºC is shown in Fig. 20.

It may be seen that varying the location of the reinforcement has practically no effect on the strength of the slab. This may be explained by examining Figs 6 and 7 where it can be seen that the temperature of the reinforcement, even when placed 10mm below the reference surface, only attained a temperature of 435ºC. At this temperature very little of the its strength has been lost. It appears, therefore, that for increased robustness in fire conditions, it is advantageous to place a larger area of reinforcement low down in concrete floor slabs. This has the effect of increasing the strength of the slab while helping ensure the steel becomes hot and so develop significant thermal strains thus helping the floor slab to survive large deflections.

CONCLUSIONS

The set of results presented demonstrate that in general the strength of concrete slabs is not straightforward when load cases that involve combined bending and membrane forces are considered. This is particularly so when fire conditions result in changing material properties. The following points may be concluded from the investigation.

- The effect of increasing temperature is to reduce the strength of concrete floor slabs. For realistic temperature gradients this loss of strength is larger when under hogging moments than under sagging moments.

- The large increase in moment capacity seen when slabs are subject to the in-plane membrane compression that may result from restrained thermal expansion in fire conditions, means that simple yield line analyses of slabs in these conditions is not easily applicable.

- The tensile strength of heated concrete slabs arises principally from the reinforcement mesh. Increasing the area of reinforcement mesh increases the tensile capacity of the slab.

- Placing reinforcement mesh low in concrete slabs may increase the slabs ability to accommodate large deflections in fire conditions without reducing its strength.

REFERENCES

1) Bravery PNR. Cardington large building test facility. Technical report, Building Research Establishment, 1993
2) Rotter JM, Sanad AM, Usmani AS and Gillie M. Structural performance of redundant structures under local fires. In *Proceeding of Interflam '99*, vol 2, Scotland 1999.
3) Sanad AM, Rotter JM , Usmani AS and O'Connor MA. Finite element modelling of fire tests on the Cardington composite building. In *Proceedings Interflam '99* ,vol 2, Scotland 1999.
4) Gillie M. Pit project research report MD3: BS/TEST1 model using FEAST with shell elements. Technical report, University of Edinburgh, 2000. Available at www.civ.ed.ac.uk/research/fire/project/reports.html
5) Gillie M. Pit project research report AM3: Analysis of results from BS/TEST1 models , part C, FEAST shell models. Technical report, University of Edinburgh, 2000. Available at www.civ.ed.ac.uk/research/fire/project/reports.html
6) O'Connor M. Pit project research report MD4: BS/TEST1 ABAQUS model using shell elements for the beam and beam general section for the slab. Technical report, British Steel, 2000. Available at www.civ.ed.ac.uk/research/fire/project/reports.html
7) Gillie M, Usmani AS and Rotter JM. Modelling of heated composite floor slabs with reference to the Cardington experiments. *Fire Safety Journal* 36(8):745-767, 2001
8) Gillie M, Usmani AS and Rotter JM. A structural analysis of the first Cardington test. *Journal of Constructional Steel Research,* 56(6):581-601, 2001
9) Gillie M. *The Behaviour of Steel-framed Composite Structures in Fire Conditions.* PhD thesis, University of Edinburgh, 2000
10) Gillie M, Usmani AS and Rotter JM. A structural analysis of the Cardington British Steel Corner test. *Journal of Constructional Steel Research* In press.
11) Bailey CG, Burgess IW and Plank RJ. Computer simulation of a full-scale structural fire test. *The Structural Engineer, 77(8):15-21, 1999*
12) Bailey CG. The behaviour of full-scale steel-framed buildings subject to compartment fires. *The Structural Engineer,* 77(8):15-21, 1999.
13) Bailey CG and Moore DB. The structural behaviour of steel frames with composite floor slabs subject to fire: Part 1: theory. *The Structural Engineer 78(11):19-27,2000*
14) Bailey CG and Moore DB. The structural behaviour of steel frames with composite floor slabs subject to fire: Part 2: design. *The Structural Engineer 78(11):28-33 ,2000*
15) Huang Z, Burgess IW and Plank RJ. Non-linear analysis of reinforced concrete slabs subject to fire. *ACI Structural Journal,* 96:127-135, Jan-Feb 1999
16) Huang Z, Burgess IW and Plank RJ. Three-dimensional modelling of two full-scale fire tests in a composite building. *Proceedings of the Institute of Civil Engineers, Structures and Buildings* 134(1):243-255,1999
17) Huang Z, Burgess IW and Plank RJ. Non-linear modelling of three full-scale structural fire-tests. In J-M Franssen, editor, *Structures in Fire-Proceedings of First International Workshop*, pages 53-70, 2000.
18) Elghazouli AY, Izzuddin BA and Richardson AJ. Numerical modelling of structural fire behaviour of composite buildings. *Fire Safety Journal, 35(4):279-297, 2000.*
19) Owens GW *Steel Designers' Manual.* Blackwell Science. 5th edition 1995
20) Sanad AM. PIT project research report AM1: Analysis of results from BS/TEST1 models, part A grillage models. Technical report, University of Edinburgh, 2000. Available at www.civ.ed.ac.uk/research/fire/project/reports.html

21) Sanad AM. PIT project research report AM6: Analysis of results from BS/TEST3 models, part A grillage models. Technical report, University of Edinburgh, 2000. Available at www.civ.ed.ac.uk/research/fire/project/reports.html

22) Usmani AS, Rotter JM, Lamont S, Sanad AM and Gillie M. Fundamental principles of structural behaviour under thermal effects. *Fire Safety Journal*, 36(8):721-744, 2001

23) Kirby BR. The behaviour of a multi-storey steel-framed building subjected to fire attacks, experimental data. Technical report, British Steel,1998.

24) Harmathy TZ *Fire Safety Design and Concrete.* Longman Scientific and Technical, 1st edition, 1993

25) Malhotra HK. The effect of temperature on the compressive strength of concrete. *Magazine of Concrete Research,* 8(85),1956

26) Scheider U. Concrete at high temperatures – a general review. *Fire Safety Journal,* 13(1):55-68, 1988

27) ENV. *Eurocode 2 Design of Concrete Structures, 1992*

28) ENV. *Eurocode 3 Design of Composite Steel and Concrete Structures, 1994*

29) Gillie M. Modelling heated composite floorslabs with ABAQUS using a UGENS subroutine. In *ABAQUS Users' Conference 2000.* Hibbett, Karlsson and Sorensen INC, 2000

30) Rose PS, Burgess IW, Plank RJ and Bailey CG. The influence of floor slabs on the structural behaviour of composite frames. In Lee, editor, *Structures in the New Millennium*, 1997

31) Wang YC. Tensile membrane action in slabs and its application to the Cardington fire tests. Technical report, Building Research Establishment, 1996. Paper presented to the second Cardington Conference 12-14 March 1996

32) Lamont S, Usmani AS and Drysdale DD. Heat transfer analysis of the composite slab in the Cardington frame fire tests. *Fire Safety Journal, 2001.* In press.

33) Bailey CG, White DS and Moore DB. The tensile membrane action of unrestrained composite slabs simulated under fire conditions. *Engineering Structures, 22:153-159,2000.*
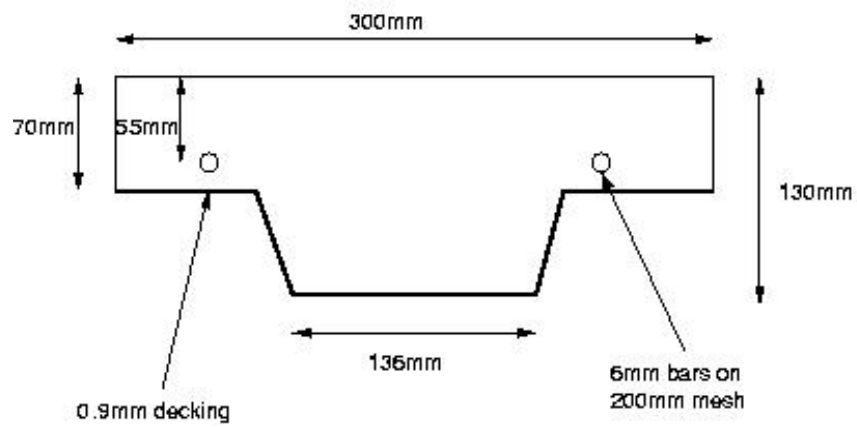
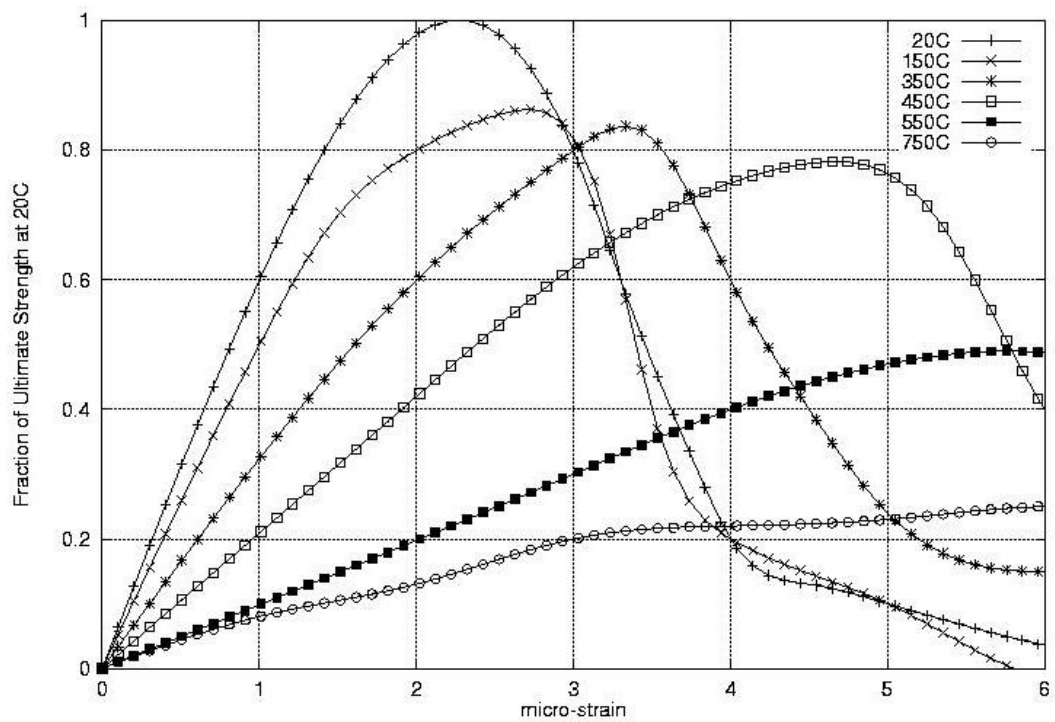**Figure 1. Cross section of the Cardington slab parallel to the ribs.**

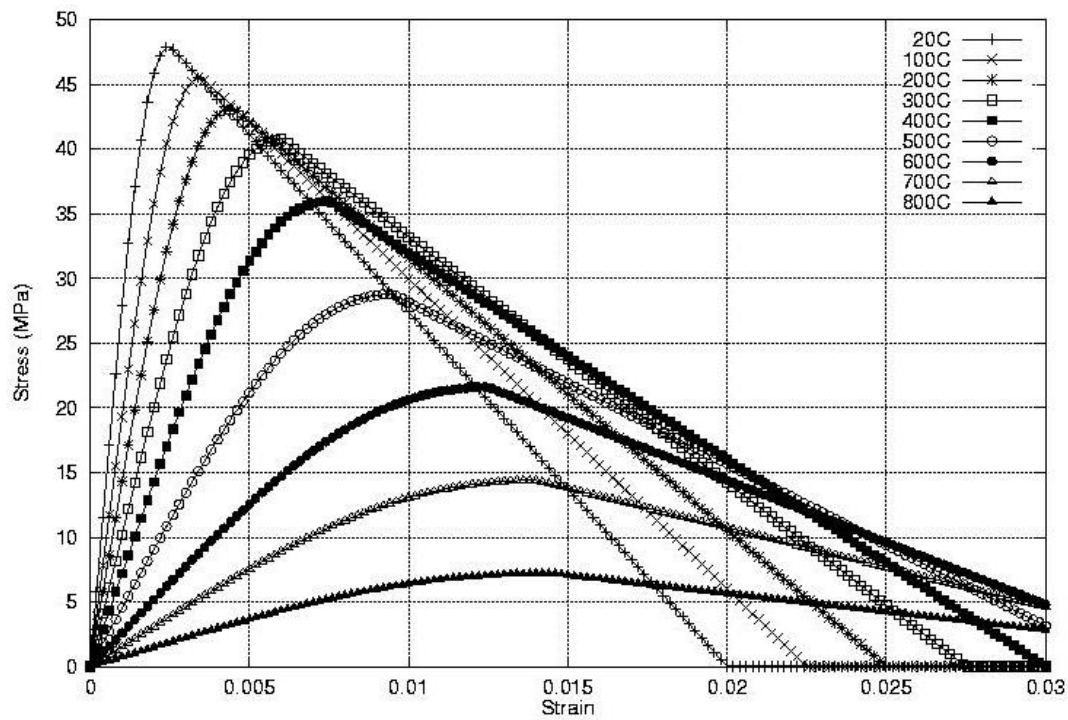**Figure 2. Concrete stress-strain behaviour at elevated temperatures[26]**

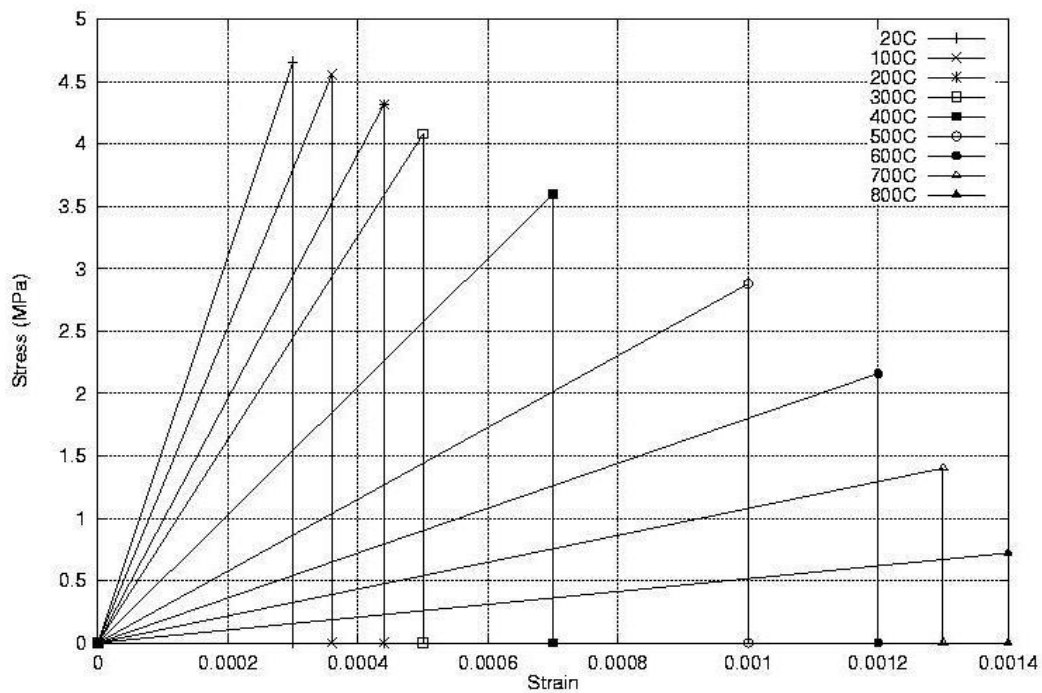**Figure 3. Concrete compressive behaviour as defined by Eurocode 2[27.]**

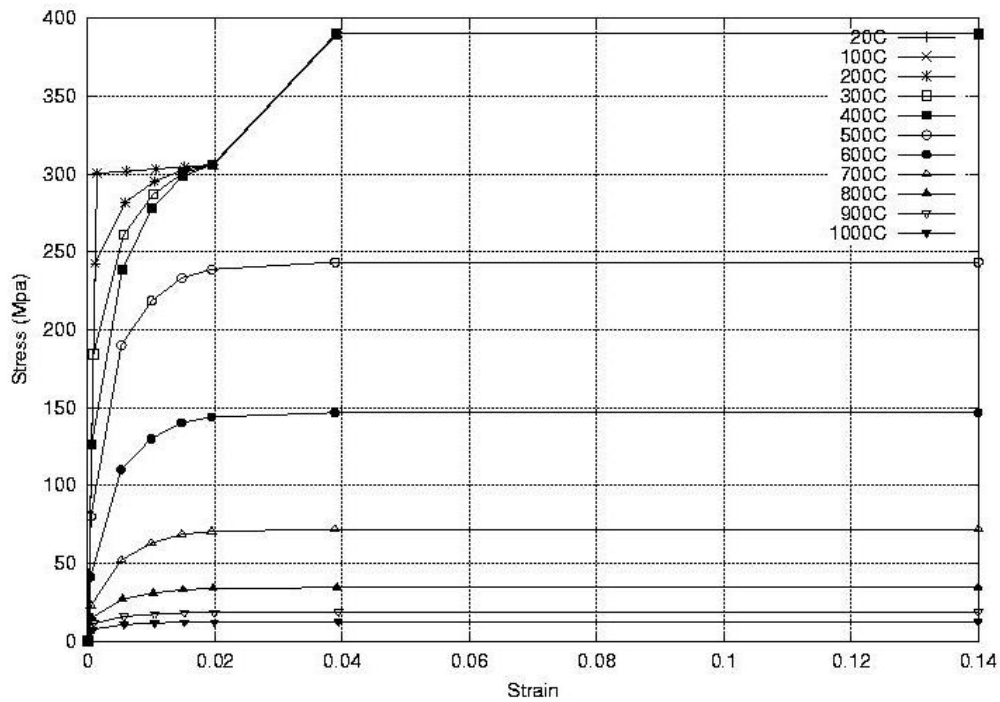**Figure 4. Concrete tensile behaviour as defined by Eurocode 2[27]**

Figure 5. Stress-strain behaviour of steel at elevated temperatures as defined by Eurocode 3 Part 1.2[28]
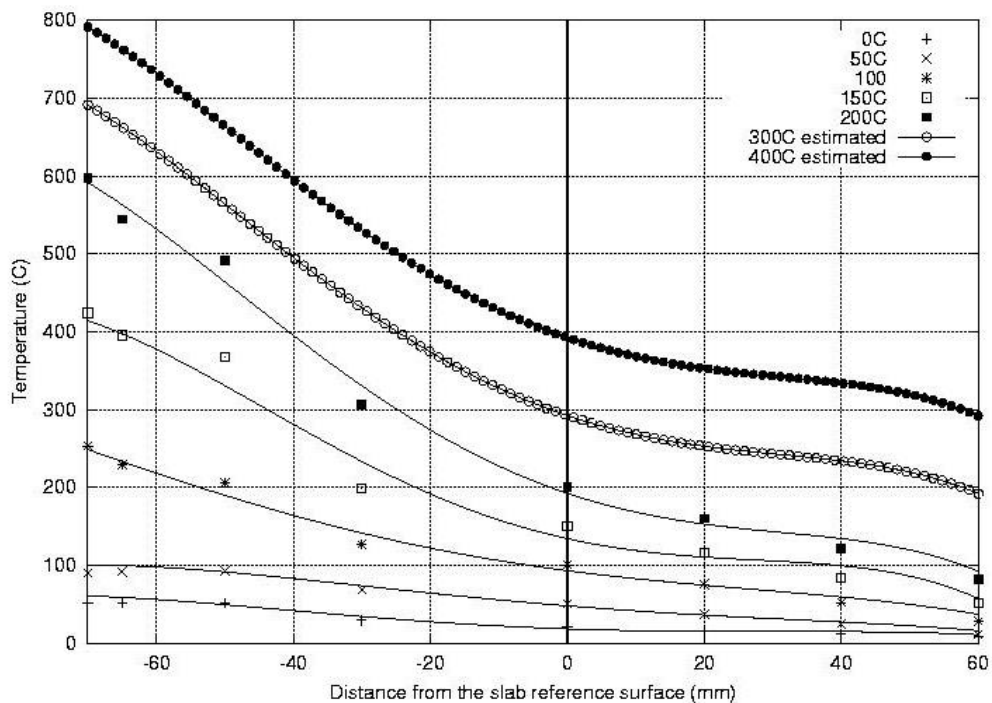

Figure 6. Experimental data from the Cardinton tests showing the variation of temperature through as typical "thick" cross-section of the floor slab, together with polynomial fits for various reference surface temperatures
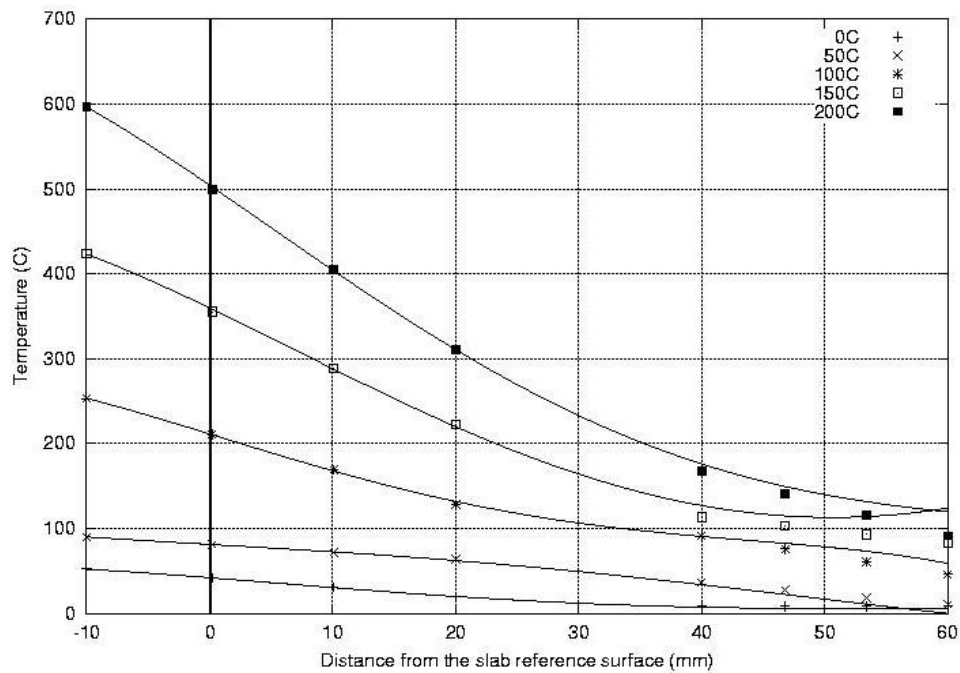
Figure 7. Experimental data from the Cardington test showing the variation of temperature through a typical "thin" cross-section of the floor slab, together with polynomial fits for various "thick" direction reference surface temperatures.
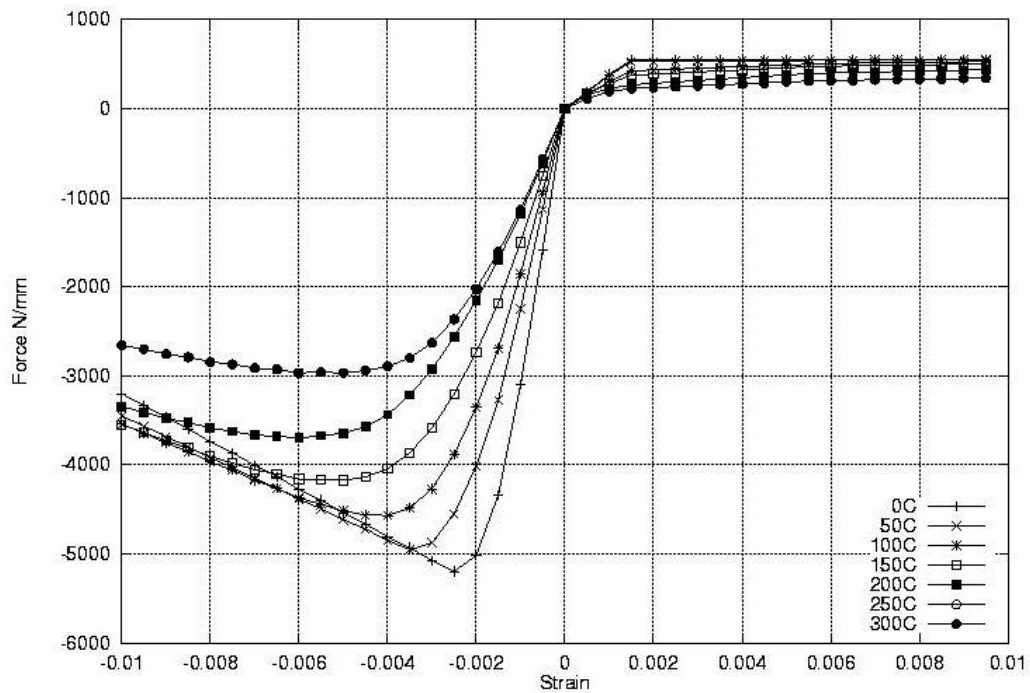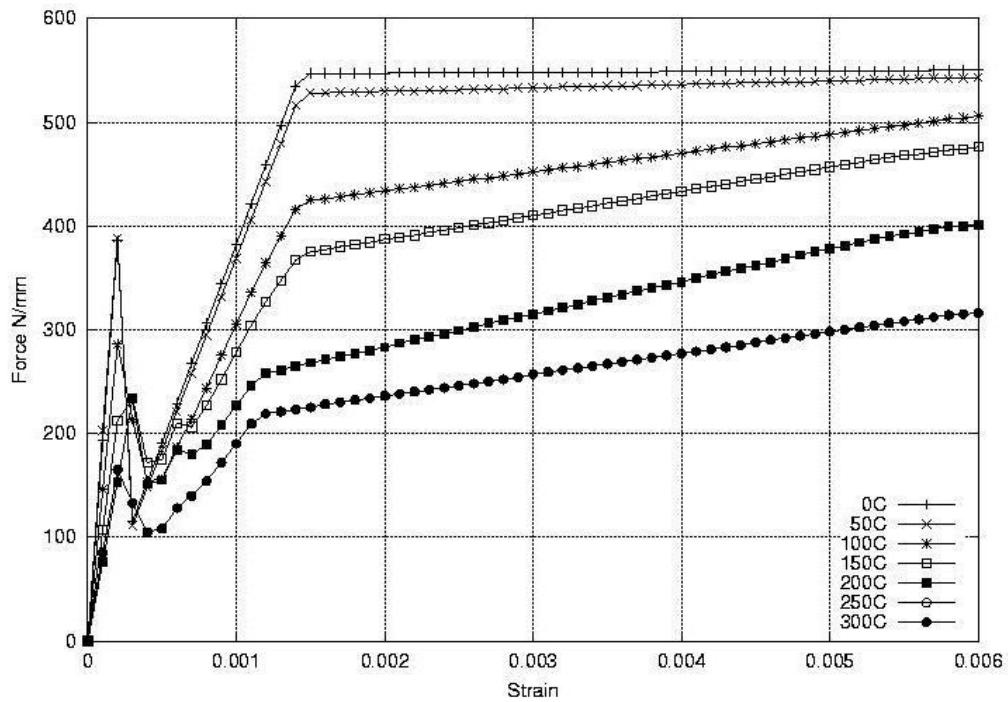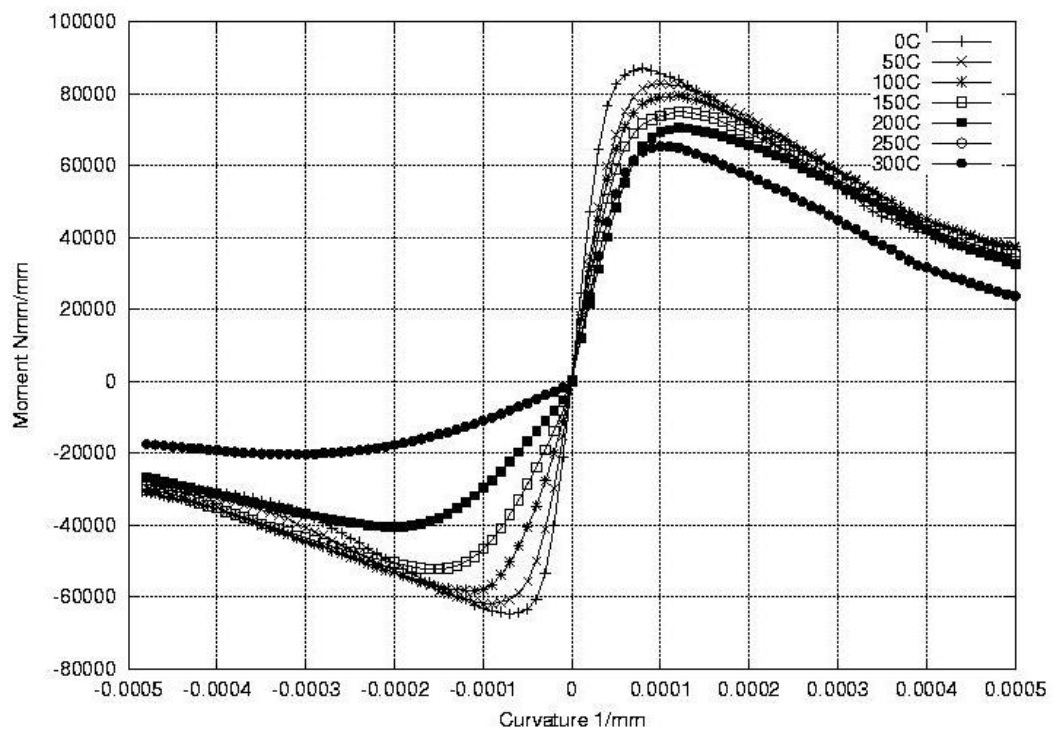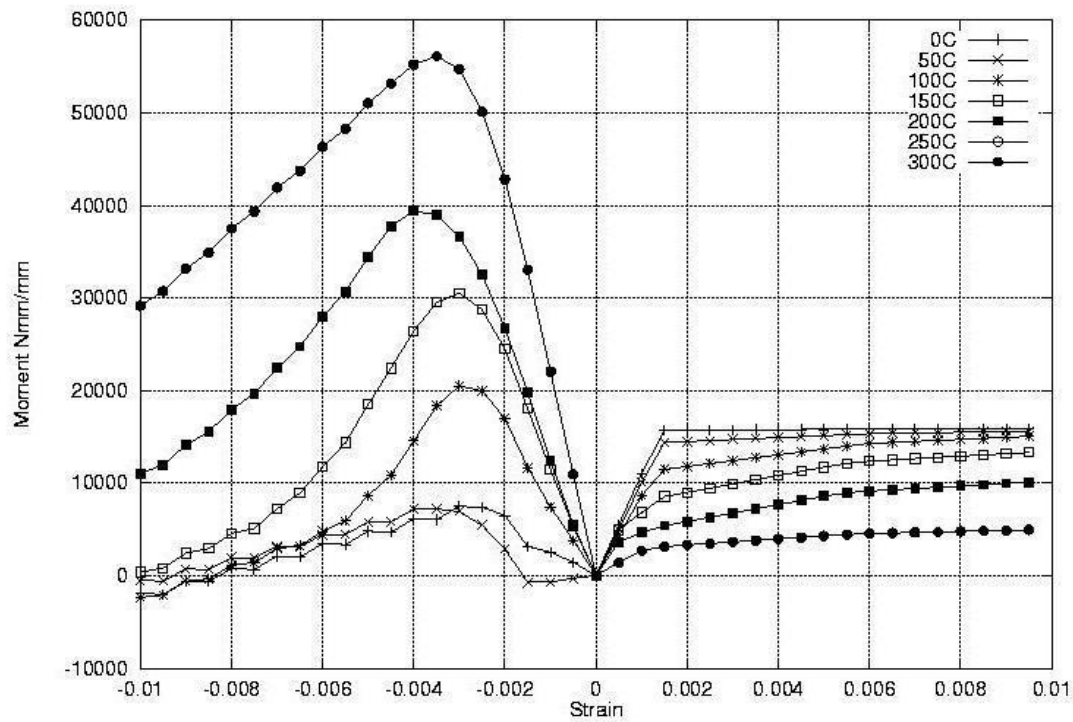

Figure 8. Force-strain diagram for the Cardinton slab parallel to the ribs
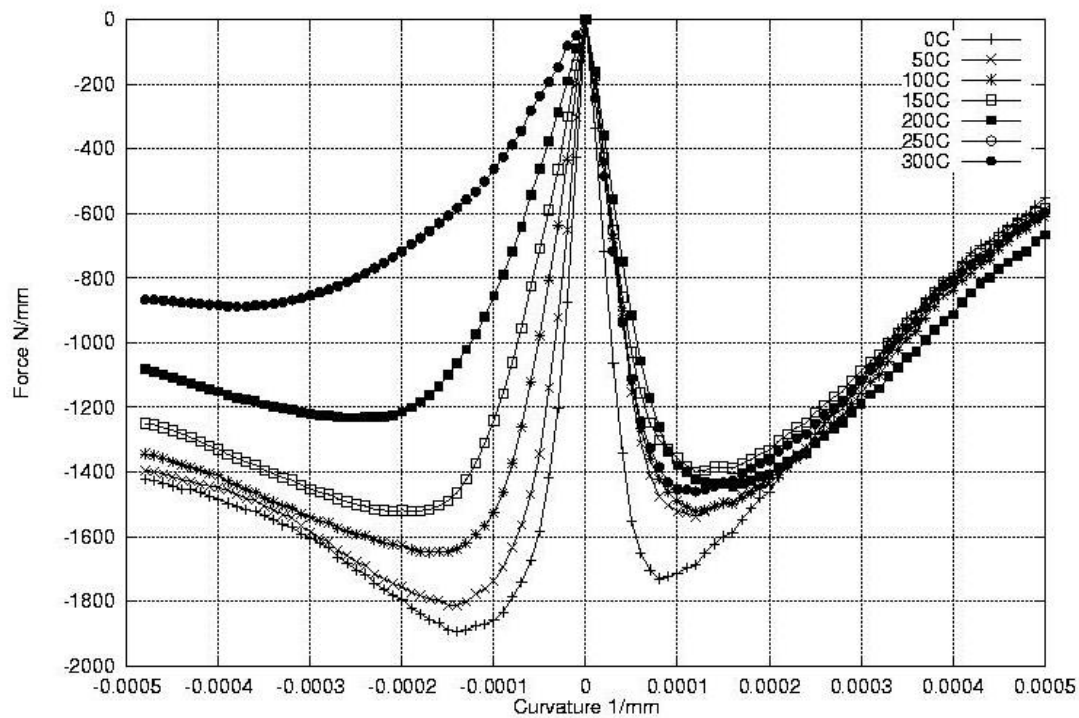
Figure 9. Force-strain diagram for the Cardinton slab parallel to the ribs (detail of tensile region).

Figure 10. Moment-curvature diagram for the Cardington slab parallel to the ribs

Figure 11. Moment-strain diagram for the Cardington slab parallel to the ribs

Figure 12. Force-curvature diagram for the Cardington slab parallel to the ribs
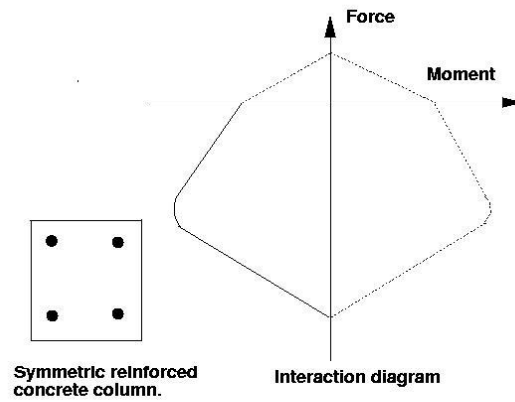
Figure 13. Sketch of an interaction diagram for a symmetric reinforce concrete column. It is common for only one quarter (shown solid) of the diagram to be shown in design charts.
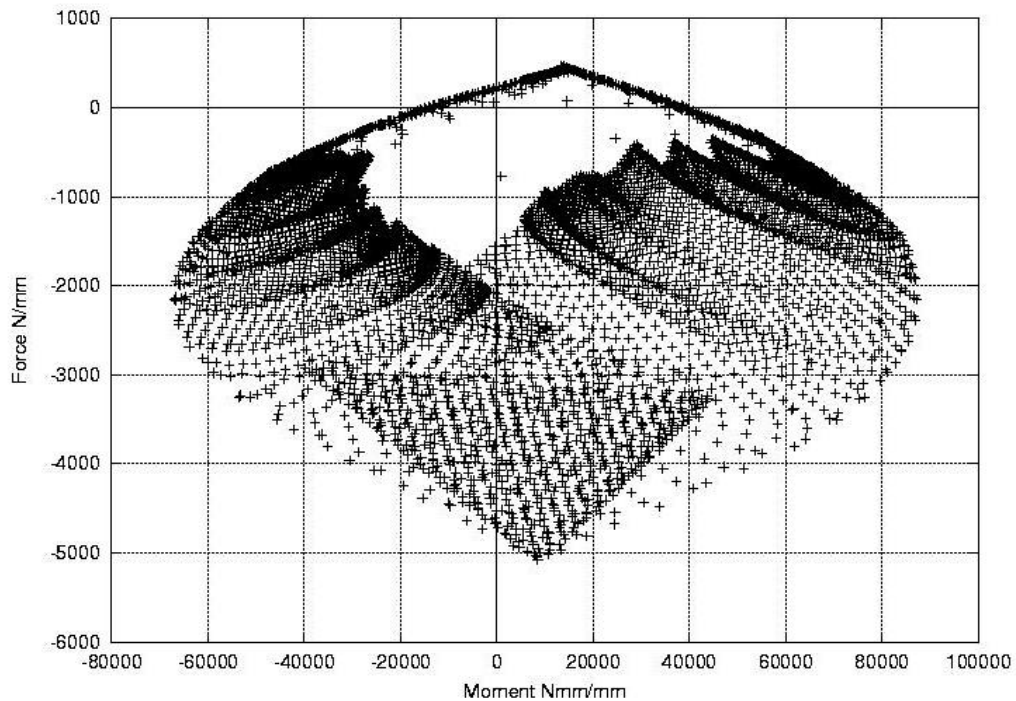
Figure 14. Interaction diagram for the Cardington slab parallel to the ribs at ambient temperature
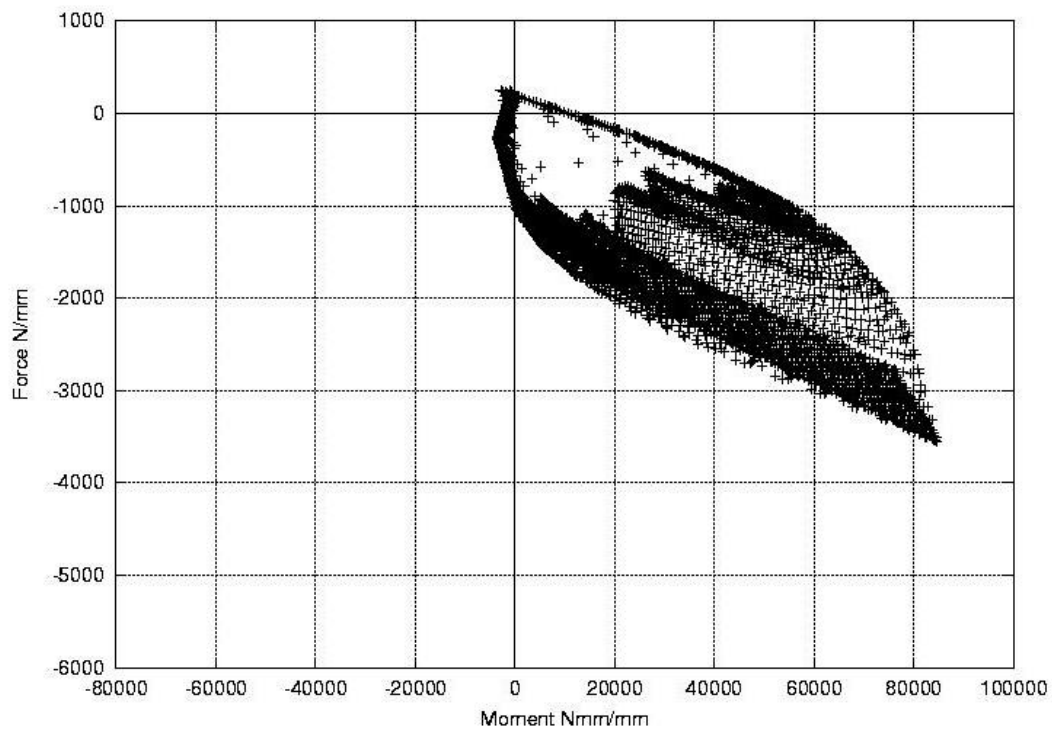
Figure 15. Interaction diagram for the Cardington slab perpendicular to the ribs at ambient temperature.
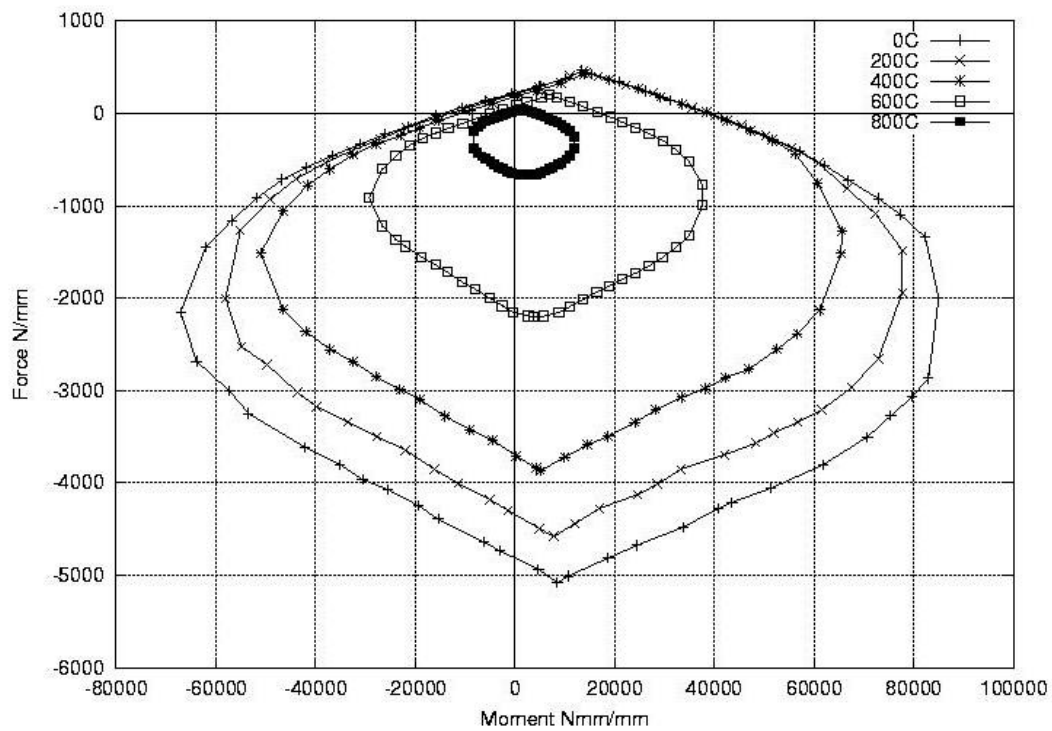
Figure 16. Interaction diagram for the Cardington slab parallel to the ribs at various uniform temperatures
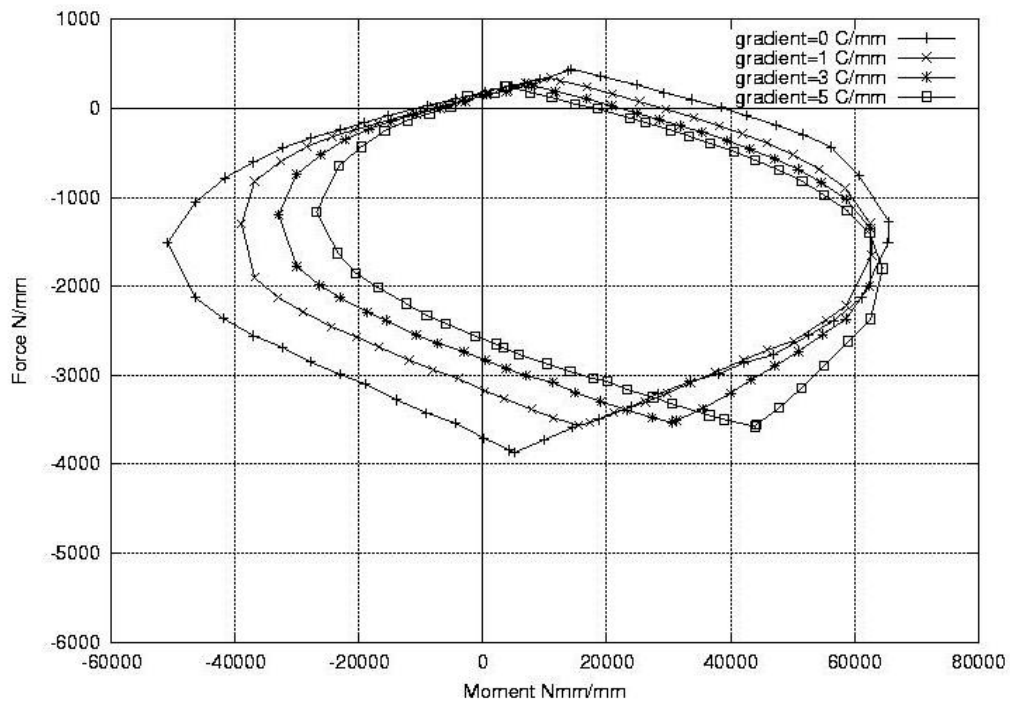
Figure 17. Interaction diagram for the Cardington slab parallel to the ribs with various linear temperature gradients.
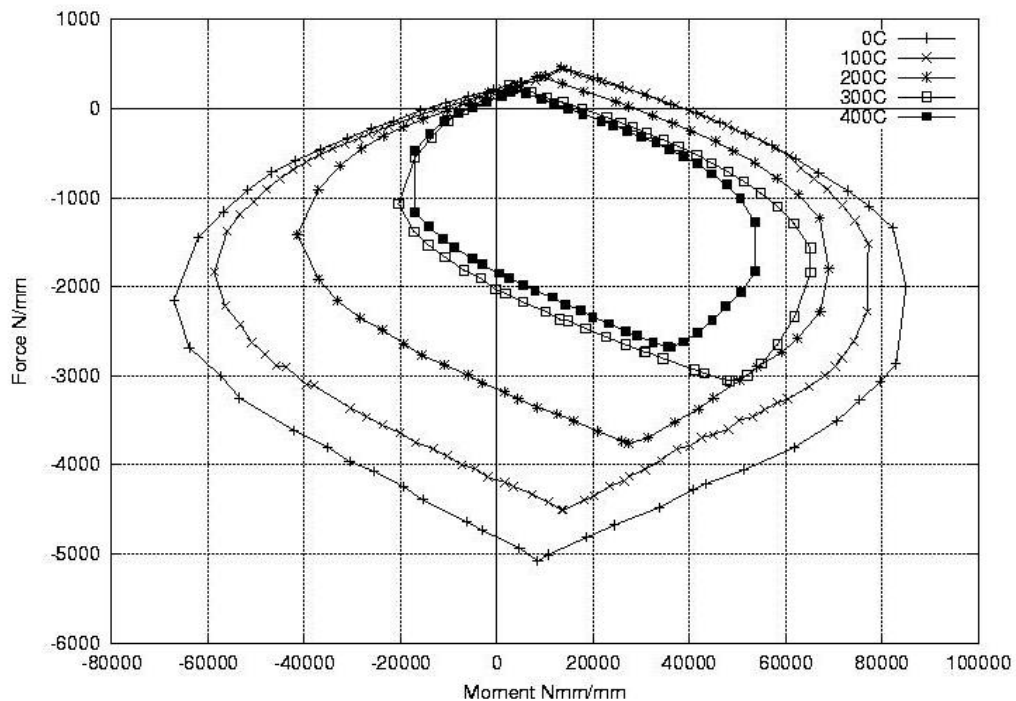
Figure 18. Interaction diagrams for the Cardington slab at various reference surface temperatures with the non-linear temperature gradients obtained from the Cardington test data.

113
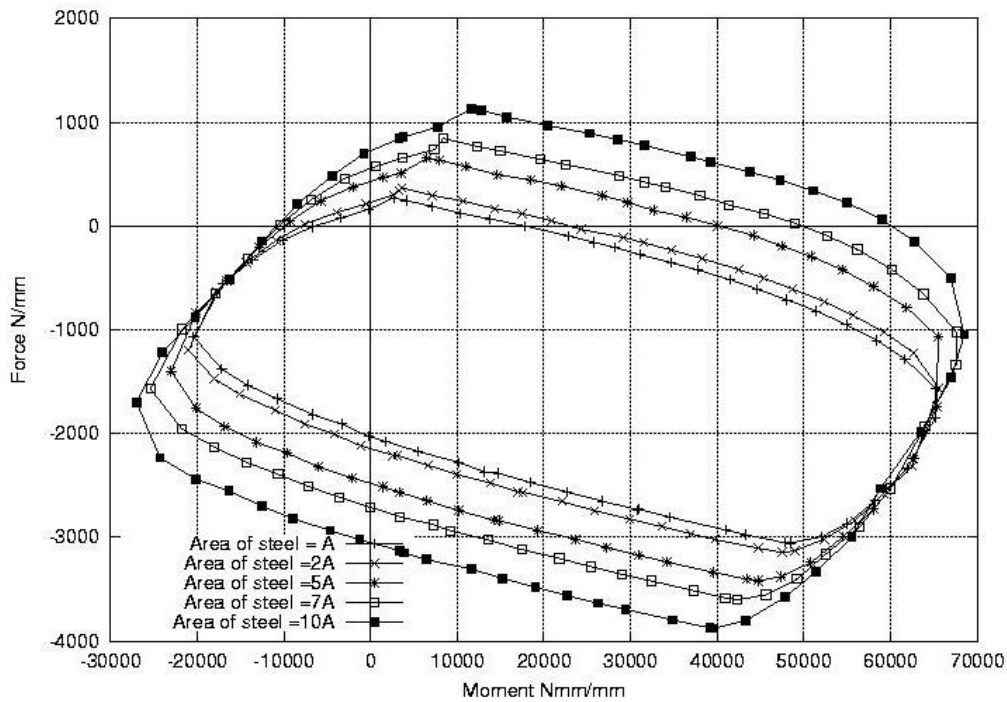
Figure 19. The effect of varying the amount of reinforcement steel on the strength of the Cardington slab with a reference surface temperature of 300C
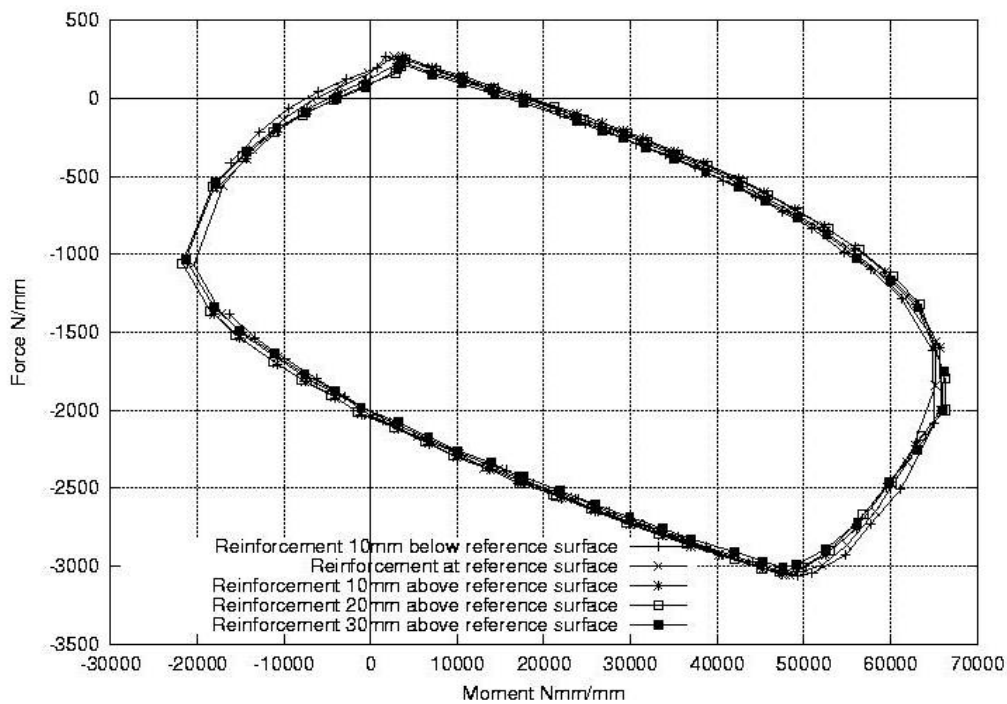
Figure 20. The effect of varying the depth of reinforcement on the strength of the Cardington slab at a reference surface temperature of 300C.

ANALYTICAL SOLUTIONS FOR FLOOR SLABS IN FIRE

N.J.K. Cameron and A.S. Usmani
School of Civil and Environmental Engineering
The King's Buildings, The University of Edinburgh, UK
n.j.k.cameron@ed.ac.uk

ABSTRACT

The computer models developed of the full-scale fire tests at Cardington greatly increased the understanding of the behaviour of composite framed structures in fire. It became clear that their structural response under thermal effects was markedly different to that under ambient conditions. In order that the behaviour of composite framed structures in fire is fully understood it is essential that the fundamental principles governing the behaviour of the frame are understood. This paper describes an elastic analysis method for determining the large-deflection behaviour of a laterally restrained floor slab in fire conditions. Both the thermal expansion of the slab and a thermal gradient through the slab are considered. When the deflections and internal forces are compared against results from analyses using the finite element package ABAQUS they compare well. The application of these results in design of structures to resist fire is highlighted.

KEYWORDS: Composite floor systems, structural behaviour in fire, analytical solutions

INTRODUCTION

From the tests at Cardington and the subsequent numerical modelling it was apparent that in a steel-framed building subject to fire the floor slabs played a key role in maintaining the integrity of the structure. Research has shown that when exposed steel temperatures are less than 400^oC the slab has little influence on the structural behaviour, however, as the temperature increases above 500^oC the effect of the slab increases[1]. As the supporting secondary beams lose their strength the slab is the main structural member which distributes the load to the surrounding structure through membrane action. It has been proven from experiments such as Cardington and subsequent numerical modelling that composite frame structures possess considerable natural fire resistance. In order that the natural fire resistance of such structures can be used it is necessary that this can be quantified. A key part of this reserve strength comes from the ability of the floor slab to redistribute loads to the surrounding cooler, stiffer structure. To be able to quantify the natural fire resistance it is therefore essential that a value can be put on the strength of the floor slab.

The finite element models of the Cardington tests were very complex. For use in a design office models of this complexity are impractical: they take a long time to construct; are computationally expensive; and require a high degree of operator expertise. Simple analytical methods for the analysis of structures in fire are required. Only a few analytical studies exist of the behaviour of floor slabs in fire, however, for a de-

sign method to be developed based on actual behaviour it is essential that this can be described analytically.

GOVERNING EQUATIONS

To calculate the distribution of membrane stresses within a plate subjectd to thermal loading it is necessary to solve two governing differential equations. For stresses under large deflections to be obtained it is necessary to retain the nonlinear terms. The two equations to be solved are the equilibrium equation and the compatibility equation which, for an isotropic flat plate subject to thermal effects can be written as follows:-

$$
D \left[\frac{\partial^4 w}{\partial x^4} + 2 \frac{\partial^4 w}{\partial x^2 \partial y^2} + \frac{\partial^4 w}{\partial y^4} \right] - h \left(\frac{\partial^2 F}{\partial y^2} \frac{\partial^2 w}{\partial x^2} + \frac{\partial^2 F}{\partial x^2} \frac{\partial^2 w}{\partial y^2} - 2 \frac{\partial^2 F}{\partial x \partial y} \frac{\partial^2 w}{\partial x \partial y} \right) + \frac{\partial^2 M^T}{\partial x^2} + \frac{\partial^2 M^T}{\partial y^2} = 0 \quad (1)
$$

$$
\frac{1}{E} \left[\frac{\partial^4 F}{\partial x^4} + 2 \frac{\partial^4 F}{\partial x^2 \partial y^2} + \frac{\partial^4 F}{\partial y^4} \right] - \left[\left(\frac{\partial^2 w}{\partial x \partial y} \right)^2 - \frac{\partial^2 w}{\partial x^2} \frac{\partial^2 w}{\partial y^2} \right] + \frac{(1 - \nu)}{E} \left(\frac{\partial^2 N^T}{\partial x^2} + \frac{\partial^2 N^T}{\partial y^2} \right) = 0 \quad (2)
$$

where w is the deflection function for the plate, F is the Airy stress function, E is the Young's modulus and D is the flexural rigidity of the plate.

Boundary conditions
The plate to be analysed is as shown in Figure 1. For a laterally restrained plate the boundary conditions to be satisfied are as follows:-

$$
\begin{aligned}
w_{x=0,L} &= w_{y=0,B} = 0 \\
u_{x=0,L} &= v_{y=0,B} = 0 \\
\frac{\partial^2 w}{\partial x^2}_{x=0,L} &= \frac{\partial^2 w}{\partial y^2}_{y=0,B} = 0
\end{aligned}
$$

where u and v are the membrane displacements in the x and y directions respectively.

Loading
When a slab is in a fire it causes a temperature distribution $T = T(x, y, z)$ within it. For this analysis it is assumed that the temperature is independent of x and y i.e. the temperature only varies through the depth z such that $T = T(z)$. The temperature distribution $T = T(z)$ can then be represented by an average temperature increase $\alpha(\Delta T)$ corresponding to the thermal expansion and an average temperature gradient $T_{,z}$ as shown in Figure 2.

The thermal loading causes a thermal moment M^T and a thermal force N^T within the plate due to the temperature gradient $T_{,z}$ and the average temperature increase ΔT respectively. The values of the thermal moment and thermal force are calculated:-

$$
M^T = E\alpha \int_{\frac{-h}{2}}^{\frac{h}{2}} (\Delta T) \, z \, \mathrm{d}z \tag{3}
$$

$$
N^T = E\alpha \int_{\frac{-h}{2}}^{\frac{h}{2}} (\Delta T) \, \mathrm{d}z \tag{4}
$$

114
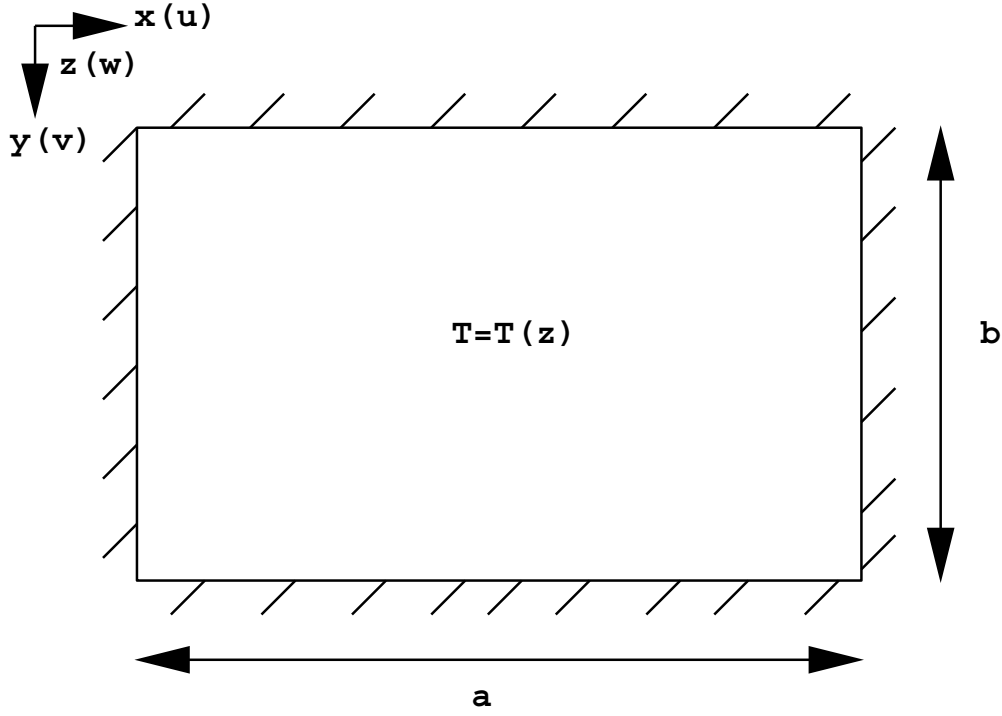
Figure 1: Laterally restrained plate subjected to temperature distribution T=T(z)

Solution for a plate subject to thermal effects

In obtaining a solution to the governing differential equations it is assumed that the deflection of the plate can be defined using a double Fourier series:-

$$w = \sum_{m=1}^{\infty} \sum_{n=1}^{\infty} w_{mn} sin \frac{m\pi x}{L} sin \frac{n\pi y}{B} \tag{5}$$

Substitution of Equation(5) into that for membrane equilibrium, Equation(2), results in:-

$$\frac{1}{E}\left[\frac{\partial^4 F}{\partial x^4} + 2\frac{\partial^4 F}{\partial x^2 \partial y^2} + \frac{\partial^4 F}{\partial y^4}\right] = \frac{m^2 n^2 \pi^4}{2L^2 B^2} w_{mn}^2 \left(cos \frac{2m\pi x}{L} + cos \frac{2n\pi y}{B}\right) \tag{6}$$

The solution of the Airy stress function F consists of two parts, a particular solution F_P and a homogeneous solution F_H. The particular solution F_P is obtained by solving Equation (6):-

$$F_P = \frac{w_{mn}^2 E}{32}\left(\frac{n^2}{m^2}\frac{L^2}{B^2}cos \frac{2m\pi x}{L} + \frac{m^2}{n^2}\frac{B^2}{L^2}cos \frac{2n\pi y}{B}\right) \tag{7}$$

The general solution of equation(2) can be described as:-

$$F = P\frac{x^2}{2} + Q\frac{y^2}{2} + \frac{w_{mn}^2 E}{32}\left(\frac{n^2}{m^2}\frac{L^2}{B^2}cos \frac{2m\pi x}{L} + \frac{m^2}{n^2}\frac{B^2}{L^2}cos \frac{2n\pi y}{B}\right) \tag{8}$$

115

Figure 2: Equivalent temperature distribution in a plate

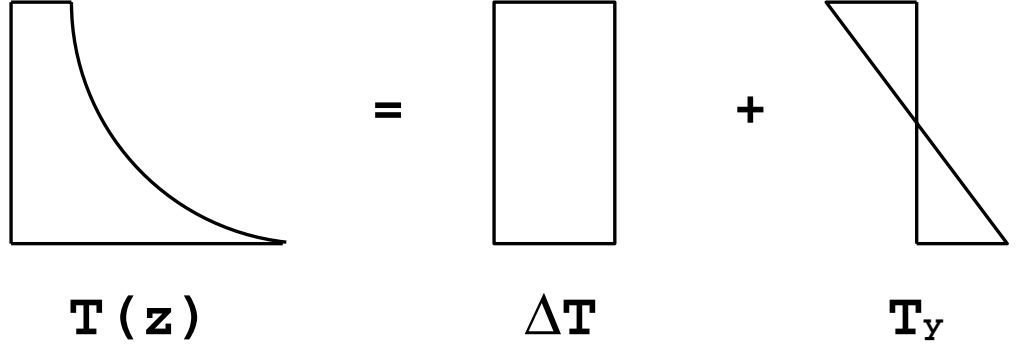In this analysis it is assumed that the plate is laterally restrained along all of its edges and that the elongations in the x and y direction are independent of y and x respectively. Considering this statement the values of P and Q are found to be:-

$$P = \frac{w_{mn}^2 \pi^2 E}{8\left(1-\nu^2\right)}\left(\frac{n^2}{B^2}+\nu\frac{m^2}{L^2}\right)-\frac{E\alpha\Delta T}{1-\nu}$$

$$Q = \frac{w_{mn}^2 \pi^2 E}{8\left(1-\nu^2\right)}\left(\frac{m^2}{L^2}+\nu\frac{n^2}{B^2}\right)-\frac{E\alpha\Delta T}{1-\nu}$$

The final solution for the Airy stress function F satisfying Equation(2) can therefore be described as:-

$$F = \frac{w_{mn}^2 \pi^2 E}{8\left(1-\nu^2\right)}\left(\frac{n^2}{B^2}+\nu\frac{m^2}{L^2}\right)\frac{x^2}{2}+\frac{w_{mn}^2 \pi^2 E}{8\left(1-\nu^2\right)}\left(\frac{m^2}{L^2}+\nu\frac{n^2}{B^2}\right)\frac{y^2}{2}$$
$$+\frac{w_{mn}^2 E}{32}\left(\frac{n^2}{m^2}\frac{L^2}{B^2}cos\frac{2m\pi x}{L}+\frac{m^2}{n^2}\frac{B^2}{L^2}cos\frac{2n\pi y}{B}\right)-\frac{E\alpha\Delta T}{1-\nu}\frac{x^2}{2}-\frac{E\alpha\Delta T}{1-\nu}\frac{y^2}{2} \qquad (9)$$

By substituting Equations (5) and (9) into the equation for bending equilibrium Equation(1) and applying the Galerkin method a cubic equation with respect to the deflection w_{mn} of the plate is obtained.

$$\left\{\frac{1}{16}\pi^4 hE\left(3-\nu^2\right)\left[m^4\frac{B}{L^3}+n^4\frac{L}{B^3}\right]+\frac{1}{4}\frac{m^2 n^2}{LB}\pi^4 hE\nu\right\}w^3$$
$$\left\{\pi^4 D\left(1-\nu^2\right)\left[m^4\frac{B}{L^3}+2\frac{m^2 n^2}{BL}+n^4\frac{L}{B^3}\right]-\pi^2 hE\alpha\Delta T\left(1+\nu\right)\left[m^2\frac{B}{L}+n^2\frac{L}{B}\right]\right\}w$$
$$-16M^T\left(1-\nu^2\right)\left[\frac{m}{n}\frac{B}{L}+\frac{n}{m}\frac{L}{B}\right]=0 \,(10)$$

The above equation allows the deflection of the plate w_{mn} to be calculated for any term mn in the series. By putting these values into the Fourier series describing the deflection, Equation(5), the deflected shape and total deflection can be calculated.

116

Compared to results from ABAQUS finite element analyses, when only the first term in the series is considered then the deflection is overpredicted. When the aspect ratio of the plate is increased above one then, when compared with results from a finite element analysis, the error in the deflection obtained is much larger. When the first fifteen terms in the series are considered the deflections are underpredicted for all aspect ratios.

When calculating the internal forces in the slab it is essential that the deflections are predicted to a reasonable degree of accuracy as the forces are very sensitive to even a slight change of deflection. In order to increase the accuracy of the forces and deflections it was necessary to change the term describing the thermal expansion ΔT in Equation(10). To simplify the calculation only the first term in the series will be considered.

A finite element parametric study was carried out and based on the results it is proposed that the term in the equation considering the thermal expansion Δ^T should be revised to:-

$$k = -\left(0.3 + \frac{L}{B}\right)\left(1 + \frac{L}{B}\right)\frac{L^2 N^T}{Eh^3} \tag{11}$$

This results in the equation becoming:-

$$\frac{3}{4}\left[(3 - \nu^2)\left(1 + \frac{L^4}{B^4}\right) + \frac{4\nu L^2}{B^2}\right]\left(\frac{w_{11}}{h}\right)^3$$

$$+ \left[\left(1 + \frac{L^2}{B^2}\right)^2 - \left(0.3 + \frac{L}{B}\right)\left(1 + \frac{L}{B}\right)\frac{L^2 N^T}{EH^3}\right]\left(\frac{w_{11}}{h}\right)$$

$$+ 192 M^T \frac{(1 - \nu^2)L^4}{\pi^4 Eh^4}\left(\frac{1}{L^2} + \frac{1}{B^2}\right) = 0 \tag{12}$$

Using the above equation plates with an aspect ratio of 1,2 and 3 were analysed for thermal bending and thermal expansion. Two thermal gradients were considered - $5^oC/mm$ and $10^oC/mm$ and the thermal expansion δT was altered from 0^oC to 200^oC in steps of 50^oC. Calculated results for displacements and membrane stresses and those from finite element analyses are contained in Figures (3)-(10). In the diagrams tensile stresses are negative and compressive stresses are positive.

When compared against the results from the finite element analyses the results using Equation(12) agree relatively well. It can be seen from the graphs that the general trend of the behaviour of the plates is captured by the above method and the error between the two sets of results is generally acceptable.

The results also agree with the findings of previous research investigating the behaviour of slabs under different heating regimes.[2,3] It can be seen that when there is no thermal expansion i.e. the plate is only subject to a thermal gradient, then there is tension across the whole plate and an increase in the thermal gradient results in an increase in the tensile stresses.[4] If the plate is heated so that there is thermal expansion as well as thermal bending then the tensile stresses start to decrease. This is due to some of the thermal expansion strain $\alpha(\Delta T)$ being absorbed by the increasing deflection of the slab. Any thermal expansion strain not contributing to deflections produces

Figure 3: Deflection at centre of plates subjected to thermal expansion and with a constant thermal gradient of 5C/mm

Figure 4: Membrane stresses at centre of plate with L/B=1 subjected to thermal expansion and with a constant thermal gradient of 5C/mm

Figure 5: Membrane stresses at centre of plate with L/B=2 subjected to thermal expansion and with a constant thermal gradient of 5C/mm

Figure 6: Membrane stresses at centre of plate with L/B=3 subjected to thermal expansion and with a constant thermal gradient of 5C/mm

Figure 7: Deflection at centre of plates subjected to thermal expansion and with a constant thermal gradient of 10C/mm

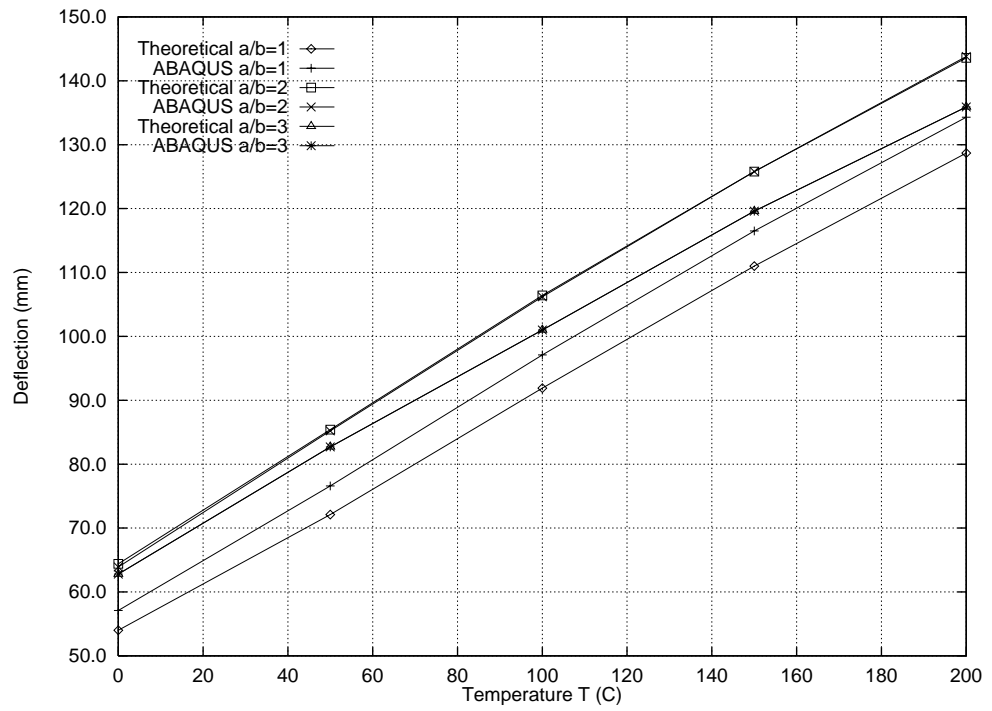Figure 8: Membrane stresses at centre of plate with L/B=1 subjected to thermal expansion and with a constant thermal gradient of 10C/mm
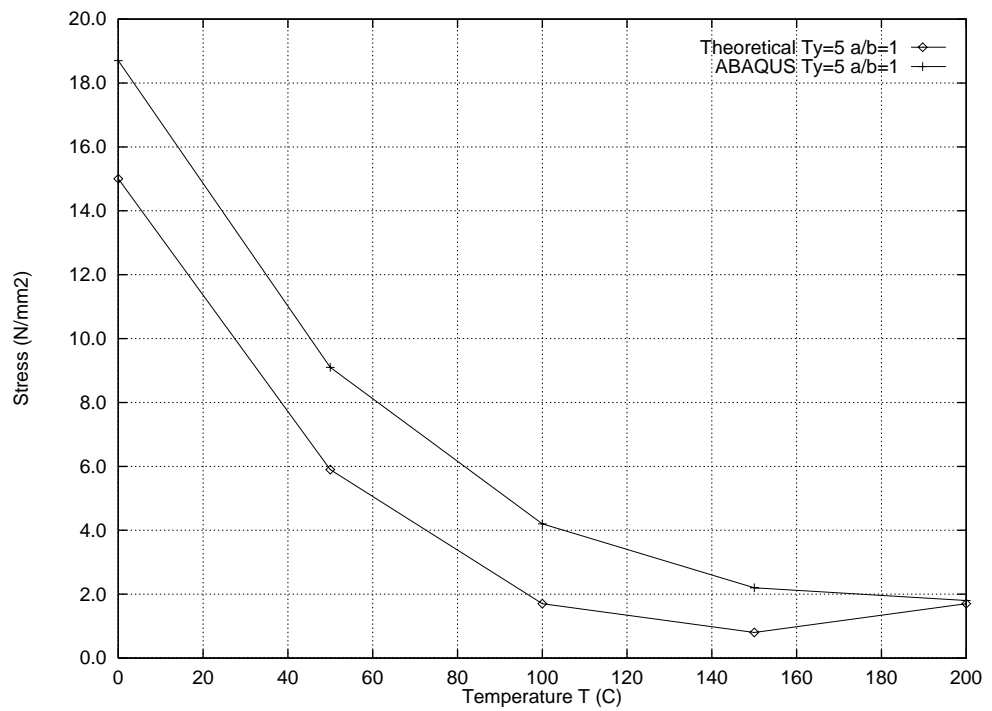
Figure 9: Membrane stresses at centre of plate with L/B=2 subjected to thermal expansion and with a constant thermal gradient of 10C/mm
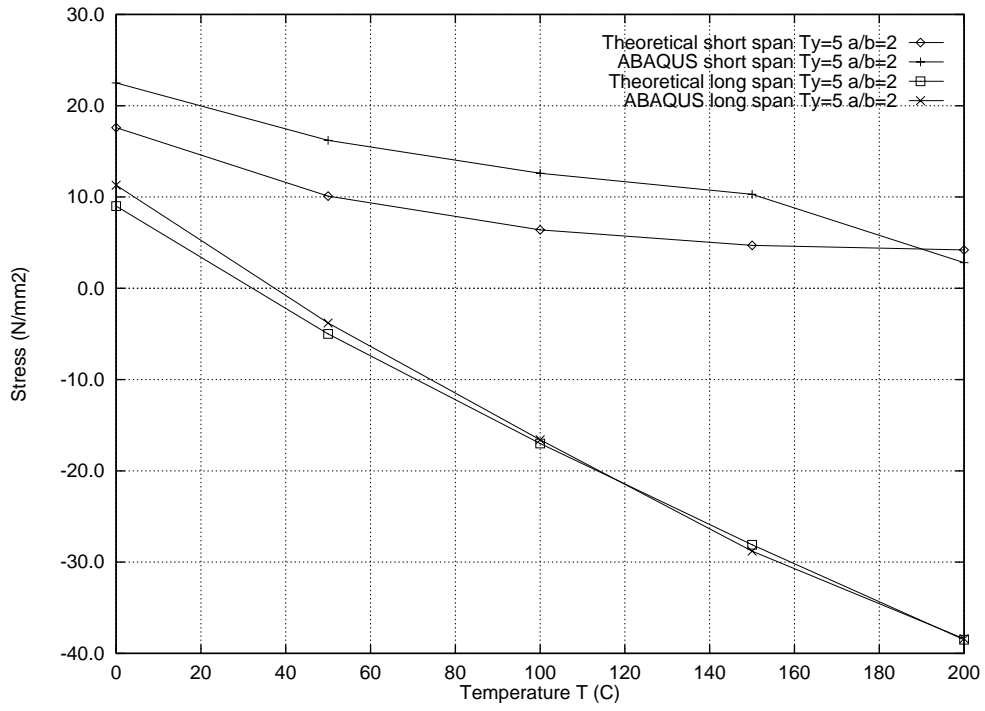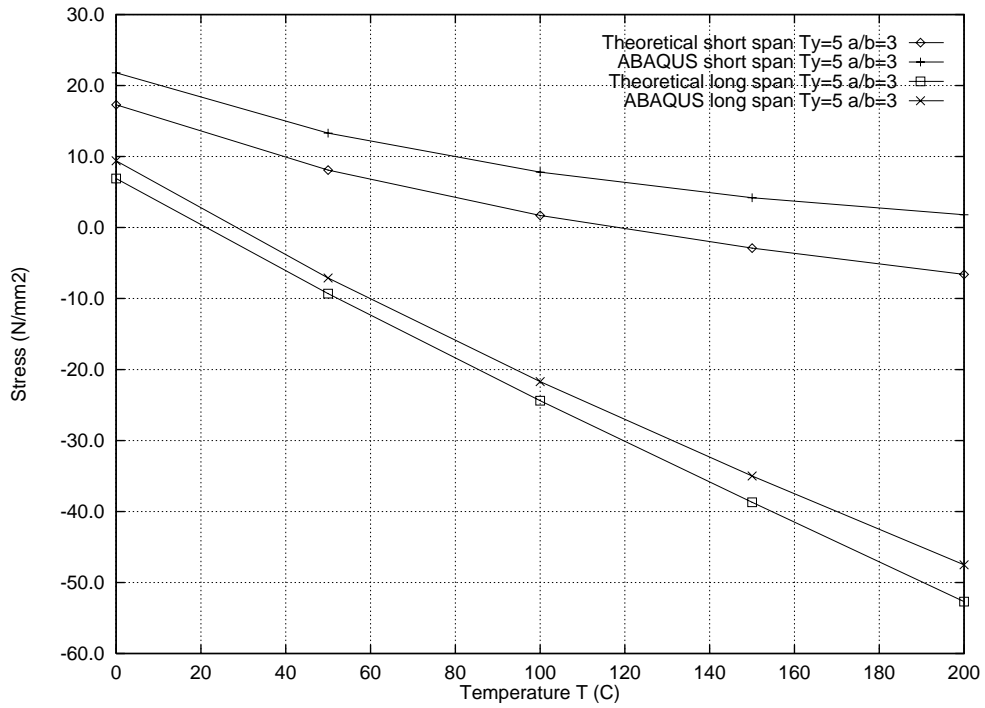

Figure 10: Membrane stresses at centre of plate with L/B=3 subjected to thermal expansion and with a constant thermal gradient of 10C/mm

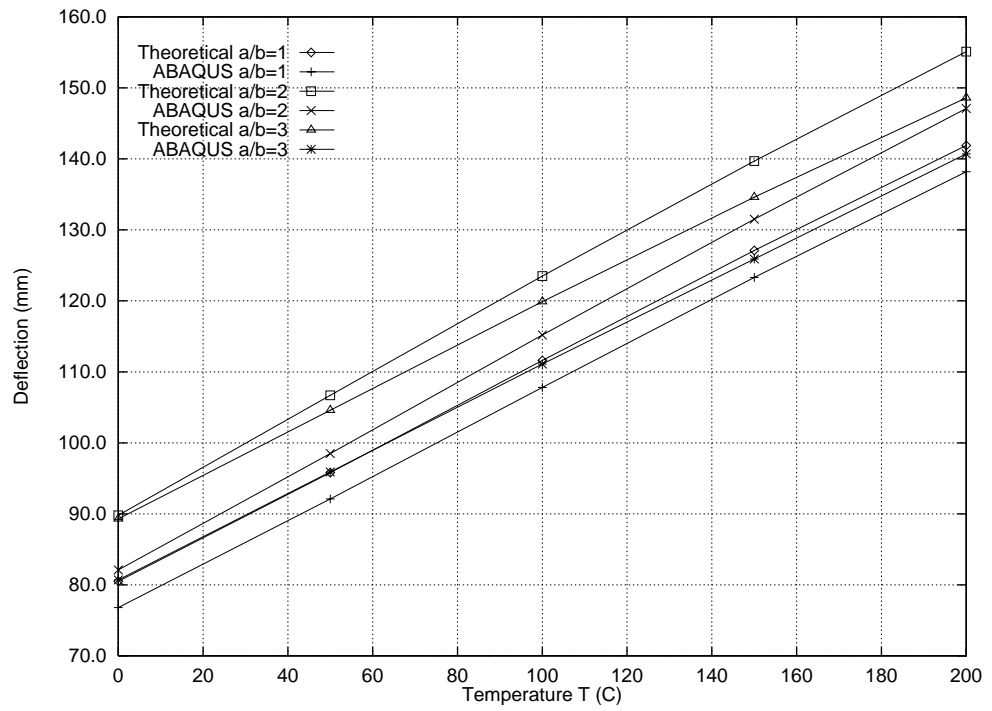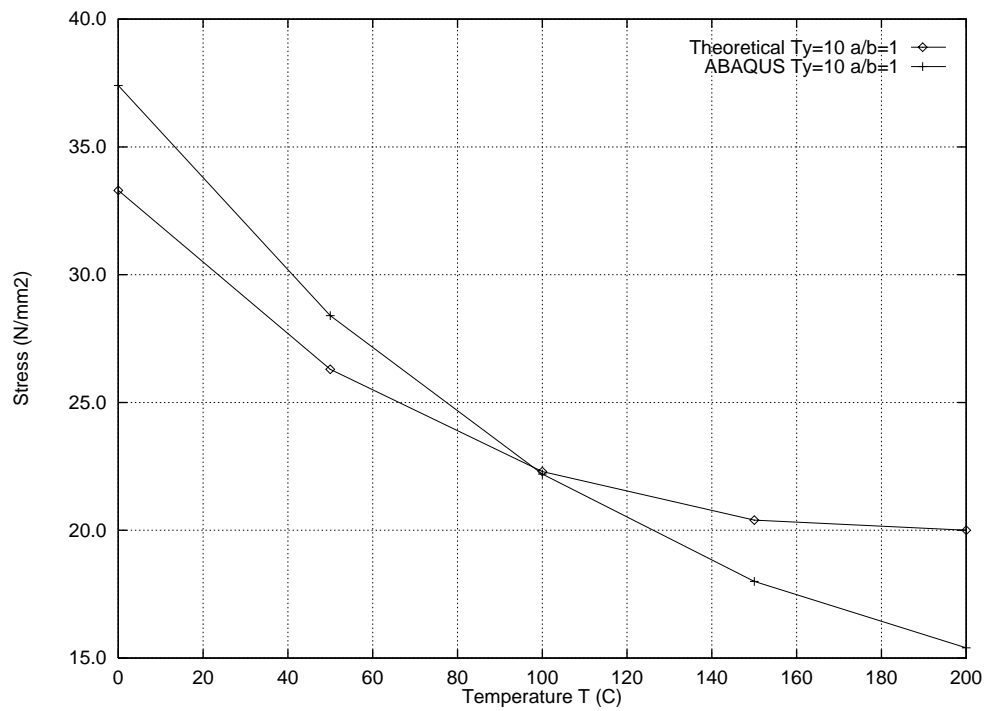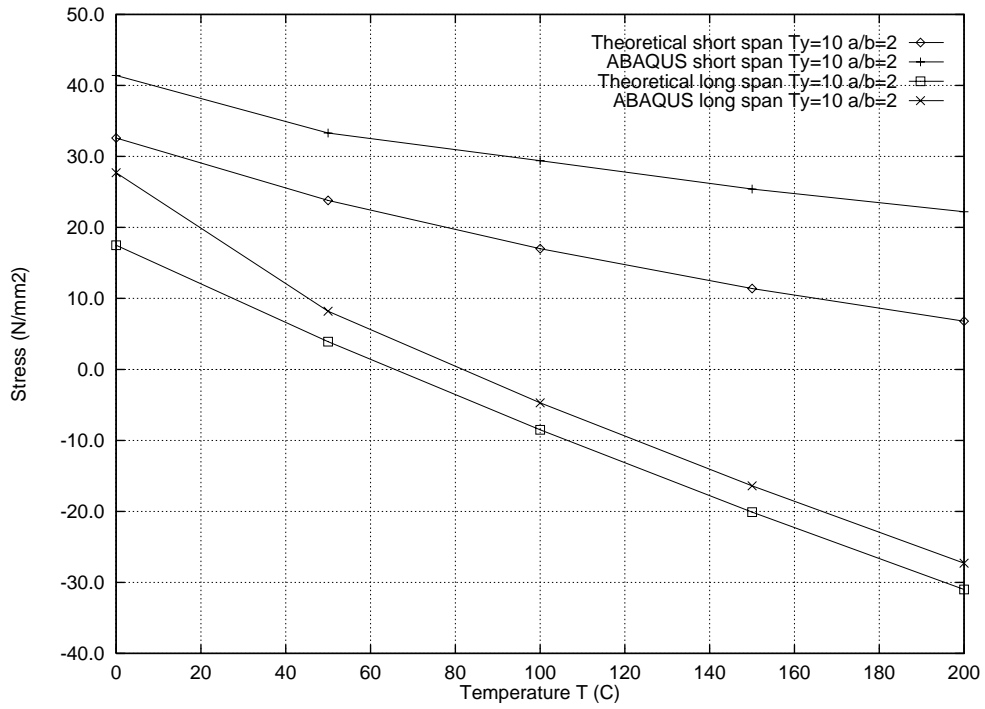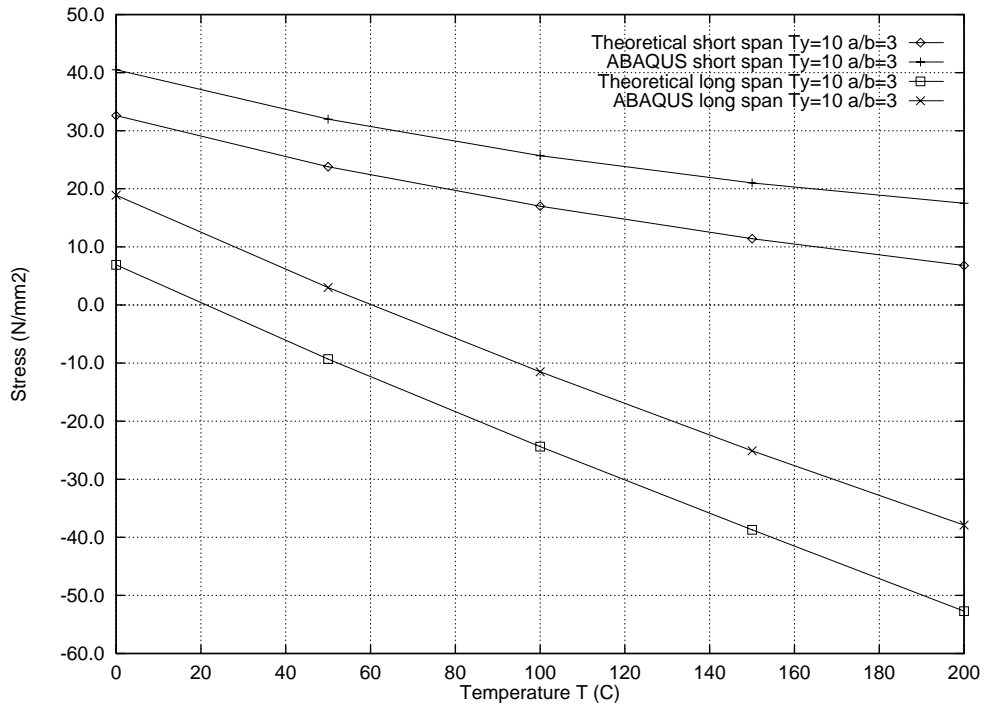compressive mechanical strains. These mechanical strains reduce the tensile stresses in the plate from the thermal bending. If the aspect ratio $\frac{L}{B} > 1$ then it can be seen that as the temperature of the plate ΔT increases the stresses in the longer span rapidly turn from being tensile to compressive. In the short span the rate of change from tensile to compressive is not so rapid. This is as expected due to the requirements of compatibility. Similar results were found when the Cardington tests were analysed.

Application to Design of Slabs for Fire

The failure limit state of a structural member is reached if the load carrying capacity is less than the applied load. As the temperature of a material increases, its strength and hence its load carrying capacity, decrease. Current design codes limit the temperature rise of a structural element so that its strength and therefore its load carrying capacity are not reduced. Although this does protect a building in the event of fire, when considered in the context of the fire resistance of the entire building, it is highly conservative. The fire resistance of a structural member in a fire resistance test is based on a limiting deflection. However, it has been shown that large deflections are largely a manifestation of the thermal strains and not a good indication of the load carrying capacity.[4] It is also important to consider the degree of redundancy of the structure. Modern buildings have a high degree of redundancy with the effect that the failure of one member will not result in the collapse of the entire building and alternative load paths will develop through membrane actions. Large deflections, due to thermal expansion, will allow load to be transferred through membrane action in the slabs from the weakening parts of the fire affected structure to the surrounding, stronger stiffer structure. It is important that this new knowledge of the real behaviour of floor slabs in fire and their importance in terms of the fire resistance of the entire building is transferred into design codes.

Current methods suggested for the design of slabs in fire do not take into account the actual behaviour of the slab in the fire. Wang[5] suggested a method for determining the tensile membrane action in floor slabs and used it to predict the fire resistance of a steel-framed building. Bailey's method[6,7] uses a yield line approach and applies an enhancement factor to the moment resistance of a section to take into account the effect of the membrane forces within the slab. Although Bailey takes into account the effect of the thermal strains within the slab he does this using a very rough approximation and only considers strains caused by thermal bowing.

For a design method to take into account the actual behaviour of a slab in a fire, good estimates of the deflected shape and internal stresses should be taken into consideration. By using the method presented in this paper to determine the magnitude of the deflection and the internal stresses in a slab it will be possible to use a 'rupture line' approach to determine the remaining strength of the floor slab and thus allow its ultimate capacity to be determined. There will be three stages involved in determining the ultimate load of the slab for a given fire.

1. Initially the deflected surface will be defined for a given temperature profile consisting of a thermal expansion ΔT and a thermal gradient $T_{,z}$

2. Define the yield capacity of a unit length of the deflected surface in both tension and flexure

3. Define probable 'rupture' patterns and calculate the most likely pattern based on the minimum energy required

This will be a significant improvement on the current methods proposed.

CONCLUSIONS

This paper has presented a nonlinear analytical method for analysing the deflections and internal forces of a floor slab in a fire. When compared to previous work it has been shown that it predicts the general behaviour of the floor well. It therefore allows a quick check to be made of results obtained from complicated finite element models or, where a finite element model is too expensive, for the behaviour to be calculated quickly and easily. Further work remains to be done to extend the method to composite floor sytems in modern steel frame structures. Preliminary ideas on the application of such a method to the design of floor systems in fire have been pesented.

REFERENCES

1. M. Gillie, A.S.Usmani and J.M.Rotter A structural analysis of the first Cardington test. *Journal of Constructional Steel Research*, 57:7581–601, 2001.

2. A.M.Sanad, S.Lamont, A.S.Usmani and J.M.Rotter Structural behaviour in fire compartment under different heating regimes - part 1 (slab thermal gradients). *Fire Safety Journal*, 35:99–116, 2000.

3. A.M.Sanad, S.Lamont, A.S.Usmani and J.M.Rotter Structural behaviour in fire compartment under different heating regimes - part 2 (slab mean temperatures). *Fire Safety Journal*, 35:117–130, 2000.

4. A.S.Usmani, J.M.Rotter, S.Lamont, A.M.Sanad and M.Gillie Fundamental principles of structural behaviour under thermal effects. *Fire Safety Journal*, 36:721–744, 2001.

5. Y.C. Wang. Tensile membrane action in slabs and its application to the cardington tests. In *Proceedings of the 2nd Cardington Conference 1996*.

6. Bailey C.G. and Moore D.B. The structural behaviour of steel frames with composite floorslabs subject to fire: Part 1: Theory. *The Structural Engineer*, 78(11):19–27, 2000.

7. Bailey C.G. and Moore D.B. The structural behaviour of steel frames with composite floorslabs subject to fire: Part 2: Design. *The Structural Engineer*, 78(11):28–33, 2000.

Session 3:
World Trade Centre and Multi-storey buildings

REVIEW OF THE PERFORMANCE OF FIRE-EXPOSED BUILDINGS IN THE WORLD TRADE CENTER INCIDENT OF SEPTEMBER 11, 2001

James A. MILKE, Ph.D., P.E.
University of Maryland. Department of Fire Protection Engineering, College Park, MD, USA

An overview of the results from the building performance study of the World Trade Center Towers will be reviewed. This review will concentrate on the performance of the twin towers, though will also describe the performance of other buildings in the area. This study has been conducted by a coalition of engineering organizations, including the American Institute of Steel Construction, Inc. (AISC), the American Concrete Institute (ACI), the Council on Tall Buildings and Urban Habitat (CTBUH), the International Code Council (ICC), the National Fire Protection Association (NFPA), the Society of Fire Protection Engineers (SFPE), the Structural Engineers Association of NY (SEAoNY), the Masonry Society (TMS) and the National Council of Structural Engineering Associations (NCSEA). The study is being led by the American Society of Civil Engineers and its Structural Engineering Institute. The study has consisted of a review of videotape records, eyewitness accounts, interviews with building design teams, a survey of the site and steel recycling centers, and the application of computer models. Based on this information, the goal of the study is to understand how the buildings collapsed and provide guidance for the future design and construction of similar structures. In order to develop the desired insights understanding, work is underway to understand how the respective buildings responded to the aircraft impact and the ensuing fire.

RESISTANCE OF TALL BUILDINGS TO LARGE AIRCRAFT IMPACT AND FIRE

Gordon M E COOKE BSc PhD CEng MIMechE MICE FIFireE
International Fire Safety Consultant, UK, London and Visiting Professor, School of Engineering, City University, London
gordon@cookeonfire.com

ABSTRACT

The demolition of the 420m high twin-towers of the World Trade Center on 11 Sept 2001 by terrorist attack has led structural and fire engineers to consider what might be done to reduce the consequences of terrorist attack against heavily-populated tall buildings by large, fuel-laden aircraft.

The paper discusses the different structural behaviour of the two principal forms of structure used in tall buildings – the cantilever core structure and, as in the WTC towers, the framed-tube structure – and comments on the susceptibility of both to massive horizontal impact and progressive collapse. Some data are presented on the missiles and the targets in the WTC incident and some estimates of local impact forces are made, and the author speculates on the effect of these impacts on the structure.

Structural features of some tall buildings in the UK, USA and Asia are given to illustrate differences in structural design. The hazard of progressive vertical collapse is considered in the context of what UK codes imposed on designers following the partial collapse of the Ronan Point block of flats in London in 1968.

 Comments are made on the vulnerability of steel and concrete to impact and fire caused by impact of aircraft, and indications are given on how vulnerability can be reduced. Finally some options are considered, ranging from the general to the specific, for protecting people in tall buildings.

KEYWORDS: *tall buildings, impact, fire, collapse, framed-tube building, cantilever core building, structure, World Trade Center, terrorism, Sept 11th*

INTRODUCTION

The demolition of the twin-towers of the World Trade Center (WTC) on 11 Sept 2001 by terrorist attack has led structural and fire engineers to consider what might be done to reduce the consequences of terrorist attack against heavily-populated tall buildings by large, fuel-laden aircraft. The combined effect of impact and fire led to collapse of both towers, the estimated loss of over 3200 lives including 350 firefighters, and estimated insurance losses of around $30 billion. It triggered world war against terrorism and retaliatory bombing in Afghanistan.

Large robust core
Structural wind-resisting core
Columns transmit no wind load
Small external column section size
Large column spacing
Small floor span
Floors act as diaphragms
Maximum daylight

Small core
Non-structural core
Non-robust core enclosure
Large external column section size
Deep external beam
Small column spacing
Floors act as diaphragms
Long floor spans
Large usable floor area
Possible shear lag effect

a) Cantilever core structure

b) Framed-tube structure

Figure 1 Comparison of cantilever core and framed-tube building

This paper does not speculate on the sequence of structural element failures in the WTC tower collapse since several sequences are possible, besides, the author does not have access to all the video footage, map of debris location, or witness statements. One scenario is that floor beams outside the core may have weakened in the fire allowing the floor slab to drop onto the floor below pancake-fashion causing progressive collapse of that area of the floor for all floors below that level. At some point the external grillage of columns , having lost the lateral support of the floors, would become unstable because of the greatly increased column buckling length, and the framed-tube, unable to sustain the load, would collapse. Another speculative, and perhaps unlikely, scenario is that several external columns were buckled outwards by a missile, e.g. an engine, exiting the façade. During the fire the out-of-plumb columns then deflected more away from the building stripping off the delicate floor-to-column connections allowing more gross deflections of the external grillage to occur and this may or may not have been compounded by later collapse of the floors pancake-fashion. A variety of comments have been made and scenarios proposed relating to the collapse of the WTC twin towers [1, 2, 3, 4].

This paper does, however, try to illustrate the main structural difference between the cantilever core structure and the framed-tube structure - forms mostly used in tall buildings - and describes, qualitatively, the vulnerability of these structures to missile attack. Figure 1 illustrates the main differences between the two types. Structural features (including external column sizes and floor depths) of actual buildings are described so that the reader can get a feel for their vulnerability to missile and fire attack.

THE WTC TOWERS

The twin towers of the WTC in New York, built in 1966/7, were roughly 60m apart and rose 420m and, in 1973, they were the tallest office towers in the world. The 110 stories contained almost 1million m^2 of office space and each tower was said to be capable of accommodating 50,000 people. Both towers were framed-tube structures in which the grillage of steel beams and columns forming the external wall carried all of the wind load.

The towers had external columns at nominally 1m centres and were prefabricated from steel plate in the form of a box with constant outside dimension 450 mm square. The wall thickness and grade of steel were varied in successive steps in the upward direction: wall thickness decreasing from 12.5mm to 7.5mm [5,6]. External beams (spandrel panels) interconnecting the columns comprised steel plate 1.2m deep. 12m below entrance level the external columns were combined, three in a group, to form single base columns spaced at three 3m centres and having an overall cross section 800 mm square. Prefabricated lightweight steel floor trusses were 900mm deep and spanned a maximum of 20m to the core. They were spaced 2m apart and laterally braced with secondary joists. Floors comprised 100mm thick lightweight concrete on profiled steel sheet decking. The service core was nominally 50m by 20m and was supported by 450mm square steel box columns which carried only gravity loads.

1993 explosion
On February 26, 1993, there was a terrorist-inspired explosion in the underground car park of the north tower which killed six people and left a crater 30m wide x 60m deep [7, 8]. There was immediate structural threat to seven columns, each nominally 450mm square, left

unbraced for distances up to 18m in some areas. These columns had been laterally braced by the car parking floor slabs which, in turn, were bracing the retaining wall**.**

To understand the possible consequence of the 1993 terrorist bomb in the North tower one must have an appreciation of the substructure. The WTC towers were founded on rock and involved the excavation of a massive volume of material and the construction of a 22m deep retaining wall around the site perimeter [9]. At the time the construction of a retaining wall of this depth in an area already well populated with buildings was a major feat and used the slurry-trench method for the 1m thick concrete wall. This involved excavating material while keeping the trench filled with Bentonite and then, when the full depth had been excavated down to bed rock, the trench was filled with concrete from the bottom up using the tremie method, and the Bentonite removed for reuse. In this way the walls of the trench were prevented from collapsing. As excavation for the towers proceeded, ground anchors (called tie-backs) were installed to provide lateral support to the exposed retaining wall. The anchors comprised steel tendons inserted into holes drilled at 45° and anchored in position by grouting them into 11m long drilled portions of the underlying rock, Figure 2. When the basement columns and floors of the towers were installed to the original ground surface, such that they provided lateral support to the retaining wall, the tie-backs were released.
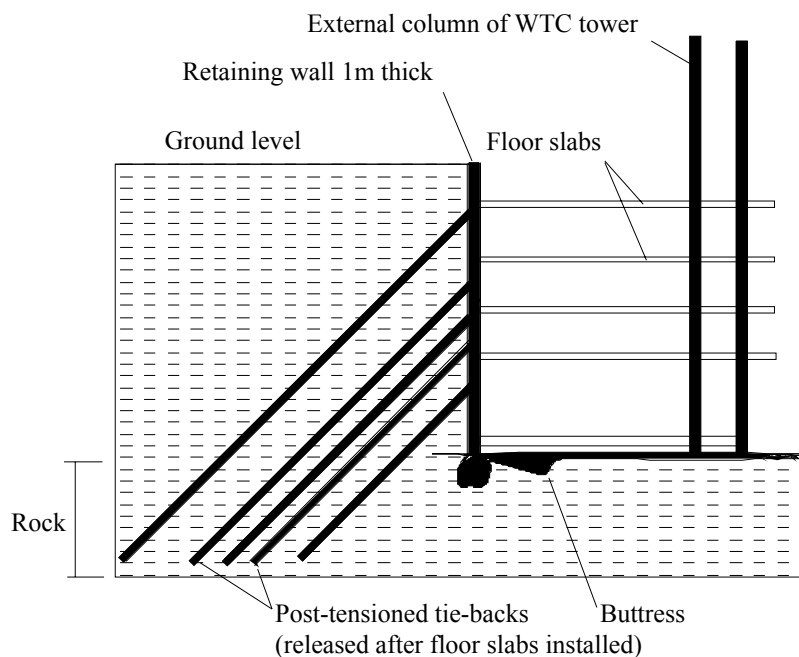
Figure 2 Section through retaining wall near WTC tower

Hence the subsequent removal of sub floors, as in an explosion, could remove the lateral support to the retaining wall which could collapse inwards putting the stability of the whole tower at risk. Fortunately this did not happen following the 1993 explosion. The explosion, however raised questions in some minds as to the wisdom of having towers so close to each other since collapse of one tower, from whatever cause, might destabilise the retaining wall and thus affect the horizontal restraint of the columns in the other tower, leading in turn to collapse of that tower, but this is, of course, highly speculative.

Sept 11th, 2001

On 11 Sept 2001 the 92nd floor of the North tower was hit at 8.45 am by a hi-jacked Boeing 767 passenger jet loaded with fuel. At 9.03 am the South tower was hit by a hi-jacked Boeing 757 at the 83rd floor. Both impacts were accompanied by a fire ball. The South tower collapsed at 10.05 am and the North tower collapsed at 10.30 am. The plan configuration of towers and aircraft is shown in Figure 3.

Site boundary and retaining wall

Impact 8.45 am
Collapse 10.28 am

North tower

Impact 9.03 am
Collapse 10.05 am

South tower
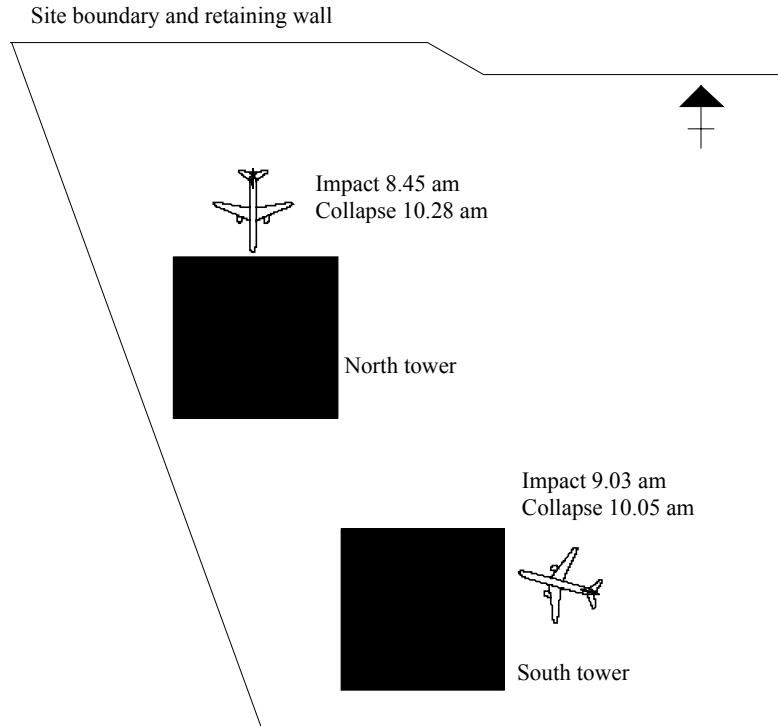
Figure 3 Location of towers and attacking aircraft

A nearby 47 storey building was also damaged, caught fire and collapsed later in the afternoon. The combined effect of impact and fire led to delayed collapse of both towers, the estimated loss of over 3200 lives including 350 firefighters, and estimated insurance losses of around $30 billion [10]. At the time of writing (4 months after the event) removal of the debris continues. It is remarkable and fortunate that so few of the potential building occupants were killed (nominally 3000 compared with a potential occupancy of 100,000)

 We can say that the towers were able to resist collapse from impact and that collapse was caused by the effects of fire on a severely distressed structure. It is difficult, however, to be sure about the mechanism of collapse or sequence of events because of the obscuring effect of the smoke and flames issuing from both towers, despite much external video footage. We believe that the floors of the WTC, like floors in most high-rise buildings, were not designed to resist progressive vertical collapse caused by one floor dropping pancake-fashion onto the floor below. We also know that vertical load bearing members i.e. columns can only support the axial load if they are laterally restrained by the floors at (usually) each floor level. Structural engineers will be aware that when the column buckling length is increased (as by the removal of lateral restraint provided by floor slabs), the Euler buckling load P reduces as the square of the effective length, assuming elastic behaviour:

$$P = \frac{\pi^2 EI}{L^2} = \frac{K}{L^2}$$

where K = Constant
　　　L = effective length of column

TWO TYPES OF BUILDING STRUCTURE

Although there are hybrid forms, the structure of tall buildings can be divided into two main types: the cantilever core building and the framed-tube building. Figure 1 shows these structural forms. For a given building foot-print the objective is to minimise the area taken up by the core in order to maximise the usable floor area outside the core. To maximise daylighting and simplify services, all the services – stairs, elevators, toilets, and circulation routes – are normally placed within the core which is positioned centrally. Floors are usually simply-supported because of their large span and, for rectangular floor areas, half the dead and live floor loads are carried by the external columns and half by the core. Live floor loads are usually in the range 5 to 8kN/m^2 for office occupancies.

Cantilever core
In the cantilever core building all of the overturning moment due to wind load is resisted by the central core; the external columns only transmit dead and live loads associated with the floors. The core is typically a heavily reinforced concrete 'tube' produced by slip-forming and penetrated by door openings at each storey level. Wind forces are transmitted by the cladding to the external beams and columns, then to floors, then, usually by diaphragm action, to the core, then by flexural action to the raft and piles. The load path is reversed if there is an earthquake. The external columns can be widely spaced around the perimeter of the building and their spacing may be dictated by the spanning capabilities of the floor system used. Since the columns are not required to transmit large bending moments (as in the framed-tube) they can also be small in section size. As in all multi-storey framed buildings, the floors give lateral stability to the columns, and the columns support the floor edge – they are mutually dependent – and this has implications for progressive collapse (see below).

Framed-tube
In the framed-tube building the external beams and columns are sized to transmit in-plane bending moments resulting from wind forces, and the columns additionally carry gravity loads from the floors. The beam/column joints in the external wall have to be moment-resisting to resist wind loads and this, together with the need for rapid erection, normally means that off-site welded fabrications of tree-columns have bolted connections at mid-column height where there is a point of contraflexure (position of zero bending moment). The nature of bending moments and shear forces for part of a framed-tube is shown in Figure 4, the bending moments, shear forces and section sizes diminishing with height above ground. Tree-columns of three-storeys height were used in the WTC towers. The service core normally transmits only gravity loads (except in hybrid forms as in the Petronas towers, which are discussed later, in which the core is also a framed-tube). Hence the service core can be constructed on simple beam and post principles and, unlike the heavily reinforced cantilever core, can be clad in lightweight construction which would be very vulnerable to damage by any horizontal missiles which managed to penetrate the external framed-tube grillage

PROGRESSIVE COLLAPSE

The removal of a primary structural element such as a column, beam or load-bearing wall, can have a disproportionate effect on the rest of the structure.
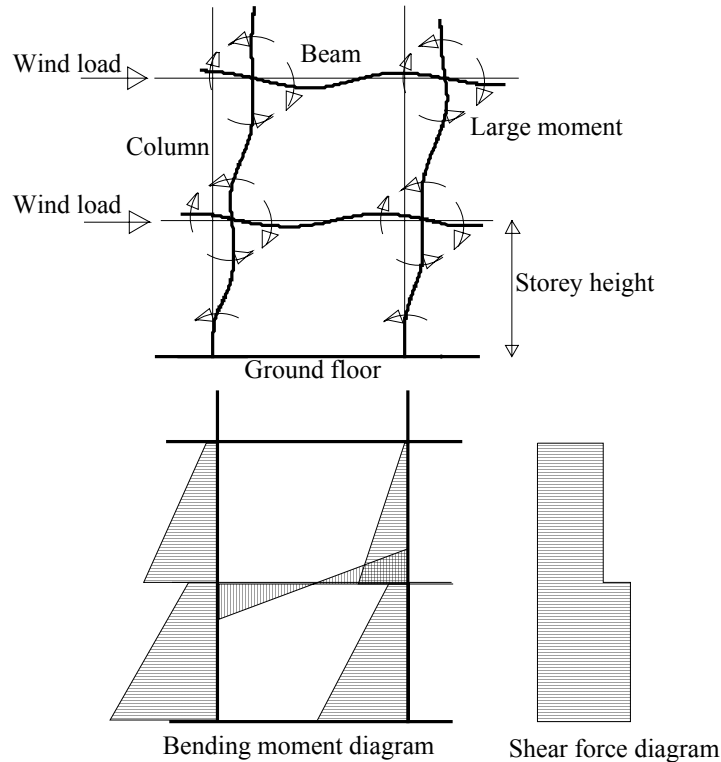
Figure 4 Nature of bending moments and shear forces in part of framed-tube

Progressive collapse is inevitable if floors collapse onto the floor below causing a dynamic load many times greater than the static load normally designed for. Once collapse begins it cannot be stopped, unless strong floors are incorporated. Many office floors are designed to carry a vertical live load of only 5kN/m^2 plus a small additional load (e.g. 1.5 kN/m^2) to allow for the weight of moveable partitions.

Progressive collapse was demonstrated in the UK by the collapse in 1968 of one corner of the 22-storey Ronan Point block of flats in London. Triggered by a gas explosion on the 18th floor, the corner of the building collapsed from roof to ground level killing four people. The building was formed from large precast wall and floor panels and the collapse revealed that the panel joints were designed to transmit wind pressure at 12 lb/ft^2 whereas explosion pressures were subsequently shown to be 30 to 100 times this pressure. The Report of the Inquiry [11] recommended that designs should take account of alternative load paths when a primary structural member was removed, and building regulations were changed to require design against progressive collapse in buildings more than 5 storeys high. These regulations mean that the designer must show that removal of a primary floor beam does not lead to collapse of the floor, and this means the floor has to be designed with a high level of reinforcing continuity steel in order to span two bays instead of one. Currently (February 2002) there are UK government proposals [12] to extend the requirements so that they additionally apply to certain buildings, e.g. hospitals, irrespective of number of storeys.

However the requirements are not intended to guard against collapse caused by one floor falling onto the floor below and so on – a scenario which seems likely in the WTC disaster - and it is, in the author's opinion, unlikely that a floor designed according to the Ronan Point recommendations would resist progressive collapse caused by one floor falling onto the floor below unless the upper floor sagged slowly onto the floor below, minimising the dynamic loading effect – a mechanism one would like to have, but is unpredictable since floors are not yet intentionally designed with this failure mode in mind.

A missile such as the engine of a passenger jet would, the author believes, easily remove a column in a cantilever core building owing to its slender shape and size. According to UK codes, removal of one column should not lead to progressive collapse, but it seems likely that removal of two or three horizontally-adjacent columns would precipitate collapse unless there was high degree of redundancy in the structure and negligible wind load acting at the time. Progressive collapse in such a building, however, would be confined to the floors outside the core, but the core and its contents would remain standing since penetration of the core such as to cause progressive collapse of floors within the core is unlikely assuming the core floors are cast insitu and thus robust. Progressive and unconfined collapse of floors outside the core could be limited by the use of strong floors placed, say, every 10 storeys. These strong floors, perhaps constructed as storey-high vierendeel girders cantilevered from the core, could also be used as safe refuges for evacuation purposes. There are strong floors in the London NatWest office tower described later, though not designed as refuges.

IMPACT FROM AIRCRAFT

To be realistic this paper considers the missiles used in the 11 Sept hi-jacking incident. The Boeing 757 and 767 passenger jets involved are very similar [13].
Both are low wing aircraft with one podded turbofan engine under each wing, and the following gives information essential to understand the missile-like properties of these aircraft. Engines are by Rolls Royce or Pratt and Witney, weigh around 4400 kg each and are roughly 3m long by 2.2m diameter. The engines are spaced roughly 10m apart. The wing span is approximately 40m, the overall length and height of the aircraft is approximately 45m and 13m respectively. Maximum take-off weight is around 100,000 kg and approach speed with flaps down is in the range 150-250 mph. The 767-400ER for example can carry 300 passengers within a maximum range of about 6000 miles. A fuel capacity of approximately 40,000 litres is possible for a 757, which corresponds to about 25 tonnes. A plan view and front view of a Boeing 757 are shown in Figure 5

The force arising from an impact can be calculated from Newton's Second Law of Motion: force = mass times deceleration,

$$F = ma \ (N) \tag{1}$$

where m = mass (kg) and a = deceleration (m/s^2)
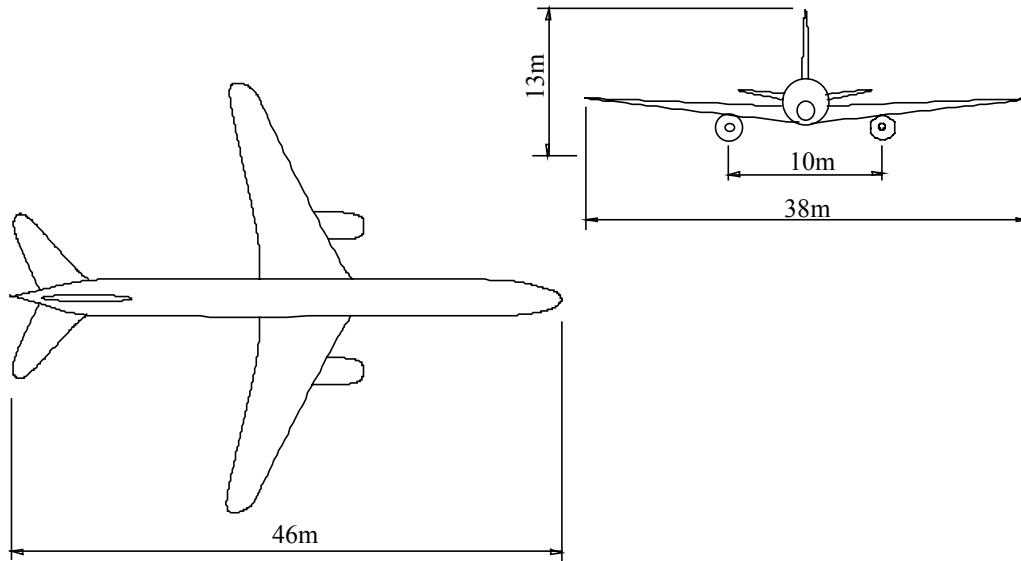
Figure 5 Main dimensions of a Boeing 757-200 twin turbofan passenger jet

Consider just one jet engine weighing say 4000kg and moving at 250mph. Assume that all parts are decelerated over a period of 10 milliseconds (this is a big assumption). Then, as 1mile = 1609m:

$$F = \frac{4000 \times 250 \times 1609}{0.010 \times 3600} = 44.7 \, MN$$

The impulse force is approximately 44.7MN (approx. 447 tonneforce). This is an enormous force. In a sense it is a theoretical force since the target would, arguably, have to be massive and unyielding to cause a deceleration of 10 milliseconds. The duration of impact is clearly important: the nose-to-tail crumpling time of a 43m long 757 aircraft fuselage travelling at 250mph perpendicular to the target is 0.384 seconds assuming the target does not move.

So we may know the mass of the missile (say an engine or a fuselage) but to quantify the force imparted by the missile we must how the missile and target interact as this affects the deceleration of the missile. Unlike a bullet which may be designed to imbed itself in a target giving all its momentum to the target, a turbofan engine contains hundreds of fan blades moving at high speed and on impact the blades would explode radially due to centrifugal force and some of the concentrated mass would be lost. Thus on impact a turbofan engine would impart its linear momentum to the target and at the same time produce many lethal fan blade missiles travelling radially outwards. The fuselage on impact would crumple from front to back and could be regarded as a large area, soft body impact.

Figure 6a shows the longitudinal distribution of mass/unit length for a Boeing 707-320 from which it is clear that most mass resides in the wing area due to the engines, the fuel tanks and the wing construction itself: compare Figure 5 with Figure 6a.
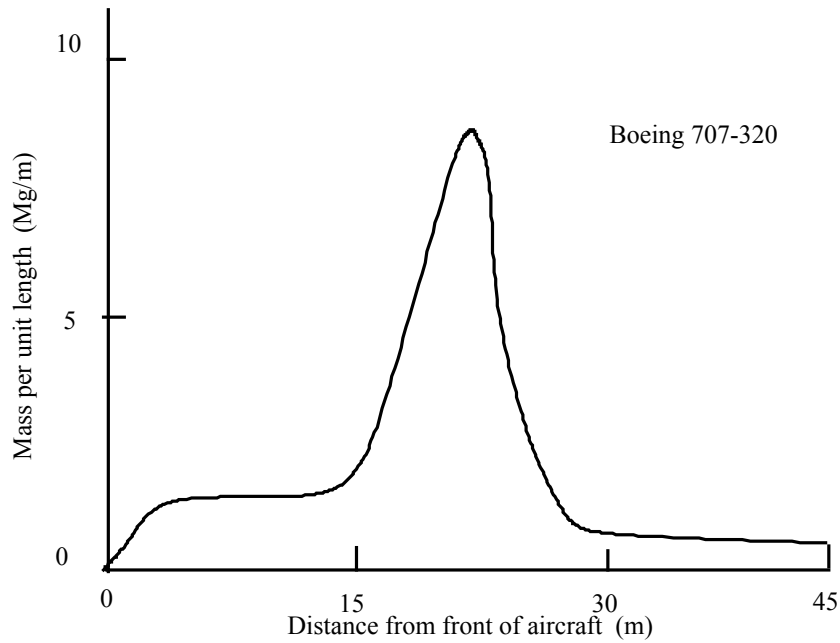
a) **Variation of mass along 707 aircaft**
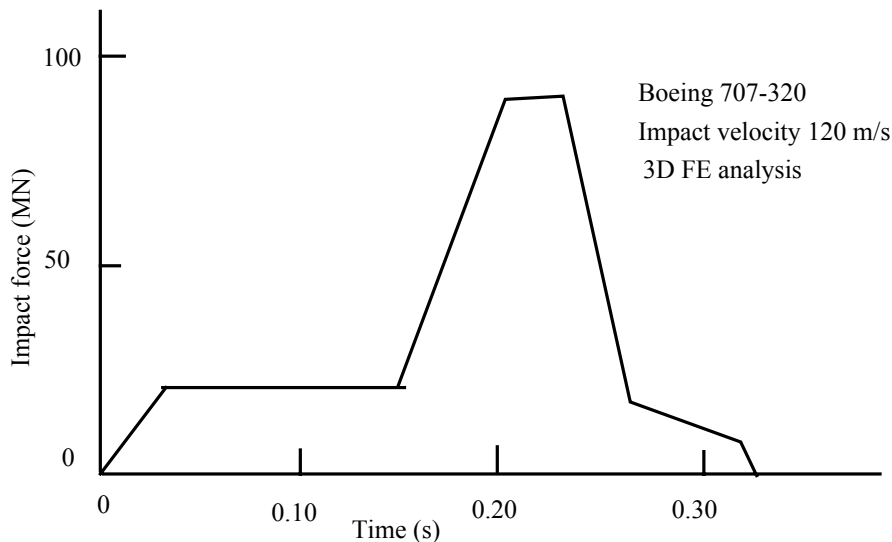
b) **Variation of impact force with length**

Figure 6 Mass and impact force data for a Boeing 707 passenger aircraft.

Since F = ma it is not surprising to find that the curve of impact force with time, Figure 6b, approximately overlays the shape of the curve of mass with longitudinal position. Figure 6b is the impact force computed with a finite element computer program assuming the target is rigid [14]

To make calculations of impact force is difficult. We may know the approach speed of the missile, say 250 mph for a hi-jacked 757 which to gain accuracy of impact position has been slowed down but is still above the stalling speed. But questions arise over the time of deceleration. Is all the linear momentum of the missile imparted to the target as when the missile is embedded in the target, or does the missile or part of it pass through the target? Does the target or part of it behave elastically, instantaneously accelerating away with the

missile so reducing the effective deceleration of the missile and the peak force imparted by it? The time period over which the impulse force acts is clearly important and depends on the crushing behaviour of the missile and target. Back-of-envelope calculations can give spurious answers because of the unknown impact duration time, and computer programs are normally used in such studies. In rare cases full size impact tests are carried out.

Figure 7 Silhouette of Boeing 757 against WTC external beam/column grid

Figure 7 gives the relative scale of the fuselage and two engines of a Boeing 757 and the array of beams and columns on the front face of the WTC tower. It will be recalled that the columns were at 1m centres and the storey height was approximately 3.75m. Without advance warning so that the building can be evacuated, it its clear that nothing can be done to avoid loss of life outside the service core within the two or three storey zone impacted by a passenger jet travelling at 250 mph. There are however a large number of columns to resist penetration
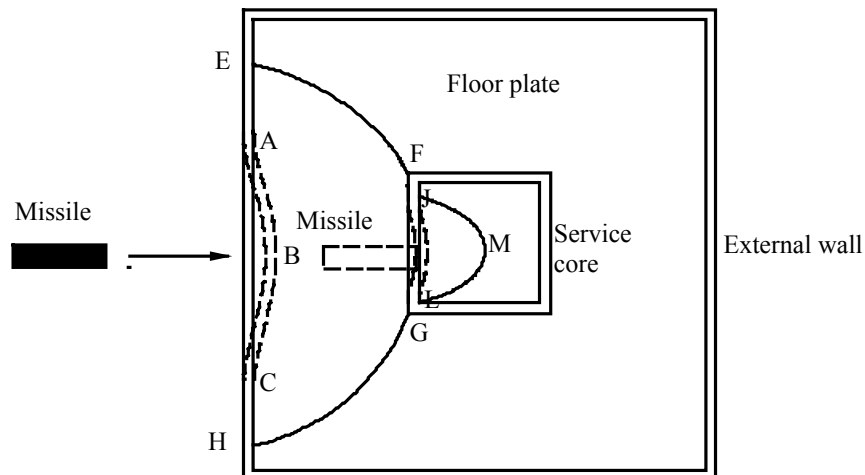

Figure 8 Missile penetrating to service core

A missile could rip through one façade and bury itself in the service core, as shown in Figure 8, or, depending on the robustness of the external columns and the trajectory of the missile

(an engine or other heavy object), the missile could conceivably rip through one façade and emerge from the opposite façade having missed the service core, Figure 9.

In the case of a framed-tube structure, the missile on entering the façade will instantaneously make the façade framework behave as a tensile network involving catenary forces in the portion ABC in Figure 8. Any bolted joints in the beam/column assembly (used at the junctions of the 3-storey tree-columns in the WTC towers) would fail since it is unlikely they would not have been designed for large catenary forces. Instantaneously the floor slab (area EFGHE in Figure 8 and its support beams would also be placed in compression and would be expected to fail in buckling. In particular, light steel floor trusses, as used in the WTC towers, would suffer torsional instability. Assuming the missile penetrated the façade it is possible that the missile would damage the core, perhaps in the area FMGF in Figure 8, but such damage

would be negligible in the reinforced concrete core of a cantilever core building. The missile might not be in line with the service core and could enter and exit the façade, Figure 9, creating catenary forces in both facades.
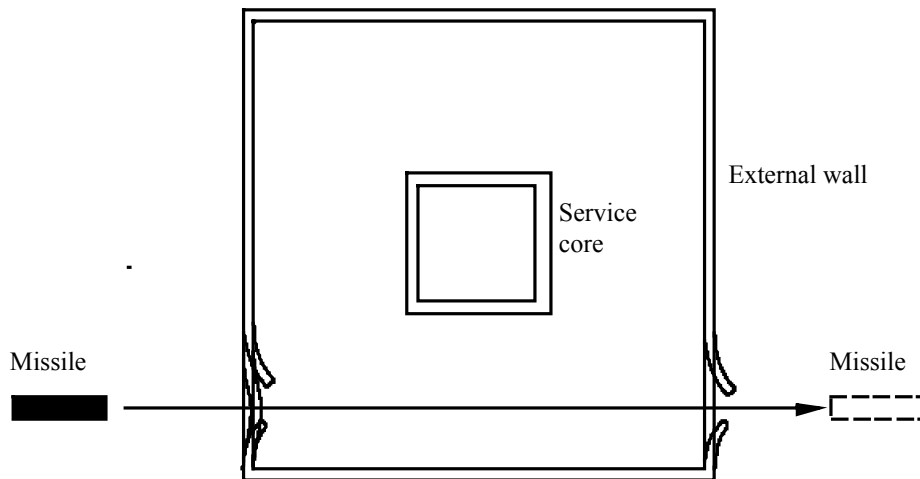
Figure 9 Missile penetrating both facades

The damage area will inevitably be large and in the case of the WTC façade many columns would be affected as shown in Figure 7. However a missile could more easily penetrate between widely spaced external columns in a cantilever core building resulting in a greater impact force on the core.

COMPARISON OF WIND AND IMPACT FORCE

It is interesting to compare the wind force acting on the WTC tower in a strong wind with the force produced by the impact of a passenger jet. The WTC tower is 420m high by 63.5 m wide. The wind pressure on a building 35m above ground level is nominally $1kN/m^2$ for a wind speed of 40m/s (90mph) [15] and if we assume for simplicity that this acts over one face of the building, we have a wind force of 27,000kN (ie 420 x 63.5 x 1.0) or 27MN. Of course, the wind pressure varies with height and terrain (BS 6399: Part 2), but the simplifying assumptions made are adequate to get a feel for the magnitude of the forces acting. We saw from Figure 6b that the computed maximum impulse force generated on

impact of a Boeing 707 was almost 100 MN for impact on a rigid target at 120m/s. A WTC tower could not be regarded as a rigid target and the impact force of a 707 would probably be less than the wind force calculated above. In the USA it is common for buildings to be designed to resist earthquakes and hurricanes with 100 mph wind gusts

POST-IMPACT FIRE

Any passenger-carrying aircraft large enough to cause serious impact damage to a tall building will be carrying a substantial amount of aviation fuel, even near the end of its planned flight. It will also carry cargo which may be commercial in nature or passenger baggage. In a strictly fire safety engineered design, the design fire – the starting point of design –should take account of the total fire load (building contents plus combustible portions of the aircraft retained in the building), the different rates of heat release of the fuels (building and aircraft) and different ventilation factors. Generally, and this is clear from the well-known equations for compartment fire severity which express the time-equivalent of fire exposure in terms of fire resistance [16], the larger the ventilation opening the lower the fire severity.

What can we say about the ventilation and fire load immediately after impact? We may assume that flying debris from aircraft impact removes most of the glazing except perhaps that shielded by the core structure, and that the fireball and the resulting thermal shock will remove the rest. It would be convenient for analysis purposes, and for peace of mind, to assume that in terms of fire severity the increased fire load imported into the building impact area by the aircraft would be compensated by the increased ventilation. However, whereas it is relatively easy to assume a ventilation factor for the external wall after impact (e.g. that all the glazing is absent in a storey), it is clearly much more difficult to estimate what the fire load density will be bearing in mind the fluid nature of aviation fuel and it's ability to flow down lift shafts and staircases, if not by other routes, into lower floors. Hence fire will occur on several floors due to the flow of fuel to lower floors, and this complicates any analysis of fire severity and the effect upon the structure. What we can say with certainty is that the ventilation formed by the removal of glazing in the external wall will be much less in the framed tube building than in the cantilever core building simply because in the former the massive beams and columns take up a larger portion of the façade area, and thus the fire severity would be greater, other things being equal.

What we can assume is that fire will only burn and produce heat if there is an adequate supply of air, and this commonplace has implications not only for fire severity but also duration of the fire. In a compartment fire with conventional fuel such as office contents, a naturally developing fire will begin in the item first ignited in one area of a floor and gradually spread to other areas perhaps over a period of 20 or more minutes, accelerating after flashover to involve all the compartment contents. The import of aviation fuel, however, will mean that a large area fire will occur instantaneously when the fire ball inevitably occurs and all the compartment contents catch fire. However it does not follow that the whole area will continue to burn if there is insufficient air to feed the innermost areas of the fire, and this was shown in experiments that the author arranged in the UK Building Research Establishment's Fire Research Station large laboratory at Cardington. In these tests, which used 33 one metre square timber cribs as the fire load in a 23m long compartment 3m high and 6m wide with a ventilation opening at one end 6m wide, it was shown that, after flashover, the burning behaviour of the cribs was the same for the test when 3 cribs at the rear of the compartment were ignited as for the test when all 33 cribs were

ignited simultaneously [17]. In the test in which the 33 cribs were ignited simultaneously (corresponding to a large area fire with limited air supply) it was observed that, after flashover, only the cribs near the ventilation opening appeared to be burning while the cribs behind stopped flaming because of oxygen starvation but continued to pyrolyse due to the heat. In other words burning remote from the air supply slowed down. In a building the size of the WTC tower (nominally 65m square) it is possible that fire near the core was not burning as severely as at the perimeter due to restricted air supply, unless the core was itself a source of air supply.
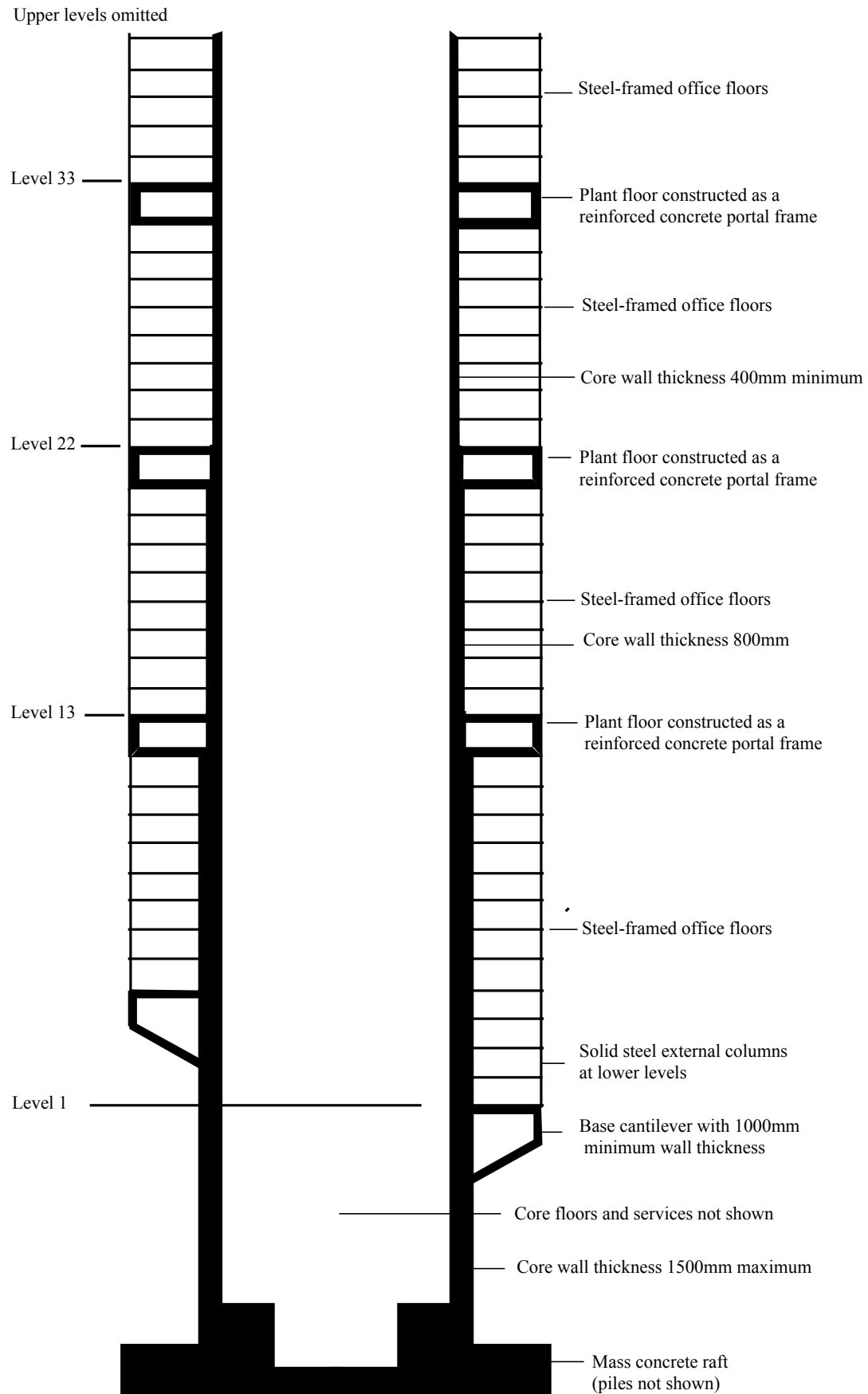
Modern tall buildings may have been designed to withstand a burnout of the contents with a hidden safety factor added to allow for the excessive height of the building, and it is common for such buildings to require a structural fire resistance of at least 90 minutes, with or without automatic sprinkler protection.

EXAMPLE OF CANTILEVER CORE BUILDING

The 173m high NatWest office tower in the city of London is a good example of a cantilever core building and probably remains the tallest cantilever core office tower in the UK even though it was completed in the 1970's. It has an unusual external appearance as it has office floors in 3 distinct leaves springing from a central core at three levels [18]. As usual the central core houses lifts, staircases and toilets. The office floors are separated at levels 13, 22 and 31 by deep intermediate plant floors designed as portal frames which serve the floors above and below, Figure 10. The tower is designed as a cantilever to withstand wind forces and periodic vortex shedding and is founded on a concrete raft supported by 27m long 1.2m diameter piles.

The heavily reinforced core wall varies in thickness from 1500mm at the base to 400mm at the top and can therefore be regarded as very robust against aircraft impact and, resulting from this, immune to progressive collapse of floors within the core. Again, the three base cantilevers are extremely robust, being 9m deep at root and 7.1m deep at tip. The office floors comprise 306mm deep I-section floor beams spanning a maximum of 10m with composite 117mm thick normal weight concrete incorporating continuity steel on profiled metal deck. The floor is designed to support a live load of 8kN/m^2 and so that, in common with other buildings designed after the Ronan Point disaster, a floor beam could be removed without affecting the stability of the system. External stanchions are 250mm x 200mm solid laminated steel at lower levels and 203mm universal column sections at upper levels and are at 3m centres. Perimeter beams are 152 x 152 x 37kg UC sections

The incorporation of a robust cantilever service core, the incorporation of immensely robust base cantilevers, robust service floors at three levels (which would probably arrest the progressive collapse of floors in between), and the use of continuity steel in the composite floor slabs, all indicate that the building is, perhaps fortuitously, likely to be very robust against catastrophic damage by large aircraft impact. Perhaps 2 or 3 floors would be demolished in the impact and fire but the building would remain standing and progressive collapse of floors minimised. It is difficult, however, to say if the stairs above the impact zone would remain usable, because of the unknown response of the fire doors to flying debris and fire.

Upper levels omitted

Steel-framed office floors

Level 33

Plant floor constructed as a
reinforced concrete portal frame

Steel-framed office floors

Core wall thickness 400mm minimum

Level 22

Plant floor constructed as a
reinforced concrete portal frame

Steel-framed office floors

Core wall thickness 800mm

Level 13

Plant floor constructed as a
reinforced concrete portal frame

Steel-framed office floors

Solid steel external columns
at lower levels

Level 1

Base cantilever with 1000mm
minimum wall thickness

Core floors and services not shown

Core wall thickness 1500mm maximum

Mass concrete raft
(piles not shown)

Figure 10 Cross section through core of NatWest cantilever tower.

EXAMPLES OF FRAMED TUBE BUILDINGS

One Canada House, commonly called Canary Wharf, is now the best known tall building in London, United Kingdom, and is a good example of a framed-tube building. The 244m high office tower with 50 floors can accommodate 11,600 people [19]. It was topped out in 1990. It employs the framed-tube concept so that the core is freed of any bracing function and is compact resulting in high rentable-to-gross floor area ratio. This means the interior framing for the service core is designed solely for gravity loads . The tube is formed from I-section steel members in grade 50 steel. The columns are typically 700mm wide by 400mm deep while the spandrel beams are 1000mm deep by 250mm wide. Like the WTC towers these members were formed into 3-storey high column-trees off-site. A typical floor beam is 456mm deep with a 140mm semi-lightweight concrete topping on trapezoidal metal decking

Three further towers are being built at Canary Wharf. [20] One is tower DS5, the 45 storey office block to be known as 25 Canada Square, and the other two are to be 33 storeys high. Interestingly, all three will incorporate a cantilevered concrete core rising from a piled raft to carry all wind loading, and the external steel framing will carry only gravity loads, unlike One Canada House, the first Canary Wharf tower. The new towers will have almost clear façades because the external columns can be much smaller and are spaced 9m apart. Typical floor beams are 457 UB sections spanning onto 610mm deep UB perimeter beams. The steelwork is spray fire protected. The floor slabs in the superstructure are formed with 130mm thick mesh-reinforced lightweight concrete on profiled metal deck to give 90 minute fire resistance. Although these buildings use cantilever cores, and in this respect are less vulnerable, in the author's opinion, to collapse from aircraft impact than their framed-tube counterparts, the cores are split-cores joined with link beams which may not be as robust as a single core of the same overall size. More importantly the 9m wide spacing of the external columns means that it will be more difficult to withstand missile damage to the external frame and this may have implications for progressive collapse of the floors.

EXAMPLE OF HYBRID FRAMED-TUBE BUILDING

The twin 452m high Petronas towers in Kuala Lumpur city centre are hybrid framed-tube buildings in which the cantilever core carries half the wind load and the external framed-tube carries the other half [21]. At the time of writing (February 2002) the towers are the tallest in the world. Each tower rests on a concrete raft 4.5m deep supported by 104 bored piles some 60 to 115m deep. The towers are circular in cross section and employ 16 large diameter cast insitu circular-section, high strength reinforced concrete columns spaced 8 to 10m apart around the perimeter together with reinforced concrete ring beams to form the framed-tube. Each core has two web walls in a cruciform arrangement and heavily reinforced corners and provides a fire rated shaft. Floors comprise long span steel beams with metal deck topped with normal weight concrete of nominal thickness 110mm for the 90 minute fire resistance needed. The perimeter columns are massive, being 2400mm diameter in grade 80 concrete at the bottom and 1200mm diameter in grade 40 concrete at the top of the towers (grade 80 means that the concrete has a cube compressive strength of 80Mpa – almost three times the strength of concrete used in most low-rise projects). The close spacing and large diameter of the columns means that windows are narrow and this reduces solar heat gain and provides much-wanted shading. The size and structural continuity of the columns therefore present, in the author's opinion, an effective barrier to missiles and, provided there was not massive

spalling following an aircraft strike, the behaviour in fire should also be good because of the slow heating rate of the massively-sized concrete members.

Each tower is fully sprinklered to NFPA 13 specification and has its own water reservoir in the basement which is mains-fed. The towers are linked by a sky bridge which serves as an egress route and refuge in case of fire. Using the sky bridge and shuttle elevators the building staff can evacuate occupants both vertically and horizontally. The strategy is to use phased evacuation of the fire floor, the floor above and the floor below. Perhaps this strategy will be reconsidered in the light of the WTC disaster.

RESEARCH NEEDED

There seems to be a paucity of published research into the severity of fires involving the burning of aviation fuel in building compartments. As far as the author is aware, fire tests have been conducted with small trays of fuel in compartments but not for the purpose of assessing fully developed fire conditions in office-like scenarios. If this is so he believes it important to make experiments to determine the heat transfer properties of the combustion gases and flames and, importantly, the heating rates of concrete and steel members exposed to such fires. If it could be shown that the severity of burning aviation fuel can be simulated, with reasonable accuracy, using the standard hydrocarbon time-temperature relation used in fire resistance testing, this would be a useful step forward.

The WTC disaster, the author believes, has shown that conventionally designed floors can collapse progressively, pancake-fashion. Floors have to stay in place if lateral instability of loaded columns is to be avoided so that whole-building collapse does not occur. Research is needed to establish if it is technically and economically viable to design floors so that they fail safe when exposed to fire. The WTC floors only collapsed well after the impact i.e. as a result of fire.

SUGGESTIONS

Every building is different. Missiles, or parts of them, are different depending on the particular aircraft design and the cargo and fuel it is carrying. It follows that it is impossible to give generic guidance that in all cases makes a building more resistant to missile damage. The following list is intended to give some ideas on what might be done, and it covers structural and non-structural measures.

- Limit the height of all tall buildings, especially icon buildings, and plan developments so that no single building rises prominently above its neighbour thus making it difficult to target an individual building.
- Perform a risk assessment for the building which includes extreme events such as accidental or malicious impact by large aircraft. This should allow for impact at any storey level and at any orientation in a horizontal plane. Arguably it should consider the worst case scenario for the additive effects of strong wind and missile impact.
- Ideally, design the building specifically to cope with large horizontal impacts. If not, at least check its vulnerability. Consider how the external wall and floors might behave as a missile enters the building and exits the building.
- Consider the effects of removing adjacent primary structural elements by a thorough understanding of alternative load paths and load effects.

- Design each tall building with a service core that acts as a laterally robust structural cantilever, e.g. as in the Natwest tower in London. Avoid designs using a delicate framed-tube construction.
- Where hybrid cantilever core/framed-tube construction is used, avoid the use of tree-columns which have stub-beam bolted connections unable to resist catenary forces arising from a horizontal impact from outside to inside and from inside to outside.
- Employ structurally robust external columns, e.g. as in the Petronas towers, so that a minimum number of columns are destroyed.
- For external columns consider the use of large diameter, high strength, reinforced concrete columns or, as practised in Australia, large welded-plate steel box columns filled with concrete[22].
- For reinforced concrete structural elements, consider including additional layers of anti-spalling steel mesh and/or the use of concrete-embedded fibres of steel or polypropylene to reduce spalling caused by impact and/or fire.
- Avoid using spray or board fire protection for structural steel beams and columns in which the protection can be easily removed by impact, flying debris or gross deformation. Do not use intumescent fire protection for primary structural elements unless it can be proved that the system is particularly robust.
- To avoid progressive collapse, design floors to behave as tension membranes in the fire limit state and check that floors are strongly connected to the external framework so that the catenary force can be carried and pancake collapse cannot occur.
- Avoid the use of lightweight structural steel members in floor construction which, stripped of their fire protection, heat up rapidly in fire.
- Avoid floor designs that have little in-plane resistance to compression caused by horizontal missile impact, eg avoid light steel truss floors which have little resistance to local buckling and torsional instability as in the WTC towers.
- Avoid floor-to-wall connections that allow the external wall framing to be easily torn away from the floor construction when a missile exits the building.
- Develop design concepts for floors so that progressive vertical collapse cannot occur. This is of the utmost importance.
- Avoid building deep basements if progressive collapse of upper floors cannot be prevented, especially if there are tall buildings nearby. Basement retaining walls can collapse inwards if basement floors collapse so removing the diaphragm action, and this may make buildings nearby unstable.
- Avoid materials used for enclosing the central services core, especially escape stairs, which can be easily penetrated by missile debris.
- Review evacuation strategy – phased or simultaneous
- Include more staircase capacity but with vertically independent zones so that any smoke logging is confined in vertical extent.
- Include safe refuges in certain storeys.
- Maximise the person-holding capacity of the service core.
- Reconsider worldwide policy not to use elevators for escape from fire. In particular, consider greater use of elevators which serve a limited number of storeys so that some remain operational after the impact.
- Avoid placing sprinkler tanks at roof level if bursting of the tanks can lead to excessive loads applied to floors below causing progressive collapse of floors.
- Discount the effect of conventional sprinklers as they would be overwhelmed in a large area fire of the kind associated with burning aviation fuel, assuming the distribution pipework had not been disrupted in the impact. To include a foam fire suppressant would

probably be considered unjustified when considering the low probability of a missile strike.

- Employ individual battery-powered emergency lighting luminaires throughout the building so that a missile strike at night would not leave occupants without light to escape. Avoid reliance on standby generators or central battery packs especially for emergency lighting systems in staircases since these are likely to be destroyed in an impact. Fortunately this is becoming common practice in the UK.
- Provide fire fighters with more education on structural aspects of building design
- Provide fire fighters with advance information on the structural form of the building and the likely resistance of the building to progressive collapse. This should be feasible for UK designers who have to prepare a fire risk assessment under the CDM regulations.
- Carry out large scale experiments in compartments to quantify the thermal severity of aviation fuel fires for a variety of ventilation conditions, for we should not assume they are simulated with the hydrocarbon fire used in standard fire resistance testing

CONCLUSIONS

It is clear from the experience of the WTC disaster that a tall building can be designed to resist collapse immediately upon impact and in the absence of fire. It is also clear that a tall building which has a severely distressed structure and a disabled fire suppression system can collapse due to the effect of fire resulting from the burning of the building contents and the imported fuel.

The susceptibility to collapse has been considered for two forms of structure commonly used in tall buildings. It is suggested that total collapse is less likely for a cantilever core building than for its framed-tube counterpart. Progressive collapse of floors appears to be the most difficult problem to solve and should be the subject of design studies and testing to quantify realistic options for preventing or limiting the extent of progressive collapse.

Some suggestions, not confined to structural measures, are made which could reduce the effects of aircraft impact and fire on tall buildings. Their adoption depends on the probability attached to the likelihood that accidental or malicious impact by large, fuel-laden aircraft will occur during the lifetime of the building – a difficult question to answer – and, of course, on the cost of the added safety measures.

REFERENCES

1   Alexander S, World Trade Center – an initial appreciation, *New Steel Construction*, Vol 9, No6, Nov/Dec 2001, p17

2   Clifton C, Demolition of the Towers, *New Steel Construction*, Vol 9, No6, Nov/Dec 2001, p 18-22

3   Pope R, Destruction of buildings by terrorism, *New Steel Construction*, Vol 9, No6, Nov/Dec 2001, p 23

4   Soane S, What future for tall buildings, *The Structural Engineer*, Vol 79, No 20, 16 Oct 2001, pp13-15

5   Godfrey G B (editor), Multi-storey buildings in steel, 2nd edition, Collins, London, 1985

6   Feld L S, Superstructure for 1350 ft World Trade Centre, *Civil Engineering – ASCE*, June 1971, pp 66-70

7   After the blast, *ASCE journal*, Vol 63, No 5, May 1993, pp 44-77

8   Ramabhushanan E and Lynch M, Structural assessment of bomb damage for World Trade Center, *Journal of performance of constructional facilities*, Vol 8, No 4, Nov 1994, ASCE, pp 229-243

9   Kapp, M S. Slurry-trench construction for basement wall of World Trade Center, *Civil Engineering – ASCE*, April 1969, pp 36-40

10   Schroeder A, Saqi V and Winans C, World Trade Center Special Review, Insurance – property – Casualty, Morgan Stanley Equity Research, North America, Sept 17, 2001, pp 29

11   Ministry of Housing and Local Government, Report of the inquiry into the collapse of flats at Ronan Point, Canning town, London, HMSO, 1968, 68pp

12   DETR, Consultation package, Proposals for amending Part A (Structure) of the Building Regulations 2000, Department for Transport, Local Government and the Regions, London, UK, 31 August 2001, pp 105

13   Jane's, All the worlds aircraft, 2001-2002

14   Bangash M Y H, Impact and explosions, Blackwell, 1993

15   Steel designers manual, 4th edition, Crosby Lockwood, London

16   Eurocode 1, Basis of design and actions on structures, Part 2.2 Actions on structures exposed to fire (DD ENV 1991-2-2), British Standards Institution

17   Cooke, G M E, Tests to determine the behaviour of fully developed natural fires in a large compartment', *Fire Note 4*, Building Research Establishment, February, 1998, pp 248, ISBN 1 86081 206 6

18   Frischmann W W et al, National Westminster Tower - design, Proc ICE, Part 1, Vol 74, 1983, pp 387-434

19   Bergmann R and Campbell R H, Office tower DS7 at Canary Wharf, The Structural Engineer, Vol 69,No 7, April 1991, pp 137-140

20   Thiemann R, The City Group tower at Canary Wharf, Building Engineer, Oct 2001, p18

21   Design of the world's tallest buildings – Petronas twin towers at Kuala Lumpur city centre, The structural design of tall buildings, Vol 6, No 4, Dec 1977

22   Uy B and Patel S B, Concrete filled high strength steel box columns for tall buildings – behaviour and design, The structural design of tall buildings, Vol 5, No 2, June 1996

FURTHER READING

Canary Wharf, *Building Supplement*, Oct 1991

Blast effects on buildings, edited Mays G C and Smith P D, Thomas Telford, 1995

Sutherland R J M, The sequel to Ronan Point, Proc. 42nd Annual Convention of Structural Engineers Association of California, 1973

Smolira M, Analysis of tall buildings by the force-displacement method, McGraw-Hill, London, 1975

DESIGN OF MULTI-STOREY STEEL FRAMED BUILDINGS WITH UNPROTECTED SECONDARY BEAMS OR JOISTS FOR DEPENDABLE INELASTIC RESPONSE IN SEVERE FIRES

Charles CLIFTON
HERA Structural Engineer, HERA, Auckland, New Zealand
structural@hera.org.nz

ABSTRACT

Design of multi-storey steel framed office and other commercial buildings for fire resistance has traditionally been undertaken on the premise that the building will suffer partial or total collapse unless the beams and columns are insulated from temperature rise under fully developed fire conditions. Since 1990, a growing body of evidence from severe fires in buildings and from the results of advanced research has shown that there is a substantial reserve of strength available from a typical composite steel beam/concrete floor slab system with uninsulated floor support beams in severe fire conditions. This reserve of strength is mobilised when the floor system undergoes inelastic response due to the effects of the fire.

The reserve of strength has been demonstrated experimentally in the landmark series of fire tests undertaken during 1995 and 1996 on an eight storey steel framed building at the former Cardington Large Building Test Facility in the UK. Those tests have shown that the floor system deforms in two way action, as a slab panel, between points of restraint that undergo minimal vertical movement under severe fire conditions.

Subsequent to these tests, a design model based on this two way slab panel action has been developed by Colin Bailey of the UK Building Research Establishment. The structural mechanisms on which that model are based have been confirmed by large-scale ambient temperature tests on concrete slab panels of various size reinforced with varying levels of mesh reinforcement.

The author has developed that procedure further into the *Slab Panel Method* of design. These developments have involved;
- Incorporating the contribution to the slab panel load carrying capacity that is made by the unprotected secondary beams and by additional fire emergency reinforcement that may be added
- Accounting for the expected elevated temperatures of all components and their reduced strength
- Determining the elevated temperature shear capacity at the supports

- Maintaining effective force transfer and integrity at the supports through suitable detailing provisions.

This paper presents an overview of the *Slab Panel Method*, covering its background, basis, general details and building structure characteristics required for its use. Following this is a critique of the procedure. The paper concludes with acknowledgments and references.

KEYWORDS: *Fire engineering, structural design, inelastic response, elevated temperatures, materials.*

INTRODUCTION & SCOPE

General Background

This paper presents an overview and general details of the *Slab Panel Method* (SPM) of floor system design, which allows for the use of unprotected secondary beams or joists supporting concrete floor slabs and exposed to severe fire conditions. It is written for application to multi-storey steel framed buildings subject to high fire severity, typical of that possible in open plan office and commercial buildings which are *Fire Hazard Category* (FHC) 2 or 3. (FHC is as defined in Comment to Paragraph 2.2 of [1]). Full details of the SPM method are presented in the *HERA Design and Construction Bulletin* (*DCB*) No. 60 [2]. Summary results of heat flow studies of slabs, protected steel beams and columns, which have been necessary to establish design elevated temperatures of floor slab components for use in the procedure, are given in *DCB* No. 59 [3].

The SPM design procedure is fundamentally different in philosophy and application to fire engineering design provisions currently used on steel framed buildings in New Zealand. This is because the procedure is written for application to buildings subject to potential high fire severity (FHC 2 or 3 to C/AS1 [1]), in which any unprotected steel members may be subjected to high temperatures and considerable inelastic demand in the event of fully developed fire. Fig. 1 shows the maximum extent of inelastic demand that could be expected; in practice it would typically be less. The extent of this inelastic demand is anticipated and a dependable proportion of the additional reserve of strength available from the building when undergoing this deformation is incorporated into the procedure.

FIGURE 1 : Deformed Floor System After Cardington Demonstration Furniture Test (from [4]).

Scope and Content

The basis of the slab panel design procedure is presented in the next section. Application is dependent on calculating the appropriate temperatures and mechanical properties of the slab panel components; how these have been determined is then described. This is followed by an overview of the method's application.

Details of the structural performance to be delivered by the procedure and the building structural characteristics and examples of the detailing required for its successful implementation are then given.

The next two sections present a brief critique of the method. This is covered in two parts; first a critique of the tensile membrane enhancement mechanism [5] developed by Bailey and secondly a critique of the New Zealand application of this mechanism.

The paper then briefly mentions future research planned or desired, before concluding with acknowledgments and references.

BASIS OF SLAB PANEL DESIGN PROCEDURE

General

Under ambient temperature conditions, the beams support the floor slab. For example, with reference to Fig. 2 herein, the load path involved in resisting dead and live loads under ambient temperature conditions is:

Slab → secondary beams → primary beams → columns (1)

Under severe fire conditions, when the secondary interior beams are unprotected, they lose most of their strength, such that the ambient temperature load path in equation (1) cannot be maintained. As a result, the beams form plastic hinges and the load-carrying mechanism changes to a two-way system. This transition is illustrated in Fig. 3, for the case of a single secondary beam supporting its tributary area of slab.

Under severe fire conditions incorporating unprotected secondary beams, two-way action prevails, involving the region of slab and unprotected beams known as a slab panel.

The slab panel resists applied load by two-way action back to the supports, through a load path involving:

Slab panel → supporting beams → columns (2)

This is illustrated in Fig. 2. The same concept is applicable to floor slabs supported on closely spaced joists, such as the *Speedfloor* system.

The slab panel develops its load-carrying capacity in the deformed state through:

Yieldline moment action, plus
Tensile membrane enhancement

The loads transferred from the slab panel into the supporting beams (ie. as given by the tributary floor slab areas contained within the yieldline patterns shown in Fig. 2) must be resisted by those supporting beams and transferred back to the columns.

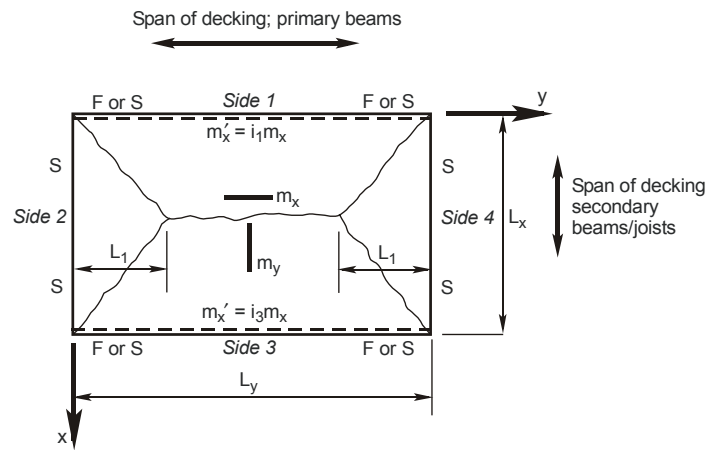The basis of the design procedure – elaborating on these points – is now briefly covered.
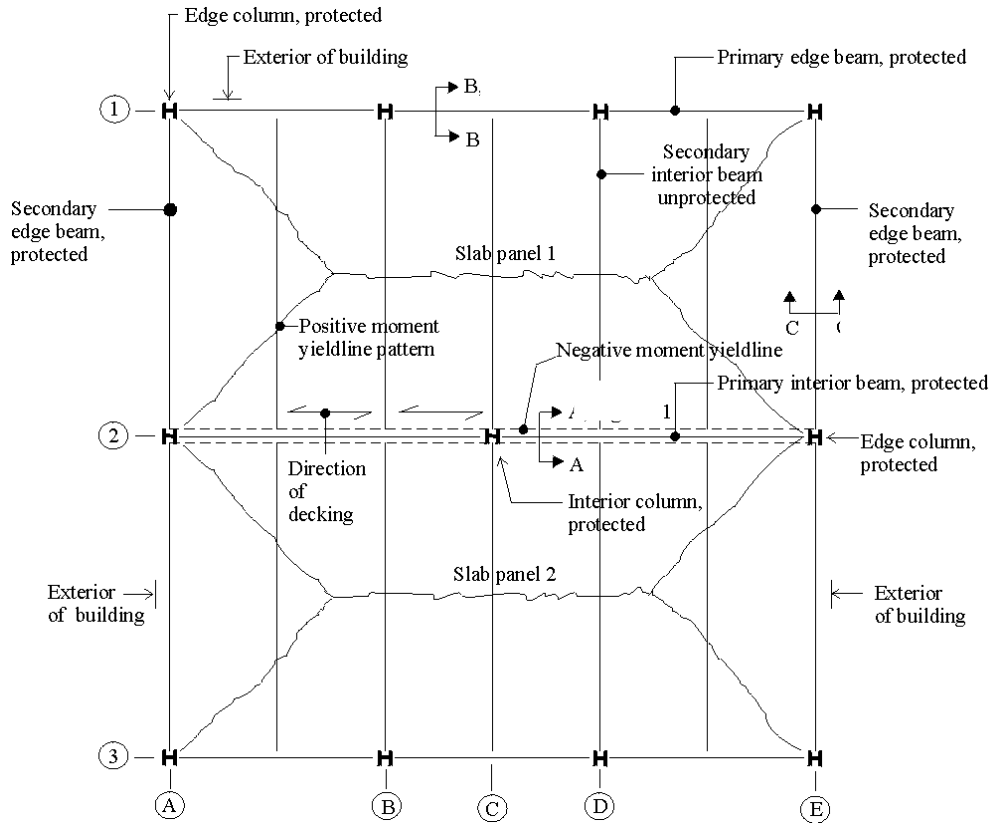
FIGURE 2 : **Reflected Floor Plan for Application of Slab Panel Fire Engineering Design Procedure to a Concrete Slab on Profiled Steel Deck Supported on Primary and Secondary Beams**

Notes to Fig. 2
1. *The beam positions shown are the centrelines.*
2. *The exterior of the building shown is the edge of the concrete slab.*
3. *A two slab panel floor system is shown; the concept is applicable to larger floor plan areas.*
4. *Lateral load-resisting systems are not explicitly shown, but their position is not restricted by the method.*
5. *The secondary interior beams are unprotected. The columns and primary interior beams will have passive fire protection. The edge beams may be unprotected if they have a suitably high reserve of strength; see details in [2].*
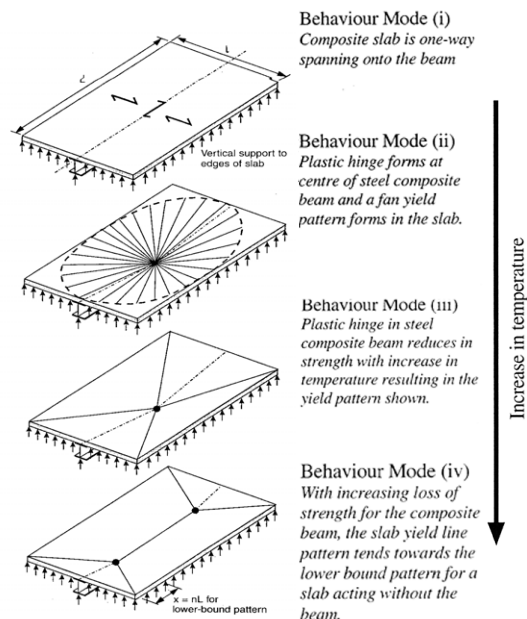

FIGURE 3 : **Slab and Unprotected Steel Beam Behaviour with Increase in Temperature (from [5])**

Span of decking; primary beams

F or S   *Side 1*   F or S   y

$m_x' = i_1 m_x$

S   S

m_x

Side 2   *Side 4* L_x

Span of decking secondary beams/joists

L_1 L_1

S m_y S

$m_x' = i_3 m_x$

F or S   *Side 3*   F or S

L_y

x

FIGURE 4 :   Uniformly Loaded Rectangular Slab With All Edges Supported (from [6])

Notes to Fig 4

_____	=	slab positive yieldline moment
--------	=	slab negative yieldline moment in the x-direction (where applicable)
m_x	=	positive moment in the x-direction per unit width along the y axis
m_y	=	positive moment in the y-direction per unit width along the x axis
m_x'	=	negative moment in the x-direction per unit width along the y axis
Side 1	=	length AD, etc.
F	=	fixed edge support (side 1 or 3, where applicable)
S	=	pinned edge support (sides 2 and 4, always)

a_x ϕ_{fire} 0.85f'$_c$

R_{cc}

$e_{r,mesh}$

$R_{ts,x}$

t_0

$R_{tsbx,tf}$

d_{sb} $R_{tsbx,w}$

$R_{tsbx,bf}$
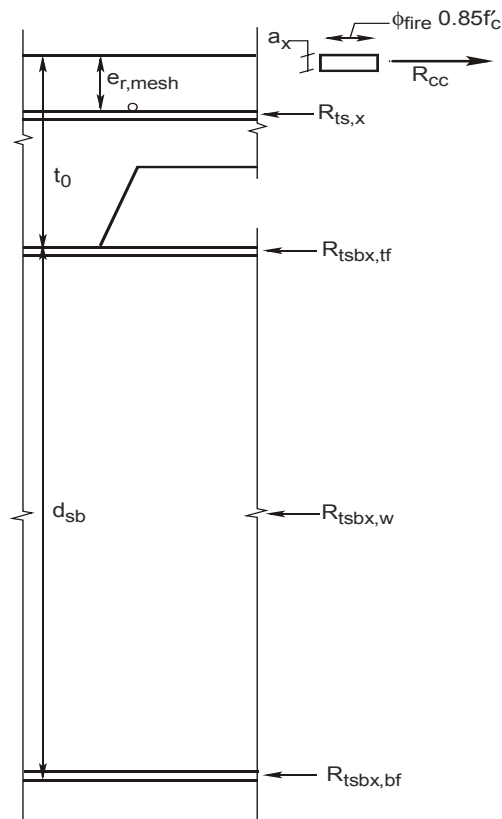
FIGURE 5 : Section Through Region of Floor Slab, Incorporating Steel Decking and Secondary Beam, Showing Development of Positive Moment Capacity Using the Mesh Reinforcement and Secondary Beams

Notes to Fig. 5
1. *This section is taken across the x-direction looking along the y-direction.*
2. *The optional deck trough bars are not shown in this section.*
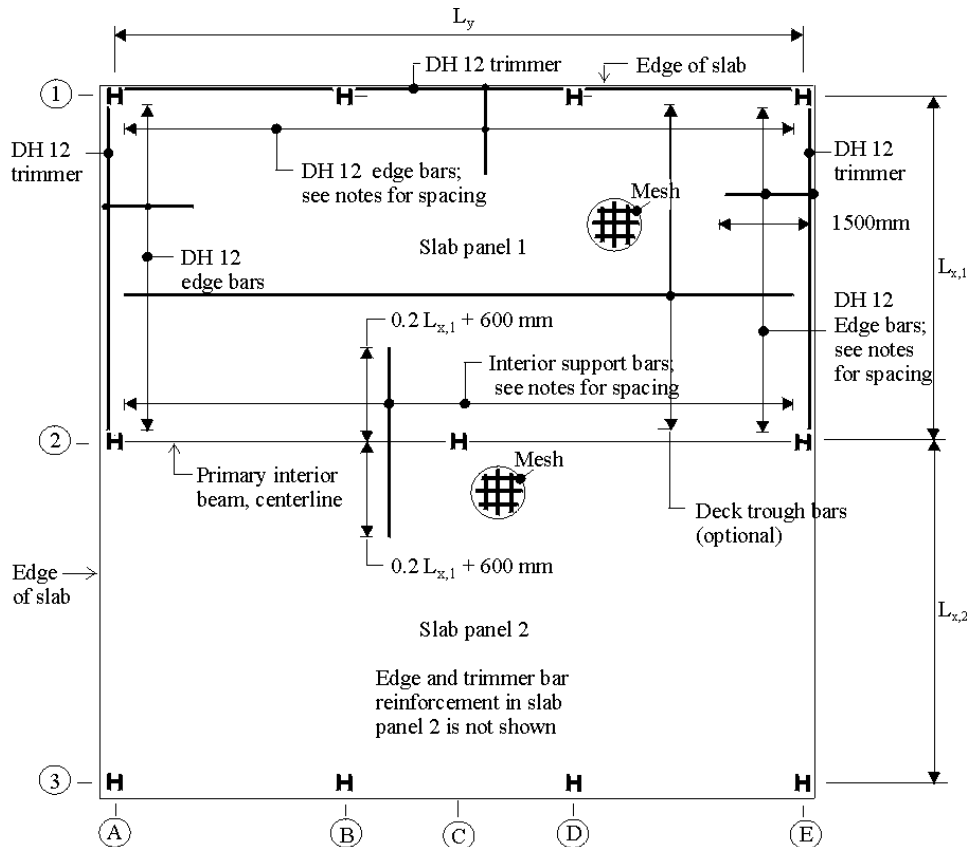
FIGURE 6 : Floor Plan Showing Reinforcement Required in the Slab Panels for Use of This Design Procedure

Notes to Fig 6
1. *The reinforcing bars shown are deformed high tensile reinforcement, with at least 15% dependable uniform elongation.*
2. *The reinforcement shown is additional to the mesh required for shrinkage and temperature control.*
3. *The edge bars, trimmer bars and interior support bars are required in all instances. They are placed on top of the slab mesh. Interior support bars are typically 12 or 16 mm diameter.*
4. *The spacing and minimum area requirements for the edge bars and interior support bars must comply with the recommendations on pages 64.33 to 64.35, DCB No. 64.*
5. *The deck trough bars are optional and are used if necessary to increase the load-carrying capacity of the slab panel. They are placed in the troughs as shown in Figs. 60.11 – 60.13 of DCB No. 60. They will typically be 12 or 16 mm diameter.*
6. *The centreline position of the primary interior beams is shown in this view, because the placing of the interior support bars is based around this position. The rest of the floor support beams are not shown herein.*

Slab Panel Behaviour

(1)   Development of yieldline capacity

When the unprotected secondary beams lose strength in severe fire conditions, the slab panel begins to deform. Under only moderate deformation, the yieldline capacity is developed. This is associated with plastic moment formation along a pattern of yieldlines, the shape and extent of which depend on the positive moment capacity which can be developed within the slab panel in each direction and the negative moments which can be developed across any fixed supports.

The general pattern of yieldlines in a rectangular slab with all edges supported vertically is shown in Fig. 4; the pattern of positive and negative moment yieldlines within a slab panel is shown in Fig. 2.

The development of the yieldline moment capacity (kNm/m length) follows conventional reinforced concrete practice, as described in [6]. All components which can dependably contribute to developing internal tension across a yieldline are included. This calculation is

156

undertaken for the two directions (x and y) seperately. The elevated temperature of each component must be determined and the appropriate material strength used.

In the x-direction (ie. the calculation of m_x shown in Fig. 4), the positive moment internal tension actions are developed by the mesh and unprotected secondary beam elements (top flange, web and bottom flange), as shown in Fig. 5. The tension contribution from the unprotected secondary beam elements are small, because of their high temperatures, however their moment contribution is significantly greater than that of the mesh, because of the large lever arm. *For the secondary beams to contribute in this manner, they must be connected to the slab with sufficient shear studs so that slip at the slab and beam interface is effectively eliminated under severe fire conditions.*

In the y-direction, the positive moment (ie. m_y in Fig. 4) is developed by the mesh and the deck trough bars; these are shown in Fig. 6. The decking spans in the y-direction but is not included in determination of m_y. This is because the decking is laid in individual lengths, which are not able to transfer tension force across the ends of adjacent sheets. Thus there is not a dependable tension load path through the decking, over the slab panel length, under normal conditions of deck laying and fixing. Its resistance is therefore ignored, however in practice it will contribute to some extent to m_y.

The internal tension force for negative moment, m_x', over interior primary beams, is developed by the interior support bars (Fig. 6).

Having determined the yieldline moments, the yieldline load carrying capacity is calculated in accordance with conventional considerations of equilbrium of external and internal work. The resulting equation used is 60.A1.1 of [2]; its derivation is given in [6].

(2)   Tensile membrane enhancement

The extent of slab panel displacement needed to develop the yieldline capacity is relatively small; typically around $L_x/100$, where L_x = slab panel width (Fig. 4).

Once the yieldline pattern is formed, the load-carrying capacity of the slab panel continues to increse under increasing panel deformation. This has been graphically observed in the Cardington fire tests [4]. A mechanism to explain and quantify this enhancement (termed the tensile membrane enhancement) has been developed by Bailey [5], based on the Cardington fire tests [4] and confirmed (for ambient temperature conditions) by a load test [8] on a 9 m x 6 m slab panel.

When a slab panel is loaded or deformed to failure, the failure mode – conservatively, if the results from [8] are generally applicable – occurs through the development of a central crack across the slab panel width, as shown in Fig. 7. The crack, shown there as occurring along the line EF, in practice does not extend to the outer edges of the slab panel, where the concrete is in compression [8].

The in-plane axial forces within part of the slab panel (one half of element 1 from Fig. 7) are shown in Fig. 8. By taking moments about point E and equating internal and external work, Bailey [5] has developed an expression for the distribution of in-plane axial forces developed immediately prior to formation of the central crack. This allows the magnitude and pattern of these forces to be determined and the extent of tensile membrane enhancement to be calculated.

This enhancement arises from two sources. The first is the influence of the in-plane axial forces on the yieldline moments. When determining the moment capacity (m_x, m_y), the slab

panel is always lightly reinforced – ie. the moment is governed by the internal tension force that can be developed across the yieldline (see Fig. 5), rather than by the compression capacity of the concrete. This is the case even with secondary beam contribution included. It follows that, if a length of yieldline is in a region of in-plane compression, the yieldline moment capacity is enhanced; if in a region of tension, it is reduced. By summing the contribution along all the yieldlines, the overall enhancement in yieldline moment capacity arising from the interaction of moment and axial load is determined. This is independent of the slab panel deflection.

The second source of enhancement comes from the downwards vertical deflection of the slab panel, displacing the membrane tension force relative to the supports, as shown in Fig. 9. This provides moment enhancement due to P-Δ effects, with the extent of enhancement dependent on the magnitude of deflection and sign of membrane force (tension enhances; compression detracts).

Bailey presents these enhancement factors normalised to the positive moment yieldline capacities; they are given as equations 60.A35 to 60.A38 in [2].

An in-depth explanation of these two tensile membrane enhancement factors is given in [5], along with the development of the full set of equations used [2] in calculating the slab panel flexural / tensile load carrying capacity. Where changes have been made in adapting the procedure to New Zealand application (in particular incorporating the additional sources of tension action in developing the yieldline moment capacities), the details of these changes are given in Appendix A of [2] and the principal changes are briefly discussed later in this paper.

Design of Supporting Beams and Columns

The supporting beams are shown in Fig. 2 and comprise:

- Primary interior beams
- Primary edge beams
- Secondary edge beams

Their design for severe fire conditions is given in section A6 of [2]. The load transfer from slab panel into these supporting beams depends on the pattern of yieldline development, with, for example, the load from Element 2 going into the beam GH (Fig. 7).

The supporting columns are also shown in Fig. 2. They are protected from direct fire exposure. Their design for severe fire conditions is given in section A7 of [2].
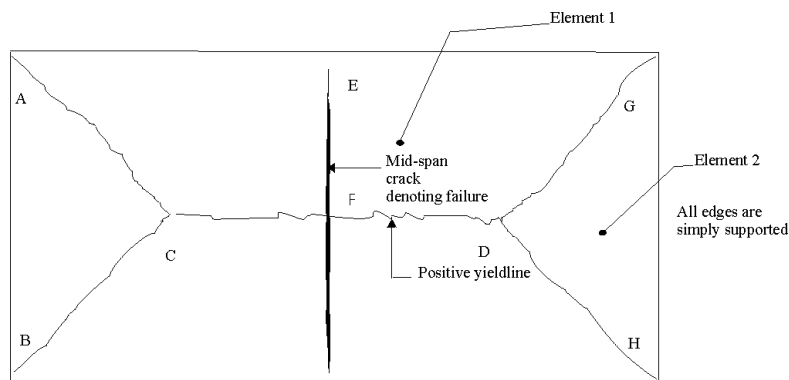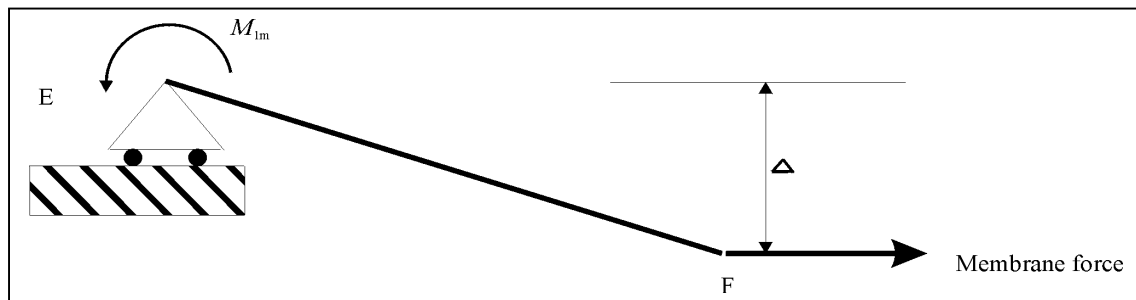

FIGURE 7 : Mode of Failure of a Slab Panel Loaded into the Tensile Membrane Regime (from [5])
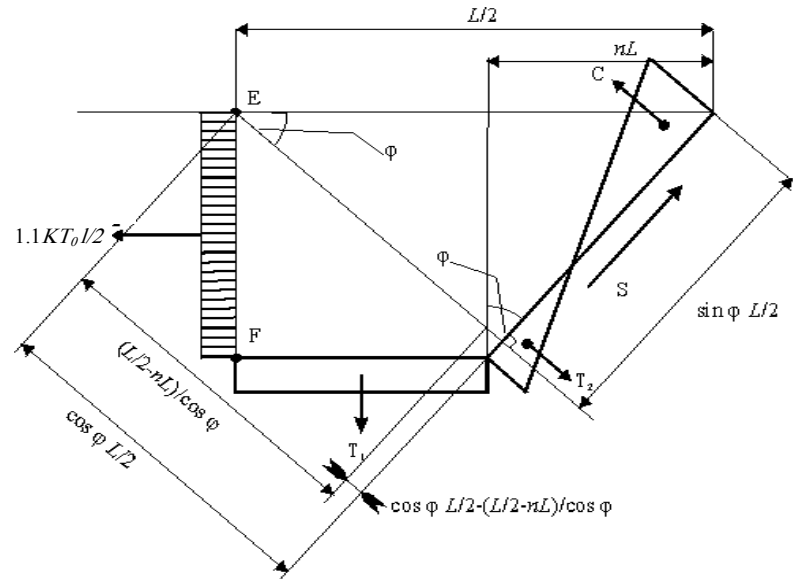
FIGURE 8 : In-Plane Axial Forces Within the Slab Panel at the Time of Failure (from [5])

Note: *The notation herein is that used in [5].*

FIGURE 9 : Enhancement of Yieldline Moment Capacity Due to Displacement of Membrane Tension Force (from [5])

Note: *This view is taken along the line EF shown in Fig. 7*

Temperatures Reached in Critical Components

As previously stated, this is a design procedure written for application under severe fire conditions, where temperatures in all components are typically sufficiently high to reduce the ambient temperature mechanical properties of the steel and concrete. It is therefore important to determine appropriate temperatures reached and the influence of those temperatures. This is undertaken as detailed in Appendix A of [2], with a background in [3].

ELEVATED TEMPERATURES OF COMPONENTS AND THEIR MECHANICAL PROPERTIES

Scope of Research

Critical to the implementation of the SPM procedure is the capability to determine, as realistically as practicable, the elevated temperatures of the slab panel structural components and their associated design mechanical properties. This has involved a research programme which is described in [3]. A brief overview of it is given in this section of this paper.

The research programme has involved the following steps:

(1)   Develop natural fire design time-temperature curves for a representative range of multi-storey enclosure and ventilation conditions.

(2.1)   Determine the maximum floor slab concrete and reinforcement temperatures reached in these fire conditions, and

(2.2)   Develop a design method, based on the use of the time-equivalent formula from [9] and the method of predicting slab reinforcement temperatures from [10], that provides a realistic prediction of the actual floor slab reinforcement temperatures reached, and hence enables:

(2.3)   Determination of the reduction in ambient design strength that is required to allow for the temperature reached in the slab reinforcement in the event of fully developed fire

(3.1)   Determine the maximum temperatures reached in the protected supporting beams and columns under the natural fire conditions

(3.2)   Compare these temperatures with the target limiting temperatures (from [3, 20]) for the different cases considered (member type, insulation type and structural fire severity give the thickness of insulation required)

(3.3)   Determine what parameter settings are necessary for design of these protected members to ensure that the target limiting temperatures are not exceeded, in practice, to an undesirable extent, nor are too conservatively underestimated.

The temperatures reached in slab reinforcement and protected steel members have been determined using SAFIR [11.1] and the pre-processor SAPPHIRE [11.2].

DCB No. 59 [3] contains the following details of this research:

- Validation test for SAFIR on the predicted temperature reached in one of the insulated columns within the Cardington Demonstration Furniture test [4] and that obtained experimentally. (The column used in this test is that shown in the left foreground of Fig. 1, which was insulated in that test with a ceramic fibre blanket.)

- The range of enclosure conditions and the natural fire time-temperature curves developed

- The modelling of the slab and reinforcement in SAFIR [11.1] and the predicted peak temperatures reached

- The modelling of the protected supporting steel primary beams and columns in SAFIR and the predicted peak temperatures reached

- The development of a design method, using readily available criteria [9, 10] that generates design temperatures for the components which are close to or in excess of those determined from the SAFIR analyses.

Owing to space limits, this paper presents only the following of this work:

(1)   Overview of the natural fire design time-temperature curves developed

(2)   Temperatures reached in slab and concrete and the corresponding material mechanical properties

(3)   Temperatures in the unprotected secondary beam elements and the corresponding material mechanical properties

Development of Natural Fire Design Time – Temperature Curves

The intention with this study was to cover a sufficiently wide range of enclosure conditions and associated structural fire severities likely to be encountered in multi-storey buildings.

An enclosure height (H) of 3.5 m was used, being a typical multi-storey enclosure height. It is slightly greater than the value used in developing the basic time equivalent (t_e) values given in Table 5.1 of C/AS1 [1].

The range of enclosure plan areas and configurations studied are shown in Fig. 10. The rationale behind choosing these configurations was based on that used by Kirby et.al. [12] in developing their large-scale compartment tests, to validate the time-equivalent equation used in the relevant Eurocode [13] (equation 5 herein). Kirby et. al.'s tests involved using a strip model to represent an enclosure of unlimited width and with a depth of twice the depth of the test compartment.
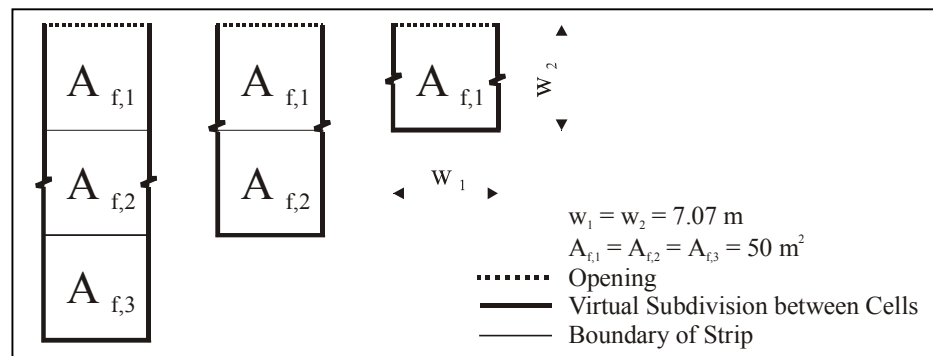
FIGURE 10 : Enclosure Conditions Used in Study

In this SPM study, three enclosure depths were used, as shown in Fig. 10 and Table 1. These cover the range of depths likely to be encountered in any multi-storey office building. The enclosure (strip) width used was 7.07 m in each instance.

Three heights of opening were used, namely 1.5 m (Low), 2.0 m (Medium) and 2.5 m (High).

The fire time-temperature curves used in this study were developed from the following:

(i)   The migrating large firecell model [14] published by HERA in 1996 and revised in 1999. For the rectangular 2 cell and 3 cell strips, this gives a time-temperature curve that accounts for the influence of the fire reaching full development adjacent to the openings and then burning back through the enclosure over time. The model utilises modified Eurocode Parametric Curves [14] to generate the time-temperature characteristics of a migrating fire for the region within the building under fully developed fire conditions.

(ii)   The time-temperature conditions generated by applying the Modified Eurocode Parametric Curves to the entire enclosure - this assumes uniform fire conditions throughout the enclosure, which is easier to consider in design but is a less accurate representation of the actual fire conditions.

(iii)   The ISO Curve, eg. as given by equation 5.12 of [9].

Fire Case No	A_f	w_2 [m]	h [m]	A_v [m^2]	OF [m$^{-0.5}$]	A_v/A_f	e_f [MJ/m^2]	t_{eq} [min]
C1LN	1x1	7.07	1.5	9.02	0.06	0.18	800	*50*
C1MN	1x1	7.07	2.0	12.02	0.09	0.24	800	*45*
C1TN	1x1	7.07	2.5	15.03	0.12	0.30	800	*45*
C1LH	1x1	7.07	1.5	9.02	0.06	0.18	1200	*80*
C1TH	1x1	7.07	2.5	15.03	0.12	0.30	1200	*65*
C2LN	1x 2	14.14	1.5	9.02	0.03	0.09	800	*100*
C2MN	1x 2	14.14	2.0	12.02	0.05	0.12	800	*75*
C2TN	1x 2	14.14	2.5	15.03	0.02	0.15	800	*60*
C2LH	1x 2	14.14	1.5	9.02	0.03	0.09	1200	*145*
C2TH	1x 2	14.14	2.5	15.03	0.07	0.15	1200	*90*
C3LN	1x 3	21.21	1.5	9.02	0.02	0.06	800	*115*
C3MN	1x 3	21.21	2.0	12.02	0.03	0.08	800	*100*
C3TN	1x 3	21.21	2.5	15.03	0.05	0.10	800	*90*
C3LH	1x 3	21.21	1.5	9.02	0.02	0.06	1200	*175*
C3TH	1x 3	21.21	2.5	15.03	0.05	0.10	1200	*130*
Column No	1	2	3	4	5	6	7	8

Table 1 : Enclosure Characteristics Used in Component Temperature Study (from [3])

Notes: Naming system for the fire case numbers:
The variable naming system for the fire case numbers for all the output presented herein is as follows:
- The first two digits represent the number of cells in enclosure
  (C1, C2 or C3; C3 ≡ 3 cell model)
- Where the second digit is either 2 or 3, and is followed by another number, that second number represents the location of the cell, as shown in Fig. 10 (eg 1 represents the cell adjacent to the opening)
- The next digit represents the height of the openings (**L**ow, **M**edium or **T**all)
- The next digit represents the fire load energy density (**N**ormal = 800 MJ/m^2 floor area, High = 1200 MJ/m^2 floor area)

The area of openings, A_v, was determined from equation 3:

$$A_v = 0.85 \ w_1 h \qquad (3)$$

where:
0.85 = reduction factor to account for presence of curtain walling, etc.
w_1 = strip width = 7.07 m
h = window height

The opening factor was calculated using equation 4, ie. in accordance with [14]:

$$OF \qquad = \quad \frac{A_v h^{0.5}}{A_t} \ \left(m^{0.5} \right) \qquad (4)$$

where:
A_v = area of openings (m^2)
h = opening height (m)
A_t = total surface area of enclosure; walls (including openings), ceiling and floor (m^2)

The time equivalent, t_{eq}, was calculated using equation 5.9 from [9], repeated as equation 5 below:

$$t_{eq} = e_f k_b w_f \tag{5}$$

where:

e_f	=	fire load (MJ/m^2 floor area)
k_b	=	0.065, being the value appropriate to an enclosure with normal weight concrete and floor and plasterboard lined walls (see Table 5.1 from [9]).
w_f	=	ventilation factor, given by Table 5.1 from [9].
	=	function of H and A_v/A_f
H	=	firecell height = 3.5 m

The normal fire load (800 MJ/m^2 floor area) is the design fire load energy density associated with Fire Hazard Category (FHC) 2 from [1]. FHC 2 covers most multi-storey office and commercial building applications. The high fire load (1200 MJ/m^2 floor area) is the design fire load energy density for FHC 3 from [1].

As can be seen from Table 1, the study incorporated a wide range of ventilation conditions, with OF from 0.02 to 0.12, A_v/A_f from 0.06 to 0.30 and a wide range of structural fire severity (t_{eq} from 45 mins to 175 mins).

There were five fire cases considered for each of the three depths of strip, as shown in Table 1. In addition, for the two cell and three cell strips using the HERA migrating fire model, the appropriate time-temperature curve for each cell was output, giving a total of 30 fire time-temperature outputs using this HERA model. An example of the output from this model, for the three cell strip, is shown in Fig. 11.
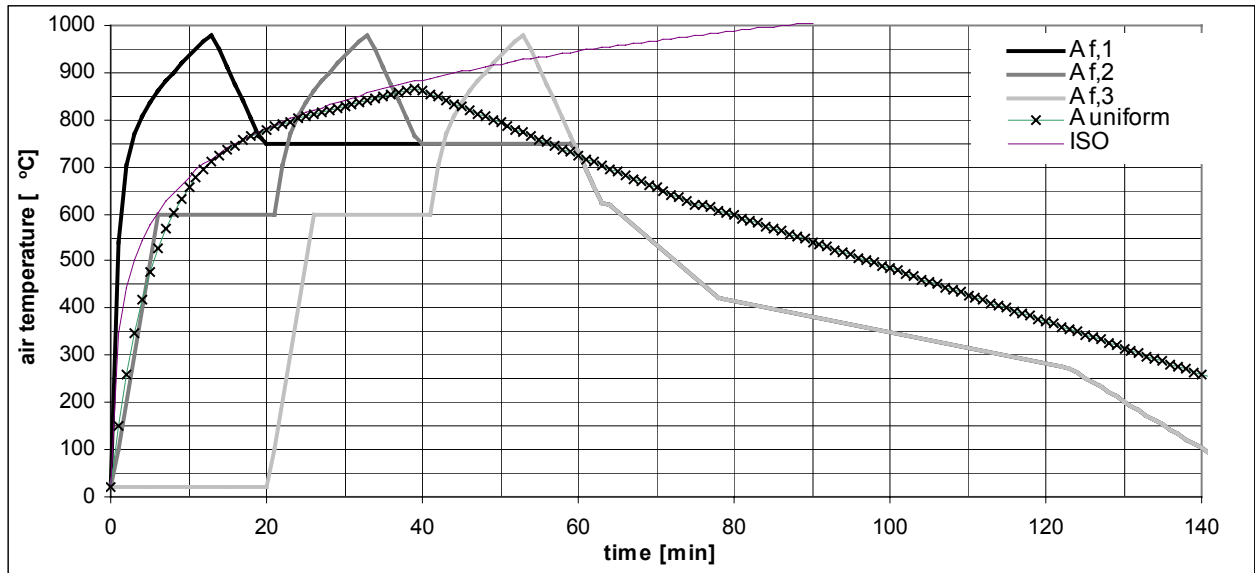
FIGURE 11 : Time-Temperature Curve for Largest Enclosure (Three Cell Model) Tall Window Height, Normal Fire Load, Normal Weight Concrete Floors

Temperature in Slab Reinforcement

The purpose of this study was to determine the "actual" slab mesh temperatures reached in a range of natural fire conditions by thermal analyses, then to compare these actual temperatures with those calculated using readily available design tools and procedures [9, 10], and, finally to introduce modifications to these tools and procedures, as required, to obtain suitable agreement between the "actual" and the calculated design mesh temperatures.

The implementation of this study is described in section 4.4 of [3] and the key results shown in Table 59.2 therein. These results show that a realistic determination of slab reinforcement temperature can be made using the established design tools of [9, 10] with the following modifications:

1. The FRR used = $0.8 t_{eq}$, where t_{eq} is as calculated in equation 5
2. The heat path procedure given in section 6.4.2 of [10] is used to calculate the temperature reached
3. For the slab mesh, the height from the centre of the mesh reinforcement to the nearest fire exposed concrete face is used for u_3, with $u_1 = u_2 = \sqrt{2} \ u_3$.

The use of this procedure generates results that, for all cases where the reinforcement temperature exceeds $300^{o}C$, err on the conservative side the (ie. the calculated temperature exceeds that from the thermal analyses).

Elevated Temperature Mechanical Properties of Slab Reinforcement

Having obtained the reinforcement temperature, the variation of mechanical properties with temperature needs to be determined. This can be obtained from a number of sources, such as NZS 3101 [15], however the values given in EC2 Part 1.2 [16] are more appropriate to use, for the following reasons:

- They differentiate between cold-worked and hot-formed reinforcement, which is desirable, given that the properties are different and both sorts are used
- Values are given for strains $\geq$ 2%, which is appropriate to the magnitude of deformation developed by the slab panel in severe fire conditions
- The relationships for cold-worked bars are given in Table A.4 of [16], while those for hot-formed bars are given in Table A.3 of [16]
- The cold-worked provisions cover low ductility welded mesh to AS/NZS 4671 [17] while the hot-formed provisions cover seismic grade mesh or bars [17].

Unportected Secondary Beam Elements

The unprotected secondary beams span the short dimension, L_x, as shown in Fig. 4.

Being unprotected, they are assumed to be directly exposed to the fire and therefore to reach very high temperatures. It has been shown from the Cardington tests [4, 21] that the bottom flange and web reach 95% of the peak fire temperature, and that the top flange, with its greater shielding and proximity to the heat sink of the concrete slab, remains at around $150^{o}C$ below the peak fire temperature.

The peak fire temperatures have been obtained as described in section CA4.1.5 of [2], with the relationship described above then used to obtain the peak steel beam element temperatures. These temperatures are a function of the Fire Hazard Category, type of concrete used in the floor slabs and position of beam element. They are as given by Table 2.

The variation of yield stress with elevated temperature for the unprotected secondary beam elements is taken from EC 3 Part 1.2 [19] for a strain ≥ 2%.

	Bottom Flange	Web	Top Flange
FHC 2, NWC	850	850	750
FHC 3, NWC	900	900	800
FHC 2, LWC	950	950	850
FHC 3, LWC	1000	1000	900

Table 2 : Design Temperatures of Unprotected Secondary Beam Elements

Notes to Table 2

1. *All temperatures are ^oC*
2. *NWC = normal weight concrete; density ≥ 2300 kg/m³*
   LWC = light weight concrete; density ≤ 1900 kg/m³
3. *FHC = fire hazard category, as given by [1]*

Secondary Beam to Primary Beam Connections: Bolts and Beam Web

Based on analyses of the Cardington test temperatures, the maximum bolt temperature,θ_f ,is taken as that for the unprotected secondary team top flange, from Table 2. The same temperature is used for the beam web at the connection.

Given the bolt design temperature, the variation of bolt tensile strength with temperature for high strength structural bolts has been established by UK testing, as detailed in section 4.3.3 of [18]. This variation is as follows, for bolts in the relevant temperature range:

$$\frac{f_{uf\theta}}{f_{uf20}} = 0.170 - (\theta_f - 680)\, 0.5312 \times 10^{-3} \tag{6}$$

for $680^oC < \theta_f \le 1000^oC$

APPLICATION OF SLAB PANEL DESIGN METHODOLOGY

United Kingdom Application

The first application of this procedure has been developed by the UK Steel Construction Institute; details are given in SCI Publication P288 [7].

The UK application is limited in scope to:

- Moderate levels of structural fire severity (60 minutes maximum time equivalent)
- Maximum panel dimension of 9m (being the secondary beam span in [4])
- Only some secondary beams are allowed to be unprotected
- The secondary beam contribution is ignored
- Mesh/steel/concrete materials and designations used are those for the UK
- The effect of elevated temperature on the material strengths is ignored.

New Zealand Application

The procedure presented herein has been developed from first principles using the Bailey method [5, 8] rather than by adapting the UK application.

In the report on the ambient temperature test, Bailey notes some factors required to be considered for general application of the slab panel method. These are [8]:

(i)   Elevated temperatures of components near the fire-exposed face need determination to account for expected strength loss of materials which are at high temperatures

(ii)   High temperature shear capacity at the slab panel supports needs to be determined

(iii) Detailing for effective force transfer and integrity at supports needs to be considered, especially under conditions of high structural fire severity.

The initial application [7] of the UK procedure puts conservative restrictions on its use to avoid these factors exerting significant influence, rather than directly taking them into account.

The New Zealand application [2] of the UK procedure addresses these factors directly and thus permits a wider range of application. It extends the methodology to:

- High structural fire severity (FHC 2 and 3)
- No explicit limitation on slab panel size (limitations are implicitly imposed by the method)
- Contribution of secondary beams to slab panel moment capacity is included
- Contribution to slab panel moment capacity of slab reinforcement that is additional to the mesh is included
- Design of all components takes account of their elevated temperature
- Shear capacity at elevated temperature is checked
- Slab reinforcement and detailing provisions are included.

Some of the recommendations from P288 [7] relating to compartmentation are also incorporated into the New Zealand application [2].

STRUCTURAL PERFORMANANCE TO BE DELIVERED BY THE PROCEDURE

Under Severe Fire Conditions

The structural performance that will be delivered by this procedure, in the event of fully developed fire conditions, is as follows:

(1)   Slab and unprotected secondary beams may undergo appreciable permanent deformation. The maximum extent of this is described in section 2.2 of *DCB* Issue No. 59 [3] and shown in Fig. 1 herein.   In practice, the inelastic demand would usually be less, for the following reasons:
- Lower fire load
- Presence of shielding linings
- Non-fire rated enclosures reducing the fire size
- Fire service intervention

(2)   Support beams and columns will undergo minimum permanent deformation

(3)   *Load-carrying capacity* and *integrity* of the floor system will be preserved.

(4)   *Insulation* requirements will be met for at least the F rating times specified by C/AS1 [1].

(5)   Local and global collapse will be dependably prevented.

In practice, structural repair and reinstatement of a steel building designed to this method will be almost as straightforward as that for a building with all floor support beams protected, based on experience from actual fires in modern, multi-storey framed buildings.

Maintaining Effective Compartmentation

Effective compartmentation will be maintained, both between floors and between firecells on the same floor. The former is a consequence of the floor system performance that will be

dependably delivered by this procedure.   The latter may require special detailing and is covered in section 6 of [2]. Where deformable fire rated separations are required, these can be provided through the use of details developed for application across seismic joints.

BUILDING STRUCTURE CHARACTERISTICS REQUIRED FOR DEPENDABLE IMPLEMENTATION OF METHOD

Floor Slabs

Floor slab characteristics required are;

(1)   Concrete is normal weight, (NWC) $f_c' \geq 20$ MPa.

The procedure is readily expandable to light weight concrete (LWC); guidance on determining component temperatures for some of the slab panel components using LWC floor slabs is already included in [2].

(2)   Mesh reinforcement
- Low ductility welded AS/NZS 4671 [17] wire mesh to can only be used if the pitch of the mesh bars is 300mm; mesh of low ductility with lesser pitches **does not have** the ductility required
- Mesh formed from welded seismic 300 or 500 grade bars to [17] must be used where the area of mesh required is such that the required bar pitch < 300mm. Otherwise use bars instead of mesh.

(3)   Bar reinforcement
- Seismic grade 300 or 500 bar reinforcement to [17].

Steel Beams/Joists

Typically all steel beams will be composite with the floor slab.

If these beams are not composite, then shear studs to NZS 3404 [20] Clause 13.3.2.3(h) are required to apply [2] as written; ie. maximum stud spacing at 4 x slab thickness.

Hot-rolled beams, welded beams, *Speedfloor* Joists, beams with web openings are all suitable. However, special considerations are required, from [2], for beams of non-uniform cross section or beams which contain web openings.

Columns

Bare steel columns are required to be passive protected full height. The limiting temperature to use and the FRR to apply are given in section 7.5 of *DCB* Issue No. 59 [3]; see page 25 therein.

For design of concrete-filled structural hollow section columns, refer to section 7.6 of *DCB* Issue No. 59 [3].

Connections

Connections to unprotected secondary beams

Connections between unprotected secondary beams and either primary beams or columns are subjected to significant inelastic rotation up to the maximum temperature, then are subject to tension force during the cooling phase. This is described in more detail on pages 9-11 of session 4, HERA Report R4-105 [21]. These connections must be designed and detailed to retain their integrity during both the heating and the cooling phases.

These requirements are similar to the severe earthquake requirement to retain integrity under seismic-generated inelastic rotation demand. The same design and detailing concepts should be used. The connections given in HERA Report R4-100 [22] will be suitable in this regard.

Connections to beams that support the slab panel edges

These will be subjected to lower rotation and axial force demands from fire, either because the beams are protected or because they possess a very high reserve of strength. However, they will typically be connections between supporting beams and columns (eg. as shown in Fig. 2) and therefore will also be subject to earthquake design and detailing requirements. These earthquake requirements will cover the fire condition. Once again, connections given in [22] are suitable.

Overall Structural Stability

The slab panel design procedure is applicable to all structural systems. There are no specific limitations on type or position of lateral load-resisting system elements imposed by the use of this method.

Lateral load-resisting systems will have protected columns, which will therefore be subject to negligible inelastic demand in fire, and either protected beams or beams with a very high reserve of strength in severe fire conditions. These systems will therefore retain their integrity under severe fire conditions.

All gravity system columns will be protected and hence subject to negligible inelastic demand in fire.

Thus local and global structural stability will be retained throughout the fire.

DETAILING REQUIREMENTS FOR USE WITH PROCEDURE

As with any system designed to deliver a dependable level of inelastic response, the detailing is as important as the design.

(1)   This especially relates to the floor slab, where:
  - Decking must be fastened to beams to NZS 3404 [20] Clause 13.3.2.4
  - Mesh must be lapped to NZS 3101 [15] Clause 7.3.21
  - Bars must be lapped to NZS 3101 Clause 7.3.17
  - Supply and positioning of the reinforcement required to develop yieldline moments and tensile membrane action, plus additional reinforcement to ensure integrity of shear transfer at the supports, is detailed in Figs. 60.10 to 60.14 of [2]. The floor plan view only of these details is shown herein as Fig. 6
  - Covers for mesh and reinforcement are important and must be placed as specified in [2].

(2)   When passive fire protection is specified, it must be placed as specified, especially:
  - Full length of beams
  - Full height of columns.

CRITIQUE OF TENSILE MEMBRANE MODEL

Structural Mechanism

Bailey postulates [5] that the slab panel develops its load-carrying capacity in the deformed state through:

  - Yieldline moment action, plus

- Tensile membrane enhancement.

Mathematical representations for both mechanisms are well established [6, 5] and are not described in more detail herein. The uniformly distributed load-carrying capacity predicted by yieldline action for a rectangular slab panel with all edges supported is developed by Park [6] and used directly in the SPM procedure. That capacity is based on equilibrium of internal and external work.

The additional enhancement due to tensile membrane action is derived [5] for a rectangular slab panel with simply supported edges (ie. no moment or axial restraint), based on the postulated pattern of in-plane axial forces shown in Fig. 8. The enhancement effect of this tensile membrane action comes from two sources:

- Influence of the in-plane axial forces on the yieldline moment capacity. (Compression enhances; tension detracts)
- P - Δ (or catenary action), as shown in Fig. 9. In this case in-plane tension generates enhanced resistance, in-plane compression generates reduced resistance.

In order to avoid over-estimating the slab panel's load-carrying capacity under flexural / tensile membrane action, it is important that lower bound solutions for both the yieldline moment and tensile membrane enhancement are developed and confirmed by experimental test. This test must include sufficient monitoring of deflections, observed patterns of behaviour and recording of internal strains at critical locations, to allow the proposed mechanisms to be validated as dependable lower bound solutions.

A large-scale (9.5 m x 6.5 m) composite slab test to failure has been undertaken [8] by BRE, to produce one example of experimental validation of the proposed mechanisms. The validation requires unobstructed observation of behaviour on both sides of the slab, recording of concrete and steel strains to failure and recording of in-plane and out-of-plane slab panel deflections. Because the first two of these cannot effectively be undertaken in fire test conditions, the test was undertaken at ambient temperature, by loading the slab panel to destruction. Only those components in the slab panel which would dependably remain cool enough to retain significant strength in fully developed fire conditions were included in the ambient temperature test – in this case the slab concrete and mesh reinforcement. The test set-up and execution is described in [8].

Failure Criteria

In terms of how closely the postulated failure criteria and deflections were met by the observed performance, the following can be said:

- The yieldline pattern developed as predicted, in terms of both applied load and geometry
- The failure mode is a mid-span fracture of the reinforcement across the short span. This postulated mid-span crack at EF (Fig. 7) visibly commenced forming at 88% of the final applied load and increased in length, with subsequent load increments, up to 94% of the applied load, whereupon that crack remained stable in length while a second crack formed between location A & F (Fig. 7)
- The mid-span crack finally reached 83% of the width of the slab, not extending into the compression ring beam region of the slab edge. It was greatest in width at midspan
- The fact that the crack does not extend full width means that slightly less than the magnitude of tension force shown along line EF is developed. However, the centroid of

this force is further from point E than assumed, so in terms of moment generated by the force about point E, the effect is minimal

- The patterns of out-of-plane and in-plane slab panel deformations were consistent with the proposed structural mechanisms. In particular, the maximum midspan deflection (measured at point F, Fig. 7), remained nearly constant at 110 mm once the yieldline pattern was formed until 9% more load had been added. It then increased from 110 mm to 220 mm as the load increased from 52% of the ultimate load to 84% of the ultimate load. As the central crack then developed, the midspan deflection increased from 220 mm to 700 mm (at 94% of ultimate load) and remained constant at 700 mm from 94% to 100% of the ultimate load

- Bailey proposes [5] an equation for limiting the mid-span deflection to just below the point at which the reinforcement will commence fracture along the mid-span crack. Its application to the BRE test [8] would limit the deflection to 216 mm, as is desired.

In terms of the reinforcement strains recorded in [8], the following can be said:

- The transverse strains recorded near the slab panel centre (point F in Fig. 7) remained near constant at 200 micro-strain from the development of the yield-line pattern until the development of the mid-span crack EF. These were recorded slightly off centre. Their magnitude, at 7% of yield strain, is low, considering their proximity to the visually observed yieldline that had developed along CFD (Fig. 7) at only 48% of the ultimate load

- The longitudinal strains recorded at the centre along the crack plane EF start below 50 micro-strain at yieldline formation and increase to 400 micro-strain at the load step immediately prior to crack EF commencing to form They then jump to 1600 micro-strain (56% of yield strain) at the next load step, as the crack commences forming, before reducing to 630 micro-strain once the crack EF is fully formed

- This pattern is consistent with the proposed tensile membrane structural mechanism [5]. The maximum recorded strain (56%) is just above the 50% limit on longitudinal mechanical strain incorporated in the slab panel deflection limit [2].

Bailey does not include a shear failure criterion in [5], nor was shear failure observed in [8]. However, that slab was lightly reinforced. He makes the point that general application of the procedure in fire engineering design requires a check for shear failure; such a check is included in the application developed in [2, 3].

In a severe fire, the vertical load on the slab panel remains constant (or decreases) while the slab panel deformation increases, due to thermal and mechanical effects. The shear capacity per unit length from the slab, as derived from [15], is independent of the percentage of flexural reinforcement supplied (ie. is a function of concrete strength only) for a wide range of reinforcement levels. However, the flexural / tensile membrane capacity is directly related to flexural reinforcement content. This means that, if the slab performance under fire conditions is being represented in an ambient temperature test by incorporating only the reinforced slab and by loading it to failure, increasing the quantity of reinforcement will linearly increase the flexural / tensile capacity, but will have negligible effect on the shear capacity. Therefore, at some point, the failure mode will change from flexural / tensile panel failure to shear failure at the supports. The author has not explored this further in ambient temperature testing, however it must be a consideration if planning such tests on more heavily reinforced slabs than [8]. The same reasoning will not apply in a fire situation.

Application to Elevated Temperature Conditions

The following factors are significant:

(i)   The influence of thermal-induced curvature needs to be included, as it potentially increases the contribution to tensile membrane resistance. This is done by including a thermal deflection term in the calculation of slab panel deflection. The derivation of that term is given in section 8.4 of [5] and in section A4.2.3 of [2]

(ii)   The effect of restrained thermal expansion of the slab panel is ignored. For slab panels with two or three free edges (ie. the edge of a building), the influence is likely to be very small. For slab panels with two or more edges restrained, the effect will be more significant, but difficult to quantify. Increased in-plane compression from restraint would increase the moment capacity along a yieldline, but decrease the P - Δ enhancement effect (Fig. 9). However the net effect is considered likely to be positive on slab load-carrying capacity

(iii)   The increase of ductility of the mesh reinforcement, as it increases in temperature, is ignored. However, a series of slab panel fire tests scheduled for June/July 2002 as part of a University of Canterbury / HERA / BRANZ research project should quantify the extent of this increase, for reinforcement to AS/NZS 4671 [17]

(iv)   For a slab panel in an actual building, the influence of the steel deck and steel secondary beams needs to be considered [8]. Bailey does this [5] by considering the load-carrying contribution from slab and secondary beams separately and summing them. The author considers that this is appropriate for slabs supported on non-composite secondary beams. However, for slabs supported on composite secondary beams, the contribution of the secondary beams should be included directly in the determination of yieldline moment capacity (see eg. Fig. 5) and tensile membrane enhancement. That is the approach used in the SPM procedure [2]

(v)   Calculation of the elevated temperature shear capacity at the slab panel supports is necessary, but not developed by Bailey. A suitable procedure is included in [2] and briefly critiqued in the following section.

CRITQUE OF THE NEW ZEALAND APPLICATION

Contributions to Yieldline Moment Capacity

All elements that can resist internal tension and hence contribute to the development of yieldline moment capacity are included in the slab panel moment / tensile membrane capacity determination. This includes the secondary beams (Fig. 2) and interior support bars (Fig. 6) for m_x and the deck trough bars (Fig. 6) for m_y. The contribution of these is calculated at a design elevated temperature, as detailed in [2].

The location and contribution of elements to developing m_x is shown in Fig. 5. These contributions apply when the slab panel has achieved the deformed shape consistent with the high temperatures and loss of strength associated with tensile membrane action. The strain/ stress history within the secondary beam and slab throughout the heating cycle and prior to this point is very complex and still not well quantified. However, given that the slab panel is operating in the inelastic regime, the stress-strain history prior to developing m_x is unimportant, provided that it does not result in premature failue of the tensile load-carrying capacity of any element or separation of the slab and beam. Furthermore, integrity of these elements must be retained throughout the cool-down phase. The material selection, design and detailing provisions of [2], coupled with the knowledge of floor system performance

gained from the LBTF tests [4, 5] and the check against shear failure required by section A4.2.6 of [2], is dependably expected to achieve this.

Elevated Temperature Shear Capacity

This is a critical check to make and is implemented in section A4.2.6 of [2]. There are two sources of shear resistance available:
- through the slab into the supports
- through the slab into the secondary beams and hence into the supports.

The former is calculated through the cover slab thickness (ie. the depth of concrete above the ribs in a ribbed slab). The shear capacity is determined using the NZS 3101 shear in slab provisions, with the participating depth of concrete, d_v , calculated neglecting the hottest layers at the fire exposed face. Experience from inelastic seismic testing of reinforced concrete members has shown that the shear capacity under monotonic inelastic rotation is maintained as long as the tension reinforcement within the yielding region does not fracture. For slab panels, this is achieved through restrictions on the material selection and positioning of reinforcement along all slab panel support lines; this reinforcement is shown in Fig. 6.

The latter is achieved from the lesser of the elevated temperature capacity of the unprotected secondary beam web or that of the unprotected bolt group. This capacity is maintained throughout the heating and cooling cycle, provided that the connections are designed to retain their integrity including their integrity under cooling-induced tension. This is a requirement of connections used in the SPM procedure and will be delivered by connections designed and detailed to [22].

The shear capacity of the slab panel at the primary beam supports is the sum of these two. Given the ductility available from each of the two mechanisms and the magnitude of support rotation expected, this summing of the two sources of shear resistance is appropriate.

No allowance is made for the contribution of the decking towards increased shear capacity. However, no allowance is made for the influence of spalling of the concrete at the supports in potentially reducing the slab shear capacity. New Zealand aggregates have been shown to be not prone to spalling under standard fire test or natural fire test conditions.

Ductility of Slab Reinforcement

This comprises either mesh or bar. Mesh is typically Grade 500L to AS/NZS 4671 [17] with a dependable minimum uniform elongation of 2%. Bar to Grade 300E or 500E has a dependable minimum uniform elongation of 15%. Based on the location of the reinforcement within the slab and the plastic rotation at the yieldlines, associated with the deformed shape shown in Fig. 9 and the limiting displacement specified in equations 60.A22 of [2], the required strain demands on reinforcement crossing the positive yieldline CD (Fig. 7) and the negative moment yieldline at the interior supports (Fig. 2) have been assessed and shown to be within the above material mechanical capabilities. Details are given in section CA4.2.3 of [2], with material restrictions in section 4. They are based on ambient temperature elongation; this will increase with elevated temperature but the extent of this increase is currently unquantified, with details expected to become available from slab panel fire tests planned in 2002 and mentioned earlier.

Requirements for Integrity

For floors comprising concrete slabs on steel deck, the requirements for integrity (prevention of the passage of hot gas or flame) through the floor are met by the deck sealing the fire exposed face of any potential crack.

For floors not incorporating a steel deck, then the potential for integrity failure through a full depth crack exists and must be controlled by limiting the crack width. Positive moment yieldlines generate maximum crack width on the fire exposed side, while the reverse holds for negative moment yieldlines. Where these two co-exist there is the maximum potential for a full depth crack; examples are regions near the supporting columns A2 and E2 in Fig. 2.

The approach currently specified by [2] is to reinforce the whole slab panel, when a steel deck is not present, to achieve the "strong crack control" provisions of AS 3600 [23]. These provisions are intended to ensure that crack widths under serviceability conditions or due to shrinkage and temperature effects do not exceed 0.2 mm [23]. To fail the integrity requirement, crack widths of 1.0 mm or more are required, hence these provisions are expected to deliver dependable performance in this regard. Their adequacy will be established in the series of slab panel fire tests in mid-2002 and mentioned below.

FUTURE RESEARCH

As previously mentioned, a series of slab panel fire tests are scheduled for June/July 2002 as part of a University of Canterbury / HERA / BRANZ research project. These tests will provide an experimental and analytical evaluation of the SPM method. Six slab panels, each measuring 4.3m x 3.3m, have been built. They will be supported on vertical supports over the BRANZ test furnace, loaded with 3.3kPa applied load and heated to failure under the Standard fire curve regime. Their performance will be monitored for load-carrying capacity, integrity and insulation. The SPM procedure will be amended, if and as required, based on the findings of this research. The results will also be used to validate the program SAFIR [11.1] for use in slab modelling, thereby allowing this program to be used to evaluate the performance of slab panels over a wider range of boundary conditions.

The author would then like to see the influence of supporting member deflection on the slab panel capacity determined. In developing the procedure to its current form [2], it is a requirement that the supporting members remain "effectively undistorted under severe fire conditions relative to the peak downwards deflection expected within the slab panel region"[3]. However evidence from the Cardington steel building fire tests [4] indicates that the mechanism will still work when the supporting beams undergo significant vertical deflection. Quantifying this through advanced analysis would be a worthwhile outcome.

REFERENCES

[1]   C/AS1: 2001, Acceptable Solution for Fire Safety; Building Industry Authority, Wellington

[2]   Clifton, GC et.al.; Design of Multi-Storey Steel Framed Buildings With Unprotected Secondary Beams or Joists for Dependable Inelastic Response in Severe Fires; HERA Steel Design and Construction Bulletin; No. 60, February 2001, pp. 1-58

[3]   Clifton, GC and Hinderhofer, M; Performance of Steel Structures in Fully Developed Fires: Fire Engineering Research Results of Interest; HERA Steel Design and Construction Bulletin, No. 59, December 2000, pp. 2-25.

[4]   Kirby, BR; The Behaviour of a Multi-Storey Steel Framed Building Subject to Fire Attack - Experimental Data; British Steel Swinden Technology Centre, United Kingdom, 1998. Also data from BRE, Cardington, on the Corner Fire Test and Large Compartment Fire Test, 1996.

[5]   Bailey, CG; Design of Steel Structures With Composite Slabs at the Fire Limit State; UK Building Research Establishment, Watford, England, 2000, Report No. 81415

[6]   Park, R; Ultimate Strength Design of Reinforced Concrete Slabs, Volume 2; University of Canterbury, Christchurch, 1970 (approx).

[7]   Newman, GM et.al; Fire Safe Design – A New Approach to Multi-Storey Steel Framed Buildings, The Steel Construction Institute, Ascot, England, 2000, SCI Publication P 288.

[8]   Bailey, CG; The Tensile Membrane Action of Unrestrained Composite Slabs Simulated Under Fire Conditions; UK Building Research Establishment, Watford, England, 2000, paper accepted for publication in Engineering Structures.

[9]   Buchanan, AH (Editor); Fire Engineering Design Guide (Second Edition); Centre for Advanced Engineering, University of Canterbury, Christchurch, 2001.

[10]   Barber, DJ; Calculation of the Fire Resistance of Composite Concrete Slabs With Profiled Steel Sheet Under Fire Emergency Conditions; HERA, Manukau City, 1994, HERA Report R4-82

[11.1] Franssen, JM et.al.; SAFIR: A Computer Program for Analysis of Structures Submitted to the Fire; University of Liege, Belgium, 1998/2001.

[11.2] Mason, J; SAPPHIRE: A Pre-Processor for SAFIR; Sinclair Knight Merz, Wellington, 2000.

[12]   Kirby, BR et.al; Natural Fires in Large Scale Compartments; British Steel Technical, Swindon, UK, 1994.

[13]   EC1-1-2/59:2001 (Third Draft) : Eurocode 1 – Actions on Structures Part 1-2: General Actions – Actions on Structures Exposed to Fire; CEN, Brussels, Belgium.

[14]   Clifton GC; Fire Models for Large Firecells; HERA Manukau City, 1996, HERA Report R4-83, plus amendments on page 20, HERA *DCB* No. 54, February 2000.

[15]   NZS 3101:1995 (incorporating Amendments 1 and 2, 1997), Concrete Structures Standard; Standards New Zealand.

[16]   DD ENV 1992-2 : 1996, Eurocode 2: Design of Concrete Structures Part 1.2 General Rules – Structural Fire Design (together with United Kingdom National Application Document); BSI Standards, London, England.

[17]   AS/NZS 4671: 2001, Steel Reinforcing Materials; Standards New Zealand, Wellington.

[18]   Clifton, GC et. al.; Draft for Development: Revision 2: Design Procedure for the Inelastic Floor System/Frame Response of Multi-Storey Steel Framed Buildings in Fully Developed Natural Fires; HERA, Manukau City, 2000, HERA Report R4-90-DD-Rev 2

[19]   DD ENV 1993-1-2 : 1996, Eurocode 3: Design of Steel Structures Part 1.2 General Rules – Structural Fire Design (together with United Kingdom National Application Document); BSI Standards, London, England.

[20]   NZS 3404: 1997, plus Amendment No. 1: 2001, Steel Structures Standard; Standards New Zealand, Wellington.

[21]   Clifton, GC and Robinson, J; Notes Prepared for a Seminar on The Behaviour and Design of Multi-Storey Steel Framed Buildings for Severe Fires, Revised June 2001; HERA Manukau City, 2001, HERA Report R4-105.

[22]   Hyland C; Structural Steelwork Connections Guide; HERA, Manukau City, 1999, HERA Report R4-100.

[23]   AS 3600, 1994, Concrete Structures; Standards Australia, Sydney, Australia.

Session 4:
Steel buildings

EFFECT OF SUPPORT CONDITIONS ON THE FIRE BEHAVIOUR OF STEEL AND COMPOSITE BEAMS

Peter MOSS, Andy BUCHANAN, Jenny SEPUTRO, Clayton WASTNEY and Richard WELSH
University of Canterbury, Christchurch, New Zealand

ABSTRACT

The fire behaviour of a structural steel beam or a steel and concrete composite beam in a fire compartment depends on many factors including the nature of the supports at the ends of the beam.

This paper describes a detailed analytical investigation into the effects of support conditions on the fire performance of steel and composite steel-concrete beams exposed to linearly increasing temperature with time, as well as standard and parametric fires.

The support conditions include simply supported, fully fixed, and a range of intermediate cases, providing varying levels of axial and flexural restraint. In each case, a comparison of the deflected shape with the evolving internal forces shows unusual but predictable behaviour, strongly dependent on the stress-strain relationship of the steel. In addition to the standard support conditions, a spring was used to simulate the effect of axial restraint provided by adjacent spans of a multi-span beam. This case showed that the spring stiffness had a very considerable influence on the behaviour of the beam and the time to failure under an increasing fire temperature.

This paper gives new insight into the structural performance of steel and composite beams, observed in recent fires such as the eight storey steel frame at Cardington. There are major implications for structural designers.

KEYWORDS: *fire engineering, steel beams, composite beams.*

INTRODUCTION

In multi-storey steel framed buildings, the floors are usually made of concrete, either precast or cast-in-situ. In the former case, the concrete floor does not usually act compositely with the steel beams but does act as a heat sink and provide fire protection for the top flange of the steel beam. In the latter case, the floor is often formed by casting concrete on sheet-metal formwork with steel shear studs welded to the top of the beams to provide composite action. Over the last ten years, developments in composite floor systems and advances in fabrication technology have made steel framed buildings with composite floor construction an extremely competitive form of construction. Fire tests on an eight storey steel framed building at Cardington [1] have shown that modern steel-concrete construction provides good inherent fire resistance.

Along with these developments in fire engineering, sophisticated finite element software has been developed to aid the design and analysis of structures at elevated temperatures [2]. Recent research carried out in several countries (e.g see [3, 14]) as well as in New Zealand [4-6] has shown that it is possible to predict the performance of steel buildings which survive typical fires, albeit with substantial deformation in the beams.

This paper describes the structural performance of unprotected single span steel and composite steel-concrete beams exposed to uniformly increasing temperatures on three sides, as well as the ISO 834 fire [7]. The beams were analysed with four different support conditions: simply-supported (*pin-roller supported*), *pin supported* at each end, *fixed and slide supported*, or *fixed* at each end, as shown in Figure 1.

(a) Pin-roller   (b) Pin-pin

(c) Fixed-slide   (d) Fixed-fixed
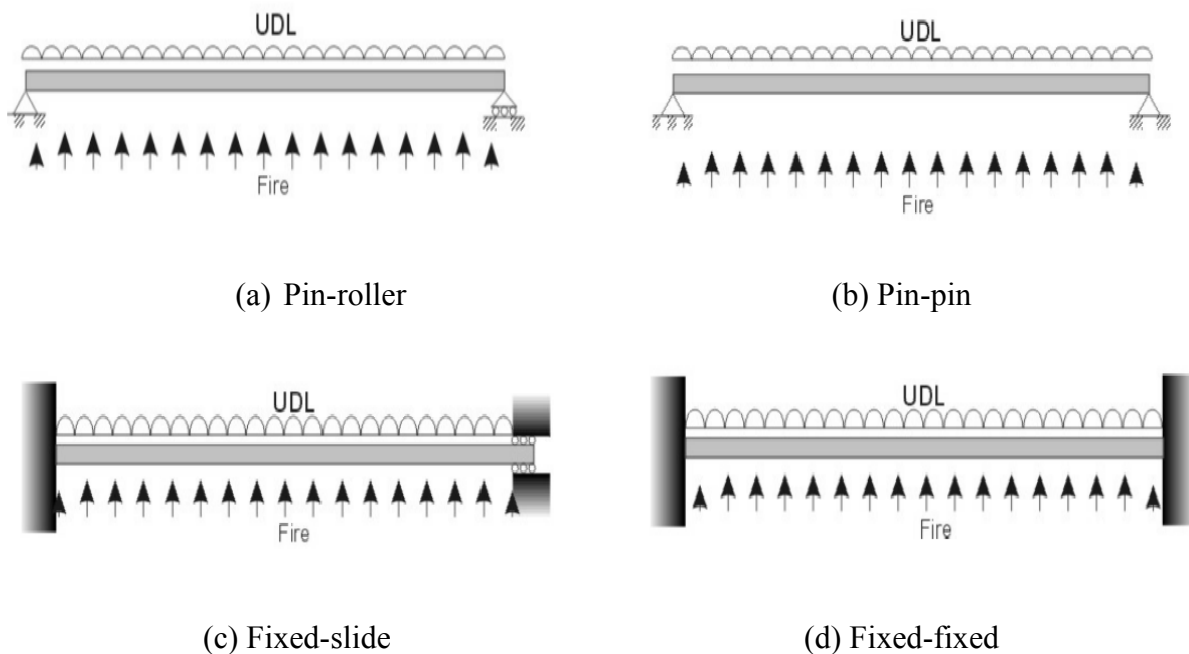
FIGURE 1   Support conditions investigated

ANALYSES CARRIED OUT

Analyses were carried out using the SAFIR computer software [8] written to analyse structures under ambient and elevated temperature conditions. SAFIR can be used for one, two and three dimensional analyses using truss, beam, shell and 2-D and 3-D solid elements in conjunction with a range of material models incorporating stress-strain behaviour at ambient and elevated temperatures.

Two beams, each having a span of 8 m, were analysed; one was a 610 UB 101 steel beam [9] with properties to EC3 [10] while the other was a composite beam [11] comprising the same steel section but with a 120 mm thick concrete slab cast on top of the top flange as shown in Figure 2. The two beams were analysed for the range of support conditions shown in Figure 1. As the analyses were two dimensional, no lateral restraint was required to prevent lateral flexural torsional buckling.

Because of the different load-carrying capacities of the two beams, the steel beam was subjected to a load of 25 kN/m while the composite beam was subjected to a load of 50 kN/m. The steel beam was subjected to a constant rate of rise in temperature of 10°C/min until collapse occurred, while the composite beam was subjected to a temperature rise of 5°C/min. These heating rates are not representative of realistic fire attack, but they have been used to show the response of the beams to increasing temperatures. Exposure to the ISO fire is also described.

(a) Steel beam   (b) Composite steel/concrete beam
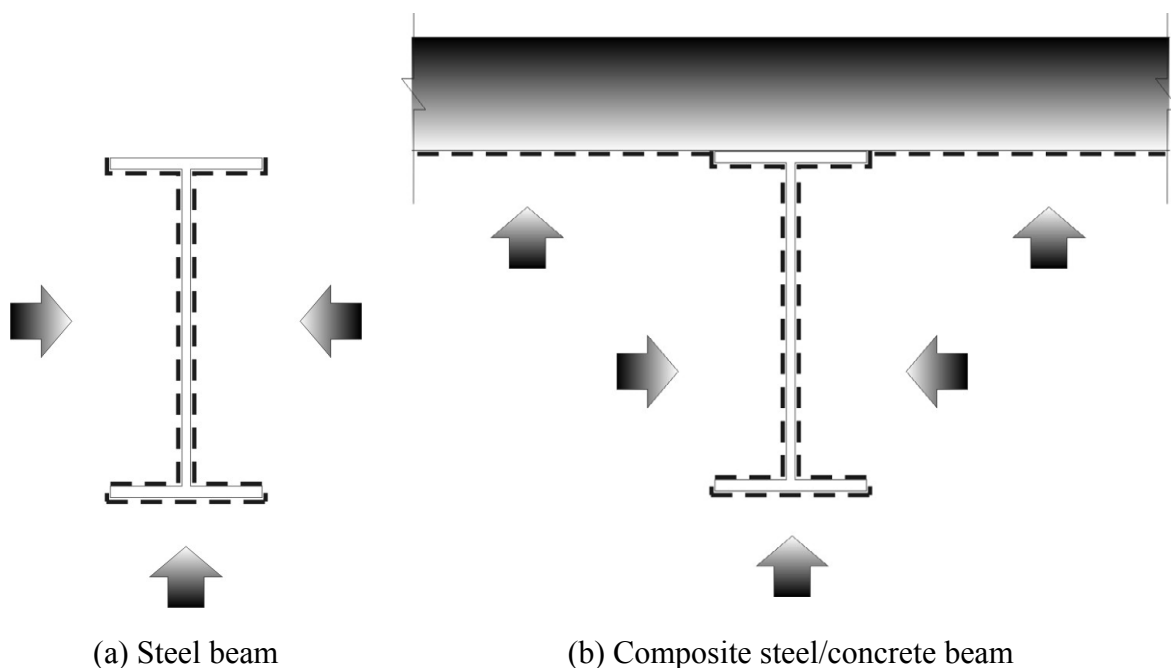
FIGURE 2   Beam cross-sections. Dotted lines indicate fire-exposed surfaces

STEEL BEAM RESULTS – uniform temperature rise

Pin-roller supports
Since the beam is free to expand, the bending moment along the beam remains constant over time as no axial force is induced in the beam. Failure occurs when one plastic hinge forms at mid-span.

The mid-span deflection of the beam is shown in Figure 3a while the average top and bottom flange stresses are shown in Figures 3b & c. In the latter figures, the dashed line is the temperature reduced yield stress from EC3 [10] while the grey line is the temperature reduced proportional limit stress, also from EC3. It can be seen that the bottom flange stresses reach the proportional limit after 62 minutes (point (a)) and the top flange stresses reach the proportional limit after 70 minutes (point (b)).

Once the bottom flange yields after 81 minutes (point (c)in Figure 3c) the section capacity reduces significantly causing runaway deflection. When the top flange yields, the failure mechanism forms (point (d) in Figure 3b).
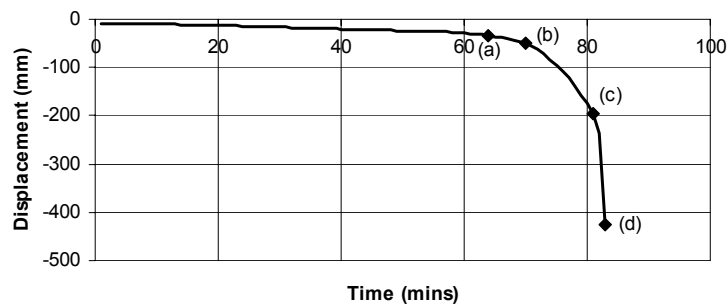
(a) Mid-span deflection
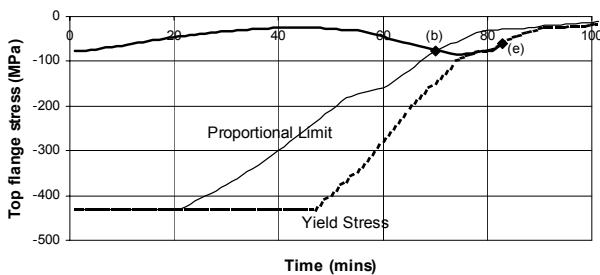
(b) Top flange stress at midspan
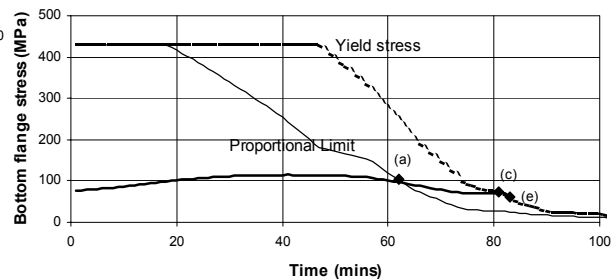
(c) Bottom flange stress at midspan

FIGURE 3   Results for pin-roller supported steel beam

Pin-pin beam supports

These supports prevent thermal elongation and consequently induce axial restraint into the beam. This axial force varies with the increasing temperature and makes the behaviour of the beam more complex. The mid-span deflection, mid-span moment, axial force and top and bottom flange stresses are shown in Figure 4.

The axial force in the beam increases due to the restraint of the thermal expansion until the beam starts to deflect significantly when the top flange stress reaches the temperature reduced proportional limit at point (a) in Figure 4d. This causes alteration to the stresses in the bottom flange and at the supports. The beam also starts to lose its stiffness as the modulus of elasticity is reduced by the elevated temperature, further increasing the deflection. This yielding and reduced stiffness causes a sudden reduction in the axial load (point (a) in Figure 4).

At 53 mins, the top flange yields at the mid-span, followed by the bottom flange reaching the proportional limit ½ min. later. At point (d) in Figures 4b-e, the bending moment begins to decrease as the mid-span plastic hinge forms and the axial force decreases faster than the deflection increases. At point (e), the bottom flange yields and the plastic deformation allows the deflections to increase further. The beam goes into axial tension after 80 mins of heating.

(a) Mid-span deflection

(b) Mid-span moment

(c) Axial force

(d) Top flange stress at midspan

(e) Bottom flange stress at midspan
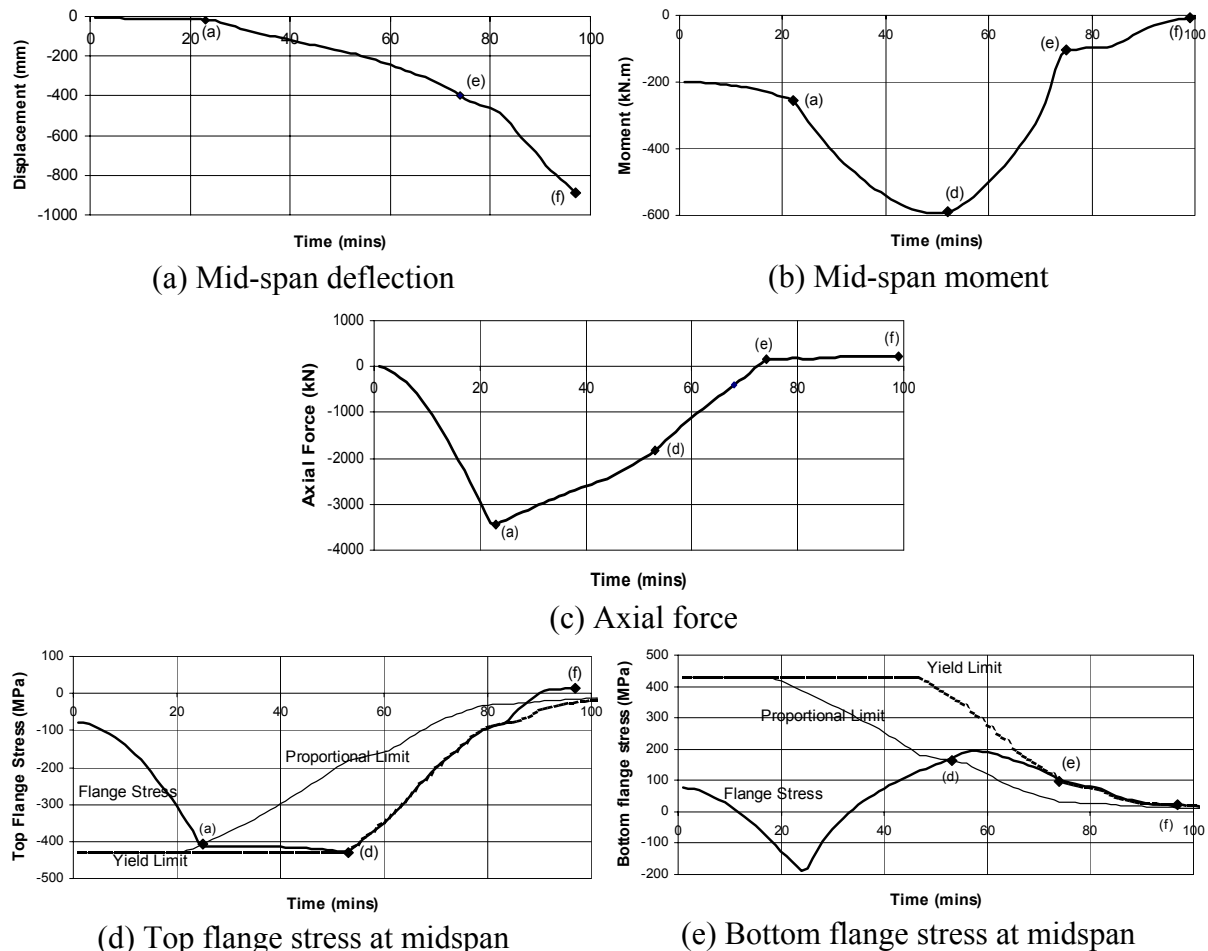
FIGURE 4   Results for pin-pin supported steel beam

Fixed-slide beam supports

The beam with *fixed-slide* supports was free to elongate and consequently no axial force was induced as a result of thermal expansion. For the first hour of heating, the beam behaved elastically with very small mid-span deflection. The the mid-span deflection, the mid-span and support moments, and the stresses in the top and bottom flanges at the mid-span are shown in Figure 5.

At 66 minutes, the top flange at the supports reached the temperature reduced proportional limit, followed three minutes later by the bottom flange. After this stage the deflection began to increase noticeably. At mid-span, the bottom and top flanges reached the proportional limit after 77 and 84 minutes respectively (points (c) and (d) in Figures 5f, e).

The bottom flange at the supports reached the temperature reduced yield stress at 85 minutes of heating and the top flange at 89 minutes. When the top and bottom flanges at the mid-span yielded at the same time after 90 minutes (point (g) in Figures 5e, f), runaway deflection occurred and the beam failed.

The changes in the bending moments in the beam are shown in Figure 5d where it can be seen that the overall shape of the bending moment remained the same throughout the fire exposure. The negative moment at the supports increased during the first 40 minutes due to thermal bowing. The amount of thermal bowing then decreased as the temperature gradient decreased, causing a reduction in the end moments. The mid-span moments changed accordingly since the sum of the mid-span moments and the support moments at any given time must equal $wL^2/8$ since there is no axial force present. At failure, the mid-span and support plastic hinge moments were both equal to $wL^2/16$.

(a) Mid-span deflection

(b) Mid-span moment

(c) End moment

(d) Moment distribution

(e) Top flange stress at mid-span

(f) Bottom flange stress at mid-span
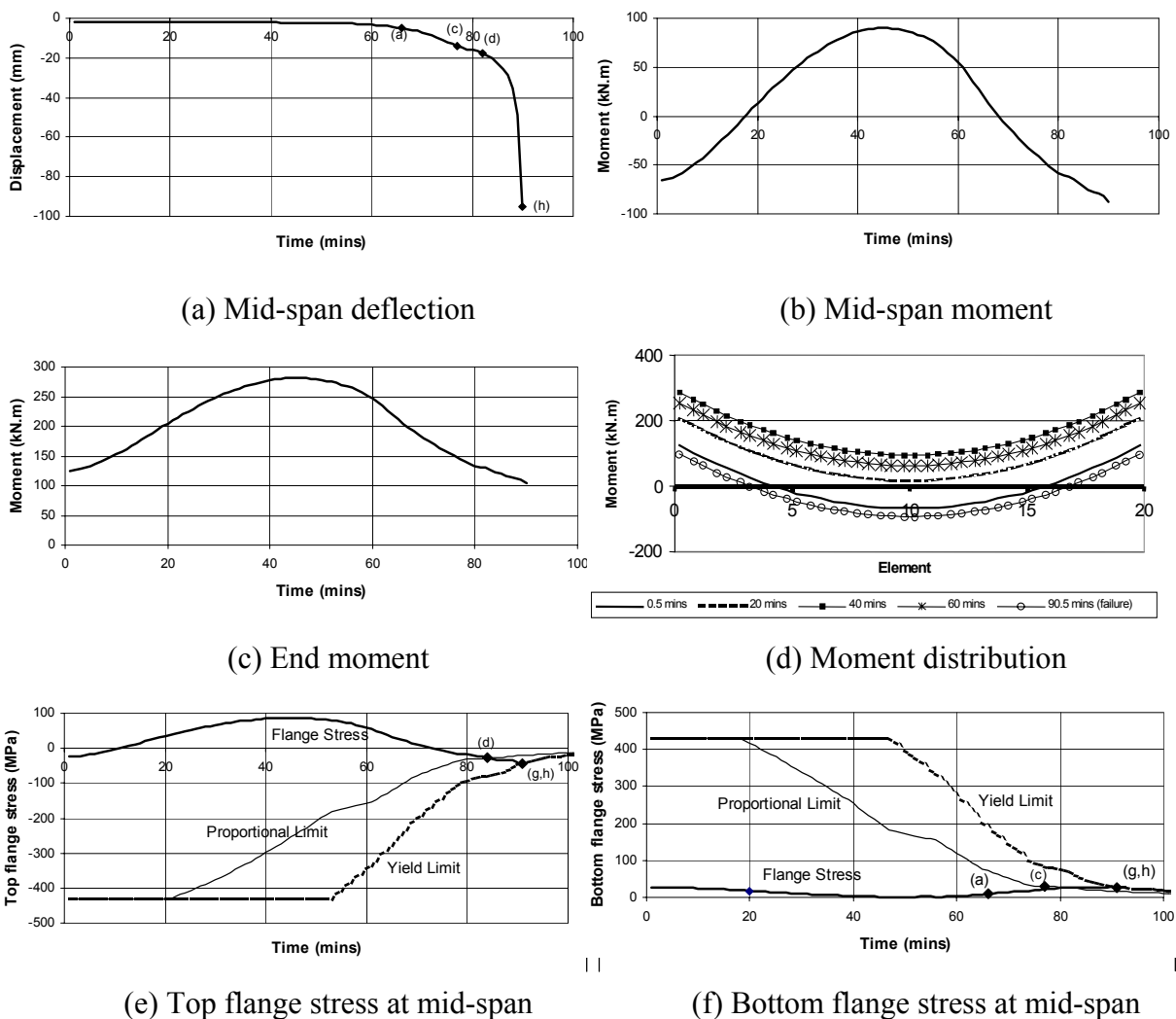
FIGURE 5   Results for fixed-slide supported steel beam

Fixed-fixed beam supports

With fully fixed supports at both ends, the beam required the development of three plastic hinges to form a failure mechanism. The changes in mid-span deflections, bending moments, axial force and top and bottom flange stresses are shown in Figure 6.

During the first 25 minutes there was almost no increase in the mid-span deflection up to point (a) in Figure 6a, when the bottom flange at the supports reached the proportional limit stress. Thermal expansion caused the development of a compressive axial force (Figure 6e) and this, together with the differential temperature, caused a change in the bending moments as shown in Figures 6b-d. The high axial compressive force caused the bottom flange at the supports to reach the proportional limit after 25 minutes leading to an increase in the rate of deflection, while the bending moment decreased (point (a) in Figures 6a,b,d,f). The maximum axial force was still well below the plastic squash load of 5590 kN.

(a) Mid-span deflection

(b) Mid-span moment

(c) End moment

(d) Moment distribution along the beam

(e) Axial force

(f) Top flange stress at mid-span

(g) Bottom flange stress at mid-span
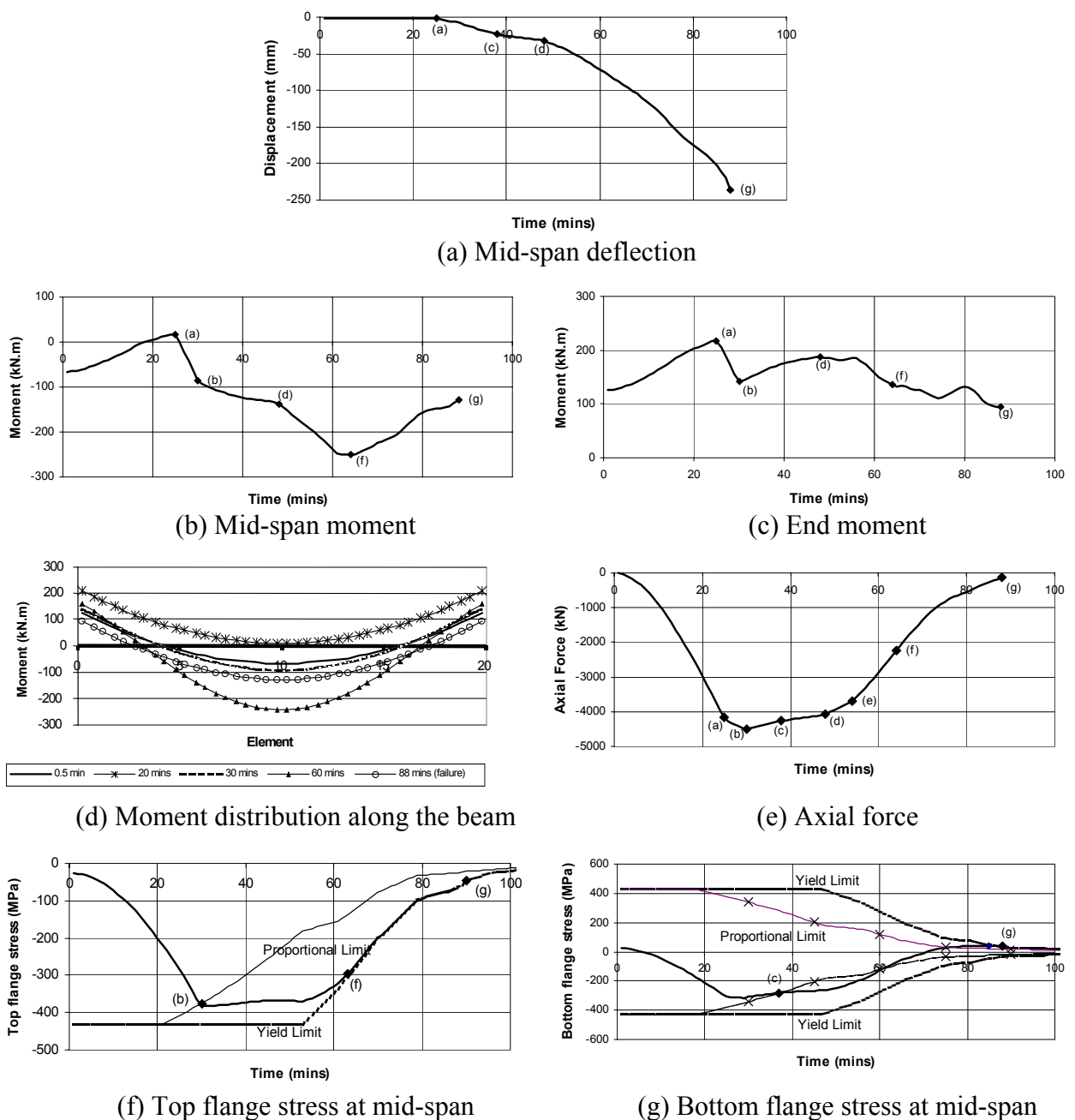
FIGURE 6   Results for fixed-fixed supported steel beam

The flanges heated up more slowly than the web on account of their greater thermal mass. Plastic hinges started to form at point (b) in Figures 6b,c,f when the top flange stress reached the temperature-reduced proportional limit. The mid-span moment grew progressively at this point and moment redistribution allowed the moment to compensate for the strength reduction at mid-span (Figures 6b,c). At the same time, the axial force began to reduce (Figure 6e) while the deflection continued to increase. The bottom flange at mid-span reached the proportional limit after 37 minutes (point (c)) but caused no obvious change in the overall behaviour of the beam. However, when the top flange at the supports reached the proportional limit (point (d) in Figure 6e), the axial load reduced more rapidly and the mid-span moment showed a sudden increase as redistribution of moment from the supports to the mid-span took place. The P-δ effect of the axial force was governed by the deflection since the deflection was increasing even though the axial force was reducing.

The bottom flange at the supports was the first flange to yield after 55 minutes (point (e) in Figure 6e, followed by the top flange at mid-span yielding (point (f). There was not much residual strength left in the beam at this point as the three plastic hinges were continuing to develop and the axial force was reducing to zero. Unlike the pin-pin case where the beam developed catenary action in tension and carried the load for 97 minutes, the fix-fix beam experienced loss of strength and stiffness earlier and failed after 88 minutes.

The moment distribution along the beam at various times of heating are illustrated in Figure 6d. The support moment can be seen to be always hogging while the mid-span moment was always sagging, except for a brief period about 20 minutes into the heating. At the beginning of the heating, the support moments were $wL^2/12$ and the mid-span moments were $wL^2/24$, and these changed with the increasing heating on account of the P-δ effects and thermal bowing. At failure, the end moments and the mid-span moment were both $wL^2/16$ with plastic hinges in three locations.

A significant finding from this analysis is that the moment restraint at the supports caused the beam to be very sensitive to the stress conditions with respect to the temperature reduced proportional limit and yield stresses. This is illustrated by Figures 6f, g where the top and bottom flange stresses at mid-span are compared with the proportional limit and yield stress envelopes.

STEEL BEAM RESULTS –ISO fire

The analysis of an unprotected steel beam carried out above for a uniform rate of heating has been repeated with exposure to the standard ISO-834 fire [7]. The results are shown to be similar, as described below. The failure times in this section are more realistic of actual fire conditions. A future study will investigate behaviour with natural fires which include a decay phase.

Pin-roller supports

The mid-span deflection of the beam subjected to the ISO fire is shown in Figure 7a while the average top and bottom flange stresses are shown in Figures 7b & c. The bottom flange of the beam reaches the proportional limit stress after 7½ minutes and the yield stress after 21½ minutes. The top flange reaches the proportional limit stress after 18½ minutes and the yield stress after 23½ minutes. At this time a plastic hinge develops fully and a run-away failure of the beam occurs after 24 minutes
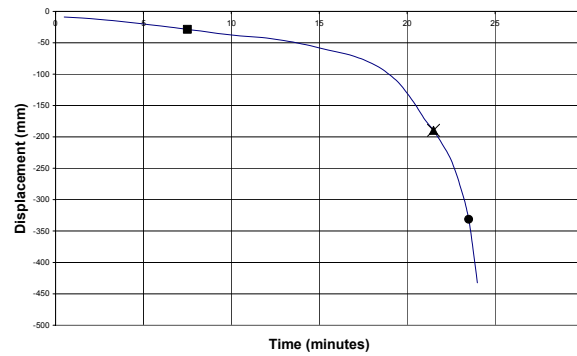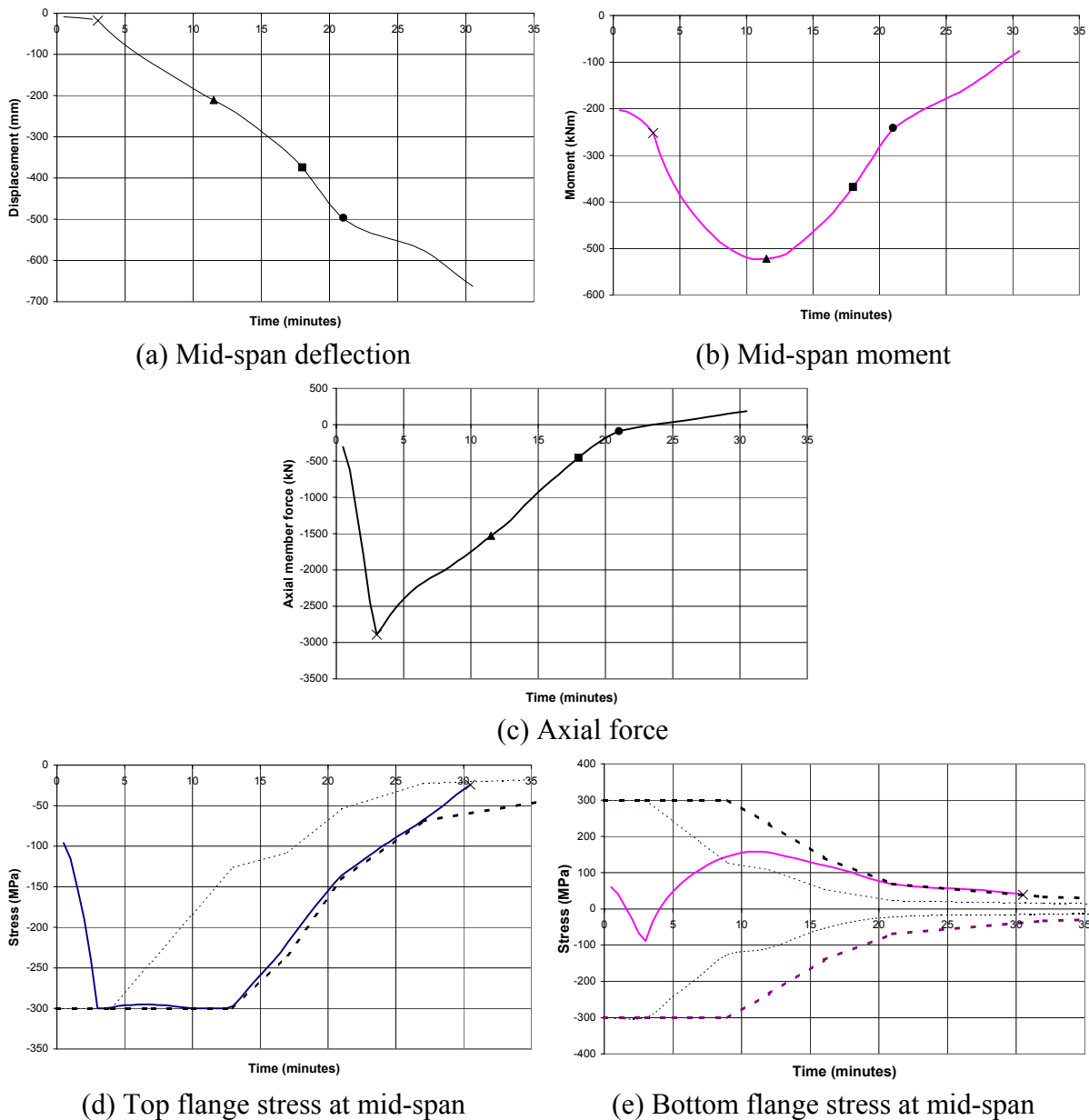
(a) Deflection
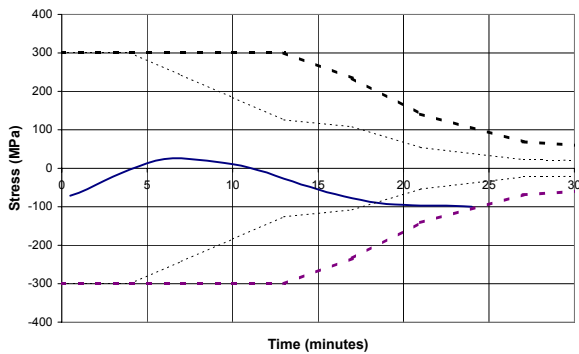
(b) Top flange stress
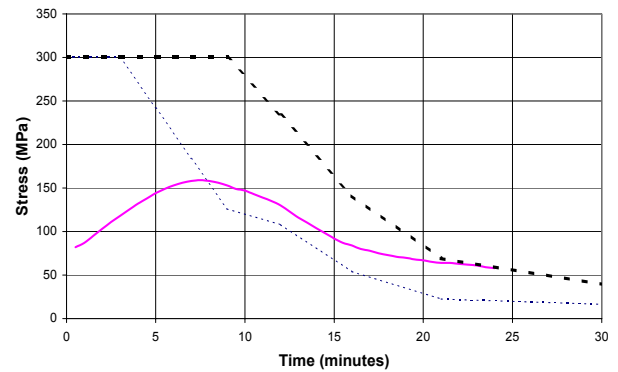
(c) Bottom flange stress

Figure 7 Results for pin-roller supported steel beam in ISO fire

Pin-pin supports

For pin-pin supports, typical output is shown in Figure 8. Over the first 3 minutes, the axial force increases very rapidly on account of the restraint against thermal expansion, then decreases when the top flange and the top portion of the web yield in compression (Figure 8d). The bottom flange yields after 18 minutes (Figure 8e), followed by the bottom part of the web to complete the formation of a plastic hinge after 21 minutes. The beam does not fail at this point as it can carry further load by developing axial tension, with final collapse occurring after 31 minutes of heating.

(a) Mid-span deflection

(b) Mid-span moment

(c) Axial force

(d) Top flange stress at mid-span

(e) Bottom flange stress at mid-span

FIGURE 8   Results for pin-pin supported steel beam in ISO fire

COMPOSITE BEAM RESULTS – uniform temperature rise

Pin-roller beam supports

The results of the analysis are shown in Figure 9. Up to point (a), the beam shows elastic behaviour with little vertical displacement since the roller support allows unrestrained thermal expansion to occur. From point (a) to (b) the section exhibits increasing plastification and the mid-span displacement increases. The bottom flange stress decreases while the bending moment remains constant. At point (b), the bottom flange reaches the thermally reduced yield stress. At this point the bottom flange is yielding in tension and the neutral axis moves up the section towards the concrete slab and the displacement shows runaway failure. As the roller

support is unable to offer any tension reaction, the member finally collapses 12 mins after the bottom flange reaches the yield stress (point (c)).

(a) Mid span displacement   (b) Mid span bending moment

(c) Mid span bottom flange stress
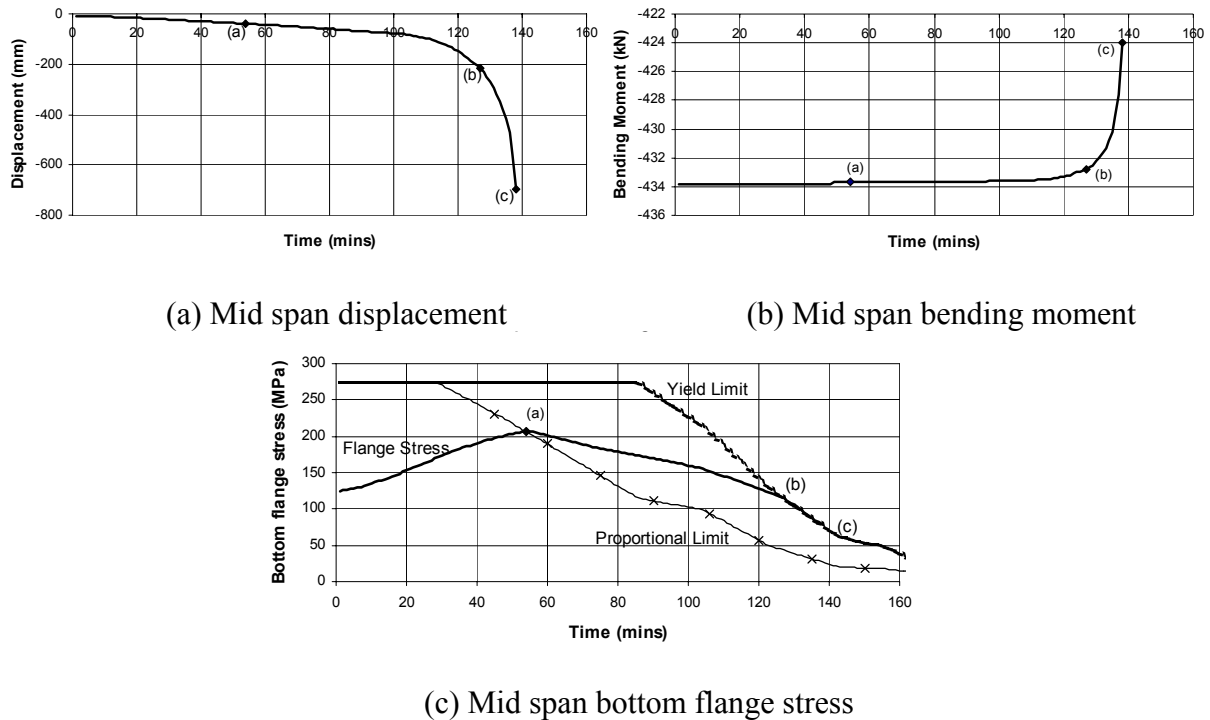
FIGURE 9   Mid span results for pin-roller supported composite beam.

Pin-pin beam supports

The results of the analyses are shown in Figure 10. Up to point (a), when the bottom flange at mid-span reaches the proportional limit, the composite beam shows elastic behaviour. With increasing axial force and displacement there is an increase in the bending moment (Figure 10a-c). The increase in compressive axial force starts to level off after 45 mins due to a loss of material strength and the displacements increase due to a loss of stiffness. The rate of increase in deflection is greater than the rate of decrease in axial force, hence the bending moment continues to increase due to P-δ effects.

After the bottom flange stress reaches the thermally reduced proportional limit stress (point (a)) the bottom flange is no longer in the elastic range hence the compressive axial force levels off and then decreases due to the yielding. The displacements increase at a constant rate up to 105 mins after which time the slope of the displacement graph increases leading up to the yielding of the entire bottom flange at point (b). The bending moment also increases up to the yielding of the bottom flange.

(a) Mid span displacement

(b) Mid span bending moment

(c) Mid span axial force

(d) Mid span bottom flange stress
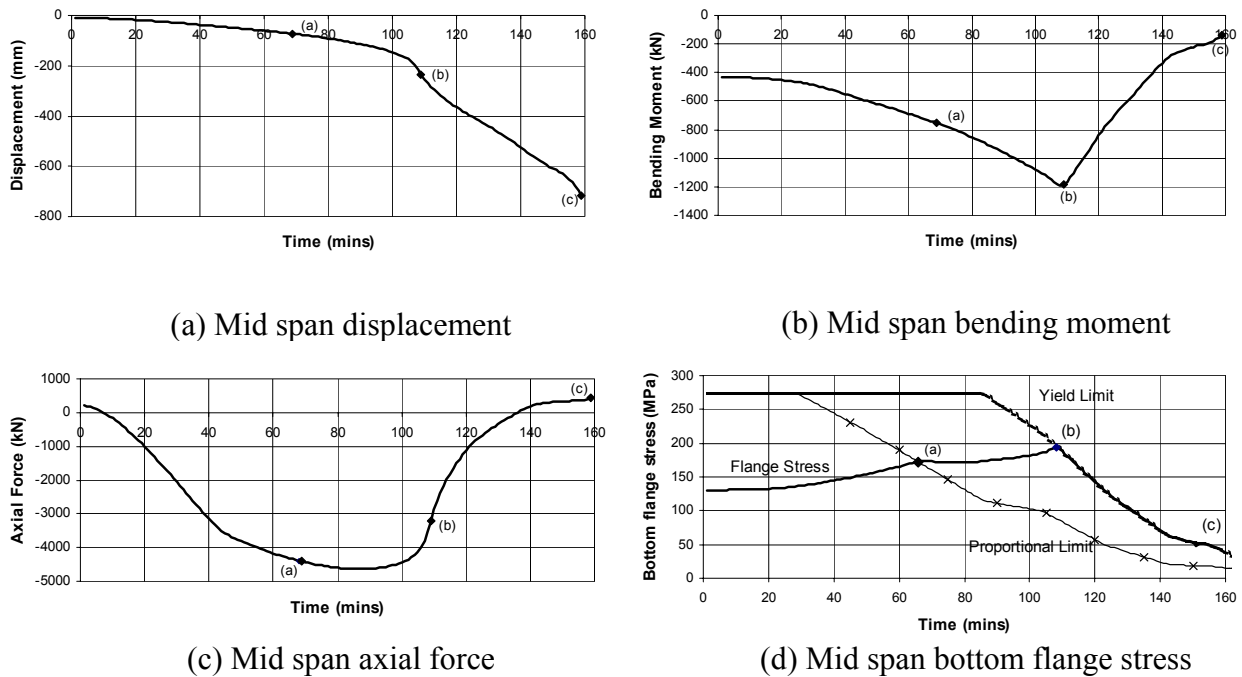
FIGURE 10   Mid span results for pin-pin supported composite beam.

After yielding of the bottom flange a plastic hinge occurs at mid-span. Figure 10d shows that from (b) onwards, the flange stress follows the yield stress envelope until collapse occurs at (c) after 159 mins. From (b) to (c) the axial force decreases to zero and then goes into tension. The displacement increases at a constant rate while the bending moment decreases to below its initial level as catenary action develops and the applied load is resisted by tension rather than by bending.

(a) Mid span displacement

(b) Mid span bending moment

(c) Mid span bottom flange stress

(d) Mid span top flange stress
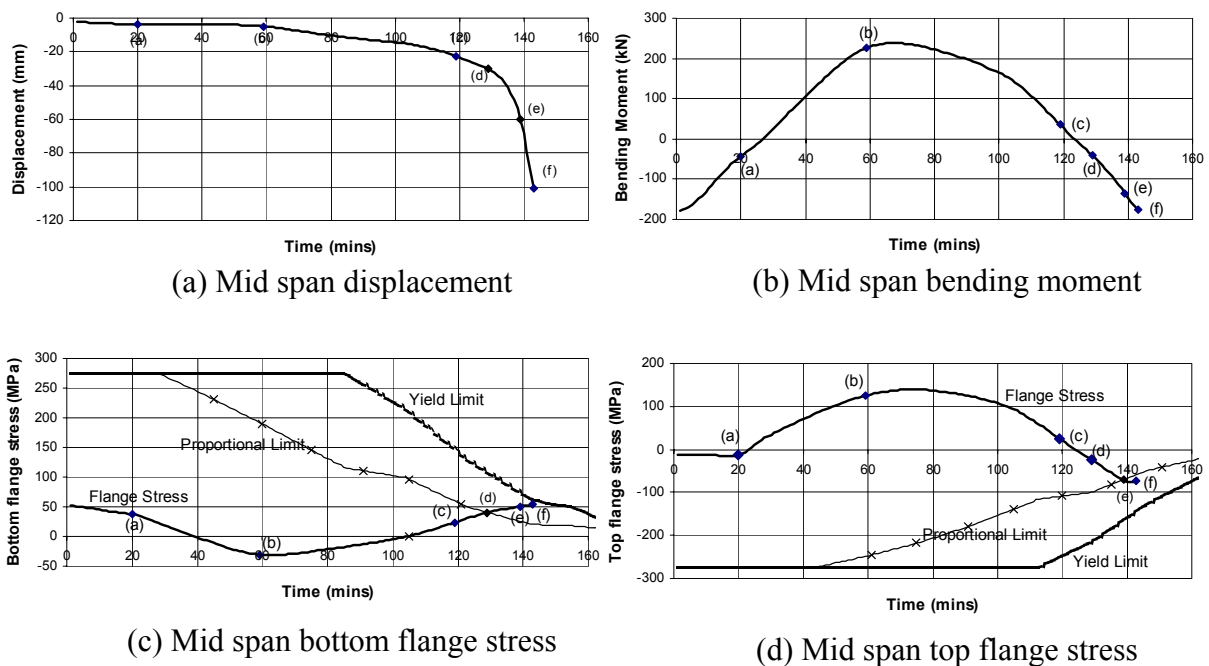
FIGURE 11   Mid span results for fixed-slide supported composite beam.

Fixed-slide beam supports

The beam with fixed-slide supports was free to elongate and consequently no axial force was induced as a result of thermal expansion. For the first hour of heating, the beam behaved elastically with very little deflection. The results for the mid-span deflection, mid-span moment, and the stresses in the top and bottom flanges are shown in Figure 11. The points (a) and (b) in Figure 11 represent the top and bottom flanges (respectively) at the ends of the beam reaching the proportional limit stress.

Fixed - fixed beam supports

The results of the thermal and structural analyses are shown in Figure 12 in terms of the displacements, axial force, bending moments and stresses at the mid-span.

(a) Axial force

(b) Mid span displacement

(c) Mid span bending moment

(d) Mid span bottom flange stress

(e) Mid span top flange stress

(f) Mid span concrete slab stress
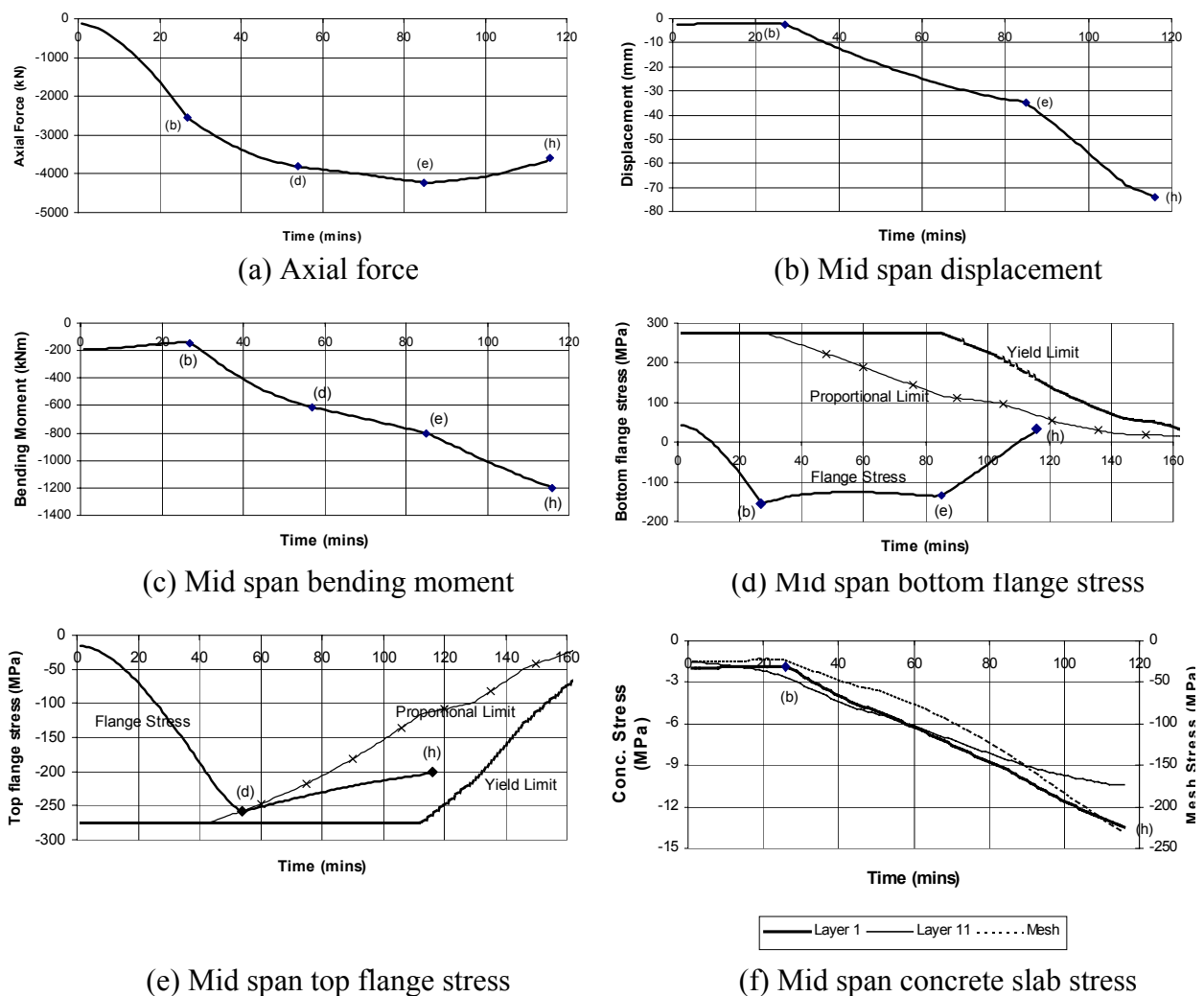
FIGURE 12 Mid span results for fixed-fixed supported composite beam.

When the bottom flange reaches the proportional limit stress at the supports at point (b), the mid-span displacements and bending moments increase as shown in Figures 12b, c & d. Up to point (b) the mid-span displacement is constant and the bending moment decreases due to increases in the end moments. Figure 12f shows that the compressive stress in the slab and the

187

mesh stay fairly constant under positive moment. Figure 12d shows that the bottom flange at mid-span goes into compression after 12 minutes.

Between points (b) and (d) in Figures 12a-c the mid-span axial force and displacements increase at a relatively uniform rate leading to an increase in the positive bending moment. At point (d) in Figure 12e the mid-span top flange reaches the thermally reduced proportional limit stress but there is no detrimental effect on the rest of the beam at this time due to stress redistribution. Between points (b) and (e) in Figures 12a & d the bottom flange shows the effects of stress redistribution where the stress stays relatively constant while the displacement increases at a uniform rate. Figures 12a & b show that the axial force increases at a diminished rate between points (d) and (e) while the displacement increases at a uniform rate. The bending moment increases at a decreasing rate due to P-δ effects.

Figures 12a-c show that after point (e) the axial force decreases due to yielding and the mid-span displacement and bending moment increase at a greater rate. The increasing mid-span displacement causes the third plastic hinge to form and the failure mechanism is achieved at point (h).

COMPOSITE BEAM RESULTS –ISO fire

Pin-roller supports

The results of the analysis are shown in Figure 13. For the first 5 minutes, the beam shows elastic behaviour with little vertical displacement since the roller support allows unrestrained thermal expansion to occur. At 5½ minutes, the bottom flange stress at mid-span reaches the tensile proportional limit stress, while the top flange reaches the compressive proportional limit after 13½ minutes. After a further 1½ minutes, the bottom flange reaches the temperature reduced yield stress, followed 4 minutes later by the top flange reaching the proportional limit in tension. At 21 minutes, the concrete slab begins to crush at the top, followed ½ minute later by the top of the steel beam reaching yield, thus forming a plastic hinge with failure of the beam.
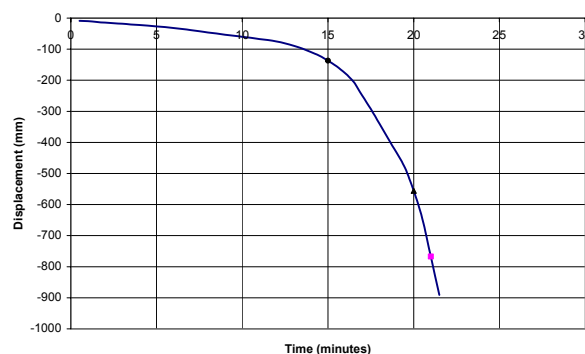
(a) Mid span displacement
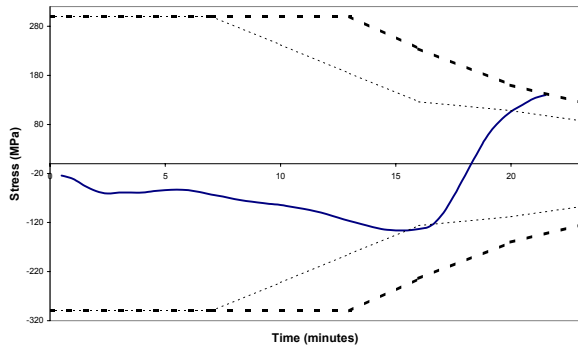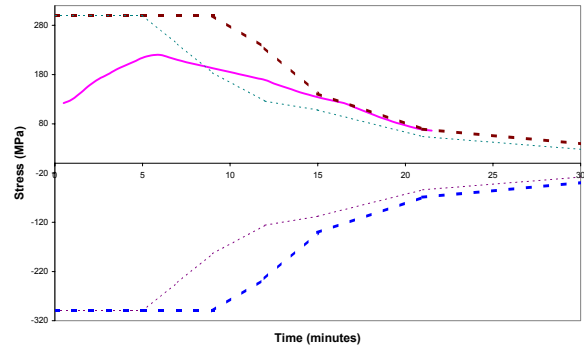
(b) Mid span top flange stress　　　　　(c) Mid span bottom flange stress

FIGURE 13　Mid span results for pin-roller supported composite beam.

Pin-pin supports

The results of the analyses are shown in Figure 14. For the first 5 minutes the composite beam shows elastic behaviour. With increasing axial force and displacement there is an increase in the bending moment (Figure 14b). The increase in compressive axial force starts to level off after 5 mins due to a loss of material strength as the bottom flange reaches the proportional limit strength and the displacements increase due to the loss of stiffness. The rate of increase in deflection is greater than the rate of decrease in axial force, hence the bending moment continues to increase due to P-δ effects.
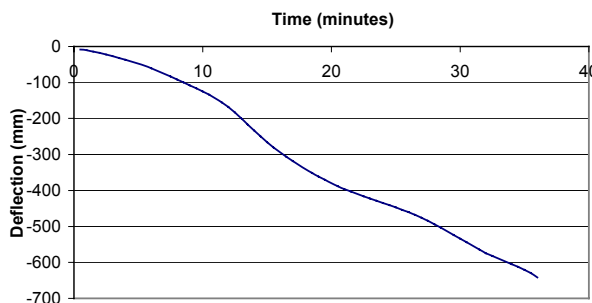
(a) Mid span displacement　　　　　(b) Mid span bending moment
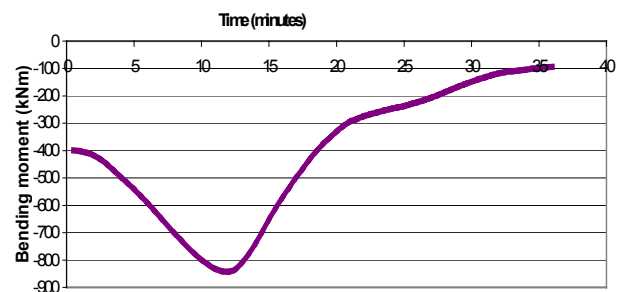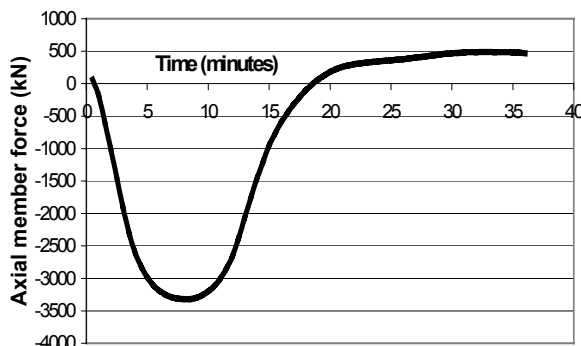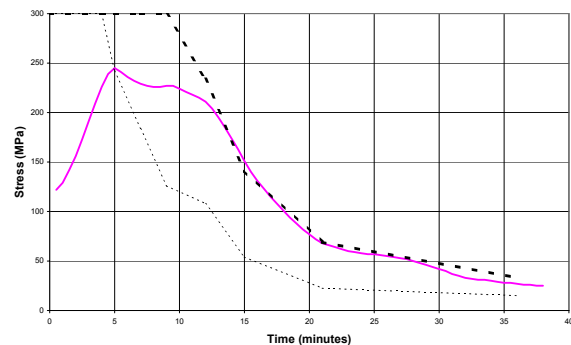
(c) Mid span axial force　　　　　(d) Mid span bottom flange stress

FIGURE 14　Mid span results for pin-pin supported composite beam.

189

13 minutes after the fire starts, the bottom flange yields, beginning the formation of a plastic hinge. After a further 3 minutes, the bottom of the concrete slab cracks, followed 2 minutes later by the sagging beam beginning to resist its load by going into axial tension. The top flange of the beam reaches the tensile proportional limit at mid-span after 20 minutes. This is followed 7-8 minutes later by tensile cracking of the concrete slab reaching the top surface. Finally, at 38 minutes, the top flange yields at mid-span, completing the plastic hinge and causing failure of the beam.

SUMMARY AND CONCLUSIONS

Steel beam

Upon heating, a *pin-roller* beam is free to elongate and there is no axial force induced in the beam due to thermal expansion. Deflection gradually increases due to the loss of strength in the steel. When the plastic hinge develops, the beam has lost most of its strength and the deflection increases greatly, pulling the roller support closer to the pin support; this is known as a runaway failure.

The axial restraint in a *pin-pin* beam prevents the beam from expanding. Thermal expansion causes large axial force along the beam resulting in greater deflection. The forming of the plastic hinge at the mid-span causes reduction in the axial load as the deflection increases. Approaching failure, when the loss of stiffness overwhelms the beam performance, the load is supported by catenary action as the whole beam is in tension.

In a *fixed-slide* beam, thermal expansion has no significant effect, as the beam is free to expand. This, together with the moment resisting supports, results in very small deflection for a considerable period of time. The moments at both mid-span and ends of the span increase initially due to thermal bowing and then decrease as the thermal gradient becomes more uniform. As there is no P-δ effect, the shape of the bending moment does not change.

Three plastic hinges form due to reduction in the steel strength leading to runaway failure shortly after the time of failure of an identical *fixed-fixed* beam.

Since a *fixed-fixed* beam is fully fixed at both ends, thermal loading induces a large axial compressive force which causes the ends of the span to yield, after which the axial force slowly reduces and the deflection starts increasing. The behaviour of the *fixed-fixed* beam changes dramatically when the stresses reach the proportional limit or the yield stress. Formation of a plastic hinge at mid-span reduces the axial force considerably, accompanied by increasing deflection. The *fixed-fixed* beam fails earlier than the *pin-pin* beam without as much deflection (Moss et al 2001).

Composite beam

For a composite steel-concrete beam, the pin–pin support case lasted the longest of the four end conditions which were analysed, followed by the pin-roller case. The pin–pin support case has the best fire resistance even though there is axial restraint causing thermal bowing and high initial deflection. This means that even though the stresses are high at the mid span the concrete slab is able to contribute to the moment capacity of the section. The bottom

flange of the steel beam yields due to the thermal degradation in steel strength but there is sufficient redistribution of stress to allow the composite beam to survive a significantly longer period.

For all support cases, the displacements and axial forces tend to change significantly when the steel stress reaches proportional limit stress or the yield stress. In the axially restrained case this causes changes in the bending moment due to P-δ effects. In the non-axially restrained cases only the displacements are affected

The *fixed–fixed* support case fails due to the compression force and bending moment causing large stresses in the flanges at the ends of the beam. The bottom flanges at the ends of the span reach their yield stress prior to the thermal degradation in strength of the steel. The top flanges soon follow causing the first two hinges of the failure mechanism. The third plastic hinge is formed at the mid span of the beam due to increased deflection caused by the end of span plastic hinges.

Conclusions

The principal findings are:

1. The behaviour of steel and composite beams during fire exposure is very much more complex than at ambient temperature, with continuous interrelated changes in the deflected shape, axial force, bending moments and internal stresses.
2. Beam behaviour is very different for the four support conditions which were analysed.
3. Beam behaviour is very sensitive to the stress condition relative to the temperature-reduced proportional limit and yield stress. Sudden changes in deflection or internal forces often occur when the stresses at a critical cross section reach the proportional limit or when yielding occurs.
4. The overall behaviour of a steel beam and a similar sized steel-concrete composite beam follow similar trends.
5. A uniform heating rate and exposure to the ISO standard fire produce similar patterns of behaviour.
6. Additional studies are necessary for more realistic fire exposure, where very large axial tensile forces are expected in the decay phase of the fire.

REFERENCES

1   Kirby, B R; The Behaviour of a Multi-Storey Steel Framed Building Subject to Fire Attack-Experimental Data, British Steel, Swinden Technology Centre, United Kingdom, 1998.

2   Buchanan, A.H. *Structural Design for Fire Safety*, Chichester: Wiley, 2001.

3   Franssen, J-M. Structures in Fire, being Proc. 1st International Workshop, Copenhagen, Denmark, 2000.

4   Moss, P.J. and Clifton, G.C. Behaviour of Multi-Storey Steel Frames in Fires, *Mechanics of Structures and Materials* (M.A. Bradford, R.Q. Bridge and S.J. Foster, eds) being Proc. 16th Australasian Conf. on the Mechanics of Structures and Materials, Sydney, Australia, Dec. 1999, Balkema, Rotterdam, 461-466, 1999.

5   Moss, P.J. and Clifton, G.C. The Effect of fire on Multi-Storey Steel Frames, *Structural Engineering, Mechanics and Computation,* (ed. A. Zingoni), being Proc. International Conference on Structural Engineering, Mechanics and Computation, Cape Town, South Africa, 2-4 April, Elsevier, Oxford, 2:1063-1070, 2001.

6   Moss, P.J. and Clifton, G.C. The Performance Of Multi-Storey Steel Frames In Fires, *Proc. Sixth Pacific Structural Steel Conference, Beijing, Oct. 2001*, 2001.

7   ISO 834, *Fire Resistance Tests - Elements of Building Construction*, International Organisation for Standardisation, 1975

8   Franssen, J.M., Kodur, V.K.R, Mason, J,. User Manual for SAFIR2000: A Computer Program For The Analysis Of Structures Submitted To Fire, University of Liege, Belgium, 2000.

9   Seputro, J. Effect of Support Conditions on Steel Beams Exposed To Fires, Fire Engineering Research Report 01/6, University of Canterbury, New Zealand, 2001.

10 EC3, Eurocode 3: Design of Steel Structures. ENV 1993-1-2: General Rules – Structural Fire Design. European Committee for Standardisation, Brussels, 1995.

11 Welsh, R. 2-D Analysis of Composite Steel-Concrete Beams in Fire, Fire Engineering Research Report 01/8, University of Canterbury, New Zealand, 2001.

12 Wastney, C. Performance of Unprotected Steel and Composite Steel Frames Exposed to Fire, Fire Engineering Research Report 02/?, University of Canterbury, New Zealand, 2002.

13 Moss, P.J., Buchanan, A.H., Seputro, J.& Welch, R. Effect of Support Conditions on the Fire Behaviour of Steel Beams. In *Proc. Pacific Struct. Steel Conf., Beijing, China, Oct. 2001.*

14 Rotter, J.M., Usmani, A.S.. Fundamental Principles of Structural Behaviour Under Thermal Effects. *First International Workshop on Structures in Fire (Copenhagen)*, 2000.

MODELLING OF THE CARDINGTON LBTF STEEL FRAME BUILDING FIRE TESTS

P J MOSS
Former Associate Professor, University of Canterbury, Christchurch, New Zealand.
p.moss@civil.canterbury.ac.nz

G C CLIFTON
HERA Structural Engineer
HERA, Auckland, New Zealand.
structural@hera.org.nz

ABSTRACT

Design of multi-storey steel framed office and other commercial buildings for fire resistance has traditionally been undertaken on the premise that the building will suffer partial or total collapse unless the beams and columns are insulated from temperature rise under fully developed fire conditions. Since 1990, a growing body of evidence has shown that there is a substantial inelastic reserve of strength available from a typical composite steel beam/concrete floor slab system with uninsulated beams. An intensive research effort is underway in a number of countries to determine the extent of this reserve of strength and the mechanisms involved in its delivery. This research involves experimental testing and advanced finite element (FE) modelling. It is leading on to design procedure development to take account of the inelastic reserve of strength available from this type of building system.

The most detailed experimental testing programme undertaken took place in 1995 and 1996 on an eight storey steel framed building at the former Cardington Large Building Test Facility in the UK. This programme included a number of large-scale fire tests using wood cribs and office furniture as the fuel.

The University of Canterbury and HERA are involved in advanced finite element modelling of multi-storey steel framed buildings subject to severe fires. In order to validate the methodology and details used in this modelling, it is being applied to three of the LBTF fire tests. These are the BRE *Large Enclosure Test,* the Corus *Corner Test* and the Corus *Demonstration Furniture Test.* The first test uses wood cribs and generates near uniform fire

conditions as a function of time throughout the 342m^2 enclosure, allowing the variation in the fire conditions from one location to another to be ignored. However, it generated relatively low peak temperatures. The second test modelled also generates near uniform fire conditions with time throughout the 75m^2 enclosure, with peak temperatures over 1000°C. This allows the structural response under uniform fire conditions and higher temperatures to be modelled. Finally, the third test generates non-uniform fire conditions and very high peak temperatures, bringing in the influence of migrating fire conditions on the structural response. The aim of this research is to tune the model to get the best agreement between the experimentally recorded deflections and the predicted deflections for the three different tests, thereby validating the model over a range of fire and structural conditions.

This paper presents an overview of the modelling of the building. The initial results will be presented at the conference.

INTRODUCTION AND SCOPE

General Background

Design of multi-storey steel framed office and other commercial buildings for fire resistance has traditionally been undertaken on the premise that the building will suffer partial or total collapse unless the beams and columns are insulated from temperature rise under fully developed fire conditions. Since 1990, a growing body of evidence from severe fires in buildings and from the results of advanced analyses has shown that there is a substantial reserve of strength available from a typical composite steel beam/concrete floor slab system with uninsulated floor support beams in severe fire conditions. This reserve of strength is mobilised when the floor system undergoes inelastic response due to the effects of the fire.

The reserve of strength has been demonstrated experimentally in the landmark series of fire tests undertaken during 1995 and 1996 on an eight storey steel framed building at the former Cardington Large Building Test Facility in the UK [1]. This programme included a number of large-scale tests using wood cribs and office furniture as the fuel.

The University of Canterbury and HERA have been undertaking advanced finite element modelling of multi-storey steel framed buildings subject to severe fires since 1998. The initial building modelled has been a seventeen storey office building situated in the central business district of Auckland, New Zealand. A view of this building is shown in Fig. 1.

The floor system of this building comprises a concrete slab cast onto profiled steel decking and supported on a network of secondary and primary steel beams. These are supported internally on two gravity load carrying columns and round the perimeter by a seismic-resisting system on each side. For all these analyses the floor beams were unprotected, the columns protected with an insulation material.

The first and most detailed results of this work were published [2] in February 1999. Ongoing results have been presented in a number of papers, the latest in 2001 [3].

A range of natural fire curves representing fires of medium and high structural fire severity were generated, from [4], for these analyses, including the effects of a migrating fire.

FIGURE 1: View of the First Building Subject to Finite Element Analysis for Fully Developed Fire Scenarios as Part of this Research Programme (from [2])

While these analyses gave results that appeared to be realistic, when compared with the experimental behaviour of floor systems with similar beam sizes, spans and loadings from [1], they could not be related to any directly comparable experimental results. The principal purposes of these analyses were therefore twofold, namely:

- To develop practicable modelling procedures for this type of advanced analysis, and
- To determine the likely influence of a range of fire, material and structural variables on the response of the building and thus get a better feel for the sensitivity of the response to a range of variables.

The next and current stage in this research involves applying the modelling concepts developed [2, 3] to the eight storey steel framed test building at the Cardington LBTF. In that instance, the building and fire characteristics are known and hence the predicted output from the model can be compared against the known experimental response. The modelling details can then be amended, as required, until the best agreement between experiment and prediction is obtained.

Once this is complete, the upgraded model can then be applied to the original test building (Fig. 1) and the predicted response compared with those obtained from the initial analyses [2, 3].

This paper addresses the current stage of the research, namely the modelling of three of the steel building fire tests from the Cardington LBTF. A view of this test building is given in Fig. 2.

Scope of Paper

The paper provides a brief overview of the development and application of the model, as of the end of February 2002. It aims to present sufficient information to enable key points of the modelling to be considered and debated by those attending the SiF02 conference. As the paper is describing work in progress, that is the most desirable outcome at the time of writing the paper (early March 2002).

The paper starts by describing the philosophy behind the modelling. It then identifies which tests have been selected for modelling and the reasons for these selections.

The modelling of the fires is then covered, followed by an overview of the heat transfer modelling.

An overview of the structural model is then given.

The paper concludes with the acknowledgments and references.

CARDINGTON FIRE TESTS BEING MODELLED

Philosophy Behind Modelling

This is as follows:

(i)   To use available fire models [4] and computer software [5.1, 5.2, and 6], rather than developing new programs, wherever possible. Also to use predictive tools, rather than the experimental results directly, wherever possible

(ii)   At each stage of the model's development, to test the accuracy of the output from these predictive tools against the experimental data and adjust the input parameters (eg. the thermal properties of concrete, steel into SAFIR [5.1]) to obtain the closest agreement between experimental and predicted outcomes

(iii)   Through the implementation of (i) and (ii), to develop a modelling approach that can be applied to a wider range of buildings than just the Cardington test building [1].

Fire Tests Chosen for Modelling

Three tests from the LBTF test series [1] have been selected for modelling. These are the BRE Large Enclosure Test, Corus Corner Test and Corus Demonstration Furniture Test. Each test took place on the second storey (ie. the fire was on level 1 and impacted on the level 2 floor). The location in plan of each test is shown in Fig. 3.

The reasons for selecting each test were as follows:

FIGURE 2: View of the Steel Test Building at the Cardington LBTF
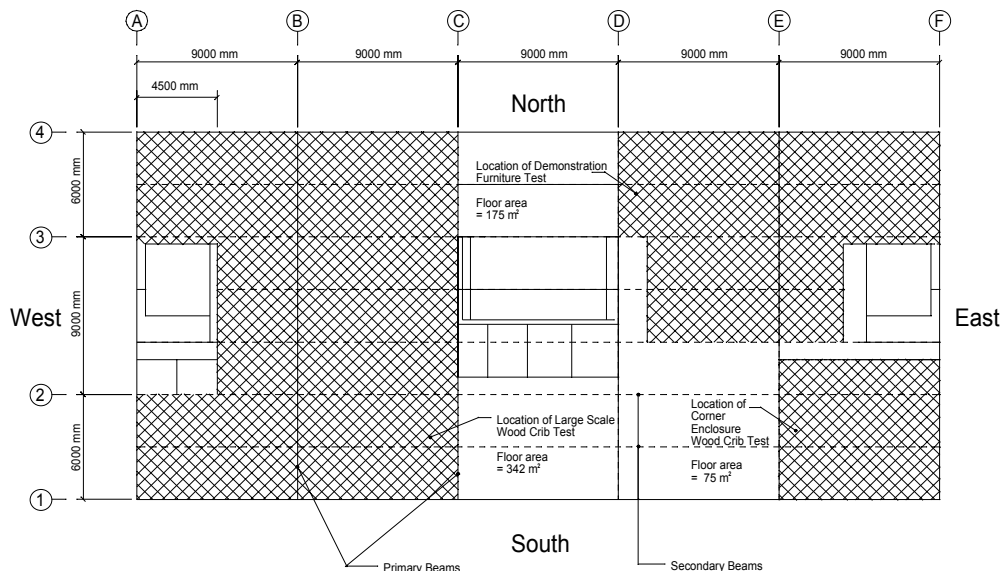
FIGURE 3: Plan of Fire Floor, Level 2, Eight Storey Steel Frame Test Building, BRE Cardington, Showing the Floor Areas Involved in the Three Large Scale Realistic Fire Tests Being Modelled.

Large Enclosure Test

This test occupied most of the floor space between grids A and C and generated near uniform fire temperature-time conditions throughout the 342 m^2 floor area enclosure. This allowed the variation in fire conditions to be ignored as a parameter affecting the structural response. It also allowed the structural model to be tested over a large region of floor involving multiple slab panels, where a *slab panel* incorporates a region of floor slab and unprotected secondary support beams which transfers load in two-way action back to supports. The supports remain effectively undistorted relative to the peak deformations that occur within the slab panel region. The slab panel concept is described in [7] and the principal slab panel mobilised in the Large Enclosure Test comprised the region bounded by gridlines 1, 4, B and C (see Fig. 3).

However, the maximum gas and unprotected steel temperatures reached in the enclosure were under 700°C (see Fig. 5), thus allowing the structural model to be tested only to this temperature.

Corner Test

This test occupied a much smaller region in the South-East corner, as shown in Fig. 3. However, the region was sufficiently large to enable slab panel action, with multiple secondary beam participation, to develop.

The fire temperature-time conditions over this enclosure were again near uniform, this time with a peak gas temperature of 1000°C and peak unprotected steel temperature of over 900°C (see Fig. 6). This allows the structural model to be tested to steel temperatures at the upper end of those expected in practice.

Demonstration Furniture Test

This test took place in the North-East quadrant of the building, as shown in Fig. 3. It generated non-uniform (migrating) fire conditions and very high peak temperatures, with the fire conditions allowing the fire model [4] to be applied (and refined).

It also generated possible failure conditions in the floor slab around column E3, as shown in Fig. 4. One of the principal objectives in the modelling of this test will be to determine if this failure can be predicted analytically.

MODELLING OF THE FIRES

Large Enclosure Test and Corner Test

It was not possible to model these fires using the Modified Eurocode Curves [4]. In the former case, the difference between experimental and predicted fire conditions is very large [8] and not explainable. In the latter case, the ventilation conditions (size of openings) were varied during the test, rendering use of [4] not feasible.

As the fire conditions were near uniform throughout the two enclosures, average values of the experimentally recorded temperature-time curves were used in the case of the Large

Enclosure Test (see Fig. 5). For the Corner Test, the variation about the average from recording points was slightly greater and 1.05 x average values were used (see Fig. 6.).

Demonstration Furniture Test

This was modelled using the migrating firecell model in [4]. Fig. 7 shows the areas of fire used. The fire model is based on the fire start in $A_{1,1}$, whereas it was in fact lit near the back right hand corner of $A_{2,1}$ and spread rapidly to the openings along grid 4, within the area $A_{1,1}$. It then progressed firstly sideways into $A_{1,2}$, and $A_{1,3}$, and finally back to $A_{2,1}$ and $A_{2,2}$. $A_{2,2}$ was the last region subjected to full fire development in this test.

The design fire temperature-time curves used are shown in Fig. 8. Their comparison with experimental results is shown in [8] and examples will be given at the conference.

FIGURE 4: View of Level 2, Demonstration Furniture Test, Showing Possible Failure in the Floor Above the Fire.
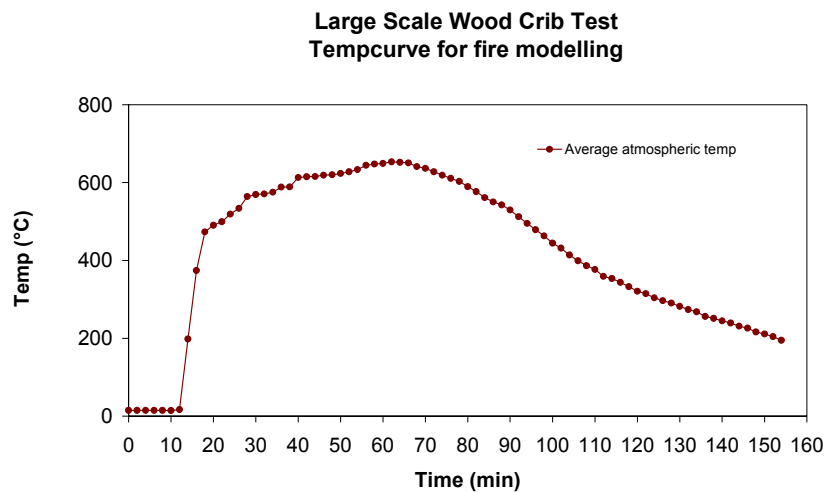
FIGURE 5: Input Fire Temperature-time Curve for the Large Enclosure Test

Experimental and Design Fire Temperatures for the Corner Test
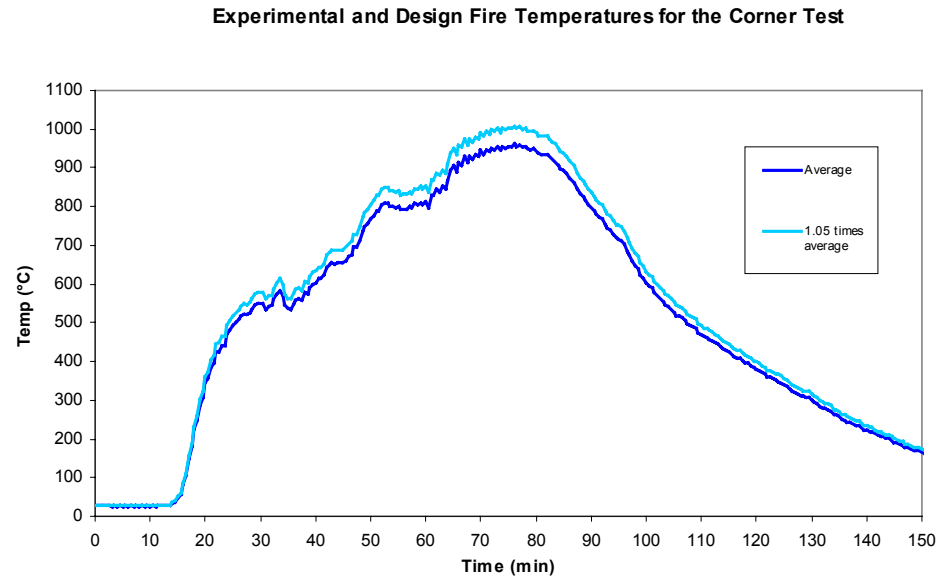
FIGURE 6: Input Fire Temperature-time Curve for the Corner Test
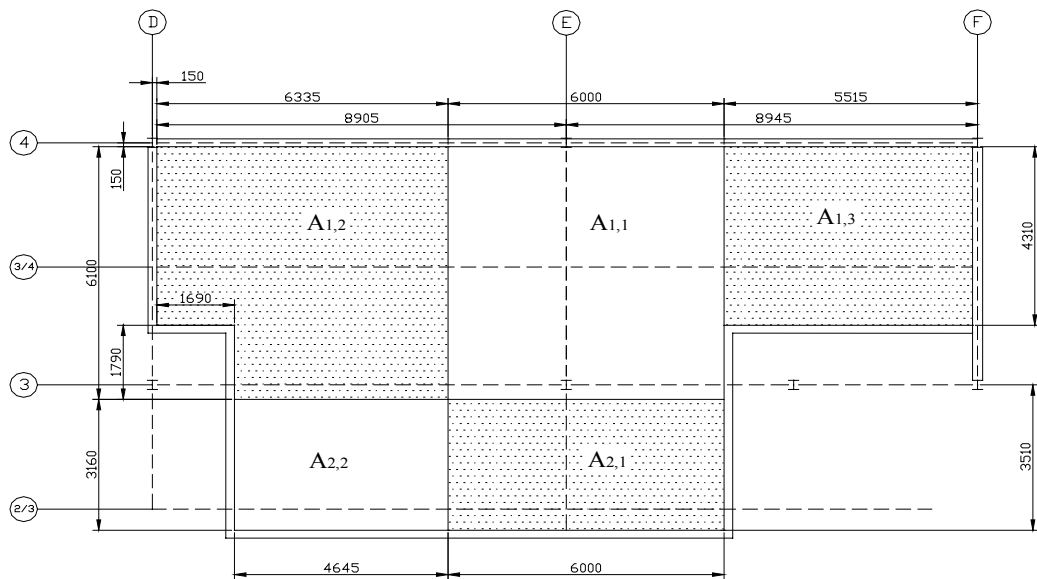
FIGURE 7: Location of Areas of Fire Used for Modelling the Demonstration Furniture Test

Note: The fire start was taken as occurring in $A_{1,1}$ The only openings were along grid 4.

Fire Curves for the Demonstration Furniture Test
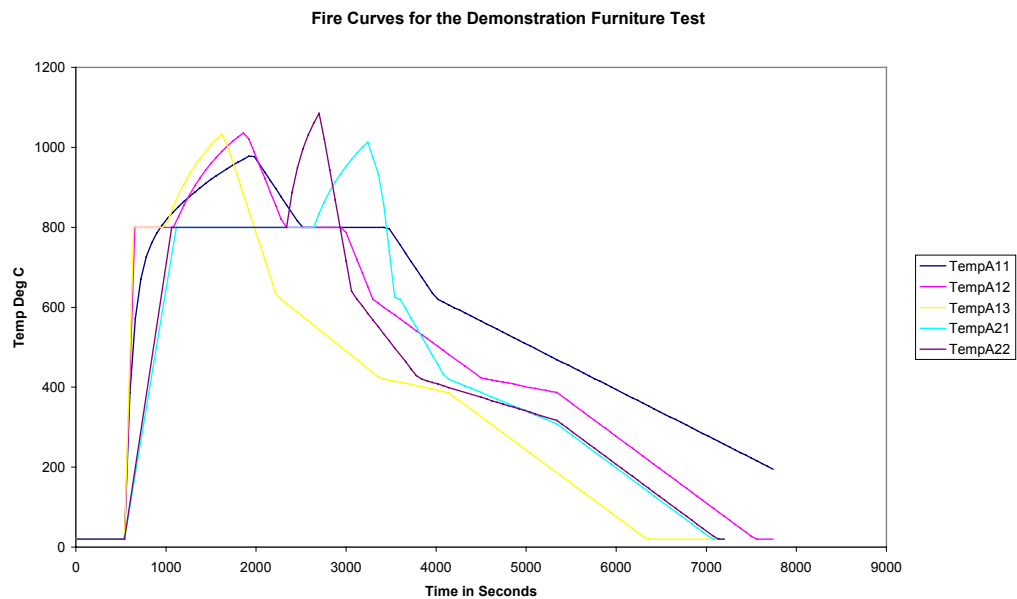
FIGURE 8: Design Fire Temperature-time Curves for the Demonstration Furniture Test

HEAT TRANSFER MODELLING

General Approach

Wherever possible, the heat transfer modelling was undertaken using SAFIR [5.1] and SAPPHIRE [5.2], with the fire curves from Figs. 5, 6 and 8 used as input and the temperatures within the structural elements determined accordingly. In each instance, the predicted results were compared with the experimental results and the input parameters in [5] were altered to obtain the closest practicable agreement.

This worked well for the floor slab and unprotected steel beams within each enclosure. It also worked reasonably well for the protected columns within each enclosure.

The approach did not work well for members on the edge of the enclosure, thereby having only partial exposure to the fire. Reasonable agreement could be obtained between predicted and experimental results for some unprotected edge beams, however the predicted temperatures for the protected edge columns were typically much greater than the experimentally determined temperatures and the latter have therefore been used directly.

Time and space limitations prevent detail being given on deriving the input temperatures for every member. General details relating to the unprotected beams and floor slab and to the columns are now given.

Slab and Beams

The slab in the LBTF test building comprised a nominal 130 mm thick LWC slab on a 55 mm deep trapezoidal steel deck, with mesh reinforcement at 35 mm cover. (Concrete density at ambient temperature was 2084 kg/m^3).

The slab was subdivided into 11 layers for modelling in SAPPHIRE/SAFIR, with the subdivisions and slab mesh used shown in Fig. 9.

The CALCONEC 2 concrete material from [5.1] was used, with the thermal properties (thermal conductivity, specific heat and specific mass) amended to account for the actual moisture content etc, such that the best practicable agreement between predicted and measured temperature-time data was obtained.

Note that the input slab temperatures were obtained independent of the beam.

The beam temperatures were then obtained using [5.1, 5.2] incorporating a 130 mm thick solid slab. The influence of deck voids increasing the secondary beam top flange temperature, above what would have been developed for a solid slab, was allowed for by placing the fire on half the top surface of the beam top flange as well as around the flange tips and on the inside bottom surface of the top flange.
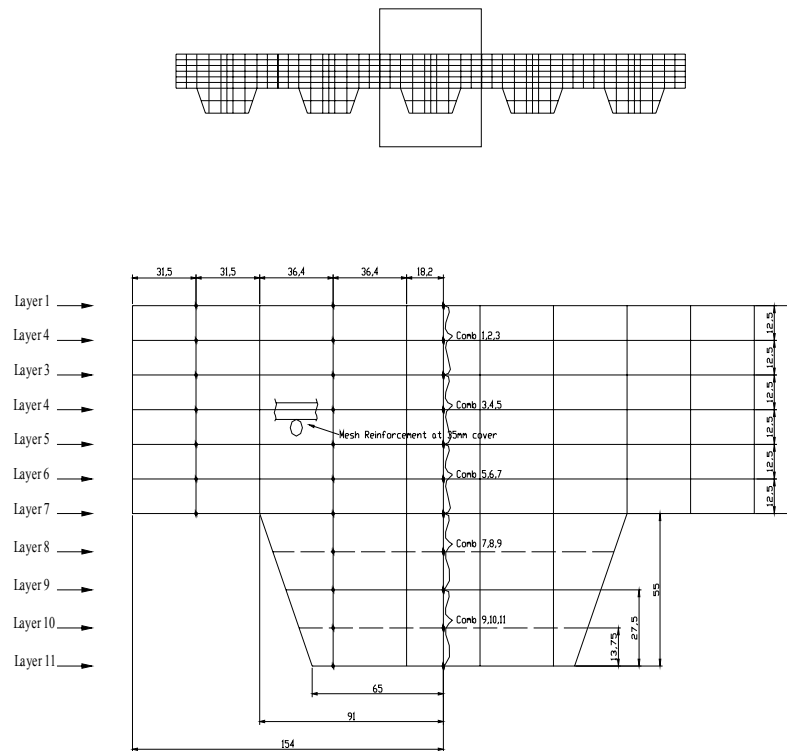
FIGURE 9: Division of the Profiled Slab into Eleven Layers for the Determination of Temperature-time Inputs

Large Enclosure Test
Beam 610UB101 - primary beam grid B - and Concrete
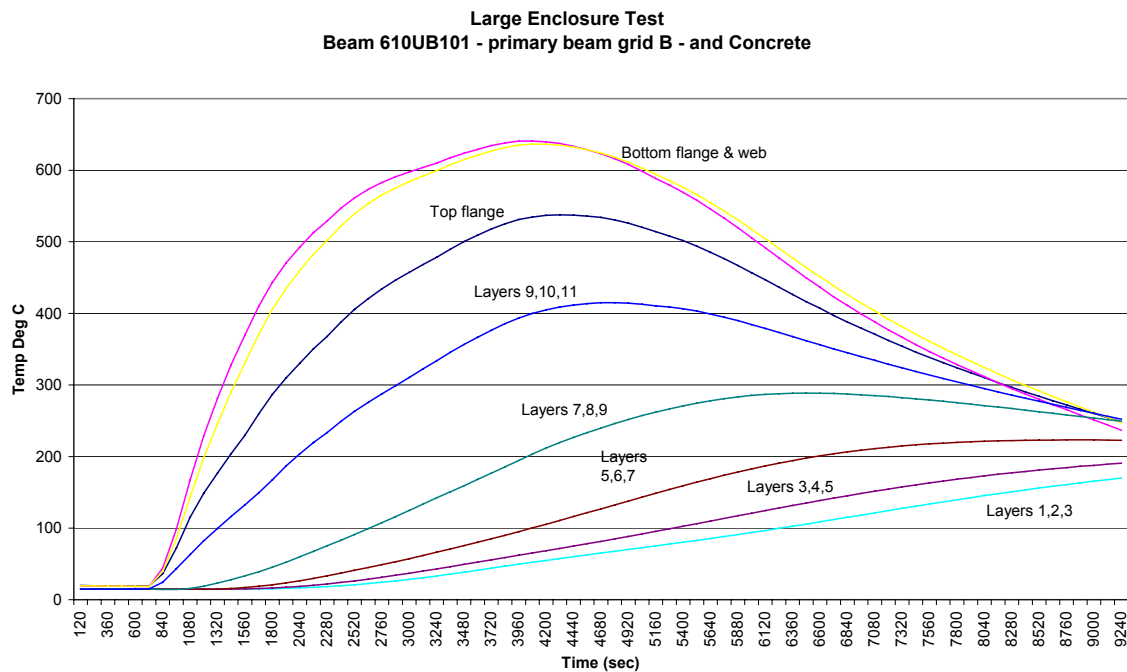
FIGURE 10:   Temperature-time Inputs for Beam and Slab, Beam B2 – B3, Large Enclosure Test

Fig. 10 shows the resulting temperatures for slab and primary beam B2-83, subjected to the large enclosure design fire shown in Fig. 5. Figure 10 shows that the bottom half of the slab rib and the beam elements follow a similar pattern of temperature change with time, while higher in the slab there is an increasing lag in the time at which the peak temperatures are reached. This is important in the structural modelling, as described later.

Columns

All columns in the test building were protected, typically with a 25 mm thick ceramic fibre blanket for interior columns. Previous work [9] has been undertaken to determine the appropriate thermal properties to use for this material; see results in Fig. 11 for column E3, Demonstration Furniture Test.

Interior column temperatures were determined from analysis involving the appropriate design fire. Temperatures in the edge columns, especially those with less than half their (insulated) profile exposed to the fire, were obtained directly from the experimentally recorded data.
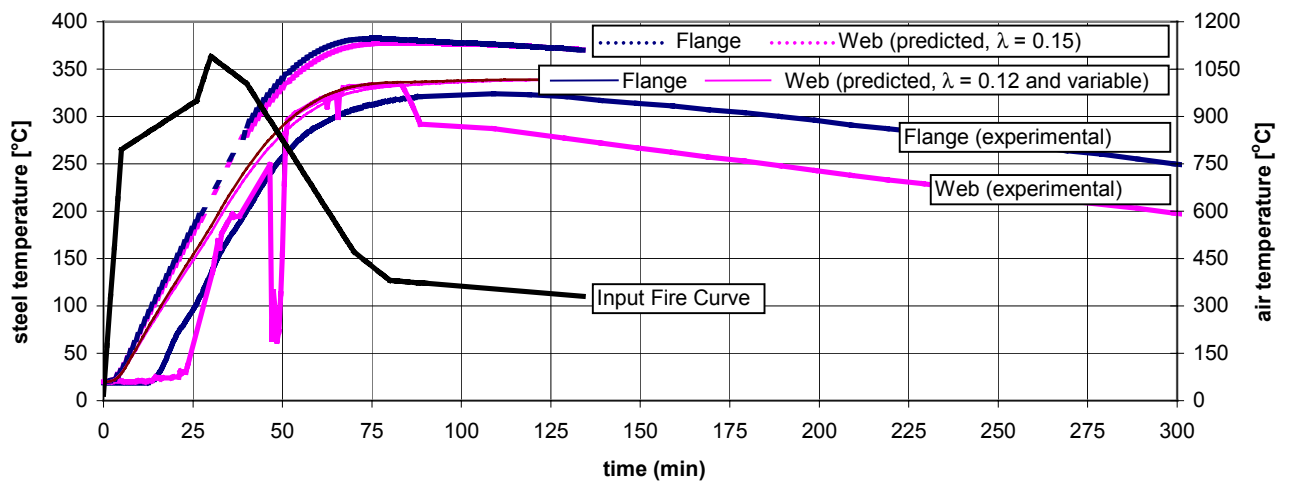
FIGURE 11: Comparison of Predicted and Experimental and Steel Column Temperatures for Column E3 (from [9]).

STRUCTURAL MODEL

Overall Structure

The entire building has been modelled in the analyses. Fig. 12 shows the arrangement of nodes and member numbers for the first suspended floor. The nodal numbering system has been developed with the following objectives in mind:

(1)   Every member is divided into at least four segments to account for second-order effects and to allow member actions and deflections to be readily output

(2)   The nodal system at the connections allows for semi-rigid, user defined rotational and axial springs to be input between secondary and primary beams and between primary beams and columns

(3)   Additional nodes have been positioned to allow for the effects of furnace walls etc. to be modelled

(4)   The beams are modelled as composite elements – more on this below

(5)   The columns members, which are steel UC sections, are modelled using the standard I-beam element supplied by ABAQUS [6]

(6)   Elevated temperature material properties are used for all steel and concrete elements; concrete properties to EC2-1-2 [10] and steel to EC3-1-2 [11]

(7)   Member sizes are those used in the test building [1]

(8)   The applied loads on level 3 and the higher levels are those used in the fire tests [1]

(9)   Ambient temperature material properties for steel, slab mesh and concrete are those derived from experimental testing of samples of each material.

All edge beams 356x171x45 (Grade 50) UB
All interior secondary beams 305x165x40 (Grade 43) UB
All beams exept as shown round stairs and lifts 356x171x51 (Grade 50) UB

General Floor Layout-BRE 8-Storey Frame
Nodes and Member Numbers
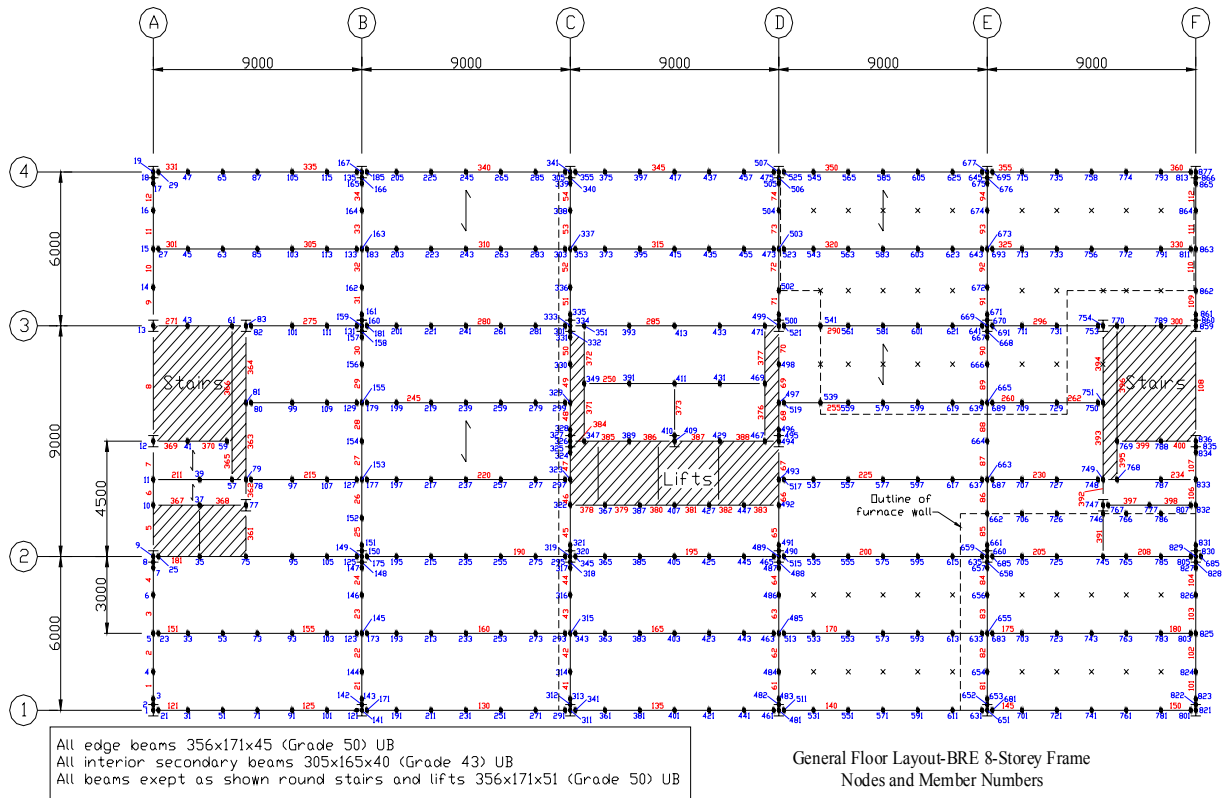
FIGURE 12: Floor Plan of Level 1 Cardington Test Building Showing Nodes and Members
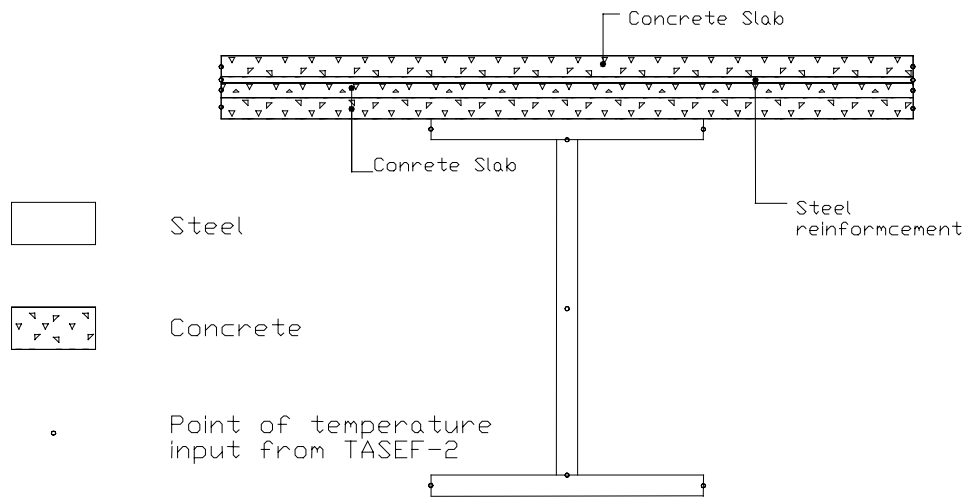
FIGURE 13: Modelling of Composite Beam Members in ABAQUS

Note: This figure is from [2], in which the heat transfer modelling was undertaken using TASEF – 2; now SAFIR [5] is used.
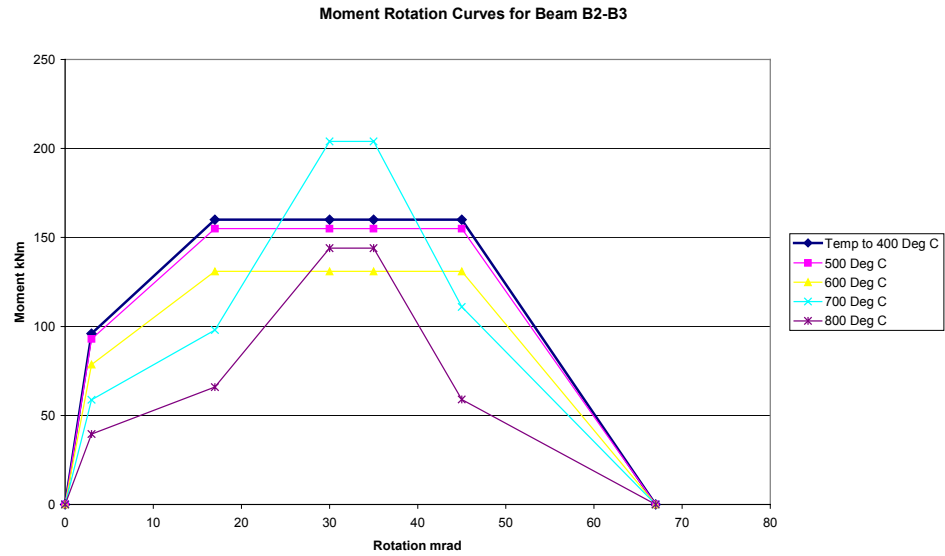
FIGURE 14: **Moment Rotation Curves for the Semi-Rigid Connections Between Beam B2-B3 and Columns**
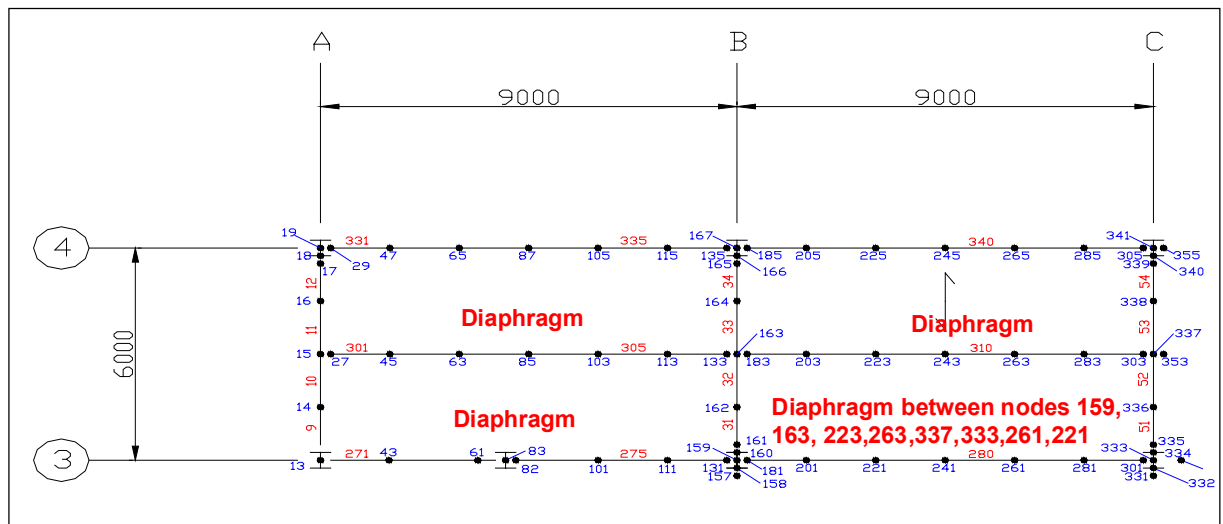
FIGURE 15: **Diaphragm Between Floor Beams , Part View of Floor at Level 2.**

Slabs and Beams

The principal components of the floor system are the composite secondary and primary beams, a generic detail of which is shown in Fig. 13. Some details of the modelling of these members follows:

(1) The cover slab is modelled with three layers of concrete and one reinforcement layer; the slab ribs are modelled with two layers of concrete. These layers are shown in Figs. 9 and 10

(2) The concrete width of the cover slab layers has been determined from NZS 3404 [12]. That of the rib layers is half the cover slab width, reflecting the trapezoidal nature of the decking

(3) The reinforcement is modelled as a 0.14 mm thick steel layer positioned at layer 4, Fig. 9 and fully bonded to the concrete

(4) No slip between the concrete slab and steel beam is modelled

(5) Each layer of the composite beam is built up as shown in Fig. 13. These layers have temperature-time histories and temperature dependent properties. However, a significant simplification of the temperature-time input data is required by ABAQUS. Each layer of the beam may reach a different peak temperature, but must reach this peak temperature at the same time and follow the same pattern of temperature variation with time in relation to that peak temperature. For example, with reference to Fig. 10, if the temperature-time history of layers 9, 10, 11 within the concrete is used to define the variation of temperature with time for the cross section, then all other layers of the cross section must follow a scaled version of that relationship. As can be seen from Fig. 10, the steel beam elements (top flange, bottom flange, web) achieve that quite closely, however the higher and cooler layers of the concrete slab do not. Given that the top layers of concrete only reach temperatures of 200°C, the effects of this simplification are not expected to be significant

(6) The temperature conditions described in (5) above are constant along the length of the beam.

Connections

The beam to beam and beam to column connections of all beams within the enclosures are modelled as semi-rigid flexural and axial springs, with temperature dependant properties. An example of the moment-rotation curves for the flexural springs connecting primary beam B2-B3 to the supporting columns is shown in Fig. 14.

The derivation of these springs is based on our knowledge of material behaviour gained from HERA's fire and seismic research programme and will be covered in more detail at the conference.

Slab Diaphragm Action

The network of floor beams is tied together with an eight node shell element within each bay of four beams. An example of this over four bays is shown in Fig. 15.

The diaphragm models the interconnecting influence of the slab and comprises a shell element material, 0.14 mm thick, with ambient temperature mild steel properties and connecting nodes on all four boundary beam elements, as shown for that example in Fig. 15.

ACKNOWLEDGMENTS

The authors would like to acknowledge the contribution of all persons/organisations involved in this research with special mention of:

(1)   The UK BRE and Corus, for supplying the fire test and slab panel load test data contained in [1]

(2)   The Foundation for Research, Science and Technology, for providing past and on-going funding of HERA's fire research programme, of which this advanced analytical work is the principal component.

REFERENCES

[1]   Kirby, BR; The Behaviour of a Multi-Storey Steel Framed Building Subject to Fire Attack - Experimental Data; British Steel Swindon Technology Centre, United Kingdom, 1998. Also data from BRE, Cardington, on the Corner Fire Test and Large Compartment Fire Test, 1996.

[2]   Clifton, GC and Moss, PJ; Key Aspects of the Behaviour of a Multi-Storey Steel Framed Building Subject to Fully Developed Natural Fires; HERA Steel Design and Construction Bulletin, No. 48, 1999, pp 3-13.

[3]   Moss, PJ and Clifton, GC; The Performance of Multi-Storey Steel Frames in Fires; Proceedings of the 2001 Pacific Structural Steel Conference; Beijing, China, 2001.

[4]   Clifton GC; Fire Models for Large Firecells; HERA, Manukau City, 1996, HERA Report R4-83. Plus amendments on page 20, HERA DCB No. 54, February 2000.

[5.1]   Franssen, JM et.al.; SAFIR: A Computer Program for Analysis of Structures Submitted to the Fire; University of Liege, Belgium, 1998/2001.

[5.2]   Mason, J; SAPPHIRE: A Pre-Processor for SAFIR; Sinclair Knight Merz, Wellington, 2001.

[6]   ABAQUS/Standard; Finite Element Analysis Program; HKS Inc, Pawtucket RI, USA, 2001.

[7]   Clifton, GC; Design of Composite Floor Systems With Unprotected Secondary Beams for Dependable Inelastic Response in Severe Fire; Proceedings of the Structures in Fire 2002 Workshop; University of Canterbury, Christchurch, 2002.

[8]   Auffinger, A; Response of Multi-Storey Steel Framed Buildings in Fully Developed Natural Fires: Revision of Fire Model and Inelastic Response Design Procedure; Report for Second Practical Term; HERA, Manukau City, 2000.

[9]   Clifton, GC and Hinderhofer, M; Performance of Steel Structures in Fully Developed Fires: Fire Engineering Research Results of Interest; HERA Steel Design and Construction Bulletin, No. 59, 2000, pp. 2-25.

[10]   DD ENV 1992-2 : 1996, Eurocode 2: Design of Concrete Structures, Part 1.2 General Rules – Structural Fire Design (together with United Kingdom National Application Document); BSI Standards, London, England.

[11].   DD ENV 1992-2 : 1996, Eurocode 3: Design of Steel Structures, Part 1.2 General Rules – Structural Fire Design (together with United Kingdom National Application Document); BSI Standards, London, England.

[12]   NZS 3404: 1997, Plus Amendment No. 1:2001, Steel Structures Standard; Standards New Zealand, Wellington.

Session 5:
Timber and Concrete Structures

MODELING OF THE THERMAL DEGRADATION OF STRUCTURAL WOOD MEMBERS EXPOSED TO FIRE

Marc L. JANSSENS
UNCC, 320 Smith, 9201 University City Boulevard, Charlotte, NC 28223-0001, USA
mljansse@uncc.edu

ABSTRACT

To accurately predict the structural performance of a wood member, knowledge is required of the rate at which it chars and the temperature distribution in the residual load-bearing section. The charring rate and temperature distribution can be calculated with a model that predicts the thermal degradation or pyrolysis of wood exposed to a high-temperature environment. More than 50 wood pyrolysis models have been developed since World War II [1-51]. They range from simple analytical expressions to complex systems of coupled partial differential equations that describe the heat and mass transfer through wood and char.

This paper presents a brief overview of the aforementioned models and provides a more detailed description of a new model. This model is referred to by the acronym CROW (Charring Rate Of Wood). Although the intent was to keep CROW as simple as possible, the model accounts for the four major factors that affect the thermal degradation of wood:

- Dry density of the wood
- Moisture content of the wood
- Lignin content of the wood
- Char contraction

The predictive capability of CROW was evaluated on the basis of ASTM E 119 furnace data obtained for a Douglas fir glulam beam tested under different loads. CROW predictions, with some adjustment for moisture effects, are in reasonable agreement with the measurements. The model will be most useful to predict performance of wood members exposed under thermal conditions that deviate from the standard fire (natural or parametric fires) and/or members that are protected by a membrane.

KEYWORDS: *charring rate, fire resistance, fire model, fire test, pyrolysis, wood*

INTRODUCTION

The charring rate, β, is an important factor in the fire design of exposed structural timbers, because it determines how quickly the size of the load-bearing section decreases to a critical level. Design procedures for fire-resistant wood members in the U.S. model building codes [52] are based on work done by Lie in the early 1970's [53]. Lie assumed a constant charring rate of 0.6 mm/min, regardless of species and moisture content.

White performed extensive measurements of the charring rate of eight wood species exposed according to ASTM E 119 [54]. He found that the data could be correlated according to the following equation:

$$t = mx_c^{1.23}$$
(1)

with t time (min),
        m char rate coefficient (min/mm$^{1.23}$),
        x_c char depth (mm).

Based on the experimental data, an empirical model was developed that expresses m as a function of density, moisture content, and a char contraction factor. The latter is the ratio of the thickness of the char layer at the end of the fire exposure divided by the original thickness of the wood layer that charred. The char contraction is primarily a function of the lignin content in the wood. Permeability was identified in a more recent publication as an important missing factor in this correlation [55].

By using White's time-location model it is possible to refine Lie's method and account for the effects of species and moisture content [56]. Moreover, application of Eq. 1 results in a more economical design if the desired fire endurance is greater than 60 min as the charring rate decreases with time.

White's model is not applicable if exposure conditions deviate from the standard fire. A limited amount of charring rate data is available for natural fire conditions and wood members covered by a protective membrane. A more universal approach to determine the charring rate of wood members involves the use of a pyrolysis model that predicts the thermal degradation under specified thermal exposure conditions.

White's data and correlation provide guidance as to the physical and chemical phenomena that need to be addressed by the pyrolysis model. A conceptual description of these phenomena is provided in the next section. A literature survey was conducted to determine whether a suitable model with the necessary features is not already available. Since the search was unsuccessful, it was decided to develop a new model. The development and experimental validation of the new pyrolysis model form the main subject of this paper.

CONCEPTUAL DESCRIPTION OF WOOD PYROLYSIS

Pyrolysis of porous char-forming solids, such as wood, exposed to fire is a very complex process. Figure 1 identifies the major physical and chemical phenomena involved in the pyrolysis of an exposed slab of wood.
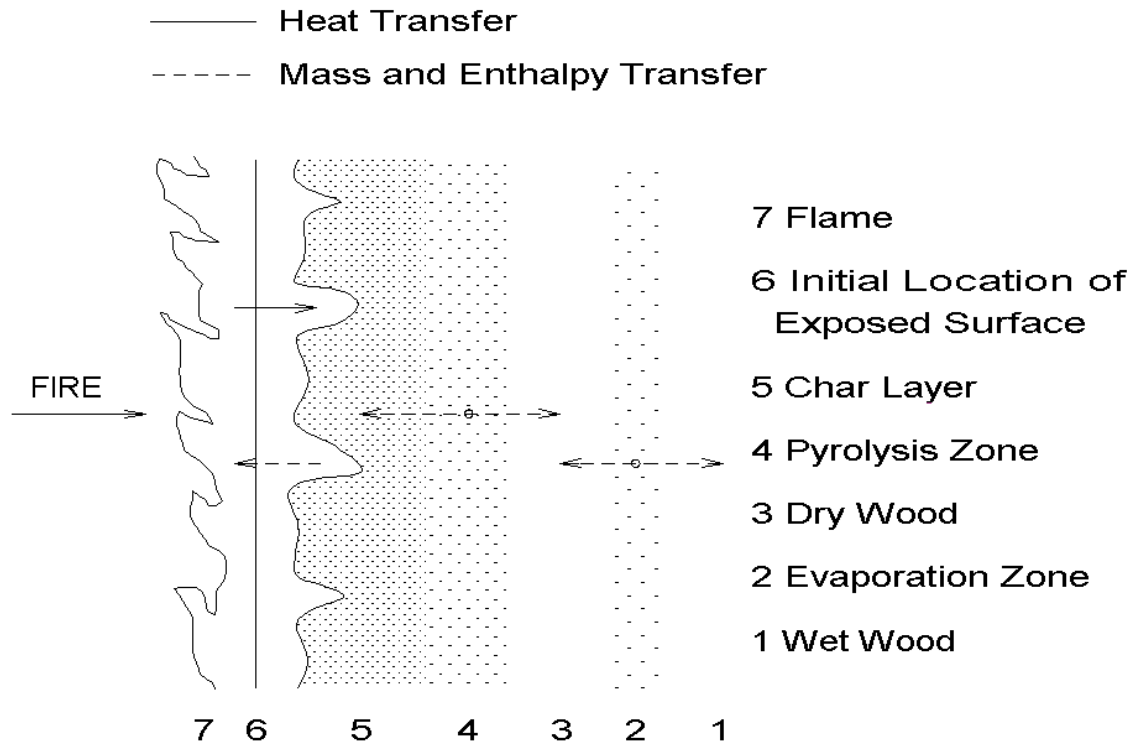
FIGURE 1 : Heat and Mass Transfer in a Pyrolyzing Slab of Wood

Under practical conditions of use, wood products always contain a certain percentage of moisture. When exposed to fire, the temperature of the wood will rise to a point when the moisture starts to evaporate. Since the water is adsorbed to the cell walls (at least if the moisture content is below the fiber saturation point, which is around 30% by mass), evaporation requires more energy than needed to boil free water and may occur at temperatures exceeding 100°C. The water vapor partly migrates toward and escapes through the exposed surface. A fraction also migrates in the opposite direction, and re-condenses at a location where the temperature is below 100°C.

The dry wood (zone 4) further increases in temperature until the fibers begin to degrade. The thermal degradation starts around 200 to 250°C. The volatiles that are generated again travel primarily toward the exposed side, but also partly in the opposite direction. They consist of a combustible mixture of gases, vapors, and tars. A solid carbon char matrix remains. The volume of the char is smaller than the original volume of the wood. This results in the formation of cracks and fissures which greatly affect the heat and mass transfer between the flame and the solid. The combustible volatiles that emerge from the exposed surface mix with ambient air, and burn in a luminous flame.

Under certain conditions, oxygen may diffuse to the surface and lead to char oxidation. The exposed surface recedes as combustion progresses due to the char contraction and possible char oxidation.

MATHEMATICAL MODELS FOR WOOD PYROLYSIS

More than 50 different mathematical models for the pyrolysis of wood have been developed since WW II [1-51]. These models range from simple approximate analytical equations to

very complex numerical solutions of the conservation equations. They vary widely in complexity depending on the physical and chemical phenomena that are included and the simplifying assumptions that are made. Some address both heat and mass transfer, while others completely ignore migration of water and/or fuel vapors. There are two main application areas for such models:

- Use of wood fuel for energy generation
- Fire performance of wood

Nine of the models in the second category were specifically developed for structural applications [9, 13, 16, 18, 26, 36, 44, 46]. The remaining models in the second category were developed to predict the flammability of wood in building fires or the burning behavior of forest fuels.

It is relatively easy to write down a comprehensive set of model equations [57]. The main equation expresses the conservation of energy as follows:

$$\rho c_p \frac{\partial T}{\partial t} + \nabla \cdot (\rho_g \overline{v}_g c_g T) = \nabla \cdot (k \nabla T) - \dot{r}_V (\Delta h_v + \Delta h_w) - \dot{r}_p \Delta h_p \tag{2}$$

with ρ density of wood, partially charred wood, or char (kg/m^3),
  c_p specific heat of wood, partially charred wood, or char (J/kg-K),
  T temperature (K),
  t time (s),
  ρ_g density of volatiles (kg/m^3),
  $\overline{v}_g$ velocity vector of the volatiles (m/s),
  c_g specific heat of volatiles (J/kg-K),
  k thermal conductivity of wood, partially charred wood, or char (W/m-K),
  $\dot{r}_V$ vaporization rate of water (kg/s),
  Δh_v heat of vaporization of water (J/kg),
  Δh_w heat of wetting (J/kg),
  $\dot{r}_p$ generation rate of pyrolyzates (kg/s),
  Δh_p heat of pyrolysis (J/kg).

Solving the equations is not so easy. Moreover, obtaining material properties can be a monumental task. For example, the thermal conductivity of wood is a function of temperature, density, and moisture content. It is hard to obtain experimental data at elevated temperature, and some models simplify this problem by using a constant that is representative for a certain density of the wood, moisture content, and temperature range. A similar challenge exists in selecting suitable values for the thermal conductivity of partially charred wood, and char.

NEW ENGINEERING WOOD PYROLYSIS MODEL

It is clear from the information provided in the previous section that a tremendous amount of work has been done in the area of pyrolysis modeling. Unfortunately, none of the models that have been developed include all the important features that need to be addressed. For

example, one of the most complete model was developed by Fredlund [36]. This model includes unique mass transfer and char oxidation algorithms, but it does not address char contraction.

In addition, there are many inconsistencies and contradictions between the different models. For example, different thermal properties are being used for similar wood species. The thermal conductivity of char varies by two orders of magnitude. Janssens developed a procedure to generate thermal properties for wood, partially charred wood, and char, but to date this procedure has not been used in any published pyrolysis model [58]. The new model incorporates properties that are calculated according to this procedure. The model is one-dimensional, and consists of the following energy conservation equation

$$\rho c_p \frac{\partial T}{\partial t} = \frac{\partial}{\partial}(k\frac{\partial T}{\partial x}) - (\Delta h_v + \Delta h_w)\rho_0 \frac{\partial u}{\partial t} \tag{3}$$

with x length coordinate (m),
       ρ_0 density of oven dry wood (kg/m^3),
       u moisture content by mass.

The primary model assumptions are as follows:

- Wood properties are used when $T \le 200°C$
- Char properties are used when $T \ge 800°C$
- Mass weighted averages are used at $200°C < T < 800°C$
- Water evaporates at $T = 100°C$
- The heat of pyrolysis is equal to 0
- Char contraction is taken into account
- The equation is solved via a finite difference method

Moisture migration to the cold side is not directly accounted for, but is addressed as discussed in the next section. To simulate the behavior under standard fire exposure conditions, Eq. 3 is coupled with a surface boundary condition that accounts for the heat transfer from the furnace and its own flame as described by Hadvig [18]. The furnace is modeled in the same way as done by Mehaffey et al.

EVALUATION OF THE PREDICTIVE CAPABILITY OF CROW

Experiments

In 1997, the American Forest & Paper Association (AF&PA) conducted a series of four experimental glued laminated (glulam) beam tests according to ASTM E 119 at Southwest Research Institute (SwRI) in San Antonio, Texas. The primary objective of the tests was to evaluate the effect of load on the fire resistance of glulam beams. Four 2400F-V4 Douglas fir beams, with an actual section of 222×419-mm, were tested under different load conditions. The clear span of the beams was 4.57 m, of which the central 3.76 m section was exposed in the furnace. Times to structural failure, measurements of beam temperature, and post-test char measurements were recorded.

The first of the four tests was conducted without external load, but with an extensive number of thermocouples distributed across the section to determine charring rates in different directions as a function of time.

In the remaining three tests, the beams were loaded at 27%, 44%, and 91% of the design load. The reported allowable stresses and stifness were F_b = 16.55 MPa and E = 11 GPa respectively. Each beam was braced against lateral translation and rotation at the supports and was loaded at 2 evenly spaced load points. The resisting moment was estimated to be 302 kN-m compared to induced moments of 25.7 kN-m, 41.6 kN-m, and 88.2 kN-m for the 27%, 44%, and 91% design load cases, respectively. The corresponding failure times were 147 min, 114 min, and 85 min respectively.

Calculations

The effects of moisture migration toward the cold side are indirectly accounted for by the CROW model. It is assumed that only part of the moisture evaporates and escapes through the exposed surface. The remaining part evaporates, moves toward the cold side where it condenses, evaporates again at a later time, etc. The energy required to initially evaporate the second fraction of the moisture is never lost from the system.

The fraction of the moisture content that evaporates and escapes in the form of steam is determined by matching CROW charring rate predictions with White's time-location model. The Douglas fir beams tested at SwRI had a density of 460 kg/m^3 and an average moisture content of approximately 9% by mass. The corresponding values for m in White's model are 0.47 and 0.58 for a moisture content of 0% and 9% respectively. Figure 2 shows that the times to reach char depths of 12.7, 25.4, 38.1, 50.8, and 63.5 mm in dry wood according to the CROW model are in good agreement with White's time–location model. Best agreement between CROW model predictions and Eq. 1 for a moisture content of 9%, was obtained by assuming that half of the moisture is conserved.

The section modulus at failure was determined for each of the three loaded beam tests conducted at SwRI based on the following equation

$$S_f = \frac{M}{k_f k_{mean} F_b} \tag{4}$$

with S_f section modulus at failure (m^3)
          M maximum load-induced moment (kN-m)
          k_f strength reduction factor to account for partial heating of the section
          k_{mean} factor to convert from allowable stress to mean failure stress (2.85)
          F_b allowable stress (16,550 kPa)
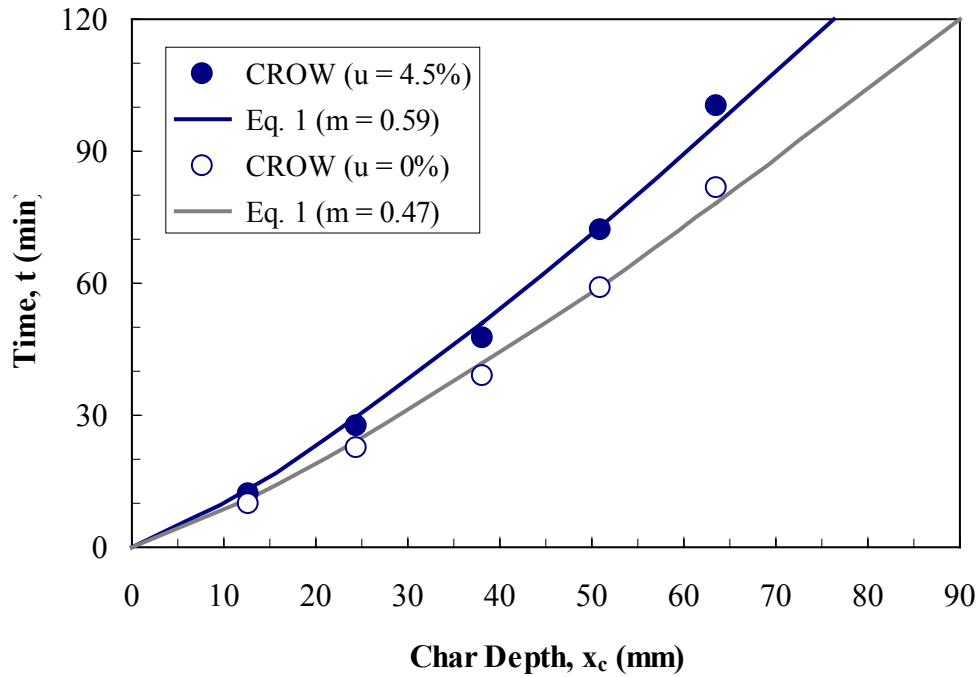
FIGURE 2 : Comparison between CROW predictions and White's time-location model

The strength reduction factor was calculated as a function of the beam perimeter P (m) and area A (m^2) according to Eurocode 5 [59]:

$$k_f = 1 - \frac{P}{200A}$$

(5)

The corresponding char depth was then obtained by solving the following equation, which accounts for corner rounding.

$$S_f = \frac{(b - 2x_c)(d - x_c)^2}{6} - 0.215x_c^2(d - x_c)$$

(6)

with b initial width of the beam section (m)
x_c char depth (m)
d initial depth of the beam section (m)

The results of these calculations are given in Table 1. Figure 2 compares CROW char depth predictions with the calculated char depth values in Table 1. It can be concluded from Figure 3 that the "calibrated" CROW model predicts charring rates that are consistent with the results of two of the three beam tests. The CROW model slightly underestimates the char depth for the beam loaded at 44% of the design load.

M *(kN-m)*	k_f	S_f *(m³)*	x_c *(mm)*
25.7	0.819	0.000666	81.1
41.6	0.849	0.001039	74.5
88.2	0.893	0.002093	57.3

Table 1 : calculated char depths at failure for the Douglas fir beam tests at SwRI
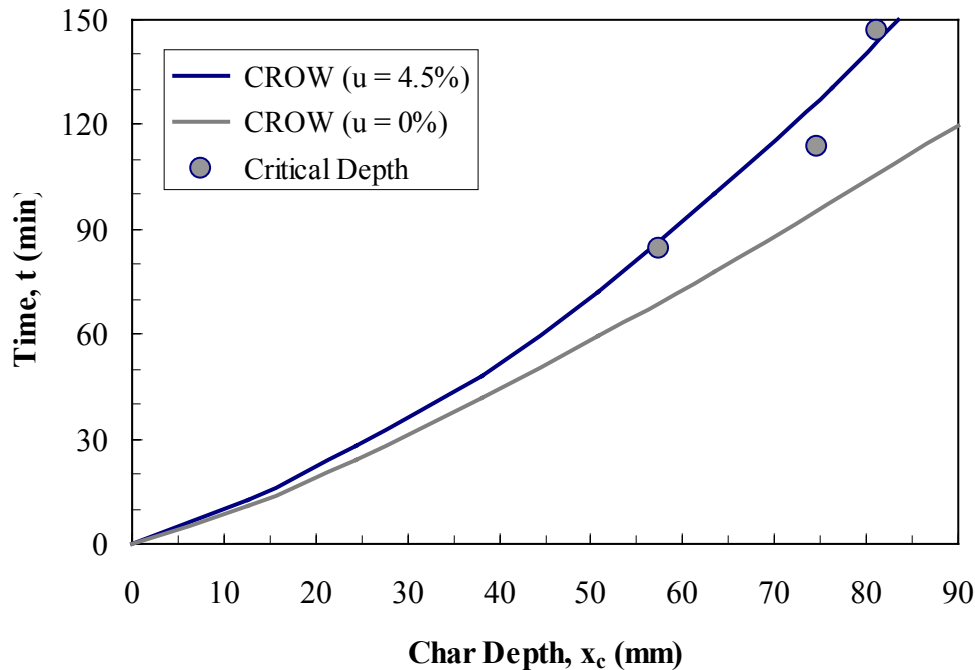
FIGURE 3 : CROW char depth predictions vs. estimated char depths at failure

CONCLUSIONS

A new pyrolysis model was developed to predict the charring rate of and temperature distribution in wood members exposed to specified fire conditions. The model is calibrated on the basis of White's correlations for the charring rate of wood members exposed to the standard ASTM E 119 fire. Model predictions are consistent with char depth estimates from Douglas fir beam tests conducted at SwRI. Additional comparisons with experimental data are needed to extend the validity of the pyrolysis model.

ACKNOWLEDGEMENT

REFERENCES

[1]   C. Bamford, J. Crank, and D. Malan, "The Combustion of Wood. Part I," *Proceedings of the Cambridge Philosophical Society*, Vol. 42, pp. 166-182, 1946.

[2]   W. Squire and C. Foster, "A Mathematical Study of the Mechanism of Wood Burning," Technical Progress Report No. 1, NBS Contract No. CST-362, Southwest Research Institute, San Antonio, TX, 1961.

[3]   E. R. Tinney, "The Combustion of Wooden Dowels in Heated Air," *Tenth Symposium (International) on Combustion,* The Combustion Institute, Pittsburgh, PA, pp. 925-930, 1965.

[4]   A. M. Kanury, "Burning of Wood - A Pure Transient Conduction Model," *Journal of Fire & Flammability*, Vol. 2, pp. 191-205, 1971.

[5]   R. Panton and J. Rittman, "Pyrolysis of a Slab of Porous Material," *Thirteenth Symposium (International) on Combustion,* The Combustion Institute, Pittsburgh, PA, pp. 881-891, 1971.

[6]   J. Havens, H. Hashemi, L. Brown, and R. Welker, "A Mathematical Model of the Thermal Decomposition of Wood," *Combustion Science and Technology*, Vol. 5, pp. 91-98, 1972.

[7]   A. M. Kanury, "Rate of Burning of Wood (A Simple Thermal Model)," *Combustion Science and Technology*, Vol. 5, pp. 135-146, 1972.

[8]   H. Kung, "A Mathematical Model of Wood Pyrolysis," *Combustion and Flame*, Vol. 18, pp. 185-195, 1972.

[9]   R. Knudsen and A. Schniewind, "Performance of Structural Wood Members Exposed to Fire," *Forest Products Journal*, Vol. 5, pp. 23-32, 1973.

[10]   P. Maa and R. Bailie, "Influence of Particle Sizes and Environmental Conditions on High Temperature Pyrolysis of Cellulosic Material - I (Theoretical)," *Combustion Science and Technology*, Vol. 7, pp. 257-269, 1973.

[11]   P. Thomas and L. Nilsson, "Fully Developed Compartment Fires: New Correlations of Burning Rates," Fire Research Note No. 979, Fire Research Station, Borehamwood, Herts, England, 1973.

[12]   F. Tamanini, *A Study of the Extinguishment of Wood Fires,* Ph.D. Thesis, Harvard University, Cambridge, MA, 1974.

[13]   S. Hadvig and O. Paulsen, "One-Dimensional Charring Rates in Wood," *Journal of Fire & Flammability*, Vol. 7, pp. 433-449, 1976.

[14]   L. T. Fan, L. S. Fan, K. Miyanami, T. Chen, and W. Walawender, "A Mathematical Model for Pyrolysis of a Single Particle," *The Canadian Journal of Chemical Engineering*, Vol. 55, pp. 47-53, 1977.

[15]   E. Kansa, H. Perlee, and R. Chaiken, "Mathematical Model of Wood Pyrolysis," *Combustion and Flame*, Vol. 29, pp. 311-324, 1977.

[16]   R. White and E. Schaffer, "Application of the CMA Program to Wood Charring," *Fire Technology*, Vol. 14, pp. 279-290, 1978.

[17]   F. Hoffman, *Study of the Thermal Behavior of Wood as Affected by Hygroscopic Moisture (in German),* Ph. D. Thesis, Carolo-Wilhelmina University, Braunschweig, Germany, 1979.

[18]   S. Hadvig, "Charring of Wood in Building Fires," Technical University of Denmark, Lyngby, Denmark, 1981.

[19]   A. Handa, M. Morita, O. Sugawa, T. Ishii, and K. Hayashi, "Computer Simulation of the Oxidative Pyrolysis of Wood," *Fire Science and Technology*, Vol. 2, pp. 109-116, 1982.

[20]   A. Atreya, *Pyrolysis, Ignition and Fire Spread on Horizontal Surfaces of Wood*, Ph.D. Thesis, Harvard University, Cambridge, MA, 1983.

[21]   M. Delichatsios and J. deRis, "An Analytical Model for the Pyrolysis of Charring Materials," FMRC Report No. RC83-BP-5, Factory Mutual Research Corporation, Norwood, MA, 1983.

[22]   D. Pyle and C. Zaror, "Heat Transfer and Kinetics in the Low Temperature Pyrolysis of Solids," *Chemical Engineering Science*, Vol. 79, pp. 147-158, 1984.

[23]   W. R. Chan, M. Kelbon, and B. Krieger, "Modeling and Experimental Verification of Physical and Chemical Processes during Pyrolysis of a Large Biomass Particle," *Fuel*, Vol. 64, pp. 1505-1513, 1985.

[24]   C. Miller and K. Ramohalli, "A Theoretical Heterogeneous Model of Wood Pyrolysis," *Combustion Science and Technology*, Vol. 46, pp. 249-265, 1986.

[25]   J. Villermaux, B. Antoine, and F. Soulignac, "A New Model for Thermal Volatilization of Solid Particles Undergoing Fast Pyrolysis," *Chemical Engineering Science*, Vol. 41, pp. 151-157, 1986.

[26]   B. Gammon, *Reliability Analysis of Wood-Frame Wall Assemblies Exposed to Fire*, Ph. D. Thesis, University of California, Berkeley, CA, 1987.

[27]   I. Wichman and A. Atreya, "A Simplified Model For the Pyrolysis of Charring Materials," *Combustion and Flame*, Vol. 68, pp. 231-247, 1987.

[28]   R. Capart, L. Falk, and M. Gelus, "Pyrolysis of Wood Macrocylinders under Pressure Application of a Simple Mathematical Model," *Applied Energy*, Vol. 30, pp. 1-13, 1988.

[29]   K. Ragland, J. Boerger, and A. Baker, "A Model of Chunkwood Combustion," *Forest Products Journal*, Vol. 38, pp. 27-32, 1988.

[30]   S. Alves and J. Figueiredo, "A Model for Pyrolysis of Wet Wood," *Chemical Engineering Science*, Vol. 44, pp. 2861-2869, 1989.

[31]   D. Purnomo, J. Aerts, and K. Ragland, "Pressurized Downdraft Combustion of Woodchips," *Twenty-Third Symposium (International) of Combustion,* The Combustion Institute, Pittsburgh, PA, pp. 1025-1032, 1990.

[32]   C. Koufopanos and N. Papayannakos, "Modeling the Pyrolysis of Biomass Particles: Studies on Kinetics, Thermal and Heat Transfer Effects," *The Canadian Journal of Chemical Engineering*, Vol. 69, pp. 907-915, 1991.

[33]   W. Parker, "Chapter 11: Wood Materials. Part A. Prediction of the Heat Release Rate from Basic Measurements," in *Heat Release in Fires*, V. Babrauskas and S. Grayson, Eds., Elsevier Applied Science, New York, NY, 1992, pp. 333-356.

[34]   M. Delichatsios and Y. Chen, "Asymptotic, Approximate, and Numerical Solutions for the Heatup and Pyrolysis of Materials Including Reradiation Losses," *Combustion and Flame*, Vol. 92, pp. 292-307, 1993.

[35]   C. DiBlasi, "Analysis of Convection and Secondary Reaction Effects within Porous Solid Fuels Undergoing Pyrolysis," *Combustion Science and Technology*, Vol. 90, pp. 315-340, 1993.

[36]   B. Fredlund, "Modelling of Heat and Mass Transfer in Wood Structures During Fire," *Fire Safety Journal*, Vol. 20, pp. 39-69, 1993.

[37]   M. Janssens, "Cone Calorimeter Measurements of the Heat of Gasification of Wood," *Interflam '93, Oxford, England,* Interscience Communications, London, England, pp. 549-558, 1993.

[38]   I. Mardini, A. Lavine, and V. Dhir, "Experimental and Analytical Study of Heat and Mass Transfer in Simulated Fuel Element during Fires," *Heat Transfer in Fire and Combustion Systems,* American Society of Mechanical Engineers, New York, NY, pp. 1-9, 1993.

[39] J. Mehaffey, P. Cuerrier, and G. Carrisse, "Model for Predicting Heat Transfer through Gypsum-Board/Wood Stud Walls Exposed to Fire," *Journal of Fire and Materials*, Vol. 18, pp. 297-305, 1994.

[40] D. Shrestha, S. Cramer, and R. White, "Time-Temperature Profile across a Lumber Section Exposed to Pyrolytic Temperatures," *Journal of Fire and Materials*, Vol. 18, pp. 211-220, 1994.

[41] E. Suuberg, I. Milosavlevic, and W. Lilly, "Behavior of Charring Materials in Simulated Fire Environments," NIST-GCR-94-645, National Institute of Standards and Technology, Gaithersburg, MD, 1994.

[42] F. Albini and E. Reinhardt, "Modeling Ignition and Burning Rate of Large Woody Natural Fuels," *International Journal of Wildland Fire*, Vol. 5, pp. 81-91, 1995.

[43] J. Caballero, R. Font, A. Marcilla, and J. Conesa, "New Kinetic Model for Thermal Decomposition of Heterogeneous Materials," *Industrial and Engineering Chemistry Research*, Vol. 34, pp. 806-812, 1995.

[44] P. Clancy, V. Beck, and R. Leicester, "Time-Dependent Probability of Failure of Wood Frames in Real Fire," *Fourth Fire and Materials Conference, Crystal City, VA, November 15-16, 1995,* Interscience Communications, London, England, pp. 85-94, 1995.

[45] B. Moghtaderi, V. Novozhilov, D. Fletcher, and J. Kent, "An Integral Model for the Transient Pyrolysis of Solid Materials," *Journal of Fire and Materials*, Vol. 21, pp. 7-16, 1997.

[46] M. Tavakkol-Khah and W. Klingsch, "Calculation Model for Predicting Fire Resistance Time of Timber Members," *Fire Safety Science, Fifth International Symposium, Melbourne, Australia, March 3-7, 1997,* International Association of Fire Safety Science, Boston, MA, pp. 1201-1211, 1997.

[47] S. Ritchie, K. Steckler, A. Hamins, T. Cleary, J. Yang, and T. Kashiwagi, "Effect of Sample Size on the Heat Release Rate of Charring Materials," *Fire Safety Science, Fifth International Symposium, Melbourne, Australia, March 3-7, 1997,* International Association of Fire Safety Science, Boston, MA, pp. 177-188, 1997.

[48] R. Yuen, R. Casey, G. DeVahl-Davis, E. Leonardi, G. Yeoh, V. Chandrasekaran, and S. Grubits, "Three-Dimensional Mathematical Model for the Pyrolysis of Wet Wood," *Fire Safety Science, Fifth International Symposium, Melbourne, Australia, March 3-7, 1997,* International Association of Fire Safety Science, Boston, MA, pp. 189-200, 1997.

[49] J. deRis and Z. Yan, "Modeling Ignition and Pyrolysis of Charring Fuels," *Fifth Fire and Materials Conference, San Antonio, TX, February 23-24, 1998,* Interscience Communications, London, England, pp. 111-121, 1998.

[50] F. Jia, E. Galea, and M. Patel, "Numerical Simulation of the Mass Loss Process in Pyrolyzing Char Materials," *Journal of Fire and Materials*, Vol. 23, pp. 71-78, 1999.

[51] M. Spearpoint and J. Quintiere, "Predicting the Burning of Wood Using an Integral Model," *Combustion and Flame*, Vol. 123, pp. 308-325, 2000.

[52] Anon., "International Building Code," International Code Council, Fairfax, VA, 2000.

[53] T. Lie, "A Method for Assessing the Fire Resistance of Laminated Timber Beams and Columns," *Canadian Journal of Civil Engineering*, Vol. 4, pp. 161-169, 1977.

[54] R. White, *Charring Rates of Different Wood Species,* Ph. D. Thesis, University of Wisconsin, Madison, WI, 1988.

[55] R. White and E. Nordheim, "Charring Rate of Wood for ASTM E119 Exposure," *Fire Technology*, Vol. 28, pp. 5-30, 1992.

[56] Anon., "Calculating the Fire Resistance of Wood Members," Technical Report 10, American Forest & Paper Association, Washington, DC, 1991.

[57] I. Wichman, "A Continuum-Mechanical Derivation of the Conservation Equations for the Pyrolysis and Combustion of Wood," Research Report 591, Technical Research Centre of Finland, Espoo, Finland, 1989.

[58] M. Janssens, "Thermo-Physical Properties for Wood Pyrolysis Models," *Pacific Timber Engineering Conference, Gold Coast, Australia,* pp. 607-618, 1994.

[59] EC5, "Eurocode 5: Design of Timber Structures," ENV 1995-1-2, CEN, Brussels, Belgium, 1994.

COMPRESSION PROPERTIES OF WOOD AS FUNCTIONS OF MOISTURE, STRESS AND TEMPERATURE

Francisco JONG and Paul CLANCY
Victoria Univ. of Technology, PO Box 14428, Melbourne City, MC 8001, Australia
Paul.Clancy@vu.edu.au

ABSTRACT

There has been considerable research in recent times in light-timber framed structures in fires. These structures have included horizontal (floor-like) panels in bending and walls under eccentric and approximately concentric vertical loading. It has been shown that compression properties are the most dominant mechanical properties in affecting structural response of these structures in fire. To date compression properties have been obtained by various means as functions of one variable only, temperature. It has always been expected that compression properties would be significantly affected by moisture and stress, as well. However, these variables have been largely ignored to simplify the complex problem of predicting the response of light wood framed structures in fire. Full scale experiments on both the panels and walls have demonstrated the high level of significance of moisture and stress for a limited range of conditions. Described in this paper is an overview of these conditions and experiments undertaken to obtain compression properties as a functions of moisture, stress and temperature. The experiments limited temperatures to 20°-100°C. At higher temperatures moisture vaporizes and moisture and stress are less significant. Described also is a creep model for wood at high temperatures and the incorporation of the creep model into a structural model for walls and panels.

KEYWORDS: *fire resistance, wood, timber, compression properties, creep, experiments, model*

INTRODUCTION

It is well known that fire degradation of light timber framed structures is more complex than the degradation heavy timber structures. Fire degradation of heavy timber members can be modeled one-dimensionally with simple constant char rates, typically 0.6 mm.min^{-1}. The degradation of light timber framed structures is two-dimensional and has to been modeled generally with heat transfer analysis and structural numerical methods. It is assumed that char occurs where temperatures exceed 300°C and that the mechanical properties of uncharred wood are a function of temperature alone. The dominant mechanical property that governs the behaviour of light timber framed walls is the elastic modulus of wood in compression, E_c, because walls tend to fail by buckling and buckling capacity is a function of E_c. It is known [1] that the compression behaviour of light-timber framed structures in fire is affected by creep which is a function of stress and moisture as well as temperature. König [1] demonstrated that wood in compression creeps far more than wood in tension.

Relationships for E_c obtained by various researchers are shown in Figure 1. White [2] and Gerhards [3] obtained their relationships from experiments involving small specimens of wood. Their relationships are similar to the relationship obtained by Young [4] for dry wood. It appears that the small specimens dried quickly when experiments were undertaken at elevated temperatures. More recent relationships incorporating the effects of moisture were obtained by Konig [1] and Thomas [5], as well as Young. These relationships were obtained by calibrating models of studs or joists against the results of full-scale experiments. The mid height deflections of a pin-supported wall predicted with various relationships mentioned, are plotted in Figure 3. The structural wall model used to obtain the plots is Young's model [6].

Young also obtained relationships by direct measurement of wood samples 300mm x 90mm x 35mm in concentric compression. These relationships are shown in Figure 2. He took measurements on specimens with 12% moisture content in a temperature range of 20°-100°C. He also tested dry specimens. The relationship he deduced for temperatures between 20°-300°C is shown as the dashed line. This relationship was substantially above the relationship obtained by calibration. The difference was attributed to creep.

It is apparent that the effect of creep is substantial. Several causes of creep seem possible. These include:
- Creep due to the presence of moisture, heat and stress in the temperature range 20°-100°C.
- Creep due to mechano-sorptive effects
- Creep due to heat and stress in the temperature range 100°-300°C.

Mechano-sorptive creep arises from changing moisture content including wetting and drying. It is common for the deflection of timber structures to gradually increase in climates of greatly varying humidity. This increase is not restricted to a maximum limit.

224

It is worth noting that these causes of creep were known centuries ago except they were not as elaborately explained as they are today. Timber framing members of galleons were bent in fire. Wood in furniture is shaped by applying water, and bending while drying.

The research described in this paper aimed to identify the causes of creep of light-timber structures in fire. In particular, it aimed to check whether all the creep observed in compression property experiments and standard fire [7] wall furnace experiments undertaken by Young [8] could be explained from the identified causes. From this check, it was desired to determine whether calibrated relationships in general needed further refinement. Finally it was desired to develop models for creep for general use and for adoption in Young's structural model [6]. To achieve these aims creep experiments on specimens of wood similar in size to Young's were undertaken.
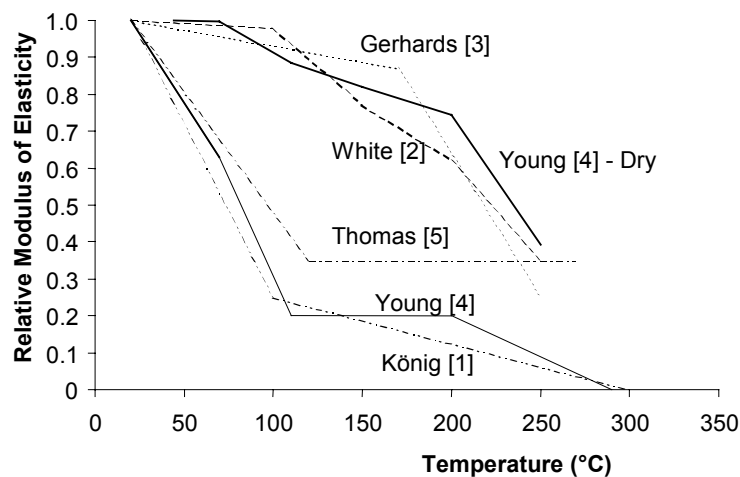
Figure 1. Relative elastic modulii versus temperature published by various researchers.
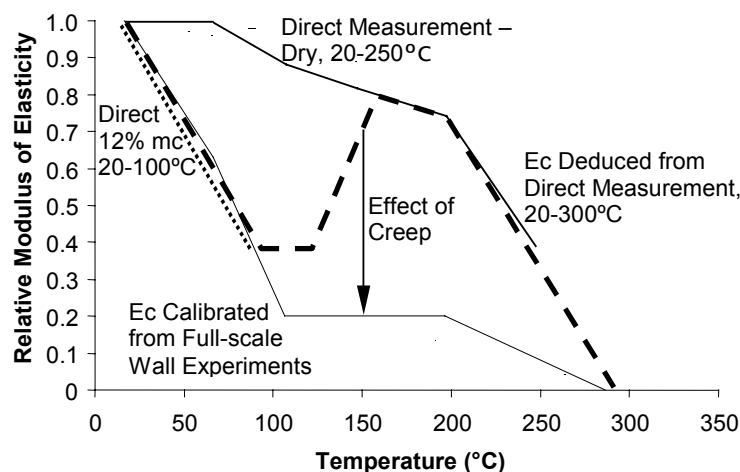
Figure 2. Effect of creep on elastic modulus deduced from measurements [8].
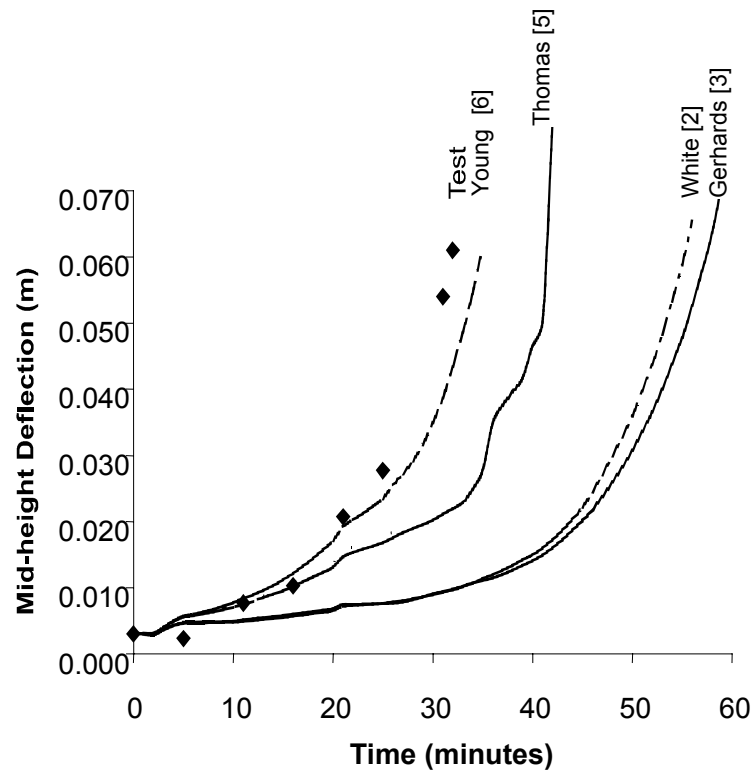
Figure 3. Deflection of composite pin-ended wall. (Plots marked Thomas, White and Gerhards were obtained using the relative moduli of elasticity in Figure 1.)

EXPERIMENTS

General

To evaluate all of the axial related compression deflection of timber members, experiments were undertaken to measure the elastic modulus and creep. For both of these types of experiments the following general procedures were adopted.

Compression deflections due to elastic and creep behaviour were measured for the following range of moisture contents and temperatures:
- Dry (0% moisture content) 20°-250°C
- 12% mc 20°-100°C
- 30% mc 20°-100°C

These moisture contents cover the full range in structural timber. The 12% value is typical for seasoned timber in most applications. In North America, 10% is perhaps more typical. The 30% value corresponds to fibre saturation conditions. Higher moisture contents are possible but will

not alter the moisture content bound in the wood fibre and thus not affect the structural response differently with any degree of significance.

The moisture content of dry specimens was achieved by oven drying at 105°C for three days. Repeated weighing of specimens showed no further weight loss after this period. The weighing and drying of these specimens showed that ordinary specimens had a moisture content of 12%. These specimens were coated with three coats of acrylic paint to seal in the moisture. The moisture content of 30% was achieved by soaking specimens in water at ambient temperature for 24 hours. The specimens were then placed in sealed plastic bags. The level of the moisture content was checked for some specimens by weighing and drying.

Specimens were cut from 90x35mm radiata pine. The moist specimens were cut to form a bone shape as shown in Figure 4. This shape was used to reduce bearing stresses and prevent crushing at the ends of the specimens which can be a problem for wood specimens with high moisture contents.

The moist specimens tested between 20°-100°C were placed in a metal tank filled with water as shown in Figure 5. The submersion in water helped maintain the moisture content at a constant level better than open air heating. The paint controlled the increase in moisture content of 12% specimens to 1-3%. It was found that the 30% specimens increased in moisture content by 1-5%.

The experiments were non-destructive. Specimens were re-used to minimize variability in the results.

The target temperatures for testing the moist specimens were achieved within 5°C in 30 minutes according to measurements taken with thermocouple wires inserted in the core of trial specimens. All specimens were heated for 40 minutes, which was similar to the period of heating of wood in wall furnace experiments [8]. Thus the heating procedure replicated the heating of wood in the wall furnace experiments well. A longer period could increase the creep in the specimens more than the creep in the wall furnace experiments. The use of water to heat specimens was much faster than the use of metal heating plates in air which took 150 minutes.

The dry specimens were heated with metal plates as shown in Figure 6. Insignificant creep was observed and hence the long period of heating with metal plates proved not to be of concern.

Loads of 6.0 and 8.0 MPa were applied. These are approximately three times the average stress and 50% greater than the peak stress applied by Young in his full-scale wall furnace experiments. The larger stresses were required to obtain measurable deflections. The larger stresses also enabled investigation of the behaviour of timber at the upper limit of practical loads.

The apparatus in Figure 7 and Figure 6 was fabricated to measure the deflection of a 100mm gauge length at the middle of specimens. The mechanism was the second one made. The first was found to be too insensitive. Despite obtaining a heat resistant LVDT, problems were encountered in using it in hot water. Sensitivity in the second apparatus was improved by

attaching the arms with circular bearing assemblies. LVDT's with long probes enabled deflection measurement to be undertaken clear of the water and overcame problems with inadequate heat resistance. Measurements were in the range of 0.01-0.07 mm.
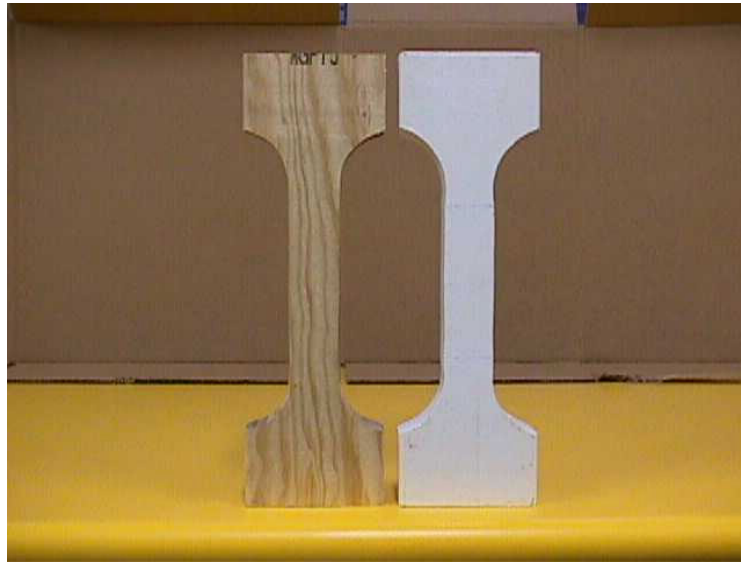
Figure 4. Moist specimens cut to form bone shapes to prevent end-crushing. A specimen with 30% moisture content is on the right, and a painted specimen with 12% moisture content is on the right.
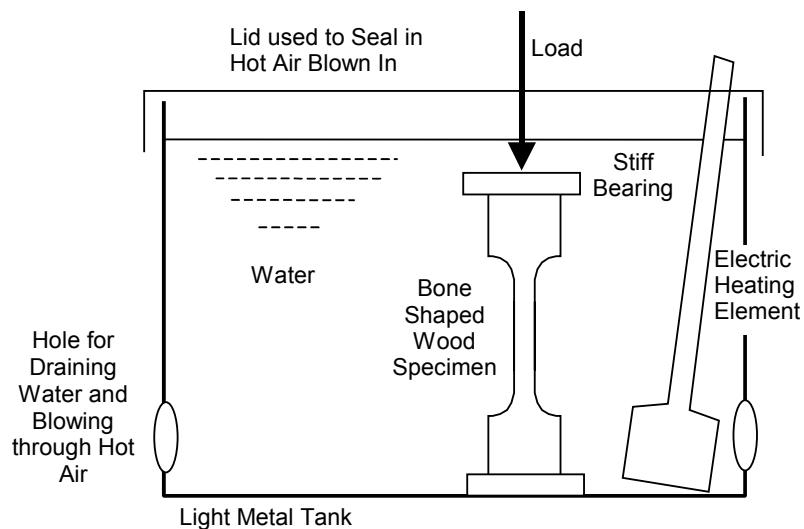
Figure 5. Schematic diagram of creep experiment on bone shaped wood specimen immersed in tank of heated water.
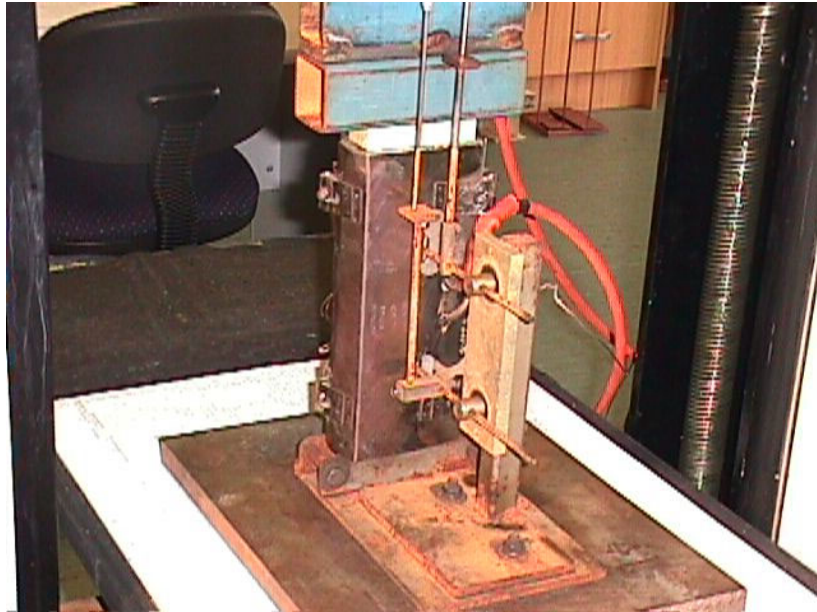
Figure 6. Experiment on dry specimen. Heating plates and deflection apparatus shown.
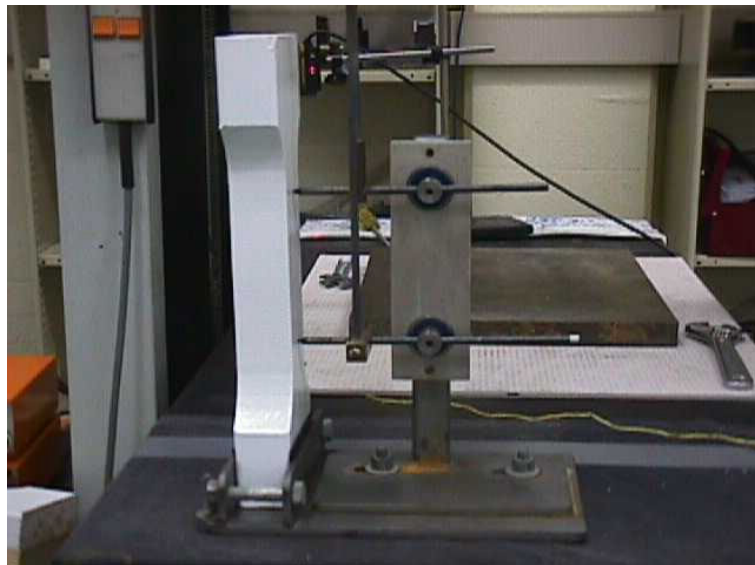
Figure 7. Deflection measurement apparatus.

Elastic Modulus of Wood in Compression

All specimens were loaded to 8MPa. The loads were applied in the minimum time that the loading apparatus could achieve, which was 1-2 minutes. Unlike Young's experiments to measure elastic modulus, the standard, ASTM D198 [9] was not used. It prescribes a rate of

0.001 strain per minute. This rate would have required a period of five minutes for the target load to be applied. It was found that creep during a period of five minutes was substantial.

To remove creep from the measurements that were taken, the procedure illustrated in Figure 8 was carried out. During the initial application of load, the gradient of the load deflection plot was low as the loading apparatus engaged the specimen. Once the specimen was engaged the gradient of the plot achieved maximum steepness. Thereafter, the plot drifted to the right, most likely due to small but significant creep. This creep was discarded by calculating the elastic modulus of steepest tangent when the specimen was engaged.
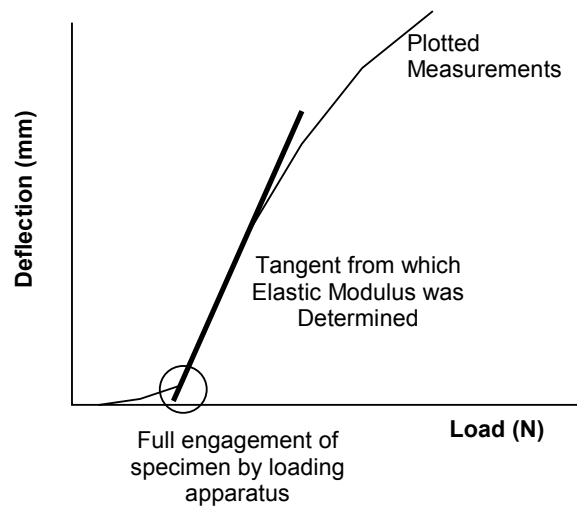
Figure 8. Graphical approach for determining the elastic modulus of wood in compression.
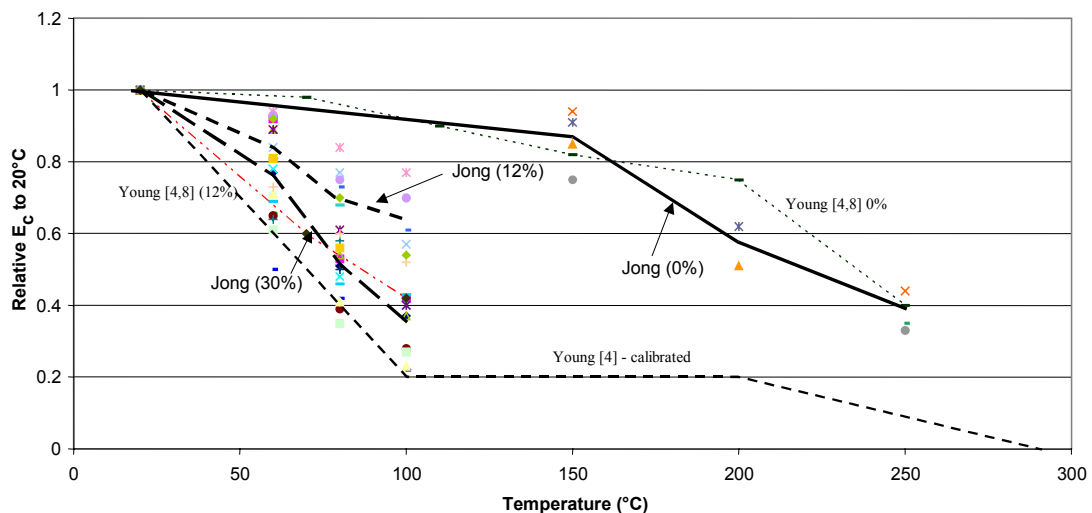
Figure 9. Relative elastic modulus versus temperature.

Elastic moduli were calculated graphically for the range of specimens listed in the previous section. Four dry specimens were tested at temperatures of 20°C, 150°C, 200°C and 250°C. Four 12% specimens and seven 30% specimens were tested at 20°C, 60°C, 80°C and 100°C. The calculated elastic modulus at ambient conditions was 15000±1300 MPa for the dry specimens; 14,500±1000 for the 12% specimens and 10200±1600 MPa for the 30% specimens. The similarity of elastic moduli for dry specimens compared with the 12% specimens is consistent with Young's findings. The elastic moduli relative to initial values for ambient conditions are plotted in Figure 9. Results from Young are shown for comparison.

Compression Creep Experiments

Experiments were designed to measure the three types of creep identified in the introduction:
- Creep due to the presence of moisture, heat and stress in the temperature range 20°-100°C.
- Creep due to mechano-sorptive effects
- Creep due to heat and stress in the temperature range 100°-300°C.

Key results for creep experiments in the temperature range 20°-100°C are shown in Figure 10, Figure 12 and Figure 13. The results shown are averages of groups of three similar experiments. The variations in the results of similar experiments was less than 10%.

Compression Creep (12% and 8 MPa- AR4) at Different Temperature
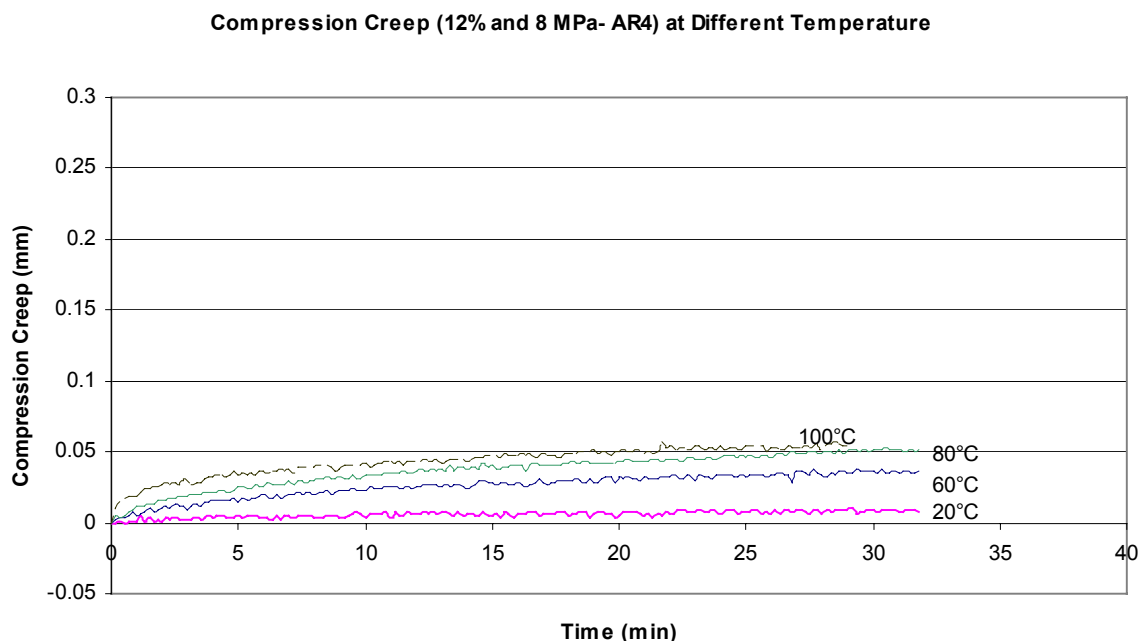
Figure 10. Compression creep for specimen with 12% moisture content and 8MPa loading.

231

The creep for a 100 mm gauge length of radiata pine with 12% moisture content and a constant load of 8MPa is shown in Figure 10. To gauge the significance of the creep, distributions of temperature obtained from thermocouple measurements in studs in walls in the furnace experiments are given in Figure 11. A pin-supported wall in the furnace experiments failed at 35 minutes of fire exposure. The temperature of the wood during the period prior to failure, 30-35 minutes, was largely 80°-100°C. From Figure 10, an estimate of the creep in the specimens is 0.05 mm. Elastic compression deflections can be deduced from Figure 9. The elastic deflection at 20°C is 0.055mm. At 80°-100°C the moisture content approximately doubles to, say, 25%. This doubling has been demonstrated experimentally and theoretically [10,11]. The moisture increases in wood at this temperature due to vaporization in nearby wood at 100°-120°C being dispersed by the pressure created and condensing in cooler regions. The elastic deflection for wood at 80°-100°C at 25% moisture content is expected to be approximately 0.07 mm. The creep due to temperature, stress and the presence of moisture would be approximately 75% of the elastic deflection. The creep experiments directly demonstrate that creep can almost double deflections.
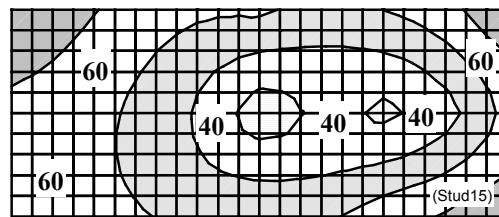
(a) At 15 Minutes
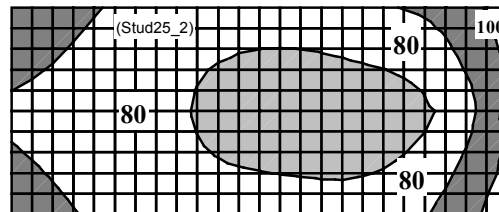
(b) At 25 minutes
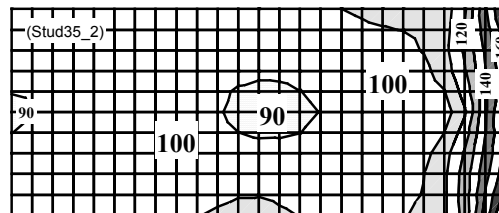
(c) At 35 minutes

Figure 11. Temperatures in studs in full scale wall furnace experiments [8]. (The plots are cropped 7.5 around all four edges.)

The creep for a 100 mm gauge length of radiata pine with 30% moisture content and a constant load of 8MPa is shown in Figure 12. The increase in creep due to the larger moisture content of 30% compared with 12% is dramatic, particularly for temperatures approaching 100°C. It appears that plastic behaviour of wood compression was approached.
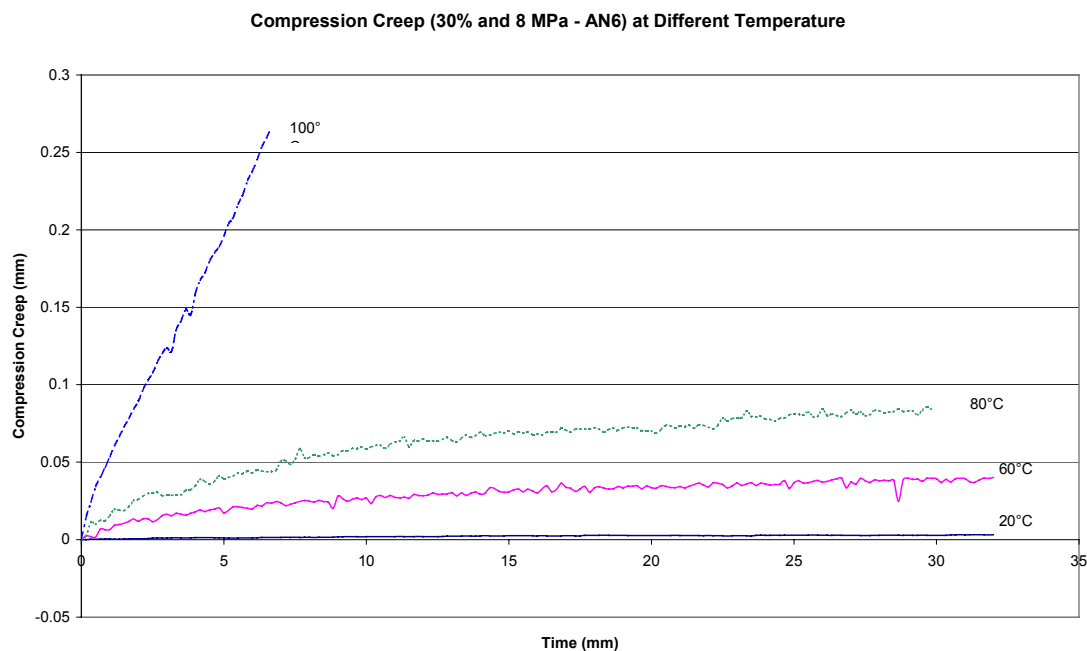
Figure 12. Compression creep for specimen with 30% moisture content and 8 MPa loading.

The creep for an experiment similar to the previous one described but with a load of 6MPa is shown in Figure 13. At this lower load no plastic behaviour is apparent and the effect of moisture on creep is substantial.

Another important observation from Figure 10, Figure 12 and Figure 13 is that the creep for a period as short as 5 minutes is highly significant compared with elastic deflections. Creep of wood is thus a significant phenomenon during the exposure of light timber framed walls in fire. Creep in this application contrasts to creep in many other structural applications in which creep is significant over long periods of time – years.

The following procedure was undertaken to evaluate the significance of mechano-sorptive creep. The scope of the testing was limited to desorption. Adsorption testing was not undertaken because the time for adsorption would greatly exceed the creep periods of interest, 5-30 minutes. Further, it has been reported [12,13,14] that desorption leads to greater creep than adsorption. Bone-shaped specimens were used with a minimum section of 30x15mm. This small size was chosen to facilitate desorption while maintaining a level of capacity that enabled measurable load to be applied. A constant load of 8MPa was maintained throughout the

experiment. The specimens had an initial moisture content of 30%. The experiment was undertaken in two stages. In the first stage the specimens were heated to 100°C in the tank. Constant moisture and load was maintained for 40 minutes. The water was drained from the tank. The tank was externally insulated. Hot air at 100°C was blown through the empty tank still containing the loaded specimen. The core temperature of specimens dropped to 65°C according to preparatory experiments used to establish the procedure. Deflections reduced substantially. After 10 minutes of blowing hot air into the tank the deflections increased and the specimens began to dry.
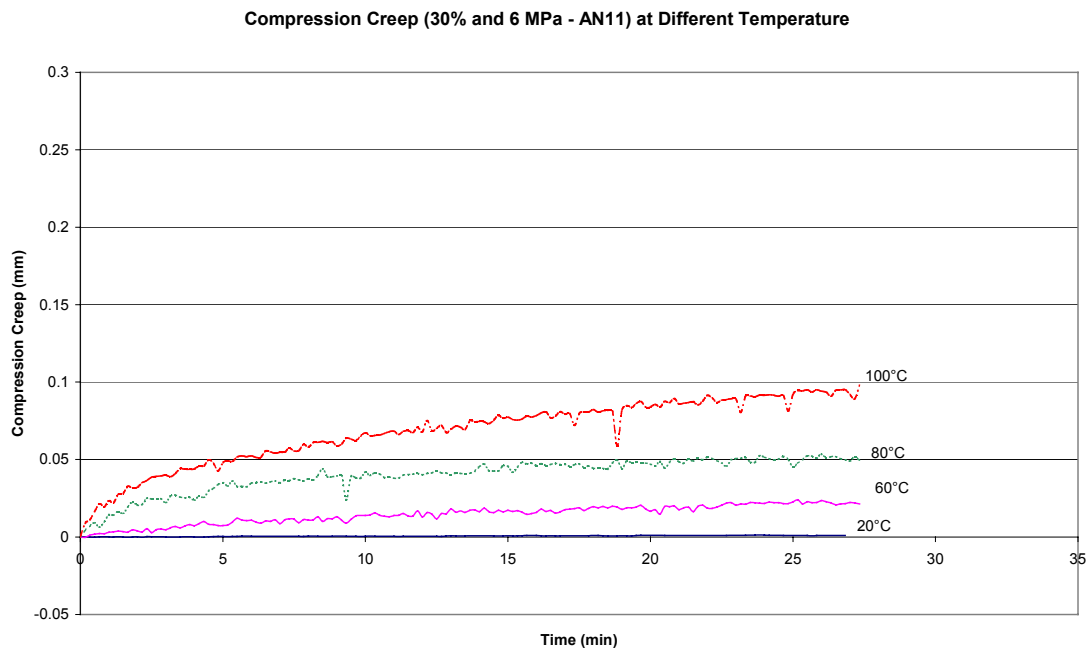
Figure 13. Compression creep for specimen with 30% moisture content and 6 MPa loading.

Developing a procedure to measure mechano-sorptive effects is difficult. Ideally, moisture content, stress and temperature should be uniform through the specimen. Maintaining uniform moisture content is virtually impossible. It may have taken up to the 100th minute in Figure 14 for sufficient moisture to evaporate for mechano-sorptive action to commence. The mechano-sorptive deflection does not appear to be significantly greater than the expected deflection projected as if stage one was continued beyond the 40th minute. From the crude mechano-sorptive experiment, it appears that the creep experiments involving constant moisture conditions, as previously described in this paper, are sufficient to predict deflections at temperatures less than 100°C.
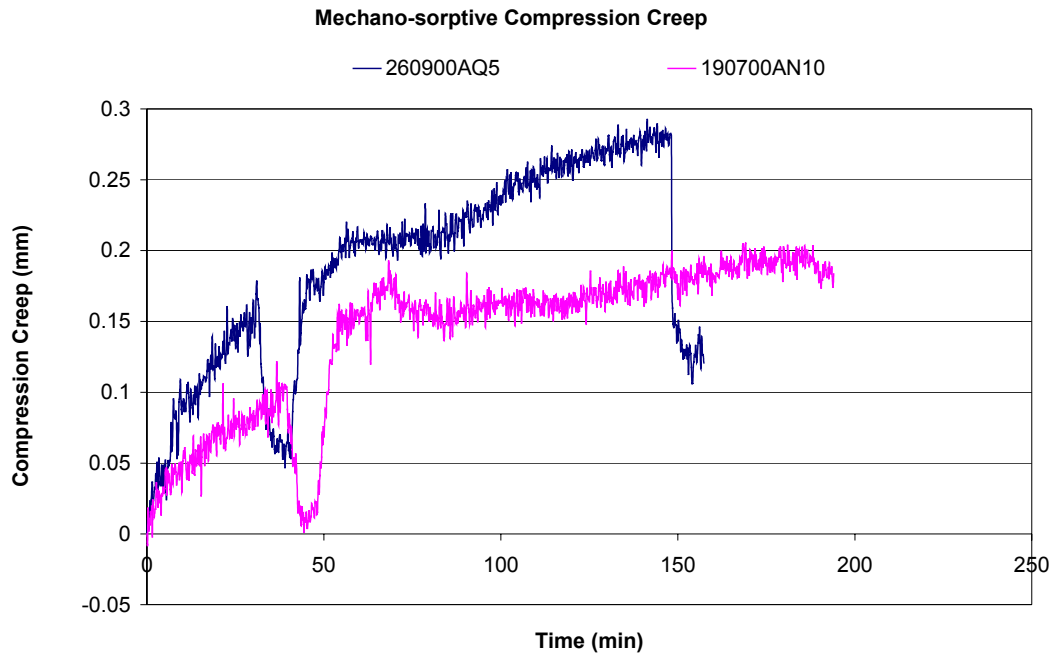
Figure 14. Compression creep for dry specimens with 8 MPa loading and temperatures at 100°C.
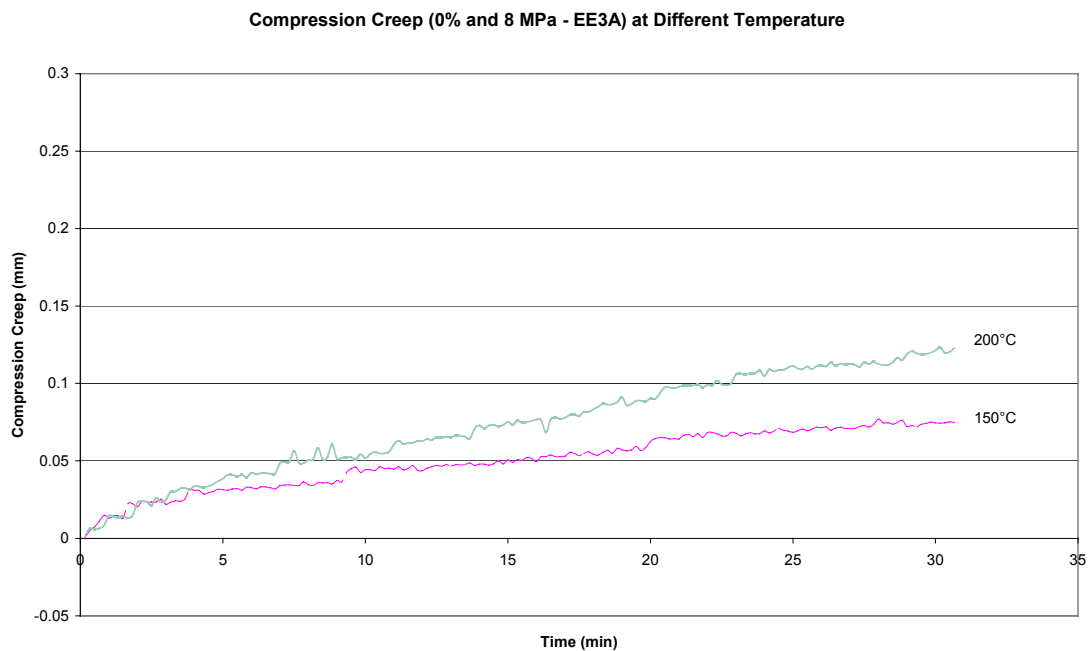
Figure 15. Compression creep for dry specimens with 8 MPa loading and temperatures above 100C..

235

The results of experiments to measure creep due to heat and stress in the temperature range 100°-300°C are given in Figure 15. Schaffer [15] documented creep of Douglas Fir in the conditions of 0% moisture content and temperatures between 150°-300°C. Creep of the radiata pine specimens was measured for these conditions. From Figure 9, the elastic deflection of a 100mm gauge length of dry wood at 200°C is approximately 0.09 mm. The creep is 0.12 mm at 30 minutes. Creep more than doubles the elastic deflection. It appears that Young's plot should be lowered further at high temperatures, to be more similar to König's plot in Figure 1.

These conditions of 0% moisture content and temperatures between 150°-300°C occurred in studs in furnace experiments on a wall with fixed supports, just prior to failure at 60 minutes. The temperature distribution, at this time, obtained from thermocouple measurements in unloaded studs, is shown in Figure 16.
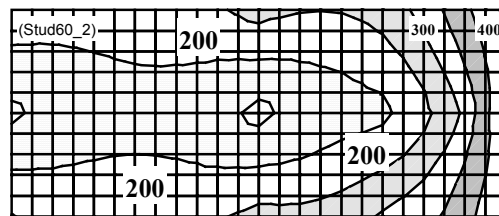
Figure 16. Temperatures in stud in wall at 60 Minutes [8].

Elasto-Creep Material Model

The simplest model of creep for general use is a reduction of the elastic modulus to allow for the additional deflection caused by creep. This type of model will be called an elasto-creep material model. The relationships for elastic modulus developed by calibration [5,1,4] in Figure 1 are effectively elasto-creep models. Discussion on such a model will address the aim of checking whether all the causes of creep discussed in the previous section could account for the difference between measured and calibrated compression properties of Young's [4] in Figure 2. This section will focus on the experimental results for radiata pine with an initial moisture content of 12% and a load of 6.0MPa.

The elastic compression deflection of a gauge length of 100 mm for such specimens at 20°C is 0.041 mm according to Jong's plot (12%) in Figure 9. The calculation of the deflection at 100°C involves elastic deflection and creep. The moisture content of wood at 100°C can be expected to double, as previously explained, to approximately 25%. Interpolation of deflections deduced from the measurements of specimens with moisture contents of 12% and 30% is required.

The elastic deflection for a specimen with 12% moisture content at 100°C is 0.065 mm. The creep deflection has been calculated in accordance with the procedure demonstrated in Figure 17. The creep deflection for a particular time period such as t_0-t_1 was deduced from an

236

experimental plot for the average stud section temperature, T_1, during the period. The average temperature was estimated from temperature distributions in Figure 11. The creep for the succeeding time period, t_1-t_2 , was deduced assuming that the creep continued at the rate measured for the average temperature, T_2, for the succeeding period. The average temperature during the first 10 minutes was estimated to be insufficient to cause any significant creep. The average temperature for 10-20 minutes was estimated as 50°C, for 20-30 minutes as 80°C and for 30-35 minutes as 100°C. The creep deduced was 0.034 mm. The total deflection deduced was 0.099 mm.

Similarly the total deflection deduced for a specimen with a 30% moisture content was 0.228 mm. By interpolation, the total deflection expected for a specimen with a moisture content of 25% was 0.192 mm. The predicted deflection for a specimen of wood subjected to temperature increasing from 20°C to 100°C is 0.041 mm increasing to 0.192mm; that is the effective elastic modulus reduced to 21% of its initial value. This result compares well with König's plot in Figure 1. The good comparison gives confidence in the accuracy of the measurements for elastic modulus and creep.

Figure 9 is repeated with the simple elasto-creep model superimposed in Figure 18. The model is simply bilinear with the linear plots intersecting at 100°C. More elaborate plots could be made. The plot could be kinked to account for the change in moisture content from 12% to 25% as temperature rose to 100°C. As well, the two linear plots could intersect at a relative modulus of 0.21 instead the value 0.20. However, such elaboration would be pretentious accuracy. The model is similar to König's in Figure 1, except the relative elastic modulus at 100°C is 0.2 instead of 0.25.

Although the model supports the results of previous research, it still suffers similar limitations. The model is applicable to light-timber framed structures which experience similar histories of temperature, moisture content and stress as the specimens in the experiments. A more rigorous model, which incorporates the variable of time explicitly, needs to be investigated.
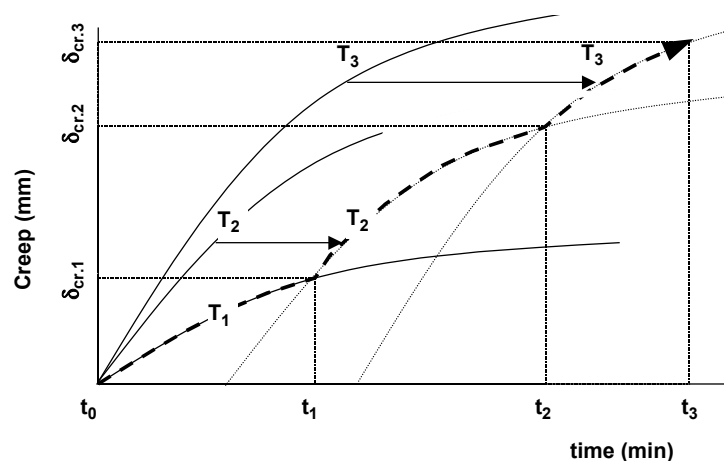
Figure 17. Calculation of creep involving changes in temperature.
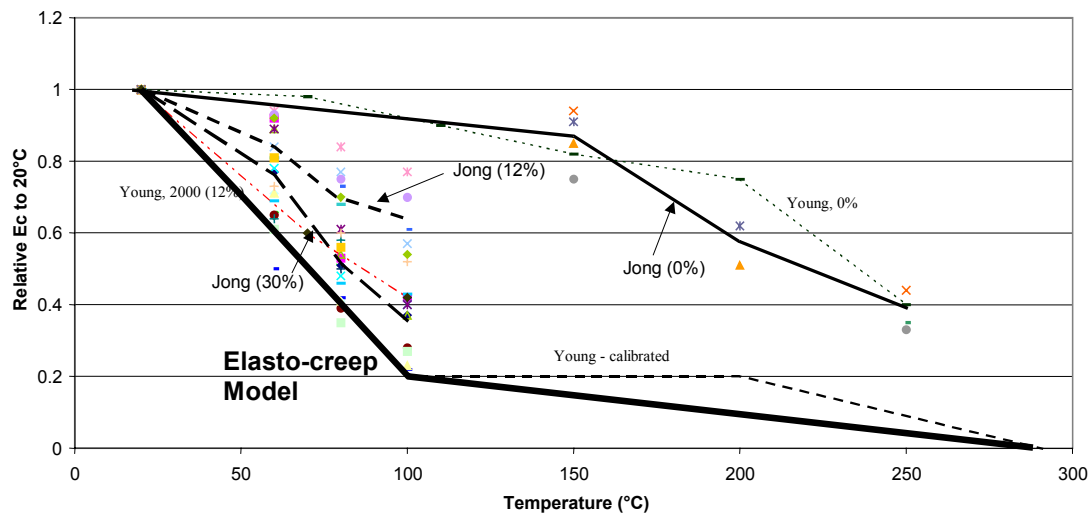
Figure 18. Elasto-creep model.

Time-Based Frame Model

The elasto-creep model numerically solved the problem of creep indirectly at the material level. Alternatively, an attempt can be made to directly model creep. Such a model is under development. It is an extension of Young's structural model [6] which can be used for light-timber framed walls and floors. The model discretizes a representative portion of the wall involving a stud and attached gypsum boards as shown in Figure 19 and Figure 20. The stiffness EI is determined for the composite action of all discrete elements in a member *ij*. The model thus represents a wall or floor as a contiguous assembly of line members. As shown in Figure 21, the assembly is analysed using the second order direct stiffness method to allow for the loss of stiffness due to large deflections of the wall as it thermally degrades and approaches collapse. The loss of stiffness comes from two sources – thermal degradation and large deflection. The model re-applies load equal to the load resistance lost due to the reduction in stiffness. In effect the model is a relaxation model rather than a creep model.

The simple nature of the discrete elements in the model makes it easy to adopt appropriate stress-strain behaviour that has been published previously [16]. The modeling of the elements is being modified to incorporate creep behaviour observed in the experiments described in this paper. It has been found that the creep of elements can be modeled with the simple expression,

$$\text{creep strain} = At^B \text{ x elastic strain}$$

Values for coefficients A and B have been found for specimens over a range of moisture contents, loads and temperatures. The model is thus essentially empirical and is being developed for radiata pine which is common in Australia. To model the effect of loads, the coefficients have been related to strain at ambient conditions in an effort to make the model more general.

238

The model will be used to deduce the range of walls for which creep is a significant problem affecting the time to failure. This range will include such variables as load and wall height. It is expected that the walls for which creep significantly affects the time to failure, would be more heavily loaded or more slender than that are typically used currently.
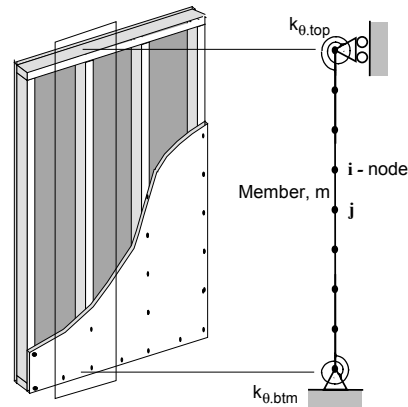
Figure 19. Discretisation of wall frame into members *ij* [6].
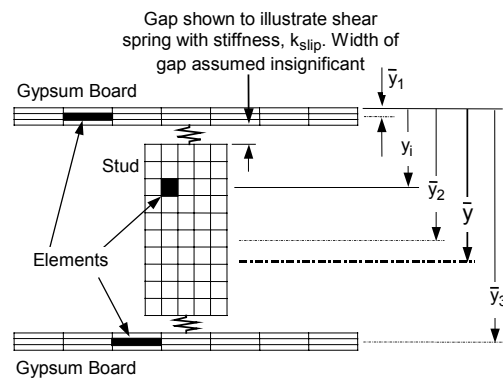
Figure 20. Discretisation of a member into elements [6].
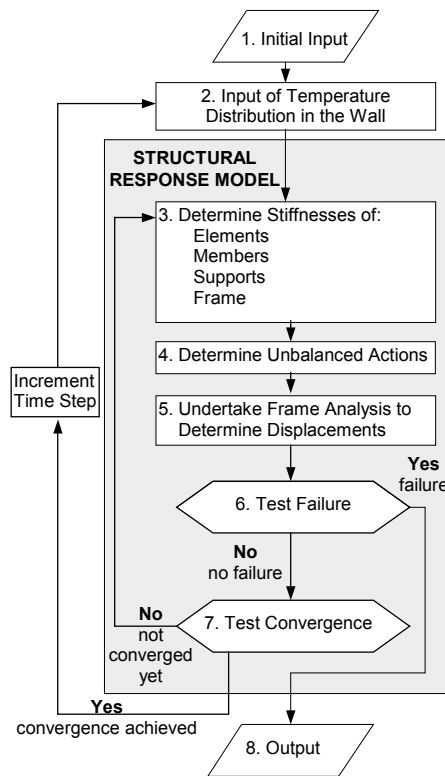
Figure 21. Flowchart showing overview of structural response model [6].

CONCLUSIONS

Creep of wood specimens has been measured for a range of loads, moisture contents and temperatures. The significant types of creep observed were:

- Creep due to the presence of moisture, heat and stress in the temperature range 20°-100°C.
- Creep due to heat and stress in the temperature range 100°-300°C.

Experimentation involving desorption of moisture in wood specimens did not reveal significant creep due to mechano-sorptive effects.

The first type of creep mentioned above was sufficient for explaining the difference between the elastic modulus obtained by calibration and direct measurement.

The relationships for the elastic modulus of wood in compression obtained by several researchers through the calibration of models to full scale experiments represent simple elasto-creep models for predicting the effects of creep of light-timber structures in fire. The models are limited to applications in which the wood is subjected to temperatures, moistures and stresses similar to values that occurred in the experiments.

Creep due to rises in temperature (above 70°C), moisture content or stress is significant compared with elastic deflections, in a time period as short as 5 minutes.

A time-based frame model has being developed. The model incorporates creep directly. It will be used to predict ranges of variables, including load and wall height, for which creep can be a problem.

REFERENCES

[1]   König J. and Walleij L., *Timber Frame Assemblies Exposed to Standard and Parametric Fires. Part 2: A Design Model for Standard Fire Exposure*, Trätek (Swedish Institute for Wood Technology Research), Stockholm, Report I 0001001, 76 pp., 2000.

[2]   White R.H., Cramer S.M. and Shrestha D.K., *Fire Endurance Model of a Metal-Plate-Connected Wood Truss*; Research Paper FPL 522; US Department of Agriculture, Forest Products Laboratory, Madison, Wisconsin, USA, 1993.

[3]   Gerhards C.C., *Effect of Moisture Content and Temperature on the Mechanical Properties of Wood: An Analysis of Immediate Effects*, Wood and Fiber, 1984; pp 4-36.

[4]   Young S.A. and Clancy P., *Compression Mechanical Properties of Wood at Temperatures Simulating Fire Conditions*, Journal of Fire and Materials, Vol 25, No 3, pp 83-93, 2001.

[5]   Thomas G.C., *Fire resistance of light timber framed walls and floors,* Fire Engineering Research Report 97/7, School of Engineering, University of Canterbury, Christchurch, New Zealand, 1997.

[6]   Young S.A. and Clancy P., *Structural Modelling of Light-timber Framed Walls in Fire*, Fire Safety Journal, Vol 36/3, pp 241-268, 2001.

[7]   ISO 834, *Fire-Resistance Tests- Elements of Building Construction*, International Standards Organisation.

[8]   Young S.A., *Structural Modelling of Plasterboard-clad Light Timber Framed Walls in Fire*, PhD Thesis, Centre for Environmental Safety and Risk Engineering, Victoria University of Technology, Melbourne, Australia, 2001.

[9]   American Society for Testing and Materials, *Standard Methods of Static Tests of Timbers in Structural Sizes: ASTM Designation: D198-84*, 1994.

[10] White R.H. and Schaffer E.L., *Transient Moisture Gradient in Fire-Exposed Wood Slab*, Wood and Fiber, vol 13 part 1 pp 17-38, 1981.

[11] Fredlund B., *A Model for Heat and Mass Transfer in Timber Structures During Fire, A Theoretical, Numerical and Experimental Study*, Lund University, Sweden, Institute of Science and Technology, Department of Fire Engineering, Report LUTVDG/(TVBB-1003), (a - p 178), 1988.

[12] Armstrong L.D. and Christensen, G.N., *Influence of Moisture Changes on Deformation of Wood Under Stress*, Nature, Vol. 191, pp. 869-870, 1961.

[13] Armstrong L.D. and Kingston R.S.T., *The Effect of Moisture Content Changes on the Deformation of Wood Under Stress*, Australian Journal of Applied Science, Vol. 13, pp. 257-275, 1962.

[14] Hearmon R.F.S. and Paton J.M., *Moisture Content Changes and Creep of Wood*, Forest Products Journal, Vol. 14, No. 8, pp. 357-359, 1964.

[15] Schaffer E.L., *Effect of Pyrolytic Temperatures on the Longitudinal Strength of Dry Douglas-Fir*, ASTM Journal for Testing and Evaluation, vol 1, part 4, pp319-329, 1973.

[16] Buchanan A.H., *Combined Bending and Axial Load in Lumber*, Journal of Structural Engineering, ASCE, Vol 112 No 12, pp2592-2609, 1986.

.

ANALYTICAL METHOD FOR THE BEHAVIOR OF A REINFORCED CONCRETE FLEXURAL MEMBER AT ELEVATED TEMPERATURES

KANG, Suk-Won
Research Engineer, Daewoo E&C, Song-Juk Dong, Jang-An Gu, Suwon, Korea
sharkang@mail.dwconst.co.kr

HONG, Sung-Gul
Seoul National University, Shillim Dong, Kwan-Ak Gu, Seoul, Korea
sglhong@snu.ac.kr

ABSTRACT

An analytical method is proposed for the thermal behavior of a reinforced concrete flexural member subjected to fire. The analysis procedure can be subdivided into two different steps; sectional analysis and member solution. A segmentation scheme is employed in the analysis for a section. It implicates uniform sectional properties and temperature distribution through the longitudinal axis of the member. The mechanical changes at the segmented section such as strain changes and corresponding stresses due to temperature increase are integrated into the member behavior at the member solution step. According to the analysis results, there exist very severe nonlinear strain changes with the depth measured from the fire-exposed surface, which are caused by a nonlinear temperature distribution at the section. Self-equilibrating stresses are manifested during heating just to let the section remain plane after deformation.

INTRODUCTION

In order to understand the behavior of the structures subjected to elevated temperatures such as fire, an information on the temperature distribution according to external heat and a full comprehension on the characteristics of the material at a given temperature condition are needed. Temperature changes vary the thermal and the mechanical properties of materials, and thus, they must be the preconsiderations for the analysis. The mechanical changes such as deformations or partial failure during heating also may affect the temperature distribution. However, it is almost true that their degrees are not remarkable and therefore, it is assumed that the temperature distribution is not affected by the mechanical changes of the member in the real applications.[1,6,11,&12] Thus, the analysis for the fire response of the structures can be subdivided into two major sequences for the reasons mentioned above; a nonlinear temperature analysis and a successive structural analysis as briefly shown FIGURE 1. It should be noted that the material properties are also subdivided into two categories following the analysis type in this study. The density, the specific heat, and the thermal conductivity are used in the temperature analysis and called as thermal properties in this study. Whilst, the thermal expansion coefficient, the initial elastic modulus, the strength, and etc. are included in the mechanical properties for the successive structural analysis.
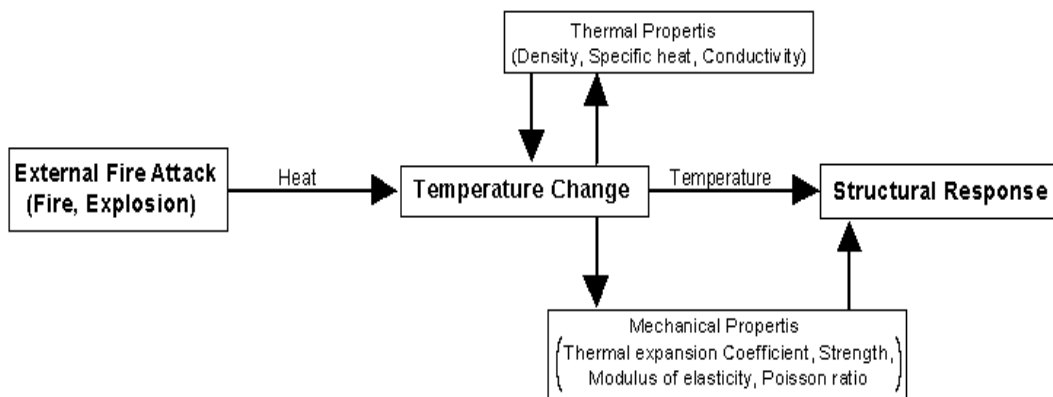
FIGURE 1. General procedure of thermal analysis

Recent rapid progress in the personal computer technology enables structural engineers to solve many complicated nonlinear problems by means of finite element method. However, the solution for a thermal response problem is still intricate and time-consuming because the solution procedure essentially requires iterative procedures for the calculation of stresses, strains, displacements, and etc. at the section and the temperature-dependent material properties of the element should be updated with the corresponding temperature. Besides, large displacement problems should be considered at higher temperature level in some cases. Thus, it is not unnatural to seek a more simple analysis technique for the members, and a simple numerical method to calculate the structural behavior during heating will be very useful for the engineers. Lie et al.(1993) suggested proposed a simple calculating the fire resistance of a vertical member by a simple illustrative way.[3] The calculation procedure is quite simple compared to finite element analysis, and the understanding of the behavior of a column under fire is very easy and clear.

This paper aims to propose a simple numerical process to analyze the thermal behavior of the horizontal members during heating. The motive is Poh's action-deformation concept and

Lie's member solution method. Poh et al. suggested an analytical formulation by their action-deformation relationships and solution procedure.[11] The solution is achieved by action and deformations with an iterative procedures. The behavior of the cross section is determined in the first loop (section analysis) and the behavior of the member is determined in the second loop (member analysis). The member solution approach for the vertical member by Lie has a similar procedure. The strength of the column is calculated by a method on the load-deflection relation.

In this study, the simple member solution procedure proposed by Poh et al., with consideration of Lie's method was extended to the horizontal members with the newly added concepts. The proposed method takes into account the material deterioration, the material nonlinearity, and nonlinear strain changes of concrete with temperature increase.

The proposed analysis procedure has some benefits. It can replace a full-scale analysis with a little effort. It can efficiently describe the structural response during heating with a simple illustration. On the other hand, the proposed method presumes a fixed shape of the section with the uniform material properties.

DEVELOPMENT OF AN ANALYSIS MODEL

The thermal response of the structure is obtained by three procedures. The temperature analysis and the stress-strain analysis at the section are carried out at the segmented section at first. Finally, the structural behavior is achieved by the member solution by integrating the section analysis result. It is assumed that the temperature distribution and the structural behavior are mutually independent. FIGURE 2 is an analysis procedure of the proposed method.
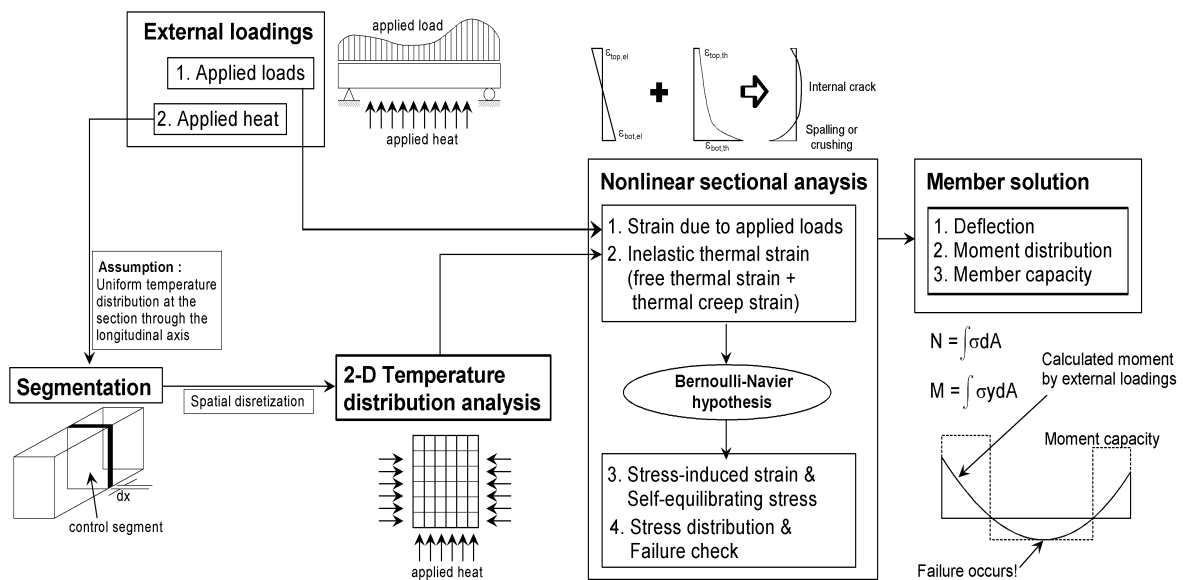
FIGURE 2. Thermal analysis procedure using with segmentation

Following assumptions are made before the structural analysis at elevated temperatures.

- Uniaxial behavior of the segmented elements

- Plane section remains plane after deformation

- Perfect bond between concrete and steel

Temperature analysis at an arbitrary segmented section is treated as a 2 dimensional problem. It has nothing to do with its position because the section properties and the shape are assumed uniform. The mechanical changes such as strain increases and corresponding stresses are obtained in the section analysis. Assumption 1 is used at the structural analysis of the section. Only uniaxial deformation is allowed and the transversal deformations and their affections are ignored. Assumptions 2 to 3 are used at the member solution procedure for the estimation of the curvature by the thermal effect.

TEMPERATURE ANALYSIS AT THE SECTION

The temperature information of the elements with time is essential for the successive solution of the structural analysis. There exist three types of the heat transferring; convection, radiation, and conduction. In general, the heat flux from the fire to the structure at fire-side is governed by convection and radiation, while the heat flow inside the element is determined by conduction.

From the first law of thermodynamics and Fourier's law, the heat conduction within the material is represented as

$$\nabla^2 T(x,\ y,\ t) + \frac{1}{k}Q(x,\ y,\ t) = \frac{1}{\alpha}\frac{\partial T(x,\ y,\ t)}{\partial t} \tag{1}$$

where

k = Conductivity $[W/m \cdot K]$

$Q(x,\ y,\ t)$ = Internal heat generation $[W/m^3]$

ρ = Density of the material $[kg/m^3]$

c_p = Specific heat of the material $[J/kg \cdot K]$

α = Thermal diffusivity $(= k/\rho c_p)$ $[m^2/\sec]$

The left side of the heat conduction equation is the second order function, which requires appropriate conditions at boundaries. The boundary conditions in this study consider convection and radiation heat flux from fire and are expressed as

$$Q = \alpha(T_e - T_s)^\beta + v\sigma(\varepsilon_e T_e^4 - \varepsilon_s T_s^4) \tag{2}$$

where α, β, v, σ, and ε are convection factor, convection power, radiative view factor, Stefan-Boltzman constant, and emissivity coefficient, respectively. Terro's research data are used for the values of the coefficients.[12]

STRUCTURAL ANALYSIS

Constitutive relationships at high temperature

It is generally accepted that the creep due to temperature change becomes more critical with temperature. Recently, it has been reported that at higher temperature level the creep strain of concrete can be modeled by using Dorn's theorem. They employed an Arrhenius plot in order to derive the activation energy of concrete for the thermal creep.[3&4]

For the simplicity of the numerical model, the strain components are assumed to be uncoupled. Then, the total strain of concrete (ε_{total}) at high temperature is assumed as the sum of three different components and can be written as

$$\varepsilon_{total} = \varepsilon_{th}(T) + \varepsilon_{\sigma}(\sigma, T) + \varepsilon_{cr}(\sigma, T, t) \tag{3}$$

where ε_{th}, ε_{σ}, ε_{cr}, T and t represent free thermal strain, stress-induced strain, thermal creep strain, temperature and time, respectively. The free thermal strain and the thermal creep strain are originated with the temperature change. Whilst, the stress-induced strain is generated by the external loads. Inelastic strain change due to moisture in concrete is neglected in this study for the reason that it is so small compared to thermal creep strain at high temperature and its effects are getting disappear at more than 400°C.[5&10]

The thermal expansion of concrete is calculated by the following simple equation.

$$\varepsilon_{th} = \int_{T_1}^{T_2} \alpha_c(T) dT \tag{4}$$

where $\alpha_c(T)$ is the coefficient of the thermal expansion of concrete, and it varies with temperature. The thermal creep strain of concrete can be defined as

$$\dot{\varepsilon}_{cr} = C \cdot \sigma^m \cdot \theta^n \quad \text{and} \quad \theta = \int_0^t \exp(-\Delta H / RT) dt \tag{5}$$

where C, m and n are the thermal creep constants. The term θ in the equation is the representative of the effective time intensified by temperature change and the internal energy of molecular phase transformation for creep behavior. It is usually called as a temperature compensated time. The coefficients, ΔH and R, are the activation energy of concrete and gas constant, respectively. They are obtained from the logarithmic graph of Arrhenius plot. More details on the thermal creep of concrete at high temperature are described in other researcher's paper.[3,4,&6]

Structural behavior at the section

The total strain in equation (3) can also be described by an illustrated way as shown in FIGURE 3. The strain of the heated flexural member is regarded as the sum of three components and represented as

$$\varepsilon_{total} = \varepsilon_{el} + \varepsilon_{thermal} + \varepsilon_{se} \tag{6}$$

where ε_{el}, $\varepsilon_{thermal}$, and ε_{se} are the strain by the external loads, the thermal strain due to the temperature change and a virtual self-equilibrating strain. The load-induced strain is simply calculated from the elastic beam theory. The thermal strain is obtained by assuming the virtual curvature. The virtual strain is derived from the planeity condition after the deformation by the nonlinear temperature gradient and gives rise to the self-equilibrating stress. It does not affect the structural behavior and just change the stress distribution at the section. In this study, the virtual thermal curvature is calculated from either the temperature difference or the strain difference. The explanation for the curvature calculation is written in the example analysis.

$$\varepsilon_{thermal} = \phi_{thermal} \cdot \overline{y} \tag{7}$$

where $\phi_{thermal}$ and $\overline{y}$ are the thermal curvature due to temperature or strain gradient and the distance from the top of the member. For a reinforced concrete flexural beam, it is not easy to derive the curvature due to the nonlinearity of the temperature distribution at the section. The differences of temperatures, strains or stresses between the top and bottom of the member can be used to calculate the thermal curvature(refer to FIGURE 3). The locations of the two points to be measured have the possibility to move depending on the severity of the nonlinearities of temperature, strains, or stresses.
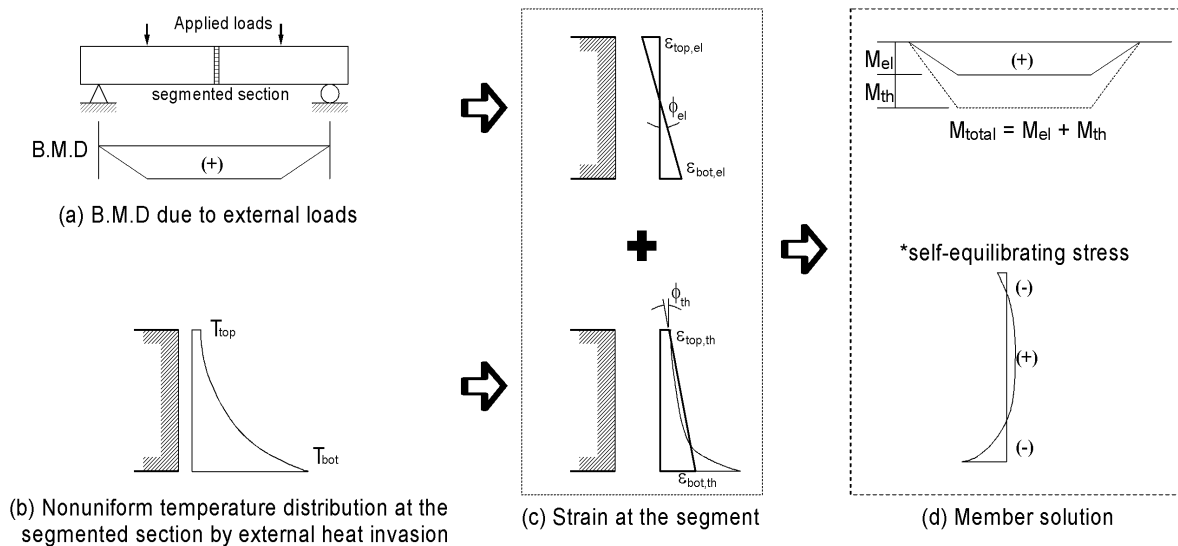
FIGURE 3. Thermal strains and curvature of a flexural member during heating

Member solution procedure

If the thermal curvature is obtained, then the whole structural response of the flexural member is achieved from the simple beam theory. The prediction of the structural behavior of the member is determined by integrating the sectional response through the longitudinal axis.

$$\phi_{total} = \phi_{el} + \phi_{thermal} \tag{8}$$

$$\frac{d^2 v}{dx^2} = \frac{M}{EI} = \phi_{total} \tag{9}$$

where ϕ_{el}, $\phi_{thermal}$, and v are the curvature by external loads that are easily obtained, the curvature by nonlinear temperature distribution at the section, and the deflection at the section, respectively. The self-equilibrating stress at a given point is also determined from the equation (6).

$$\sigma_{se} = E(T) \cdot (\varepsilon_{tot} - \varepsilon_{el} - \phi_{thermal} \cdot \overline{y}) \tag{10}$$

APPLICATION OF THE PROPOSED METHOD

A simply supported beam with 4-point loading was analyzed by the proposed method. The specimen was fire-tested at PCA by T. D. Lin et al. (1981).[9] The geometry of the specimen is shown in FIGURE 4. Average yield strength measured is about 435.8MPa. Compressive strength and modulus of elasticity are 29.46MPa and 25.91Gpa, respectively. The span loading is kept almost constant during fire test, and its value is 20.0kN. Furnace temperature followed ASTM E 119 specification.
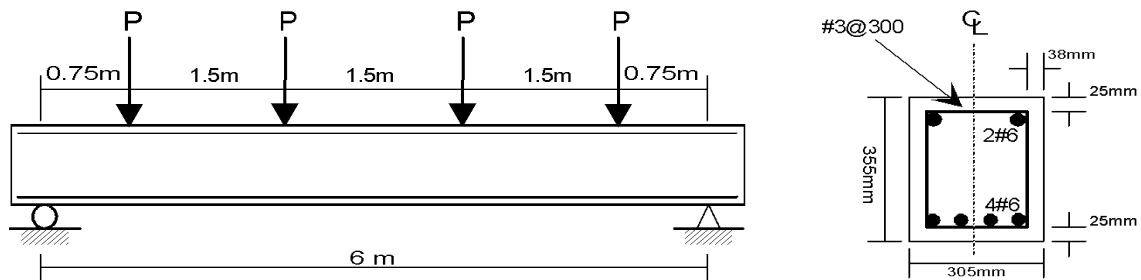
FIGURE 4. Geometry of a simply supported beam (elevation and section at center. Lin et al., (1981))

Temperature analysis on the segmented section was carried out as a 2 dimensional heat conduction problem with the boundaries having convection and radiation. Half of the section was analyzed with symmetry condition of the section. In the analysis, the contribution of the steel was ignored as the reinforcement ratio is so small and the temperature drop at the interface between concrete and steel sets off the high conductivity of the steel. The thermal properties needed for temperature analysis followed the numerical models presented in the ASCE Recommendation[2].

The results of the temperature analysis are shown in FIGURE 5. It is clearly shown that there exists a nonlinearity of temperature distribution with the depth and the nonlinearity gradually increases with temperature.

The thermal curvatures are calculated in three ways. The first and the second assumptions are the temperature and the strain differences at both ends of the member, respectively.
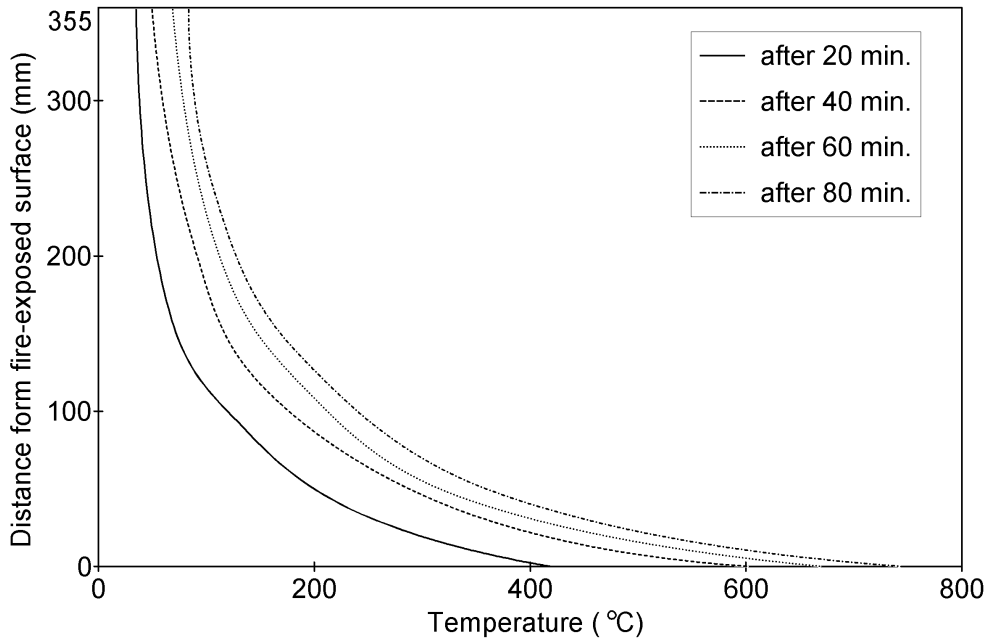
FIGURE 5. Temperature distribution at the segmented section with time

Case 1: $\Delta\phi_{th} = (\overline{\alpha}_{bot} \cdot \Delta T_{bot} - \overline{\alpha}_{top} \cdot \Delta T_{top}) / h$ (11a)

Case 2: $\Delta\phi_{th} = (\Delta\varepsilon_{bot} - \Delta\varepsilon_{top}) / h$ (11b)

where ϕ_{th} and h are the thermal curvature due to nonlinear temperature distribution and the depth of the member. $\overline{\alpha}_{bot}$ and ΔT_{bot} are and the average thermal expansion coefficient of the two successive time step at the bottom of the member, respectively. The section is discretized with uniform length as was done in Poh's method in order to make it easier to sum up the total strain and stress at the section, which enables using the personal computer as shown in FIGURE 6. The predicted deflections are compared with the test result (FIGURE 7).

As seen in the figure, the assessments by the assumed curvatures are somewhat unstable in some cases and are not compatible with test result. The predictions according to the temperature and the strain differences are about   times and   times the test result after 80 minutes. In order to improve the reliability of the assessment of the deflection, more adequate assumption for the thermal curvature is needed and the following suggestion is used.

Case 3: $\Delta\phi_{th} = (\Delta\varepsilon'_{bot} - \Delta\varepsilon'_{top}) / h'$ (11c)

where ε'_{bot}, ε'_{top} and h' are the effective strains and the distance between the points where the strains are measured, respectively. The locations for the strain calculations in case 3 by which the analysis lies the nearest to the test result in the figure is not obtained explicitly and determined by trial and error method using an iterative procedure. The implicit iteration procedure for the location should be repeated until the total stress at the section is zero according to the planeity condition. This iteration is two-folded for the geometrical problem

unlike others in a one-way because it should find two optimum locations. In this study, the iteration is stopped when the sum of the stresses is the smallest due to the coarse discretization of the section and another iteration is begun after the location of one of them is changed. The difference between the test result and the case 3 is about 30% at 80 min. of the fire.
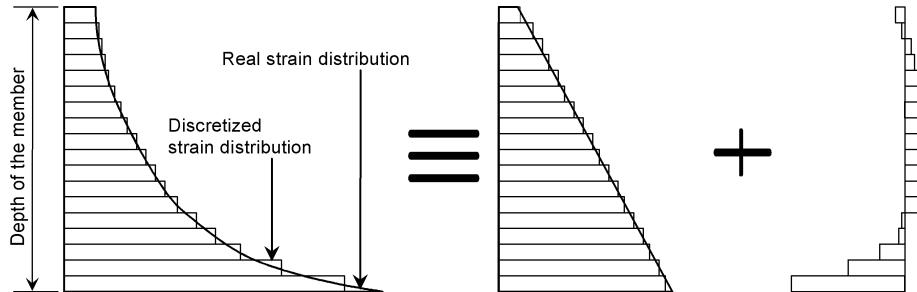
FIGURE 6. Discretized strain distribution at the section
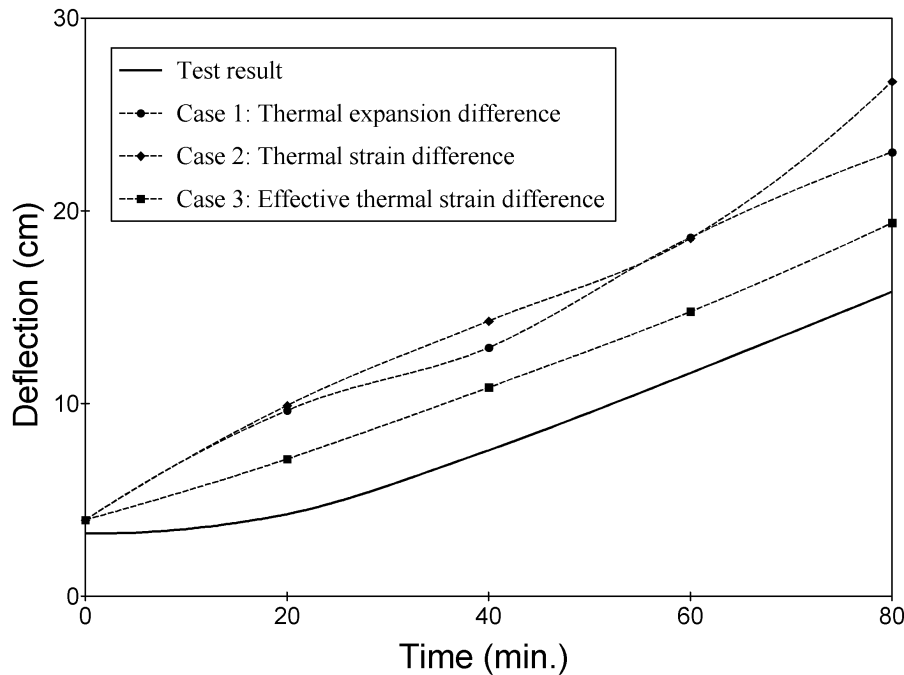
FIGURE 7. Deflections of the beam at the center

DISCUSSIONS

This study presented a simple analysis model for the behavior of a reinforced concrete flexural member at elevated temperatures. The analysis process is subdivided into temperature analysis of the section and structural analysis of the member. The nonlinear temperature distribution at the section causes a nonlinear strain distribution which results in the change of the curvature of the member with the self-equilibrating stress. The successive structural response of the member is obtained from the integration of the curvature

An application of the proposed method shows a relative good tendency compared to the experimental results. The structural analysis of the member is achieved as a 1 dimensional problem. The extension of the method for 2 dimensional analysis of the section will be more

useful to the analysis of the member in a real fire situation such as an unsteady or 3 sided fire. A more reliable temperature-dependent material model, a more reliable temperature analysis, a more finer discretization of the section, and a comprehension of the effects of the failure of the material during heating will also improve the reliability of the analysis method.

ACKNOWLEDGEMENT

REFERENCES

[1] American Concrete Institute, Guide for Determining the Fire Endurance of Concrete Elements, ACI 216R-89

[2] American Society of Civil Engineers, Structural Fire Protection, ASCE Manuals and Reports on Engineering Practice No. 78

[3] Dias W. P. S, Khoury G. A., and Sullivan P. J. E, "An Activation Energy Approach for the Temperature Dependence of Basic Creep of Hardened Cement Paste," Magazine of Concrete Research, Vol. 39, No. 140, September 1987, pp. 141-147

[4] Dias W. P. S, Khoury G. A., and Sullivan P. J. E, "The Thermal and Structural Effects of Elevated Temperatures on the Basic Creep of Hardened Cement Paste," Materials and Structures, Vol. 23, No. 1990, pp. 418-425

[5] Kang S. W. and Hong S. G., "Thermal Stress of Concrete Structure at High Temperature Considering Inelastic Thermal Strain Change," Proceedings of the Korea Concrete Institute, 2000, pp. 1145-1150

[6] Kang S. W. and Hong S. G., "Material Model and Thermal Response Analysis of Concrete at Elevated Temperatures, "Journal of the Korea Concrete Institute, Vol. 13, No. 3, June 2001, pp. 268-276

[7] Lie T. T. and Irwin R. J., "Method to Calculate the Fire Resistance of Reinforced Concrete Columns with Rectangular Cross Section," ACI Structural Journal, Vol. 90, No. 1, January-February 1993

[8] Lin T. D., Ellingwood B., and Piet O., "Flexural and Shear Behavior of Reinforced Concrete Beams during Fire Tests," PCA R&D Serial No. 1849, December 1988

[9] Lin T. D., Gustaferro A. H., and Abrams M. S., "Fire Endurance of Continuous Reinforced Concrete Beams," PCA R&D Bulletin RD072.01B, 1981

[10] Noumowe A. N., Clastres P., Debicki G., and Costaz J.-L., "Thermal Stresses and Water Vapour Pressure of High Performance Concrete at High Temperature," 4th International Symposium on Utilisation of High-Strength/High-Performance Concrete, 1996, pp. 561-570

[11] Poh K. W. and Bennetts I. D., "Analysis of Structural Members under Elevated Temperature Conditions," Journal of Structural Engineering, Vol. 121, No. 4, April 1995, pp. 664-675

[12] Terro M. J., "Numerical Modeling of the Behavior of Concrete Structures in Fire," ACI Structural Journal, March-April 1998, pp. 183-193

THERMAL SPALLING OF HIGH-PERFORMANCE CONCRETE DURING FIRE

Fumie ARITA[1], Kazunori HARADA[2]
Dept. of Architecture & Environmental Design ,Kyoto University
Yoshida-honmachi, Sakyo-ku, Kyoto 606-8501 Japan
[1]*be.fumie@archi.kyoto-u.ac.jp,* [2]*harada@archi.kyoto-u.ac.jp*

Keiichi MIYAMOTO
Kajima Techenical Research Institute
19-1, Tobitakyu 2-Chome, Chofu-shi, Tokyo 182-0036, JAPAN
keiichi-miyamoto@kajima.com

ABSTRACT

Investigations were made to clarify the mechanism of thermal spalling of concrete during fire by experiments and numerical calculations. The experiments were carried out for two sizes of cylinders (50mm diameter by 100mm length and 100mm diameter by 200mm length) and small cubic columns (100mm by 100mm by 400mm length). The compressive strength was 30MPa and 108MPa. The specimens were heated by small electrical furnace to see the degree of spalling. The influences of compressive strength, water content, age, diameter, length/diameter ratio (*L/D* ratio) and axial load were analysed to show that the degree of spalling would be increased as compressive strength, *L/D* ratio are increased. The effect of axial loading is negative. As the axial load is increased, degree of spalling seemed to be decreased.

Based on the experimental results, the mechanism of spalling is discussed. During experiments, some sounds of crack propagation were heard for several minutes before spalling took place. However specimens had almost no surface crack as seen after the test. Thus it is suspicious that internal crack takes place in prior to explosive spalling, which suggest that the explosive spalling in small specimens might be caused by buckling of surface layer that was split from the internal core due to shear stress caused by thermal gradient.

Considering the state-of-the-art of spalling study, the influence of pore pressure rise by water vapor is still suspicious. To investigate the degree of force caused by pore pressure, heat and mass transfer analysis was carried out to obtain time-dependent profiles of temperature, pore pressure (vapor pressure plus pressure of air entrapped in the pore) and water content. The stress caused by pore pressure was compared with the thermal stress calculated by simple thermal stress theory based on Navier's hypothesis. It was found that thermal stress is by far larger than the stress caused by pore pressure. The maximum thermal stress is of the order of 10% of compressive strength in case of unrestrained cylinders. However the order of pore pressure is less than 1% of concrete of it. It is suggested that the main cause of spalling is thermal stress, not pore pressure alone.

KEYWORDS: *Thermal Spalling, Thermal Stress, Pore Pressure, Internal Crack, Buckling of Surface Layer*

INTRODUCTION

Utilization of high-performance concrete has been increasing due to its superior structural performance and durability. However, its application is limited to buildings where severe fire is not expected to take place because of its weakness in fire resistance. Spalling is one of the main concerns that obstacles the design and construction of high performance concrete. Lacking of understanding the mechanism of spalling is the reason to make rational design difficult.

Existing studies show that compressive thermal stress[1] or pore pressure[2] causes spalling. However, the theory is not enough to explain many of the spalling patterns that actually take place. Corresponding with pore pressure, inclusion of short-length polypropylene fiber is *believed* to be beneficial because melting of fiber would release pore pressure. The other measure is to apply intumescent paint in order to reduce thermal gradient that arises in the early stage of heating.

However the generality of these measures is in question. For designing high-performance concrete against fire, it is necessary to clarify the mechanism of spalling. This study was activated by the needs to extend the use of high performance concrete for buildings. As a preliminary stage, fire tests of small scale specimens were carried out to investigate the general tendency of spalling and sequence of spalling mechanism. Numerical analysis is followed in order to investigate the relative magnitude of thermal stress and pore pressure. Through the investigation of experimental and numerical analysis, possible failure mechanism is suggested for future research.

EXPERIMENTAL PROGRAMS

Small scale experiments were carried out to investigate: 1) the factors influencing the degree of spalling, for example compressive strength and loading 2) the behaviour of failure. For the purpose of 1), a systematic series of experiments were planed and carried out for varying parameters. Compressive strength, water content, age, degree of axial loading were the parameters in question. For the purpose of 2), behaviour of specimen was observed by video

camera throughout the tests. Sounds of crack and fallout of small pieces were recorded manually. This type of information is valuable to discuss the mechanism of spalling.

Specimens

Specimen sizes, mix proportions and properties of concrete are shown in Table.1. To examine the difference by size, three types of specimens were tested. Namely, two sizes of cylinders (S: 50mm diameter, 100mm length, M: 100mm diameter , 200mm length) and one cubic small column (100mm x 100mm, 400mm length). In some of the tests, two small cylinders (S) were connected in axial direction in order to study the influence of length – diameter ration (*L/D* ratio).

To study the influence of compressive strength, two mix proportions were designed. Design strength was aimed to 100MPa and 30MPa at 28 days. To exclude the influences of material-dominated instability, no silica fume was used for either 100MPa nor 30MPa mixture. All the specimens were cured in water. Compressive strength (cylinder strength) of 100MPa- and 30MPa- mixtures are shown in Table 1 together with average water content

Testing Furnace

Two types of furnace were used in these experiments: furnace –1 is a small electric furnace (290 x 310 x 275mm) shown in Fig.1. Furnace –2 is a full-scale testing furnace for building elements (3.0 x 3.0 x 3.0m).

Furnace –1 is equipped with uni-axial loading system. Specimens were axially loaded to a designated level ($0-1/3F_c$) during heating. To check the special distribution of heating temperature, sixteen thermocouples were placed. Because of the size and loading capacity limitation, only cylinders (S, M) were tested. As will be shown later, temperature profile is not uniform, which might increase the degree of spalling.

In case of Furnace-2, several specimens were put in center of it. As a result, heating temperature was fairly uniform. No loading was applied.

TABLE 1. Sizes, Mix Proportions and Properties of Concrete

Name	Size[mm]	w/c[%]	Water[kg/m³]	Cement[kg/m³]	s/a*[1]	Compressive Strength[MPa]*[2]	Water Content[mass%]*[3]
108S	ϕ 50×100						4.3
108M	ϕ 100×200	25	165	660	41.2	108	2.4
108L	100×100×400						3.8
30M	ϕ 100×200	63.8	165	259	46.8	30	5.0

*1: s=fine aggregate, a= fine aggregate + coarce aggregate, s/a=volume percentage
*2: obtained from cylinders (108M, 30M) at 28 days
*3: average of experimented specimens

Heating Condition

Heating temperature was controlled so as to fit to ISO 834 standard time- temperature curve. When spalling took place, heating was stopped. Fig.2 shows the furnace temperature measured at 16 points in Furnace-1. Furnace temperatures started to rise at 2 minutes after initiation of heating. After 10 minutes, average temperature almost agreed with ISO834 curve. It should be noted that temperature measured by TC4 (lower part of furnace) was about 100-150°C than that measured by TC1 (upper part of furnace). It is suggested hat specimen was heated intensely from bottom side, mildly from topside. Even though the figure is omitted, temperature in Furnace-2 was precisely controlled to ISO 834 curve. Special temperature difference was negligible.
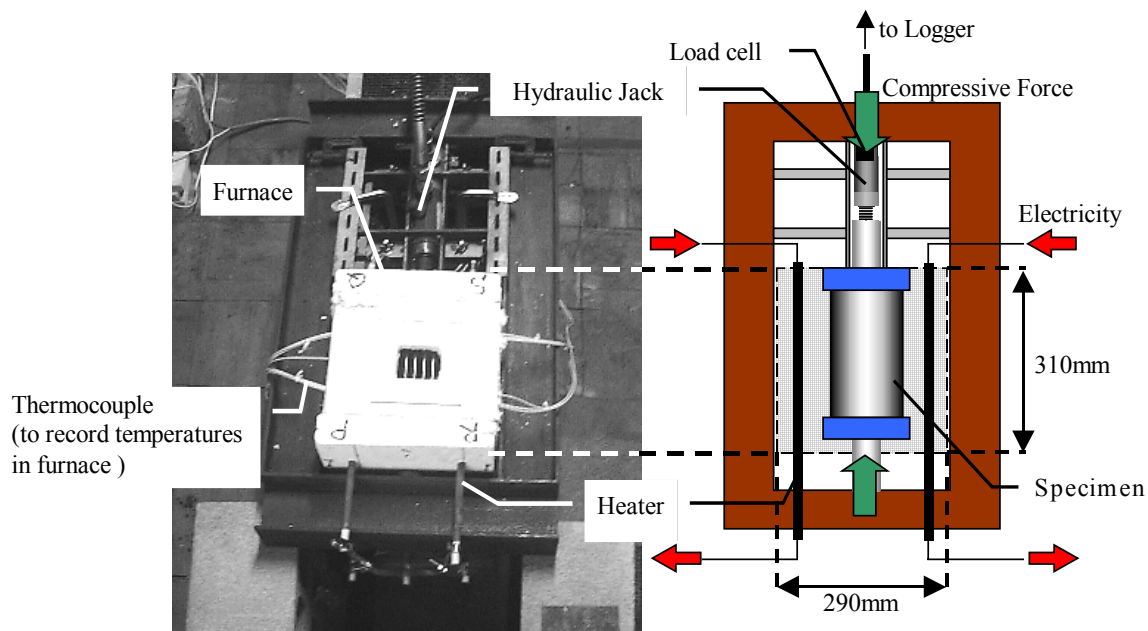
FIGURE 1. Furnace Type-1
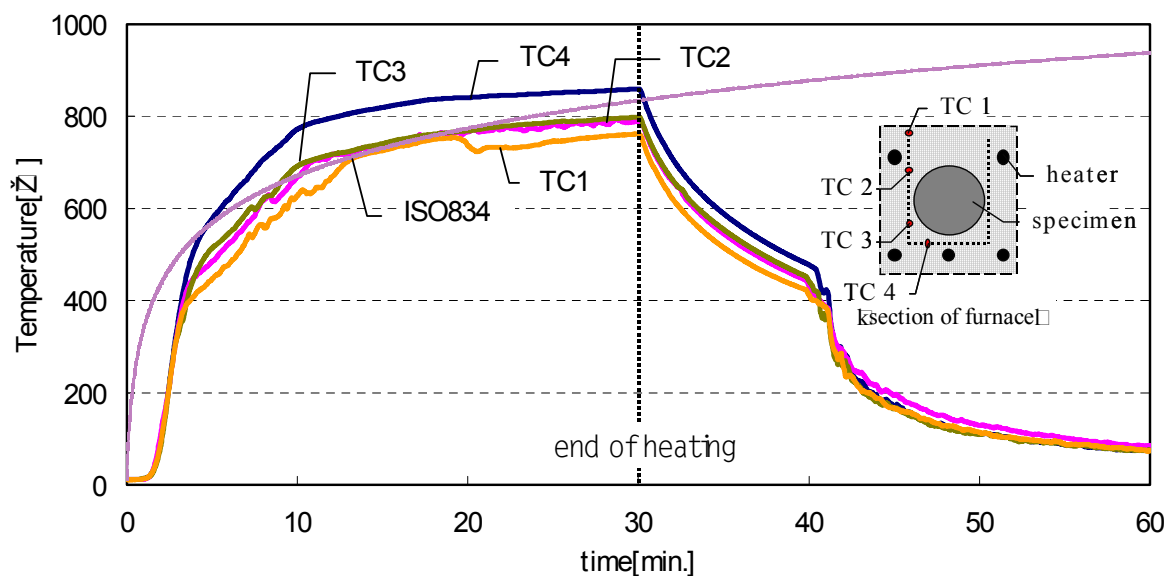
FIGURE 2. Measured Temperatures in Furnace Type-1

EXPERIMENTAL RESULTS

Experimental results are shown in Table 2. Spalling took place only in cases of high strength concrete (108MPa) heated by Furnace-1. Even though the number of tests is not enough to discuss general tendency of spalling, the followings can be stated qualitatively.

Factors Influencing the Degree of Spalling

Fig.3 shows the relationships between experimental parameters and degree of spalling expressed in terms of the fraction of spalling volume over total weight, e.g., (decrease of volume after heating)/(volume before heating). By analyzing the results, the following tendency is shown:

Influence of Compressive Strength

Among the specimens, only 108MPa specimens spalled. High-strength concrete can spall easily and extensively than normal-strength concrete. This result agrees with many previous studies.

Influence of Axial Loading

Some of the non-loaded specimens spalled more deeply and widely than axially loaded specimens of identical strength. It is suggested that proper loading may reduce the degree of spalling. In the point of possible mechanisms, tensile failure such as internal cracking may be mitigated by axial loading.

Influence of Diameter

The influence of diameter was not clear from experimental results. However, the clear

TABLE 2. Conditions of Tested Specimens and Results

	Furnace	Compressive Strength[MPa]	Ages[days]	Water Content[mass%]	Axial Load Ratio[-]	Diameter[cm]	L/D Ratio[-]	Fraction of (spalling volume)/(total volume)[%]
1)	1	110.954	45	3.749	0.333	2.5	2	0
2)	1	112.9124	57	3.948	0	2.5	2	0
3)	1	113.0756	58	3.351	0.1	5	2	2.842377437
4)	1	113.2388	59	1.575	0	5	2	3.875969233
5)	1	34.6498	64	5.616	0.333	5	2	6.318682239
6)	1	34.6498	64	5.616	0	5	2	0
7)	1	38.6686	98	5.616	0	5	2	0
8)	1	39.3778	104	4.039	0.333	5	2	0
9)	1	121.0724	107	4.452	0	2.5	4	10.68733916
10)	1	121.0724	107	4.471	0.333	2.5	4	0
11)	2	113.7284	62	3.948	0	2.5	2	0
12)	2	113.7284	62	4.699	0	2.5	2	0
13)	2	113.7284	62	2.012	0	5	2	0
14)	2	113.7284	62	2.648	0	5	2	0
15)	2	113.7284	62	3.674	0	5.643	3.544	0
16)	2	113.7284	62	3.84	0	5.643	3.544	0
17)	2	118.7876	93	4.579	0	2.5	2	0
18)	2	118.7876	93	4.579	0	2.5	2	0
19)	2	38.0776	93	4.597	0	5	2	0
20)	2	118.7876	93	2.623	0	5	2	0
21)	2	118.7876	93	2.749	0	5	2	0
22)	2	118.7876	93	2.42	0	5	2	0
23)	2	118.7876	93	4.072	0	5.643	3.544	0
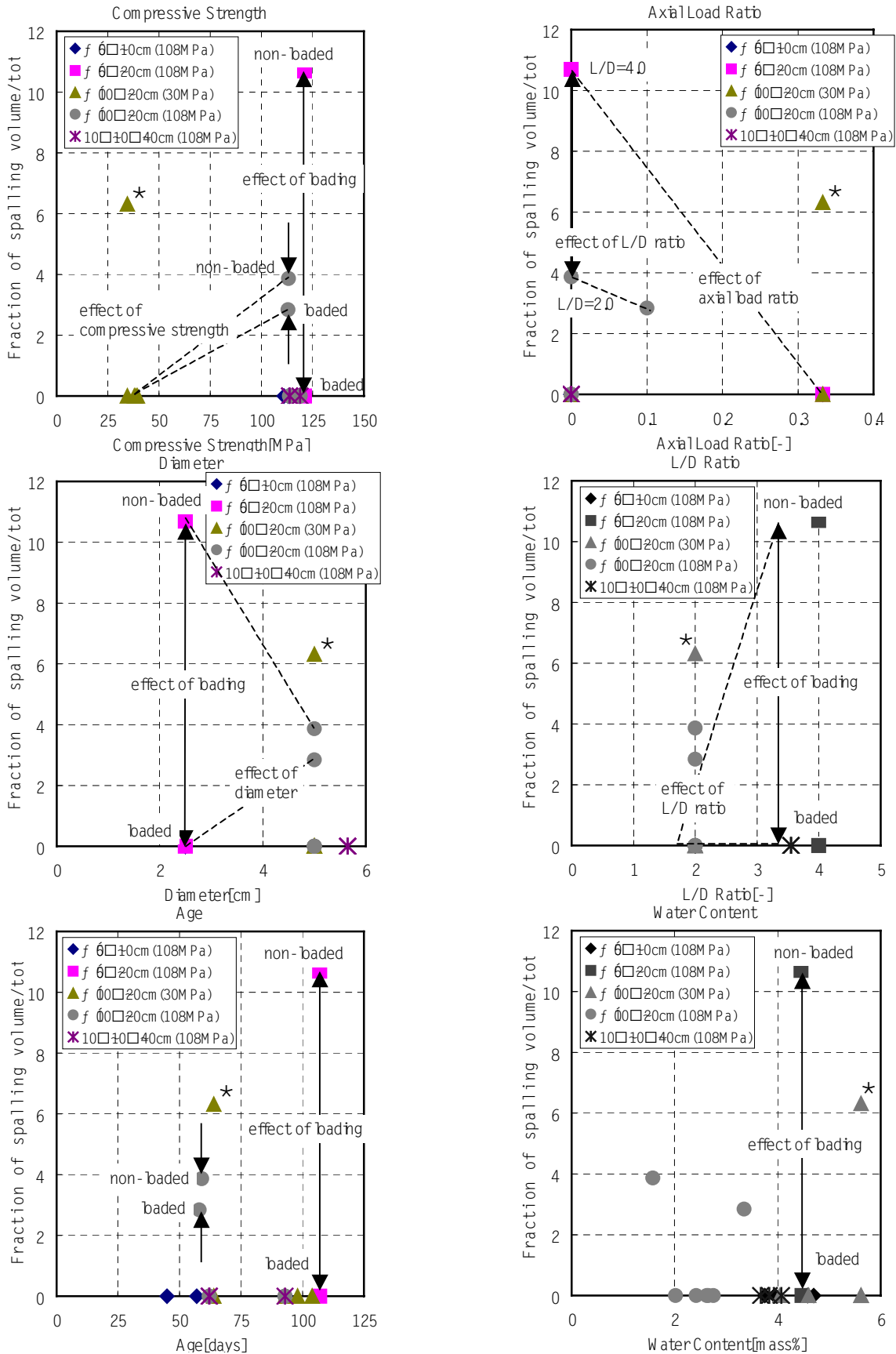
FIGURE 3. Factors Influencing The Degree of Spalling

*:The spalled 30M specimen isn't considered because the control system was in bud condition and temperatures in the furnace were very different from other cases

dependence was observed when we correlated the data with *L/D* ratio. Large *L/D* ratio may bring non-uniform temperature distribution along specimen's axis, which cause secondary thermal stress.

Influence of Water Content and Age

It was investigated by Morita *et al* [3], Nishida *et al* [4] and many other authors that existence water increases the degree of spalling. However the tendency was not clear in this result.

Possible Spalling Mechanism from Experimental Observation

Sequence of Spalling

During the experiments, video observation and sound recording was made. By analyzing the results, the following sequence was observed in most of the cases where spalling took place.

    (1) Sound of crack propagation for during 3 – 10 minutes
    (2) Fallout of small pieces from surface layer
    (3) Explosive spalling at around 11 minutes

After the spalling, and subsequent cooling down,

    (4) Almost no surface crack observed
    (5) No shape change other than fallout part

Thus it is suspicious that internal crack takes place in prior to explosive spalling.

In case of non-spalled specimens, crack started at 3minutes. At 15 minutes, crack sound alost ceaced. Surface crack was observed after cooling.

Shape of Spalling and Surface Crack

The degree of spalling and surface crack are categorized in Figure 4,5,6. In case of high strength concrete, spalling shape is trapezoidal, rather than cone. Comparing between loaded and non-loaded specimens, the depth of spalling differs almost twice. Almost no change was observed in overall size in case of spalled specimens.

In case of small specimens, no spalling was observed but extensive net-like crack was observed in non-loaded specimens. Elongation and shrinkage in diameter was observed after cooling down to normal temperature. In case of loaded specimens, large surface crack was observed in the direction parallel to axis.

In case of normal-strength specimens, major crack are observed only in part of the surface.
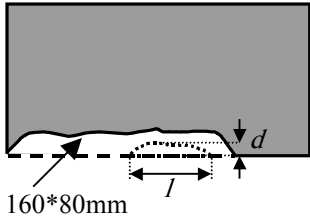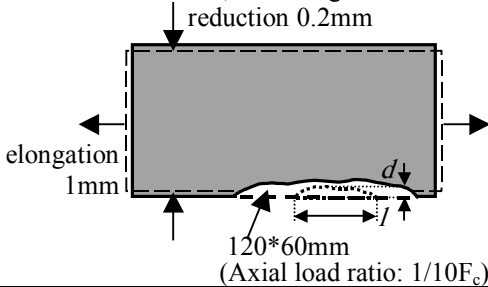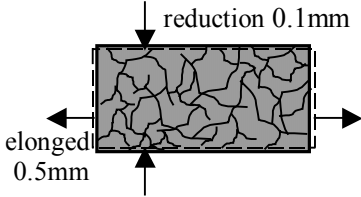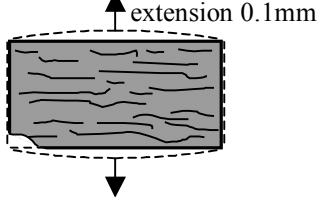
Suggested Mechanizm of Spalling

By summarizing the above-mentioned tendency, it is suggested that spalling is proceeded by internal crack. Partial splitting of surface layer from core of specimen is suspicious.
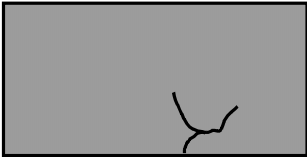
Considering that there is no significant damage on the surface, buckling of split layer might be a reason of spalling that took place in this experimental test series. Throughout this process, thermal stress plays dominant role, rather than pore pressure.

This hypothesis cannot be verified at this stage of research development at least by experimental evidence. At the same time, the effect of pore pressure rise is also of concern as is stated in many papers. Therefore numerical analysis was carried out to check if the above-mentioned hypothesis (crack-split-buckling) is realistic or not, and to compare the stress developed by thermal gradient with that by pore pressure.

TABLE 3. Specimen Conditions after Heating

Compressive Strength=108MPa		
Size \ Load	non-loaded	axially loaded
100mm diameter by 200mm length	✧ Spalling occurred at 10'25". ✧ The deepest and widest spalling occurred. ✧ The largest fall-out piece: 50*25*9mm. (*l/d*=2.0) ✧ The length and diameter didn't change after heating 160*80mm	✧ Spalling occurred at 10'26". ✧ Less spalling than non-loaded case ✧ The largest fall-out piece: 50*22*4.5mm. (*l/d*=2.0) ✧ Reduced diameter, and elonged. reduction 0.2mm elongation 1mm 120*60mm (Axial load ratio: $1/10F_c$)
50mm diameter by 100mm length	✧ No-spalling. ✧ Extensive net-like crack. ✧ Reduced diameter, and elonged. reduction 0.1mm elonged 0.5mm (Heating stopped at 30'00")	✧ No-spalling. ✧ Dropped out about 30*20mm at edge. ✧ Cake along axis. ✧ Diameter expanded along axis. extension 0.1mm (Heating stopped at 35'00". Axial load ratio: $1/3F_c$)

Compressive Strength=21MPa		
Size \ Load	non-loaded	with axial load
100mm diameter by 200mm length	✧ Non-spalling. ✧ Net-like crack in part. ✧ The length and diameter didn't change after heating (Heating stopped at 30'00")	✧ Non-Spalling. ✧ Some large cracks like nets. ✧ The length and diameter didn't change after heating (Heating stopped at 30'00")
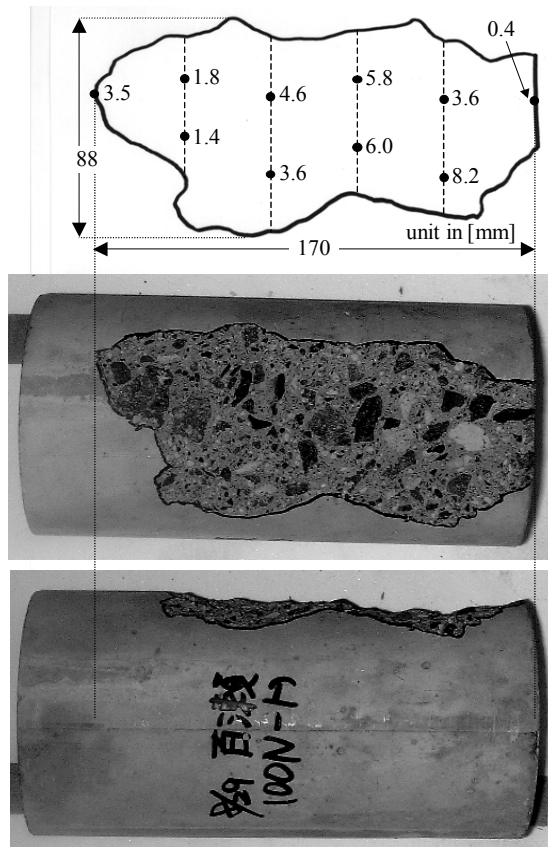
FIGURE. 4 Spalled Specimen

(108M, non-loaded)
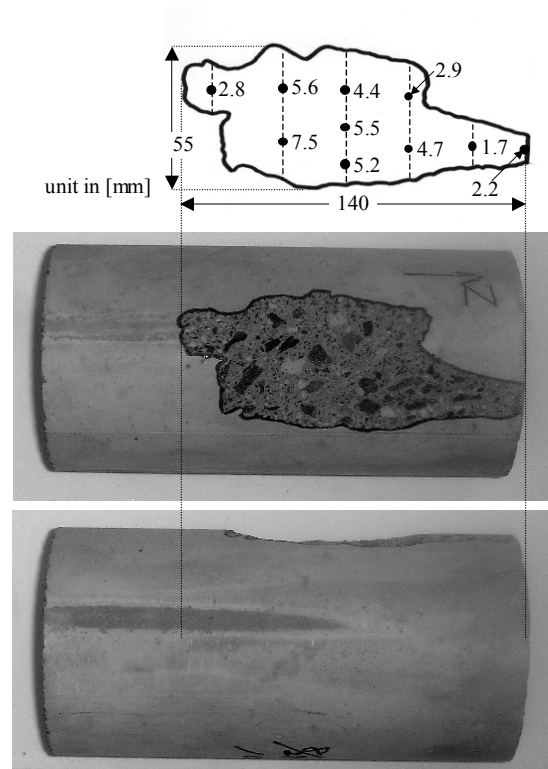
FIGURE5. Spalled Specimen

(108M, loaded)
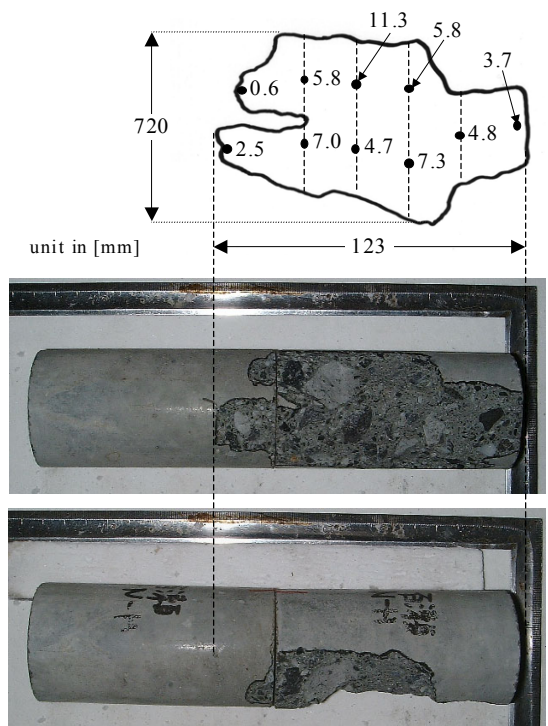
FIGURE6. Spalled Specimen

(108S $\times$ 2, non-loaded)

ANALYSIS OF PORE PRESSURE AND THERMAL STRESS DEVELOPEMENT

Experimental results suggest the importance of thermal stress to discuss the reason of spalling. At the same time, the contribution of pore pressure to stress profile is still suspicious.

Usually, experimental study tries to correlate the mechanical properties and water content with the degree of spalling. However, as shown in Figure 7, strength (density) and water content are inter-related. High density concrete tends to contain vapor, which cause pore pressure rise. At the same time, high density concrete suffers from large thermal stress. Quite often, large water content is said to bring large pore pressure. However, large water content delays temperature rise of the core, which results in large temperature gradient. Therefore, large water content contributes to increase thermal stress as well.

The above-mentioned relationships are hard to be investigated by experimental study. To discuss the relative importance of thermal stress and pore pressure and to discuss the effect of corresponding factors, analytical method is necessary. In this section, numerical calculations were carried out for pore pressure rise and temperature gradient. The impact on resulting stress profile was discussed. The results are compared qualitatively with experimental evidence.

Method of Analysis

Fig.8 shows the method of analysis. At first, heat and mass transfer analysis was carried out to obtain time-dependent profiles of temperature, pore pressure and water content. Using the results, effective temperature (temperature to give same amount of thermal strain under the existence of pore pressure) was calculated to take into account both thermal stress and stress caused by pore pressure. Finally, stress profile was calculated using Navie's hypothesis. Simple analytical solution for plane stress condion was applied. All the calculation was carried out for axially symmetric body.
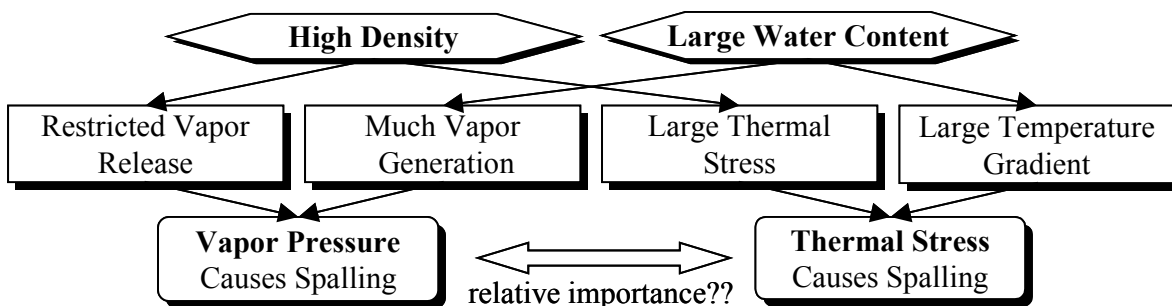
FIGURE 7. Relation between Factors and Reasons Concerning Spalling

Heat and Mass Transfer Analysis

To calculate time-dependent profiles of temperature and pore pressure, simultaneous transfer of heat and mass was considered. The prototype model was developed earlier [5]. However, simplification was made for convenience. The governing equations for heat, vapor, air and liquid water transfer are ;

Heat: $\dfrac{\partial(\rho_0 c T)}{\partial t} = \dfrac{1}{r}\left\{\dfrac{\partial}{\partial r}(\lambda r \dfrac{\partial T}{\partial r})\right\} - L m_v,$ (1)

Vapor: $\dfrac{\partial(\varepsilon \rho_v)}{\partial t} = \dfrac{1}{r}\left\{\dfrac{\partial}{\partial r}(\kappa \rho_v r \dfrac{\partial P}{\partial r})\right\} + m_v,$ (2)

Air: $\dfrac{\partial(\varepsilon \rho_a)}{\partial t} = \dfrac{1}{r}\left\{\dfrac{\partial}{\partial r}(\kappa \rho_a r \dfrac{\partial P}{\partial r})\right\},$ (3)

Water Content: $\rho_0 \dfrac{\partial w}{\partial t} = -m_v.$ (4)

These equations are coupled with the equation of state for vapor and air

$p_v = \rho_v RT/M_v, \ p_a = \rho_a RT/M_a,$ (5)

and Dalton's Law,

$P = p_v + p_a.$ (6)

The hygro-thermal properties are listed in Table 4.
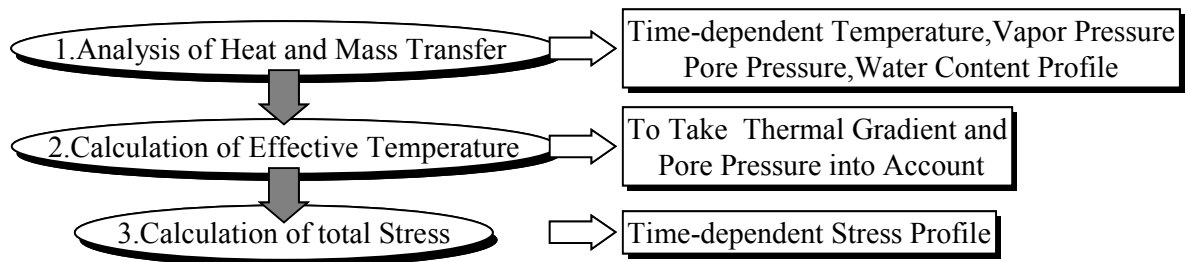
FIGURE 8. Flow of Analysis

TABLE 4. Material Properties

Thermal Concuctivity[W/m K]	$\lambda = 1.75 - 0.58 \times (T/500)$
Density[kg/m³]	$\rho = 2500$
Specific Heat[J/kg K]	$C = 2500$
Void Fraction[-]	$\varepsilon = 0.14 - 7.14 \times 10^{-4} \times F_c$
Permeability[m³/Pa S]	$\kappa = 4.77 \times 10^{-9} \times \left\{\varepsilon^3 / (1 - \varepsilon^2)\right\}$

Calculation of Effective Temperature

In general sense, free thermal strain is calculated using coefficient of linear expansion,

$$\varepsilon_{th} = \alpha \Delta T. \tag{7}$$

Under the existence of pore pressure, it is proposed that additional strain $\varepsilon_{pres} = f\Delta P / E$ is developed as a interaction between fluid and skeleton [6]. As a result, it is practical to determine effective temperature so that the sum of thermal strain and pore pressure- induced strainwould be eqral,

$$\Delta T_{eff} = \Delta T + f\Delta P / \alpha E. \tag{8}$$

Using effective temperature, the stress-strain relationship would be

$$\begin{Bmatrix} \varepsilon_z \\ \varepsilon_r \\ \varepsilon_\theta \end{Bmatrix} = \frac{1}{E} \begin{Bmatrix} \sigma_z - v(\sigma_r + \sigma_\theta) \\ \sigma_r - v(\sigma_z + \sigma_\theta) \\ \sigma_\theta - v(\sigma_z + \sigma_r) \end{Bmatrix} + \alpha \Delta T_{eff}, \tag{9}$$

which is identical with conventional formula for the calculation of thermal stress. In the succeeding calculations, conservative approximation $f = 1$ was applied.

Calculation of Axial Stress

The actual stress field is three dimensional. However, simple analytical calculation method was adopted. Assuming no axial restraint and loading, cylinder is primarily deforms in axial direction. Letting the average strain be $\varepsilon_{th,z,ave}$, and neglecting Poisson effect by radial (r) and tangential (θ) directions, we get

$$\varepsilon_{th,z,ave} = \frac{\int_0^{r_0} E(r)\alpha(T)\Delta T(r)r\,dr}{\int_0^{r_0} E(r)r\,dr}. \tag{10}$$

Resultant stress in axial direction at r is calculated by

$$\sigma_z(r) = E(r)\big(\varepsilon_{th,z,ave} - \alpha(r)\Delta T(r)\big). \tag{11}$$

Calculation of Radial and Tangential Stress

Under plane stress approximation, stress distribution in a circular plate is calculated by

radial direction: $\sigma_r = \dfrac{E_0\alpha_0}{r^2}\left(\dfrac{r^2}{r_0^2}\int_0^{r_0} \Delta Tr\,dr - \int_0^r \Delta Tr\,dr \right),$ (12)

tangential direction: $\sigma_r = \dfrac{E_0\alpha_0}{r^2}\left(\dfrac{r^2}{r_0^2}\int_0^{r_0} \Delta Tr\,dr + \int_0^r \Delta Tr\,dr - Tr^2 \right).$ (13)

The above equations assume uniform material properties and no axial stress. Thus two types of correction were made.

Correction due to the Poisson effect was accounted by adding temperature that cause the same amount of free thermal strain. The Poisson strain due to the strain in axial direction is $-\nu\sigma_z(r)/E(T)$. Thus we added,

$$\Delta T_v(r) = -\frac{\nu\sigma_z(r)}{\alpha(T)E(r)},\tag{14}$$

to equivalent temperature determined by equitation (8).

Further correction is made to account for non-uniform properties. Equivalence in free thermal strain gives,

$$\alpha(T)E(T)\Delta T_{th,e} = \alpha_0 E_0\big(\Delta T_{eff}(r) + \Delta T_v(r)\big)\tag{15}$$

effective temperature for radical and trangential direction. The final form for the description is

$$\Delta T_{th} = \frac{\alpha_0 E_0\big(\Delta T_{eff}(r) + \Delta T_v(r)\big)}{\alpha(T)E(T)}.\tag{16}$$

Results of Analysis

Analysis were carried out to correspond with 108M, 30M and 108S as shown in Table 5.

Temperature

The results are shown in Figures 9-11(a). The difference between 108M and 108S is not significant. Clearly, the thermal gradient depends largely upon radius. In case of 108S, quick migration of heat is observed.

Pore Pressure

The results are shown in Figures 9 – 11(b). In all the cases, pore pressure rise starts in the zone of surface layer. Peak position of pore pressure moves towards center with time. Largest pore pressure is experienced in case of 108S, because of the quick migration of heat toward core. The difference between 108M and 108S are attributed to the difference of permeability.

TABLE 5. Analyzed Objects

Name	Diameter[cm]	Compressive Strength[MPa]	Water Content[mass%]
108*S*	5	108	5.5
108*M*	10	108	3.0
30*M*	10	30	4.0

Water Content

The results are shown in Figures 9 – 11(c). In all the cases, moving of drying front is observed. It is noteworthy that water content rises up at first. Then after that, it drops down to zero.

Stress Profile

Calculated stress profiles are shown in Figures 12-14 . The profiles are shown in every three minutes. In case of 108M (right side), compressive stress is developed at the early stage of heating in the surface layer. At 6 minutes, shear stress exceeds shear octahedral stress proposed by Kotsovos [6], which corresponds with cracking at the center core ($\tau_0 > \tau_{0cr}$). After 6 minutes, cracking zone expands toward surface layer. This cracking process is in accordance with experimental observation (crack sounds before spalling).

In case of 30M, cracking does not take place until 18 minutes. After that, stress is decreased as the temperature gradient is reduced. In case of 108S, the behavior is similar to the case of 108M. It can be said that the occurrence of internal cracking depends on strength of concrete.

Discussion

From the analytical calculation results, it was pointed out that internal crack takes place much easier in high strength concrete than in normal-strength concrete. To examine the cause of cracking, sensitivity analysis was carried out.
For the case of 108S, same calculation was carried out putting the effective temperature rise by pore pressure ΔT_{pres} equal to zero. The results are shown in Figure 15 for 9 and 15 minutes. It is clear that the effect of pore pressure upon stress field is sufficiently small for this size and strength of concrete. Neglecting pore pressure in stress calculation would bring slight over estimation of tensile stress in the core part. It is too early to draw general conclusions, however, it is supposed that thermal stress is a dominant force to cause spalling.

CONCLUSIONS

The spalling of concrete was analyzed by experiments and theoretical analysis. It was confirmed that high strength concrete is much easier to spall than normal strength concrete. At this stage, the results are summarized as follows:

(1) In experiments, sound of internal crack was heard in prior to destructive spalling.
(2) Theoretical analysis showed that high strength concrete is likely to suffer from internal crack in the early stage of heating.
(3) The effect of pore pressure is not significant compared with the effect of thermal gradient.

By summarizing the findings, a hypothesis is proposed that the spalling is caused by internal crack propagation, followed by buckling of surface layer. This hypothesis is still need to be examined, however, experimental evidence and theoretical results are in accordance.
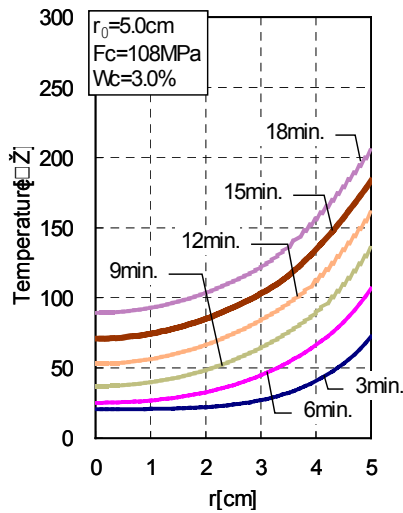
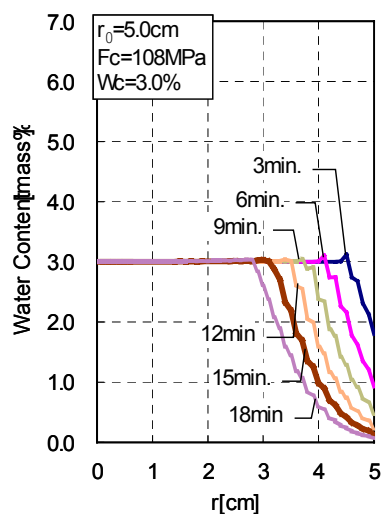(a) Temperature
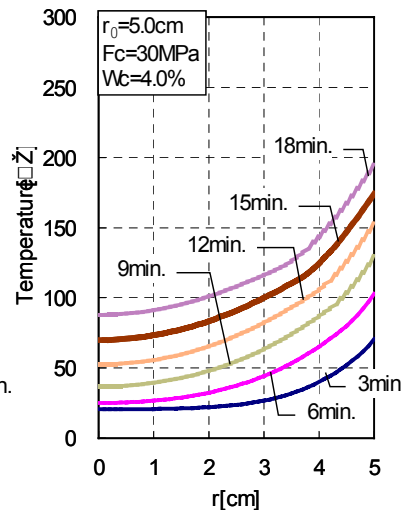
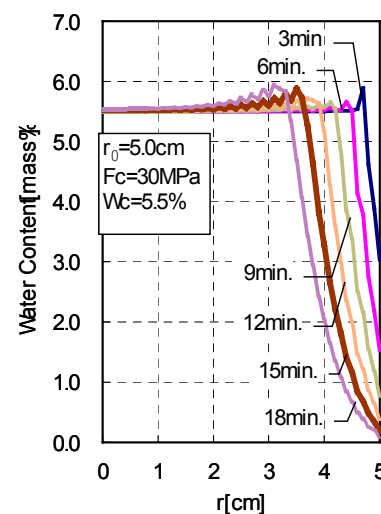(a) Temperature
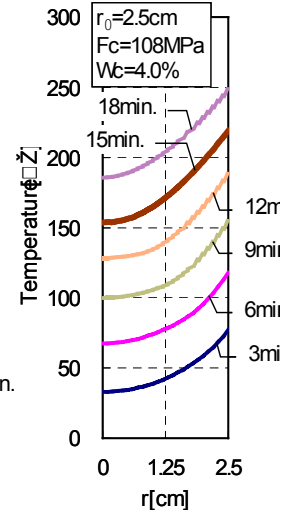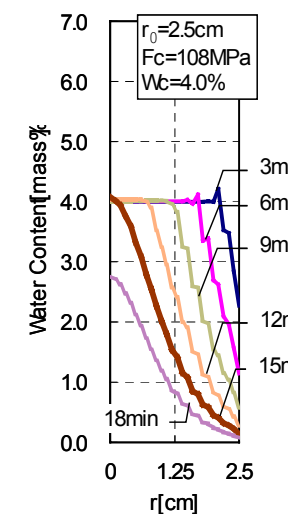
(a) Temperature
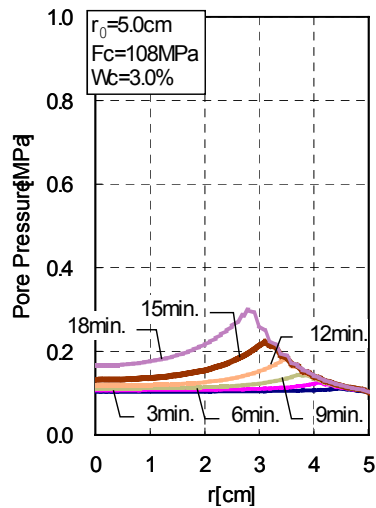
(b) Pore Pressure
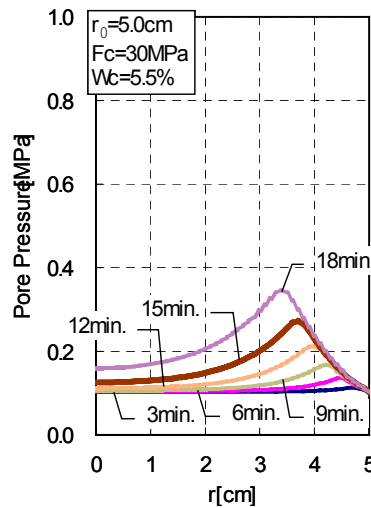
(b)Pore Pressure
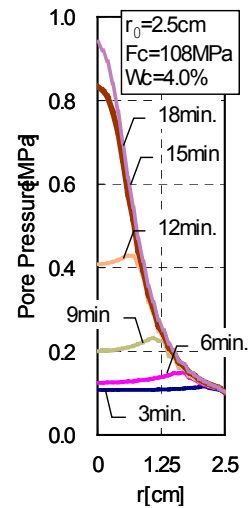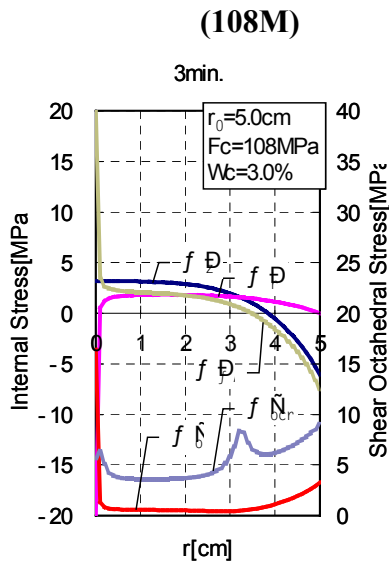
(c) Pore Pressure
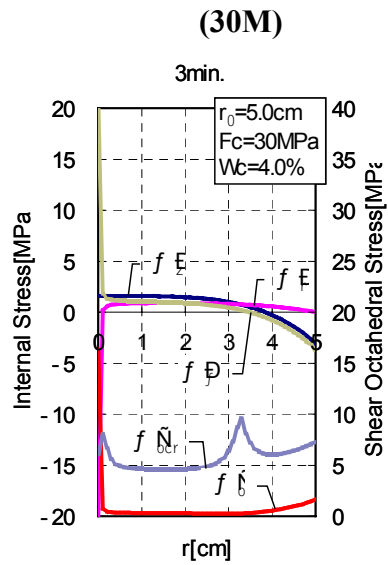

(c) Water Content

(c) Water Content

(c) Water Content

Fig.9 Analytical Results (108M)

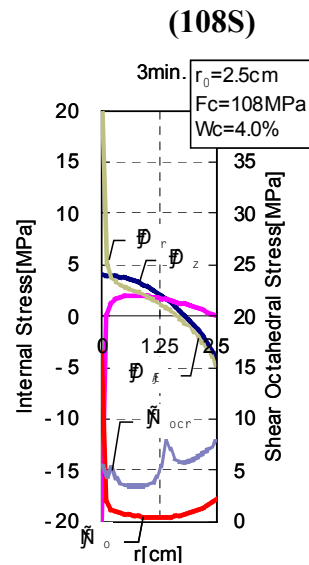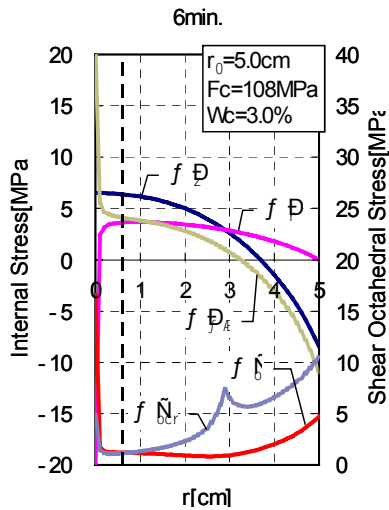**Fig.10 Analytical Results (30M)**
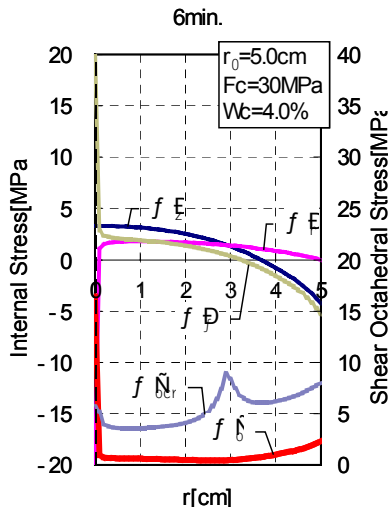
Fig.11 Analytical Results (108S)
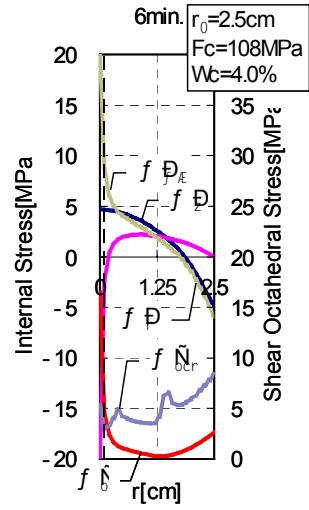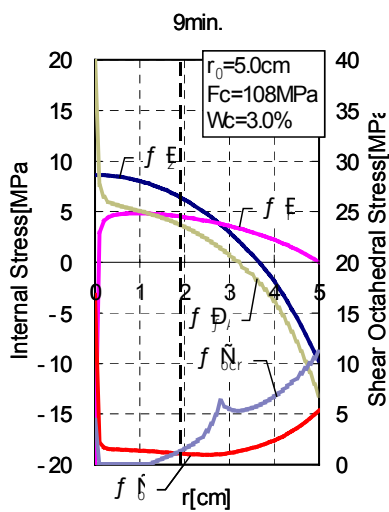
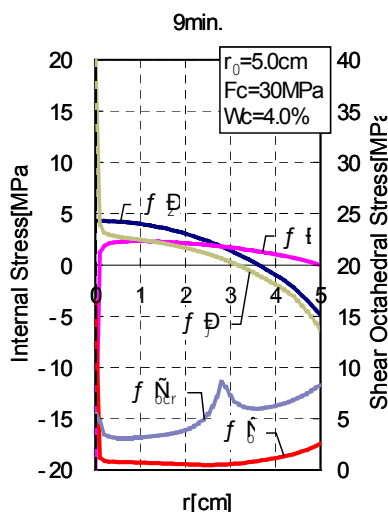(a) 3min. (108M)

(a) 3mni. (30M)

(a) 3min. (108S)

(b) 6min. (108M)

(b) 6mni. (30M)

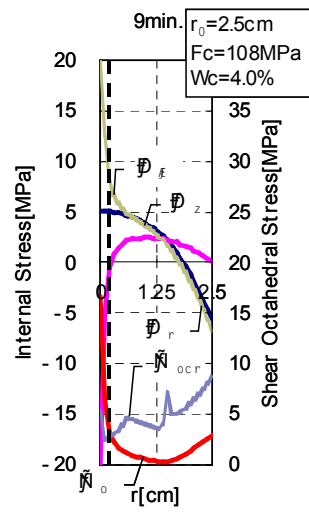(b) 6min. (108S)
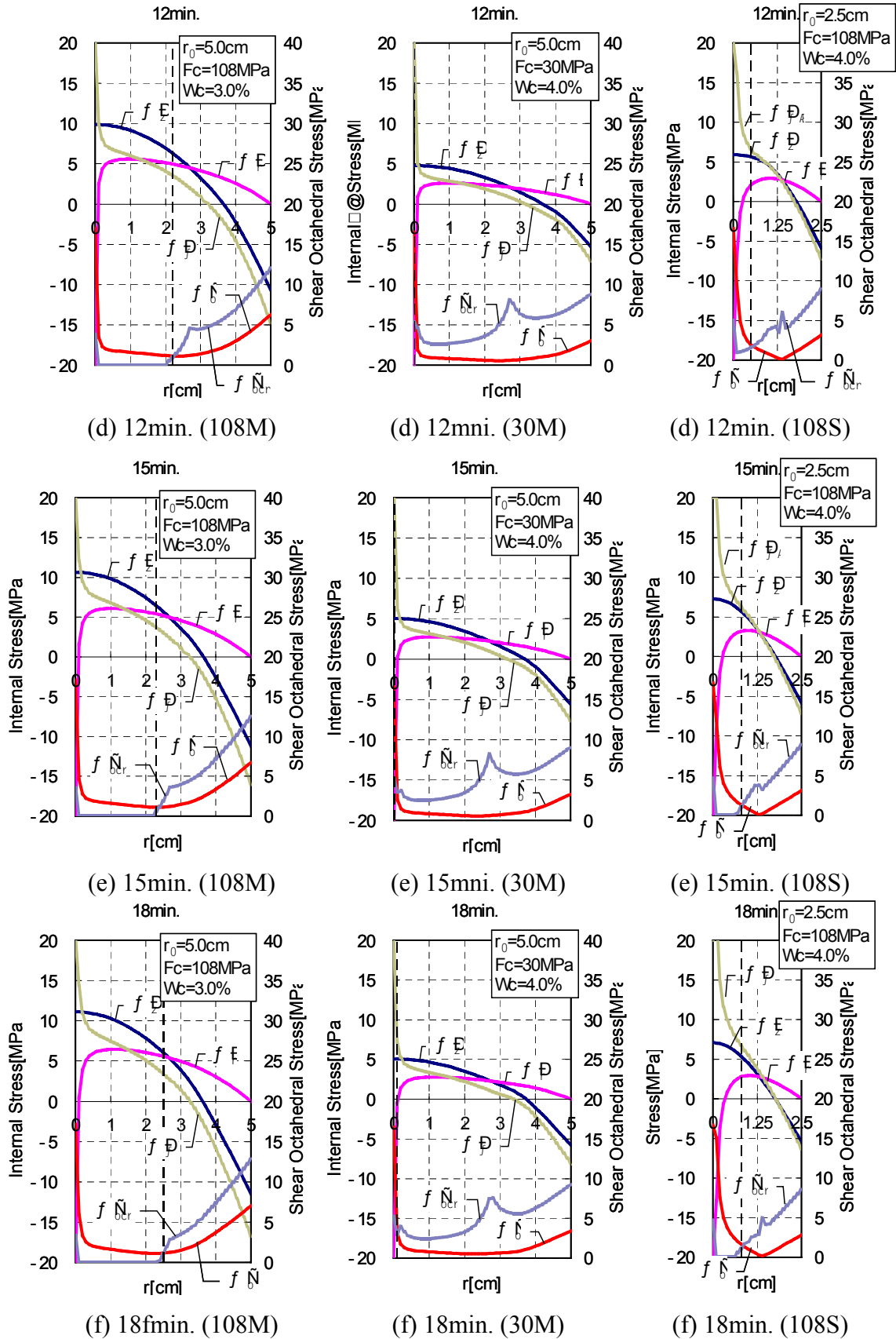
(c) 9min. (108M)

(c) 9mni. (30M)

(c) 9min. (108S)

(d) 12min. (108M)

(d) 12mni. (30M)

(d) 12min. (108S)

(e) 15min. (108M)

(e) 15mni. (30M)

(e) 15min. (108S)

(f) 18fmin. (108M)

(f) 18min. (30M)

(f) 18min. (108S)

FIGURE. 12 Stress Profiles (108M)

FIGURE. 13 Stress Profiles (30M)

FIGURE. 14 Stress Profiles (108S)

269
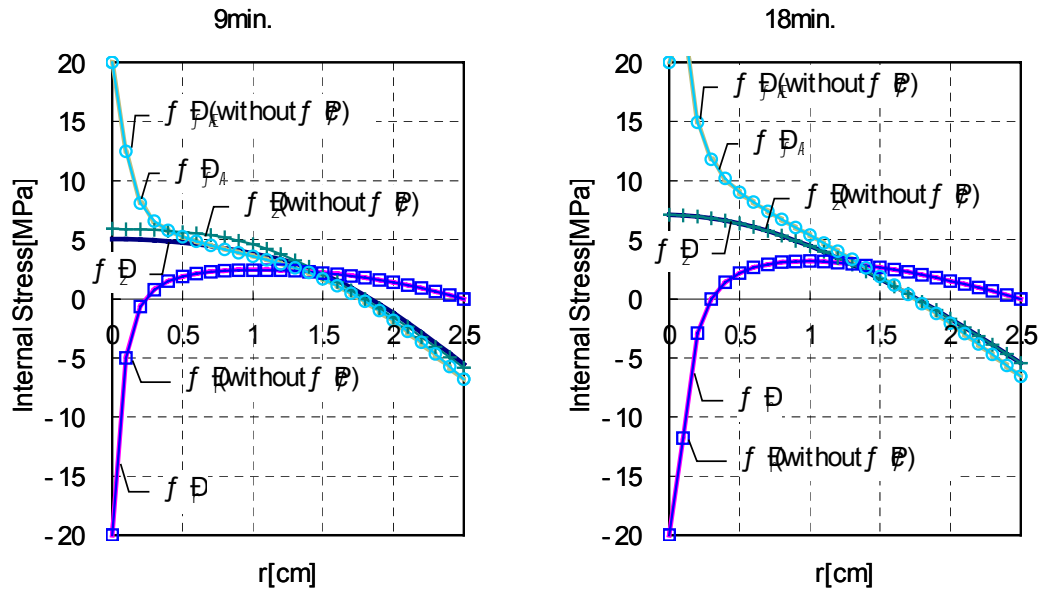
FIGURE. 15 Influence of Pore Pressure on Stress Profile(108S)

NOTATIONS

T: temperature [K], *P*: total pressure [MPa], p_v: vapor pressure [MPa], p_a: air pressure [MPa], m_v: rate of vapor generation [kg/m³s], *w*: water concent [kg/kg], λ: thermal concuctivity [W/m.K], ρ_0: density of concrete [kg/m³], ρ_a: density of air [kg/m³], ρ_v: density of air [kg/m³], *c*: specific heat [J/kg.K], κ: permeability[m³/Pa.s], ε: void fraction [-], *R*: universal gas constant [J/kmol.K], M_v molecular weight of water [kg/kmol], M_a molecular weight of air [kg/mol], ϕ_v: mole fraction of vapor, F_c: compressive strength [MPa], r_0: radius [m], *E*: elastic modulus [MPa] (E_0: at room temperature), α: coefficient of thermal expansion [K⁻¹] (α_0: at room temperature), σ_z: axial stress [MPa], σ_r: radial stress [MPa], σ_θ: tangential stress [MPa],: ε_{pres} : strain caused by pore pressure rise [-], ΔT_{eff}: effective temperature [K], ΔT_v : effective temperature due to Poission's effect [K] τ_0: shear octahedral stress [MPa], τ_{0cr}: critical shear octahedral stress for cracking [MPa], ν : Poisson's ratio [-],

REFERENES

[1] Saito, H., <u>Bulletin of Fire Prevention Society of Japan</u>, Vol. 15(2), 1966
[2] Walraven, J., "<u>The Future of High Strength/ High Performance Concrete</u>", Proceedings of the 5th International Symposium on Utilization of High Strength/ High Performance Concrete", pp. 25-36, 1999
[3] Morita, T., Nishida, A., Yamazaki, N., Schneider, U. and Diederichs, U., "<u>An Experimental Study on Spalling of High Strength Concrete Elements under Fire Attack</u>", Procedddings of the Sixth International Symposium on Fire Safety Science, July 1999
[4] Nishida, A., Yamazaki, N., Inoue, H., Schneider, U. and Diederichs, U., "<u>Study on the Properties of High Strength Concrete with Short Polypropylene Fiber for Spalling Resistance</u>", Proceeding of the International Conference on Concrete under Service Conditions, CONSEC '95, E&FN SPON, August 1995

[5] Harada, K., Terai, T., " Heat and Mass Transfer in an Intensely Heated Mortar Wall", Fire Safety Science, Vol. 3, (Proceedings of the third International Symposium on Fire Safety Science, Edgingburh) pp. 781-780, 1991

[6] Scheidegger, A., "The Physics of Flow through Porous Media", University of Toronto Press, 1960.

[7] Kotsovos, M., D., "A Mathematical Description of the Strength Properties of Concrete under Generalized Stress", Magazine of Concrete Research, Vol. 31(108), pp. 151-158, 1970

Session 6:
Steel Structures

MECHANICAL PROPERTIES OF STRUCTURAL STEEL AT ELEVATED TEMPERATURES AND AFTER COOLING DOWN

Jyri OUTINEN and Pentti MÄKELÄINEN
Laboratory of Steel Structures,
Department of Civil and Environmental Engineering,
Helsinki University of Technology
P.O. Box 2100, FIN-02015 HUT, Finland
jyri.outinen@hut.fi
http://www.hut.fi/Units/Civil/Steel/

ABSTRACT

Experimental research program has been carried out during the years 1994-2001 in the Laboratory of Steel Structures at Helsinki University of Technology in order to investigate mechanical properties of several structural steels at elevated temperatures by using mainly transient state tensile test method. The aim is to produce accurate material data for the use in different structural analyses. The main test results are public and they are available for other researchers.

In this paper the experimental test results for the mechanical properties of the studied steel grades S350GD+Z, S355 and S460M at fire temperatures are presented with a short description of the testing facilities. A test series was also carried out for cold-formed material taken from rectangular hollow sections of structural steel S355J2H and these test results are also given in this report.

The mechanical properties of structural steel after cooling down have also been shortly examined and these test results are given in this report.

The test results were used to determine the temperature dependencies of the mechanical properties, i.e. yield strength, modulus of elasticity and thermal elongation, of the studied steel material at temperatures up to 950°C. The test results are compared with the material model for steel according to Eurocode 3: Part 1.2.

KEYWORDS: *mechanical properties, strength, high-temperature testing, structural steel*

INTRODUCTION

The behaviour of mechanical properties of different steel grades at elevated temperatures should be well known to understand the behaviour of steel and composite structures at fire. Quite commonly simplified material models are used to estimate e.g. the structural fire resistance of steel structures. In more advanced methods, for example in finite element or finite strip analyses, it is important to use accurate material data to obtain reliable results.

To study thoroughly the behaviour of certain steel structure at elevated temperatures, one should use the material data of the used steel material obtained by testing. The tests have to be carried out so, that the results can be used to evaluate the behaviour of the structure, i.e. the temperature rate e.g. should be about the same that is used in the modelling assumptions.

Extensive experimental research has been carried out since 1994 in the Laboratory of Steel Structures at Helsinki University of Technology in order to investigate mechanical properties of several structural steels at elevated temperatures by using mainly the transient state tensile test method. The basic material research programme is still going on, but the main test results so far were published in 2001 in the Laboratory of steel structures' publication series [1]. The publication is freely available from the laboratory's website: *http://www.hut.fi/Units/Civil/Steel/Publications/jsarj.html.* Some of the test results were also presented in the previous 'Structures in Fire' –workshop in Copenhagen [2].

The test results have recently been used in some research projects studying the behaviour of e.g. cold-formed steel members in fire [3] [4]. The results seem to work quite well with the structural analyses carried out within these projects.

In this paper the transient state test results of structural steel grades S355, S355J2H, S460M and S350GD+Z are presented with a short description of the testing facilities and comparisons with ENV1993-1-2 [5].

In addition to the original plan, some tests were also carried out for structural steel material taken from that have been tested at elevated temperatures. This was to find out the remaining strength of the material after fire. The preliminary test results are presented in this paper.

274

STUDIED MATERIALS

The studied materials were common structural steel grades with nominal yield strength varying from 350N/mm^2 to 460N/mm^2. The actual yield strength varied significantly from the nominal values and this has to be taken into account. The materials are listed in the Table 1 below with the nominal and measured values at room temperature.

Steel Grade	Nominal f_y [N/mm^2]	Measured f_y [N/mm^2]	Material Standard
S350GD+Z	350	402	SFS-EN 10 147
S355	355	406	SFS-EN 10 025
S460M	460*	445*	SFS-EN 10113
S355J2H	355	539-566**	SFS-EN 10219-1

Table 1: Studied steel grades

* The nominal yield strength is dependent on plate thickness. The nominal yield strength for steel plates with 20mm thickness that was studied in this research is 440N/mm^2.

** The measured yield strength values are for test specimen taken from the face of square hollow sections 50x50x3, 80x80x3 and 100x100x3.

TEST METHODS

Two types of test methods are commonly used in the small-scale tensile tests of steel at high temperatures; transient-state and steady-state test methods. The steady state tests are easier to carry out than the transient state tests and therefore that method is more commonly used than the transient state method. However, the transient state method seems to give more realistic test results especially for low-carbon structural steel and that is why it is used in this research project as the main test method. A series of steady state tests were also carried out in this project.

Transient-state test method
In transient-state tests, the test specimen is under a constant load and under a constant temperature rise. Temperature and strain are measured during the test. As a result, a temperature-strain curve is recorded during the test. Thermal elongation is subtracted from the total strain. The results are then converted into stress-strain curves as shown in Figure 1.
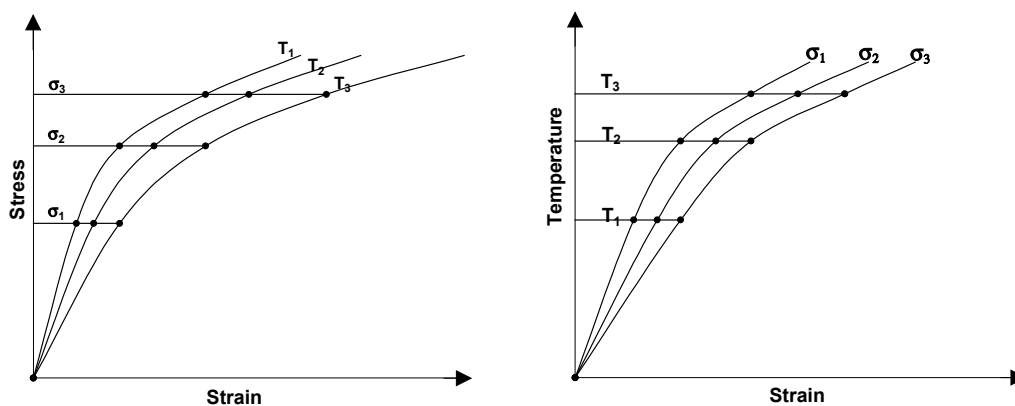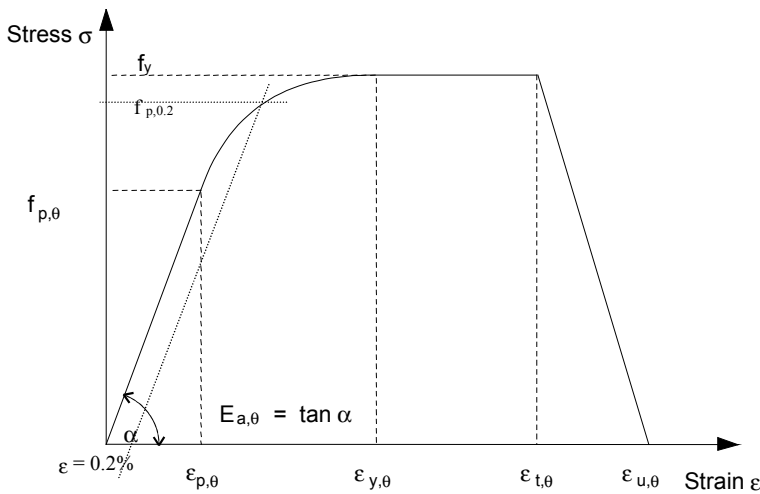

FIGURE 1: Converting the stress-strain curves from the transient state test results.

The mechanical material properties i.e. elasticity modulus and yield strength, can be determined from the stress-strain curves. This is illustrated in Figure 2. The strain value of $\varepsilon_{y,\theta}$ stands for 2 % total strain.

**FIGURE 2: Stress-strain relationship for steel at elevated temperatures.**

The transient-state test method gives quite a realistic basis for predicting the material's behaviour under fire conditions. The transient-state tests were conducted with two identical tests at different stress levels. Heating rate in the transient state tests was 20°C min^{-1}. Some tests were also carried out using heating rates 10°C min^{-1} and 30°C min^{-1}. In addition some tests were carried out with a high heating rate close to the ISO-curve to compare the real behaviour of the material with this heating rate. Temperature was measured accurately from the test specimen during the heating.

Steady-state test method
In the steady-state tests, the test specimen was heated up to a specific temperature. After that a tensile test was carried out. In the steady state tests, stress and strain values were first recorded and from the stress-strain curves the mechanical material properties could be determined. The steady state tests can be carried out either as strain- or as load-controlled. In the strain-controlled tests, the strain rate is kept constant and in the load-controlled tests the loading rate is kept constant.

TESTING DEVICE

The tensile testing machine used in the tests is verified in accordance with the standard EN 10 002-2 [6]. The extensometer is in accordance with the standard EN 10 002-4 [6]. The oven in which the test specimen is situated during the tests was heated by using three separately controlled resistor elements. The air temperature in the oven was measured with three separate temperature-detecting elements. The steel temperature was measured accurately from the test specimen using temperature-detecting element that was fastened to the specimen during the heating. The testing device is illustrated in Figure 3.
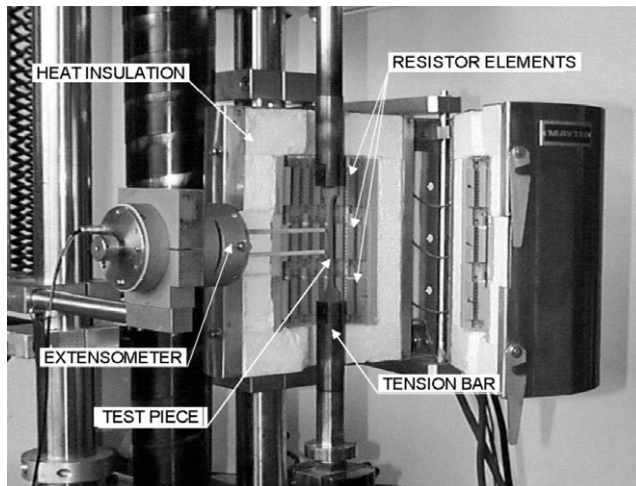
FIGURE 3: High-temperature tensile testing device.

TEST RESULTS OF STRUCTURAL STEEL S350GD+Z

The behaviour of structural steel S350GD+Z at elevated temperatures was studied with 30 high-temperature tests. The test results were combined with an earlier test series of 60 tests that were carried out in the same laboratory. The aim was to add the test results of the mechanical properties at temperatures from 700°C to 950°C to the earlier test results. On the basis of these test results a suggestion concerning the mechanical properties of the studied material was made to the Finnish national norm concerning the material models used in structural fire design of unprotected steel members. The test results were fitted to ENV1993-1-2 material model and the results are illustrated in Table 2.

In Figure 4 the experimentally determined yield strength f_y is compared with ENV1993-1-2 material model. In Eurocode, the nominal yield strength is assumed to be the constant until 400°C, but in the real behaviour of the studied steel it starts to decrease earlier.

Additionally room-temperature tests were also carried out for material taken from members that have been tested at elevated temperatures. This was to find out the remaining strength of the material after fire. In Figure 5 the tensile test results are compared with the test results for unheated material.

Steel Temp. θ_a [°C]	Reduction factor for the slope of the linear elastic range $k_{E,\theta} = E_{a,\theta}/E_a$	Reduction factor for proportional limit $k_{p,\theta} = f_{p,\theta}/f_y$	Reduction factor for satisfying deformation criteria (**informative only**) $k_{x,\theta} = f_{x,\theta}/f_y$	Reduction factor for yield strength $k_{p0,2,,\theta} = f_{p0,2,\theta}/f_y$	Reduction factor for yield strength $k_{y,\theta} = f_{y,\theta}/f_y$
20	1.000	1.000	1.000	1.000	1.000
100	1.000	0.970	0.970	1.000	0.970
200	0.900	0.807	0.910	0.863	0.932
300	0.800	0.613	0.854	0.743	0.895
400	0.700	0.420	0.790	0.623	0.857
500	0.600	0.360	0.580	0.483	0.619
600	0.310	0.180	0.348	0.271	0.381
700	0.130	0.075	0.132	0.106	0.143
800	0.090	0.000	0.089	0.077	0.105
900	0.068	0.000	0.057	0.031	0.067
950	0.056	0.000	0.055	0.023	0.048
1000	0.045	0.000	0.025	0.014	0.029

TABLE 2: Reduction factors for mechanical properties of structural steel S350GD+Z at temperatures 20°C-1000°C. Values based on transient state test results.
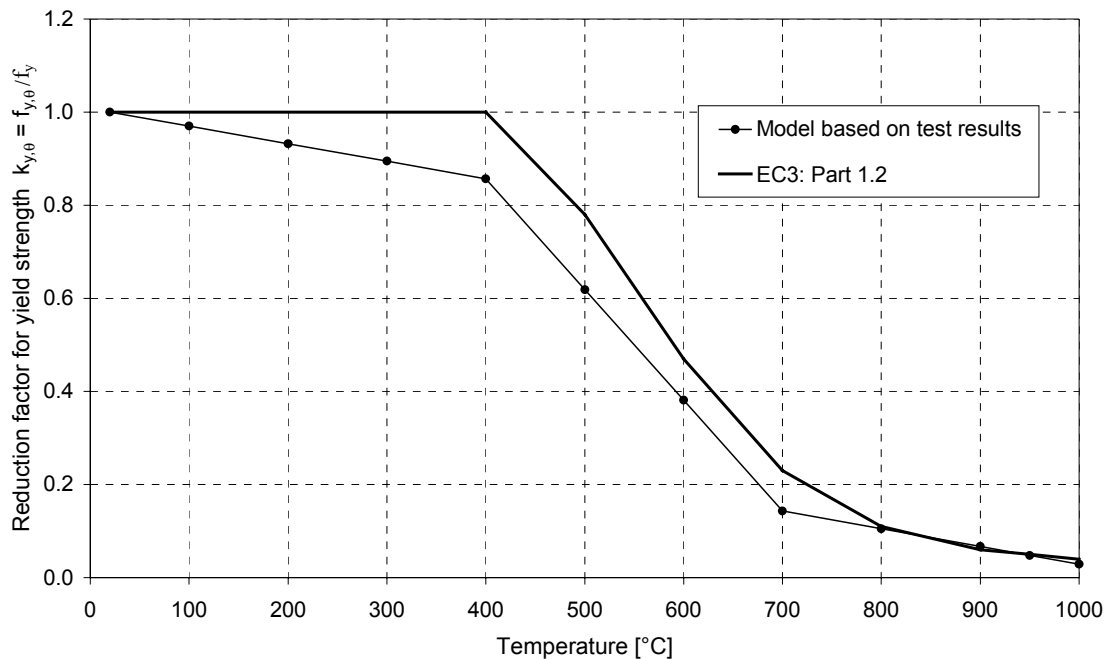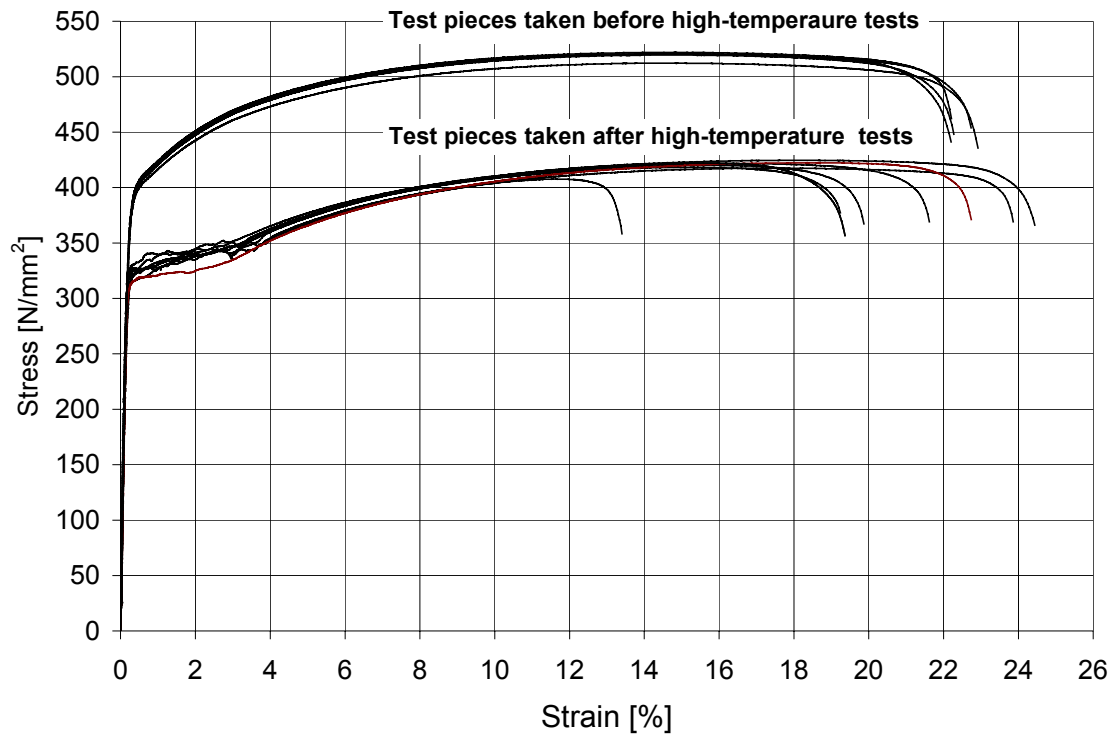

FIGURE 4: The reduction factor for effective yield strength f $_{y,\theta}$ of structural steel S350GD+Z determined from test results compared with the values given in Eurocode 3: Part 1.2.

F**IGURE 5: Tensile test results for structural steel S350GD+Z. Test pieces taken before and after high-temperature compression tests.**

From Figure 5 it can be seen that the increased yield strength of the material due cold-forming has decreased back to the nominal yield strength level of the material. It has to be noted that the material has reached temperatures up to 950C in the compression tests. The temperature histories from the compression tests are illustrated in Figure 6. The tensile test specimen were taken from compression members 24,27 and 30. The compression tests were carried in a research project of VTT, the Techcnical Research Centre of Finland.
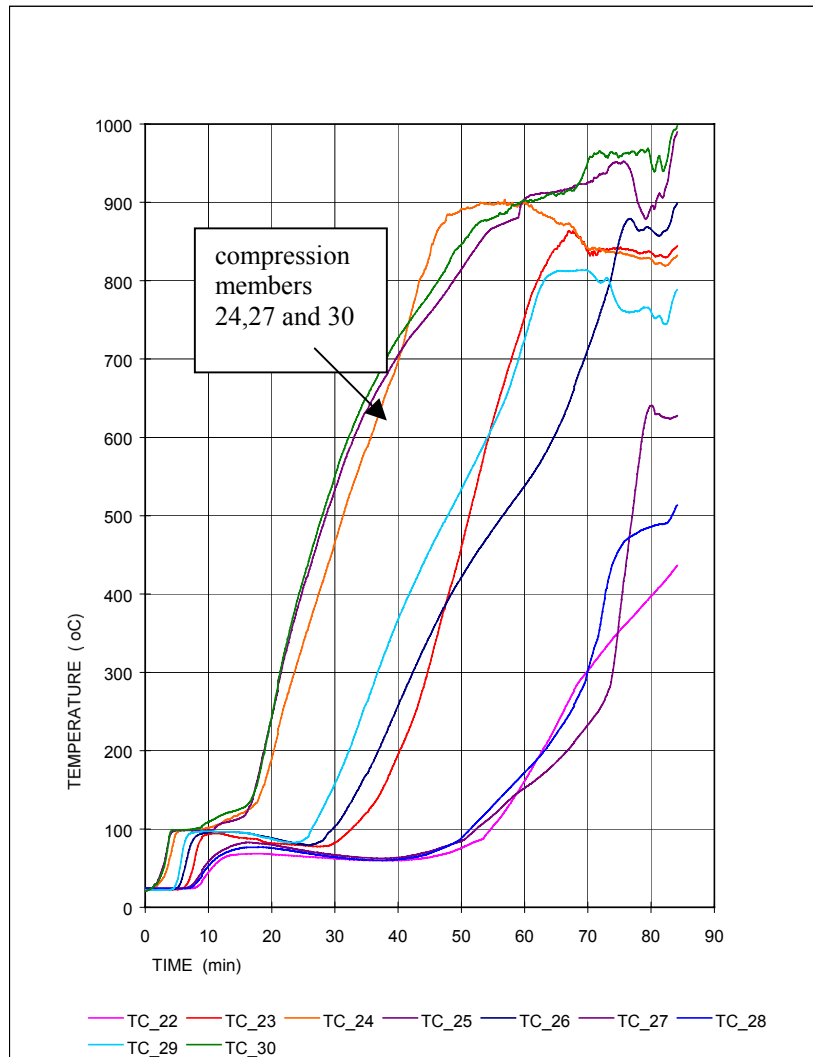
FIGURE 6: Temperature histories of the compression test specimens, from which the tensile test specimens were taken after cooling down.

The members that were in the compression tests were quite distorted after the tests. Despite this, the mechanical properties of the steel material were preserved in the nominal strength level of the material. This kind of phenomenon should be taken into account when considering the load bearing capacity of steel structures that have been in fire and are otherwise still usable, i.e. not too badly distorted.

TEST RESULTS OF STRUCTURAL STEEL S355J2H

Normal tensile tests according standard SFS-EN 10002-1 were carried out for the cold-formed material. The test results for yield strength are illustrated in Table 3. It can be seen from the test results that the increased strength caused by cold-forming is significant for all studied hollow sections. The nominal yield strength for the material is 355N/mm^2. The tensile tests at room temperature were carried out for the specimens taken from the corner part of SHS 50x50x3. The average yield strength fy for these specimens was 601 N/mm2.

	Yield strength f_y [N/mm^2]	Yield strength $R_{p0.2}$ [N/mm^2]	Yield strength $R_{t0.5}$ [N/mm^2]
50x50x3	566	520	526
80x80x3	544	495	502
100x100x3	539	490	497

Table 3: Tensile test results for structural steel S355J2H at room temperature. Test pieces from SHS cross-sections.

A test series of over 100 tensile tests was conducted for the material taken from SHS-tubes 50x50x3, 80x80x3 and 100x100x3. The heating rate in the tests was 20°C/minute. Some tests were also carried out with a heating rate 10°C/minute and 30°C/minute. A small test series was also carried out with a heating rate 45°C/minute.

The tensile tests for structural steel S355J2H were carried out using test specimens that were cut out from SHS-tubes 50x50x3, 80x80x3 and 100x100x3 longitudinally from the middle of the face opposite to the welded seam. A small test series with test specimen taken from the corner parts of the SHS-tube 50x50x3 was also carried out as an addition to the original project plan. The test results have been fitted into the EC3: Part 1.2 material model using the calculation parameters determined from the transient state tests.

The high-temperature tensile testing has to be carried out using the rules given in testing standard SFS-EN 10002 : Metallic materials. Tensile testing. Parts 1-5. In this standard there are limitations for the strain rate and the loading rate used in high temperature tensile testing. The test results that are given in this report are based on tests carried out according this testing standard.

From the test results it was clearly seen, that with this used heating rate 20°C/minute the increased strength caused by cold forming starts to vanish in temperatures 600°C-700°C. For the test specimen with a higher heating rate the increased strength seems to remain to higher temperatures. The test results at temperatures 20°C – 1000°C are illustrated in the following tables.

Temp. [°C]	Modulus of Elasticity E [N/mm^2]	Proportional limit f_p [N/mm^2]	Yield strength f_y [N/mm^2]	Yield strength $R_{p0.2}$ [N/mm^2]	Yield strength $R_{t0.5}$ [N/mm^2]
20	210000	481.1	566	520	526
100	210000	481.1	566	520	526
200	189000	441.48	549.02	485	496
300	168000	367.9	537.7	439	455
400	147000	311.3	481.1	381	399
500	126000	169.8	367.9	255	280
600	65100	67.92	181.12	118	132
700	27300	39.62	101.88	66	72
750	23100	28.3	67.92	46	51
800	18900	19.81	42.45	29	33
850	16537.5	11.32	31.13	20	23
900	14175	6.792	22.64	13	17
950	11812.5	5.66	19.81	12	14
1000	9450	4.528	22.64	10	11

Reduction factors relative to the values at temperature 20°C:

Temp [°C]	Modulus of Elasticity $k_{E,\theta} = E_{a,\theta} / E_a$	Proportional limit f_p $k_{p,\theta} = f_{p,\theta} / f_y$	Yield strength f_y $k_{y,\theta} = f_{y,\theta} / f_y$	Yield strength $R_{p0.2}$ $k_{p0.2,\theta} = f_{p0.2,\theta} / f_y$	Yield strength $R_{t0.5}$ $k_{t0.5,\theta} = f_{t0.5,\theta} / f_y$
20	1,000	0,850	1,000	0,919	0,929
100	1,000	0,850	1,000	0,919	0,929
200	0,900	0,780	0,970	0,867	0,876
300	0,800	0,650	0,950	0,795	0,804
400	0,700	0,550	0,850	0,693	0,705
500	0,600	0,300	0,650	0,468	0,495
600	0,310	0,120	0,320	0,217	0,233
700	0,130	0,070	0,180	0,124	0,127
750	0,110	0,050	0,120	0,088	0,090
800	0,090	0,035	0,075	0,053	0,058
850	0,079	0,020	0,055	0,039	0,041
900	0,068	0,012	0,040	0,025	0,030
950	0,056	0,010	0,035	0,021	0,025
1000	0,045	0,008	0,030	0,018	0,019

Table 4: Mechanical properties of structural steel S355J2H at elevated temperatures. Test pieces from SHS 50x50x3

| Temp [°C]	Modulus of Elasticity E [N/mm²]	Proportional limit f_p [N/mm²]	Yield strength f_y [N/mm²]	Yield strength $R_{p0.2}$ [N/mm²]	Yield strength $R_{t0.5}$ [N/mm²]
20	210000	462,4	544	500	525
100	210000	462,4	544	500	505,4882
200	189000	424,32	527,68	473	478,1146
300	168000	353,6	516,8	432	438,4486
400	147000	299,2	462,4	379	384,3109
500	126000	163,2	353,6	255	270,426
600	65100	65,28	174,08	117	128,1229
700	27300	38,08	97,92	67	70,38595
750	23100	27,2	65,28	44	48,80605
800	18900	8,16	35,36	21	24,87326
850	16537,5	7,344	29,92	16	22,46505
900	14175	6,528	16,32	11	12,67555
950	11812,5	5,44	13,6		

Reduction factors relative to the values at temperature 20°C:

Temp [°C]	Modulus of Elasticity $k_{E,\theta} = E_{a,\theta}/E_a$	Proportional limit f_p $k_{p,\theta} = f_{p,\theta}/f_y$	Yield strength f_y $k_{y,\theta} = f_{y,\theta}/f_y$	Yield strength $R_{p0.2}$ $k_{p0.2,\theta} = f_{p0.2,\theta}/f_y$	Yield strength $R_{t0.5}$ $k_{t0.5,\theta} = f_{t0.5,\theta}/f_y$
20	1,000	0,850	1,000	1,016	1,000
100	1,000	0,850	1,000	1,016	0,963
200	0,900	0,780	0,970	0,961	0,911
300	0,800	0,650	0,950	0,878	0,835
400	0,700	0,550	0,850	0,770	0,732
500	0,600	0,300	0,650	0,518	0,515
600	0,310	0,120	0,320	0,238	0,244
700	0,130	0,070	0,180	0,136	0,134
750	0,110	0,050	0,120	0,089	0,093
800	0,090	0,015	0,065	0,043	0,047
850	0,079	0,014	0,055	0,033	0,043
900	0,068	0,012	0,030	0,022	0,024
950	0,056	0,010	0,025		
1000	0,045	0,008	0,020		

Table 5: Mechanical properties of structural steel S355J2H at elevated temperatures. Test pieces from SHS 80x80x3

Temp [°C]	Modulus of Elasticity E [N/mm²]	Proportional limit f_p [N/mm²]	Yield strength f_y [N/mm²]	Yield strength $R_{p0.2}$ [N/mm²]	Yield strength $R_{t0.5}$ [N/mm²]
20	210000	458,15	539	496	500,9744
100	210000	458,15	539	496	500,9744
200	189000	420,42	522,83	469	473,8989
300	168000	350,35	512,05	427	434,6986
400	147000	296,45	458,15	373	381,0532
500	126000	161,7	350,35	252	268,1464
600	65100	64,68	172,48	117	127,0427
700	27300	37,73	86,24	53	64,46188
750	23100	26,95	59,29	38	45,50802
800	18900	18,865	40,425	23	25,24635
850	16537,5	10,78	29,645	17	22,26879
900	14175	6,468	16,17	11	12,56227
950	11812,5	5,39	13,475		

Reduction factors relative to the values at temperature 20°C:

Temp [°C]	Modulus of Elasticity $k_{E,\theta} = E_{a,\theta}/E_a$	Proportional limit f_p $k_{p,\theta} = f_{p,\theta}/f_y$	Yield strength f_y $k_{y,\theta} = f_{y,\theta}/f_y$	Yield strength $R_{p0.2}$ $k_{p0.2,\theta} = f_{p0.2,\theta}/f_y$	Yield strength $R_{t0.5}$ $k_{t0.5,\theta} = f_{t0.5,\theta}/f_y$
20	1,000	0,850	1,000	1,012	1,008
100	1,000	0,850	1,000	1,012	1,008
200	0,900	0,780	0,970	0,957	0,954
300	0,800	0,650	0,950	0,871	0,875
400	0,700	0,550	0,850	0,761	0,767
500	0,600	0,300	0,650	0,514	0,540
600	0,310	0,120	0,320	0,239	0,256
700	0,130	0,070	0,160	0,108	0,130
750	0,110	0,050	0,110	0,078	0,092
800	0,090	0,035	0,075	0,047	0,051
850	0,079	0,020	0,055	0,035	0,045
900	0,068	0,012	0,030	0,022	0,025
950	0,056	0,010	0,025		
1000	0,045	0,008	0,020		

Table 6: Mechanical properties of structural steel S355J2H at elevated temperatures. Test pieces from SHS 100x100x3

The test results with heating rates 10°C/minute and 20°C/minute don't differ from each other, but the heating rate 30°C/min seemed to give higher test results. This is illustrated in Figure 6 This led to the decision to carry out additional tests with a higher heating rate. Also the behaviour of the corner parts of the profile was studied.

Three small test series were carried out. One with corner specimens with a heating rate 20°C/minute, one with corner specimen with a heating rate 45°C/minute and one with flat specimen with a heating rate 45°C/minute. The used temperature history of this new test series is illustrated in Figure 7. The test results at temperatures 600C and 700 are illustrated in Figures 8 and 9.
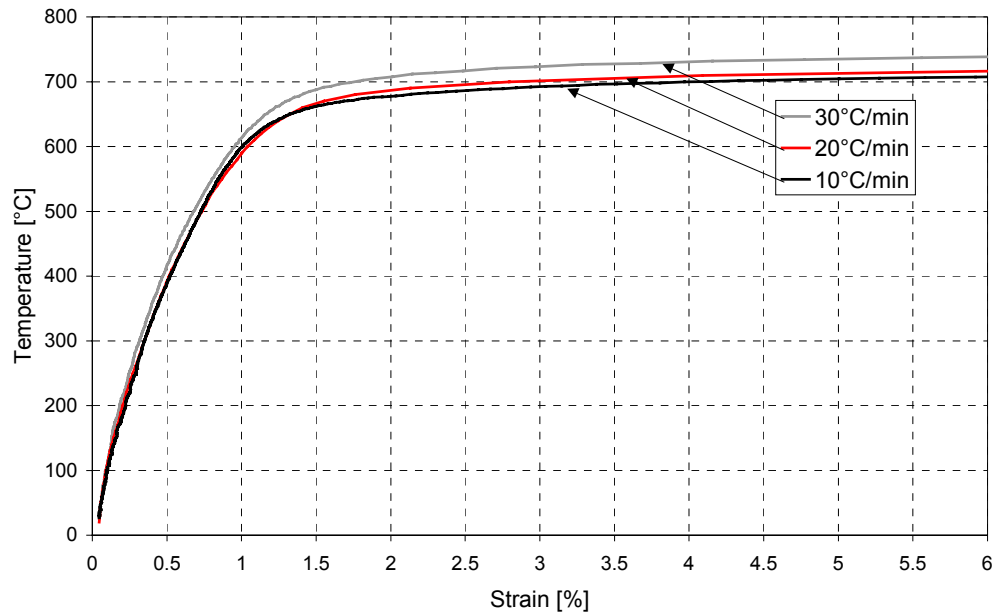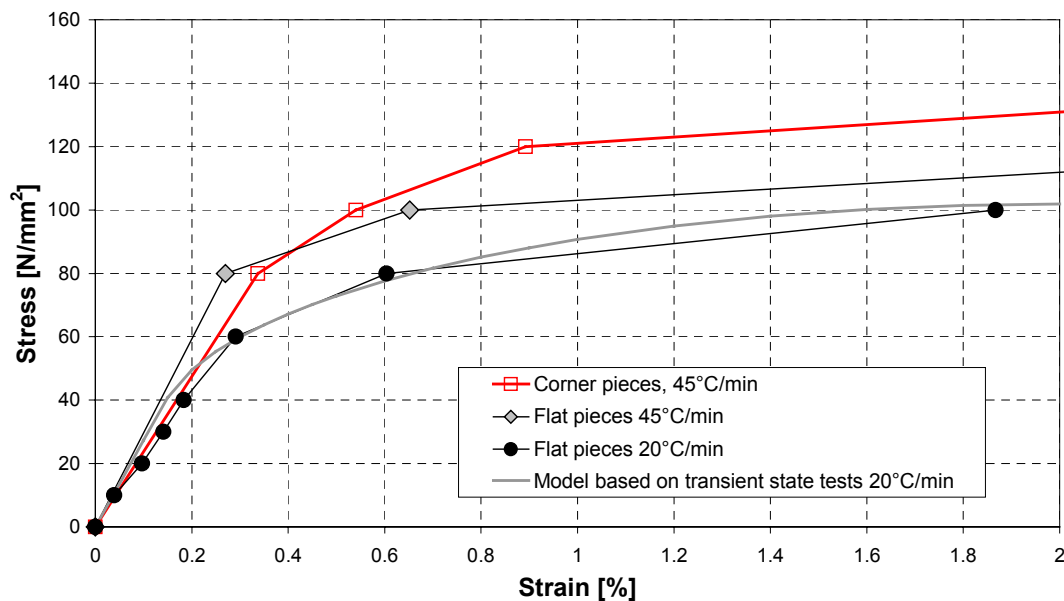
FIGURE 6: Temperature-strain curves of structural steel S355J2H at stress level 100N/mm2 with heating rates 10°C, 20°C and 30°C/min. Test pieces taken from SHS 50x50x3.
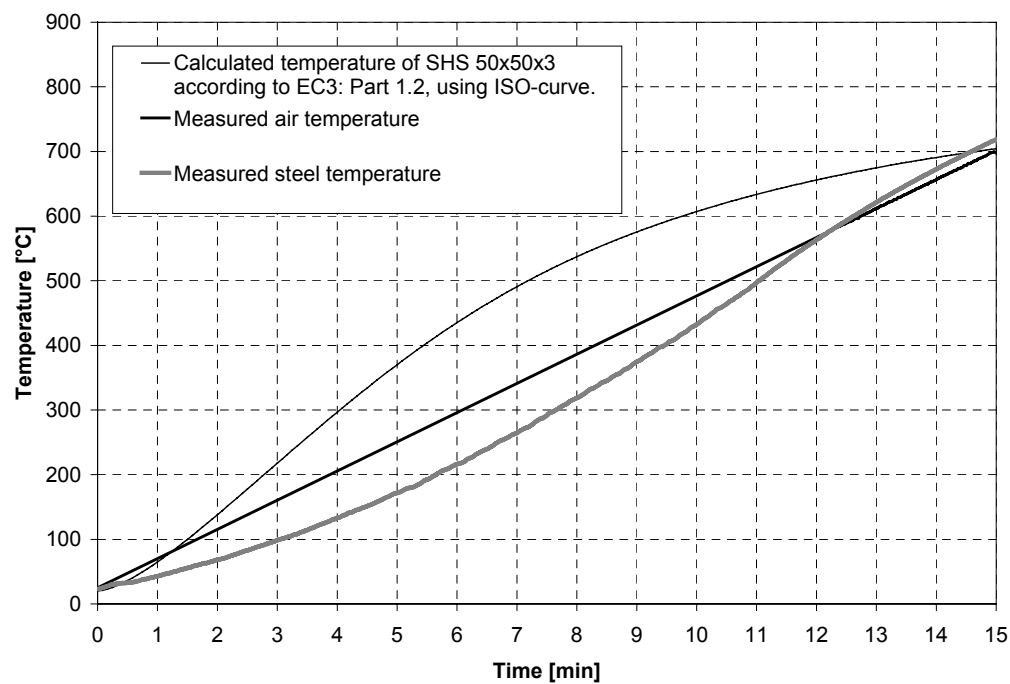
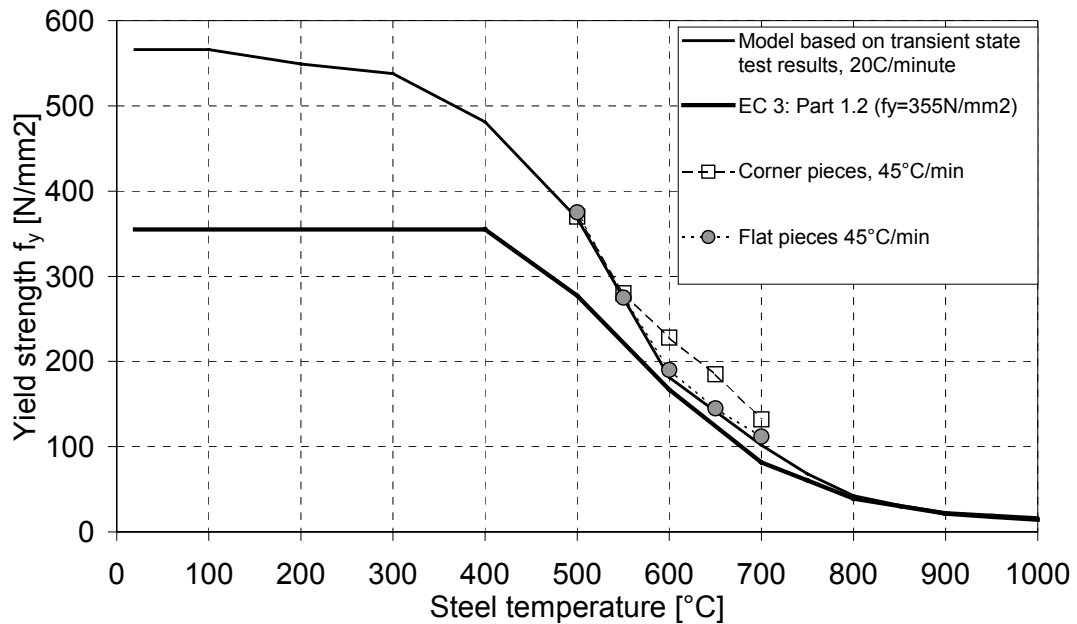**FIGURE 7: Temperature history of the new test series compared with the ISO-curve.**
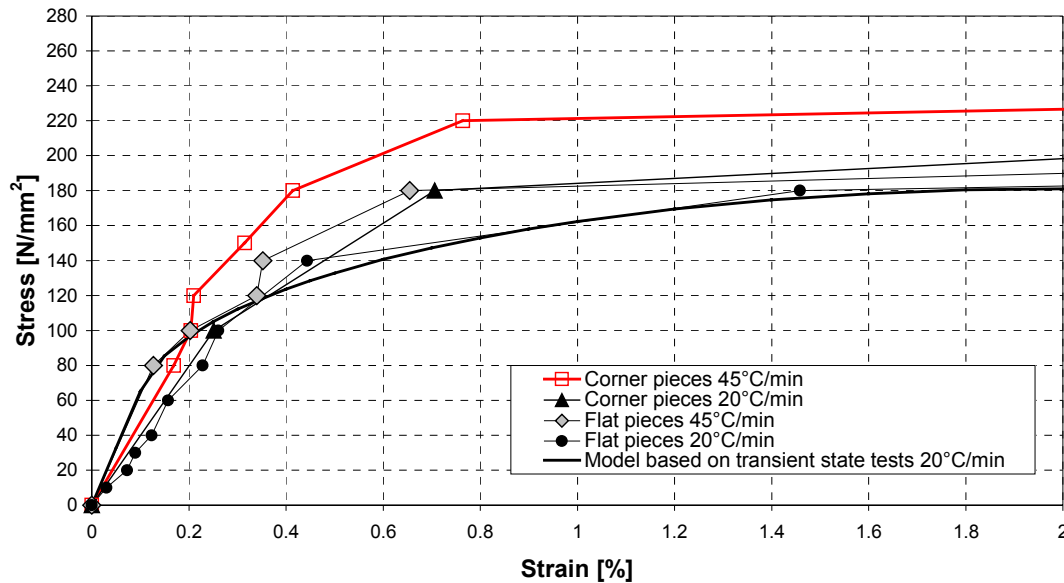
FIGURE 8: Stress-strain curves of structural steel S355J2H. Test results with different specimens and different heating rates at temperature 600°C.


FIGURE 9: Stress-strain curves of structural steel S355J2H. Test results with different specimens and different heating rates at temperature 700°C.

The difference between the test results with heating rates 20°C/minute and 45°C/minute seems not to be as big as was assumed before for the specimens taken from the face of the square hollow section. Also the difference between the test results with flat specimens and corner specimens with a heating rate 20C/minute was not very big. The test results for the corner pieces are significantly higher with heating rate 45°C/minute. In Figure 10 the yield strength f_y determined from these test results is illustrated.

FIGURE 10: Yield strength f$_y$ of structural steel S355J2H. Test results with different specimens and different heating rates at temperatures 20-700°C.

Some tests for structural steel S355J2H were carried out at room temperature with test specimens that had been heated unloaded up until temperature 950°C and let cool down to ambient temperature after that. The mechanical properties of the material seemed to return back to the nominal values of structural steel S355. In Figure 11 the test results of these tests are compared with the normal room temperature test results.
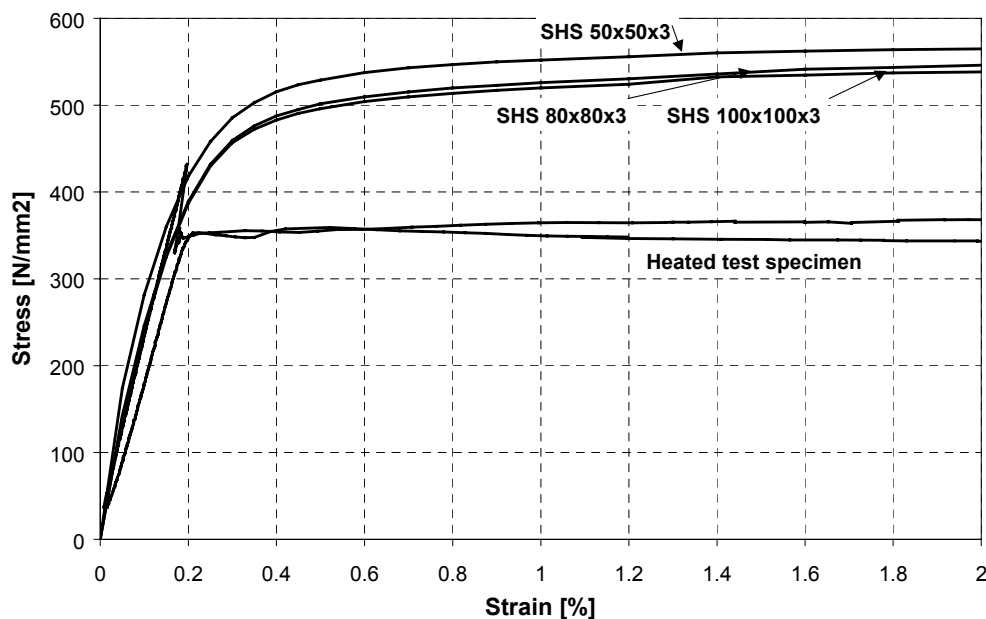
FIGURE 11: Comparison between the tensile test results of heated and non-heated test specimen on structural steel S355J2H at room temperature.

In addition to this project a small tensile test series was carried out to determine the yield strength of the material used in high-temperature stub column tests. The specimens were taken out from SHS 50x50x3 tubes after they had been tested at elevated temperatures. The average yield strength of the material before high-temperature tests was 529N/mm^2 and the nominal yield strength 355N/mm^2. The test results are illustrated in Table 6 and in Figure 12.

specimen	Max. temperature during stub column test	Yield strength f_y	Modulus of Elasticity, E
	[°C]	[N/mm^2]	[N/mm^2]
A1	602	478	148942
A2	674	527	186318
A3Y	611	482	201951
A3A	611	497	185999
A4Y	498	469	323808
A4A	498	465	214593
A5A	532	520	179985
A5Aa	532	499	210465
A6A	369	520	184878
Y1	658	-----	225715
Y2	710	464	213532
Y3	643	474	181901
Y4	569	508	184246
Y5	617	492	164970
Y6	334	538	224360

Table 6: Tensile test results at temperature 20°C for structural steel S355J2H. Test pieces from SHS 50x50x3 after high-temperature stub column tests.
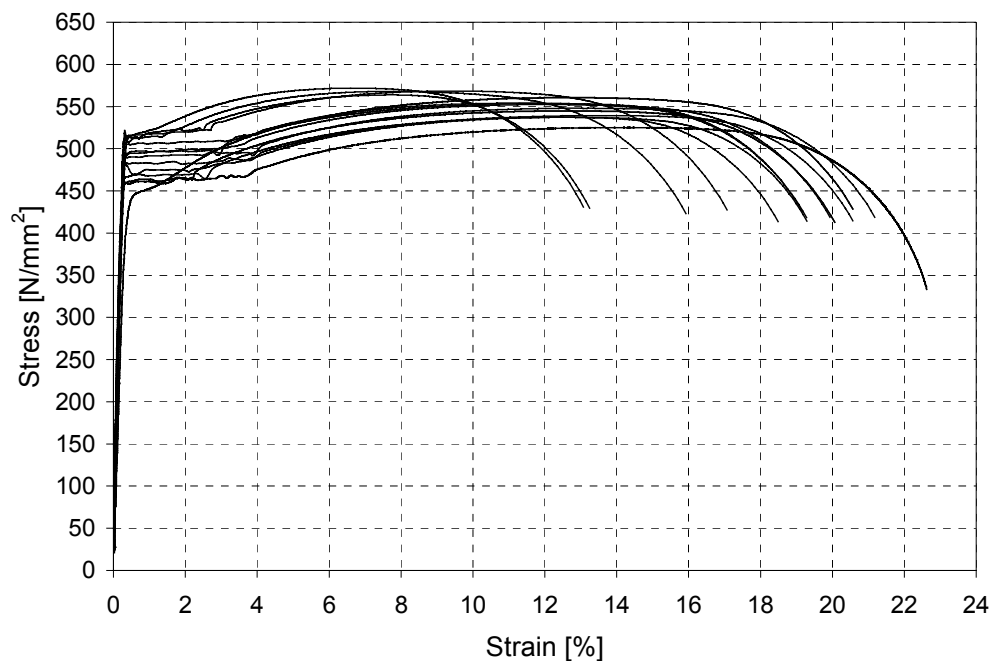
FIGURE 12: Tensile test results at ambient temperature for structural steel S355J2H. Test coupons taken from SHS 50x50x3 tubes after high-temperature stub column tests.

The temperatures used in the column tests are given in the table. It can clearly be seen that the tested yield strength of the specimen is more than the nominal yield strength of the used material.

CONCLUSIONS

An overview of the test results for structural steels S350GD+z and S355J2H were given in this paper. The high temperature test results were fitted to the 'Eurocode 3 model' to provide the data in a useful form to be used in e.g. finite element modeling of steel structures. The aim of this research is mainly to get accurate information of the behaviour of the studied steel grades and to provide useful information for other researchers.The test data is presented more accurately in Ref.[1], which can be downloaded from: *http://www.hut.fi/Units/Civil/Steel/Publications/jsarj.html*.

The behaviour of structural steel S350GD+Z differed from the EC3 model and a new suggestion was made on the basis of the high-temperature tests. The mechanical properties after heating seemed to be near the nominal values of the material, which is good, when thinking of the remaining strength of steel structures after fire.

The behaviour of steel S355J2H seemed also to be very promising. The increase of strength due to cold-forming seemed to remain quite well at elevated temperatures. This should naturally be taken into account when estimating the behaviour of cold-formed steel structures. Also the strength after high-temperature tests seemed to remain quite well.

ACKNOWLEDGEMENTS

REFERENCES

[1] Outinen, J., Kaitila, O., Mäkeläinen, P., *High-Temperature Testing of Structural Steel and Modelling of Structures at Fire Temperatures*, Laboratory of steel structures publications, TKK-TER-23, Finland, 2001.

[2] Outinen J., Kaitila O., Mäkeläinen P., *A Study for the Development of the Design of Steel Structures in Fire Conditions*, 1st International Workshop of Structures in Fire, Copenhagen, Denmark, 2000.

[3] Feng,M., Wang,Y.C., Davies,J.M., *Behaviour of cold-formed thin-walled steel short columns under uniform high temperatures,* Proceedings of the International Seminar on Steel Structures in Fire, pp.300-312, Tongji University, China, 2001.

[4] Kaitila, Olli, *Imperfection sensivity analysis of lipped channel columnsat high temperatures*, Journal of Constructional Steel Research, vol.58, no.3, pp. 333-351, 2002.

[5] EN1993-1-2 European Committee for Standardisation (CEN), Eurocode 3: Design of steel   structures, Part 1.2 : Structural fire design, Brussels 1993.

[6] SFS-EN 10002 : Metallic materials. Tensile testing. Parts 1-5

FIRE DESIGN OF A NEW SLIM FLOOR BEAM SYSTEM USING FEM-ANALYSIS

P. SCHAUMANN and S. HOTHAN
Institute for Steel Construction, University of Hannover,
Appelstraße 9A, D-30167 Hannover, Germany
www.stahlbau.uni-hannover.de

ABSTRACT

This paper deals with the application of general calculation models in structural fire design. Computer simulations enable new possibilities in assessing fire resistance of load bearing composite members.

The finite element modelling of the heating and its effects on the load bearing capacity are demonstrated and discussed via the example of a new slim floor beam system. The cross section features a cavity and special regard is paid to the modelling of heat transfer by radiation in this cavity. Typical pitfalls are regarded and checking methods are suggested. The influences of several parameters are studied and an evaluation of these parameters has been worked out.

It will be demonstrated that the radiative heat transfer in the cavity is of significant influence on the temperature development and as a consequence on the load bearing capacity of the cross section. Neglecting the radiation in the cavity can be conservative or unsafe depending on the fire duration. The effects of possible future modifications in the Eurocodes are presented, concerning the surface emissivity of the member.

KEYWORDS: *Fire design, composite structure, slim floor beam, FEM, fire resistance, Eurocodes, configuration factor, cavity radiation*

INTRODUCTION

In the past, the fire resistance of load carrying members was determined only by tests. The test conditions referred to the standard fire tests. In the last two decades, computer models have been developed for the simulation of structural members and even global structures exposed to fire. The improvements concerning numerical methods were forced particularly by research work on composite steel and concrete structures.

This development may also be recognised in the "hot Eurocodes". Thus, the assessment of structural behaviour in a fire design situation according to Eurocode 4 Part 1-2 [8] (EC4-1-2) shall be based on one of the following approaches:

- level 1:
  recognised design solutions called tabular data for specific types of structural members,
- level 2:
  simple calculation models for specific types of structural members,
- level 3:
  general calculation models to simulate the behaviour of the global structure, of parts of the structure or only of a structural member.

Only in those cases where none of the above mentioned approaches is applicable, it is necessary to use a method based on test results.

Up to now, general calculation models for practitioners are less important than tabular data or simple calculation models. There are two main reasons for this. First, the use of sophisticated computer programs requires a high level of education and training. The second reason is that even if these conditions are fulfilled, the application of general calculation models is costly. Thus, general calculation models are mainly used to develop tabular data or simple calculation models. On the other hand the cost of general calculation models are less than that of fire tests, so that computer simulation supersedes more and more traditional fire tests for structural fire design.

In the following, as an example for the application of general calculation models, the finite element modelling of a new slim floor beam system is presented.

GENERAL CALCULATION MODELS

The basic requirements for general calculation models are written down in the "hot Eurocodes" [4,6,8]. Generally these calculation models comprise adequate numerical models for both the thermal and the mechanical response under the action of fire. An important improvement was the definition of temperature-dependent material properties of structural steel, reinforcement steel and concrete in the Eurocodes. According to the new European codes, general calculation models may be used for individual members, for subassemblies or for entire structures. The numerical analyses presented in this contribution are carried out with the finite element computer program ABAQUS®.

Verification of the programme for heat transfer analysis has been carried out, using the evaluation scheme presented in [11].
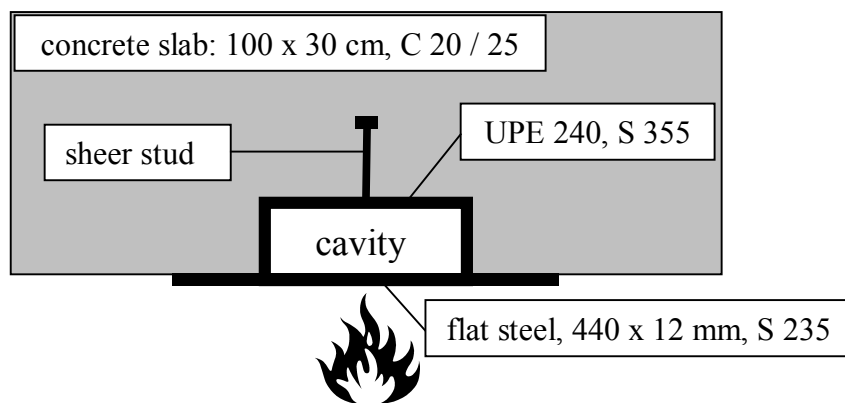
MODELLING OF A NEW SLIM FLOOR BEAM CROSS-SECTION

General

Kuhlmann & Fries & Leukart [10] designed a new single span slim-floor beam for multi-storey buildings with spans up to 10 m. The development was initialised and supported by the German steel producer Salzgitter AG. The cross section comprises a two-part, welded steel section connected to the concrete slab by shear stud connectors. The steel section is assembled welding a U-profile to a steel plate by a filled weld, so that it forms the shape of a hat. Therefore this beam is called hat-profile.

Both, the cold and the fire design of this beam, has been performed on the basis of the Eurocodes. A level-3 method (general calculation model) was applied to calculate the temperature distributions in the beam cross section. The calculation of the load bearing capacity was based on these temperature distributions using a level-2 method. The authors were involved checking the results of the calculation.

First, the temperature distribution in the cross section was calculated at different standard fire durations (ISO-fire): 30, 60, 90 and 120 minutes. Second the plastic bending moment M_{pl} and the shear resistance V_{pl} of the composite beam was calculated, considering the reduction of strength caused by elevated temperatures. A detailed discussion is given further on. At the end, a series of more than 100 sections has been studied. Figure 5 shows the example presented in this report.

concrete slab: 100 x 30 cm, C 20 / 25

sheer stud

UPE 240, S 355

cavity

flat steel, 440 x 12 mm, S 235

Figure 1:
Cross section of the slim-floor composite beam

Thermal analysis

The temperature dependant thermal material properties like specific heat, thermal conductivity and mass density of steel and concrete was implemented according to the Eurocodes. To produce conservative results moisture content of the concrete was neglected. In order to satisfy German building regulations the German National Application Documents for the Eurocodes [5,7,9] had to be considered.

To analyse the heat transfer the calculations were performed with a two dimensional model of the cross section. Four-node linear solid elements (DC2D4) were applied. Figure 2 shows the FEM-mesh of the model.
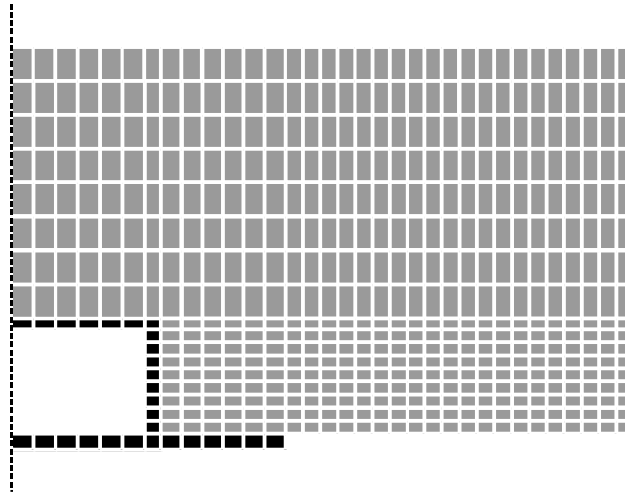
Figure 2:
FEM-mesh of the cross-section used in the ABAQUS® analysis

The axial symmetry was used to reduce the number of elements so that only one half of the cross section was modelled. Normal to the symmetry axis no heat is transferred. Therefore adiabatic boundary conditions were applied on the vertical borders of the model. To model the heat transfer by radiation a special radiation symmetry boundary condition was used, which is discussed later on. Special attention was paid to the heat transfer within the cavity and the effect on the heating process of the beam section.

On the fire-exposed underside of the section the heat transfer due to convection and radiation had to be considered. For the fire-exposed steel and concrete surfaces the emissivity is

$$\varepsilon_{res} = 0,56 \tag{1}$$

for the fire-exposed steel and concrete surfaces corresponding to Eurocode 1 Part 2-2 (EC1-2-2) and EC4-1-2. And the convective heat transfer coefficient is

$$\alpha_c = 25 \ W/(m^2K). \tag{2}$$

According to EC1-2-2 a convective heat transfer coefficient of

$$\alpha_c = 9 \ W/(m^2K) \tag{3}$$

on the unexposed top of the slab is assumed. The heat flow due to radiation has been neglected on this side. The studies showed, that in this case the heat loss at the unexposed slab side is of minor influence and an adiabatic boundary condition on the upper edge of the slab could have been applied.

Heat transfer by radiation between the interior surfaces was calculated. The value of $\varepsilon_{res} = 0,56$ is also assumed for the interior surfaces of the steel section which are not directly exposed to fire.
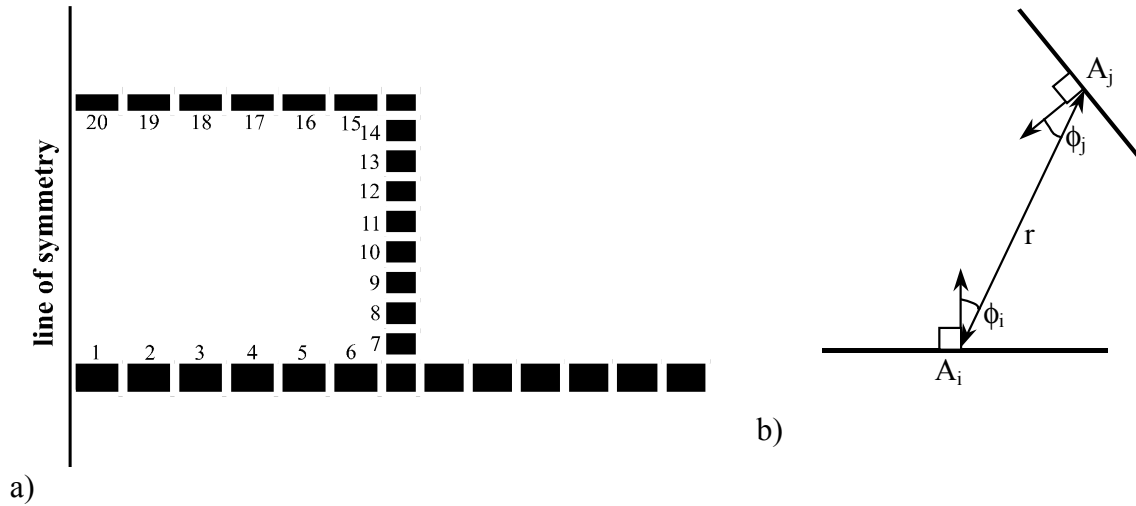
Figure 3:
a) Numbering of the surfaces composing the cavity
b) Radiative heat transfer between two surfaces

The thermal conductivity of the air and the heat transfer by convection in the cavity was neglected.

Cavity radiation is active when surfaces of the model can "see" each other, see Figure 3a). Such heat exchange depends on viewfactors that measure the relative interaction between the surfaces composing the cavity. The viewfactor F_{ij} between two surfaces A_i an A_j, see Figure 3b), is calculated as

$$F_{ij} = \int_i \int_j \frac{\cos\phi_i \cos\phi_j}{\pi r^2} dA_i dA_j, \quad F_{ij} = F_{ji}, \quad (4)$$

where r is the distance between the two areas and ϕ_i, ϕ_j are the angles between r and the normals to the surfaces of the areas. The viewfactor is a purely geometrical quantity. The symmetry line acts like a mirror, so that a radiation symmetry boundary condition could be implemented. In an ABAQUS® analysis the configuration factor is calculated and used specifying the radiative heat leaving the emitting surface and the radiative heat arriving at the receiving surface. According to ECCS Model code on Fire engineering [2] the configuration factor is calculated as

$$\Phi_{ij} = \frac{1}{A_i} F_{ij}, \quad \Phi_{ij} \neq \Phi_{ji}. \quad (5)$$

By definition, the configuration factor is between zero and unity. The configuration factors of the system are written in a matrix. In this example there are 20 surfaces composing the cavity, see Figure 3a), which leads to a 20 x 20 configuration factor matrix. This matrix can be used to control the accuracy of configuration factor calculation. In a completely enclosed cavity any ray from surface A_i in whatever direction it leaves the surface will reach another surface. Therefore the sum of each line in the matrix must be 1:

$$\sum_j \Phi_{ij} = \frac{1}{A_i} \sum_j F_{ij} = 1 \quad (6)$$

and the total sum of all lines must be the number of elementary surfaces composing the cavity, which in this example is 20.

The matrix of viewfactors (Equation 4) can be calculated from the configuration factor matrix using Equation 5 by multiplying the values in each line with the corresponding elementary surface area A_i. The resulting matrix must be symmetric, see also Equation 4.

The influence of heat transfer in the cavity is shown in Figure 4. The heating curves of the top and the bottom flange of the hat-profile are compared. The black curves show the results with and the grey curves without cavity radiation. Figure 5 illustrates the temperature gradients in the beam cross section without (a, c) and with cavity radiation (b, d) for fire duration of 30 and 90 minutes.
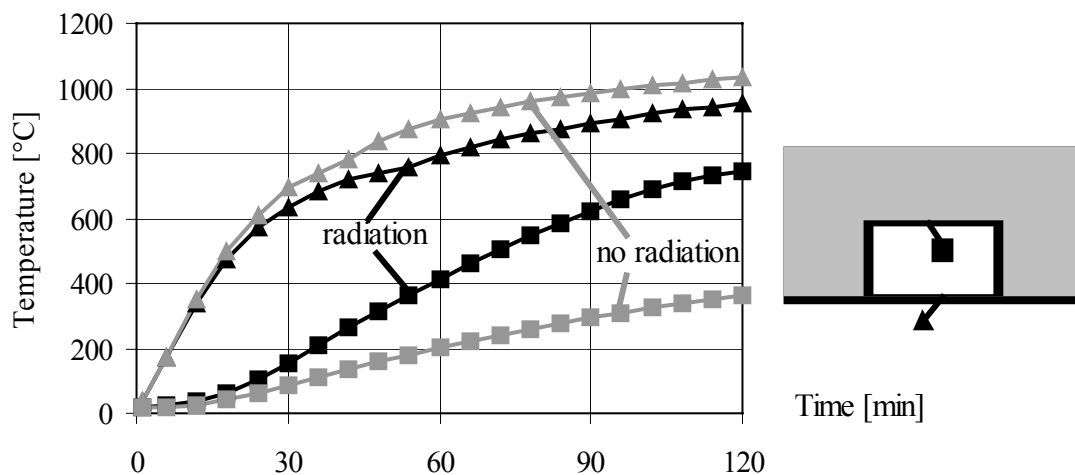
Figure 4:
Comparison of the heating curves of the bottom an the top flange
of the steel section with (black) and without (grey) cavity radiation

The effect of different assumptions concerning the radiation in the cavity is limited to the local area of the steel section. The concrete temperatures differ only marginally. As shown in Figure 4 the cavity radiation leads to dramatic higher temperatures in the top flange (black square) and lower temperatures in the bottom flange (black triangle). The different heating of the member causes a different performance of the load bearing capacity. This effect is discussed in detail in the following section.

Calculation of the load bearing capacity

Plastic theory has been used to determine the load bearing capacity. A level 2 approach was applied to calculate the bending and shear resistance. The temperature distributions were analysed using a self-made post-processing tool. The basis for the calculations are the temperature dependent mechanical material properties according to EC4-1-2 [8]. The calculation tool consists of a spreadsheet programmed in MS Excel®. The mean values of nodal temperatures related to each element are calculated and used to specify the temperature reduction factors k_t for the material strength.
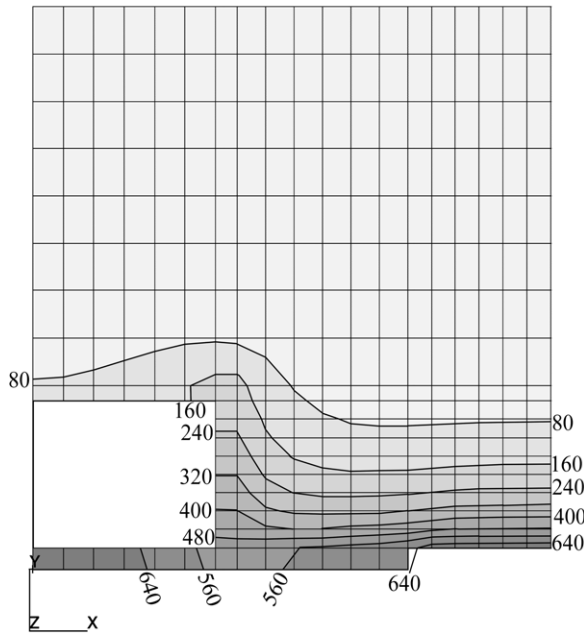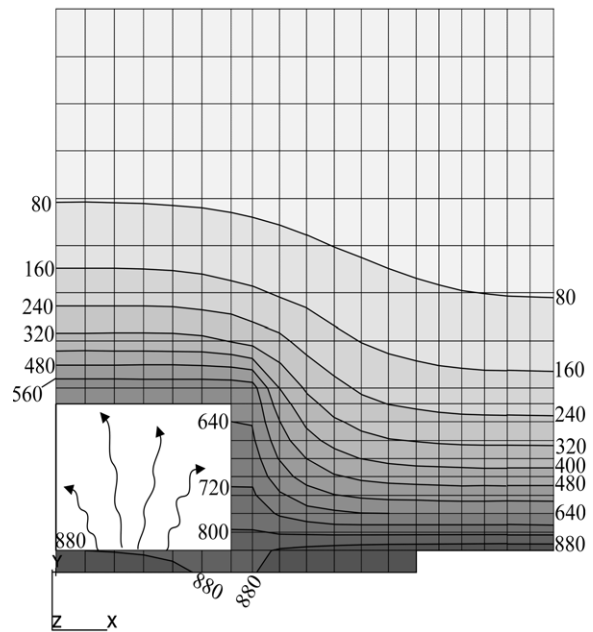
30 min, no radiation
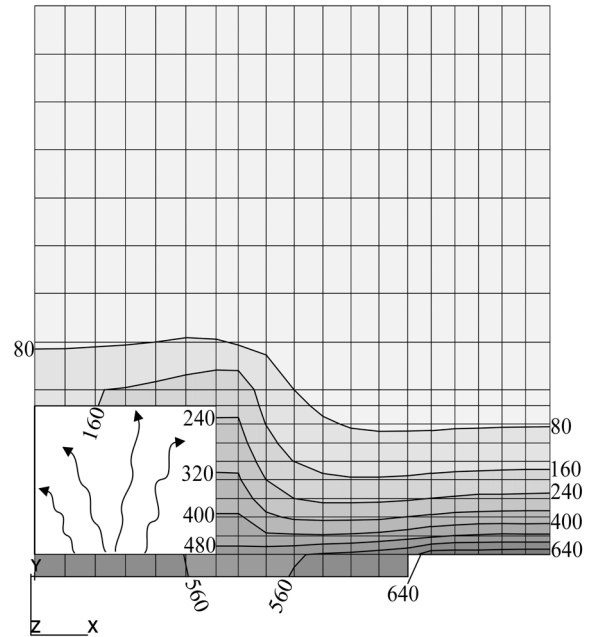
30 min, radiation
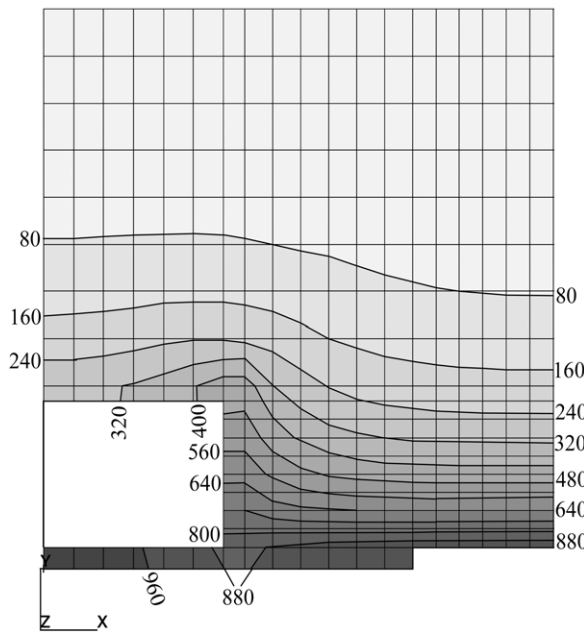
90 min, no radiation

90 min, radiation

Figure 5:
Temperature gradient in °C in the beam cross section
without (a, c) and with cavity radiation (b, d)

The plastic neutral axis is determined from

$$\sum_{s=1}^{n} A_s k_{max,\theta,s} \frac{f_{y,s}}{\gamma_{M;fi}} + 0.8 \sum_{l=1}^{m} A_l k_{c,\theta,l} \frac{f_{c,20,l}}{\gamma_{M,fi,c}} = 0, \quad (7)$$

where:

A_s, A_l are the elemental areas in the steel and concrete parts of the cross section.

$k_{max,\theta,s}$ is the reduction factor for the yield strength of steel related to the steel elemental area A_s.

$k_{c,\theta,l}$ is the reduction factor for the compressive strength of concrete related to the concrete elemental area A_l.

$f_{y,s}$ is the nominal yield strength f_y for the elemental steel area A_s and

$f_{c,20,l}$ the design strength $f_{c,20}$ of concrete at a temperature of 20°C for the elemental concrete area A_l. For concrete parts A_l tension is ignored.

$\gamma_{M,fi}, \gamma_{M,fi,c}$ are the partial safety factors for the material strength of steel and concrete in the fire design situation ($\gamma_{M,fi,} = \gamma_{M,fi,c.} = 1,0$).

The coefficient 0.8 is an additional reduction factor for the compressive strength of concrete. It is applied when calculating the bending moment capacity of composite slabs, using stress blocks without limiting the concrete strains. The plastic bending moment resistance is determined from

$$M_{fi,t,Rd} = \sum_{s=1}^{n} A_s z_s k_{max,\theta,s} \frac{f_{y,s}}{\gamma_{M,fi}} + 0.8 \sum_{l=1}^{m} A_l z_l k_{c,\theta,l} \frac{f_{c,20,l}}{\gamma_{M,fi,c}}, \quad (8)$$

where z_s and z_l are the moment arms of the steel and concrete elemental areas, measured from the centroids of the elemental areas. Only the vertical parts of the steel cross section forming the two webs are considered to calculate the transverse shear resistance of the beam:

$$V_{fi,t,Rd} = \sum_{s=1}^{n} A_s k_{max,\theta,s} \frac{f_{y,s}}{\gamma_{M,fi} \sqrt{3}}. \quad (9)$$

Table 1 shows the plastic load bearing capacities according to different fire resistance classes. It demonstrates clearly, that neglecting the radiation effect leads to unsafe results, in spite of higher temperatures in the bottom flange.

TABLE 1:
CALCULATED PLASTIC BENDING AND SHEAR RESISTANCE
WITH CAVITY RADIATION TAKEN INTO ACCOUNT
AN WITHOUT CAVITY RADIATION

			Fire duration [min]				
			0	30	60	90	120
radiation	$V_{fi,t,Rd}$	[kN]	434	421	255	103	49
	$M_{fi,t,Rd}$	[kNm]	498	393	252	125	65
no radiation	$V_{fi,t,Rd}$	[kN]	434	421	306	194	129
	$M_{fi,t,Rd}$	[kNm]	498	389	265	212	182

The influence of cavity radiation increases with higher fire resistance classes. This

performance is explained regarding the temperature gradients in Figure 5. After a fire exposure of 30 minutes the temperature in the bottom flange without cavity radiation is higher than that with cavity radiation (see also Figure 4), because there is no heat loss due to radiation. At this time the material strength of the bottom flange is of significant influence on the plastic bending resistance of the beam section. The influence of temperature and material strength of the top flange is not so important because the moment arm of the corresponding force is small compared to that of the bottom flange. Because of the lower temperatures in the bottom flange, the plastic bending moment capacity resulting from the calculation with cavity radiation taken into account is a little bit higher than calculated without cavity radiation (see Figure 6). For a fire exposure of 30 minutes neglecting the influence of cavity radiation produces conservative results.
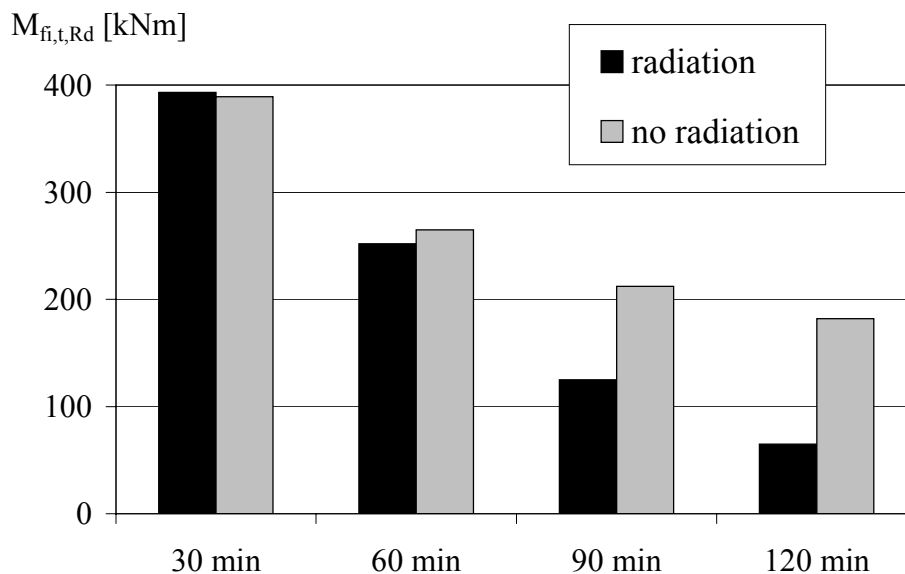
Figure 6:
Comparison between the calculated plastic bending resistance
with and without cavity radiation

The situation changes completely after 90 minutes of fire exposure. In both cases, with and without cavity radiation, the bottom flange has reached high temperatures and the material strength is reduced strongly. Therefore the strength of the bottom flange is of minor influence on the bending capacity. Now the temperature reduced material strength of the top flange is responsible for the bending resistance of the beam section. The plastic bending moment capacity calculated with cavity radiation is about 60 % of that calculated, neglecting the effect of radiation. The effect is even stronger for a fire exposure of 120 minutes. Neglect of radiation in the cavity leads to higher calculated resistance and therefore is unsafe for higher fire resistance classes.

Further calculations with cavity radiation were carried out to quantify the influence of the emissivity ε_{res} on the load bearing capacity. In one calculation the emissivity of the fire exposed surfaces and the interior surfaces of the cavity were increased to $\varepsilon_{res} = 0,70$ and in another case the emissivity was $\varepsilon_{res} = 0,80$. The second assumption corresponds to a new proposal discussed in the project team of Eurocode 4 part 1-2. Figure 7 shows a comparison of the resulting plastic bending moment resistance. It is obvious, that a higher emissivity leads to higher temperatures and as a consequence to lower load bearing capacities. For a fire duration of 30 minutes and an emissivity of $\varepsilon_{res} = 0,80$ the plastic bending moment resistance is reduced to 88 % of the value calculated with $\varepsilon_{res} = 0,56$. The reduction is even

stronger for higher fire durations. For instance after 90 minutes the bending moment capacity is reduced to 66 %.

$M_{fi,t,Rd}$ [kNm]
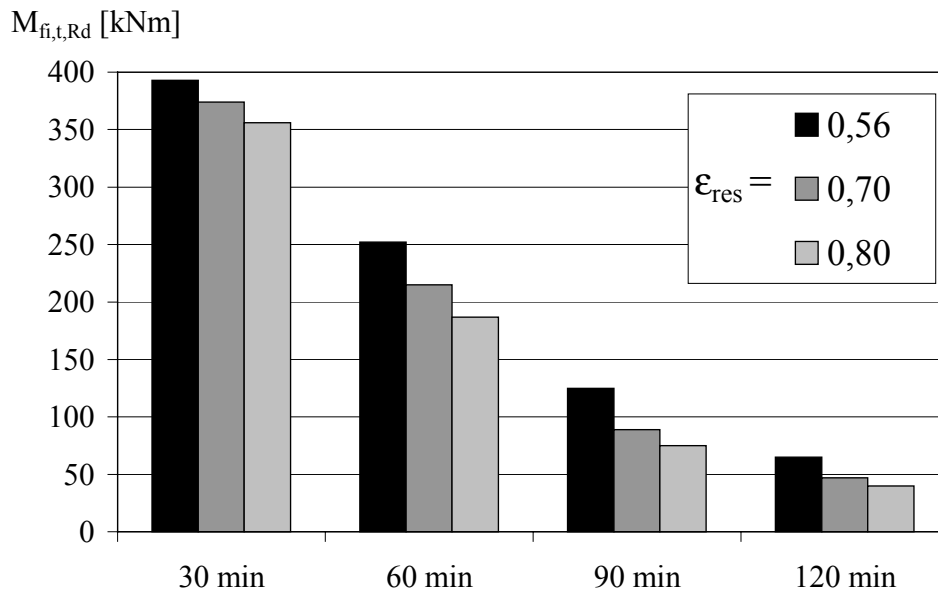
Figure 7:
Comparison of the plastic bending moment resistance resulting
from different assumptions for the emissivity ε_{res}

In general the demand for a higher value of emissivity results in more restrict requirements of the members, especially for higher fire resistance classes. It should be mentioned, that using the same value of emissivity for the interior surfaces as for the surfaces directly exposed to fire, is only an assumption. There is no regulation in the Eurocodes concerning this subject. Anyway it would be difficult to find a value for the emissivity in cavities, which is conservative for all possible types of applications. As shown in the example of Figure 6, considering the radiation in a cavity can be conservative or unsafe, depending on the duration of fire exposure.

Another aspect of the studies was to identify out the influence of different steel grades used for the UPE-profile and the flat steel to assemble the hat-profile. Three additional sections were studied supplementary to the section presented in Figure 1 (section 1). Based on this cross section only the steel grades were modified (see Table 2). Cavity radiation was considered with $\varepsilon_{res} = 0,56$. Table 2 illustrates that higher steel grades (especially for the flat steel forming the lower flange) lead to higher bending moment capacities at ambient temperatures.

TABLE 2:
STEEL CROSS SECTIONS AND BENDING MOMENT RESISTANCE
AT AMBIENT TEMPERATURES

	UPE-profile	Flat steel	$M_{fi,Rd,0}$ [kNm]
section 1	S 355	S 235	498
section 2	S 235	S 235	451
section 3	S 235	S 355	543
section 4	S 355	S 355	572

Figure 8 shows the bending moment resistances of the different sections under fire

conditions. For a comparison, the bending moment resistances are given in % of the corresponding values at ambient temperature.
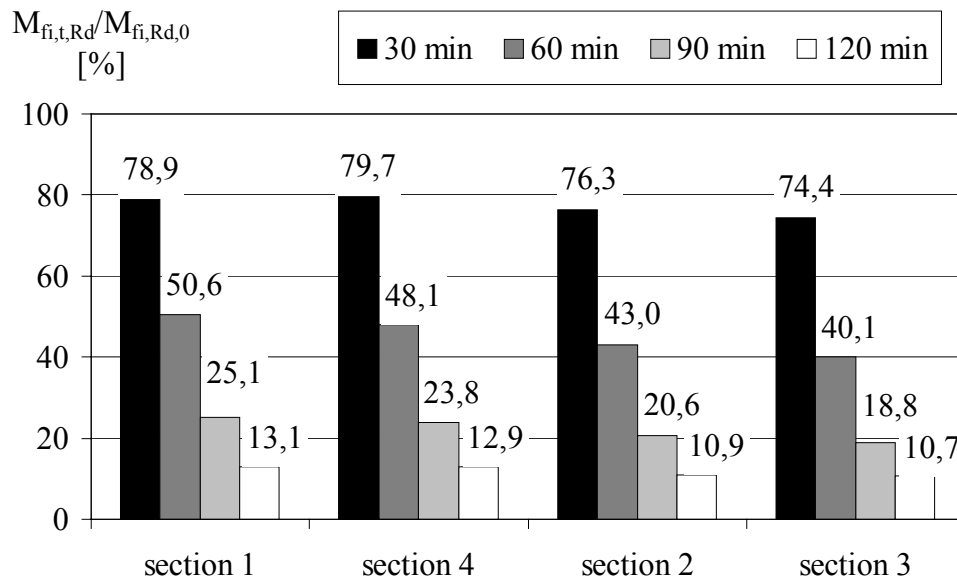
Figure 8:
Bending moment resistance for different fire duration in % of the
corresponding values at ambient temperature

Regarding the remaining bending moment resistance after certain duration of fire exposure, section 1 with a steel grade S355 for the UPE-profile and an S235 for the directly fire-exposed flat steel, shows the best performance. Section 4 with S 355 for both, the UPE-profile and the flat steel, ranges on the second position. This counts for all studied duration of fire exposure except 30 minutes. Compared to section 1 in section 3 the steel grades are inverted and now the directly fire-exposed flat steel has the higher steel grade. This leads to worse performance of section 3 compared to that of section one. This study shows that, concerning the bending moment capacity, a hat profile featuring a lower steel grade for the directly fire-exposed lower flange, shows a better performance in case of fire.

CONCLUSION

This paper deals with the application of general calculation models in structural fire design. Computer simulations enable new possibilities in assessing fire resistance of load bearing composite members.
The finite element modelling of the heating and its effects on the load bearing capacity of a new slim floor beam system are demonstrated and discussed. The cross section features a cavity and the radiative heat transfer in this cavity is of significant influence on the temperature development and as a consequence, on the load bearing capacity of the cross section. The emissivity of such cavity surfaces which are not directly exposed to fire is not regulated by the Eurocodes. In the presented example the same emissivity as for the directly fire exposed surfaces was assumed for the interior surfaces of the cavity. The calculations showed, that it would be difficult to find a value for the emissivity in cavities which is conservative for all possible types of applications. Neglecting the radiation in the cavity can be conservative or unsafe depending on the fire duration.

In general the demand for a higher value of the emissivity of fire exposed surfaces results in more restrict requirements of the members, especially for higher fire resistance classes.

ACKNOWLEDGEMENT

REFERENCES

[1] Hibbit and Karlsson and Sorensen Inc., ABAQUS[®] Theory Manual, Version 6.2, Pawtucket, USA, 2001

[2] ECCS (European Convention for Constructional Steelwork) – Technical Committee 3, Model Code on Fire Engineering, First Edition, May 2001

[3] Eurocode 1, Actions on structures – Part 1-2: General actions – Actions on structures exposed to fire, Final draft, August 2001

[4] Eurocode 1, Actions on structures – Part 2-2: Actions on structures exposed to fire, German version ENV 1991-2-2, May 1997

[5] National Application Document for Eurocode 1 Part 2-2 (Richtlinie zur Anwendung von DIN V ENV 1993-1-2), German Institute for Standardisation, Germany, September 1999, in German

[6] Eurocode 3, Design of Steel Structures – Part 1-2: General Rules – Structural Fire Design, Draft ENV 1993-1-2, July 1995

[7] National Application Document for Eurocode 3 Part 1-2 (Richtlinie zur Anwendung von DIN V ENV 1993-1-2), German Institute for Standardisation, Germany, September 1999, in German

[8] Eurocode 4, Design of composite steel and concrete structures – Part 1-2: General rules; structural fire design; German version ENV 1994-1-2:1994

[9] National Application Document for Eurocode 4 Part 1-2, (Richtlinie zur Anwendung von DIN V ENV 1994-1-2), German Institute for Standardisation, Germany, September 1999, in German

[10] Kuhlmann U. and Fries J. and Leukart M., Design of slim-floor beams with hat-profiles (Bemessung von Flachdecken mit Hutprofilen), Stahlbau Kalender 2000, Verlag Ernst & Sohn, Berlin, Germany, in German

[11] Wickström U. and Palsson J., A Scheme for verification of Computer Codes for Calculating Temperature in Fire Exposed Structures, SP Swedish National Testing and Research Institute, Fire Technology, SP Report 1999:36, Boras, Sweden

[12] CEN (European Committee for Standardisation), European prestandard, prEN1994-1-2:2000, Eurocode 4 – Design of Composite Steel and Concrete Structures, Part 1.2 : Structural Rules - Structural Fire Design, October 2001

ADVANCED ANALYSIS OF STEEL FRAMEWORK EXPOSED TO ACCIDENTAL FIRE

J.Y. Richard LIEW and K.Y. MA
Department of Civil Engineering, National University of Singapore
Blk E1A, 1 Engineering Drive 2, Singapore 117576
cveljy@nus.edu.sg

ABSTRACT

This paper describes the use of advanced analysis which accounts for both material and geometric nonlinearity to assess the performance of the steel structures exposed to natural compartment fire. The analysis requires only one line element per physical member of the structure to obtain a realistic representation of the global non-linear effects of the structure. The transient heat transfer is computed using a refined finite element mesh. The accuracy of the proposed advanced analysis is validated and its advantage over the conventional prescriptive approach in fire-resistance design is demonstrated. Natural fire curve is used in contrast to the ISO standard fire, representing the real fire development in the compartment. The simulation of natural fire time-temperature curve is according to the latest Eurocode prEN 1991-1-2 (released in July 2001) which provides a simplified but reasonable way to derive the parametric compartment fire curves based on several fundamental parameters such as fire load, ventilation factor and properties of surrounding surfaces. Performance-based assessments are carried out on 3D multi-storey frames subjected to natural compartment fire. The computed results are compared to those from the conventional approach based on ISO standard fire curve and the advantage of the advanced analysis is highlighted. The effect of fire load and ventilation on the structural response of the frames is studied and the worst fire scenarios are identified. The design implications on the requirement of fire protection are discussed.

KEYWORDS: *Advanced analysis, Eurocode parametric fire, fire resistance design, nonlinear analysis, performance-based design, plastic hinge, steel structures.*

INTRODUCTION

The use of standard ISO fire (ISO, 1992) and the prescriptive methods for fire resistance design provides only crude pointers to the actual performance of structures in fire. In reality, the individual components exposed to any fire are part of a larger structure, and a large part of which remains cold. The intact part of the structure supports the fire-weakened components. To design a structure safely and economically, it should be considered as a complete entity instead of a collection of isolated components. Moreover, the present prescriptive codes are limited to the type of structure where the influence of global instability is small. They may not be applicable for complex and flexible structures, such as the unbraced 3D frame with asymmetrical geometry and loading as studied in this paper.

Experiment-based fire research, as reported in Harris (1972) and ECCS (1993), was limited to certain types of structures. The long preparation, large expense and difficult operation of fire experiments raise the interest to develop advanced analysis techniques for studying the behaviour of steel structures in fire. Computational research wok has been carried out in the recent year to study the performance of steel structures at elevated temperatures (Saab and Nethercot, 1991; EI-Rimawi et al., 1995; Wang et al., 1995, Wang and Kodur, 2000; Bailey et al., 1999; Tang et al., 1999; Huang et al., 2000; Zhao, 2000; Toh et al., 2001; Wong, 2001). Liew et al (1998) applied the second-order plastic hinge analysis to study the global behaviour of semi continuous steel frames subjected to compartmental fires. The study was carried out over a wide range of parameters including various restraint conditions, buckling interaction between members and frames, spread of fire from one compartment to another, various fire scenarios, and different frame configurations. The fire model adopted by Liew et al. (1998) considered real fire loads, ventilation conditions, temperature delay effect of insulation material, and non-uniform heating of members.

In this paper, studies are carried out on a multi-storey unbraced frame structure to examine the effects of various fire scenarios on the overall performance of the structures. Advanced fire analysis is also carried out to investigate its sensitivity to non-symmetric heating under various load combinations. Design implications associated with the effects of compartment fires on multi-storey unbraced frame are discussed.

SIMULATION OF HEAT TRANSFER AND STRUCTURAL RESPONSE

In heat transfer analysis, the thermal effects on the structural elements are considered by subdividing the structural element into a number of quadrilateral heat transfer elements as shown in Figure 1. Heat conduction, heat accumulation and exchanges of radiation are calculated on the basis of the heat transfer element. A transformation of the "true" temperature state is required prior to the structural response calculation in order to represent the thermal expansion forces in a realistic manner. The temperature history in each structural member is first calculated. The equivalent nodal expansion forces for the line element are evaluated based on the incremental temperature change. The thermal effects on the structural element include reduction of yield stress, reduction of elastic modulus, and thermal expansion at elevated temperatures. Consistent nodal forces are produced on an elastic element at elevated temperatures due to the axial expansion and temperature gradient increment over the cross-section.
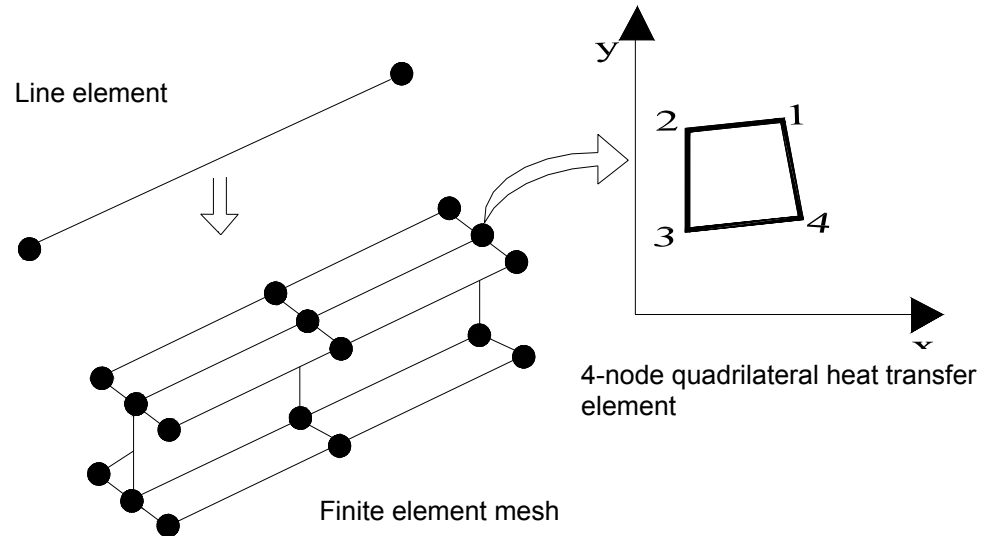
FIGURE 1: Re-meshing of line element to surface element for heat transfer analysis.

The structural response analysis is carried out using the beam-column plastic hinge approach (Liew and Tang, 2000). The element displacement fields are derived from the exact solution of the fourth order differential equation for a beam-column subjected to end forces (Liew et al., 2000). Material non-linearity is modelled by yield hinges at element mid-span and element ends. The yield hinge model, which is formulated according to the bounding surface plasticity concept, represents the inelastic cross section behaviour by considering the interaction of axial force and bi-axial bending. The initial yield surface is assumed to be a scaled down version of the bounding surface that is fixed in size and translates without rotation in stress-resultant space (El-Tawil and Deierlein, 2001). The gradual translation of the initial yield surface towards the bounding surface provides a smooth transition from initial yield to full plastification of cross section.

The initial yield surface and the bounding surface are allowed to contract at different rates reflecting the degradation of cross-section capacity due to increasing temperature. The temperature at the element's axis is taken as the reference point for determining the current values of yield strength and the modulus of elasticity. Verification studies were carried out on individual members and 2D multi-storey frames subjected to natural fire. The predicted results were found to agree well with the established results fire (Tang, 2001). The main focus of this paper is to extend the study to unbraced three-dimensional structure.

EUROCODE PARAMETRIC FIRES

The Eurocode (Draft prEN, 2001) has recommended equations for parametric fires, allowing a temperature-time curve to be produced for any combination of fire load, ventilations and boundary materials.

Equation for Heating Phase
The Eurocode equation for temperature T (°C) during the heating phase is:

$$T = 20 + 1325(1 - 0.324 e^{-0.2 t^*} - 0.204 e^{-1.7 t^*} - 0.472 e^{-19 t^*}) \tag{1}$$

where t* is the fictitious time given by

$$t^* = t.\Gamma \tag{2}$$

t is the time (hr) and

$$\Gamma = \frac{(O/b)^2}{(0.04/1160)^2} \tag{3}$$

where b = $\sqrt{\rho c \lambda}$ (J/m²s$^{1/2}$K) is the square root of thermal inertial of the boundary material of the compartment and O is the opening factor (m$^{1/2}$) given by

$$O = A_v \sqrt{h_{eq}} / A_t \tag{4}$$

A_v is the total area of vertical openings on all walls; h_{eq} is the weighted average of window heights on all walls and A_t is the total area of enclosure (walls, ceiling and floor, including openings).

In case of $\Gamma = 1$, equation (1) approximates the ISO834 standard temperature-time curve.

Duration of Heating Phase
Depending on whether the fire is fuel controlled or ventilation controlled, the duration of the heating phase t_{max} (hr) is given as:

$$t_{max} = MAX [(0.2x10^{-3}q_{t,d}/O); t_{lim}] \tag{5}$$

$q_{t,d}$ is the design value of the fire load per total surface area A_t of the enclosure. For slow fire growth rate, t_{lim} = 25 minutes; for medium fire growth rate, t_{lim} = 20 minutes and for fast fire growth rate, t_{lim} = 15 minutes. The advice on fire growth rate is given in Table E.5 in Annex E (Draft prEN, 2001).

In case of fuel-controlled fire, t_{max} is given by t_{lim} and if t_{max} is given by $(0.2x10^{-3} q_{t,d} /O)$, the fire is ventilation controlled. The introduction of t_{lim} is to avoid unrealistic very short fire duration when the ratio between the fire load and the opening factor decrease. Any object or fire load needs a certain amount of time to burn, even if there is unlimited presence of air (Franssen, 1997).

Fuel-Controlled Fire
When the fire is fuel controlled, i.e., $t_{max} = t_{lim}$, t* used in equation (1) is replaced by:

$$t^* = t.\Gamma_{lim} \tag{6}$$

with

$$\Gamma_{lim} = (O_{lim}/b)^2/(0.04/1160)^2 \text{ and } O_{lim} = 0.1x10^{-3} q_{t,d} /t_{lim} \tag{7}$$

The limiting opening factor O_{lim} is to slow down the fire in case of large openings and reduce the temperature level, because not all the air entering through the openings is used for combustion (Franssen, 1997).

When the fire is fuel controlled and large opening presents, the heat produced by the fire will be evacuated outside by mass transfer between the compartment and the exterior, which tends to further limit the elevation of the temperature in the compartment. To take this effect into consideration, a k factor is introduced (Franssen, 1997).

If O>0.04 and $q_{t,d}$ <75 and b<1160,

$$k = 1 + (\frac{O - 0.04}{0.04})(\frac{q_{t,d} - 75}{75})(\frac{1160 - b}{1160}) \tag{8}$$

and $\Gamma_{lim} = k(O_{lim}/b)^2/(0.04/1160)^2$

Equation for Cooling Phase

The temperature-time curve during the cooling phase is given by:

$$
\begin{array}{llll}
T = T_{max} - 625(t^* - t^*_{max}.x) & \text{for} & t^*_{max} \le 0.5 \\
T = T_{max} - 250(3 - t^*_{max})(t^* - t^*_{max}.x) & \text{for} & 0.5 < t^*_{max} < 2 \\
T = T_{max} - 250(t^* - t^*_{max}.x) & \text{for} & t^*_{max} \ge 2 & (9)
\end{array}
$$

in which
$t^* = t.\Gamma$
$t^*_{max} = (0.2 \times 10^{-3} \, q_{t,d} /O).\Gamma$
$x = 1.0$ if $t_{max} > t_{lim}$
$x = t_{lim}.\Gamma/ t^*_{max}$ if $t_{max} = t_{lim}$

Time- Temperature Curves

Figure 2 shows the parametric fire curves plotted for a range of ventilation factors, fuel loads and materials. Fire curves were produced for three fire loads and two types of construction, showing the significant dependence of fire temperature on the thermal properties of the bounding materials. The fire load are 400, 800 and 1200 MJ/m² floor area, for a room 5×5 m in plan and 3 m high. The materials are normal weight concrete (b = 1900 J/m²s$^{1/2}$K) and plaster board (b = 1033 J/m²s$^{1/2}$K).
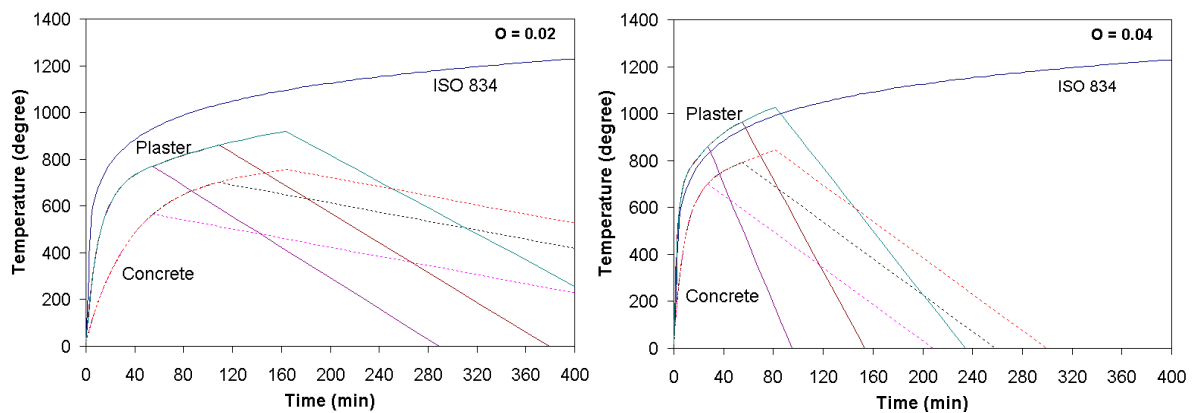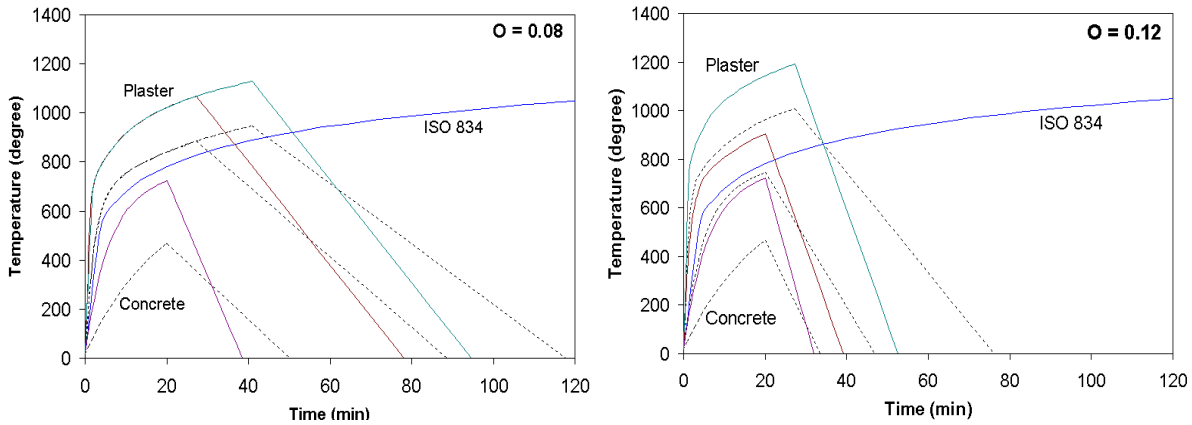
FIGURE 2: Parametric time-temperature curves (fuel load is 400, 800, 1200 MJ/m² floor area)

MODELLING OF FLOOR BEAMS EXPOSED TO FIRE

In the event of the beam being exposed to fire, the temperature distribution within the steel cross-section becomes non-uniform, with the top flange remaining considerably cooler than the rest of the cross-section due to the heat-sink effect of the concrete slab. The importance of the shielding effect of concrete floor slabs to the beam has been confirmed by the tests (Burgess et al., 1991). In this section, the behaviour of different beam models under fire conditions is compared between a bare beam exposed to uniform heating, a bare beam subjected to 3-side heating and a steel beam 3-side heated with concrete slab attached. The different beam models are illustrated in Figure 3.
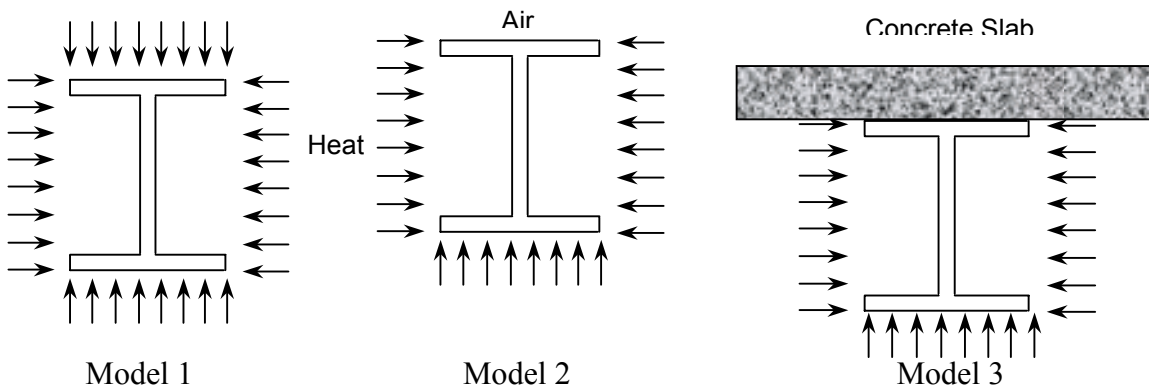
FIGURE 3: Different beam models under fire attack

The air temperature in model 2 is maintained at 20ºC and the heat dissipation from the top flange of the beam is mainly through radiation to the air. While in model 3, heat is dissipated through concrete by conduction at top flange. The purpose of studying these two models is to verify the suitability of using simplified model 2 in the analysis. The solid concrete slab is represented by 4-node quadrilateral elements in FAHTS, which have an equivalent mass as the solid. The beam web and sides of the concrete are further subdivided into a finer mesh to capture the temperature variation across the height.

A 6m span beam of 356 × 171 UB 51 kg/m Grade 43 steel section is considered and is subjected to a uniformly distributed load of 27.33 kN/m representing a load ratio of 0.5. All the beams are heated up at a rate of 10ºC per minute.

Figure 4 shows the time-deflection and temperature-deflection relationship for each beam model.
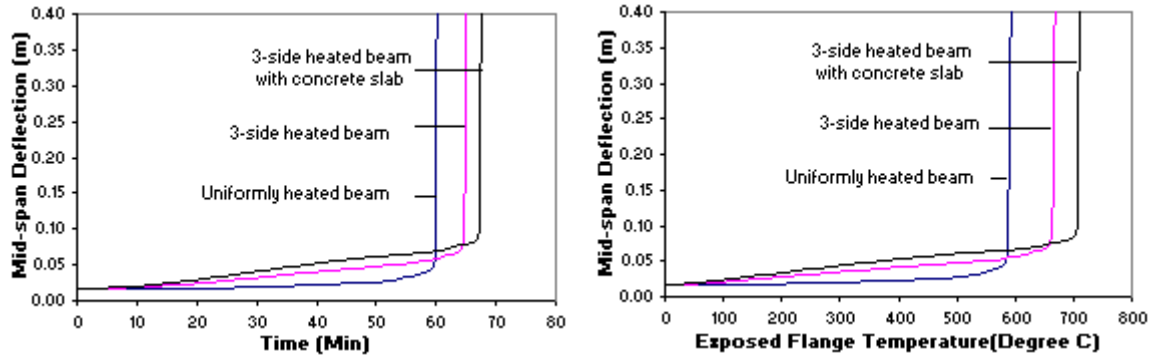
FIGURE 4: Time-deflection & temperature-deflection relationship for different beam model

Up to a temperature of about 500ºC, the uniformly heated bare beam shows very little change in deflection whilst that for the two 3-side heated beams increases steadily. This suggests that the effect of material softening in this temperature range is relatively small and that the deformation is largely due to thermal bowing effect resulting from differential thermal expansion over the cross-section of the non-uniformly heated beams. The beam with concrete slab has highest initial thermal bowing, as its temperature gradient over the cross-section is the largest.

At higher temperatures the deflection of all beams increases dramatically. For the beam attached with the concrete slab, because the slab is maintaining a lower temperature in the top flange of the beam, it loses strength and stiffness less rapidly than the bare beam. The effect of this is to delay collapse of the beam, which is typified by runaway deflection behaviour. A criterion based on a limiting deflection of span/20 (300mm in this case) is used to define failure, which is in general accordance with the definition of failure used in physical testing. Based on this criterion, the critical time and temperature at failure of 3 beam models are summarised in Table 1.

Table 1: Critical time and temperature of different beam models

	3-side heated beam with slab	3-side heated beam without slab	Uniformly heated beam
Critical Time	67 min	65 min	60 min
Critical Temperature	709ºC	667ºC	590ºC
Deflection at 500ºC	60.1mm	47.5mm	27.1mm

The beneficial effect of concrete slab is clearly demonstrated from above table. The critical temperature of the beam attached with concrete slab is 119ºC higher than that of the uniformly heated bare beam, an increase of about 17% and the critical time improves by approximately 10.5%. When comparing the two non-uniformly heated beams, the one with the concrete slab attached has a critical temperature 42ºC higher and the critical time is 2min higher. This may not seem a dramatic increase, but if the simplified model without slab is adopted based on the reason that no much increase in critical time is observed by modelling the slab, it will lead to non-conservative estimation of the deflection. By ignoring the presence of the slab, the deflection is underestimated by 21% at a temperature of 500ºC, and this order of discrepancy is too large to be neglected. Thus the more rigorous model is used for the subsequent case studies.

SIX-STOREY BUILDING FRAME

Figure 5 shows a six-storey unbraced space frame to be analysed under fire attack using the proposed advanced analysis. The building is classified as office building.
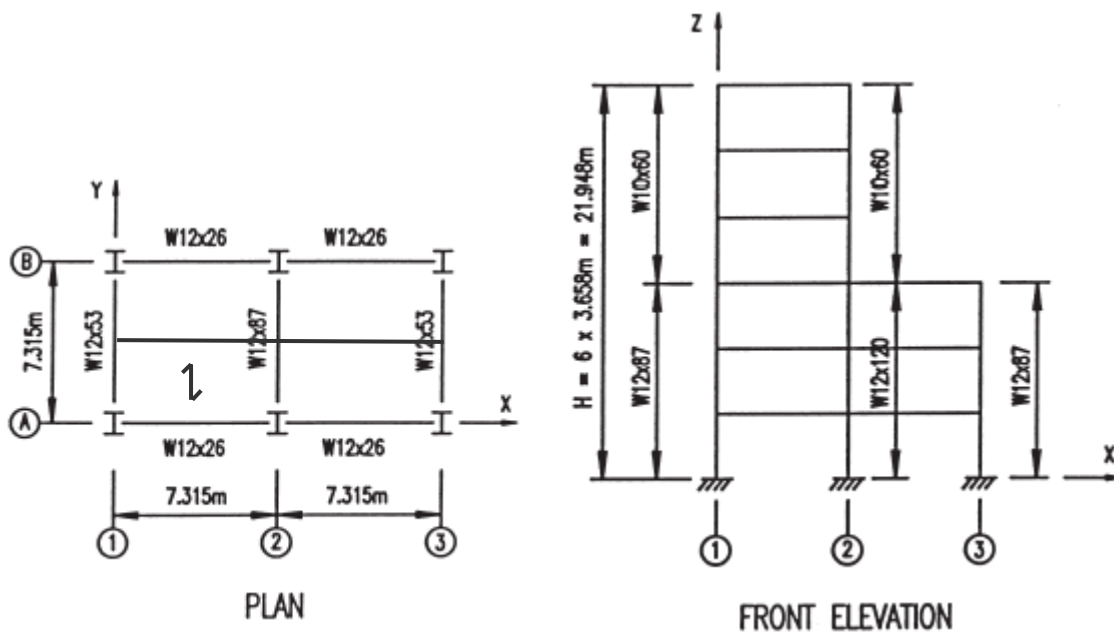
FIGURE 5: Six-storey space frame

Ultimate Limit State
The frame is designed for ultimate limit state at ambient temperature according to Eurocode 3. Various actions considered are:

Permanent actions G_k:	Dead load	3.6 kN/m^2
	Permanent imposed load	1.9 kN/m^2
Variable actions Q_k:	Variable imposed load ($Q_{k,1}$)	1.6 kN/m^2
	Wind load ($Q_{k,2}$)	593 kN (in Y-direction)

The worst combination of actions is found to be $1.35\Sigma G_k + 1.35\Sigma Q_k$. The size of beams and columns are indicated in Figure 5. A36 steel is used for all sections. In the advanced analysis, only main beams are modelled. The dead load is distributed to the main beams as uniformly distributed load and point load accordingly. Each beam is modelled using 4 elements and 1 element is used for column. Wind load is simulated by applying point load in Y-direction at every beam-column joint of the front elevation. The factored loads are proportionally applied until the frame collapse. A total of 20 plastic hinges are detected at the frame's limit load. The limit strength of the frame is reached at a load ratio of 1.044, suggesting that the size of beams and columns are adequate under ultimate limit state design.

Fire Limit State

At the fire limit state, which is treated as an accidental situation in Eurocode, the design effect of the actions is expressed as (BSI, 1994):

$$E_{fi,d,t} = G_k + \psi_1 Q_{k,1} + \psi_2 Q_{k,2} \tag{10}$$

Where ψ_1, ψ_2 are factors due to the probability of loads acting individually or in combination. Depending upon which variable load is the dominant action, two load combinations are possible under fire limit state:

Load combination 1: $E_{fi,d,t} = G_k + 0.5Q_{k,1} + NL$ (Notional Load)
Load combination 2: $E_{fi,d,t} = G_k + 0.3Q_{k,1} + 0.5Q_{k,2}$

In load combination 1, notional load is taken as 0.5% of the factored gravity load at each storey, applied in Y-direction and is distributed to the beam-column joints as point load. In both cases, the structure is subjected to gravity load or the combination of gravity load and wind load first, followed by the fire.

Fire Simulation

Parametric fire recommended in prEN 1991-1-2 is used to simulate the fire in the compartment by considering the type of building, floor layout, realistic fire load and possible fire fighting measures. Fire load density per floor area $q_{f,k} = 420$ MJ/m^2 is adopted for common office building (Draft prEN: Table E.4, 2001). The design fire load $q_{f,d}$ is defined as:

$$q_{f,d} = q_{f,k}. \, m. \, \gamma_{q1}. \, \gamma_{q2}. \, \gamma_n \tag{11}$$

m is the combustion factor and is assumed as 0.8; γ_{q1} is the partial factor taking into account the fire activation risk due to the size of the compartment. For floor area from 25 m^2 up to 250 m^2, γ_{q1} is equal to 1.5 (in this case the floor area A_f is 53.5 m^2). γ_{q2} is 1.0 for occupancies such as office, residence and hotel. It is assumed that no automatic fire suppression and detection system is installed but an off site fire brigade is available from which γ_n is calculated as 0.78. The design fire load $q_{f,d}$ is thus computed as 393 MJ/m^2, which is equivalent to 98 MJ/m^2 per total area ($q_{t,d}$). A plot of fire curves for a range of opening factors is shown in Figure 6.
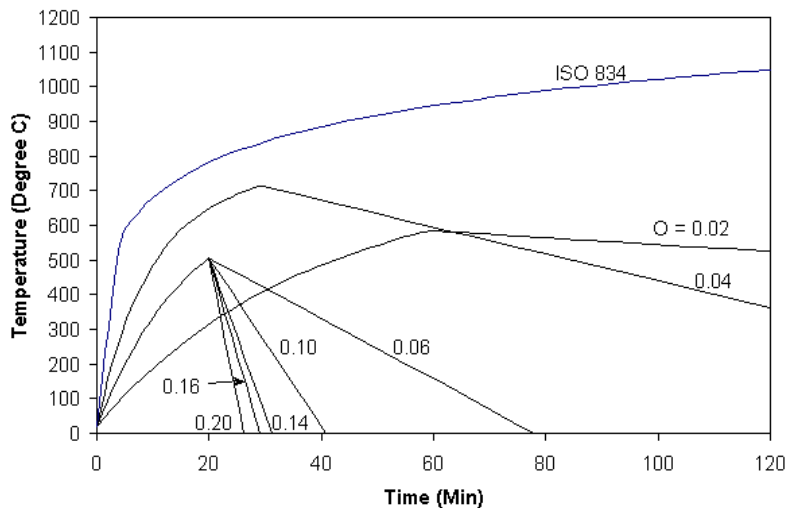
FIGURE 6: Parametric time-temperature curves for six-storey space frame

It can be seen from Figure 6 that all the fire curves for different opening factors are below the standard ISO 834 fire curve, providing the possibility of reducing passive fire protections. The fire at an opening factor of 0.04 corresponds the most sever fire scenario and this will be used in the subsequent analysis. Two compartments are considered as shown in Figure 7. The columns in compartment 1 are most heavily loaded and size of columns reduces starting from compartment 2.
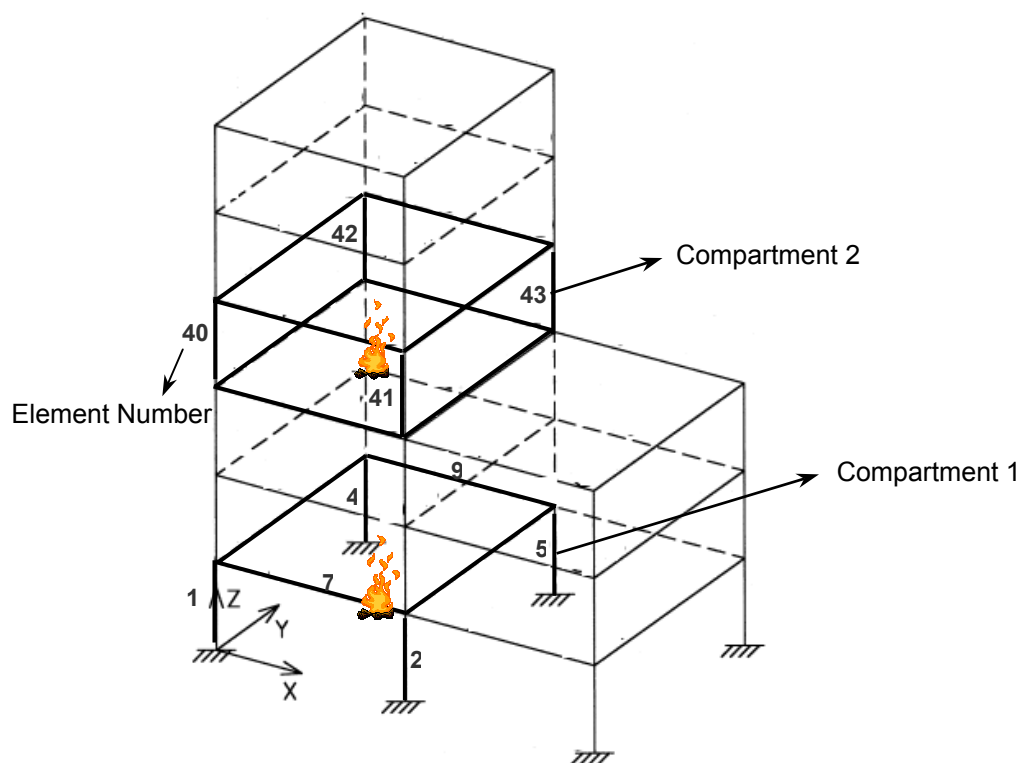
FIGURE 7: Fire compartments in 6-storey space frame

Fire at the First Storey Compartment

Case 1: All beams and columns are unprotected
It is found that load combination 2 is more critical as the structure fails at a critical time of 33.7 min while it can survive the fire attack under load combination 1. The deformed shape of the structure under fire for each load combination is shown in Figure 8.

Under load combination 1, as the beams expand under fire, column heads are forced to open up in both X and Y directions. When the frame is subjected to load combination 2, effect of wind load in Y-direction becomes pronounced, causing the frame to deform in a twisting mode. Despite the expansion of the heated beams, all columns (1, 2, 4 and 5) sway to the same direction as the wind load. The center of gravity of the frame thus shifts to the leeward columns (4 and 5), producing large axial force in the columns (Figure 9). It is the failure of the column 4 which triggers the collapse of the frame under fire.

Load Combination 1 (no collapse)   Load Combination 2
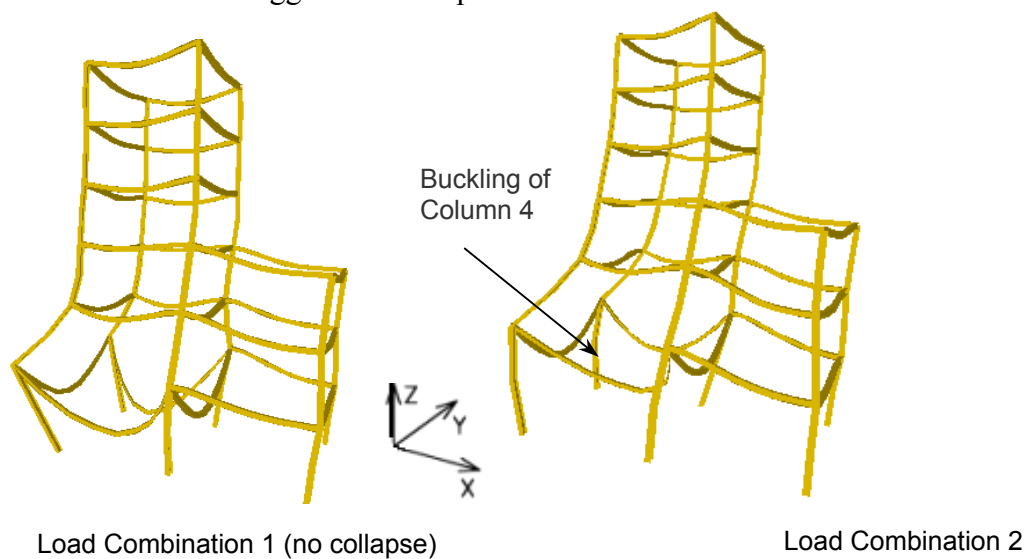
FIGURE 8: Deformed shape of 6-storey frame at fire
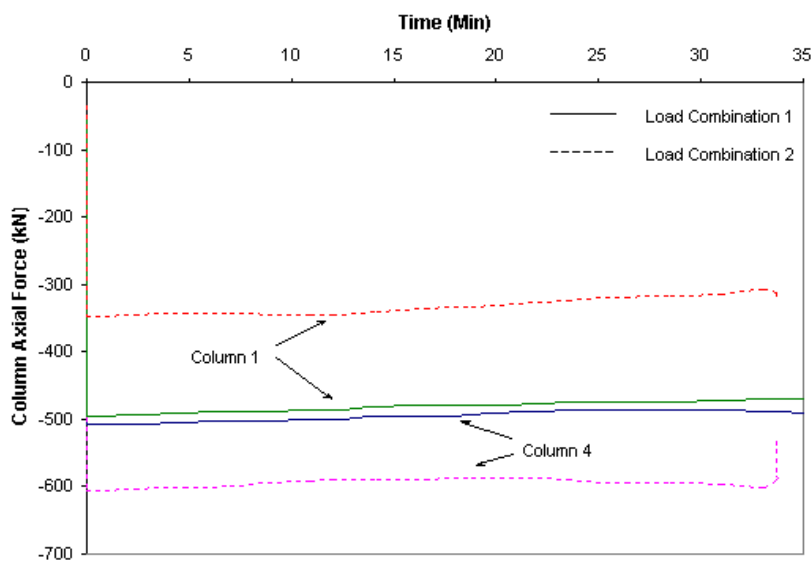
FIGURE 9: Column axial force under different load combinations

From Figure 9, it can be observed that the axial force in column 1 and 4 are almost the same under load combination 1, while there is about 250 kN difference between them when subjected to load combination 2 due to the shift of the center of gravity. The axial force in the leeward column 4 increases by 100 kN approximately.

Load combination 2 is found to be most critical, therefore subsequent analyses are carried out using only this load combination.

Case 2: Columns are protected and beams are unprotected

As columns are found to be the critical members, in case 2, all four columns are protected and assumed not to be affected by the fire. The displacement of the column head in Y-direction is greatly reduced (see Figure 10), in contrast to the runaway deflection of column 4 when approaching failure in case 1. However, the critical time has only marginal improvement, from 33.7 min to 35.5 min. In case 2, beam mechanism forms at beam 7 and 9 (the smallest beams) in X-direction due to large restraint force from intact columns (Figure 11), causing larger mid-span deflection as shown in Figure 12.
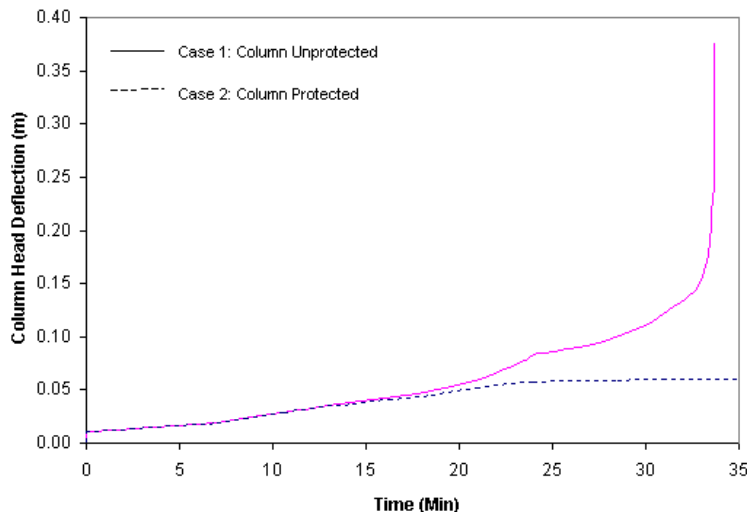
FIGURE 10: Column 4 head displacement in Y-direction at fire
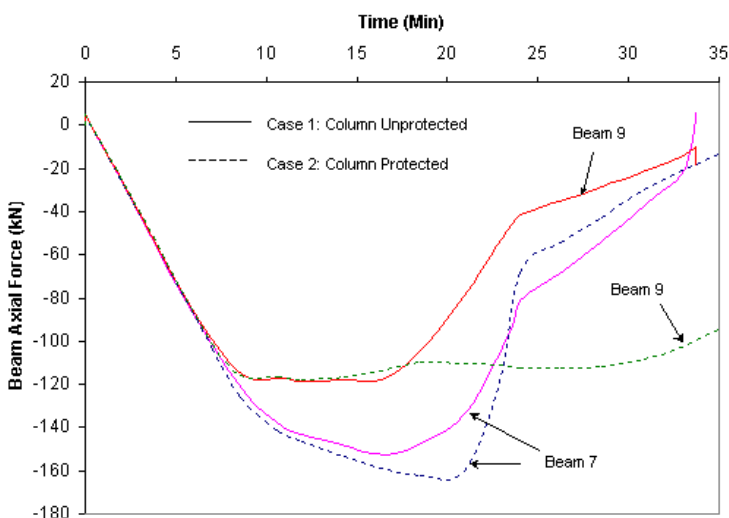
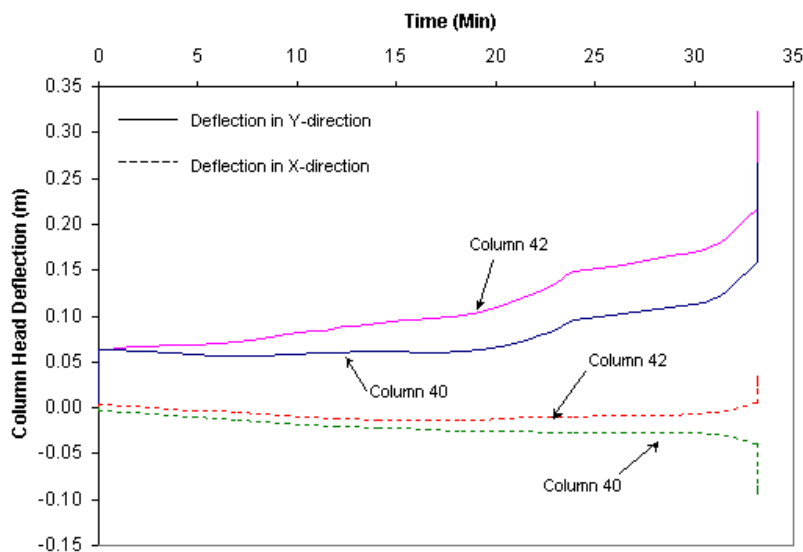**FIGURE 11: Beam axial force at fire**
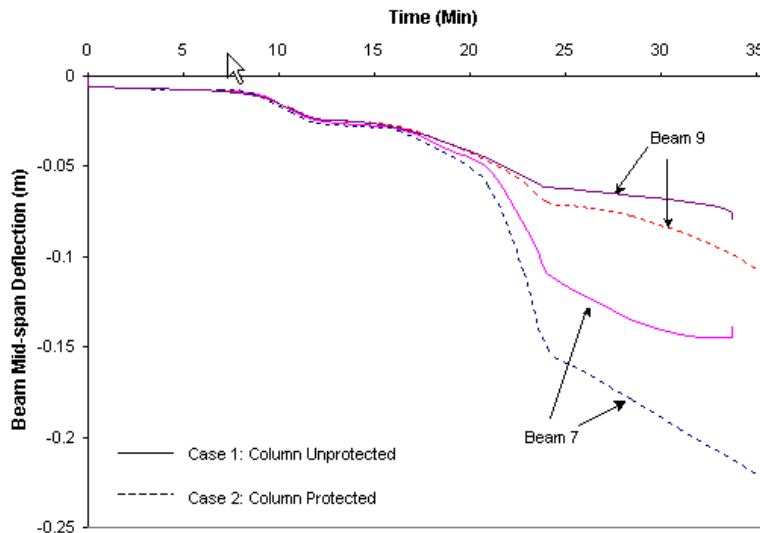
FIGURE 12: Beam mid-span deflection at fire

*Case 3: Columns and beam 7 & 9 are protected*
The next logical step is to provide fire protection to beams 7 and 9. In this case, the building survives the fire successfully with plastic hinges concentrated at beams in Y-direction.

Fire Occurs at the Fourth Storey Compartment
Fire is assumed to occur at the 4th storey's compartment as shown in Figure 7. When all the members are unprotected, extensive plastic hinges form at the four columns, triggering the collapse of the frame during the fire. Although the loading on the columns is smaller comparing to that on the first storey columns, the size of the columns is also smaller. At a critical time of 33 min, columns experience runaway deflections in both X and Y directions (Figure 13), symbolizing the failure of the columns. Figure 14 shows the axial force in windward and leeward columns. The shift of the center of gravity due to wind load produces larger axial force in the leeward column.

FIGURE 13: Column 40 & 42 head displacement in X and Y directions at fire (case 1)
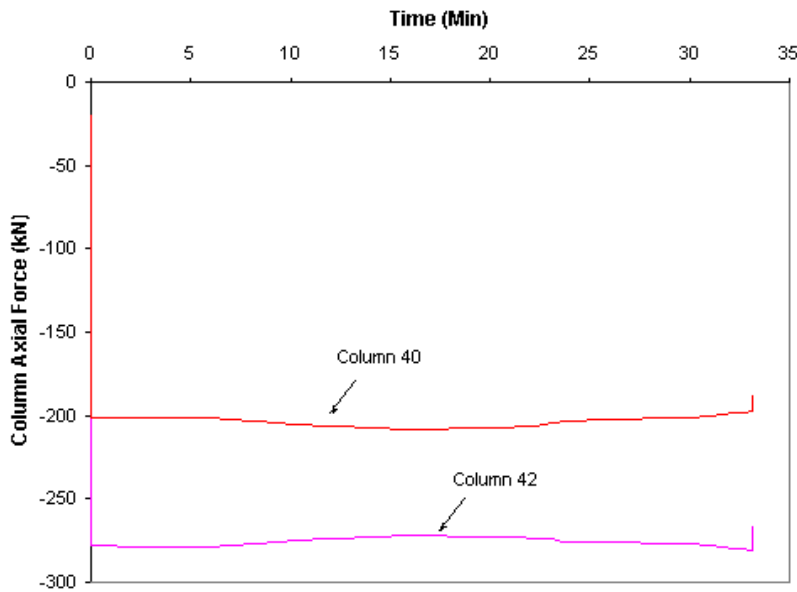
FIGURE 14: Column axial force at fire (case 1)

When all the columns are protected from the fire, no collapse of the frame occurs during the course of the fire. Fire protection is therefore not required for all the beams above the third storey.

Compartments Subjected to ISO Standard Fire

ISO 834 standard fire curve is used instead of parametric fire to carry out the same analysis on compartments 1 and 2. The results are summarized in Table 2.

Table 2: Comparison of critical time under ISO 834 and parametric fire

Load Combination 2		Critical Time (Min)	
		ISO 834	Parametric Fire
Compartment 1	Case 1	15.7	33.7
	Case 2	15.5	35.5
	Case 3	22.9	No Collapse
Compartment 2	Case 1	20.1	33.2
	Case 2	19.5	No Collapse
	Case 3	26.8	No Collapse

If a realistic fire model is considered, it is possible to reduce the fire protection and hence the cost. In the 6-storey space frame, columns and beams in X-direction require passive fire protection from 1st storey to 3rd storey. But from 3rd storey onwards, only columns need to be protected while all the beams can be left unprotected. However if ISO standard curve is used irrespective of layout of the building, fire loads and ventilation condition, all the members need to be fire protected as can be seen from Table 2.

Further study should be carried out on high-rise buildings where the savings in passive fire protection may become more significant if realistic fire is considered.

CONCLUSIONS

This paper illustrated how advanced analysis can be used in various situations to assess the performance of structures exposed to accidental fire. Parametric fire is useful for design if for compartment that is simple in geometry and layout. For complex problem, the CFD simulation model can be used to give detailed information with regard to fire and structural interaction and the heat, smoke, gas velocity and pressure distribution within the boundary of the affected zone.

Performance-based assessments were carried out on the multi-storey unbraced frame. The assessments were carried out based on a set of parameters considering various fire scenarios and passive fire protection of these structures was found to be unnecessary at some structural elements. The most distinctive feature of advanced analysis is that it can be used to predict the global behaviours of large structures subjected to fires. Direct relationship between the heating time and the fire resistance of the structure in term of its strength and stability can be established.

Improved understanding of the real behaviour of natural fire and buildings opens new ways of integrating fire safety and structural design. Prescriptive codes without considering the system's limit states behaviour are considered to be very approximate in nature. With the advance in computing technologies, there will be an increasing demand for robust and efficient nonlinear analysis methods for performance-based design of structures exposed to fire. The techniques presented herein are a step in this development.

REFERENCES

Bailey C. G., Lennon T. and Moore D. B. (1999), The Behaviour of Full-scale Steel-framed Building subjected to Compartment Fires, *Journal of the Structural Engineer*, Vol. 77, No. 8, pp. 15-21.

BSI (1994), *BS ENV 1991: Eurocode 1: Basis of Design and Actions on Structures Part1: Basis of Design,* British Standards Institution, London, UK.

Burgess I. W., Rimawi J. EI. and Plank R. J. (1991), Studies of the Behaviour of Steel Beams in Fire, *J. Construct. Steel Research*, Vol. 19, pp. 285-312

Chan S L and Chan B.H.M (2001), Refined plastic hinge analysis of steel frames under fire, *Int. J. of Structural and Composite Structures*, Techno-Press, 1(1), 111-130.

Draft prEN 1991-1-2 (2001), Eurocode 1: Actions on Structures Part 1-2: General Actions – Actins on Structures Exposed to Fire, European Committee for Standardization, Brussels.

ECCS (1993), *Fire safety in open car parks,* Modern Fire Engineering, Technical Committee 3, European Convention for Constructional Steelwork, Brussels, Belgium.

El-Rimawi J. A., Burgess I. W. and Plank R. J. (1995), The Analysis of Semi-Rigid Frames in Fire - a Secant Approach, *Journal of Constructional Steel Research*, Elsevier Science, UK, vol. 22, pp. 125-146.

El-Tawil, S and Deierlein G.G (2001) Nonlinear Analysis of mixed steel-concrete frames I: Element Formulation, *Journal of Structural Engineering, ASCE,* 127(6), 647-655.

Franssen J. M. (1997), Improvement of the Parametric Fire of Eurocode 1 Based on Experimental Test Results, *Fire Safety Science – Proceedings of the Sixth International Symposium*, pp. 927-938.

Harris L. M. (1972), *Survey of Fire Experience in Automobile Parking Structures in the United States and Canada*, Marketing Research Associate, Report January 1972, Published by the American Iron and Steel Institute, Washington D. C., USA.

Huang Z. H., Burgess I. W., and Plank R. J. (2000), Three-Dimensional Analysis of Composite Steel-Framed Buildings in Fire, *Journal of Structural Engineering*, ASCE, Vol. 126, No. 3, pp. 389-397.

ISO (1992), *Fire resistance tests- elements of building construction*, International Organization for Standardization, ISO-834 Part 1, Switzerland.

Liew J. Y. R. and Tang L. K. (2000), Advanced Plastic-Hinge Analysis for the Design of Tubular Space Frames, *Engineering Structures*, Elsevier Science, UK. 22(7), 769-783.

Liew, J. Y. R., Tang, L. K., Holmaas T., and Choo Y. S. (1998), Advanced Analysis for the Assessment of Steel Frames in Fire, *Journal of Constructional Steel Research*, Elsevier Science, UK, Vol. 47, No. 1-2, pp. 19-45.

Liew, J. Y. R., White, D.W., and Chen, W.F. (1994), Notional load plastic hinge method for frame design, *Journal of Structural Engineering*, ASCE, USA, vol. 120(5), May, pp. 1434-1454.

Liew, R J Y, H Chen, N E Shanmugam and W F Chen (2000), Improved nonlinear plastic hinge analysis of space frames. *Engineering Structures,* Elsevier Science 22, 1324-1338.

Saab H. A. and Nethercot D. A. (1991), *Modelling Steel Frame* Behaviour under Fire Conditions, *Journal of Engineering Structures*, vol. 13, No. 4 pp. 371-382.

SINTEF (1995), *Fire and Heat Transfer Simulations (FAHTS) of Frame Structures, Theory and User's Manual*, SINTEF Structures and Concrete, Trondheim, Norway.

Tang L. K. (2001), *Advanced Analysis for the Assessment of Steel Structure in Fire*, Ph. D. thesis, Department of Civil Engineering, National University of Singapore, Singapore.

Tang L. K., Liew J. Y. R. and Choo Y. S. (1999), *Advanced Analysis of Localised Fires In a Large-span Arched Framework*, Proceedings of Sixth International Conference on Steel and Space Structures, 2-3 September, 1999, Singapore, pp. 163-170.

Toh W. S., Tan K. H. and Fung T. C. (2001), Strength and Stability of Steel Frames in Fire: Rankine Approach, *Journal of Structural Engineering*, ASCE, Vol. 127, No. 4, pp. 461-469.

Wang Y. C. and Kodur V. K. R. (2000), Research Toward Use of Unprotected Steel Structures, *Journal of Structural Engineering*, ASCE, Vol. 126, No. 12, pp. 1442-1450.

Wang Y. C., Lennon T. and Moore D. B. (1995), The Behaviour of Steel Frames Subject to Fire, *Journal of Constructional Steel Research*, Elsevier Science, UK, vol. 35, pp. 291 - 322.

Wong M. B. (2001), Elastic and plastic methods for numerical modelling of steel structures subject to fire, *Journal of Constructional Steel Research*, Elsevier Science, UK, Vol. 57, No. 1, pp. 1-14.

Yao Z. P., Wang R. J. and Zhang X. J. (1995), *Heat Transmission*, Published by Beijing Science and Technology University, Beijing, P. R. China.

Zhao J. C. (2000), Application of the direct iteration method for non-linear analysis of steel frames in fire, *Fire Safety Journal*, Vol. 35, No. 3, pp. 241-255.

STRUCTURAL BEHAVIOUR AND DESIGN OF PARTIALLY FIRE-EXPOSED SLENDER STEEL COLUMNS

Yngve ANDERBERG
Fire Safety Design, P.O. Box 3061, SE-200 22 Malmö, SWEDEN
Yngve.anderberg@fsd.se

ABSTRACT

Practical experience of the behaviour of partially (along the horizontal circumference) fire-exposed "slender" columns ($\lambda > 0{,}75$) seems to be completely missing. Only results on "short" columns are presented in literature. Due to this lack of knowledge a theoretical study on partially fire-exposed steel columns was performed in a major project "Multi-storey Structures, Behaviour in Case of Fire" /1/ was carried out 1998-2001. This paper presents the main results from this analytical study on slender columns.

Comprehensive analyses performed with the software's Super-Tempcalc and Global Collapse Analysis (GCA) have shown that partially fire-exposed slender columns suffer considerably from a thermal gradient over the cross-section causing thermal bowing and increasing load eccentricity (see figure 4). The thermal moment caused by this cross-sectional gradient was found to be too large to be neglected. Exposure of about 50% of circumference was found to be the worst scenario for slender columns. It can be concluded that the collapse time will be reduced up to 75% at a load utilization degree of 60 %. At a load utilization of 25 % the reduction is "only" 35 % at 50 % exposure. Thus the fire resistance is also increasing by load utilization level.

The best way to avoid the negative influence of partial fire exposure between 20 and 100% is to avoid this kind of exposure for slender columns. Otherwise the passive fire protection must be designed to resist partial fire exposure. In the design of partially fire-exposed slender columns figure 8-11 can be used for load utilization levels 25-60% and a slenderness ratio up to 1.5.

In this study was also design methods of Eurocode 3 /2/ compared with non-linear FE-analysis (GCA) and fire test results with the following conclusions.

Design methods of beams and columns, e.g. according to Eurocode 3, were found to be too advantageous compared with GCA simulations. In computer simulations of fire tests the simplified design methods of Eurocode gave in all calculations better fire resistance than results from FE-software. This is for beams mainly due to the fact of using full plastic moment capacity and a design strength related to 2% strain in combination. Similar discussion can be made for columns.

KEYWORDS: *fire resistance, slender columns, Eurocode, computer simulation, software, fire test*

INTRODUCTION

In literature no full-scale fire tests on partially exposed columns of slenderness ≥ 0,75 ("slender columns") have been reported. Fire tests on partially exposed columns with slenderness < 0,75 ("short columns") have been performed but no negative influence on the load-bearing capacity compared with fully exposed columns have been observed /9/. This is mainly due to the fact that the tested columns have been too short to be seriously influenced by a bowing effect due to the thermal gradient over the cross-section. Computer simulations indicate that there may exist a considerable problem for slender columns partially fire-exposed along its circumference.

This paper describes the results of a theoretical study on partially fire-exposed steel columns performed in a major project "Multi-storey Structures, Behaviour in Case of Fire" /1/ which is a project financed by the Swedish board of Fire Research. The results are discussed and a design proposal is presented.

DESCRIPTION OF ANALYSES

Parameter Study for columns

A parameter study was carried out to analyse how different factors effect the load-bearing capacity for geometrical differences of fire:

- Fire exposure (ISO 834)
- Slenderness
- Axial load levels with different eccentricities
- Partially restrained elongation (not presented in this paper)
- Insulation (intumescent paint)

Simulation of fire tests

Simulations of fire tests were performed for verification of the non-linear Global Collapse Analysis (GCA) approach and corresponding, applicable design approach. Measured results from fire tests of unloaded and loaded steel columns and beams in terms of stress, strain and deformations are compared to the results from computer simulations of identical conditions. This concerns profiles that are exposed on all surfaces and cases where the degree of fire exposure vary.

Full scale fire tests of a beam and a fully exposed column conducted at Firto Borehamwood, U.K. 1984 /7/ have been simulated successfully.

PROPERTIES OF STEEL

The knowledge of thermal and mechanical properties are necessary in the thermal and structural analysis of fire-exposed steel columns. The temperature-dependence of the material properties are described in this section.

Thermal properties are essential to heat transfer calculations. These are, essentially, heat conductivity, heat capacitivity and thermal expansion, all of which vary with increasing temperature.

Stress-strain relationships (σ-ε curves) at elevated temperatures must be known to be able to calculate stress and deformations of fire exposed steel structures. Tension and compression strength and modulus of elasticity as function of temperature can be derived from σ-ε curves. All properties needed for computer calculations are taken from /2/

FIRE EXPOSURE

Definition of ~1/4, 1/2, ~3/4 and 1/1 fire exposure

In order to protect the exposed surfaces of the steel profiles, HEB300 and HEB200, a layer of intumescent paint (Hensotherm 4 Ks) is applied. This means that the temperature increase of the steel will be delayed and a fire resistance of about 50-60 minutes for 100% exposure and 40 % load is obtained. Four cases of partial fire exposure are studied viz. ~1/4 (19 %), 1/2 (50 %) , ~3/4 (83%) and 1/1 (100%), all defined as percentages of exposed surface for the profile HEB300. 19% exposure means that only the lower part of the bottom flange is exposed and the rest is not in contact with fire. This is arranged by surrounding the unexposed part with a material of concrete-type, which is illustrated in figure 1. 50% means that half of the profile is exposed and ~3/4 (83 %) means that only the upper part of the upper flange is not exposed to fire.

$$\sim\!1/4\ (19\%) \qquad 1/2\ (50\%) \qquad \sim\!3/4\ (83\%) \qquad 1/1\ (100\%)$$
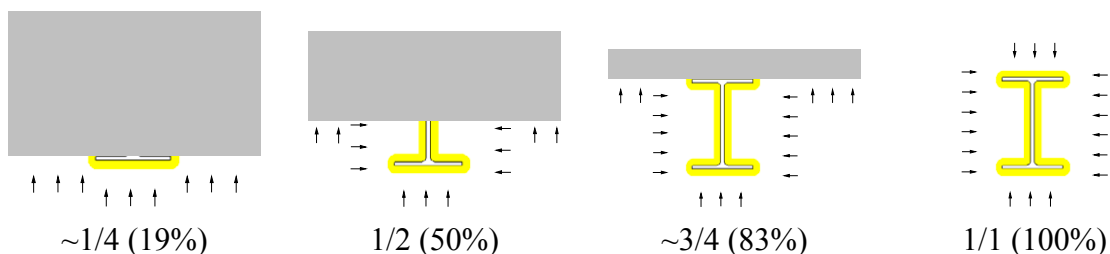
Figure 1   Four cases of fire exposure studied.
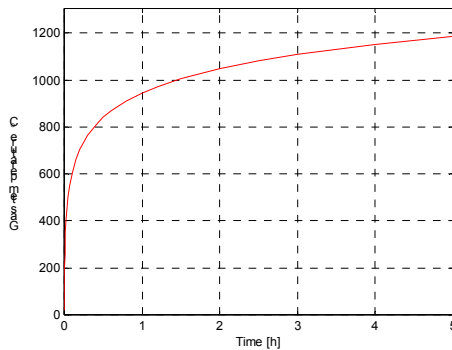
ISO 834 standard fire exposure

The standard ISO 834 time temperature development is described by

$$T(t) = 345 \cdot \log(480t + 1) + T_0 \qquad t > 0 \qquad\qquad (1)$$

where

t = time (h)
$T(t)$ = gas temperature at time t (°C)
T_0 = initial temperature (°C)

The time temperature development is presented in a chart in figure 2.

Figure 2   Time-temperature development of ISO 834 fire exposure /2/.

Boundary Conditions

The heat is transferred from the fire gases to the exposed structure through radiation and convection. The radiation, which dominates at high temperatures, is expressed by the resultant emissivity factor. The convection is calculated from the temperature difference between the structure and ambient gases, depending on the gas velocity. Resulting emissivity and convection factors used, are shown in table 1. These are in accordance with recommendations by ISO and Eurocode 1 /4/.

Emissivity/Convection	ε_r [-]	H_c [W/m^{2}K]
Exposed surface	0.56	25
Unexposed surface	0.8	9

Table 1   Resulting emissivity and convection factor for ISO 834 fire
            exposure /2/.

A boundary where no heat is allowed to pass ($q_n = 0$) is often referred to as an adiabatic boundary. These are for example symmetry lines.

MODELLING STEEL COLUMNS

Four magnitudes of slenderness have been studied, viz. λ = 1.5, 1.0, 0.75 and 0.5. Since the cross-section profile has been selected (HEB300) and the material parameters are determined, the corresponding lengths are 8.7 m, 5.8 m and 2.9 m respectively for a column restrained at the bottom and free at the top.

Steel cross-sections are generally divided into four classes depending on their ability to form a plastic hinge. The method is practically the same in all design codes; here the Eurocode version is represented.

Definition of Slenderness

Slenderness expresses the degree of sensitivity to the buckling phenomenon (flexural buckling), and links the strength, the length, the stiffness and the cross-section dimensions together. The slenderness ratio, λ, is defined in equation 2. The ratio relates the characteristic compression resistance, $N_{c.R}$, to the critical axial buckling force, N_{cr}, according to the Euler buckling theory.

$$\lambda = \sqrt{\frac{A \cdot f_y}{N_{cr}}} = \frac{l_c}{\pi i}\sqrt{\frac{f_y}{E}}$$

(2)

$$N_{c.R} = A \cdot f_y$$

(3)

$$N_{cr} = \frac{\pi^2 EI}{l_c^2}$$

(4)

where
l_c = buckling length of column

Equation 2 indicates the turning point between two different modes of failure. Values of λ exceeding 1.0 applies to a buckling failure mainly in accordance with equation 4 (flexural buckling). For lower values of λ the failure will be governed by the cross-sectional stress reaching the yield strength. Relating the loading to the characteristic compression resistance and making it a function of the slenderness ratio, the curve N_{cr}/N_{pl} shown in figure 3 will be obtained.

The following parameters are all affecting steel columns in one way or the other:

- initial out of straightness
- unintentional eccentricity
- secondary geometrical effects
- initial stresses
- plasticizing during the buckling process

Taking these effects into account, the principal reduction curve in figure 3 is obtained.
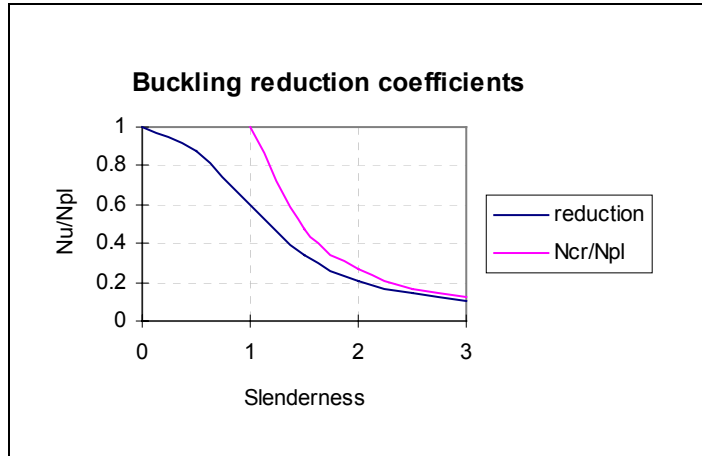
Figure 3   Load-bearing capacity for steel columns as a function of the slenderness ratio.

The reduction parameter in figure 3 is denoted χ. It is defined by the ratio between the characteristic buckling compression resistance and the characteristic plastic compression resistance (equation 5).

The characteristic buckling resistance of a compression member can be defined as:

$$N_{b.R} = \chi \cdot N_{c.R}$$

(5)

Slenderness and stiffness, defined as the product *EI*, are two essential parameters concerning columns. A decrease in stiffness will cause an increase in slenderness, and vice versa.

Eccentricities

Eccentricities as initial out of straightness and thermal bending will vary along the length of the column. These eccentricities influence the behaviour of fire exposed columns because it will implicate a moment due to the axial load in accordance with equation 6.

$$M = N \cdot e$$

(6)

The columns were modelled structurally with a geometrical eccentricity in the nodes to compensate for initial out of straightness, as indicated in figure 4. The initial out of straightness is modelled according to the first eigenmode with the maximum deflection taken as the system length divided by 400.

The difference in temperature over the cross-section implies a varying desire to expand thermally. The Bernoulli assumption states that the cross-section plane remains perpendicular to the beam axis during the progress of deformation. It is thus concluded that the beam axis must bend and a thermal eccentricity is obtained. The stress contribution from the moment will be superposed to the compression stress generated by the axial force. During the progress of the fire scenario the temperature gradient grows larger and the

"thermal eccentricity" is increasing continuously, with escalating stresses as a result, and finally the critical design strength will be attained. This is the reason why partial fire exposure is so critical to a column's load-bearing capacity and thus needs to be investigated thoroughly in order to determine the most appropriate approach of design. Presuming a structural model as showed in figure 4 the total thermal eccentricity, e_{th}, is indicated.
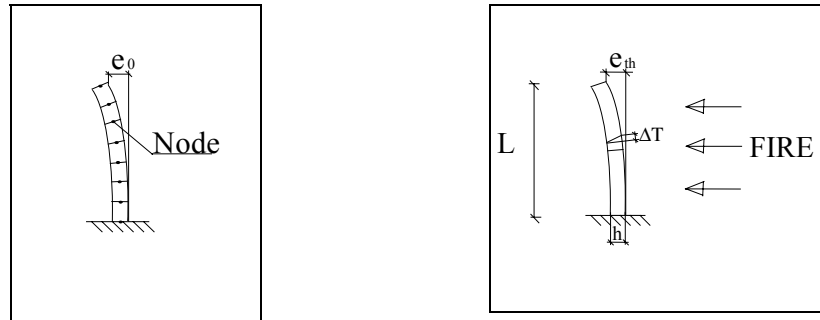
Figure 4 **Structural model of studied columns. Lower end fixed, upper end free. Initial eccentricity modelled in the nodes.** **Indication of thermal eccentricity, ε_{th}, descending from the temperature difference between the flanges, ΔT, caused by partial fire exposure.**

Degree of Loading

The degree of loading is taken as a percentage of the characteristic buckling resistance load in the fire state, represented by the expression defined in equation 2. Appropriate magnitudes of relative loading were found to be 25%, 40%, 50% and 60%. Supplementary analyses were done with a relative loading between 0-80% (see table 1).

Slenderness λ	~0	0.5	0.75	1.0	1.5
Column length	(0.3 m)	2.37 m	3.56 m	4.74 m	7.11 m
0 % load	-	-	-	0 MN	-
25 % load	1.39 MN	1.23 MN	1.03 MN	0.80 MN	0.45 MN
40 % load	2.23 MN	1.96 MN	1.66 MN	1.28 MN	0.71 MN
50 % load	2.78 MN	2.45 MN	2.07 MN	1.60 MN	0.89 MN
60 % load	3.34 MN	2.95 MN	2.48 MN	1.92 MN	1.06 MN
70 % load	-	-	-	2.24 MN	-
80 % load	-	-	-	2.56 MN	-

Table 2   Applied degrees of loading for HEB 300 column and steel with a characteristic strength of 390 MPa.

THERMAL ANALYSIS

The information about thermal properties, boundary conditions and fire exposure are essential when calculating nodal temperatures as function of time during a specified fire scenario:

The key engineering tool in this analytical procedure is the finite element temperature calculation program, Super-Tempcalc /6/, which facilitates calculations of heat transfer, temperature redistribution and temperature development in modelled materials. The features and background theory of Super-Tempcalc are described in detail in section 5.

The difference between the four cases is the modelling technique in the temperature simulations. Figure 5 illustrates how ~1/4, 1/2, ~3/4 and 1/1 exposure are being modelled in the temperature calculation.

1/1 (100%) ¼ symmetry	~3/4 (83%) ½ symmetry	1/2 (50%) ½ symmetry	~1/4 (19%) ½ symmetry
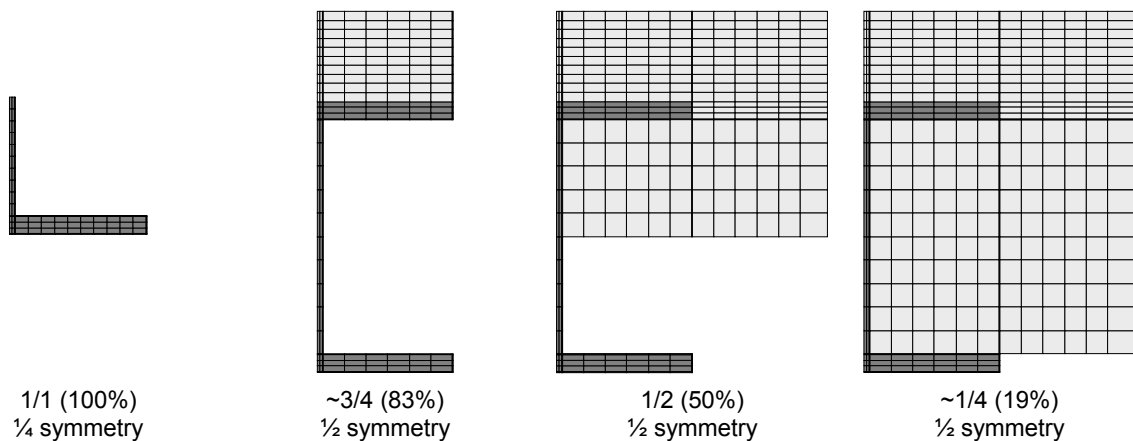
Figure 5   Modelling of the four fire exposure degrees (insulation alternatives). Exposed steel is insulated with intumescent paint.

Super-Tempcalc

Super-Tempcalc /6/ is a fire-adapted two-dimensional finite element program developed by FSD for use on personal and mainframe computers. It is a further development of Tempcalc, originally developed in 1985.

The program is widely used in the field of passive fire protection, and as part of structural analysis, in buildings and on offshore platforms. It is accepted for North Sea applications by a number of countries and organisations.

The program solves the two-dimensional, transient, heat transfer differential equation,.incorporating thermal properties that vary with temperature. The program allows the use of rectangular or triangular finite elements, in cylindrical or rectangular co-ordinates. Heat transferred by convection and radiation at the boundaries can be modelled as a function of time. Structures comprising several materials can be analysed and the heat absorbed by any existing void in the structure is also taken into account. Falling off of boards attached to structural members and spalling of concrete of concrete-based material can be simulated.

When the geometry is changed the calculation stops and the new geometry is automatically updated and the calculation continues.

Results from Thermal Analyses

The steel profile has been subjected to a heat transfer calculation for a given fire scenario, resulting in a cross-sectional temperature gradient over time. The temperature development of the profile denotes an essential input data for the subsequent global collapse analysis. Gradients over the HEB 300 profile height can be found for the four different exposure alternatives in figures 6 – 7.
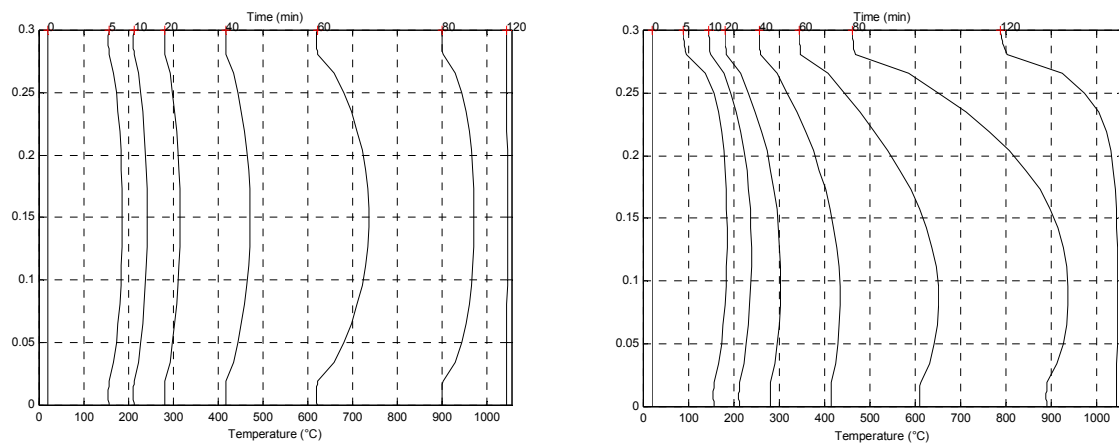
a)   b)

Figure 6   a) 100 % and b) 83 % fire exposure. Temperature gradient along the height of the HEB300 profile after 0, 5, 10, 20 40, 60, 80 and 120 minutes.
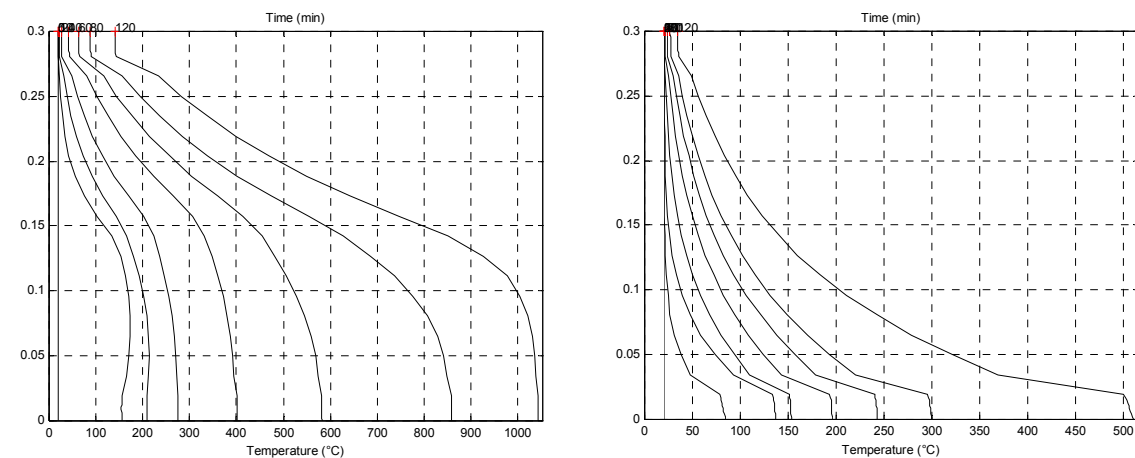
a)   b)

Figure 7   a) 50 % and b) 19 % fire exposure. Temperature gradient along the height of the HEB 300 profile after 0, 5, 10, 20 40, 60, 80 and 120 minutes.

327

SOFTWARE FOR STRUCTURAL ANALYSIS

The results of the thermal analysis are incorporated in the structural ditto for computerised prediction of structural stability. Elevating temperatures affect the steel by reduced strength and modulus of elasticity, stress-strain relationship and the ability to expand thermally.

The main tool for current analyses has been the program Global Collapse Analysis. Comparisons of tests have been done with the software Fire Design, the beam and column tools integrated in TCD/7/.

Columns differ significantly from other structures, being subjected to effects from instability. This means that failure generally occurs from the axial load reaching the critical load, and not from the cross-sectional strain attaining the yield limit. The primary task of a column is generally to transfer loads vertically down to the foundation, i.e. columns in structures are carrying axial loads. This makes the column a very essential part of a structure.

Global Collapse Analysis (GCA)

In some elastic solid mechanics problems the governing differential equations are linear and with a linear form of stress-strain relationship. However, in fire-related structural problems the linearity of constitutive relations is not preserved. The problem is actually a combination of material non-linearity together with geometrical non-linearity.

Global Collapse Analysis (GCA) is a finite element program providing computer prediction of the structural behaviour of load-bearing systems.

Essential input to the program comprise:

- cross-sectional geometry
- cross-sectional time-temperature fields from thermal analysis
- geometry (column and beam geometry)
- boundary conditions (rigidity, external attachments)
- material data (steel strength, variation of stress-strain relationship)
- external loads

GCA is integrated with the temperature calculation program Super-Tempcalc, thus incorporating steel temperature field data versus time of the adopted fire scenario.

The overall stability of a structure, due to a local fire, can be analysed and global progressive and local collapse respectively, can be predicted. Upgrading of identified separate critical members provides possible extension of initially calculated fire resistance time.

Generation of restraint stresses and strains, due to rigid external connections combined with the thermal expansion in the steel, makes the model reasonably accurate.

Results in terms of stresses, strains, cross-sectional stiffness, deflections, displacements, forces and moments may be presented at selected times through out the fire scenario. The 2-dimensional Bernoulli beam element with 6 degrees of freedom is used in the finite element

model. The kinematical assumption of this element is that plane sections normal to the beam axis remain plane and normal to the beam axis during the deformation.

TCD - FIRE DESIGN

FIRE DESIGN is a set of structural fire design tools that are interfaced with SUPER-TEMPCALC in the application TCD (Temperature Calculation and Design) /7/. The tools are SBEAM, CBEAM and COMPRES. The governing equations and the background theory for the calculations undertaken in FIRE DESIGN are outlined in this section. Output from SUPER TEMPCALC provides the essential heat transfer data upon which the FIRE DESIGN calculations are based. The design principals follow the intentions in the Eurocode documents ENV 1991-1-2 /4/, ENV 1992-1-2, ENV 1993-1-2 /2/ and ENV 1994-1-2 /3/.

SBEAM

For beams and slabs no second order geometry effects apply and thus the load bearing capacity (moment capacity) of a member can be calculated solely by studying the cross-section and its temperatures and strength relations.

SBEAM calculates the moment capacity of fire exposed structural steel beams in the ultimate limit state. Steel is an isotropic material with equal tensile and compressive properties. Hence the plastic sagging bending moment capacity of a beam is calculated based on the tensile capacity at elevated temperatures in the lower part of the beam cross-section and similarly the compressive capacity in the upper part.

COMPRES

COMPRES calculates the plastic yield compression resistance, critical Euler buckling load and design load of fire exposed structural steel compression members in the fire limit state in accordance with the guidelines in Eurocode 3 and 4 /2, 3/. Each individual material is accounted for by considering its contribution to the overall strength and stiffness of the composite structure.

STRUCTURAL ANALYSIS

### Structural Behaviour for Partially Exposed Columns

The behaviour and collapse mode of partially exposed columns have been studied in 80 computer simulations with centric loading. In the simulations of no eccentricity, the combinations of percent exposed area, slenderness and axial load are presented in figures 8 – 11. In these tables the times at collapse obtained from the GCA-analysis are presented.

The fire exposure was 120 minutes ISO 834. Modelled steel profile was HEB 300 that was insulated with 0.93 mm of intumescent paint in order to extend the overall time to collapse for the purpose. Structural steel with a yield strength of 390 MPa was chosen. The degree of loading in the fire limit state is expressed as a percentage of the characteristic buckling compression resistance load at room temperature.

From the figures 8-11 it can be observed that minimum time for collapse occurs at about 50% of partial exposure with a slenderness exceeding 0.5. The reason for this exception is that virtually no buckling occurs but only axial compressive stresses arise. However, the thermal gradient causes thermal bending and an extra eccentricity for the axial load. Due to that the horizontal deformation and the eccentricity increases when exposed area decreases from 100 % to 50 %. This means that partial exposure causes much earlier collapse of the column compared with full exposure. The fire resistance is furthermore decreasing with increasing load. These figures can be used in the design or redesign of partially fire-exposed slender columns.
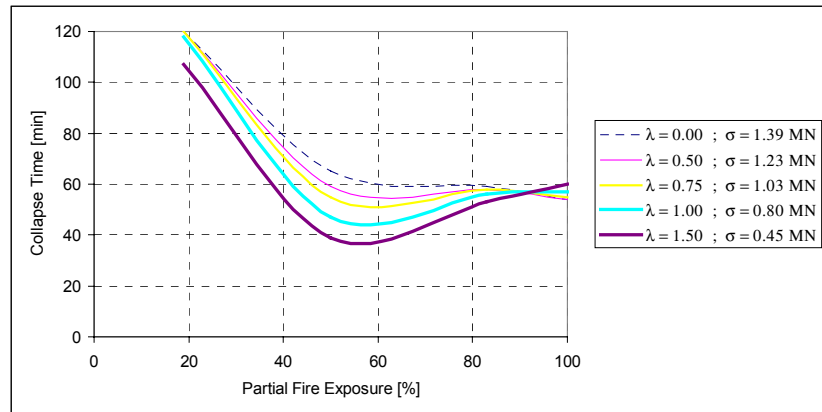
Figure 8   Calculated column fire resistance times with a degree of loading of 25%.
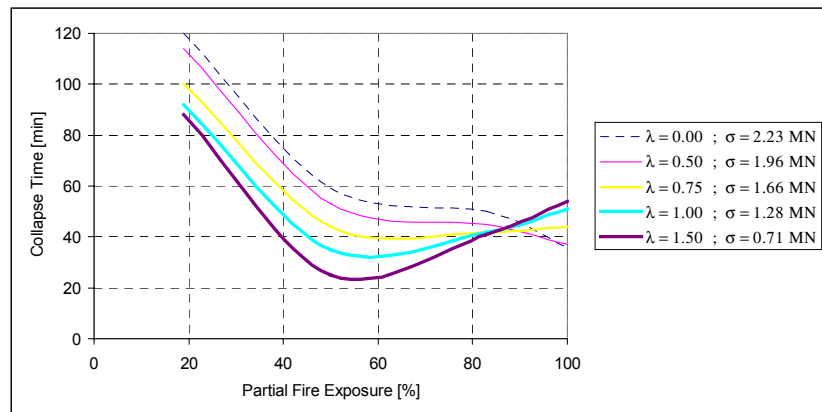
Figure 9   Calculated column fire resistance times with a degree of loading of 40%.

330
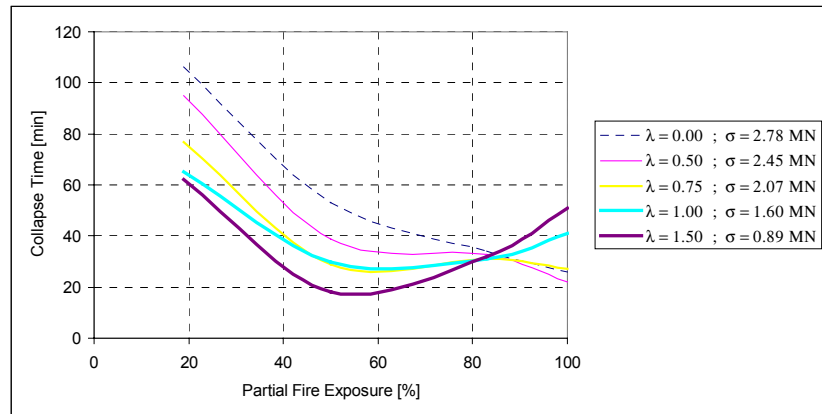
Figure 10   Calculated column fire resistance times with a degree of loading of 50%.
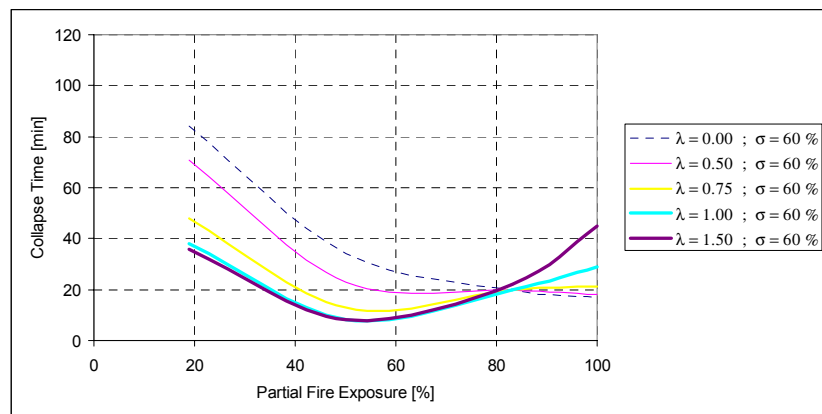
Figure 11   Calculated column fire resistance times with a degree of loading of 60%.

Fire tests and computer simulations – A comparison

Computer Simulation of Steel Column Fire Test Conducted in UK

A full scale fire test on a steel column exposed to fire on 100 % of the profile circumference that was tested at Firto Borehamwood, U.K. in 1984 /9/ has been simulated (see Figure 12). The test will be referred to as fire test 41. The column has an exposed length of 3 m. The temperature as function of time over the cross-section has been calculated by Super-Tempcalc. The fire exposure curve has been taken from documented readings during the tests and has been used in the calculations. The temperature for the 100 % exposure is presented in figure 13a where measured and computed temperatures are compared for the exposed web and unexposed flange respectively. The agreement between calculated and measured temperatures is considered adequate.
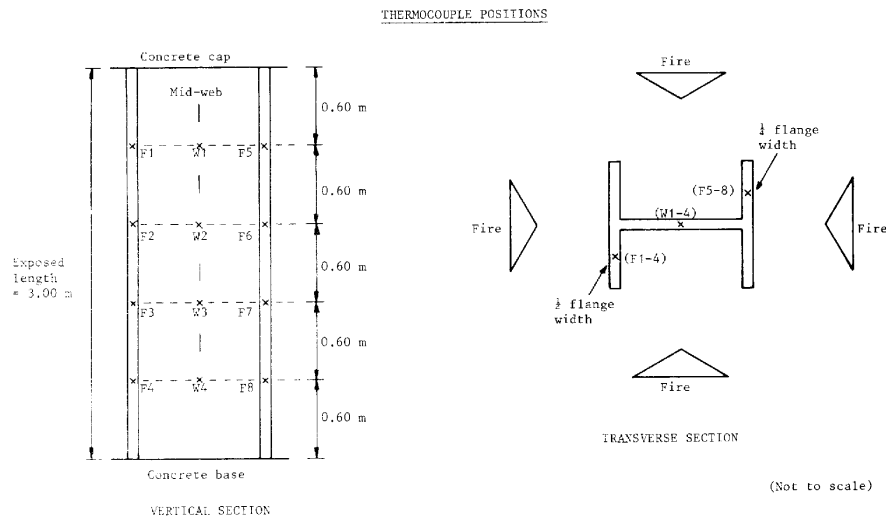
Figure 12 Description of fire test 41 on steel column (h*w*t$_w$*t$_f$ =206x204x8x12.5 mm) fully fire exposed /9/

The tested steel column has an effective length of 2.1 m (fully exposed). The slenderness ratio is 0.45 (weak axis) and 0.24 (strong axis) respectively i.e. a short column with almost no buckling influence. The deformation behaviour and the collapse time for the fire tested column (100% fire exposure and 60% of allowed maximum load according to test standard) has been predicted by Global Collapse Analysis and compared with measured results.

The measured value of steel strength was 349 MPa, to be compared with the design value of 255 MPa. The actual degree of loading is therefore less than the allowed 60%. The actual, measured value of strength was used in the simulations. The modulus of elasticity modulus was set to 210 GPa since it was not measured during the test.

In figure 13b the predicted and measured axial deformation as function of time is compared. The concordance in deformation process is good and the collapse time from GCA is predicted to 19 minutes compared to the measured 23 minutes. Due to all testing uncertainties and the normal variation of results (sometimes up to 50% for columns) from fire testing on identical specimens this difference is quite acceptable.
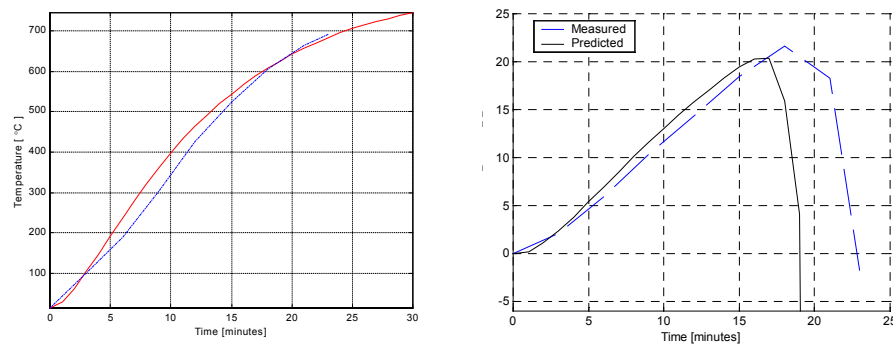
Figure 13   a)   b)
Comparison of predicted and measured a) temperature and b) axial deformations of fire exposed steel column (w*h*t$_w$*t$_f$ =204x206x12.5x8 mm) for fire test 41 under 100 % fire exposure of column /1/. (Dotted line = measured, solid line = predicted)

A comparison was done with the column analysed using the tool COMPRES. With a measured initial value of steel strength the resistance time was determined to 21.7 minutes. This value is almost 15 % greater than the GCA-calculation and ought to be less than 19 min because it is a simplified method copared with an "accurate" method.

Computer Simulation of Steel Beam Fire Test Conducted in UK

A full scale fire test on a simply supported steel beam exposed to ISO fire on three sides and with a concrete slab cast onto the upper flange that was tested at Firto Borehamwood, U.K. in 1984 /9/ has been simulated (see figure 14). This test will be referred to as fire test 11. The length of the beam was 4.5 m.

The standard ISO 834 gas temperature curve was used to simulate the fire test. The temperature as function of time over the cross-section has been calculated by Super-Tempcalc. The temperatures at top flange, web and exposed bottom flange were applied to the structural analysis.

The structural resistance has been calculated using both the non-linear approach of GCA and the Eurocode 3 design method implemented in SBEAM. This was done in order to get an indication of whether the Eurocode 3 method, which does not include the effect of added thermal moment due to temperature gradient, can be considered relevant.
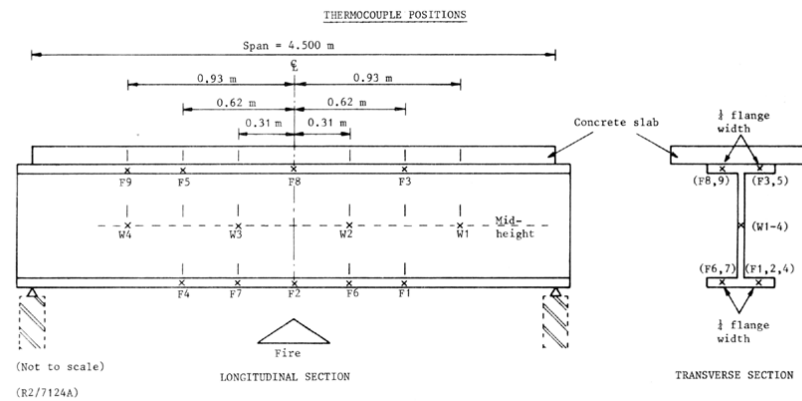
Figure 14 Description of fire test 11 on steel beam h*w*t_w*t_f = 256x145x7.47x12.79 mm. /9/

A maximum allowed deflection of L/30 was used as stability criteria. With a span of 4.5 m this means a maximum deflection of 150 mm. A comparison of measured deflections and deflections as calculated with GCA is presented in figure 15a. The fire resistance of the tested beam was 21.7 minutes and corresponding GCA calculation resulted in 19.6 minutes of fire resistance.

a)   b)
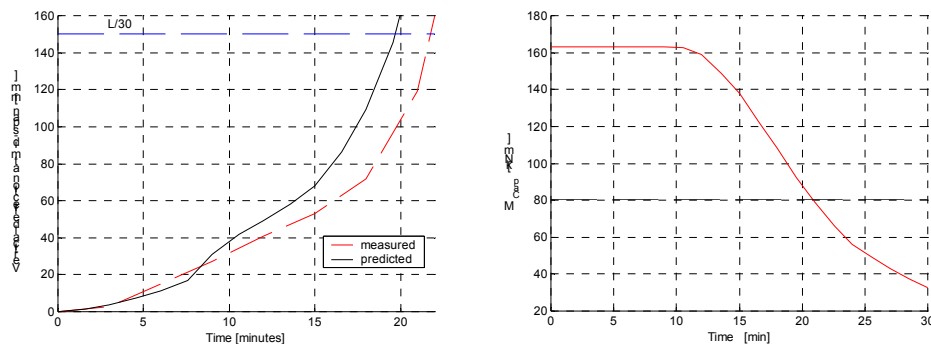
Figure 15 Deflections at centre of beam. The collapse time of the GCA simulation was 19.6 minutes. The resistance time of the test was 21.7 minutes./1/   Moment capacity as calculated using SBEAM. The fire resistance time was 20.8 minutes, to be compared with 21.7 minutes of the test./1/

A comparison to design with the tool SBEAM is shown in figure 15b. The SBEAM calculation, that does not consider deflections, resulted in 20.8 minutes of structural stability during fire. Compared with the GCA analysis this value is too advantageous for a simplified method depending on the use of design strength based on 2% strain and plastic theory. This corresponds to the time when the load bearing capacity reached the value of the load effect of 80 kNm.

The deviation between measured results and simulations is too small to conclude that the effect of the thermal moment would be significant for beams in general.

334

REFERENCES

/1/   Jeansson S. & Anderberg Y., Multi-storey Structures, Behaviour in Case of Fire-Initial Theoretical Analyses. Project no 99-018, Fire Safety Design, Lund, December 2001.

/2/   Eurocode 3 Design of steel structures, Part 1.2 Structural Fire Design, Draft prENV 1993-1-2, August 1993.

/3/   Eurocode 4 Design of composite steel and concrete structures, Part 1.2 Structural Fire Design, Draft prENV 1994-1-2, August 1994.

/4/   ENV 1991-2-2, Basis of design and actions on structures, Part 2-2 Actions on structures exposed to fire, CEN Brussels 1994.

/5/   Pettersson, Magnusson, Thor: Fire Engineering Design of Steel Structures, Swedish Institute of Steel Construction, Stockholm 1976.

/6/   Anderberg, Y.: SUPER-TEMPCALC, A Commercial And User-friendly Computer Program With Automatic FE-Generation For Temperature Analysis Of Structures Exposed To Heat. Fire Safety Design AB, Lund 1991.

/7/   Jeansson S.: TCD 5.0 manual (rev 4). An integrated software package for temperature calculations and structural design in accordance with the Eurocodes. Fire safety Design, Lund 2001

/8/   NAD(S)/SS-ENV 1993-1-2, National Application Document for Eurocode 3 - Design of steel structures Part 1-2:General rules - Structural Design.

/9/   Wainman D.E., Kirby B.R.: Compendium of UK Standard Fire Test Data. Unprotected Steel 1.British Steel Corporation 1988

Session 7:
Composite structures

STRUCTURAL BEHAVIOUR OF AN OPEN CAR PARK UNDER REAL FIRE SCENARIOS

Bin ZHAO & Joël KRUPPA
CTICM –Fire and Testing Division
Domaine de Saint Paul, BP 64
78470 Saint-Remy-Lès-Chevreuse, FRANCE

ABSTRACT

Within two successive European research projects involving CTICM (France), ARBED (Luxembourg) and TNO (Netherlands), several fire tests have been performed on cars and on a real car park made of steel columns and steel beams connected to composite slabs. Although a drastic increase of combustible product in cars, the experimental results have given convinced evidence that fire protection of the steel structure is not necessary to get an overall stability.

Parallel to above experimental investigations, numerical analysis has also been performed in which the fire development, the heating of the structure and structural behaviour during the fire are studied with different numerical models. However, the present paper will be focused mainly on the modelling of structural behaviour. It will be shown that the global structural behaviour (composite floor and steel column) subjected to localised heating from cars may be very accurately predicted by a 3D modelling in which the lateral buckling of steel beam, the membrane and diaphragm effects of the floor are taken into account.

In addition, results of a parametric study is presented in which it is shown that the use of 3D modelling in the analysis leads to the possibility of building open car parks with a more economical steel and concrete composite structures.

KEYWORDS: *fire resistance, fire test, composite structure, car park, numerical modelling*

1. INTRODUCTION

In some countries, the fire resistance requirements -based on the ISO-fire- for open car parks are rather high [1]. In this respect it is worth to analyse the expected behaviour of the loadbearing structures in case of real car fires.

One of the most common designs of such loadbearing structures is based on composite steel-concrete beams and steel columns.

The analysis of the fire behaviour of such car parks needs to consider four steps of modelling: fire model, structural model, heat transfer model and mechanical model [2,3].

From previous experimental and theoretical studies, detailed knowledge was obtained on both :
- the heat release of burning cars, for the fire model [4,5],
- the mechanical behaviour of composite beams, for structural and mechanical models [6].

These allowed the numerical modelling of the fire behaviour of car park structures for various fire scenarios, showing that, with some constructional details, open car parks needn't fire protection of steel section to have the necessary level of fire resistance.

In order to scientifically prove these conclusions, a European research project involving CTICM (France- coordinator), ARBED (Luxembourg) and TNO (Netherlands) was launched in 1999. Within this research project, an open car park using unprotected steel and concrete composite structure was specially built in France under which two main fire tests were carried out.

These tests have provided very encouraging and proving results about the fire structural behaviour of open car parks and the accuracy of numerical calculation methods. However it was found that the use of 3D modelling in the analysis could be necessary. In fact, this advanced approach has been largely used in another European research project [7, 8] with famous Cardington fire tests.

2. CAR BURNING

Regarding the energy release in case of fire, European cars can be sorted in 5 categories (table 1). For each category an average mass and energy released can be given (table 2).

Trade-marks	Category 1	Category 2	Category 3	Category 4	Category 5
Peugeot	106	306	406	605	806
Renault	Twingo-Clio	Mégane	Laguna	Safrane	Espace
Citroën	Saxo	ZX	Xantia	XM	Evasion
Ford	Fiesta	Escort	Mondeo	Scorpio	Galaxy
Opel	Corsa	Astra	Vectra	Omega	Frontera
Fiat	Punto	Bravo	Tempra	Croma	Ulysse
Wolkswagen	Polo	Golf	Passat	//	Sharan

Table 1 : Definition of European car categories (of the 90's)

Category	Car mass (kg)	Mass of combustible materials (kg)	Released energy (MJ)
1	850	200	6000
2	1000	250	7500
3	1250	320	9500
4	1400	400	12000
5	1400	400	12000

Table 2 : Average car mass, mass of combustible materials
and energy available to be released versus category

Car fires have been studied since numerous years. But the study of the rate of heat release of cars has begun only with car tests of VTT in Finland (1991) [4, 9] and by the Fire Research Station in UK and INERIS in France [10].

Comparing to these previous results, the aim of a new series of tests performed at CTICM (Maizières-Lès-Metz - France) within a European research project [3] was to record rate of heat release by considering other parameters:

- new generation of cars,
- real configuration of cars in a park: existing ceiling above the car, car close to a wall or in a corner,
- spread of fire from one car to another.

The experimental device is summed up in the figure 1.

Figure 1 : Calorimeter hood for testing two cars

In general, during the tests, the cars were equipped as in practice with oil, 4 tyres and a spare tyre, and the fuel tank was 2/3 full.

10 tests were carried out in 1995 and 1996, involving 15 cars of old (70ies/80ies) and new generation (90ies): 5 tests were performed with one car and the 5 others with 2 cars.

In the first 7 tests, the car was ignited with 1.5 l of the petrol in an open tray under the left front seat. The left front window was completely open, and the right front window was half open. All doors were closed. In the case of test with two cars, the doors and windows of the second one were closed.

In the last 3 tests, the cars were ignited under the car at the gear box level with 1 litre of petrol, as a testing procedure sometimes used by car manufactures.

Results in terms of rate of heat released using oxygen consumption technique [11], on a car of the 3rd category (of old and new generation) are shown on figure 2.
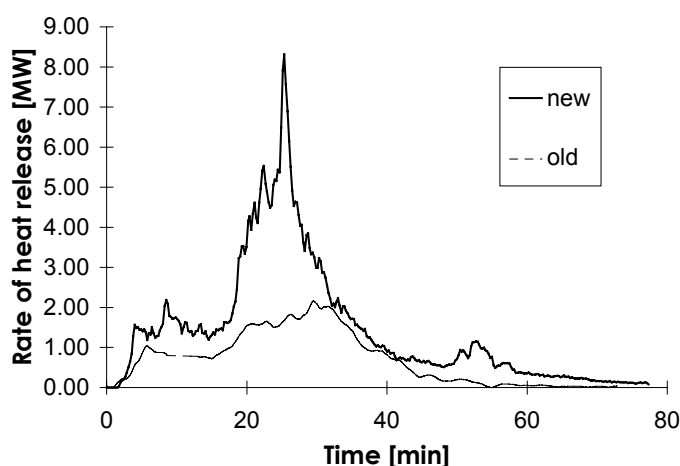
Figure 2 : Heat released from cars of category 3, old and new generation

In tests involving two cars, to study the possible fire spread from one car to another, it appeared that the second car, at approximately 70 cm from the burning car (average distance in European car parks), ignited in all cases, about 12 min after the ignition of the first car. This ignition is either due to the tyres or the rubber around doors.

3. EXPERIMENTS IN AN OPEN CAR PARK

3.1 Structure of tested open car park

So as to perform fire tests as close as possible to reality, an open car park with a floor surface of 480 m² (15m x 32 m) and a height of 3m (see figure 3) was built.
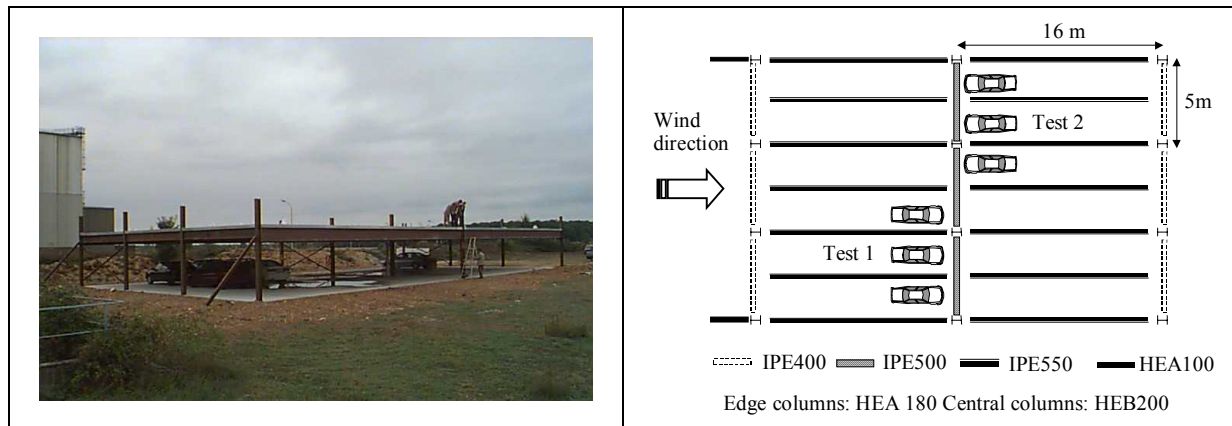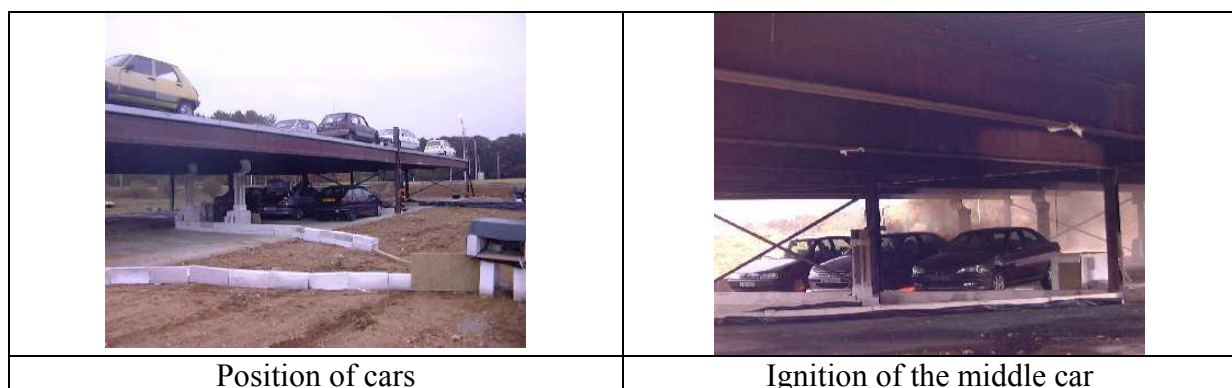
Figure 3 : Tested open car park

Its structure is composed of :

- unprotected steel columns HEA180 (edge columns) and HEB200 (central columns),
- steel and concrete composite beams, composed of unprotected steel beams (IPE 550, IPE 400 and IPE 500) connected to the steel and concrete composite slab,
- steel and concrete composite slab with a total thickness of 120 mm (COFRASTRA40).

Two main fire tests were carried out during which cars of latest generation were burned under the structure in order to investigate the fire behaviour (fire development as well as structural behaviour). The fire scenario used involves three cars parked together (see figure 3), corresponding to the most severe fire scenario according to statistic results obtained from fire brigade concerning open car parks [12].

3.2 Test results

During tests, the fire started always by ignition under the mid-car at the level of the gearbox and the fire continued until the full burn out of the three cars. This test procedure is illustrated in figure 4.

| Position of cars | Ignition of the middle car |

| Full development of car fire | Burn-out of all three cars |
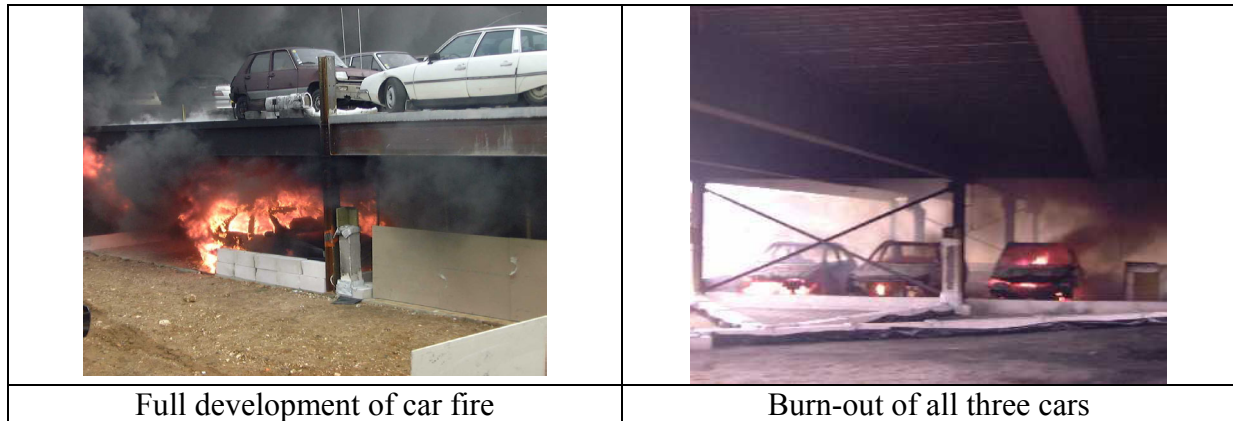
Figure 4 : Summary of a fire test involving three cars

The main observations of test results can be summarised as follows:
- the fire spread from one car to another always occurred but the propagation time is quite different according to wind condition and the orientation of the cars with respect of the wind direction. It was found that with strong wind condition, from engines towards rears, of cars (test 2), fire spreads quite quickly from one car to another and with weak wind condition, from rears to engines of cars, (test 1), it takes much longer time (figure 5), so the fire duration is very different. However, in both cases, the maximum heating of the structure is quite the same.
- measured maximum vertical displacement is different between test 1 and test 2 (figure 6). This is due to the fact that in test 1, the fire shifted from one car to another quite slowly and the wind pushed the flames outside the span of beams, so that the heating area of the structure remained small. But in the second test, the quick fire spread from one car to three cars and the wind pushing the flames towards the mid-span, created a much larger simultaneous heating area of the structure especially for the secondary beams leading to much important deformation of the structure.
- even if the fire spread is quite different, these deformations were far from leading to the collapse of the structure.
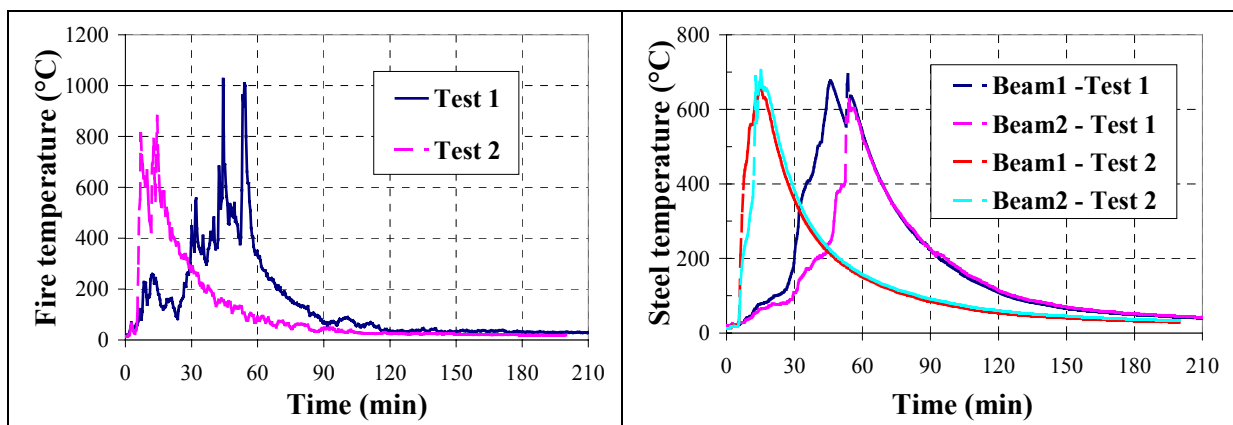

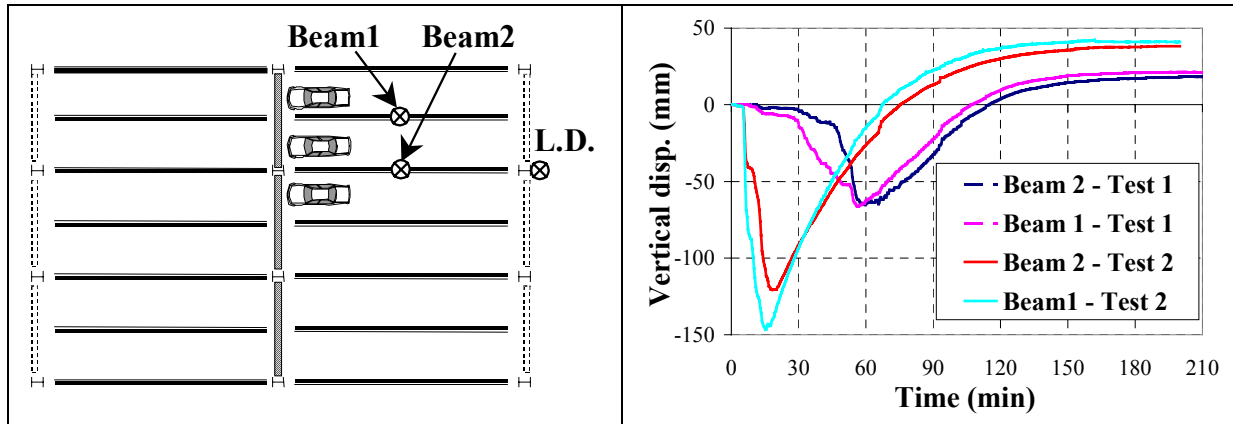Figure 5 : Measured temperature of both hot gases (fire) and steel beams versus time

Figure 6 : Measured vertical displacements of steel beams versus time

4. NUMERICAL ANALYSIS OF FIRE TESTS

Since test 2 was obviously more severe than test 1, this test is specially used as a reference example for comparison with numerical analysis results to check the validity and the accuracy of numerical models.

The numerical analysis is carried out with both computer codes SISMEF (2D) [6, 13, 14] and ANSYS (3D) [15]. The 2D modelling with SISMEF uses only beam elements (composite beams and columns) and 3D modelling combines several types of elements. The detailed 3D modelling in shown in figure 7. In this modelling, used principal elements are as follows:
- multi-layer shell element for solid part of composite slab
- beam elements for both concrete ribs and steel decking
- beam elements for additional reinforcing steel in concrete slab
- beam elements for steel members (beams and columns)

In this analysis, all steel beams are considered to have a full rigid connection with composite slab in both 2D and 3D modellings.

The calculated results of 3D modelling for test 2 are given in figures 8 and 9 in terms of vertical displacement field respectively at 15 and 70 minutes of fire. The maximum deflection obtained at 15 minutes of fire is about 177 mm. At this moment, the opposed span of structure in general went up (figure 9).
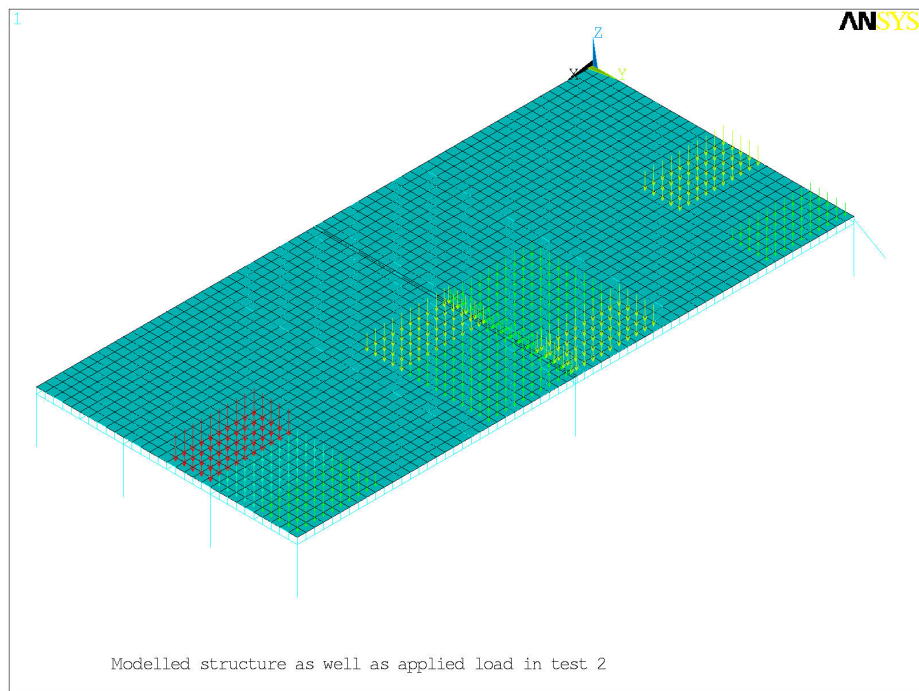
Figure 7: Modelled structure of tested open car park as well as applied load in test 2
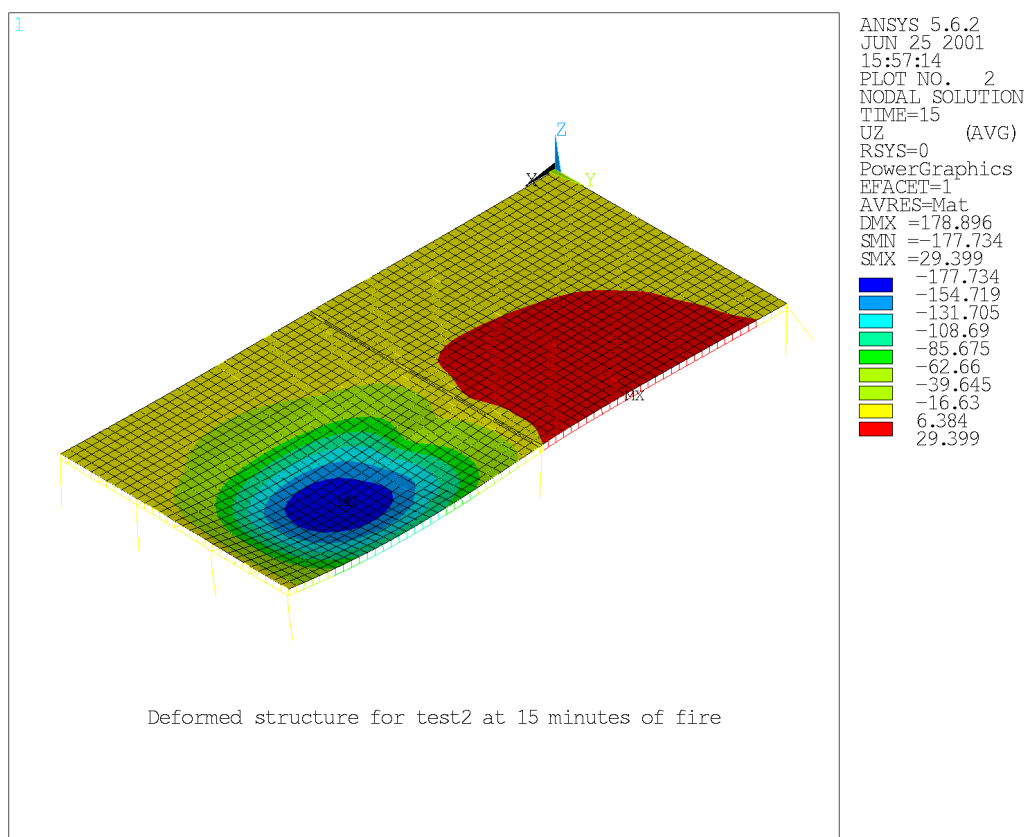

Figure 8: Simulated deformed structure for test 2 at maximum heating phase

However, this structural behaviour is fully different after the fire went out at 70 minutes (figure 10). Since at this moment, the part of the structure initially heated by car fire went up, in particular for the secondary beam rigidly connected to steel columns. On the contrary, the

cold part of the structure along the length of the structure went down for about 60 mm. This structural behaviour led certainly to a very important force at the level of beam to column joint causing the rupture of some bolts (in particular those located at the lower part of steel beams), phenomenon observed during the cooling phase of tests.
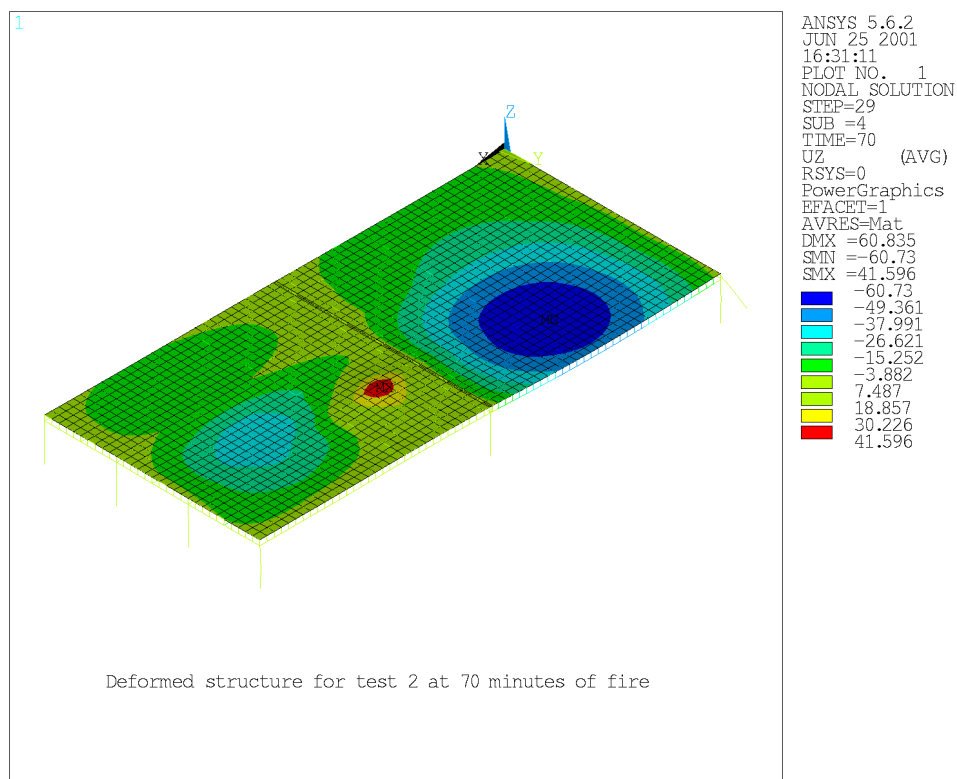
Figure 9 : Simulated structure for test 2 at cooling phase of fire

A comparison has been made between calculated displacement results and measured displacement results (figure 10 and 11). It can be found in this comparison that:

- 3D numerical modelling agrees quite well with experimental results for both heating and cooling phases. The slight differences may be explained by the fact that for some part of the structure, for instance for beam 2, the temperature measurement is not enough detailed to give an accurate temperature field for numerical simulation and the approximation made would create the difference leading to a slightly different structural behaviour. However, these differences are quite small so the adopted numerical modelling is considered accurate enough for predicting the structural behaviour of open car park.

- The results obtained with 2D numerical modelling are in general much more onerous than experimental results for both vertical and transversal displacements.
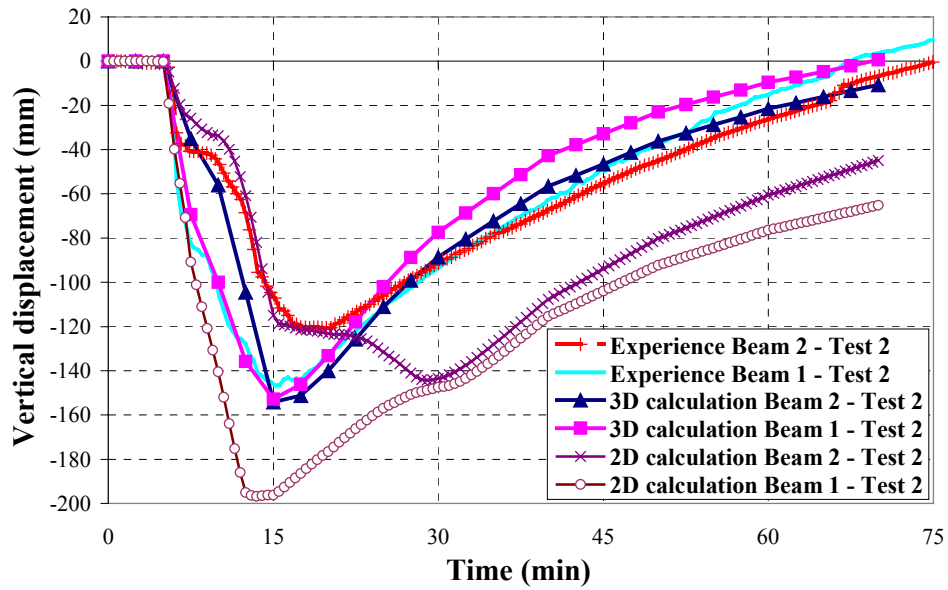
Figure 10 : Comparison of vertical displacement between calculation and experience for test 2
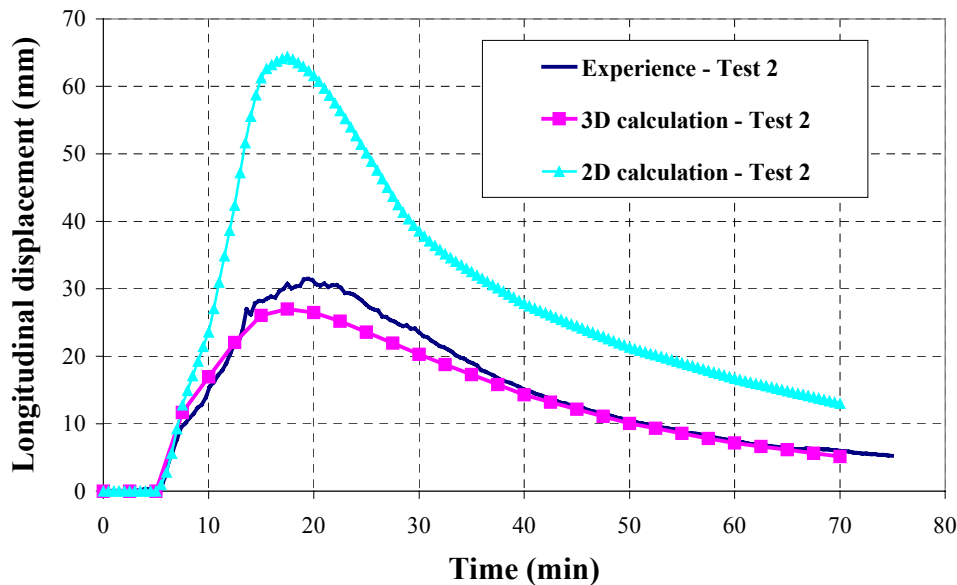

Figure 11 : Comparison of longitudinal displacement at end of secondary beam 2 between calculation and experience for test 2

This comparison shows that 3D modelling is more appropriate for predicting the structural fire behaviour of composite floor system.

5. PARAMETRIC STUDY

Regarding the tested open car park, on the one hand, its structure was designed with the worst fire scenario according to previous experimental results [3], in which the predicted maximum heating of steel members was more than 900 °C (which as shown before, was not reached during the test). On the other hand, 2D numerical modelling was adopted in the design. As a consequence, this design leads to a quite conservative structure which requires not only

additional steel reinforcement for all secondary beams through the central part of composite slab but also rigid joints between secondary beams and steel columns. In this case, it becomes interesting to know the influence of these structural parameters in case of 3D numerical modelling. A short parametric study is then carried out in which following parameters are investigated:

- additional reinforcement for secondary beams
- joint condition between secondary beam and columns

The heating of the structure is considered as the same as obtained during the test 2. The first investigated parameter is the additional reinforcing steel for secondary beams aimed for increasing the fire resistance of these beams. In order to study it, another calculation was carried out without these reinforcing steels (for tested open car park, these reinforcing steels are about 965 mm²/m with a length of 12 m). The vertical displacements of beam 1 and beam 2 obtained with this option are compared to those with real structure. It can be found that the contribution of these additional reinforcing steel is quite small under this fire scenario since the displacement difference is only about 7% (see figure 12).
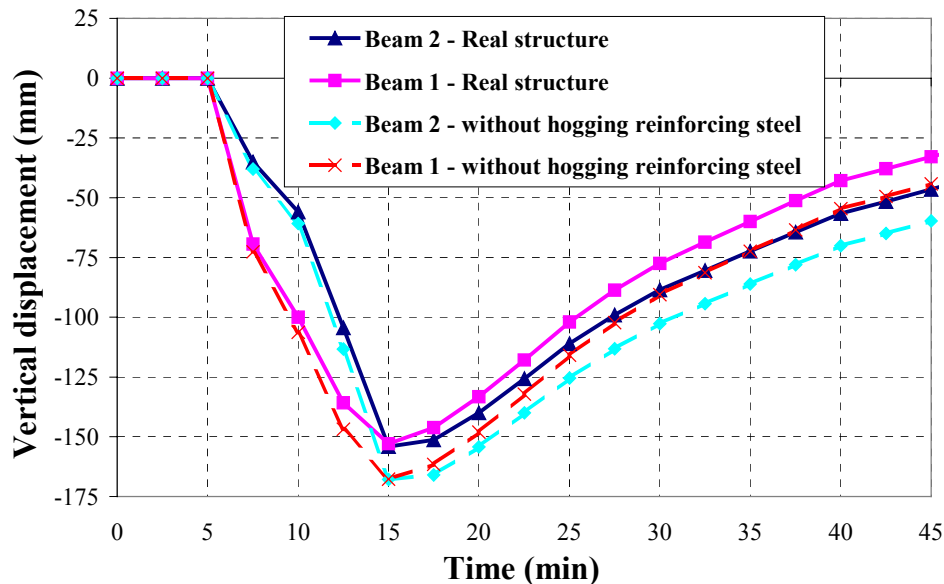

Figure 12 : Comparison of vertical displacement of both beam 1 and beam 2 with different condition of reinforcement

The second parameter is the joint condition between secondary beams and columns, for the tested structure, all secondary beams are rigidly connected to steel columns. Certainly, it would give better fire resistance for these beams during the heating up of the structure. However, during cooling phase, these beams because of their plastic deformation creates very important internal forces leading to some damages of joint elements, in particular the rupture of bolts. This type of damage is very troublesome for the repair of the structure after fire. If simple joint is used, a more important rotation capacity of steel beam in respect to steel column could avoid the damage related to joint elements (phenomenon observed at the joints between secondary beams and primary beams). But the question is how the structural will behave under fire development if simple joints are adopted. So a numerical analysis is also carried out using a modified structure for which the additional reinforcing steel for secondary beams are neglected and in particular simple joints are used between all secondary beams and

steel columns. The corresponding results are illustrated in figure 13. One can find easily that the difference is very small between rigidly and simply jointed structures.
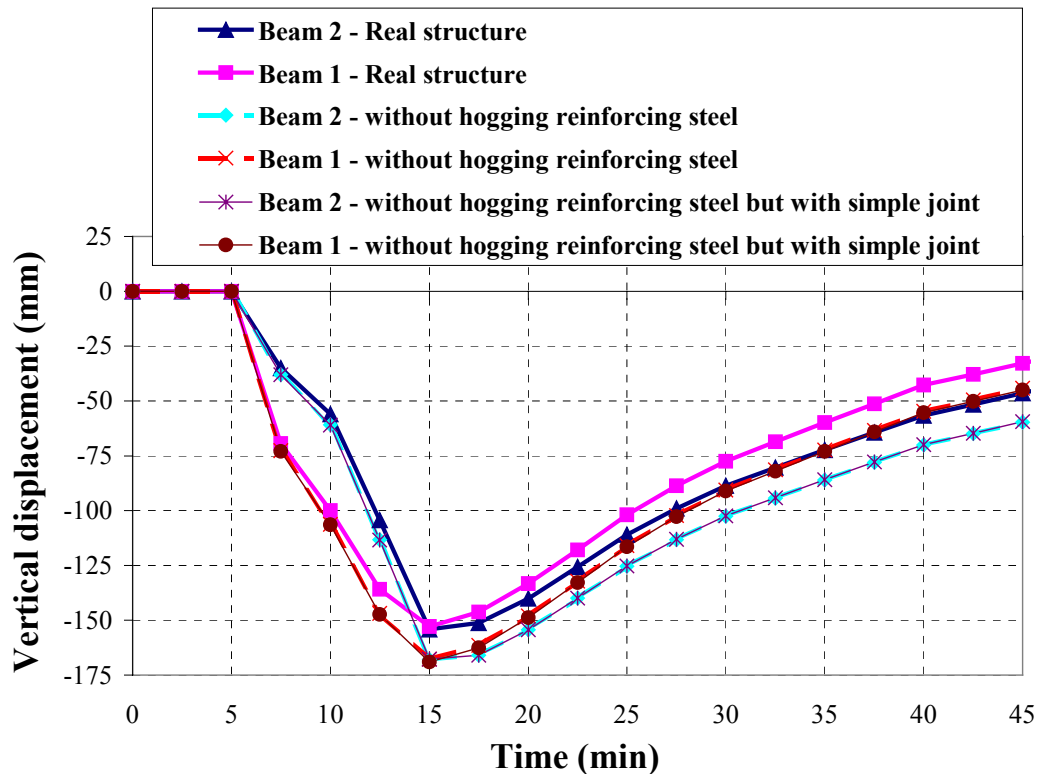

Figure 13 : Comparison of vertical displacement of both beam 1 and beam 2 with different joint condition between steel beams and columns

This phenomenon can be explained by the fact that even the steel beam has a simple joint with steel column, the continuity of composite beam and the transmission of hogging moment are still available through the concrete slab. This result has a large importance. It means that simple joints could be used between steel beams and columns while the same fire resistance is being provided, for the fire conditions recorded during the test 2.

6. CONCLUSION

Fires involving car are more severe with the current cars that they were in the 70's and 80's due to the strong increase of combustible products. Nevertheless fire tests performed in a real open car park have shown that unprotected steel structure can still be used without risk of collapse.

Fire tests results were also used for checking accuracy of numerical simulations with both 2D and 3D numerical modelling. It can concluded that:
- 2D analysis may be used to predict the structural behaviour of composite floor exposed to fire in a conservative way,
- if steel beams are connected to concrete floor, it is possible to avoid the use of rigid joints between steel beams and columns which could be much benefit for structural repair after fire,

- in order to make full use of the advantages of composite floor under fire situation, 3D numerical investigation is necessary.

7. ACKNOWLEDGMENTS

REFERENCES

[1] "Sécurité incendie dans les parcs de stationnement ouverts"
      Application de l'ingénierie du feu
      Note de la CECM N° 75- 1993

[2] J. KRUPPA
      "Performance based code in fire resistance : a first attempt by Eurocodes"
      Ottawa 1996

[3] "Development of Design Rules for Steel Structures Subjected to Natural Fire in Closed Car Parks", ECSC Agreement N°. 7210.SA/211/318/518/620/933
      Final Report - March 1997

[4] J. MANGS & P. LOIKKANEN
      "Average rate of heat release curve deduced from car fire tests"
      VTT Research Report n° PAL00455A/90
      Espoo - Finland - 1992 "Oxygen consumption calorimetry"

[5] D. JOYEUX
      "Development of design rules for steel structures subjected to natural fires in closed car parks"
      Car burning tests
      CTICM - December 1996

[6] B. ZHAO - J. KRUPPA
      "Fire resistance of composite concrete slabs with profiled steel sheet and of composite steel concrete beams"
      Part 2 : composite beams
      CTICM - July 1995

[7] Swinden Tecnology Centre, British Steel plc, "Behaviour of a Multistorey, Steel Framed Building Subjected to Natural Fire Effects", ECSC Agreement N°. 7215.CA/806, 1998

[8] C. BOTH, L. TWILT, "The Real Behaviour of Modern Largely Unprotected Steel Framed Buildings Under Natural Fire Conditions", TNO Report No. 98-CVB-R0457, January 1998

[9] "Fire tests in passengers cars"
MANGS J. and LOIKKANEN P.
VTT research report N°TSPAL00455/90
Espoo, Finland - 1991

[10] "Measurements of the severity of fires involving private motor vehicles"
SHIPP M. and SPEARPOINT M.
Fire Research Station, Building Research Establishment, Bucknalls Lane, Garston, Watford WD2 7JR, UK

[11] M. JANSSENS - W.J. PARKER
Chapter 3 - Heat Release in Fires
V. Brabauskas & S.J. Grayson
Elsevier Applied Science

[12] D. Joyeux, "Statistiques sur les feux de parking en France", INC-99/1-DJ/NB, January 1999

[13] ZHAO B. "Modélisation numérique des poutres et portiques mixtes acier-béton avec glissements et grands déplacements", Thèse de docteur en Génie Civil, INSA de RENNES, 1994

[14] ZHAO, B. and ARIBERT, J.M., "Finite Element Method For Steel-concrete Composite Frames Taking Account of Slip and Large Displacements", European Journal of Finite Elements, Vol. 5, n°2, 221-249 (1996)

[15] Swanson Analysis Systems, Inc., " ANSYS User's Manual for Revision 5.0 - Volume IV - Theory ", Houston U.S.A., 1992

KEY EVENTS IN THE STRUCTURAL RESPONSE OF A COMPOSITE STEEL FRAME STRUCTURE IN FIRE

A.S. Usmani* and S. Lamont**
*School of Civil and Environmental Engineering
The King's Buildings, The University of Edinburgh, UK
asif.usmani@ed.ac.uk
**Arup Fire, Ove-Arup & Partners, 13 Fitzroy Street, London, UK
susan.lamont@arup.com

ABSTRACT

The structural design of composite steel frame buildings in fire has traditionally been based on single element behaviour under standard fires. This approach is widely recognised as unsatisfactory and there is a general consensus that it leads to excessive fire protection being applied to the steel members based on grossly inaccurate assumptions about whole structure behaviour in fire. A great deal of research has been carried out to understand the mechanics of whole structure behaviour in fire. This paper presents a summary of this research by computational analysis of a small but realistic steel-frame composite structure with mainly unprotected beams and fully fire-protected columns.

The main purpose of this paper is to highlight a number of key events that define the response of the steel frame structure in fire. Some of these events can be observed in real fire tests (such as Cardington), however others have only been discovered by careful analysis of the output data from computational analyses supported by fundamental theoretical analysis. For instance, an event has been discovered entirely from computational modelling of the above-mentioned small structure with no similar events observed in experiments or reported in literature. This particular event involves a sudden and sharp increase in deflection of the whole floor at particular steel temperatures during the fire. If this event occurred in a real structure, it might cause an overload of the floor because of the dynamic effect of this instability (unaccounted for in the static analysis performed here) leading to compartment breach or collapse.

All of these events will be presented in order of appearance as the compartment fire progresses and the member temperatures increase. The reason of occurrence of each event will be discussed supported by simple analysis of the relevant structural mechanics and brief discussion of design implications.

KEWORDS: Composite floor systems, Cardington fire tests, structural behaviour in fire, steel-frame composite structures

INTRODUCTION

This paper draws upon the authors' experiences on modelling the Cardington frame fire tests[1] which provided a wealth of information about the behaviour of composite

structures in fire. During the Cardington frame fire tests the structure survived a number of compartment fires ranging in location and geometry, from a highly restrained internal compartment test on a single beam, to a large compartment test over half of a whole floor. The fire temperature-time histories were different in each test and in all but one of the large compartment tests all the steel beams were left unprotected. Undoubtedly the work at Cardington has provided a greater understanding of whole composite frame behaviour in fire. This behaviour has many interesting features, the occurrence of which depends primarily upon the temperature evolution in the compartment, the boundary and restraint conditions of the structural assembly and the composite behaviour.

The purpose of this paper is to highlight some of the key events that punctuate the various behaviour regimes when a composite floor slab is exposed to fire. In a recent paper,[2] Usmani *et. al.* presented some of the fundamental mechanics governing the thermal response of beam and slab type structural members under fire. This was based upon the assumption that any any thermal regime can be resolved as two geometric effects in unrestrained beam and slab type structural members: an equivalent mean temperature increase leading to thermal expansion; an equivalent thermal gradient through the depth leading to thermal curvature. If restraints to these effects were present, a large range of internal force and displacement combinations existed. A summary of the main principles outlined in[2] is as follows:

1. Unrestrained thermal expansion caused by a rise in mean temperature causes ends to move apart. The thermal strain producing this expansion is

$$\epsilon_T = \alpha \Delta T$$

   where α is the coefficient of thermal expansion and ΔT is the average temperature increment.

2. Thermal expansion in the presence of restraint to lateral translation from the surrounding structure produces compression forces leading to yielding or buckling (both the restraint and the temperature rise do not have to be large for buckling or yielding to occur).

3. Thermal bowing caused by the through depth thermal gradient leads to curvature,
$$\phi = \alpha T_{,z}$$
   where $T_{,z}$ is the average temperature gradient through the beam depth. The thermally induced curvature results in the pulling in of the ends in a simply supported beam. The reduction in distance between the ends can be written as a "contraction" strain,
$$\epsilon_\phi = 1 - \frac{\sin \frac{l\phi}{2}}{\frac{l\phi}{2}}$$
   where, l is the length of the beam.

4. Restraint to end translation produces tensions in the beam which grow with growth in the thermal gradients.

5. Rigid restraint to end rotation produces a hogging moment of $EI\phi$ over the whole length of the beam with no curvature. Finite rotational restraints produce combinations of hogging moments and curvature.

6. Compatibility of displacements in compartments with orthogonal stiffness distribution and orthogonal temperature distribution (for instance, steel only in one direction) influences the forces and displacements in the members.

These principles were indispensable in analysing the often confusing and voluminous output data from computational models of the Cardington tests and will be used here to understand the structural events to be discussed.

Estimation of equivalent temperature effects on the model
Given that the cross-sections of composite structural members and the temperature distributions over their depths can be quite complicated, the issue of equivalent thermal loading that must be applied to the members is not straightforward. A procedure has been developed based upon ideas used in estimating the effects of thermally induced stresses in bridge decks.[3] Figure 1 shows a general composite
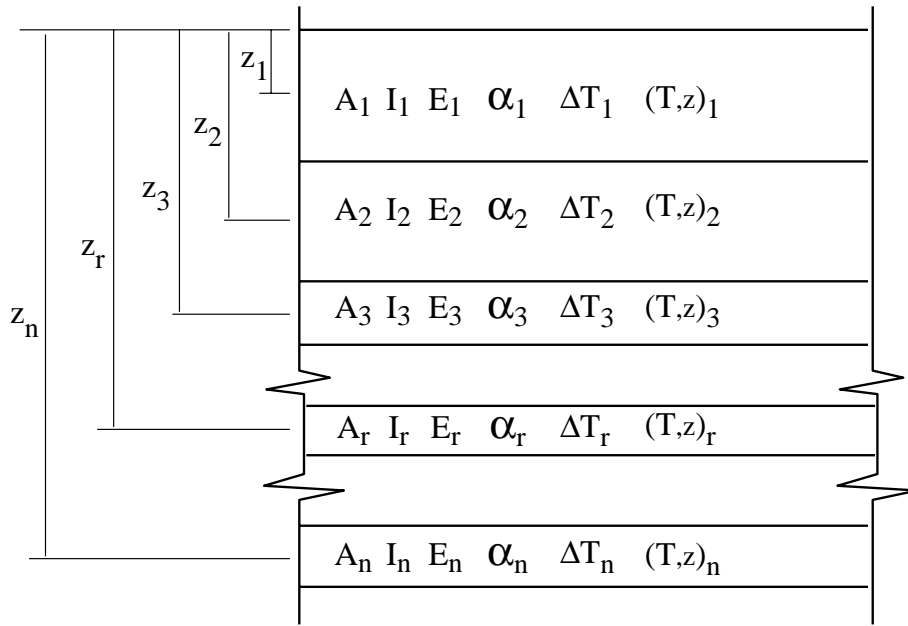

Figure 1: A general composite section divided into n slices

section with the indicated properties and temperature conditions, as defined by a uniform temperature increment $\Delta T, r$ and a through depth thermal gradient $T_{,z}$ for a given slice. If the beam that the section belongs to is fully restrained (both end translations and end rotations) then each slice will have a force and moment associated with it, defined as,

$$F_r = E_r A_r \alpha_r \Delta T_r = E_r A_r (\epsilon_T)_r = E_{\max} \hat{A}_r (\epsilon_T)_r \tag{1}$$

and,

$$M_r = E_r I_r \alpha_r (T_{,z})_r = E_r I_r \phi_r = E_{\max} \hat{I}_r \phi_r \tag{2}$$

It is convenient to write the above quantities using a transformed area (by defining modular ratios m_r based on the highest modulus in the composite), this is what $\hat{A}_r$ and $\hat{I}_r$ represent. The resultant force $\bar{F}$ and resultant moment $\bar{M}$ can now be determined from,

$$\bar{M} + \bar{F}\bar{z} = \sum F_r z_r + \sum M_r \tag{3}$$

where, $\bar{z}$ is the centroid of the composite. This If the total (transformed) area and second moment of area of the composite are denoted by $\bar{A}$ and $\bar{I}$, then the equivalent expansion $\bar{\epsilon}_T$ and curvature $\bar{\phi}$ can be written as,

$$\bar{\epsilon}_T = \frac{\bar{F}}{E_{\max}\bar{A}} \tag{4}$$

and,

$$\bar{\phi} = \frac{\bar{M}}{E_{\max}\bar{I}} \tag{5}$$

This procedure can also be used to determine the thermally induced strains and stresses in a composite beam. This can be done by releasing the restraint applied to determine the resultant force and moment in the composite. Which, of course, is the same as applying the negatives of $\bar{F}$ and $\bar{M}$, bringing the restraint forces to zero. This is illustrated using an example in Figure 2. The total strain distribution in the beam can then be determined by,

$$\epsilon(z) = \bar{\epsilon}_T + (z - \bar{z})\bar{\phi} \tag{6}$$

and the stresses are,

$$\sigma(z) = \frac{E_{\max}}{m_r} \left[(\epsilon_T)_r + (z - z_r)\phi_r + \epsilon(z) \right] \tag{7}$$

Figure 2 shows the distributions of stresses and strains computed using this procedure for a simple example of a composite beam.

KEY EVENTS DURING HEATING

The following sections will describe the key events during the heating regime in a fire, either by using previous models of the Cardington tests or models produced for various parametric studies undertaken so far. Where appropriate, an analytical treatment will also be presented. In this discussion, the structural elements considered are the composite secondary and primary beams (steel secondary and primary beams in composite action with the slab) and the composite slab on its own. The temperature is assumed to vary with time only over the depth of the composite section and not along the length.

Compressive membrane action in composite slab beam systems

Although composite members in steel frame structures are designed primarily for flexure, they have a considerably greater load carrying capacity than that predicted by Johansen's yield line theory, due to the "arching" or compressive membrane action, arising from the presence of edge restraints in such structures. Figure 3 shows the typical details of the end connections of the primary beams in the Cardington
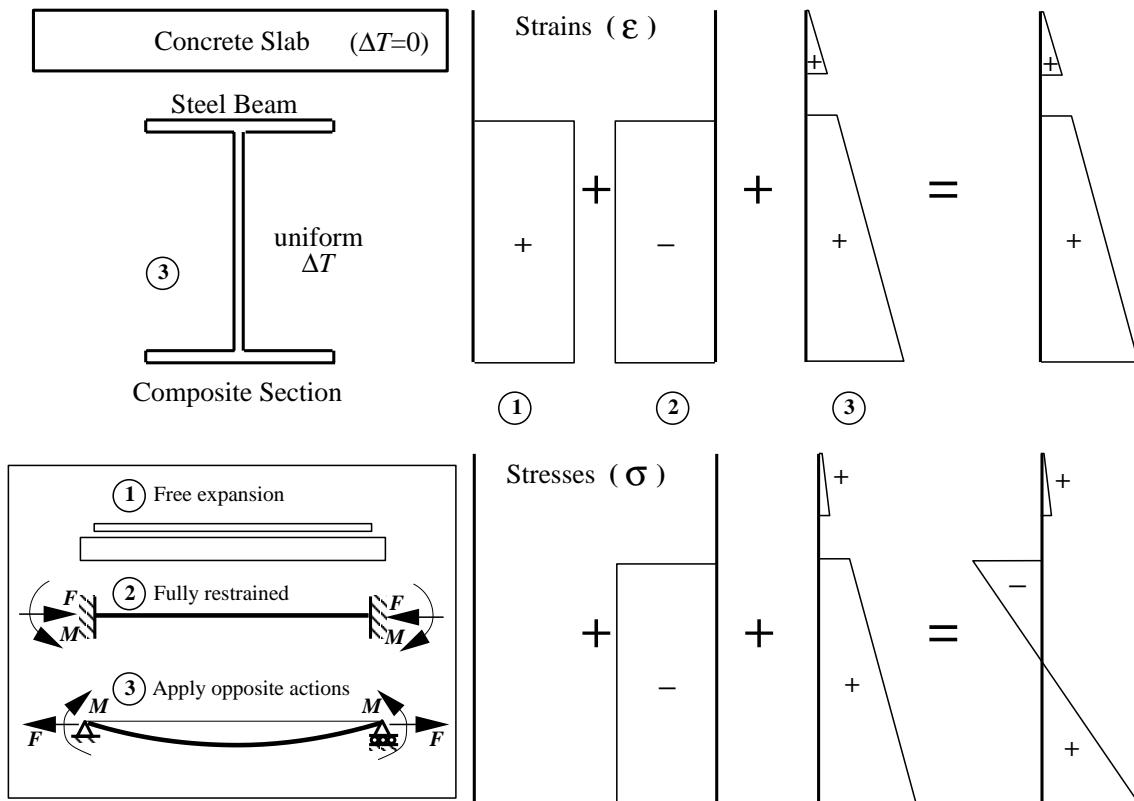
Figure 2: Analysis of thermal actions on a composite beam

structure. All beams are effectively restrained from both translation and rotation at the ends at ambient temperature. This kind of detail is common to most composite steel frame construction. The extra capacity due to compressive membrane action, depending upon a number of factors can range from 2 to 10 times that predicted by the yield line theory. Finite element models of the Cardington tests does indeed predict a uniform compression over the length of a composite beam (steel beam and RC deck)[4] (see Figure 3.3).

Local buckling of the lower flange of steel beams composite with the RC slab

The first interesting structural event that occurs is local buckling of the bottom flange of the steel beams. The explanation of this phenomenon is quite simple keeping in mind the end restraint conditions of the composite beams (as shown in Figure 3) and the fundamental principles outlined earlier.

As the temperature in the compartment increases, there are three cumulative effects that contribute towards the increase in compressive stresses along the steel beam bottom flange. The first of these is the load itself, which produces an initial hogging moment, leading to compression at the beam bottom flange. The second is the increasing mean temperature of the composite beam leading to overall compression across the equivalent composite section. Finally the thermal gradient over the depth of the section (cool slab and hot steel) leads to a uniform hogging moment developing along the length of the section, again leading to compression in the steel bottom
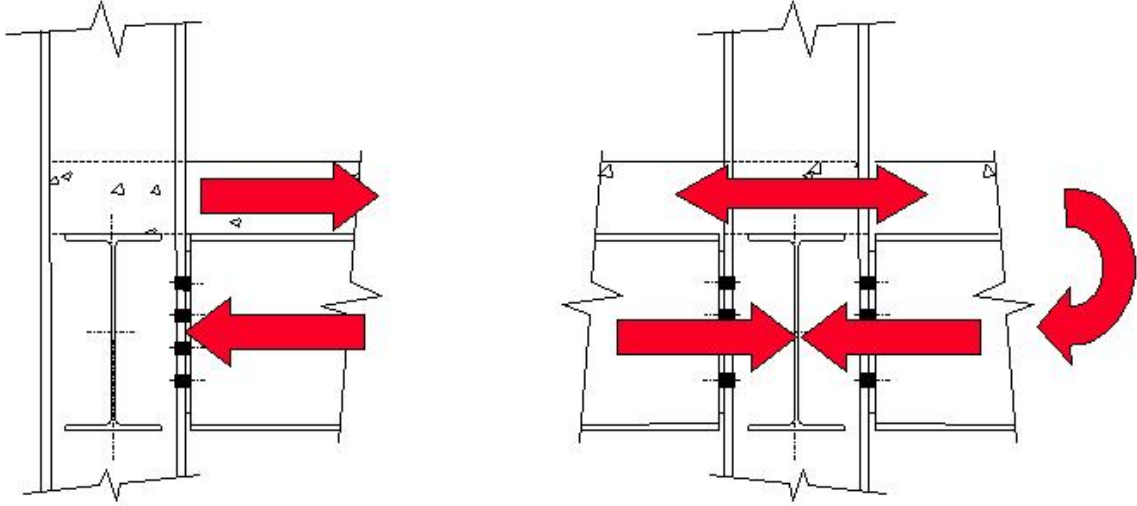
Figure 3: Typical end restraint conditions for composite members

flange. So the stress at the bottom flange of the steel beam may be written as:

$$\sigma(z) = \frac{M_w z}{\bar{I}} + E_{\max}\alpha\Delta T + E_{\max}\bar{\phi}z \tag{8}$$

Where, M_w is the fixed end moment from udl w and z is the distance from the centroid. As the temperature goes on increasing, the overall compression in the composite beam increases as well as the overall hogging moment and the the stress at the beam bottom flange rises steadily, until this stress exceeds the local buckling stress. At this point the local buckling changes the composite end conditions so that end rotations may take place, and therefore the increase in growth of axial force in the composite stabilises (to a plateau), because the thermal expansion can now be absorbed in increased deflections instead of increasing compression.

To examine this event in detail, let us consider the composite secondary beam from Cardington restrained beam test. Figures 4 and 5 show, the layout of the test and the active structural sections spanning in the two directions. Table 1 shows the equivalent section properties for the two directions.

	Area	2nd Moment	Centroid depth	Modulus	α
	$(A)\,\mathrm{mm}^2$	$(I)\,\mathrm{mm}^4$	$(\bar{z})\,\mathrm{mm}$	$(E)\,\mathrm{kN/mm}^2$	$(\alpha)\,/^\circ\mathrm{C}$
x-Slab	157500	$257{\times}10^6$	35	7.5	$8.0{\times}10^{-6}$
Steel beam	5150	$85{\times}10^6$	282	200	$12.0{\times}10^{-6}$
x-Composite	10900	$250{\times}10^6$	148	200	$10.0{\times}10^{-6}$
y-Slab (1 rib)	30700	$38{\times}10^6$	55	7.5	$8.0{\times}10^{-6}$

Table 1: Section properties of composite slab in x and y directions

For the composite beam section temperatures and gradients were calculated for three different reference temperature states of the steel beam, for both directions
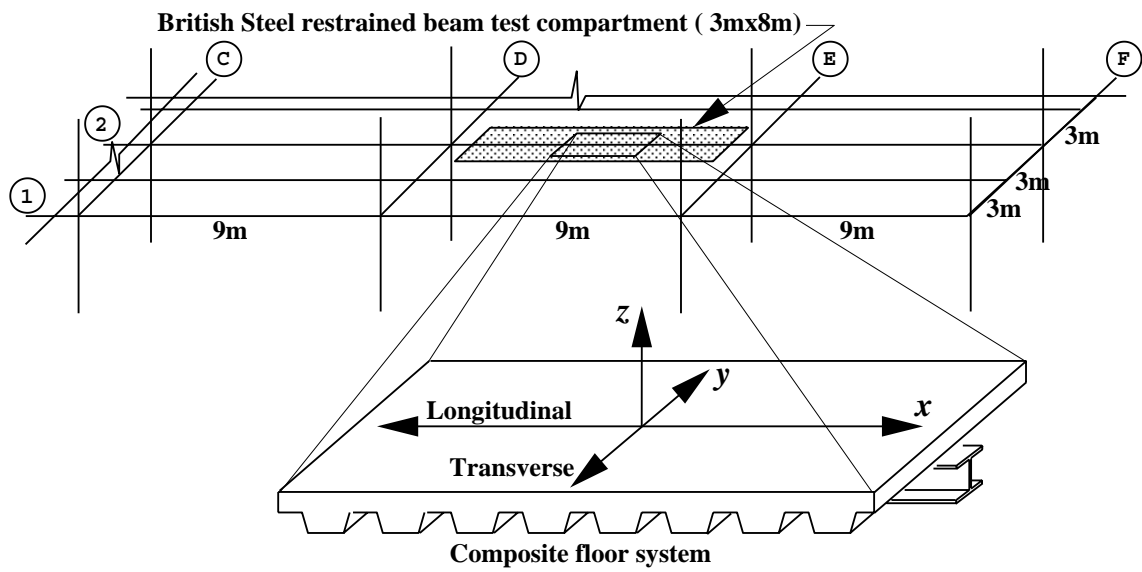
354

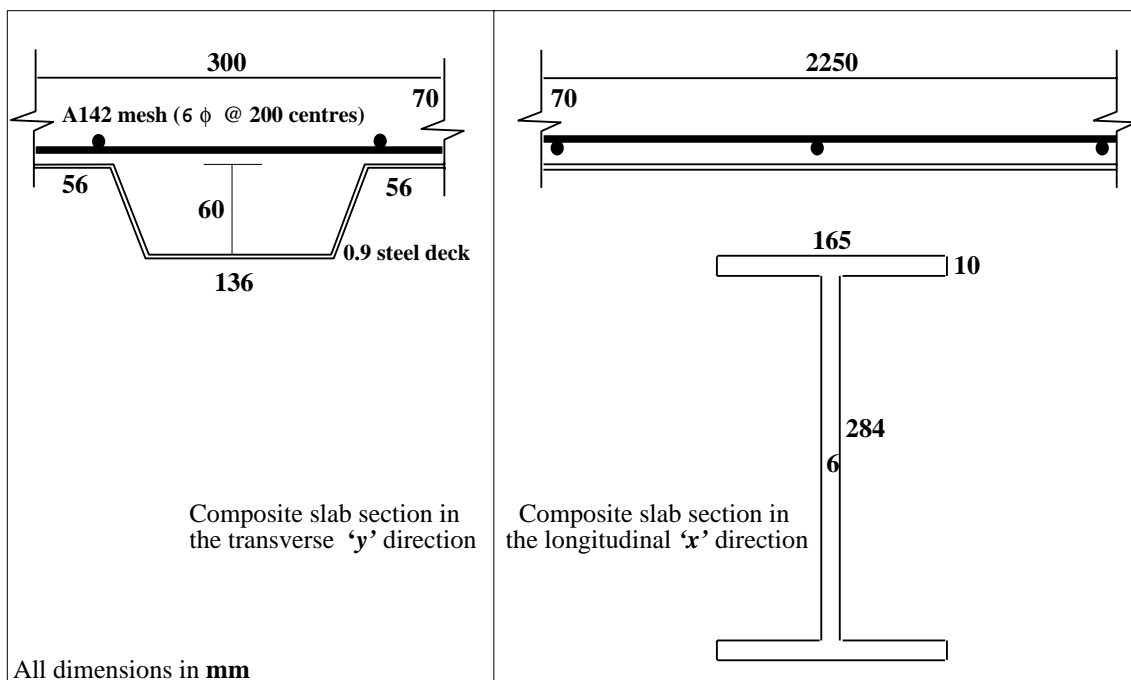Figure 4: Layout of the restrained beam test at Cardington

Figure 5: Active composite cross-sections in x and y directions

(longitudinal and transverse), using the procedure outlined earlier. The results are tabulated in Tables 2 and 3, along with other data that will be used in the analysis. It may be noted that the temperature distributions in the real structure are complicated by the effect of the ribs, and therefore appropriate averages have been used in these calculations. λ denotes slenderness ratio, and $\bar{z}$ denotes the depth of centroid of the transformed composite sections, subscripts x and y have been used to indicate longitudinal or transverse directions. Most other quantities in the tables should be self-explanatory.

Steel Temp.	E_s kN/mm^2	E_c kN/mm^2	A_x mm^2	I_x mm^4	$\bar{z}_x$ mm	λ_x	ΔT_x °C	$(T_{,z})_x$ °C/mm
150°C	200	7.5	10900	250×10^6	148.0	60	80	0.5
500°C	100	7.5	16800	300×10^6	108.5	67	260	1.6
800°C	0	7.0	124000	48×10^6	30.0	450	240	5.0

Table 2: Properties of composite slab in x direction at different temperatures

Steel Temp.	E_c kN/mm^2	A_y mm^2	I_y mm^4	$\bar{z}_y$ mm	λ_y	ΔT_y °C	$(T_{,z})_y$ °C/mm
150°C	7.5	30700	38×10^6	55.0	170	-	-
500°C	7.5	30000	37×10^6	54.0	170	85	1.4
800°C	7.5	19200	17×10^6	39.0	200	250	4.8

Table 3: Properties of composite slab in y direction at different temperatures

Previous analysis[5] has shown that for this test rigid restraint to end translation may be safely assumed. Also, Usmani *et. al.*[2] have indicated that restraint stiffnesses may not have to be very large for most of the these phenomena to be observed. Therefore assuming rigid restraint to end translation for the composite beam, the stress in the bottom flange at 150°C is calculated as 573 MPa (127 MPa from udl of 16.5 kN/m, 160 MPa from an the equivalent mean temperature rise over the composite and 286 MPa from the equivalent thermal gradient over the depth). This is clearly over the reported maximum yield stress of the steel (318 MPa) and the flange would certainly have buckled at a temperature lower than this. It is interesting to note that the thermal bowing contribution is the greatest to local buckling. Therefore, one may expect this phenomena to occur earlier (at lower temperatures) in short-hot fires (with larger gradients) than in long cool fires (with larger mean temperatures). The local buckling stress for an I-section in bending can be approximately calculated by[6]

$$\sigma_{\mathrm{cr}} = \frac{\pi^2 E}{12(1 - \nu^2)} \frac{0.425}{(b_f/t_f)^2} \tag{9}$$

Where, ν is the Poisson's ratio, b_f is half the overall flange width and t_f is the flange thickness. This equation produces a very large value of buckling stress, suggesting that the local buckle observed must have actually occurred at the yield stress, which seems to have occurred approximately around 120°C from looking at the test results.[7]

Tensile cracking of slabs over highly restrained composite members
The restrained beam test shows clearly the effect of high end restraints (both rotational and translational). From the analysis in the previous section, it is clear

that the rotational restraint because of the composite behaviour contributes significantly to the local buckling of the steel beam. Clearly the compressions in the steel must be balanced by tensions in the concrete slab. However the magnitude of the tensions depends upon the stiffness of the rotational restraint and the area of concrete available. The rotational restraint can be assumed to be very stiff in the restrained beam test (as the slab is continuous over the primary beams and loaded) the tension can be assumed to be large. Even though this tension can dissipated over a much larger area of the slab, the examination of the Cardington test shows a clean transverse crack just above the edge of the compartment. A simple calculation as described above also suggests that the top fibre stresses in concrete could have been high enough to cause this cracking. It may be mentioned here, that most real compartments are unlikely to possess the level of restraint stiffness of this test and therefor it is unlikely that these type of cracks will occur commonly. Most of the large cracking on the top of the slabs seen in Cardington is attributable to the cooling regime.

Ultimate yielding of steel beams

After the local buckling event, deflections begin to grow at a higher rate and P-Δ moments increase rapidly as a consequence. The rise in hogging moments at the ends approaches its peak value and the end rotational restraint is completely lost and moment redistribution to midspan begins[7] The next major event is caused by the steel beam reaching its ultimate axial capacity around approximately 500 C, beyond which the compressions follow the path determined by steel capacity. Figure 6[8] shows the axial forces at various points in the heated steel beam, all of which begin to decline as the steel strength and stiffness degrades as a result of heating. The ultimate axial capacity of the steel beam at 500°C is approximately 1184 kN (based on the EC3 temperature dependent properties), which is what is seen in the second curve of Figure 6 (the first curve is outside compartment).

This event signals the beginning of the end of the conventional composite flexure mechanism that is relied upon in design to carry loads at ambient temperatures. This mechanism is gradually replaced by the tensile and compressive membrane mechanisms supplied by the reinforced concrete composite deck slab. This event also marks the rise in the mean temperature of concrete to large enough levels, so that the concrete slab now begins to experience some of the compressive stresses by expanding against the restraints. The thermal gradient still stays high due to the low thermal conductivity of concrete.

RC slab under thermal pre-stress and boundaries and tensile membrane behaviour in the span

The compressive stresses developing in concrete enhance its load carrying capacity, rather like pre-stressing. This effect depends upon three factors: a) restraint: in regions where the restraint to expansion is high; location: in low deflection regions where the thermal strains are unable to be absorbed in deflections, such as regions near the support boundaries; fire scenario: a short-hot fire will cause larger gradients and lower compressions or tensions while a longer-cooler fire will produce higher mean temperatures and therefore greater compressions against restraints. Figure 7[8] shows strains in the slab at reinforcement level in the restrained beam test in the longitudinal direction (at the end of heating) which are practically all compressive.
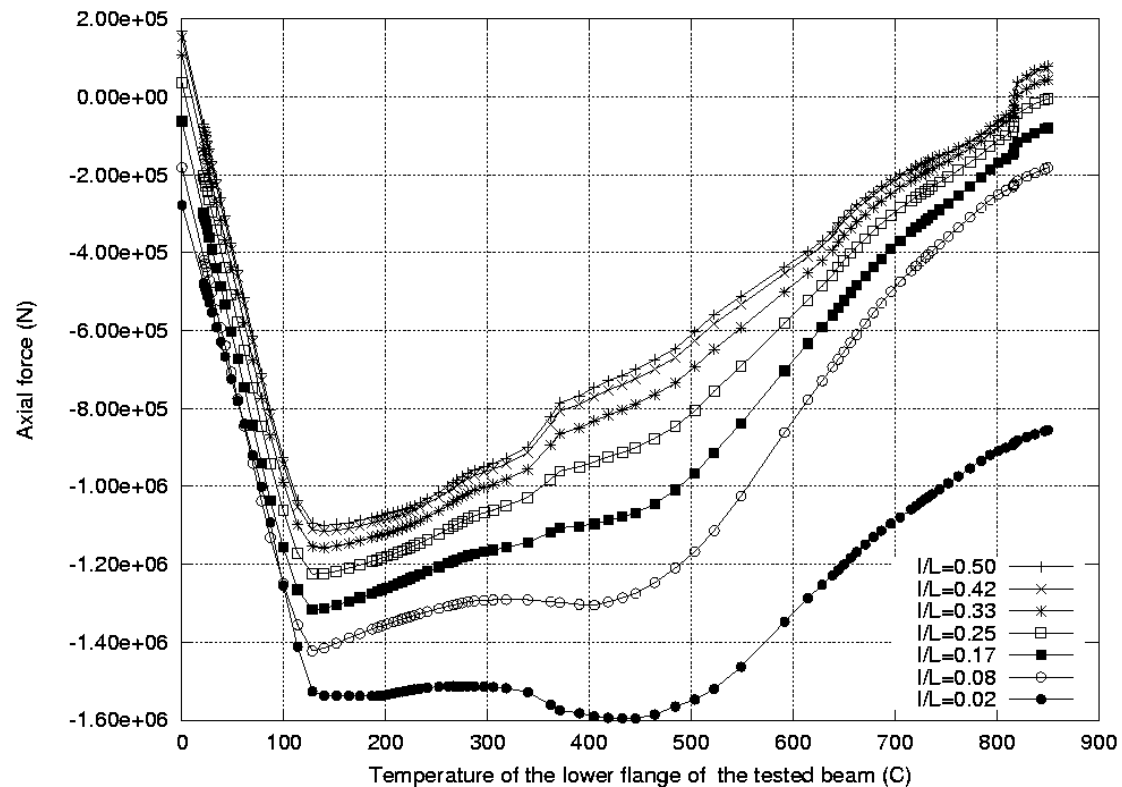
Figure 6: Axial forces at different locations in the steel beam of the restrained beam test

The strains in the transverse direction (Figure 8) shows compressions in the low deflection regions, near the ends of the compartment and tensions in the large deflection region near midspan. In this case of a highly restrained system, the tensions are not caused by the loading, but by the compatibility requirements of a large aspect ratio (8:3) compartment.

Figure 9[8] shows the reinforcement level strains in the longitudinal direction (along secondary beams) in the British Steel corner test (at the end of heating), which are also all compressive, suggesting that even for corner columns protected edge beams can provide considerable restraint and thermal pre-stress to the slab thus enhancing capacity. Figure 8 shows a small area of tension in the transverse direction, which could be because of compatibility or because of loads. Although compatibility is a good explanation, as even though the aspect ratio in this case is not as big (10:8), the mean temperature in the longitudinal direction can be considerably higher over the length of the heating.

Finally, Figure 11[1] shows principles stresses at the end of heating from an explicit analysis of the Britsh Steel Demonstration test (simulated office fire), which shows the evidence of a compressive ring around the periphery of the compartment, with tensile membrane stressed in the interior. This is simply a manifestation of the same phenomena as above, namely thermally induced pre-stress in the low deflection regions (near supports) and tensile membrane behaviour in the span.

---

[1]Courtesy of Dr. Mark O'Connor and Dr. David O'Callaghan at Corus, Swinden Technology Centre
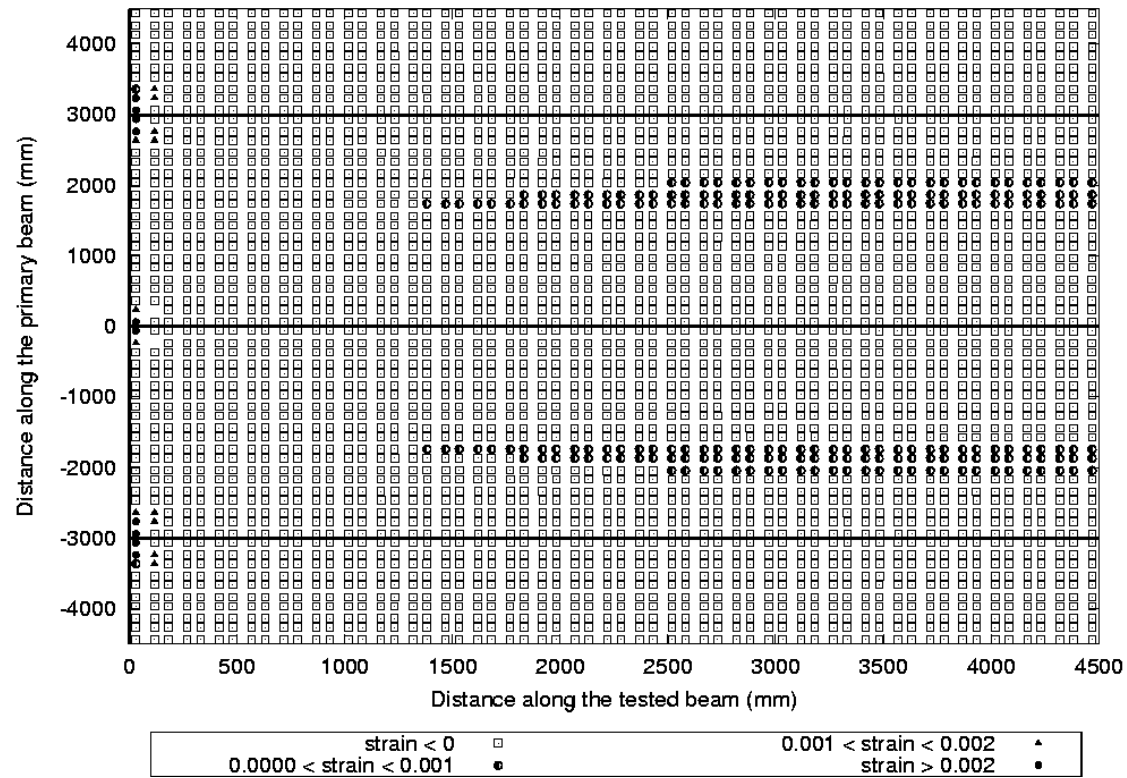
Figure 7: Reinforcement level longitudinal strain patterns in the restrained beam test
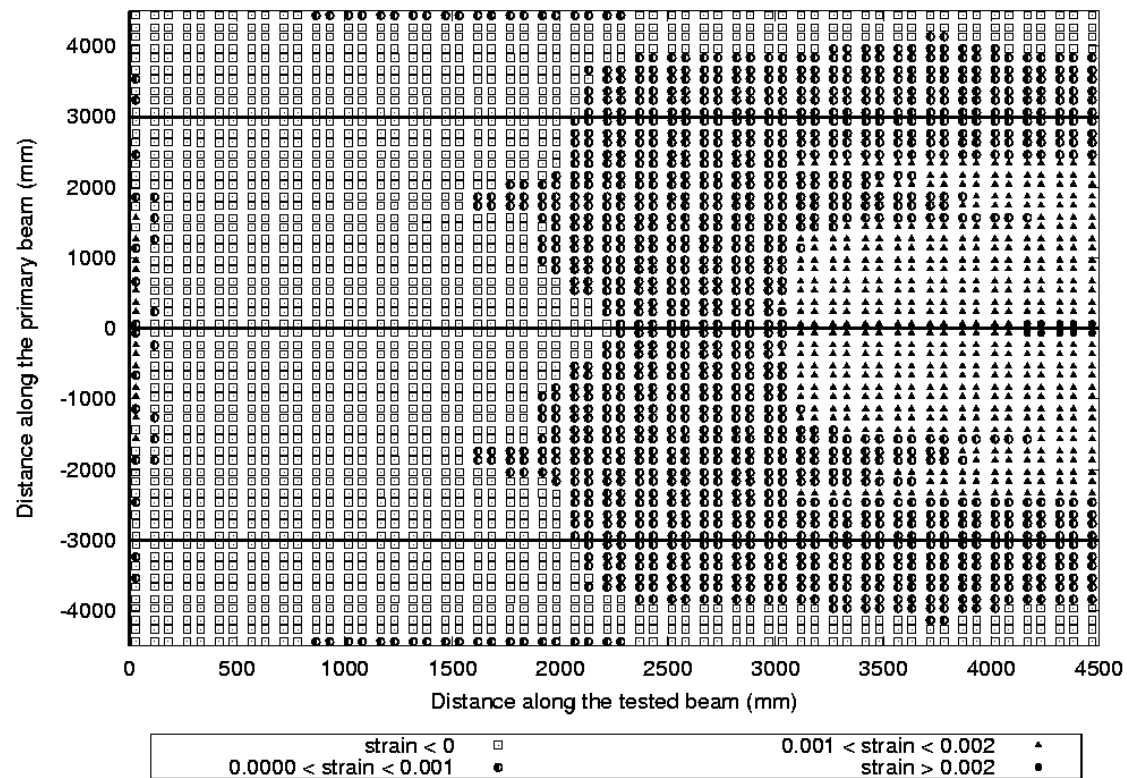

Figure 8: Reinforcement level transverse strain patterns in the restrained beam test
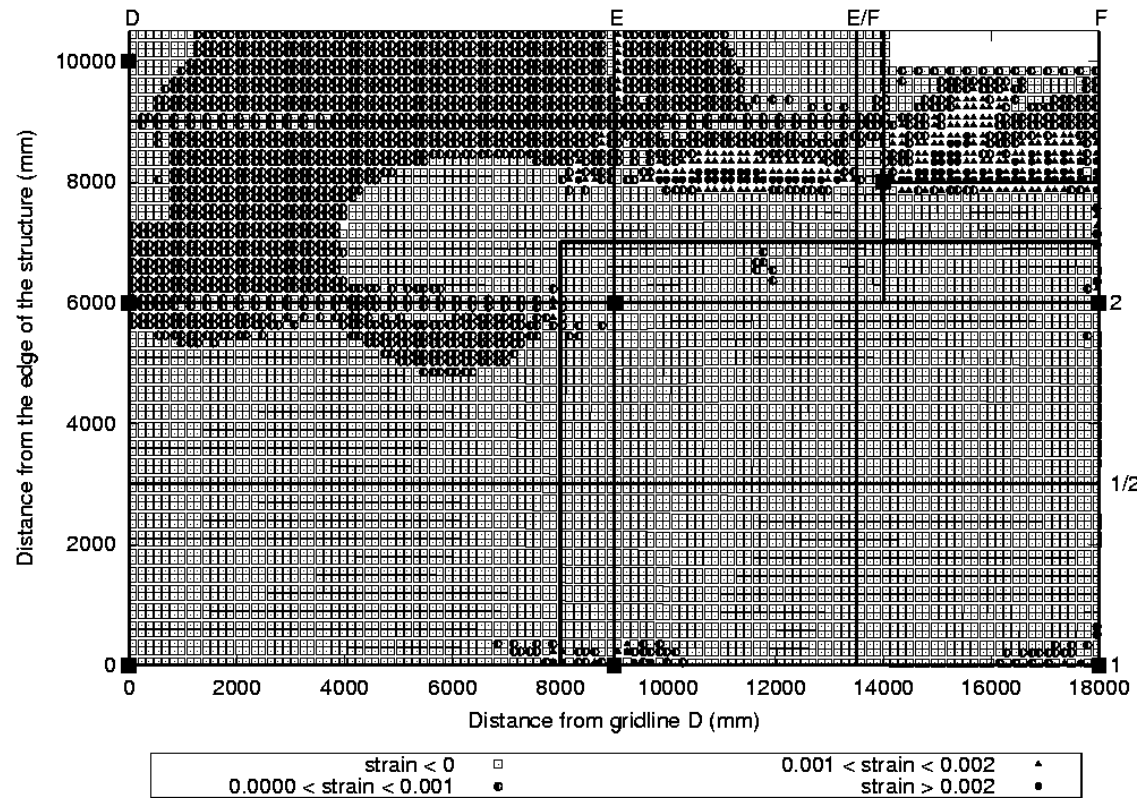
Figure 9: Reinforcement level longitudinal strain patterns in the BS corner test
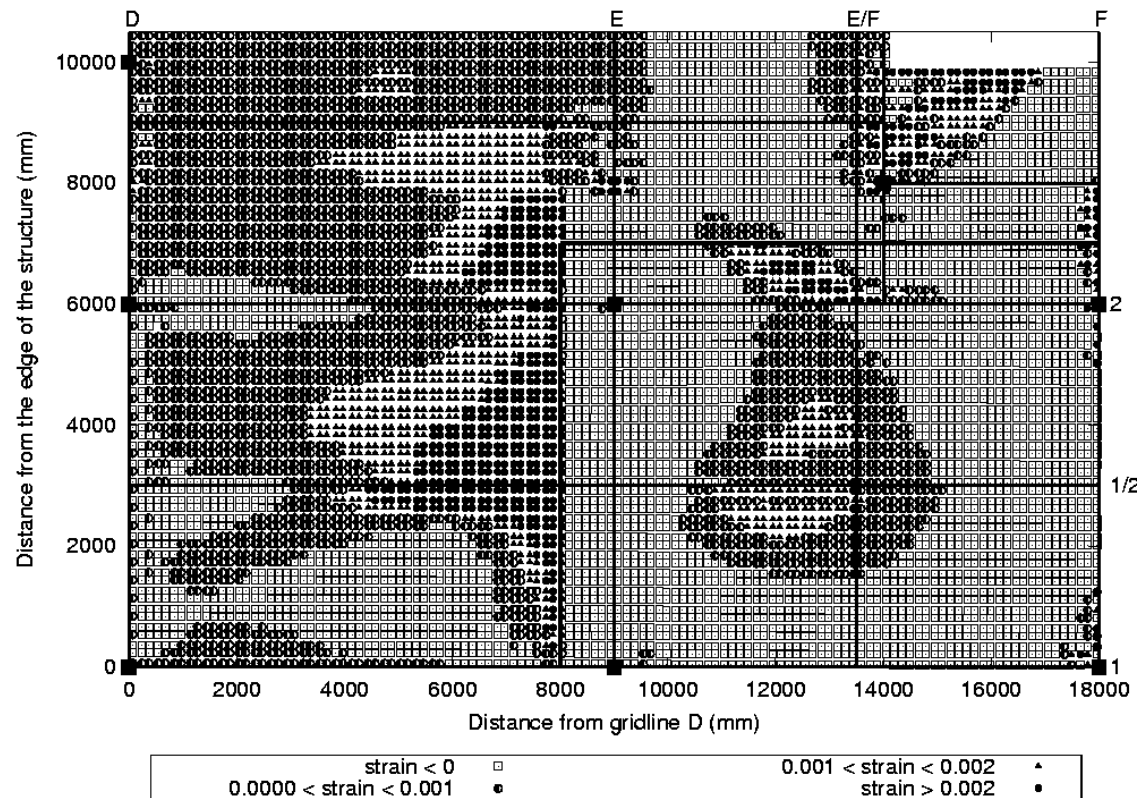

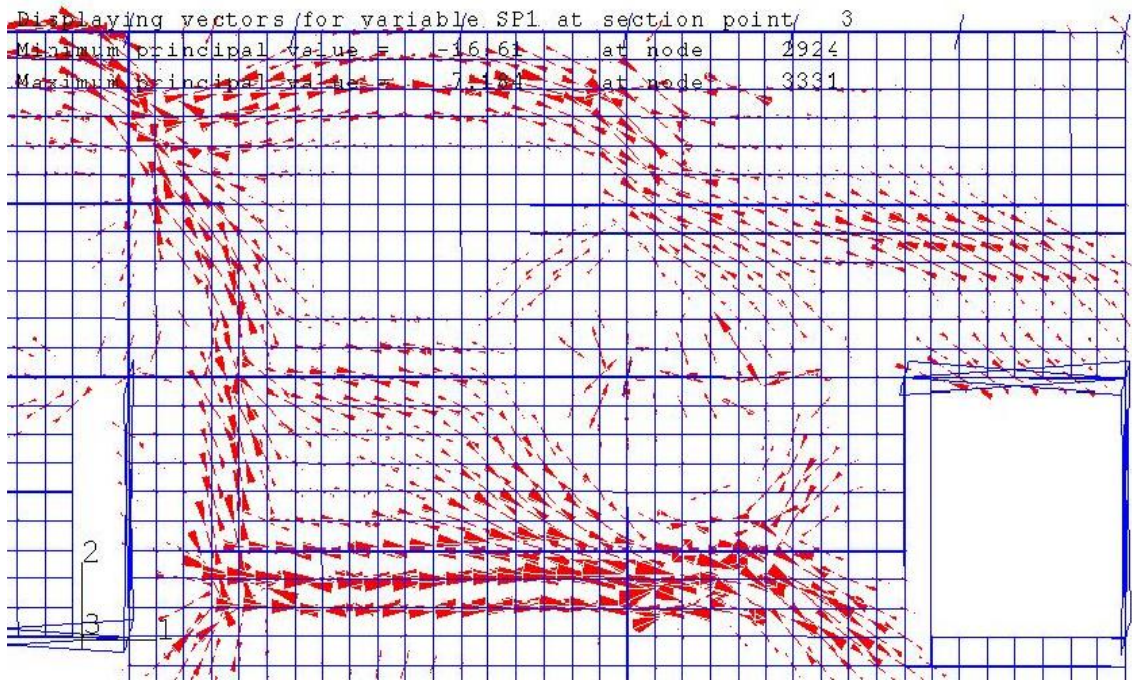Figure 10: Reinforcement level transverse strain patterns in the BS corner test

Figure 11: Principle stresses in the slab for the British Steel "demonstration" test

Panel instability

The above events and phenomena have been reported in previous publications[4,8,9] and have been observed or deduced from analysing experiments such as the Cardington tests. While extending some of the Cardington modelling work and carrying out parametric studies on models of generic composite frames the authors discovered an interesting event (phenomenon) that could occur in a real system as well and must be investigated further to assess it implications on the overall stability of such structures.

Figure 12 shows the plan of small 2×2 bay composite frame.[9] Using the natural fire curves described by Pettersson[10] and assuming a constant fire load but different opening factors two design fires were derived (See Figure 13). With an opening factor of $0.08m^{1/2}$ the post-flashover fire is short in duration reaching high maximum compartment temperatures. The fire with an opening factor of $0.02m^{1/2}$ is characterised by lower maximum compartment temperatures but relatively longer duration. For the purposes of this discussion the fires will be referred to as the "*short-hot*" fire and the "*long-cool*" fire respectively. In both cases the fire load is equal to 250MJ/m^2. Figures 14 shows the midspan deflections of the primary beams B14 and B46 for the two fire scenarios. Two sets of "kinks" can be noted in the deflection plots, one just before 90°C (for the short-hot fire) and the other at about 450°C (for the long-cool fire). These "kinks" in deflection are accompanied by a large change in the axial forces that the primary beams experience as shown by Figures 15 and 16 in the short-hot and long-cool fires respectively. This phenomenon is a sort of a "gigantic" version of the local buckling phenomenon discussed earlier, and occurs at a much larger scale involving the whole composite slab panel in a sudden deflection accompanied by a large axial force release in the primary beams. The same three
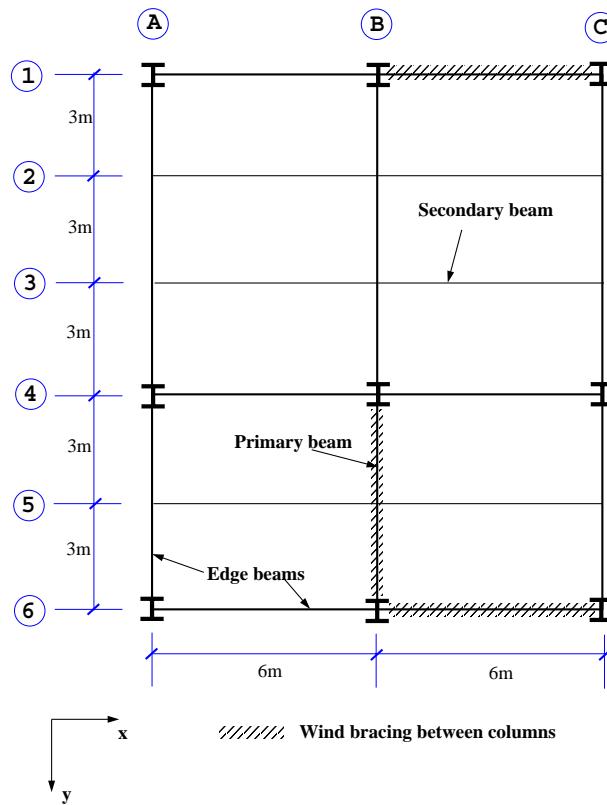
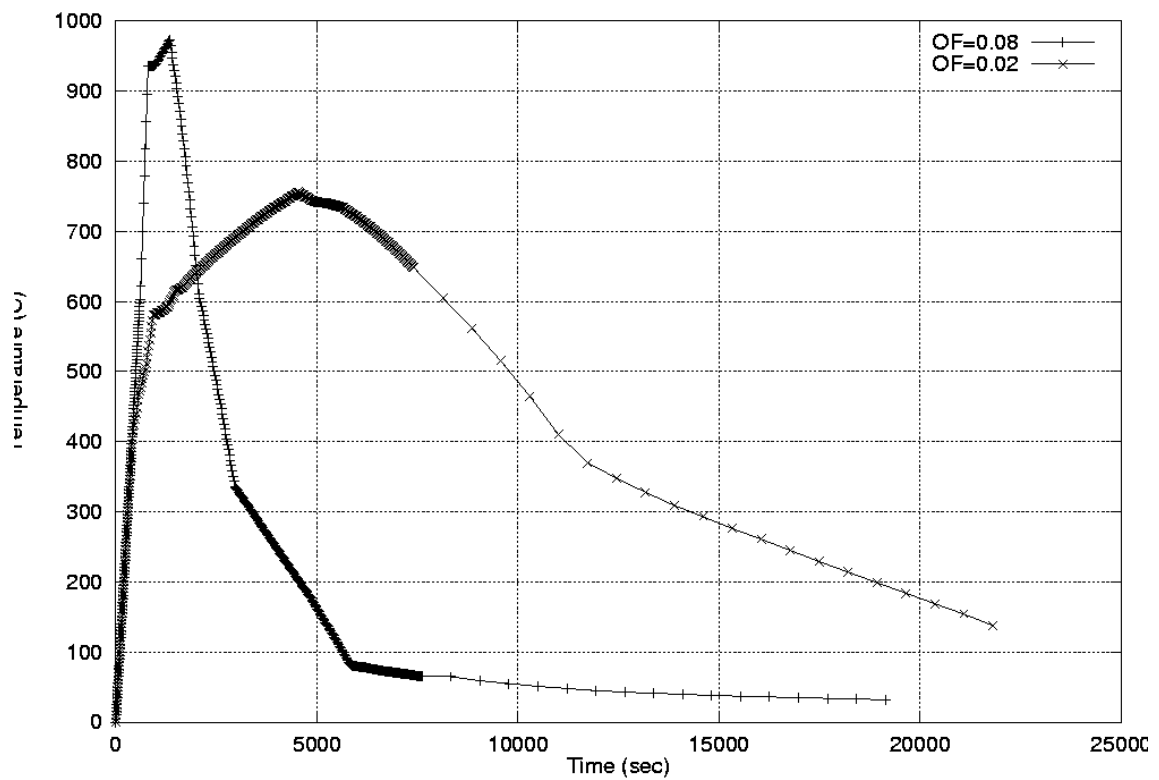Figure 12: Plan of 2×2 bay generic composite steel frame
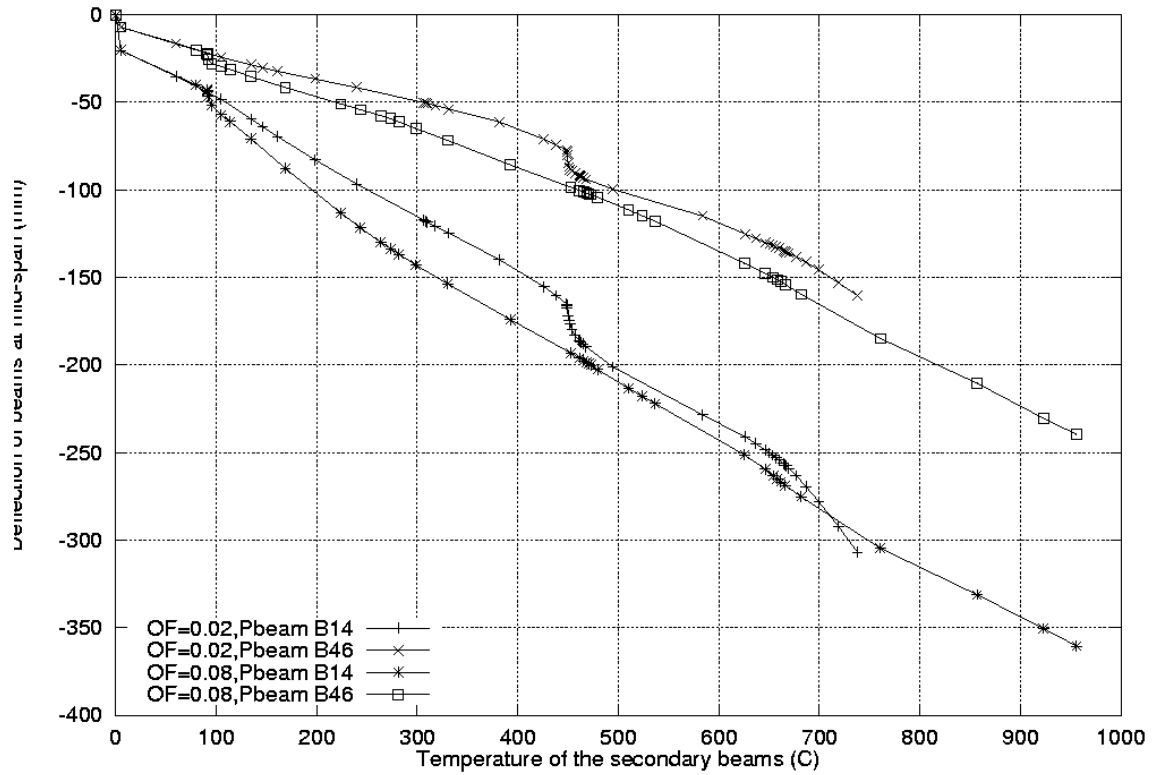

Figure 13: The two design fire scenarios

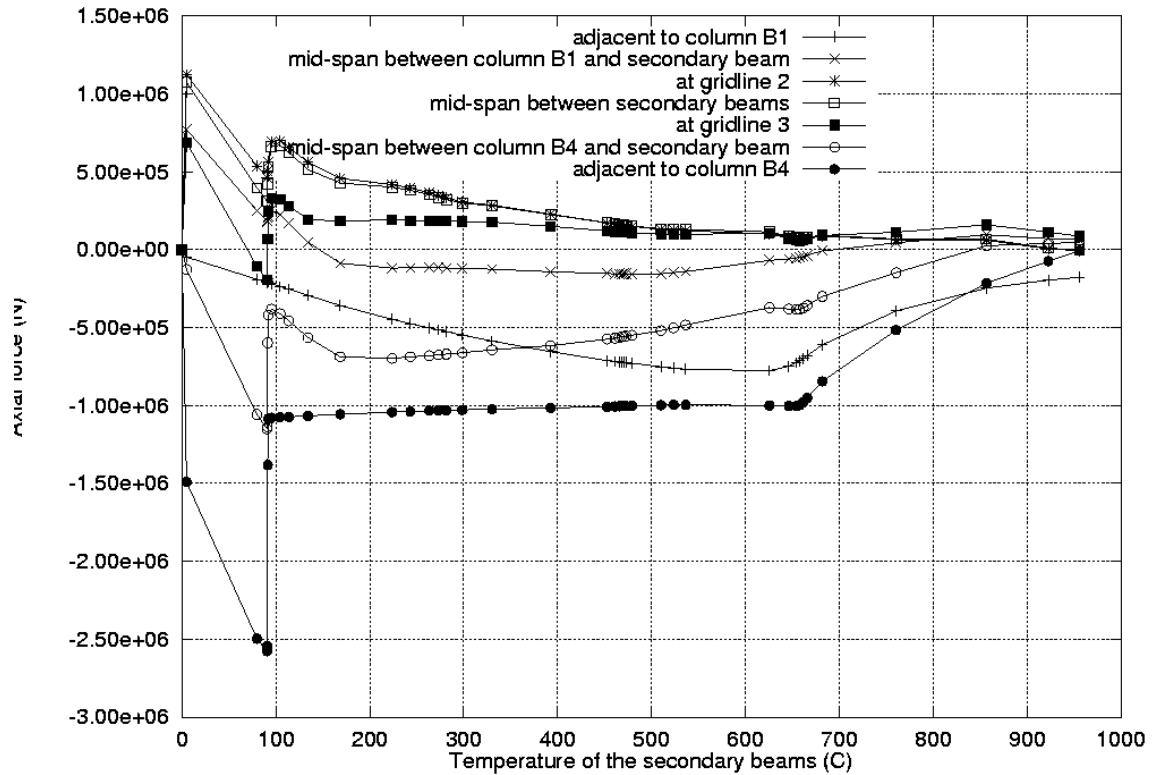Figure 14: Midspan deflections of primary beams B14 and B46

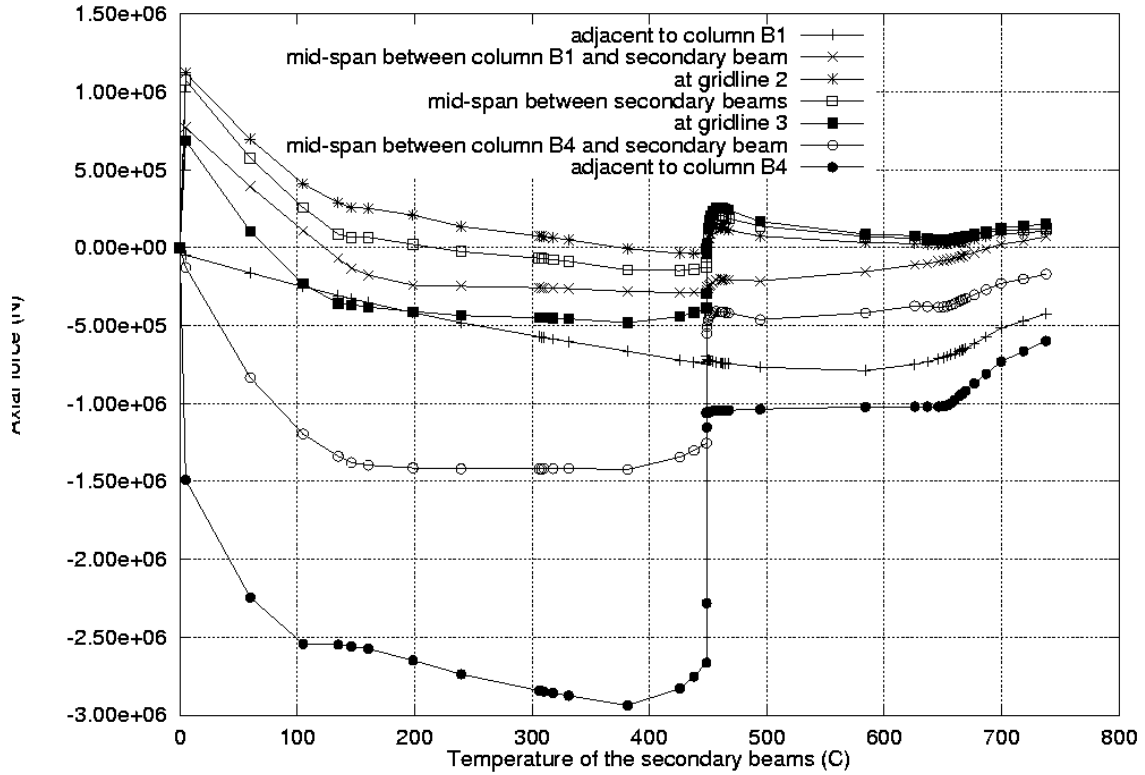Figure 15: Axial forces in the primary beam B14 for the short-hot fire

Figure 16: Axial forces in the primary beam B14 for the long-cool fire

components (loads, thermal expansion and thermal bowing) combine to create a local yielding of the bottom flange of the primary beams. The primary beams have before this event been restrained both in end translation and end rotation because of the end fixity detail shown in Figure 3. The rotational fixity does not allow the primary beam to deflect much and because of this large compressions build up in the beam. Also, these beams are supporting the secondary beams, which are also under the effect of thermal expansion and gradients and therefore are exerting downward forces on the primary beams. Once the local yielding of the primary beam bottom flange occurs, the end conditions change to allow rotation, which frees the secondary beams to push down on the primary beams increasing their deflection suddenly (and therefore length), resulting in a release of the compressive forces stored in the primary beam. This is shown schematically in Figure 17. There is a lot more to this phenomenon and detailed exposition is beyond the scope of this paper, however the second author's thesis[9] gives a much more comprehensive account of this phenomenon. The authors have discovered this phenomenon as result of computational modelling of generic Cardington like frames and are not aware of any physical evidence supporting this finding. However, as this event involves a sudden movement of a whole slab panel, it is possible that if this occurred in a real situation it could result in generating damaging dynamic forces. This event was not seen in the modelling of the Cardington tests. This may be because the live loads in this analysis were larger (when the same live loads as Cardington were applied to this analysis, this phenomenon disappeared).
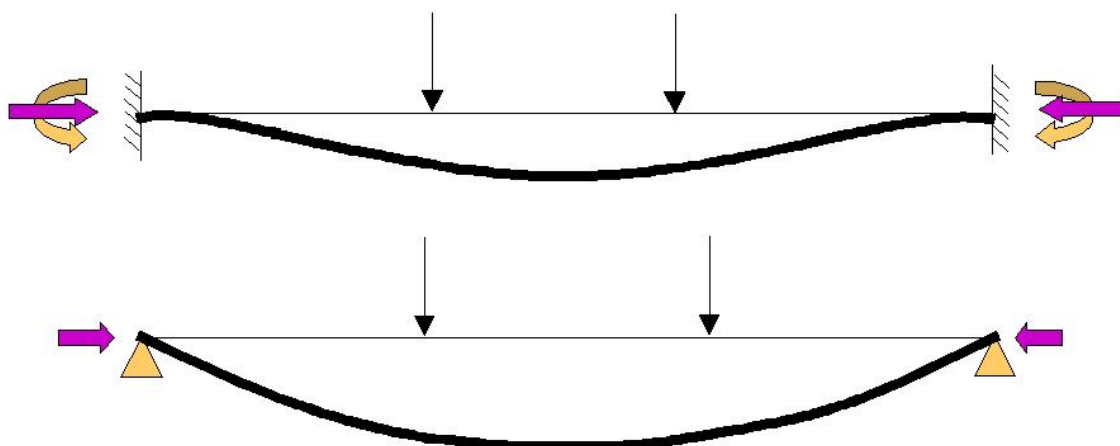
KEY EVENTS DURING COOLING

Figure 17: Schematic of "panel instability" phenomenon

There has been relatively little modelling of the cooling regime, because of a number of challenges, not least of them is the lack of material constitutive data during cooling and the much more computationally troublesome problem of fracture and strain localisation in concrete. Large cracks in the slab near supports have indeed been seen after some of the Cardington fire tests, which are generally attributed to the cooling regime. The other very important event is the rupture of end-plate connections when shortened beams experience large tensions on cooling.

CONCLUSIONS

A number of important features of behaviour of composite floor systems in fire have been analysed and explained, using simple calculation models. It is clear that this structural behaviour has many interesting and subtle features, which can to a lesser or greater extent generalised to most structures of this type. This provides the understanding necessary for developing improved ways of designing such structures for fire.

There are also as yet unanswered questions that must be investigated further, such as an experimental investigation of the "panel instability" event. The cooling regime also needs a thorough investigation and it still is one of the big unknowns in this research. The final failure mechanism of such slab systems in fire needs to be investigated. No current data exists that could be used to address this issue.

REFERENCES

1. G.S.T. Armer and T. O'Dell, editors. *Fire Static and Dynamic Tests of Building Structures.* E and FN SPON, Chapman and Hall, 1999.

2. A.S. Usmani, J.M. Rotter, S. Lamont, A.M. Sanad, and M. Gillie. Fundamental principles of structural behaviour under thermal effects. *Fire Safety Journal*, 36(8):721–744, 2001.

3. R.P.Johnson and R.J.Buckby. *Composite structures of steel and concrete - Volume 2: Bridges.* Collins, London, U.K., 1986.

4. The University of Edinburgh. Final report of the DETR-PIT project: Behaviour of steel framed structures under fire conditions. Technical report, The University of Edinburgh, 2000.
http://www.civ.ed.ac.uk/research/fire/project/main.html.

5. A.S. Usmani. Application of fundamental principles to Cardington restrained beam test. Technical report, The University of Edinburgh, 2000. PIT Project Research Report TM4.

6. N.S.Trahair and M.A.Bradford. *The behaviour and design of steel structures to AS 4100.* E. & F.N.Spon, London, U.K., 1998.

7. A.M. Sanad, J.M. Rotter, A.S. Usmani, and M.A. O'Connor. Composite beams in large buildings under fire-numerical modelling and structural behaviour. *Fire Safety Journal*, 35:165–188, 2000.

8. M.Gillie. *The behaviour of steel-framed composite structures in fire conditions.* PhD thesis, The University of Edinburgh, 2000.
http://www.civ.ed.ac.uk/research/fire/project/main.html.

9. S.Lamont. *The behaviour of multi-storey composite steel framed structures in response to compartment fires.* PhD thesis, The University of Edinburgh, 2001. http://www.civ.ed.ac.uk/research/fire/project/main.html.

10. O. Pettersson, S.E. Magnusson, and J. Thor. *Fire Engineering design of Steel Structures.* Swedish Institute of Steel Construction, Publication 50, Stockholm, 1976.

STABILITY OF LIGHTWEIGHT STRUCTURAL SANDWICH PANELS EXPOSED TO FIRE

Gordon M E COOKE BSc PhD CEng MIMechE MICE FIFireE
International Fire Safety Consultant, UK, London and Visiting Professor, Dept of Civil Engineering, City University, London
gordon@cookeonfire.com

ABSTRACT

Sandwich panels comprising flat metal faces and a lightweight structural core are increasingly used as walls and ceilings in buildings where their long-span capabilities, high thermal insulation, clean design, rapid installation and low maintenance often make them the preferred choice of designers and building owners.

The fire performance of sandwich panels can be excellent if the correct core material is used and, importantly, if the metal facings are adequately restrained. For example, fire resistance in excess of 2 hours can be easily achieved using panels with sheet steel faces and a non-combustible rock wool core.

Where sandwich panels are used in cold stores there is the potential problem of cold-bridging between the facings wherever there is a metallic through-fixing, and this has led to designs which work well in normal conditions but allow panels to collapse very early when exposed to fire because the facings are not tied back to the supporting structure. Such collapse is a fire hazard to fire-fighters as proven in the 1993 fire in the Sun Valley poultry factory in Hereford, UK in which two firemen lost their lives.

The paper describes what can happen if panel facings are not mechanically restrained with steel fastenings. It then introduces a fire safety engineering method for assessing the stability of ceiling sandwich panels exposed to fire. The method assumes that the ends of panels are restrained and the panel behaves as a catenary after delamination. The paper quantifies the variation of catenary force as fire develops and takes account of the initial beneficial sag which is present at the time of delamination. The method is currently being considered in the work of European committee CEN TC 127 on the development of rules for extended applications for construction products.

KEYWORDS: *Fire resistance, sandwich panel, stability, fire scenarios, ceilings, cold stores, catenary*

INTRODUCTION

Sandwich panels are being increasingly used in single-storey and multi-storey buildings because they are lightweight, energy efficient, aesthetically attractive and can be easily handled and erected. When constructed with non-combustible structural rock wool cores, panels have good airborne sound insulation and levels of fire resistance which can exceed two hours.

Many panels employ combustible cores of foamed plastic e.g. polyurethane, polyisocyanurate and polystyrene, which, in a fire, can delaminate and produce large amounts of heat, smoke and toxic gases which can be a hazard to life, property, business continuity and the environment.

Most sandwich panels in the UK have sheet steel facings and are bonded to the core using a thermosetting adhesive such as polyurethane. Small scale tests by the UK Fire Research Station, Building Research Establishment have shown that delamination temperatures are likely to be in the range 130-350 $^{\circ}$C. This means that panels can delaminate and collapse before flashover unless the panel facings are adequately restrained.

Sandwich panels used as external wall and roof cladding are usually attached to a supporting structure which prevents both panel facings from falling down in a fire. However, when used as ceilings and free-standing internal walls (as in some cold stores), bonded sandwich panels can collapse if the facings are not adequately restrained.

If a fire resistance test on a representative specimen has been made successfully it is unlikely that collapse in the building context will occur for an equivalent fire severity, similar size of panel and adequate panel restraint. However not all sandwich panels are tested for fire resistance and an assessment then needs to be made for panel stability, especially if the panel is much larger than its fire-tested counterpart.

This paper deals solely with theoretical aspects of structural behaviour in fire. Information on other aspects such as fire load, fire scenarios, fire testing and a check list for fire safe design is available [1-3] while some preferred panel attachment methods are given in [4]. Following a number of damaging fires associated with plastic foam cored sandwich panels in the food industry two codes of practice have been published in the UK [5, 6]. A book on sandwich panels [7] has recently been published which has useful practical guidance on ways of designing panels to resist fire. The author has made an in-depth study [8] of the problems of making a risk assessment which properly takes account of the problems associated with panels having combustible cores, and he contends that present official UK technical guidance in the government's Approved Document B remains unsatisfactory. Some inadequacies in ad-hoc fire tests for combustible-cored sandwich panels are reported elsewhere [9].

FREE-STANDING INTERNAL WALLS

The stability of free-standing sandwich panels forming a wall is achieved by attaching both facings of the panel at the top, e.g. to a roof beam, which has the required fire resistance. In a fire the panel loses its flexural strength when the facing delaminates from the core and the panel then becomes suspended from the top.

370

Adequate suspension is achieved if:

a) the fastenings at the top of the fire exposed face carry the dead load of that facing,
b) the fastenings at the top of the unexposed face carry the dead load of that facing and the core, and
c) the top support member is capable of carrying the panel dead load.

Fire is an accidental limit state and because the simultaneous occurrence of fire and snow is unlikely in most countries, the reserve of strength needed to carry the snow load can be utilised to carry the panel dead load in the fire condition so that the strength of the roof structure does not have to be increased.

CEILINGS

Structural sandwich panels rely on an adhesive layer between the flat metal faces and the core material for their flexural strength. Most adhesives used in proprietary panels delaminate at quite low temperatures - in the range 130 to 300 ^{o}C according to tests carried out by the Fire Research Station of the BRE. These temperatures are reached in less than 5 minutes in the ISO 834 fire resistance test exposure and well before flashover in a real fire. If panels simply rest on supports with no horizontal restraint the panels will, on delamination, sag and slip off the supports. Since panels can be more than 1 m wide and 12 m long a collapsing panel is a substantial potential missile threat to occupants making their escape or fire-fighters performing their search, rescue and firefighting duties. To prevent collapse the ends of the panel faces must be fastened to the supporting structure and horizontally restrained so that they act as catenaries (cable-like) structures. This can be done without forming a thermal bridge between the upper and lower facings and a suitable detail is shown in Figure 1.
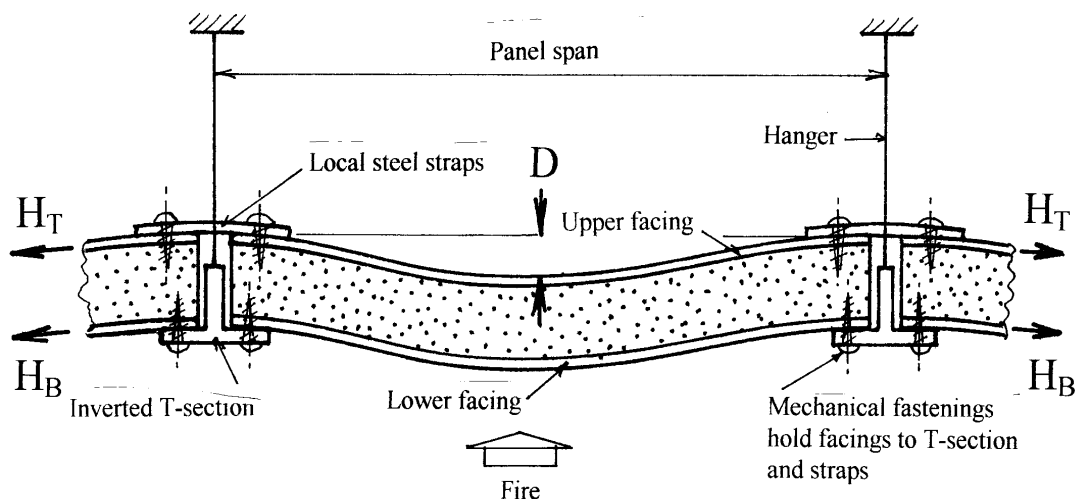

Figure 1

The catenary forces, H_T and H_B, can be large and some attempt should be made to calculate them to ensure that the panel end fastenings do not fail. For a simply supported panel of span L, the horizontal force H needed to support the catenary is
given by equation 1) and this is derived in Annex A

$$H = wL^2/8D \qquad\qquad (1)$$

where w = uniformly distributed load per unit length

Deflection D may be caused by thermal expansion of the facing and by inward displacement of the panel ends due to in-plane flexibility of the panel assembly. Both effects are beneficial .

Before equation (1) can be used, D must be calculated or estimated. This can be done if the temperature of the facing and/or inward end movement is known or can be estimated, and it is assumed in the following equations that the facings hang in the shape of a circular arc. It can be shown that, due to temperature rise alone:

$$D = L(0.375\alpha T)^{1/2} \qquad\qquad (2)$$

where α = coefficient of thermal expansion, and
T = temperature rise

Due to inward end movement alone:

$$D = (0.375Lp)^{1/2} \qquad\qquad (3)$$

where p = relative inward movement of panel ends

Using equations (1) and (2) calculations have been made for the catenary force as a function of span and temperature rise for one steel facing which is 1200 mm wide by 0.5 mm thick. Two panel spans were chosen - 6 m and 12 m. The results are given in Figure 2. The higher the failure temperature of the adhesive, the lower the catenary force and the easier it is to design the panel end fastenings. The same kind of calculations can be made for the effect of panel inward end movement.

Fire attack from below the ceiling

When the lower face is exposed to fire each panel bows downwards. Delamination of the fire exposed face occurs when the strength of the adhesive layer is lost. The flexural strength of the panel assembly then approaches zero and collapse will occur unless one or both faces are restrained horizontally at the panel ends so that they become catenaries.

If only the lower face is horizontally restrained the catenary force in that face is a maximum because the dead load of the whole panel (upper face, core and lower face) has to be carried by the lower face and its fastenings to the support structure. The catenary force can be beneficially shared between both faces if both faces are horizontally restrained.
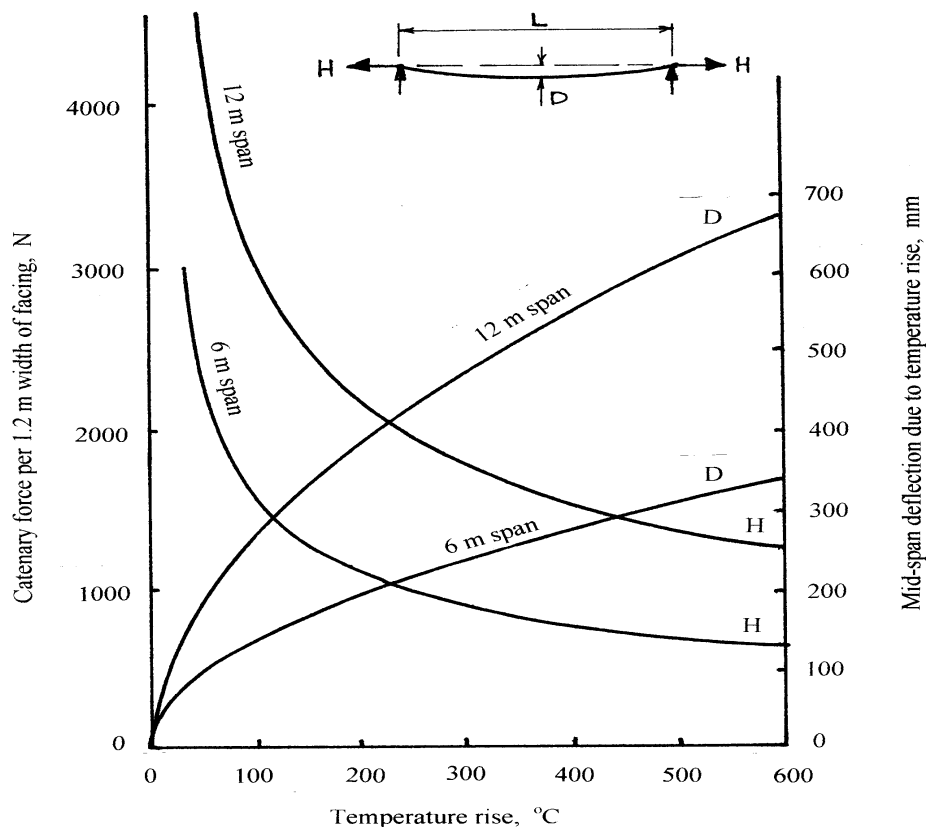
Figure 2 Variation of catenary force with temperature

Fire attack from above the ceiling

When the upper face is exposed to fire each panel initially bows upwards. Delamination of the fire exposed face occurs when the strength of the adhesive layer is lost. The flexural strength of the assembly then approaches zero and collapse will occur unless at least the lower face is restrained horizontally at its ends so that it becomes a catenary

If only the lower face is horizontally restrained the catenary force in that face is a maximum because the dead load of the whole panel (upper face, core and lower face) has to be carried by the lower face and its fastenings to the support structure. The catenary force can be beneficially shared between both faces if both faces are horizontally restrained. It should be noted that the catenary force in the lower face will be high because there is no beneficial sag in the lower face in the absence of a temperature rise in the lower face. However the transfer of the dead load of the upper facing and core onto the lower face will cause some beneficial sag due to in-plane flexibility of the whole panel assembly e.g. by dragging together the panel end support structure, by slippage of the fastenings and/or elongation of the fastening holes in the panel facing. The estimate of inward end movement requires professional judgement.

Of the two conditions, i.e. fire exposure from above or fire exposure from below, fire exposure from above causes the largest catenary forces. Note also that fire from above may be unseen by people, e.g. fire fighters, below the ceiling and collapse could present a life

risk. The realistic assessment of catenary force and the use of properly designed and tested fastenings is therefore of great importance.

LOADING AND MATERIALS DATA FOR ELEVATED-TEMPERATURE CALCULATIONS

The dead load of the facing and core can be calculated from information on the volume and density of the construction materials. The density of steel sheet can be assumed to be 7850 kg/m³. The density of other metal sheets can be obtained from national standards. The density of the core material at elevated temperature should be assumed to be the density at room temperature unless a) there are appropriate data available on the time-dependant change in density due to the effects of fire exposure e.g. due to charring or significant reduction in moisture content or b) the core material is consumed in the heating process, as with expanded polystyrene foam.
The reduction in strength properties of steel at elevated temperature may be assumed to vary according to the relevant national standard e.g. in the United Kingdom by reference to BS 5950: Part 8: 1980 which gives strength reduction factors for hot rolled steel and cold formed steel at different temperatures. Alternatively, information in the structural Eurocodes could be used, for instance, Eurocode 3: Design of steel structures, Part 1.2 General rules: Structural fire design (DD ENV 1993-1-2). Strength reduction factors for other metals may also be obtained from national standards or laboratory tests.

CONCLUSIONS

Sandwich panels have many advantages. Care is needed however to ensure that premature instability does not occur in a fire. Ways of retaining panel stability have been shown and a theory developed for ceiling panels. Assessment of panel stability forms a part of the overall fire risk assessment for a building. The panel support structure must have at least the same fire resistance as the panel assembly.

Making calculations of the structural behaviour of a sandwich panel in fire is only necessary if the panel is to be used in an application which involves a span which is greater than the fire tested span. Most fire resistance test furnaces adopt a span of approximately 4.5m whereas sandwich panel ceiling spans can reach 12m

Without a calculation of the catenary forces acting on a ceiling sandwich panel it is possible for the fasteners at the ends of the panels to fail allowing collapse at an early stage in a fire. A calculation method has been proposed which enables the catenary force to be calculated for fire attack from above or below the ceiling.

To reduce the magnitude of catenary force developed when fire attack is from below the ceiling, it is advantageous to use an adhesive for bonding the core to the facing which weakens at a high a temperature as possible consistent with economy and panel production method.

Fire attack from above the ceiling will lead to the development of large and perhaps unsustainable catenary forces unless there is sufficient in-plane flexibility in the total ceiling

assembly to allow some sagging of the lower facing. This requires an assessment using professional judgement.

REFERENCES

1   Cooke G M E, When are sandwich panels safe in fire ?- Part 1 An overview, *Fire Engineers Journal*, July 1998, pp 37 - 41

2   Cooke G M E, When are sandwich panels safe in fire ?- Part 2 Avoiding collapse, *Fire Engineers Journal*, Sept 1998, pp 25 - 33

3   Cooke G M E, When are sandwich panels safe in fire ?- Part 3 Fire scenarios, fire tests and checklist, *Fire Engineers Journal,* January 1999, pp 18 - 25

4   Cooke G M E, The behaviour of sandwich panels exposed to fire, *Building Engineer*, July 1997, p 14-29

5   Code of practice for fire protection in the food and drink industry, pub Loss Prevention Council, London, 1999

6   Guidelines for the design, specification, construction, maintenance and fire management of insulated envelopes for temperature controlled environments, pub The International Association of Cold Storage Contractors (European Division), 1999

7   Lightweight sandwich construction (edited J M Davies), published Blackwell Science, Oxford, UK, 2001

8   Cooke G M E, Sandwich panels for external cladding – fire safety issues and implications for the risk assessment process. Published by Eurisol, UK, November 2000, pp 60

9   Cooke G M E**,** Design fires for testing combustible-cored sandwich panels, Interflam 2001, International fire science and engineering conference held in Edinburgh on 17-19 Sept 2001, Pub Interscience Communications Ltd, London , 2001, pp 1189-1195

ANNEXES

Annex A

A simply supported, unrestrained member of length L and depth d is subjected to a linear temperature distribution across its depth which does not vary along the length, Figure A1. The temperature difference, T_1, causes the member to bow upwards in a circular arc resulting in each end rotating through an angle θ. It remains free of internal stresses. For an element of length dx, the expansion of the uppermost fibre is

$$de = \alpha \frac{T_1}{2} dx$$

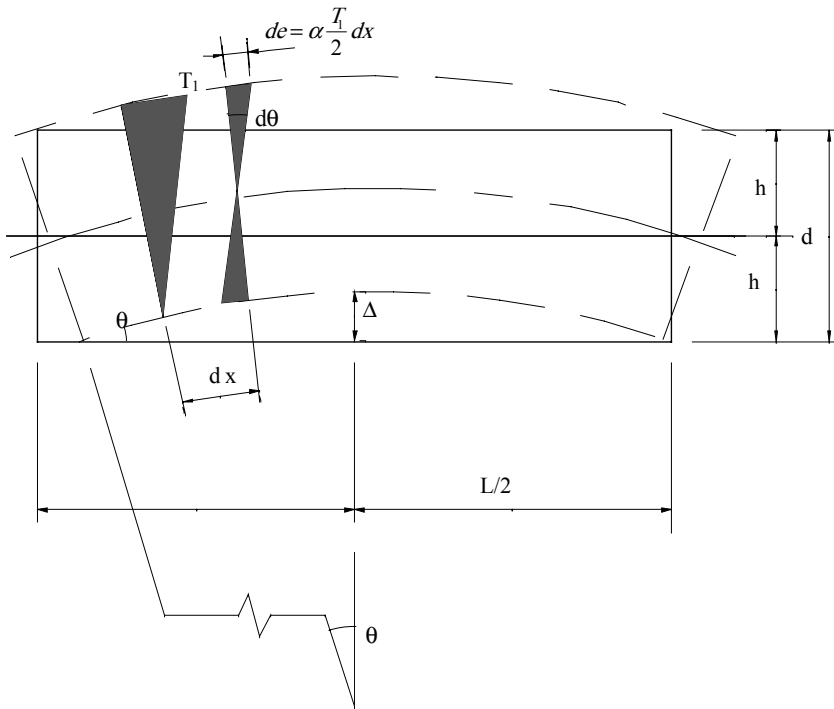The angular change in element dx is:

Figure A1 Displacements of a simply supported member subjected to a linear temperature gradient

$$d\theta = \frac{de}{h} = \alpha \frac{T_1}{2h} dx \qquad (A1)$$

Integrating Equation (A1) gives:

$$\theta = \int d\theta = \frac{\alpha T_1}{2h} \int_0^{L/2} dx = \frac{\alpha T_1}{2h} \frac{L}{2} = \frac{\alpha T_1 L}{2d} \qquad (A2)$$

376

Using the properties of similar triangles and referring to Figure A2, CB/AC = ED/EB. For small angle θ, CB = L/4 so that:

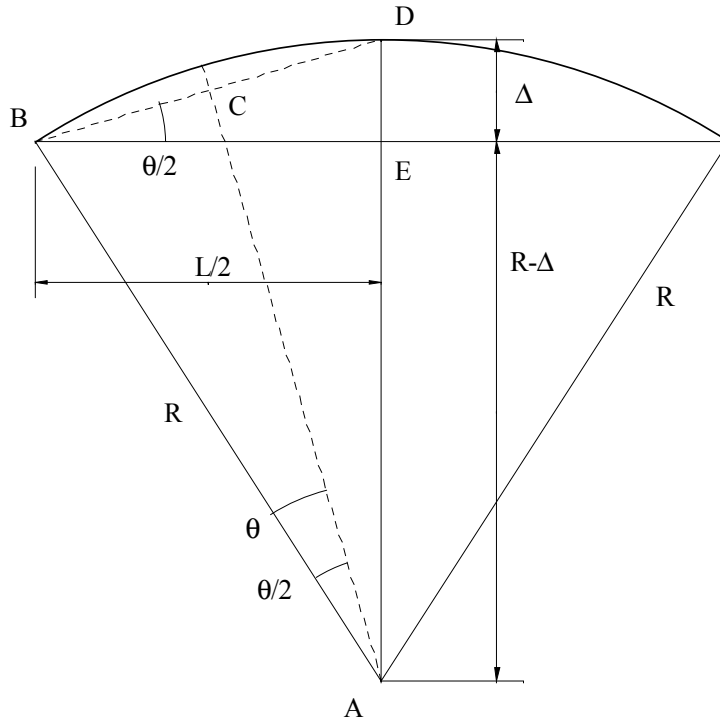Figure A2 Diagram relating Δ, θ and R

$$\frac{L/4}{R} = \frac{\Delta}{L/2} \quad \text{from which}$$

$$R = \frac{L^2}{8\Delta} \tag{A3}$$

Ignoring Δ which is small compared with R,

$$\theta = \tan^{-1}\frac{L/2}{R} \quad \text{from which, for small angles:}$$

$$\theta = \frac{L}{2R} \tag{A4}$$

Substituting R from Equation (A3) in Equation (A2) gives $\theta = \dfrac{4\Delta}{L}$ and substituting in Equation (A2) gives:

$$\theta = \frac{\alpha T_1 L}{2d} = \frac{4\Delta}{L} \tag{A5}$$

so that

$$\Delta = \frac{\alpha T_1 L^2}{8d} \qquad (A6)$$

Annex B

The classical text book equation for the horizontal restraint force H needed to support a catenary (cable-like structure) of span L carrying a uniformly distributed load w per unit length having a mid-span deflection D, Figure B1, is simply derived in the following way. For equilibrium $\sum M = 0$ where M = moment. Taking moments about point A for the right hand half of the catenary,

$$w\frac{L}{2}\frac{L}{2} = Hd + w\frac{L}{2}\frac{L}{4} \qquad \text{from which}$$

$$H = \frac{wL^2}{8D} \qquad (B1)$$

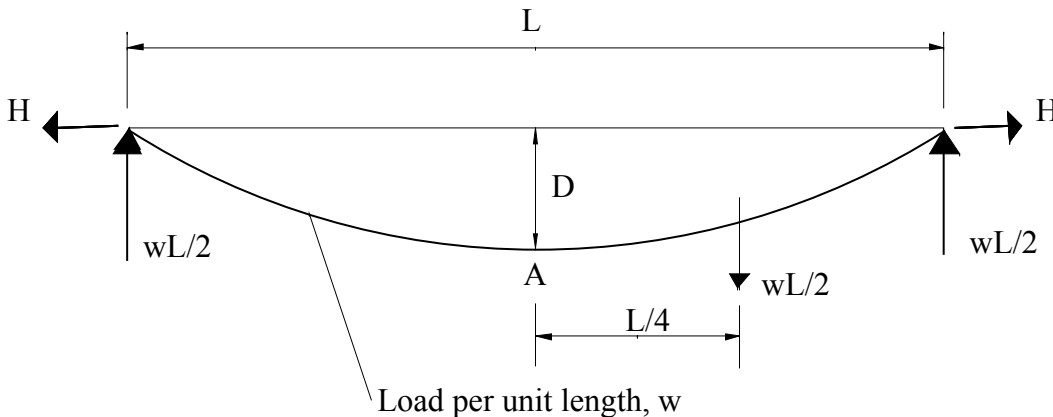Note that H becomes infinite as D becomes small

Figure B1 Catenary force diagram

Annex C

The equation derived below relates the axial shortening Δ_L to the mid-span deflection Δ_N for a flexible member when the member bows into a circular arc. Consider an initially straight member AB of length L, Figure C1, in which end A is position fixed. The member is slender so that the application of an axial compressive force P at end B causes negligible elastic compressive strain in the material but causes it to bow into a circular arc ACD.
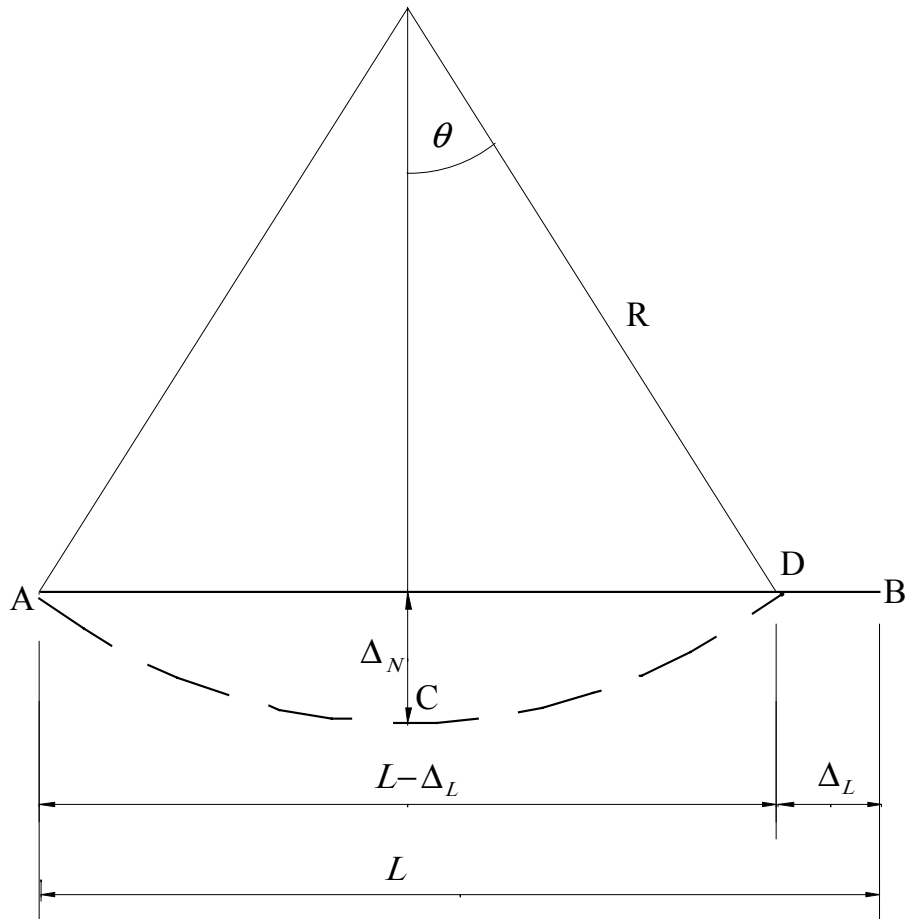From Figure C1

Figure C1   Geometry of bowed member

$$L = 2R\theta \tag{C1}$$

$$\frac{L - \Delta_L}{2} = RSin\theta \tag{C2}$$

$$R - \Delta_N = RCos\theta \tag{C3}$$

From Equations (C1) and (C2)

$$\Delta_L = 2R(\theta - Sin\theta) \tag{C4}$$

Substituting for R from (C2) in (C4)

$$\Delta_L = (L - \Delta_L)\frac{(\theta - Sin\theta)}{Sin\theta} \tag{C5}$$

By Maclaurin's series, $Sin\theta = \theta - \theta^3/3! + \theta^5/5! \approx \theta - \theta^3/3!$

Substituting in Equation (C5)

$$\Delta_L = (L - \Delta_L) \frac{\theta^2}{6} \tag{C6}$$

From Equation (C3)

$\Delta_N = R(1 - Cos\theta)$ and substituting for R from Equation (C2) gives:

$$\Delta_N = (L - \Delta_L) \frac{(1 - Cos\theta)}{2 Sin\theta} \quad \text{and as } Cos\theta \approx 1 - \theta^2 / 2!$$

$$\Delta_N = (L - \Delta_L) \frac{\theta}{4} \tag{C7}$$

Form Equation (C6)

$$\theta = \sqrt{\frac{6\Delta_L}{L - \Delta_L}} \quad \text{and substituting for } \theta \text{ in Equation (C7) gives:}$$

$$\Delta_N = \frac{(L - \Delta_L)}{4} \sqrt{\frac{6\Delta_L}{L - \Delta_L}} \quad \text{and ignoring 2nd order terms}$$

$$\Delta_N = \sqrt{0.375 L \Delta_L} \tag{C8}$$

If, instead of pushing end B of the slender member in by an amount Δ_L, the member is heated through a temperature T, the longitudinal expansion will be αLT where α is the coefficient of linear thermal expansion. If both ends of the member are position fixed before heating, the member will bow due to the expansion. In this case $\Delta_L = \alpha LT$ and substituting in Equation (C8) gives:

$$\Delta_N = L\sqrt{0.375 \alpha T} \tag{C9}$$

Session 8:
Fire Severity

EXAMPLES OF FIRE ENGINEERING DESIGN FOR STEEL MEMBERS, USING A STANDARD CURVE VERSUS A NEW PARAMETRIC CURVE

C R BARNETT
Macdonald Barnett Partners Ltd, Consulting Engineers, Auckland, New Zealand.
cliff@macbar.co.nz

G C CLIFTON
HERA Structural Engineer, HERA, Auckland, New Zealand
structural @hera.org.nz

ABSTRACT

This paper presents examples of the differences that can occur when a standard time-temperature curve and a parametric time-temperature curve are used to determine temperatures likely to be reached by uninsulated and insulated steel members during a fire. For low and moderate structural fire severity situations, determination of the adequacy of a steel member by comparing the temperature reached in a "design fire" with the limiting temperature based on the member heat sink characteristics, extent of insulation and utilisation factor is becoming increasingly common fire engineering design practice. For this it is important to have as accurate and widely applicable parametric fire model as is practicable.

The standard time-temperature curve used in the examples is the ISO 834 Curve. The two parametric time-temperature curves used in the paper are the Eurocode Parametric Curve [1] and a recently developed one termed the "BFD Curve" [2]. The latter has been found to fit the results of a wide range of actual fire tests more closely than do existing parametric curves and is mathematically simpler in form.

The shape of the BFD Curve and the parameters used to define it bear a strong relationship to both the pyrolysis coefficient ($R/A_v h_v^{0.5}$) and the opening factor, F_{02}. The curve also models the development of fire without the need for time shifts. It uses a single and relatively simple equation to generate the temperature of both the growth and decay phases of a fire in a building and only three factors are required to derive the curve. These factors are (i) the maximum gas temperature, (ii) the time at which this maximum temperature occurs, and (iii) a shape constant for the curve. If desired, the shape constant can be different on the growth and the decay sides to model a very wide range of natural fire conditions and test results.

Other parametric curves such as the current Eurocode Parametric Curve [1] require at least two relatively complex equations and both seem to have time shifts involved in their original derivations.

KEYWORDS: *Fire engineering, fire compartment temperatures, structural fire engineering design, fire modelling.*

INTRODUCTION

For low and moderate structural fire severity situations, determination of the adequacy of a steel member by comparing the temperature reached in a "design fire" with the limiting temperature for the member is becoming increasingly common fire engineering design practice. More details on this practice and examples where it is applied are given in section 1.3 of [3].

For applications to enclosures where the fuel can be considered cellulosic in nature and uniformly distributed over the enclosure area, one of the most commonly used natural design fire curves is the *Eurocode Parametric temperature–time curve,* given in Appendix A of prEN1991-1-2 [1]. Once the fire time-temperature curve has been generated, the temperature rise in a steel member can be determined using the heat transfer method given in section 3 of [1] or section 5.7 of the *Fire Engineering Design Guide* [4]. The adequacy of the steel member can then be determined in accordance with NZS 3404 [5] Clauses 11.3, 11.4 and 11.5, by determining whether the maximum temperature reached, T_{max}, is less than the limiting temperature, T_l, calculated from Clause 11.5.

The Eurocode Parametric Curve comprises up to three equations for the heating side of the curve and one of three equations for the cooling side. This makes it complex to implement in a spreadsheet. Furthermore, the decay curve has been found not to well represent the exponential time-temperature cooling characteristics of experimental fire tests. The cooling conditions can be modified to give better agreement with experiments, eg. as presented in the Modified Eurocode Curves [6], however at the cost of adding a further two equations on the cooling side.

A new parametric natural fire curve has been developed that fits the results of a wide range of natural fire tests more closely than do the Eurocode Parametric Curves and is mathematically simpler in form. It is called the "BFD Curve" and full details of its development are given in [2]. It has been developed from curve fitting to a wide range of experimental tests.

The first two sections of this paper present the equations describing the BFD Curve and examples of its fitting to some natural fire tests.

The method of limiting steel temperature determination to the New Zealand standards (NZS 3404 [5] and NZS 4203 [7]) is then illustrated, through an example involving a steel floor support beam.

This is followed by a check on the adequacy of the steel floor support beam under the natural fire conditions – first to the Eurocode Parametric Curves [1] and then to the BFD Curve [2]. The purpose of these checks is to illustrate the minimum effect that the shape differences between these two curves has on the temperature reached in an unprotected steel beam and a protected steel beam exposed to the two different parametric fire curves. For this comparison, the BFD Curve is fitted as closely as is practicable to the Eurocode Parametric Curve in terms of peak gas temperature and the time from $t = 0$ at which that peak temperature occurs.
As the BFD Curve [2] is still awaiting formal publication, the timing is opportune to make some suggestions as to how it might be used to generate design fires for a range of enclosure conditions in a simple but realistic manner. This is followed by a comparison between the two temperature-time curves when applied to a given enclosure.

Finally, some general conclusions are given, followed by the acknowledgments and references.

THE BFD CURVE EQUATIONS

The two basic equations that describe the BFD Curve are:

$$T_g \quad = \quad T_a + T_m e^{-z} \tag{1}$$

$$z \quad = \quad (log_e t - log_e t_m)^2 / s_c \tag{2}$$

where:
T_g = gas temperature at any time t (^{o}C)
T_a = ambient temperature (^{o}C)
T_m = maximum gas temperature generated above T_a (^{o}C)
t = time from start of fire (mins)
t_m = time at which T_m occurs (mins)
s_c = shape constant for the time-temperature curve (-)

In equation 2, the log_e is the natural log.

The input parameters for the BFD Curve are T_m, t_m and s_c. Detailed guidance on determining each of them is given in [2] and briefly described below.

The maximum temperature, T_m, can be derived as specified in [8] and described in section 7.1 of [2]. However, analyses of a number of natural fire tests by the authors, eg. [9], and analyses undertaken as part of HERA's fire research programme have shown that the maximum average temperature reached in a "real" enclosure, with a wide range of combustible material, is nearly constant over a range of ventilation conditions. Maximum average gas temperatures have been developed as part of implementing the SPM procedure for floor system design [10], where they have been used to derive design temperatures in unprotected steel beam elements. These average gas temperatures are given in Table 1 and could be used as T_m in the BFD Curve.

	Maximum Average Gas Temperature
FHC 1, NWC	800
FHC 2, NWC	900
FHC 3, NWC	950
FHC 1, LWC	900
FHC 2, LWC	1000
FHC 3, LWC	1050

Table 1 : Possible Values of T_m for the BFD Curve

Notes to Table 1:
1.   FHC1, FHC 2 and FHC 3 are as defined by C/AS1 [11]
2.   NWC ≡ normal weight concrete; density ≥ 2300 kg/m³
    LWC = light weight concrete; density 1500 – 1900 kg/m³

Determination of t_m (the time at which T_{max} occurs) is described in section 7.2 of [2]. If a plot of heat release rate Q (MW) versus time is plotted for a fire, the time t_m is the time at which Q_{max} occurs for a fuel surface controlled fire or the time at the end of the peak heat release rate plateau for a ventilation controlled fire.

Barnett [2] also gives two equations for calculating t_m.

As an alternative, t_m can be obtained from the Eurocode EC1-1-2/59 Annex A Parametric temperature–time curve provisions, where t_{max} is given by equation (A.7) of [1]. To obtain the correct units from that source:

$$t_m \quad = \quad 60\ t_{max} \tag{3}$$

where:
t_m =   time for input into BFD Curve (mins)
t_{max} =   time from equation (A.7) of [1] (hours)

Note also when calculating the opening factor, O, for use in [1] that $A_t = A_{t1}$ (surface area of enclosure including openings).

The shape constant, s_c, has been shown [2] to be a simple relationship between the degree of insulation of the enclosure, c, and the pyrolysis coefficient, k_p. The equation is;

$$s_c \quad = \quad ck_p \tag{4}$$

where:
    $c =$ 38 for enclosures with minimum insulation (corresponding to $k_b = 0.045$ from Table 5.1 of the FEDG [4] and applying to an enclosure with steel sheet roof and walls of any construction).

    c =   16 for enclosures with maximum typical insulation (corresponding to $k_b = 0.09$ from [4] and applying to an enclosure with timber floors and plasterboard lined walls and ceiling)

$$
\begin{aligned}
k_p \quad &= \quad 1/(148\ F_{02} + 3.8)\ (\text{-}) &\tag{5}\\
F_{02} \quad &= \quad A_v h_v^{0.5} / A_{t2} \quad (\text{m}^{0.5}) &\tag{6}\\
A_{t2} \quad &= \quad A_t - A_v \quad\quad (\text{m}^2) &\tag{7}
\end{aligned}
$$

A_t =   total internal surface area of enclosure including openings (m^2)
A_v =   sum of areas of vertical openings (m^2)
h_v =   weighted mean height of vertical openings (m)

For natural fires, s_c varies from around 0.5 to 5. The shape constant is a significant variable and can also be varied between the heating and cooling side, to generate a range of curves from equations (1) and (2) that range from representing a well ventilated natural fire to the ISO 834 standard curve. This makes the formulation a powerful mathematical tool.

There is scope for developing a relationship between c and k_b for the full range of insulation values typically encountered in practice. To date this has not been done, however for an enclosure with NWC floors and roof, corresponding to $k_b = 0.065$ from Table 5.1 of [4], c = 25 provides a suitable answer.

**FITTED EXAMPLES OF THE BFD CURVE TO FIRE TEST RESULTS**

General

In developing the BFD Curve formulation, Barnett [2] has fitted the curve to a wide range of natural fire tests; ranging from car fires, through enclosure fires with a range of fuels and enclosure materials of construction, to the Cardington large enclosure tests [12]. (These latter tests were undertaken to determine the appropriateness of the equivalent time of fire exposure provisions in Annex D of [1]). While a wide range of these results are presented in [2]; only two sets are given below.
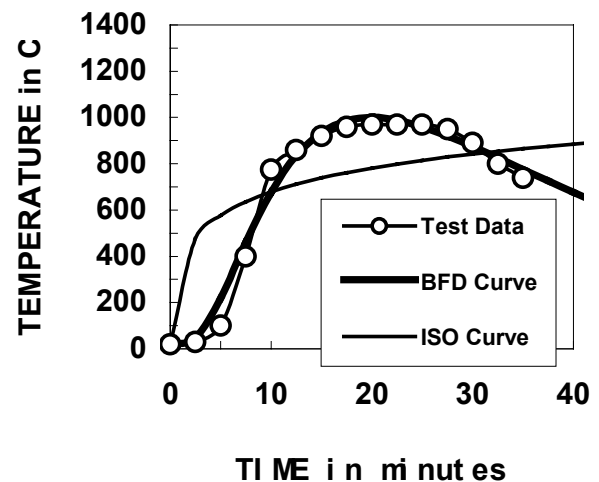
CIB/W14 Temperature–Time Curves

During the period 1964-1974, 321 experiments were carried out and the results were summarised by Thomas and Heselden [13]. Out of these 321 experiments, temperature-time information was provided therein for only four of the tests.

BFD Curves have been fitted to these four tests. Figs.1(a) and 1(b) below are the results taken from Figs. 2 and 3 of [13]. As can be seen, the BFD agreement is good.
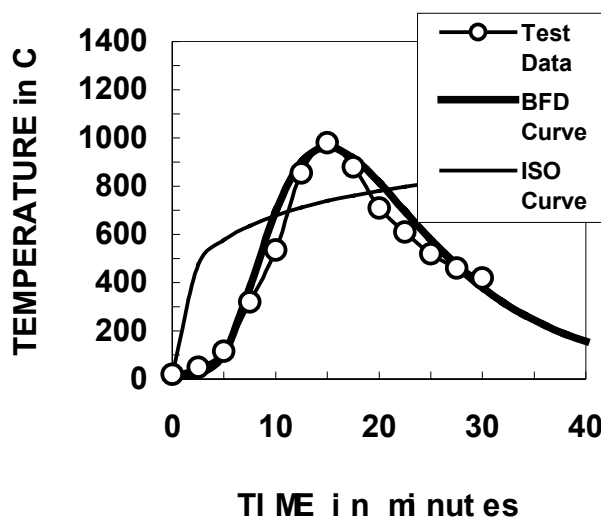

(a) Ref [13] Fig. 2   (b) Ref [13] Fig. 3

FIGURE 1: BFD Curves Fitted to CIB/W14 Temperature-time Curves

CTICM Temperature-Time Curves

Ref. [14] describes 44 fire tests for both insulated and non-insulated fire compartments, BFD curves were fitted to these and graded for fit. Six tests were rated as Category 1 (excellent fit), 15 tests as Category 2 (very good), and 15 tests as Category 3 (satisfactory). In all cases where the fire burnt in a near uniform manner throughout the enclosure, the fit was very good or excellent. The eight cases where the fit was poor were tests where the behaviour of the fire was markedly non-uniform. In such instances the fit between any parametric curve and the experimental fire temperature-time curve will not be good. Two of the insulated CTICM tests (tests 35 and 53) rated as Category 1 are illustrated below.
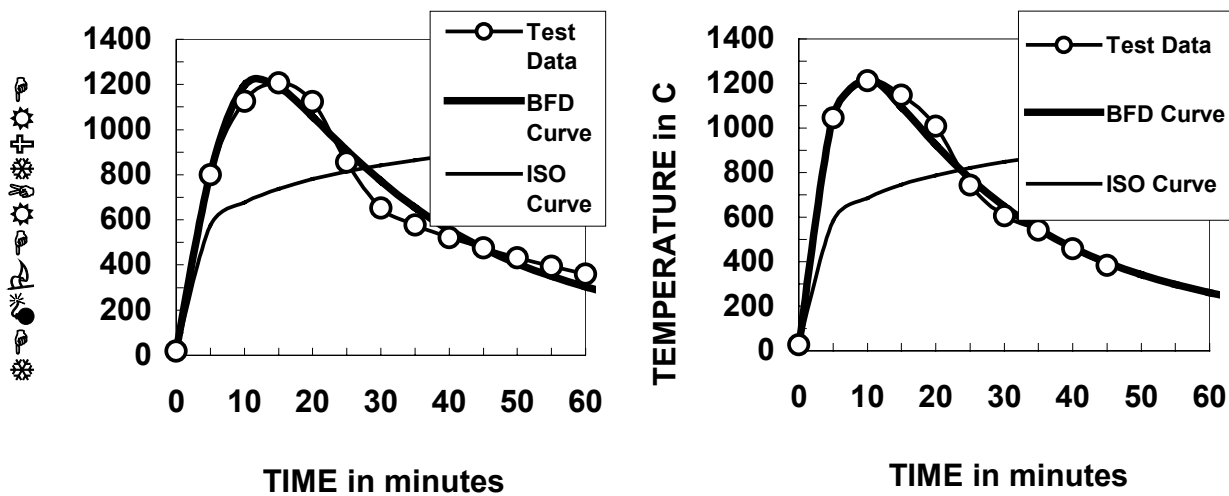
(a) CTICM Test 35	(b) CTICM Test 53

FIGURE 2: BFD Curves Fitted to CTICM Temperature-time Curves.

DETERMINATION OF LIMITING STEEL TEMPERATURE AND PERIOD OF STRUCTURAL ADEQUACY FOR STEEL BEAM

Scope of Example

This example illustrates application of the NZS 3404 [5] provisions for determining the limiting temperature and period of structural adequacy of an unprotected secondary beam supporting a profiled concrete slab. The same beam and exposure configuration is then used, in both protected and unprotected applications, to determine the maximum steel temperatures reached under the Eurocode Parametric Curve [1] and the BFD Curve [2].

Structural Floor System Characteristics and Loading

The floor system subjected to the fire comprises a composite floor with concrete slab on a profiled steel deck, supported on primary and secondary steel beams, which are designed to act compositely with the floor slab. In this example, only the slab and secondary beam elements are given, these being the components relevant to this design example:

- normal weight concrete slab, 120 mm thick on Dimond *Hi-Bond* [15]
- secondary beams are at 2.8 m centres
- secondary beam size, grade is 310UB40, Grade 300
- secondary beam is composite with the floor slab
- secondary beams are unprotected against fire
- connections to secondary beams are WP30 from [16]
- beam span is 8.3 metres
- dead load, $G = 2.4$ kPa
- basic live load, $Q = 2.5$ kPa
- the live load combination factor for the ultimate limit state, from [7], is 0.4

Determination of the NZS 3404 Limiting Temperature for the Beam in a Simply Supported Condition.

(1)   Fire emergency loading and moment on beam

$G + Q_u$ = $2.4 +$ $2.5 \times 0.4 = 3.40$ kPa

$w^*_{u,lineload}$ = $3.4 \times 0.5 \, (2.8 + 2.8) + 0.4 = 9.92$ kN/m

$$M^*_{ss} = \frac{w^*_u \, L^2}{8} = \frac{9.92 \times 8.3^2}{8} = 85.4 \text{ kNm}$$

(2)   Determination of beam limiting temperature in a simply supported condition

This uses NZS 3404 [5] Clause 11.5

$\phi_{fire} M_{pos}$ = $1.0 \times 1.5 \times M_{sx}$

          = $1.0 \times 1.5 \times 202$ =   303 kNm

ϕ_{fire} =   1.0 (NZS 3404 [5] Amendment No. 1)

1.5   = factor accounting for the minimum increase in moment capacity due to composite action from that for the beam alone (see HERA *DCB* No. 2, p.2)

$M_{sx,310UB40}$ =   202 kNm (for the beam alone, from [17] but multiplied by $1/\phi$)

$$r_f = \frac{M^*_{ss}}{\phi_{fire} M_{pos}} = \frac{85.4}{303} = 0.28$$

$T_{l,ss}$ $= 905 - 690 \, r_f = 711^{\circ}C$

**Some points in regard to this check are as follows:**

(i)   The utilisation factor, r_f, is quite low. This is typical for composite secondary beams, whose size is often controlled by serviceability considerations. For example, in this instance, the span of 8.3 m for the 310UB40 size is controlled by deflection limitations. The *Composite Floor Preliminary Design Charts* [18] Tables 2 and 3 illustrate this point.

(ii)   That publication [18] also lists the design moment capacity for 50% and for 75% partial composite action. That can be used to determine $\phi_{fire} M_{pos}$ instead of the approach in (2) above, which uses a factor of 1.5 on the bare steel beam section moment capacity and gives a lower bound value.

(iii)   The fire emergency loading is determined from NZS 4203 [7] Clause 2.4.3.4 Load Combination (7).

(iv)   If the limiting temperature associated with simple support considerations was too low, in comparison with T_{max} reached for given fire conditions, then the additional resistance available from the connections, as given by *DCB* No. 46 pp. 14 & 15 [19], could have been used to determine the increased fire resistance. However, this increased resistance is associated with increased permanent post-fire deformation, as described in [3].

Temperatures Reached Under Standard Fire Test

Fig. 3 shows the standard temperature-time curve, given by section 3.2.1 of [1] as well as the temperatures in the bottom flange for the 310UB40 floor beam unprotected and with 20 mm of profile applied insulation material.
Thermal exposure details are as follows:

(1)   For the steel beam
- Hp/A for 310UB40, top flange shielded, = 206 m^{-1}
- Specific mass of steel = 7850 kg/m^3
- Relative emissivity = 0.5
- Coefficient of heat transfer by convection = 25 W/m^{2}K

(2)   For the insulation material
- Specific mass = 840 kg/m^3
- Specific heat = 1700 J/kgK
- Thermal conductivity = 0.80 W/mK
- Thickness = 0.020 m
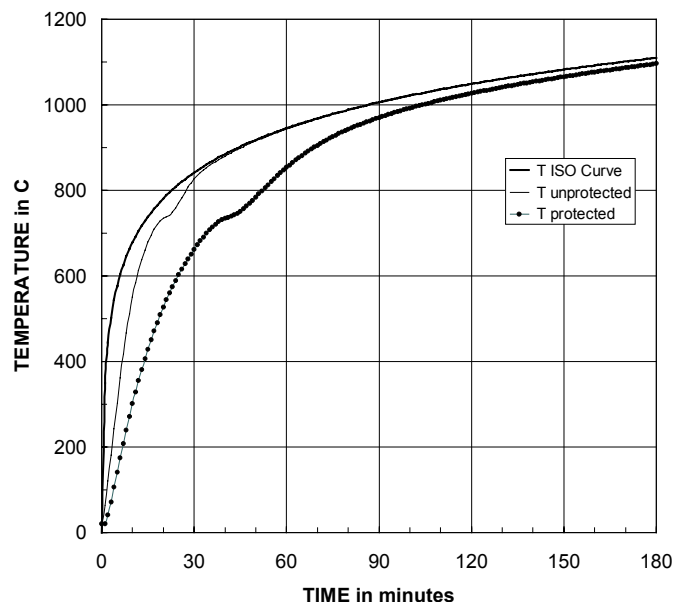
FIGURE 3: Temperatures of Fire and Steel Beam Bottom Flange

The local deviation in the steel temperature at between 700°C and 800°C is due to the increased specific heat of steel over that temperature range when the steel internal structure undergoes a phase change at around 720°C.

Period of Structural Adequacy for Unprotected Steel Beam

Having obtained the section factor and limiting temperature for an unprotected steel beam or column, its time to failure conditions as defined in the standard fire test can be determined from Equations 11.6.1 and 11.6.2 of NZS 3404. The latter is for column (4 sided exposure), the former for beams (3 sided exposure; 1 flange shielded). These curves are derived directly from standard fire tests, as referenced in Commentary Clause C11.6 of [5].

This time to failure conditions in the standard fire test is called the *period of structural adequacy* (PSA) by NZS 3404. In the design for fire resistance it is compared with a specified Fire Resistance Rating (FRR).

If PSA ≥ FRR, then the steel member is satisfactory for the fire exposure. If PSA < FRR, then the fire resistance of the member needs to be increased. This can be done by increasing the member load carrying capacity, which increases the limiting temperature, decreasing the section factor or adding insulation material to slow down the temperature rise in fire.

CHECK ON BEAM ADEQUACY UNDER THE EUROCODE PARAMETRIC CURVE

This is given in Fig. 4, for an enclosure with the following characteristics:

enclosure floor area (m^2)	A_f	48.0
enclosure height (m)		3
total enclosure surface area: walls, ceiling, floor and openings (m^2)	A_t	180.0
total area of vertical openings (m^2)	A_v	8
weighted mean height of vertical openings (m)	h	2
fire load energy density related to the floor area A_e (MJ/ m^2)	$q_{e,d}$	400
fire load energy density related to the total surface area A_t ((MJ/ m^2)	$q_{t,d}$	107
	A_v / A_f	0.167
thermal characteristic	b	1700
opening factor	OF	0.063

Fig. 4 shows the results for the beam under the pre-2001 version of the Eurocode Parametric Curve. In this instance:

$T_{\text{max, fire}}$ = 736°C at 13 mins
$T_{\text{max, unprotected steel}}$ = 687°C at 17 mins
$T_{\text{max, unprotected steel}}$ = 555°C at 29 mins
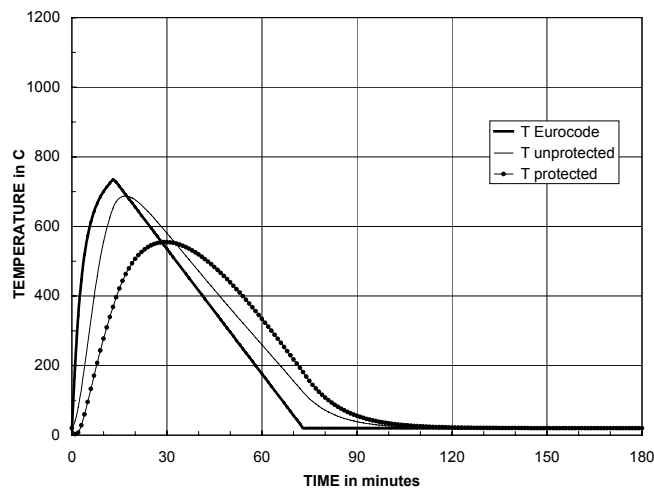
FIGURE 4: Temperatures of Fire and Steel, Pre-2001 Eurocode Parametric Curve for Fire

By comparing $T_{\text{max, steel}}$ with $T_{l, ss}$ from the earlier section, the beam can be seen to be satisfactory without insulation to support the applied load, under this fire temperature-time curve.

## CHECK ON BEAM ADEQUACY UNDER THE BFD CURVE REPRESENTATION OF THIS FIRE

This is shown in Fig. 5. The parameters used for developing the BFD Curve are as follows:

T_m = 716°C =maximum temperature from the Eurocode Curve - 20°C ambient
t_m = 13 mins (as determined from the Eurocode Curve)
S_c = 2.0

These parameters have been chosen to get the best fit between the two curves; a comparison between the current Eurocode Parametric Curve and the BFD Curve using the recommended design parameters is given in the next section.

In this instance:

$T_{max, fire}$ = 736°C at 13 mins
$T_{max, unprotected steel}$ = 694°C at 18 mins
$T_{max, unprotected steel}$ = 552°C at 29 mins
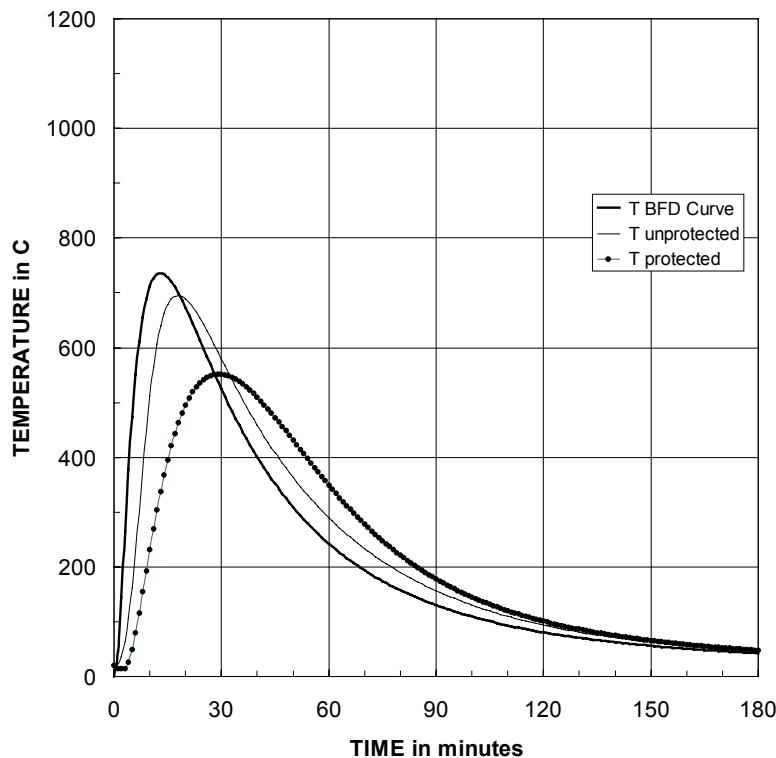
FIGURE 5: Temperatures of Fire and Steel, BFD Curve for Fire

The reason for showing Fig. 4 and Fig. 5 is to show the similarity in steel temperatures given by the two fire curves. The differences arise from the slightly different shapes of the curves and they are minor. However, this does not illustrate how well the two parametric fire curves compare when applied to a given enclosure. That comparison is made in the next section.

SOME SUGGESTIONS FOR GENERATING DESIGN FIRES USING THE BFD CURVE

Determination of Input Variables

As previously stated, there are three input variables required for generating the BFD Curve. These are T_m, t_m, and s_c, which in turn comprises c and k_p.

The maximum temperature, T_m, can be obtained from Table 1 herein, for the given Fire Hazard Category and type of concrete. When generating the BFD Curve, the value of T_a must be subtracted. The time to maximum temperature, t_m, can be obtained through Equation (A.7) of Eurocode 1-1-2 Annex [3] (see equation (3) herein).

The thermal insulation coefficient, c, varies from 16 to 38 as previously described. For enclosures with normal weight concrete ceiling and floor and plasterboard lined walls, $c = 25$ is an appropriate value.

The pyrolysis coefficient, k_p, is determined from equations (5) to (7).

Comparison Between Current (Modified) Eurocode Parametric Curve and BFD Curve

There have been some significant changes made to the Eurocode Parametric Curve between the 1994 edition and the current (2001) edition [1]. Therefore, any comparison between the two parametric curves must use the latest formulation of the Eurocode Curve against the BFD Curve.

However, as mentioned back in the introduction, the second author has found that the temperature-time relationship in the cooling regime can be better predicted through modification of the Eurocode Curve and has introduced these modifications in [6]. He has therefore used the modified curve incorporating the changes to the basic curve introduced via (1).

(1) **Modified inputs to the Eurocode Curve** (Equation A.7 from [1])

$$t_{max} = \max(2 \times 10^{-3} \, q_{t,d} / OF; \, t_{lim})$$

$$q_{t,d} = 400\frac{A}{A_t} = 106.7 \text{ MJ/m}^2 \text{ surface area}$$

$$OF = 0.063$$

$t_{lim} = $ 20 mins, from [1], for a medium growth fire

$$\Rightarrow t_{max} = \max(0.339 \, ; \, 0.333) = 0.339 \text{ hours}$$

$$\Gamma = [OF/b]^2 / (0.04/1160)^2 = 1.15$$

$$t^*_{max} = t_{max}\Gamma = 0.390 \text{ hours}$$

(this is the variable t^*_d from the pre-2001 formulation of the Eurocode Parametric Curve)

(2) **Inputs to the BFD Curve**

$$T_m = 800 - 20 = 780^oC$$

800 is from Table 1, for FHC1, NWC

$$t_m = 60 \, t_{max} = 60 \times 0.339 = 20 \text{ mins}$$

$c = 25$

$F_{02} = 8\sqrt{2} / (180 - 8) = 0.066$

$k_p = 1 / (148\, F_{02} + 3.8) = 0.074$

$s_c = ck_p = 25 \times 0.074 = 1.85$
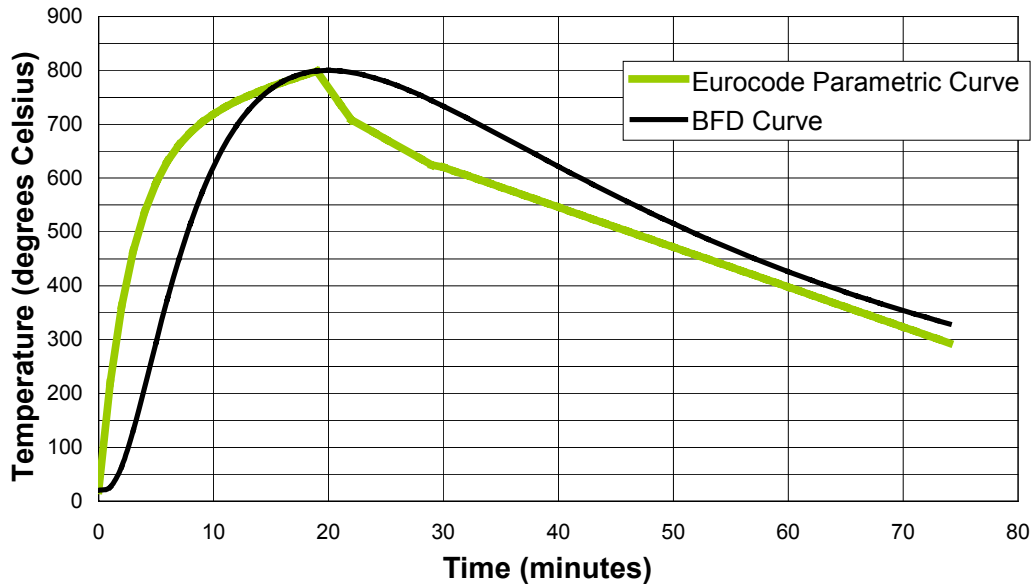
FIGURE 6 : Comparison of Parametric Curves for Given Enclosure

The comparison in Fig. 6 is for the first 74 minutes only. The agreement is good from a steel temperature design viewpoint, such that either curve could be used to determine steel member temperatures with sufficient accuracy for structural design purposes.

As a final point of interest, note that the changes to the Eurocode Parametric Curve formulation have made the results more severe, in the case of a relatively short duration fire. This can be seen by comparing the Eurocode fire curves from Figs. 4 and 6, which gives, for the maximum fire temperature reached and the associated time:

- Old Eurocode formulation : $T_{max,\ fire}$ = 736°C at 13 mins
- New Eurocode formulation : $T_{max,\ fire}$ = 798°C at 20 mins
- BFD Curve : $T_{max,\ fire}$ = 800°C at 20 mins

CONCLUSIONS

Increasing use is being made of "design fire" curves to represent the natural fire temperature-time conditions in fire engineering design.

The paper has illustrated examples of this approach and introduced a new parametric curve for such applications. Although a detailed description of this new curve is given elsewhere [2], sufficient detail is presented herein to allow its application in design. When compared with the Eurocode Parametric Curve [1] in regard to the predicted temperature reached in exposed unprotected and protected steel members, the differences are minor. When used as a design tool, an example of its application shows good agreement with the Eurocode

Parametric Curve, even though the BFD Curve is mathematically much simpler and more versatile to use in design, especially in spread-sheet based design.

ACKNOWLEDGEMENTS

REFERENCES

[1] EC1-1-2/59:2001 (Third Draft) : Eurocode 1 – Actions on Structures Part 1-2: General Actions – Actions on Structures Exposed to Fire; CEN, Brussels, Belgium.

[2] Barnett, CR; BFD Curve – A New Empirical Model for Fire Compartment Temperatures; Fire Safety Journal; Elsevier Science, paper accepted for publication 2002.

[3] Clifton, GC; Fire Design Advice Article 65: Various Examples Covering the Design of Structural Members for Fully Developed Fires; HERA Steel Design and Construction Bulletin No. 65, December 2001, pp. 4-13.

[4] Buchanan, AH (Editor); Fire Engineering Design Guide, Second Edition; Centre for Advanced Engineering, University of Canterbury, Christchurch, 2001.

[5] NZS 3404: 1997, plus Amendment No. 1: 2001, Steel Structures Standard; Standards New Zealand, Wellington, New Zealand.

[6] Clifton GC; Fire Models for Large Firecells; HERA Manukau City, 1996, HERA Report R4-83, plus amendments on page 20, HERA DCB No. 54, February 2000.

[7] NZS 4203:1992, General Structural Design and Design Loadings for Buildings; Standards New Zealand, Wellington, New Zealand.

[8] Law M and O'Brien T; Fire Safety of Bare External Structural Steel; Constrado, London, England,1968.

[9] Auffinger, A; Response of Multi-Storey Steel Framed Buildings in Fully Developed Natural Fires: Revision of Fire Model and Inelastic Response Design Procedure; Report for Second Practical Term; HERA Manukau City, New Zealand 2000.

[10] Clifton, GC et.al.; Design of Multi-Storey Steel Framed Buildings With Unprotected Secondary Beam or Joists for Dependable Inelastic Response in Severe Fires; HERA Steel Design and Construction Bulletin; No. 60, February 2001, pp. 1-58.

[11] C/AS1: 2001, Acceptable Solution for Fire Safety; Building Industry Authority, Wellington, New Zealand.

[12] Kirby, B. R. et al.; Natural Fires in Large Scale Compartments – A British Steel Technical, Fire Research Station Collaborative Report, British Steel Technical, Swinden Laboratories, United Kingdom, 1994.

[13] Thomas PH and Heselden AJM; Fully-developed Fires in Single Compartments; Fire Research Note No. 923, Fire Research Station, Borehamwood, England, 1972.

[14] Arnault P, Ehm H and Kruppa J; Report Experimental sur les Essais Avec Des Naturels Executes Dans La Petite Installation; Maiziers-La-Metz Centre Technique Industrial De La Construction Metallique, Puteax, France, Doc C.E.C.M – 3.73-11-F, 1973.

[15] Hi-Bond Design Manual; Dimond Structural, 1999, Auckland, New Zealand.

[16] Hyland C; Structural Steelwork Connection Guide Incorporating Amendment No. 1; HERA, Manukau City, New Zealand, 1999/2001, HERA Report R4-100.

[17] Design Capacity Tables for Structural Steel, Third Edition, Volume 1 : Open Sections; Australian Institute of Steel Construction, Sydney, Australia, 2000.

[18] Composite Floor Preliminary Design Charts; Steltech Structural Ltd, Auckland, New Zealand, 1999.

[19] Clifton GC; Fire Design Advice Article 46: Eliminating the Need for Passive Fire Protection in Aulti-Storey Apartment and Hotel Buildings By Using the Shielding Effects of the Linings; HERA Steel Design and Construction Bulletin, No. 46, October 1998, pp.10-16.

TECHNICAL BASIS ON STRUCTURAL FIRE RESISTANCE DESIGN IN BUILDING STANDARDS LAW OF JAPAN

Kazunori HARADA
Dept. of Architecture & Environmental Design, Kyoto University,
Yoshida-Honmachi, Sakyo-ku, Kyoto 606-8501, Japan
harada@archi.kyoto-u.ac.jp

Yoshifumi OHMIYA
Building Research Institute, Tatehara 1, Tsukuba 305-0802, Japan
ohmiya@kenken.go.jp

Akiko NANBU
Property and Casualty Insurance Rating Organization of Japan
Banzai Bld., Shiba 2-31-19, Minato-ku, 105-0014, Japan
Akiko_nanbu@sonsan.or.jp

Akiko NAKAMICHI
General Building Research Corporation of Japan,
Fujishirodai, 5-8-1, Suita, 565-0873, Japan
nakamichi@gbrc.or.jp

ABSTRACT

Structural fire resistance design method became in effect due to the revision of Japan's building code (Building Standards Law of Japan) on June 2001. The method includes standard methods to calculate 1) fire exposure to structural elements, 2) temperature rise of steel and RC elements during fire exposure and 3) structural end points such as ultimate steel temperature for buckling of columns, bending failure of beams and so on. This paper discusses the technical basis for design methods especially focused on steel framed buildings. The calculated values in each design equation were compared with experimental values in order to examine the redundancies implied. In the final stage, all the redundancies were combined by Monte-Carlo method and first-order moment method. Target safety index and corresponding partial safety factors were discussed.

KEYWORDS: *Structural Fire Resistance, Ultimate Temperature, Strength Reduction Factors, Buckling Temperatures, Bending Failure Temperatures, Target Safety Index*

INTRODUCTION

The building code of Japan (Building Standards Law of Japan, BSLJ, hereafter) was revised in 1998 to include functional requirements in place of detailed technical specifications of materials and constructions. Even though it is not perfect, the law has shifted towards performance-based manner. Following the changes in law, enforcement order (detailed items of regulation) and notifications (technical specification) were revised in June 2000. The changes in fire safety requirements were reported by Yusa and Tsujimoto [1].

Concerning with the structural fire resistance, performance evaluation framework and a set of simplified calculation formula have been added as *Kenshoho* (verification method for fire resistance). By using verification method, it is possible to check the adequacy of fire resistance of structural elements easily and quickly.

Verification method brought us the benefit of design convenience. However its technical basis is not well verified by engineering standpoint yet. This paper intends to discuss the technical basis of verification method and clarify safety level implied in verification method.

BRIEF SUMMARY OF CODE CHANGES IN 1998-2000

Functional Approach

Changes of BSLJ was made during 1998-2000. After the revision, it is possible to adopt functional approach in fire resistance design. The objective implied in BSLJ is to prevent;
  (1) collapse due to fires that are <u>foreseeable</u> to take place in the building,
  (2) fire spread to the buildings during fires that <u>normally</u> takes place around the building.

The functional requirements to satisfy the objective are;
  (1) Load bearing structural part shall sustain load throughout the complete process of fire.
  (2) Building envelope (exterior walls and roofs) shall not create a gap that may penetrate flame from inside to outside
  (3) Floors and internal partition walls shall not create a gap to penetrate flame nor transmit heat enough to ignite combustibles in the opposite side of fire compartment in both directions.
  (4) Exterior walls shall not transmit heat enough to ignite combustibles in the building.

The above requirements are summarized in Figure 1. Two kinds of fires are referred. One is the internal fire applied to structural frame (columns, beams and floors) for checking load-bearing capacity and to compartment boundaries for checking integrity (external walls and roofs) and insulation (floors and partition walls). The severity of internal fire is deemed *foreseeable*, because the fire severity depends only on the condition of the building itself. In the evaluation method, the calculation method of internal fire is provided.
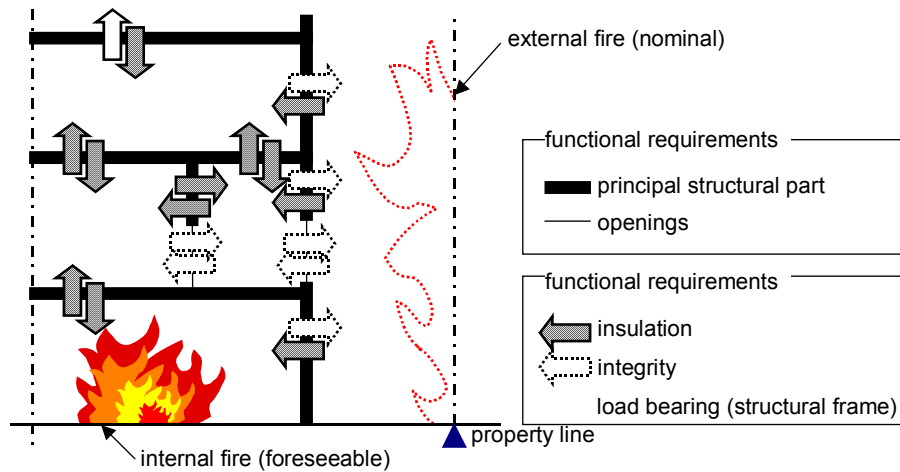
Figure 1 Functional requirements for fire resistance

The other is the external fire that may take place around the building. It is referred *normal* (unforeseeable) because the severity depends on neighboring conditions that the owner of building cannot control. In the evaluation method, no calculation method for external fire is provided, but ISO 834 fire is assured.

Performance Evaluation

To satisfy the requirement of BSLJ[1], planning body can choose among Route A, B and C. as shown in Figure 2.

Route A is a conventional method that follows prescriptions in the code. Code specifies required fire resistance time of principal structural part depending on number of stories of buildings. The principal part shall be made of fire resistive constructions listed in approved constructions. There is little chance of designing fire resistance but of selecting fire-insulating materials as to steel-framed buildings.

By adopting the performance route, they can get the freedom of building design and chance to cost reduction without loss of safety. Performance-based routes were provided as in Route B and Route C. Route B is to apply simplified design formula specified in MoC notification 1433(2000). The chance is at most increased if they choose Route C. The difference between Route B and C are the degree of sophistication and complicity of design process, and the body that would review design solution. In the Route B, design process is simplified enough so that local building authority can review the solutions. In practice, it means that review and approval process is finished quickly, but at the same time, the design would have to be conservative. In route C submittals, it is possible to adopt any design procedure as long as it follows the requirements of law and is correct in engineering sense. The appropriateness is judged by peer- review body, followed an approval by MLIT (Minister of Land, Infrastructure and Transportation).

---

[1] Article 2,21,27,61,62 of Building Standards Law of Japan
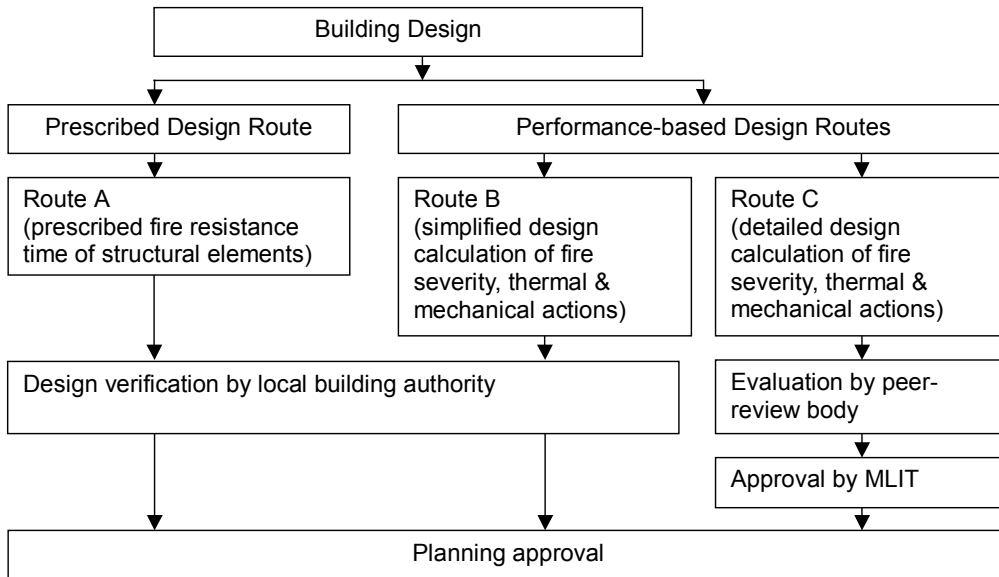
Figure 2 Three Routes to Conform with Fire Resistance Requirements in BSLJ

TECHNICAL BASIS OF VERIFICATION METHOD FOR FIRE RESISTANCE

In the followings, technical basis for verification method (Route B) is discussed. Verification method includes design equations for reinforced concrete and timber structure. However, focus is put on steel structures.

General Principle

The general principle for structural fire resistance is to limit the strength reduction of load bearing elements. Namely the strength (resistance) R must be larger than the service load S throughout the fire process,

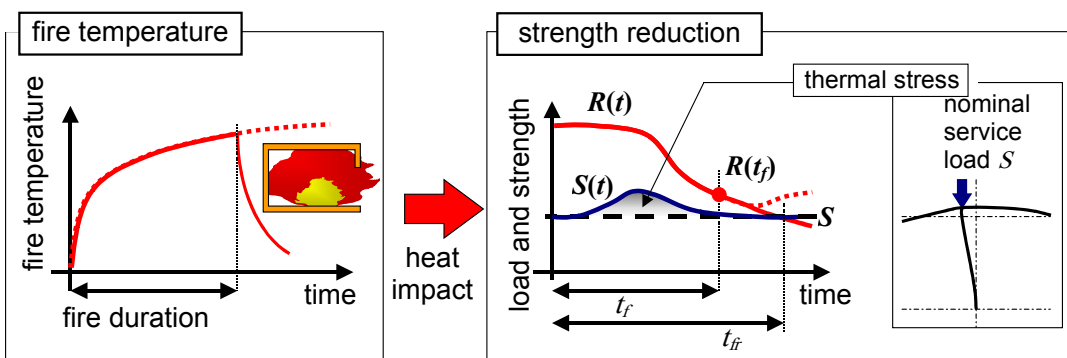$$R(t) > S(t), \; t = 0 \sim \infty .$$
(1)

Figure 3 Typical changes in load and strength of steel column during fire

The typical changes in strength and service load are shown in Figure 3. Service load increases due to the thermal stress in the early stage of fire. As steel temperature is increased, steel strength is reduced. At the same time, thermal stress is reduced. At the critical condition to structural failure, thermal stress is negligible[2]. This assumption is valid for steel structures designed against wind and earthquake motion. As a result of seismic

resistance design, structural frame is equipped with large deformation capacity so that the frame is insensitive to perturbations caused by thermal stress in the early stage of fire.

Simplified Performance Evaluation Methods (Route B)

Following above assumption, it is practical to check the strength at the fire duration time (plus some post fire period) $t = t_f$. Equation (1) could be

$$R(t_f) > S, \tag{2}$$

where S is the load applied by external force. It is more convenient to express by time margin,

$$M = t_{fr}(S) - t_f > 0 \tag{3}$$

where $t_{fr}(S)$ is the critical time to failure under the service load S.

Calculation procedure consists of two parts. The first half is to calculate the fire severity of possible fire rooms (Figure 4). The second half is to calculate the time to failure of structural element. The checking is made element by element (Figure 9). In the followings, main points are briefly reviewed followed by technical evidence. The detailed method of application [3] and practical design examples [4] are not described in this paper.

Calculation of Fire Severity and Duration

The calculation procedure is shown in Figure 4. First of all, fire compartment boundaries are to be fixed. At the same time, principal structural part is identified. Calculations are carried out for all the identified fire rooms.

For each fire room, total fire load (Q_r), heat release rate (q_b), fire temperature coefficient (α) and local fire temperature coefficient (α_l) are calculated. Summarizing the calculation results, we can identify the fire- temperature time curve as shown in the last box of Figure 4. Two fires are identified for each room. One is an average fire temperature rise whose severity is characterized by (α, t_f). The other is a local fire temperature that takes into account of the high temperature area close to combustibles. Its severity is characterized by (α_l, 20).

(1) Total fire load (Q_r)

To calculate the fire severity and duration in accordance with Figure 4, we start with total fire load of a room. It consists of movable and fixed fire load. The characteristic values of movable are shown in Table 1. These values were selected so as to cover existing survey results of fire load. For example, characteristic value for office use is 560 MJ/m^2. As shown in Figure 5, characteristic value corresponds with suffuciently large values for office area.
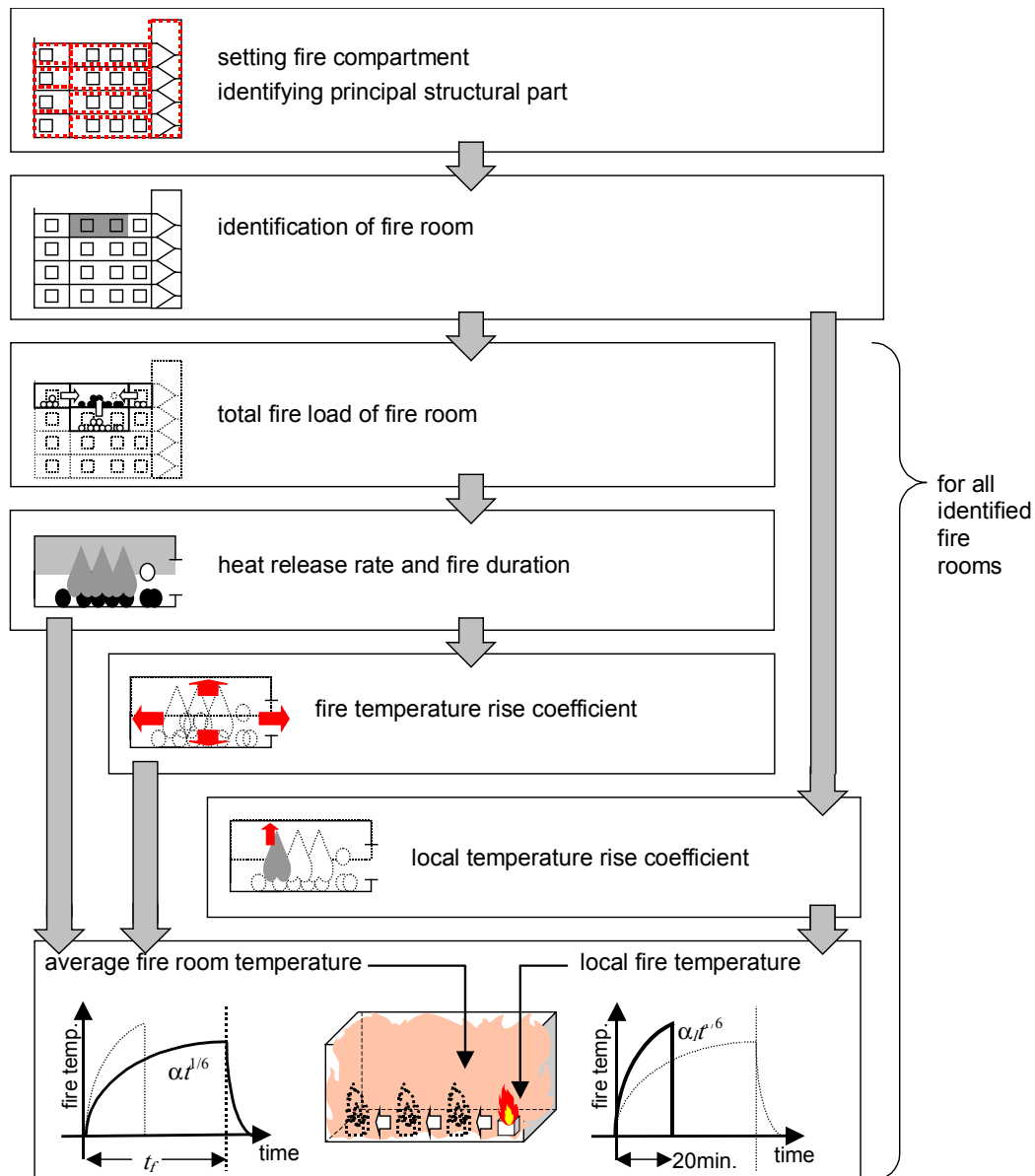
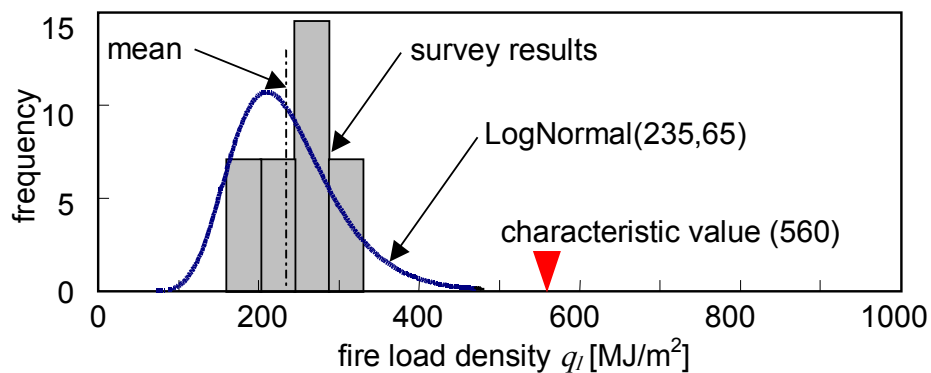Figure 4 Calculation procedure of fire severity adopted by Route B

Figure 5 Charactersitic Fire Load Density and Survey Results for Office Area

Table 1 Design Fire Load Density (Movable Load)

group	room usage			fire load density [MJ/m²-floor]	structural load density [N/m²-floor]
1	dwelling			720	1,300
	bedroom except those in dwelling			240	
2	office or similar use			560	1,800
	meeting room or similar use			160	
3	classroom			400	2,100
	athletic hall			80	
	museum or similar use			240	
4	market store or similar use	furniture shop, booksellers or similar use		960	2,400
		others		480	
	restaurant	cafeteria		240	
		others		480	
5	theater, cinema, assembly hall or similar use	seat area	fixed seating	400	2,600
			others	480	3,200
		stage		240	
6	car park	parking lot		240	3,900
		runway or similar use		32	
7	corridor, staircase or other pathways			32	-
	entrance lobby or similar use	those in group 5		160	
		others		80	
8	hoist ways or other machinery room			160	
9	roof terrace or balcony			80	1,300 (2,400)
10	warehouse or similar use			2,000	-

(2) Heat release rate (q_r)

Heat release rate is described by burning type index (air supply rate per unit fuel surface area). An empirical formula is fitted to ventilation-controlled and fuel-controlled fires of wood fuels. As shown in Figure 6, the accuracy is fair for wood fuels.

$$q_b = \begin{cases} 1.6 \times \chi \times A_{fuel} & (\chi \leq 0.081) \\ 0.13 \times A_{fuel} & (0.081 < \chi \leq 0.1) \\ (2.5 \times \chi \times \exp(-11 \times \chi) + 0.048) \times A_{fuel} & (0.1 < \chi) \end{cases} \qquad (4)$$
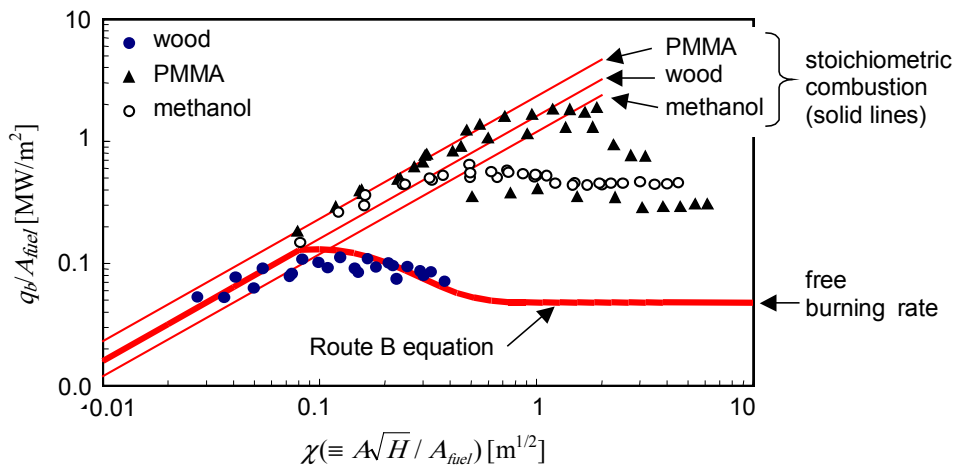

Figure 6 Heat release rate in compartment fires for various type of fuels as a function of burning type factor[5] and Route B design formula

(3) Fire duration (t_f)

Assuming constant heat release rate, the fire duration is calculated by dividing total fire load by heat release rate,

$$t_f = Q_r / 60 q_b. \tag{5}$$

(4) Fire temperature rise coefficient (α)

McCarffery's equation for compartment fire temperature is well studied that it can be applied also to post flashover fires [6]. It gives,

$$T_f = \alpha t^{1/6}, \ \alpha = 1{,}280(q_b / \sqrt{\Sigma A \sqrt{k\rho c}} \sqrt{\Sigma A \sqrt{H}})^{2/3}. \tag{6),(7}$$

The accuracy of calculation was checked against full scale experiments. The results are summarized in Figure 7. For most cases, calculation gives conservative estimate of fire temperature rise coefficient α.
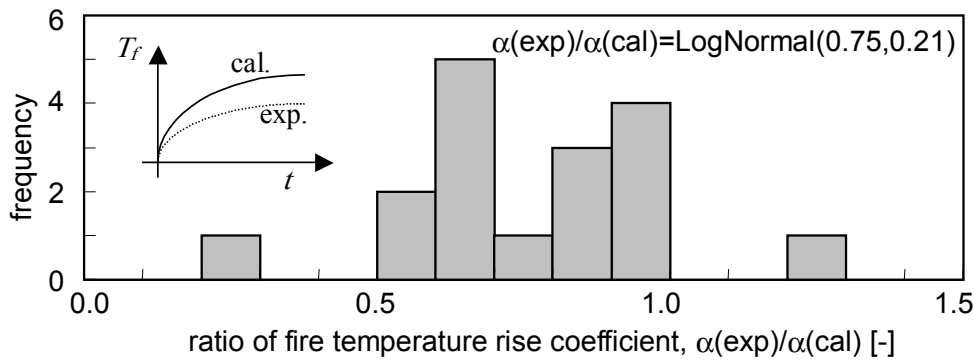

Figure 7 Comparison between experimental and calculated fire temperature rise coefficient

(5) Local fire temperature rise coefficient (α_l)

Local fire temperature rise coefficient is introduced to take into account of the spatial distribution of fire temperature. As shown in Figure 4 in the last box, temperature might be considerably higher than the average temperature. The time- dependence is assumed to be similar to equation (6), but the local temperature rise coefficient (α_l) is determined to correspond with a localized fire that grows to 3MW at 20 minutes.

$$T_f = \alpha_l t^{1/6}, \ \alpha_l = \begin{cases} 500 & (z \leq 2) \\ 500 - 100(z-2) & (2 < z \leq 7), \ 0 \leq t \leq 20 \\ 0 & (7 \leq z) \end{cases} \tag{8}$$

The maximum temperature by the design equation (8) is compared with axial flame temperature of 3MW-localized fires in Figure 8. Comparing with the axial temperature profile of unconfined (apart from wall) fire, the design equation gives higher temperature.
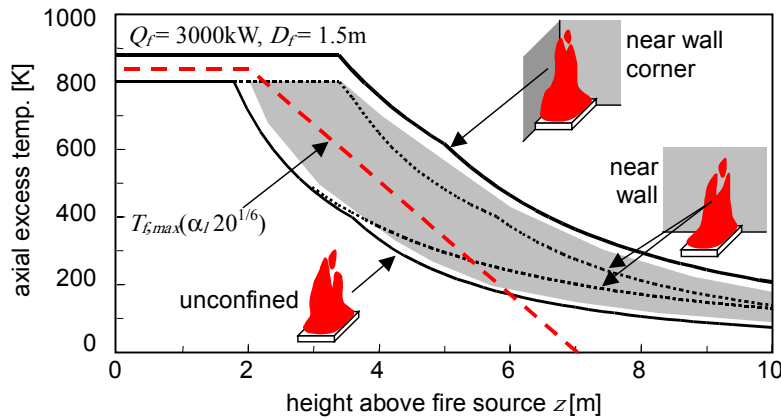
Figure 8 local fire (flame) temperature by 3MW source and the Route B formula

Calculation of Critical Time to Failure of Structural Steel Element

Figure 9 shows the calculation procedure for time to structural end point The procedure starts with calculation of structural forces during normal condition. Using the results, calculation is carried out element by element. The ultimate steel temperature is calculated in accordance with possible structural failure modes. Then steel temperature rise is calculated considering the construction of steel and insulation. Finally the time to critical condition is calculated and compared with fire duration.
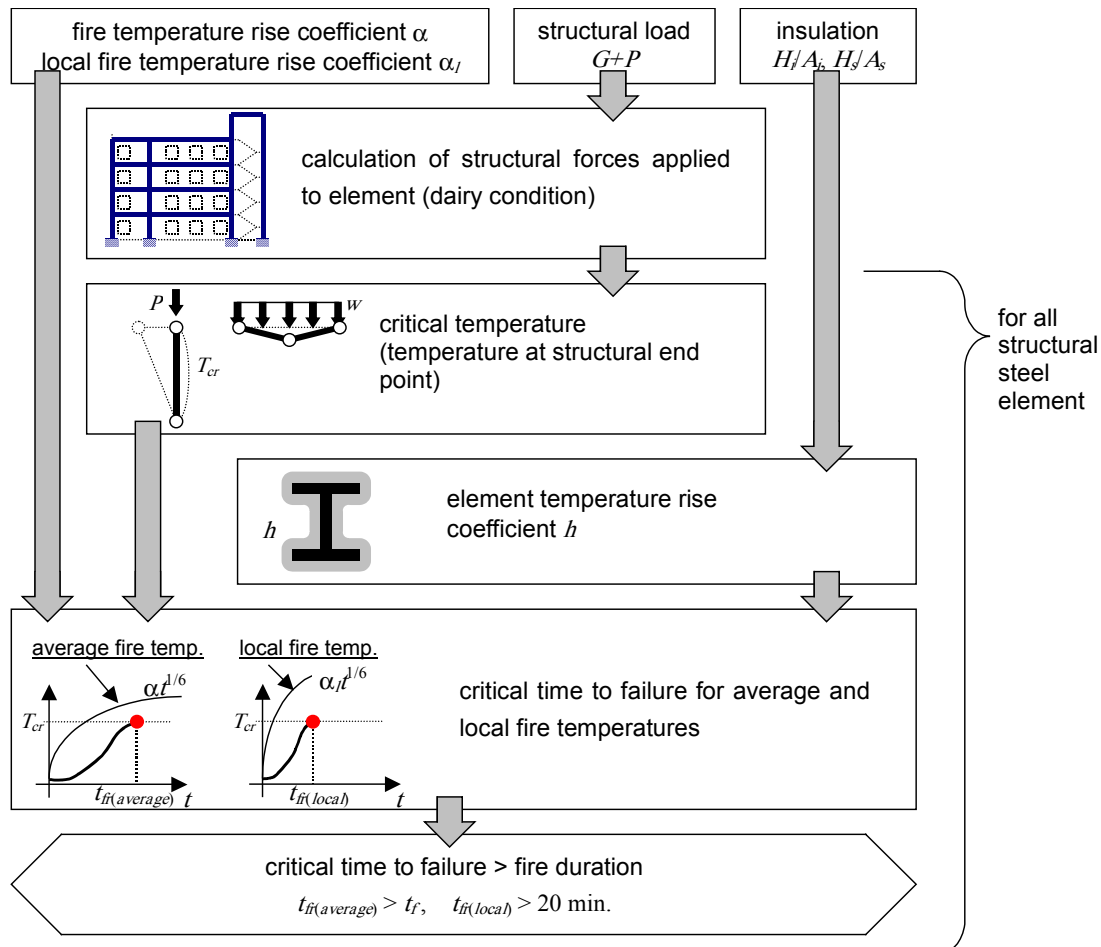

Figure 9: Calculation procedure of critical time to failure adopted by Route B.

(1) Critical temperature

strength reduction factor (κ)

In calculating strength reduction of load-bearing elements, reduction of strength with temperature rise was approximated by

$$\kappa(T) = (700 - T)/375, \ (T > 325), \ \kappa(T) = \sigma_y(T)/F \tag{9}$$

where F is the nominal design strength at normal temperature [N/mm^2], $\sigma_y(T)$ is the effective yield stress (1%- stress) at temperature T[^{o}C]. In Figure 10, equation (9) is compared with existing coupon test results that were carried out at high temperatures. It is clear that design equation corresponds with lower bound of measured results.
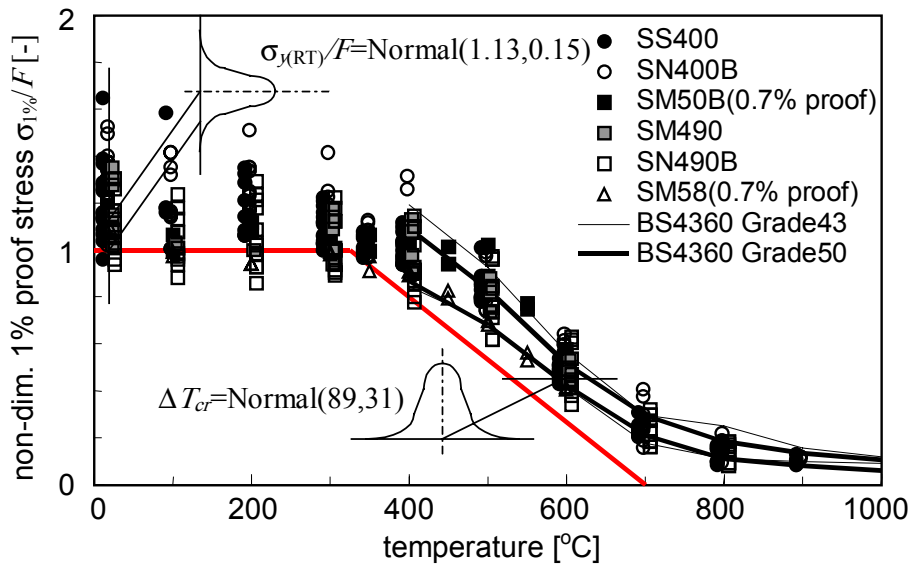

Figure 10 Strength reduction of 1%-stress, normalized by nominal strength at room temperature F [SM50B(presently SM490B)[7], SM58 (presently SM570)[7], SS400[8,9], SM490 [8,9], SN400B [9], SN490B [9], BS4360 Grade 43 and Grade 50[10]

Critical Temperature of Steel Columns

Critical temperatures of steel columns are determined by total buckling and by local buckling. For each failure mode, analytical formula is provided to calculate critical temperatures.

a) total buckling,

For most cases, inelastic buckling takes place rather than elastic buckling[2]. The buckling stress is calculated by a design equation identical with normal temperature design [11],

$$\frac{\sigma_B}{\sigma_y(T)} = \frac{1 - 0.24\lambda^2}{1 + 0.267\lambda^2} \tag{10}$$

---

[2] In practice, normalized slenderness is limited in less than unity to apply route B formula.

where $\lambda = (i/l)/3.14\sqrt{E/F}$ is the normalized slenderness ratio [-]. The design equation is shown in Figure 11 in comparison with numerical analysis results[12]. As is shown, conservative buckling temperature is predicted when slenderness ratio and load ratio are large. In case of small load ratio, equation (10) gives too conservative estimate. Thus the tangential modulus theory was applied to extrapolate to the limit $\lambda \to 0$. The final result is

$$T_B = \begin{cases} 700 - 375p & (\lambda < 0.1) \\ \max \begin{cases} 700 - 375p - 55.8(p + 30p^2)(\lambda - 0.1) \\ 500\sqrt{1 - \dfrac{p(1 + 0.267\lambda^2)}{1 - 0.24\lambda^2}} \end{cases} & (0.1 \le \lambda \le 1) \end{cases} \tag{11}$$
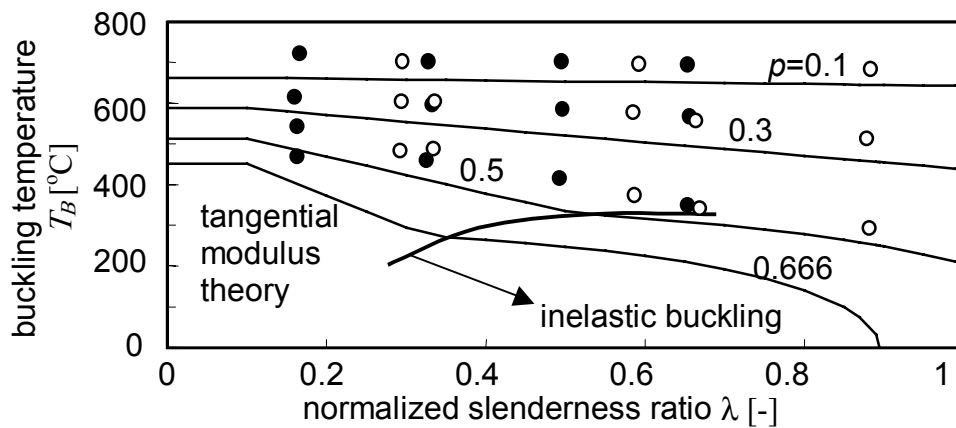

Figure 11 Design formula for Critical Temperature of Total Buckling of Columns

b) local buckling

Considering large deformation, local buckling may take place, which results in reduction of axial strength. The reduction factor is defined by B/t ratio (width/ thickness ratio of flange element of steel).

$$p = R_{LB}\kappa(T), \ R_{LB} = \min(21/(B/t), 0.75), \tag{12}$$

from which the critical temperature is

$$T_{LB} = 700 - 375 \ p/R_{LB}. \tag{13}$$

c) comparison with experimental data

Comparison was made between design formula for critical temperature and existing experimental data of load-bearing fire resistance tests. In order to check the redundancy included in formula (11) and (13), actual yield stress was used instead of the design value in equation (9). The results are summarized in Figure 12. The critical temperature is calculated conservatively both for total and local buckling.
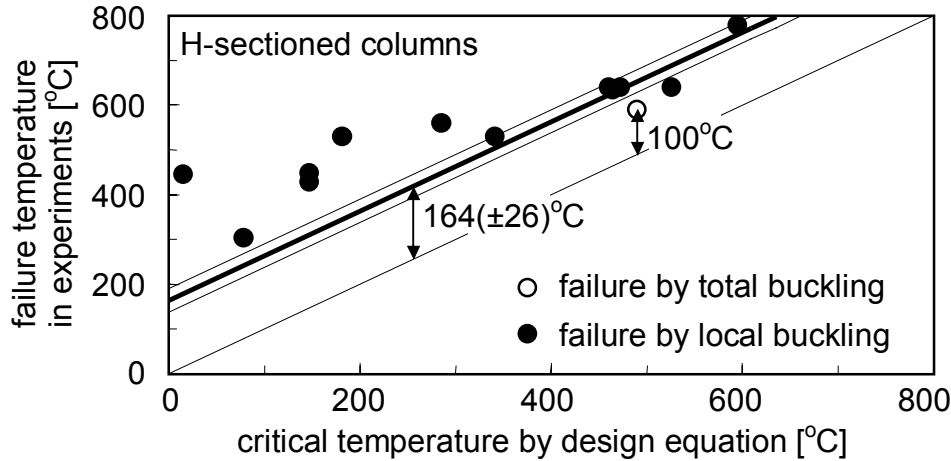
Figure 12 Comparison with fire resistance test results[13, 14] and critical temperature calculated by Route B design formula (H-sectioned columns, SN400B)

Critical Temperature of Steel Beams

For beams, critical temperature for bending failure is considered. As shown in Figure 13, a beam (span=$2l$) is applied uniform load w. At the ultimate state, ($T=T_{Bcr}$),plastic hinges are developed at both ends and center. The balance of moment gives,

$$wl^2 = M_a + 2M_c + M_b. \tag{14}$$

Assuming that beam temperature is uniform, $M_a = M_b = M_c = \kappa(T_{Bcr})M_{pB}$ holds, where M_{pB} is the full plastic moment of beam section at normal temperature. Solving for temperature, we get

$$T_{Bcr} = 700 - 375(\frac{wl^2}{4M_{pB}}) \tag{15}$$

as a design formula for critical temperature of beams[3].

In Figure 14, results of comparison with fire resistance test data is shown. Similar to the case of columns, actual yield stress was used instead of the design value in equation (9). The critical temperature is calculated fairly conservative.
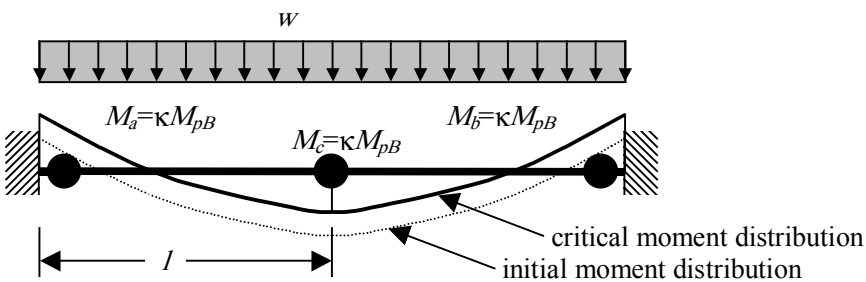

Figure 13 Ultimate Condition of Beams with Uniform Load

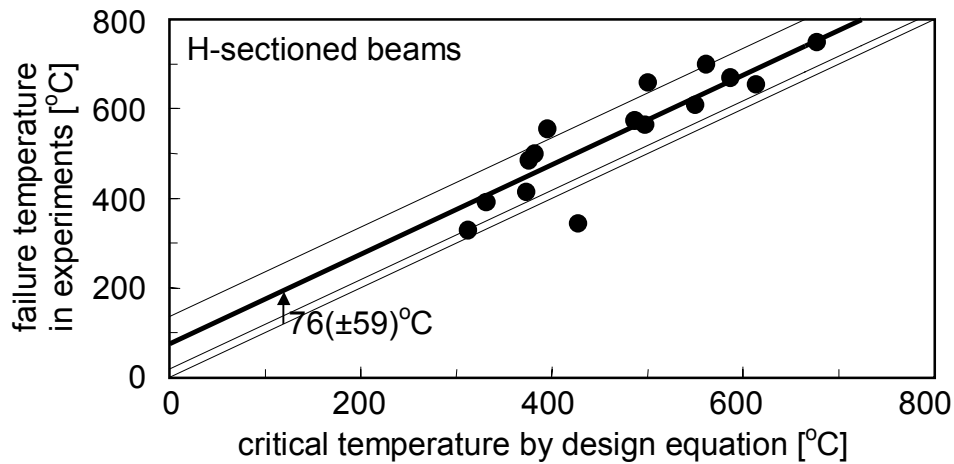[3] Factor 4 is altered in accordance with end-support conditions.

Figure 14 Comparison with fire resistance tests results[13,15] critical temperature calculated by Route B design formula (H-sectioned beams, SS400 and SN400B)

Critical Temperature of Exccesive Deformation

To prevent layer stability, excessive deformation is checked as shown in Figure 15. Part of steel frame is heated by fire. Assuming the temperature of all the beams are increased to T_{DP}, thermal elongation would be

$$\sum \Delta l_i = 0.4a(T_{DP} - T_0)\sqrt{S}$$ (16)

where $\sqrt{S}$ is the characteristic beam length heated in one compartment, $a = 1.2 \times 10^{-5}$ [K^{-1}] is the coefficient of linear expansion of steel. Factor 0.4 is assumed.

To limit horizontal displacement angle less than 1/50,

$$T_{DP} = T_0 + \frac{1}{50}\frac{h}{0.4 \times (1.2 \times 10^{-5})\sqrt{S}} \approx 20 + \frac{4500h}{\sqrt{S}} = 20 + \frac{18000}{\sqrt{S}}.$$ (17)

where simplification was made $h = 4$ m as a default.

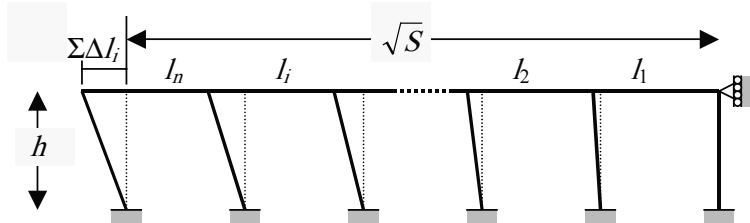Figure 15 Limitation of Excessive Deformation.

Critical Temperature for Joint Failure

No explicit design formula is defined, but 550°C is applied as a limiting temperature for joints.

(2) Steel temperature rise and critical time to failure

As shown in Figure 16, the steel temperature rise under ISO 834 standard fire is give by

$$T_s(t) = \{345\log_{10}(8t+1)\}[1-\exp\{1-h(t-t_w)\}] + T_0,\qquad(18)$$

where the steel temperature rise coefficient h and delay time are given by

$$h = \frac{\phi K_0(H_s/A_s)}{\left\{1+\dfrac{\phi R}{(H_i/A_i)}\right\}\left\{1+\dfrac{\phi}{2}\dfrac{(H_s/A_s)}{(H_i/A_i)}C\right\}},\qquad(19)$$

$$t_w = a_w/(H_i/A_i)^2.\qquad(20)$$

where H_s, H_i are the heated perimeter of steel and insulation, respectively. A_s, A_i are cross sectional area of steel and insulation. $\phi(\equiv H_i/H_s)$ is the ratio of heated perimeter length. The parameters are given in accordance with steel section geometory and insulation method. For example, K_0=0.00089[m/min.], R=310[m^{-1}], C=0.081[-], a_w=22000[min/m^2] for steel columns insulated by spray rockwool as shown in Figure 18.
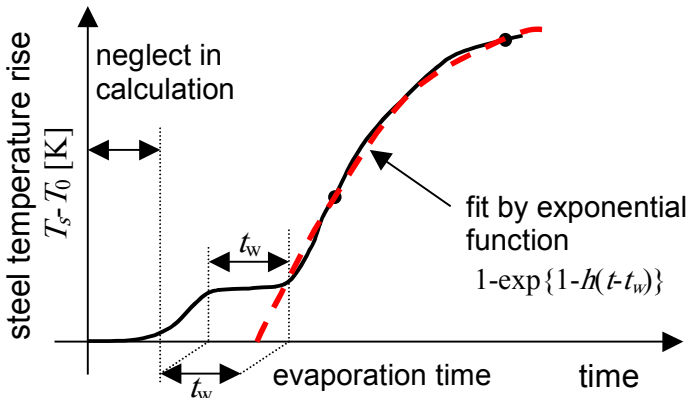
Figure 16: Steel temperature rise during standard fire [16]
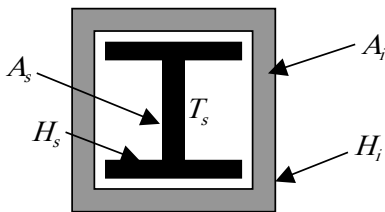
Figure 17 Definition of Parameters to Calculate Steel Temperature Rise

The critical time to failure is calculated as a time for the steel temperature to reach critical temperature. By putting $T_s(t_{fr}) = T_{cr}$, and applying the correction for fire severity $(460/\alpha)^{3/2}$ [17], the following formula is used in the calculation of critical time.

$$t_{fr} = (\frac{460}{\alpha})^{3/2}\frac{2}{h}\left\{\frac{1}{\log_e\{h^{1/6}(T_{cr}-T_0)/1250\}} + t_w\right\}^2\qquad(21)$$

408

Figure 18 Regression Results for Thermal Resistance Factor R and Evaporation Time Coefficient a_w in case of H-sectioned Steel Column Insulated by Spray Rockwool

ANALYSIS OF TARGET SAFETY LEVEL

The Route B verification method was developed by bridging existing knowledge to derive conservative estimation. Verification method itself says nothing about its intended safety level. However, in engineering sense, structural engineer should know how much safety is implied in his/her design solution. In the future, we should be able to show target safety level before carrying out structural fire safety design. So-called reliability based design could be our new goal of developement.

As a first step to reliability-based design, we tried to analyse safety level implied in verification method. A systematic analysis was carried out to combine all the type of uncertainties (type A) and redundancy in design equations (type B) for a prototype building.
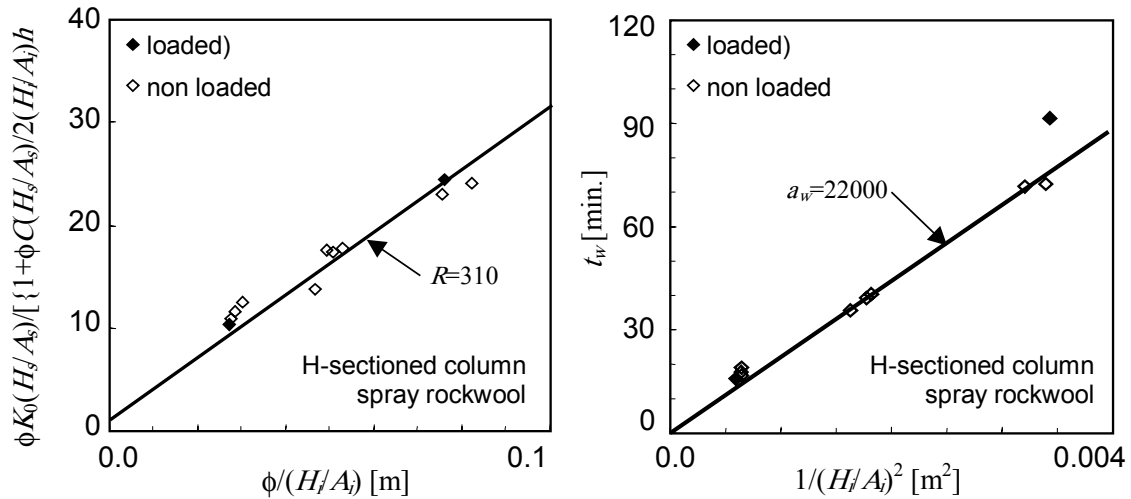
Method of Analysis

As is usually applied in reliability based method, the degree of uncertainties were described by probability density function (PDF). As long as possible, PDF's were developed based on survey results and results of experiments. Using the PDF's as input value to design formula, PDF of margin of fire resistance time is obtained, from which we can discuss safety index β

$$\beta = \mu_M / \sigma_M. \tag{22}$$

Monte-Carlo simulation method was applied to calculate PDF. However in some of the cases, analytical method (AFORM) was used to calculate the safety index directly. Similar approach are adopted in structural engineering, but to be expanded to fire safety engineering [18].

Sources of Uncertainty

The degree of safety is affected by two types of variations, type A and B. Type A (stochastic variability) corresponds with the uncertainties in the difference between characteristic design input values and actual conditions of fire. Fuel load density is a typical parameter that is

classified in type A. Type B (knowledge uncertainty) corresponds with the errors in predicting physical behavior. All the parameters were classified into either type A or B as shown in Table 2.

Table 2 Classifications of Parameters and Corresponding PDF's

type A parameters		L/N	mean	s.d.
fire load density (office area) q_l [MJ/m^2]		L	235	65
structural load intensity (office area) L_0 [N/m^2]		L	706	296
modulus of elasticity of steel E [MPa]		N	204036	17738
yield stress at room temp. σ_{yRT}/F [-]		N	1.14	0.15
type B parameters		L/N	mean	s.d.
correction in strength reduction temperature ΔT_κ [^{o}C]		N	89	31
correction factor for fire temperature rise coefficient α_{exp}/α [-]		L	0.71	0.21
basic temperature rise coefficient K_0 [m/min.]	(Box-column)	N	0.00116	0.0001
	(H-sectioned beam)	N	0.00067	0.00006
thermal resistance factor R [m^{-1}]	(Box-column)	N	419	267
	(H-sectioned beam)	N	45	31
evaporation time coefficient a_w [min/m^2]	(Box-column)	N	17435	7659
	(H-sectioned beam)	N	23052	6163
redundancy in critical temperature formula [^{o}C]	(total buckling) ΔT_B	N	164	26
	(local buckling) ΔT_{LB}	N	100	26
	(bending failure) ΔT_{Bcr}	N	76	59

L=LogNormal, N=Normal

Analysis [19]

As shown in Figure 19, typical office building was considered. Fire was assumed in the office area. Analysis is made for a column on outer row. The column is made by hollow box section. Outer diameter is 450mm. Flange thickness is 25mm. Spray rockwool is applied by 20mm thick. Evaluating by Route B formula gives the results shown in Table 3.

Table 3 Calculation Results by Route B Formula (Deterministic Calculation Results)

fire temperature rise coefficient	686°C/min$^{1/6}$
fire duration	26 min
load ratio	0.34
critical temperatures	550 ^{o}C
for total buckling	594 ^{o}C
for local buckling	578 ^{o}C
for excessive deformation	1128 ^{o}C
for joint failure	550 ^{o}C
Minimum of the above	550 ^{o}C (joint failure)
margin of fire resistance time	60 min
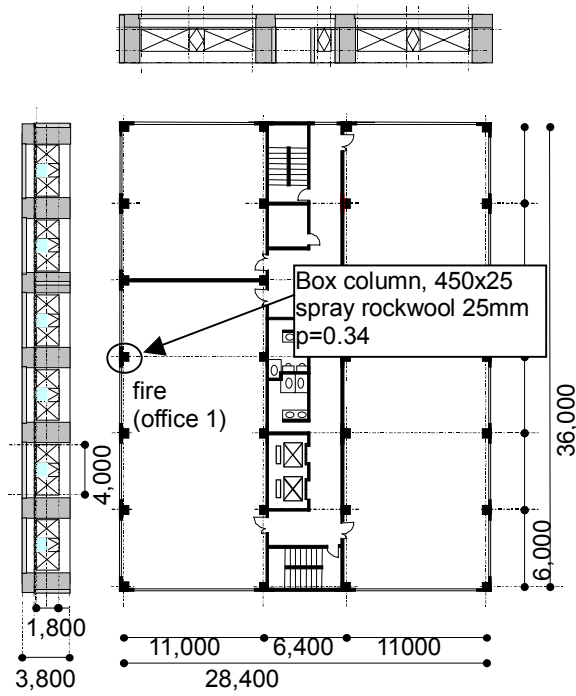
Figure 19 Analyzed Office Area (Fire in Office 1)

Results – Type A Variation

Monte-Carlo simulation was carried out for the same column using the stochastic input for type A parameters in Table 2. Type B parameters were fixed to deterministic values suggested in verification method. The result is shown in Figure 20. The mean value of margin of fire resistance time is 75.1 minutes, while the standard deviation is 3.4 minutes. It can be said that this specific design has large redundancy. It is true because the deterministic calculation results in M_D=60 minutes of margin.

Margin by deterministic calculation M_D can be set equal to zero if the design is optimized. Thus the mean value of intrinsic margin is 75.1-60=15.1 minutes. Corresponding safety index is

$$\beta_{t\arg et} = (\mu_M - M_D)/\sigma_M = 15.1/3.4 = 4.31, \tag{23}$$

which can be regarded as target safety index of verification method when considering only type A uncertainties. The value 4.31 corresponds with unrealistic safety requirement. It is expected that type B uncertainty is still important.
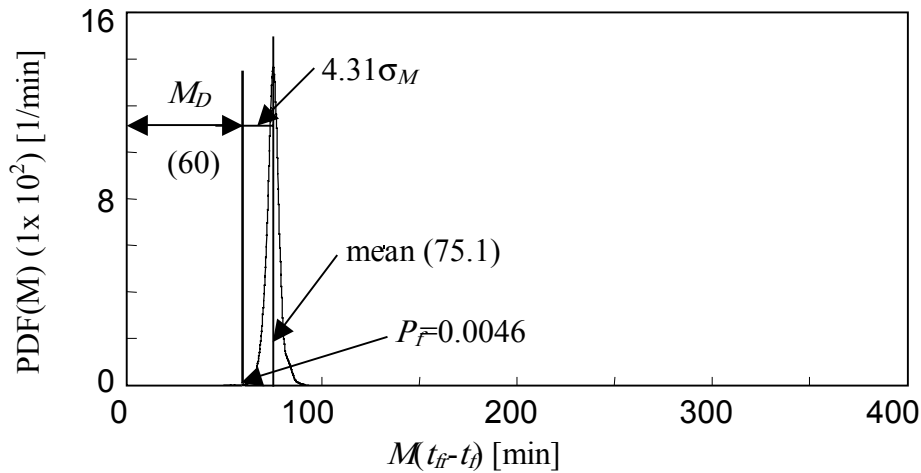
Figure 20 PDF of the Margin of Fire Resistance Time (Type A analysis)

Results – Type A+B Variation

The same analysis was made considering both type A and type B uncertainties. The result is shown in Figre 21. As the design equation is developed so as to give conservative results, margin is considerably increased. However, at the same time, standard deviation is increased. As a result, target safety index is reduced to 1.23. The probability of failure is increased to 0.045. It is interesting that the value is close to 1/20, which corresponds with the low frequency that 'normally negligible'. To derive rigid conclusion, further analysis is neccessary, but it is suggested that target safety level might be around 1/20 of probability of failure. Comparing the type A variation result, there is a room to reduce the prediction acuracy in design formula.
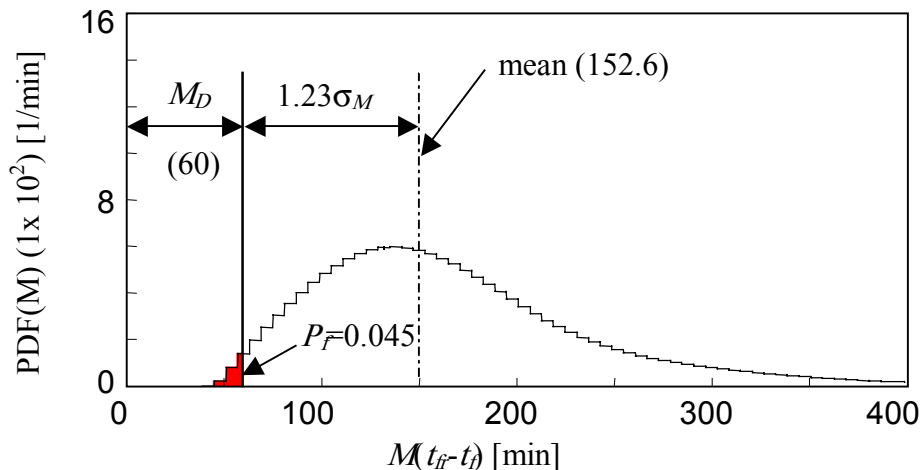
Figure 21 PDF of the Margin of Fire Resistance Time (Type A+B analysis)

CONCLUSIONS

This paper made a review of technical basis of simplified verification method for fire resistance, which has been implemented in Building Standards Law of Japan in June 2000. The design equation is simple enough to give conservative results. Preliminary analysis of

the target safety level was carried out to find that target safety level might be around 1/20 of failure.

NOMENCLATURE

A_{fuel}	surface area of combustible fire load (wood equivalent) [m^2]
p	axial force ratio $p = P / F A_c$ [-]
A_c	cross sectional area of steel element [mm^2]
$A\sqrt{H}$	ventilation parameter of fire room [m$^{5/2}$]
$\Sigma A \sqrt{k\rho c}$	heat absorption conductance to bounding walls [W.s$^{1/2}$/ K]
E	modulus of elasticity at normal temperature [MPa]
F	nominal design strength at normal temperature [MPa]
h	steel temperature rise coefficient [min^{-1}]
l	column length , half length of beam [mm]
M_{pB}	full plastic moment of beam section at normal temperature [Nmm]
M	margin of fire resistance time ($t_{fr} - t_f$) [min.]
p	load ratio (service load / nominal strength at room temperature)
P	axial force [N]
q_b	heat release rate [kW]
Q_r	total fire load of fire room [MJ]
R_{LB}	strength reduction factor for local buckling [-]
t_f	fire duration [min.]
t_{fr}	critical time to structural failure [min.]
t_w	delay time due to moisture evaporation in insulation material [min.]
T_B	critical temperature of steel column for overall buckling [^{o}C]
T_{Bcr}	critical temperature of steel beam for bending failure [^{o}C]
T_{cr}	critical temperature of steel element [^{o}C]
T_{DP}	critical temperature of steel element for over deformation [^{o}C]
T_{LB}	critical temperature of steel column for local buckling [^{o}C]
T_0	ambient temperature (=20) [^{o}C]
z	height above floor [m]
α	fire temperature rise coefficient [K/min$^{1/6}$]
α_l	local fire temperature rise coefficient [K/min$^{1/6}$]
κ	strength reduction ratio [-]
λ	normalized slenderness ratio $(l/i)/\pi\sqrt{E/F}$ [-]
σ_y	effective yield stress [MPa]
χ	burning type index [m$^{1/2}$]

REFERENCES

[1]   Yusa, S., Tsujimoto, M., "Outline of Reforming the Building Standards Law in Japan", NISTIR 6588, Fifteenth Meeting of the UJNR Panel on Fire Research and Safety, March 1-7, 2000, pp. 181-187

[2]   Architectural Institute of Japan, Recommendation for Fire Resistant Design of Steel Structures (in Japanese), 1999

[3]   Ministry of Construction, Ed., *Taika Seinou Kenshouhou no Kaisetu Oyobi Keisanrei tosono Kaisetu* (A Guideline on Verification Method for Fire Resistance and Examples) (in Japanese), *Inoue Shoin*, 2001

[4]   JSCA, *Taika Sekkei Sinpojiumu* "*Kouzou Sekkeisha niyoru Taika Seinou Kenshoho (Kokuji) no Juturei to Kaisetu*" (Symposium on Design Examples using Route B Verification method Conducted by Structural Engineers, in Japanese), Japan Structural Consultants Association, 2001

[5]   Ohmiya, Y., Sato, M., Tanaka, T., Wakamatsu, T., (in Japanese) Transaction of AIJ, 469, pp. 149-158, 472, pp. 169-176

[6]   Matsuyama, K., Fujita, T., Kaneko, H., Ohmiya, Y., Tanaka, T., Wakamatsu, T., (1998) S Simple Predictive Method for Room Fire Behavior, Fire Science and technology, 18(1), pp. 23-32, Science University of Tokyo

[7]   Japan Society of Steel Construction (JSSC) Technical Committee, Durability subcommittee, Fire Resistance Team, "*Kouzouyou Kouzaino Kouonji Narabini Kanetugono Kikaiteki Seisitsu* (Mechanical Properties of Structural Steel at High Temperature and after Heat Exposure)", JSSC, Vol. 4(33), pp. 4-74, 1968 (in Japanese)

[8]   Building Center of Japan, Total Fire Safety Design System of Buildings, Vol. 4, Fire Resistance Design, Chapter 3, 1989 (in Japanese)

[9]   Ministry of Construction, Development of Performance Evaluation Methods of Fire Safety, Project Report, Jan., 1999 (in Japanese)

[10]   Kirby, B. R., Preston, R., R., "High Temperature Properties of Hot-rolled, Structural Steels for Use in Fire Engineering Design Studies", Fire Safety Journal, Vol. 13, pp. 27- 37, 1988

[11]   Architectural Institute of Japan, Design Standard for Steel Structure, 1995 (in Japanese)

[12]   Architectural Institute of Japan, Recommendation for Fire Resistant Design of Steel Structures, Chapter 6, 1999 (in Japanese)

[13]   Ministry of Construction, Development of Performance Evaluation Methods for Fire Safety, Final Report, 1999 (In Japanese)

[14]   Motegi, T., Yusa, S., Nishida, I., Okamura, Y., Nayaka, I., "Experimental Study on Buckling Loads of Steel Columns under Elevated Temperatures in Large Scale", Journal of Structural and Construction Engineering, Architectural Institute of Japan, No. 538, pp. 187-194, Dec., 2000 (in Japaneses)

[15]   Motegi, T., Yusa, S., Nishida, I., Nayaka, I., "Experimental Study on Load Bearing Capacities of Steel Simple Beams under Elevated Temperatures", Journal of Structural and Construction Engineering, Architectural Institute of Japan, No. 536, pp. 193-200, Oct., 2000 (in Japaneses)

[16]   Harada, K., "A Simple Formula for Steel Temperature Rise" (in Japanese), Annual Metering of the Japan Society for Fire Safety Engineering, pp. 360-363, 2000

[17]   Harada, K., Kogure, R., Matsuyama, K., Wakamatsu, T., "Equivalent Fire Duration Based on Time- Heat Flux Area", Proceedings of the Fourth Asia- Oceania Symposium on Fire Science and Technology, pp. 513- 524, 2000

[18]   Magnusson, S., E., Frantzich, H., Harada, K., "Fire Safety Design Based on Calculations: Uncertainty Analysis and Safety Verification", Fire Safety Journal, Vol. 27, pp.305- 334, 1997

[19]   Akiko Nanbu *et al.*, An Analysis of Safety Margins Embedded in the Performance Verification Methods Based on Reliability Engineering, Summaries of Technical papers of Annual Meeting, 3059, 3076-3078, Architectural Institute of Japan, 2001

FIRE RESISTANCE OF STRUCTURAL COMPONENTS PROTECTING ESCAPE ROUTES

Geoff THOMAS and Delwyn LLOYD
School of Architecture, Victoria University of Wellington, PO Box 600, Wellington
geoff.thomas@vuw.ac.nz

ABSTRACT

Generally fire resistant structures are expected to survive a fire in a compartment. Some structures such as floors may be designed to provide time for occupants to escape from other compartments. A common misconception is that the fire resistance rating (FRR), the time an assembly will survive in a test furnace is the time available to escape. In small compartments such as those in residential accommodation the FRR is significantly longer than the time the assembly will survive in a real fire in the compartment. Some fire engineering designs for retrofitted accommodation buildings use FRR times for light timber frame walls and floors as the available egress time. The method of time equivalence can provide a prediction of the FRR required to survive a compartment burnout. The ratio of the total burning time of the fire to the time equivalent can be used to provide an estimate of the time taken for an assembly of given fire resistance to fail by multiplying the ratio by the FRR. This method is shown to be non-conservative when a computer model of light timber frame wall assemblies is run using both realistic time-temperature curves and the ISO-834 standard fire test time-temperature curve. This method is more conservative than assuming that an assembly will last as long in a compartment fire as predicted by the FRR.

KEYWORDS*:*

INTRODUCTION

When carrying out a fire engineering design for egress, calculations of detection time and detection time lag, estimates of occupant response and calculations for travel and queuing time are added together to give a required safe egress time (RSET). In order to determine whether a factor of safety is reached, then an available safe egress time (ASET) must be determined. In the room where are fire originates, or adjacent rooms open to the room of fire origin, then a computer model such as CFAST[5] can be used to determine the time to untenable conditions. In some situations, for example a hotel, or high-rise building, fire rated barriers such doors between hotel bedrooms and corridors or floor/ceiling systems protecting upper floors the time the barriers remain in place in a fire is the available safe egress time.

A common approach among designers is to assume, that in this situation the ASET is the fire resistance rating (FRR) of the assembly. The FRR however is the time an assembly will survive in a standard test furnace such as ISO834[4]. The standard test furnace follows a specified time-temperature curve. The temperature reaches 834 degrees Celsius after 30 minutes and increases gradually with time after that. The furnaces are also lined with firebricks and are relatively small with a volume of about 10 m^3. In a real fire in a real compartment, the fire will tend to have a growth phase until flashover occurs. Flashover is an almost instantaneous rise in temperature typically starting at about 50 degrees Celsius and may reach as high as 1300 degrees Celsius, although temperatures of 1000-1100 degrees Celsius are more common. In larger compartments lower temperatures are likely. In addition to the temperature being higher and higher temperatures being reached more quickly in a real fire compared with a test furnace, the size of the furnace and types of lining materials also result in differences between the thermal environment in a furnace and real fire.

Anecdotal evidence suggests that real fires are more severe than furnace tests, particularly in smaller compartments, however designers appear to ignore this. I have reviewed a design where an office building was hotel was retrofitted as a hotel and the original office doors were retained. Old furnace test data suggested these doors would achieve an FRR of about 12 minutes and the ASET was given as 12 minutes. In another instance when I queried a design saying a floor with an estimated FRR of 20 minutes would give occupants 20 minutes to escape I was told that everyone does it this way, with the implication that this design approach was acceptable.

In order to alter this simplistic approach by designers, a simple method of estimating the actual time an assembly will survive in a real fire is proposed. The method is not likely to be highly accurate and may be unconservative in some instances. However it is considerably safer than the current design approach assuming the FRR is the available safe egress time.

DESIGN APPROACH

In order to calculate the ASET based on the FRR rating the following procedure may be followed.

1. Determine the total fuel load. Multiply the floor area by the Fuel Load Energy density.

$$E = A_F e_f$$

where E is the total fuel load
A_F is the floor area (m²)
e_f is the fuel load energy density (MJ/m²)

2. Determine the window area and height (or total window area and a weighted average of the window heights if there is more than one opening). As fire resistance is a post-flashover phenomenon, assume that all windows are broken.

3. Calculate the burning rate based on the ventilation using the Severity Correlation[2]

$$Q_v = 1.5 A_V \sqrt{H}$$

Where Q_v is the ventilation controlled burning rate (MW)
A_V is the area of openings (m²)
H is the height of the windows (m)

4. Calculate the burn time by dividing 90% of the total fuel load by the burning rate (assumes 10% of fuel present is not burnt within the compartment)

$$t_b = 0.9 * E/Q_v$$

where t_b is the total burn time (s)

5. Calculate the time equivalent, t_e . The Eurocode 1996 formula is recommended with values for the conversion factor as used in the Zealand Acceptable Solutions for Fire, 2000[3] and also in the Fire Engineering Design Guide[2].

$$t_e = e_f k_b w_f$$

where k_b is a conversion factor given below

Construction Materials	k_b
Very light insulating materials	0.10
Plasterboard ceiling and walls, timber floor.	0.09
Lightweight concrete ceiling and floor, plasterboard walls.	0.08
Normal concrete ceiling and floor, plasterboard walls.	0.065
Thin sheet steel roof	0.045

6. w_f is the ventilation factor given by

$$w_f = \left(\frac{6.0}{H}\right)^{0.3}\left[0.62 + \frac{90(0.4 - \alpha_v)^4}{1 + b_v\alpha_h}\right] > 0.5$$

where $\alpha_v = A_v/A_f$ $0.025 \leq \alpha_v < 0.25$

$\alpha_h = A_h/A_f$ $\alpha_h < 0.20$

$b_v = 12.5(1 + 10\alpha_v - \alpha_v^2)$

A_h is the area of horizontal openings in the roof

7. Ascertain the FRR of the assembly being considered. If the FRR is significantly greater than the time equivalent for the compartment, then the assembly will not fail and is therefore adequate.

8. Multiply the FRR by the ratio of the burn time over the time equivalent to give a more realistic indication of the ASET

$$ASET = FRR * (t_b/t_e)$$

Example

A Hotel room is separated from a corridor with a door that haves a nominal FRR of 15 minutes. The room is 8.0 m long, 2.4 m high and 3.6 m wide. There is a window at one end

2.0 m high and 3.0 m long. A hotel room has a fire hazard category of 1, hence the New Zealand Acceptable Solutions[3] assume a design FLED of 400 MJ/m². Other sources suggest a value of 300 MJ/m² for this occupancy[2].

Running though the steps above:-

1. Total Fuel load, $E = A_F e_f$ =8.0*3.6*400=11520 MJ

2. A_v=2.0*3.0=6.0 m², H=2.0 m

3. Burning rate, $Q_v = 1.5 A_V \sqrt{H}$ =1.5*6.0*$\sqrt{2.0}$ =12.7 MW

4. Burn time, $t_b = E/Q_v$ = 0.9*11520/12.7=816 s (or 14 minutes)

5. time equivalent, t_e

   e_f= 400 MJ/m²

   k_b=0.065 (normal concrete ceiling and floor, plasterboard walls)

   $\alpha_v = A_v/A_f$ =6.0/(8.0*3.6)=0.21

   $\alpha_h = A_h/A_f$ =0/(8.0*3.6)=0

   $b_v = 12.5\left(1 + 10\alpha_v - \alpha_v^2\right)$=12.5(1+10*0.21-0.21²)=38.2

   $$w_f = \left(\frac{6.0}{H}\right)^{0.3}\left[0.62 + \frac{90(0.4 - \alpha_v)^4}{1 + b_v\alpha_h}\right] = \left(\frac{6.0}{2.4}\right)^{0.3}\left[0.62 + \frac{90(0.4 - 0.21)^4}{1 + 38.2*0}\right] = 0.97$$

   $t_e = e_f k_b w_f$=400*0.065*.97=25.2 minutes or 1514 seconds

6. FRR is 15 minutes

7. $ASET = FRR*\left(t_b/t_e\right)$=15*816/1514=8 minutes.

This design approach is very simple but this example shows that using the FRR of 15 minutes as ASET is unconservative. If we assume a detector response time of 90 seconds, an occupant response time of 4 minutes and a travel time of 1 minute for occupants of other doors to leave the corridor outside we have a required safe egress time of 6.5 minutes. Using the nominal FRR this gives a factor of safety of 15/6.5 or 2.3. Using this method the factor of safety is 8/6.5 or 1.2.

Obviously there are a number of assumptions in this method. The most critical assumption is that the severity of both the furnace test and the compartment fire is constant throughout both the furnace test and the compartment fire, or that the severity varies throughout the duration of the furnace test in the same manner that it varies throughout a compartment fire. This assumption will now be tested using computer modelling of a range of assemblies.

VARIATION OF FIRE SEVERITY

The time to failure is derived for a compartment fire curve derived for a range of opening factors. The time-temperature curve used assumes an infinite fuel load, so the fire carries on until the boundary fails. We are attempting to find the failure time early in a fire not the maximum fire severity for a given compartment, ventilation and fuel load.

The compartment fires are modelled using COMPF-2[1]. The methodology is that used by Thomas[8]. The time-temperature curve includes an additional growth phase at a rate of 100 Celsius/minute added on to the fire curve. This growth phase makes little difference in the

time to failure[9]. The boundary conditions are as appropriate for the compartment being considered. A sample COMPF-2 input file is included in Appendix 1.

At this stage failure is determined based on a temperature criteria. For timber walls and floor systems this is defined as the onset of charring at 300 Celsius, at a depth of 10 mm into the assembly a conservative measure of structural failure[10]. For steel structural elements failure is assumed to occur when any part of the steel reaches 550 Celsius. Similarly in reinforced concrete structures failure is deemed to occur when the reinforcing reaches 550 Celsius.

At failure the time to failure is recorded. The actual time equivalent is calculated by comparing the same thermal model with that run with an ISO834 time-temperature or test data where available. The value for the actual time equivalent is at failure and is therefore the same as the FRR. The time equivalent is calculated using the BIA formula[2,3] and the burning time is calculated using the severity correlation. The ratio of the severity correlation to time equivalent is then compared with the ratio of the actual time to failure to the FRR. If the methodology is perfectly accurate the value of the calculated ratio divided by the actual ratio should be 1.0. If it is less than 1.0 the method is unconservative and if it is greater than 1.0 the method is conservative. This value can therefore be referred to as a factor of safety for the method.

Previous work by Thomas[7] used the heat transfer model TASEF[6] for thermal analysis of timber walls, floors, insulted steel beams and concrete slab walls and floors. This data has been reanalysed to get the information required.

This modelling was based on the small compartment (figure 1).
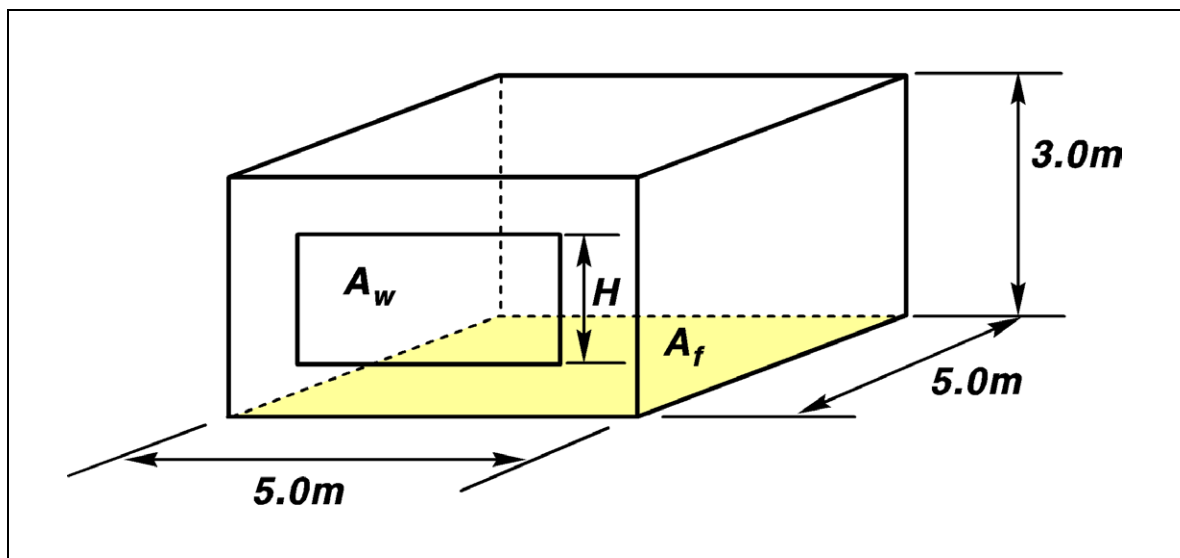
Figure 1. Compartment Used for Initial Analysis.

The following ventilation parameters are used. The restriction of window size being not more than 25% of the floor area in the BIA ventilation factor calculation has been taken into account by using the value for the ventilation factor when the window area is 25% of the floor area.

Table 1 Ventilation parameters.

WINDOW			Law Burning	Ventilation Factor
Height	Width	Area	Rate	BIA
(m)	(m)	(m²)	(MW))	(Dimensionless)
1.0	2.75	2.75	4.125	1.544
1.5	3.00	4.50	8.267	1.020
2.0	3.00	6.00	12.728	0.833
2.0	4.00	8.00	16.971	0.816
2.0	5.00	10.00	21.213	0.816
2.0	6.00	12.00	25.456	0.816

The first structure is a 360UB57 in a compartment lined with 100 mm concrete all round. The UB is directly under the ceiling slab and is protected on 3 sides with 16 mm fyreline Gib[11] board in a box profile. The time to failure for the various ventilation parameters, and ratios of actual and calculated burn times and time equivalents is shown in Table 2. When calculating the burn time and time equivalent, only the ratio between them is of significance, so both values are normalised with fuel load energy density (FLED). The value of both calculated burn time and calculated time equivalent is directly proportional to fuel load, so in the ratio between the two calculated values the fuel load cancels out. The FRR rating is taken as being that fro the thermal model exposed to the ISO834 time-temperature curve and not the actual furnace test result.

Table 2 Results for Analysis of 360UB57, lined with 16 mm GIB in concrete compartment

WINDOW Area	Actual Time to Failure	FRR	Actual Fail. Time/FRR	Calc. Burn Time/ Fuel Load	Calc. Time Equivalent/ Fuel Load	Calc. Time Equiv./Calc Burn Time	FoS Calc./Actual Ratios
(m²)	(min.)	(min.)	( )	(min.m²/MJ)	(min.m²/MJ)	( )	( )
2.75	88.5	84	0.95	0.09	0.10	1.10	1.16
4.50	55.5	84	1.51	0.05	0.07	1.46	0.97
6.00	43.5	84	1.93	0.03	0.05412	1.84	0.95
8.00	37.5	84	2.24	0.02	0.05305	2.40	1.07
10.00	34.5	84	2.44	0.02	0.05305	3.00	1.23
12.00	33.0	84	2.54	0.01	0.05	3.60	1.42

The factor of safety for the method varies from 0.95 to 1.42. It is slightly unconservative for two opening sizes, however if the FRR time had been used directly as an estimate of time to failure the answers would be unconservative by 51% and 93% of the FRR. It is highly conservative when the openings are large, however this is outside the range of the BIA formula and it is conservative whereas using the FRR directly would be unconservative.

Analysis was also carried out on a 150 mm concrete floor slab in a concrete compartment with a D20 reinforcing bar with 20 mm cover, a light timber frame stud wall with 90*45 mm studs and a 9.5 mm GIB fyreline lining, a light timber frame joist floor with 240*45 mm joists and a 16 mm GIB fyreline lining and a steel 250UC73 column lined with 16 mm GIB fyreline in a box profile. The compartment for the last three structural elements had light timber frame bounding surfaces and therefore the calculated time equivalent changes as the value for the conversion factor k_b in the time equivalence formula changes to 0.09.

The factor of safety for the method varies from 0.82 to 2.14. When only the range of validity of the BIA formula is considered, the maximum value is 1.20. Again the method appears to be unconservative in some instances, in this case for the insulated steel column in a light timber framed lined room. However it is far more conservative than using the FRR directly, being unconservative by 18% compared with an FRR that is up to 2.9 times the time to failure.

This analysis uses a crude method to determine time to failure that is in most instances conservative. Further analysis using detailed structural modelling may show that this method is more conservative.

Table 3. Results for other Structural Elements

Description	Window Area (m²)	2.75	4.50	6.00	8.00	10.00	12.00
100 mm Concrete Slab Conc. Compt	Actual Failure Time	92.4	66.6	58.2	55.2	54.0	52.8
	FRR (min.)	89	89	89	89	89	89
	FRR/Actual	0.96	1.34	1.53	1.61	1.65	1.69
	FoS (Calc/Actual Ratios)	1.15	1.09	1.20	1.49	1.82	2.14
90 mm stud LTF wall 9.5 GIB LTF Compt.	Actual Failure Time	25.6	20.4	19.2	19.1	19.0	16.2
	FRR (min.)	38	38	38	38	38	38
	FRR/Actual	1.48	1.86	1.98	1.99	2.00	2.34
	Calc. Burn Time/Fuel Load	0.09	0.05	0.03	0.02	0.02	0.01
	Calc Time Equiv./Fuel Load	0.10	0.07	0.05	0.05	0.05	0.05
	Calc. Time Equiv./Calc. Burn Time	1.10	1.46	1.84	2.40	3.00	3.60
	FoS (Calc/Actual Ratios)	1.15	1.09	1.20	1.49	1.82	2.14
290 mm joist LTF Floor 16 mm GIB LTF Compt.	Actual Failure Time	37.0	28.3	26.2	25.5	25.3	25.2
	FRR (min.)	55	55	55	55	55	55
	FRR/Actual	1.49	1.95	2.10	2.16	2.17	2.18
	FoS (Calc/Actual Ratios)	1.03	1.04	0.87	1.11	1.38	1.65
250UC73 Column 16 mm GIB LTF Compt.	Actual Failure Time	46.0	35.0	30.0	29.0	28.0	28.0
	FRR (min.)	86	86	86	86	86	86
	FRR/Actual	1.87	2.46	2.87	2.97	3.07	3.07
	FoS (Calc/Actual Ratios)	0.82	0.82	0.89	1.12	1.35	1.62

Effect of Compartment Size

The effect of compartment size was analysed by running the COMPF2 fire model with two larger compartments. The second compartment was 8 m long, 10 m wide and 4 m high. The compartment is intended to represent a small shop in a larger building such as a mall or a shop under a hotel or crowd space. It was assumed to have concrete boundaries and the structural element being considered is the 150 mm reinforced floor slab described previously. The window heights were 1m, 1m, 1.5m and 2.5 m respectively for the four runs respectively shown in Table 4.

Table 4. Results for Concrete Floor Slab in Concrete Lined 8.0m by 10.0m by 4.0m high Compartment

WINDOW Area	Actual Time to Failure	FRR	FRR/Actual Fail. Time	Calc. Burn Time/ Fuel Load	Calc. Time Equivalent/ Fuel Load	Calc. Time Equiv./Calc Burn Time	FoS Calc./Actual Ratios
(m^2)	(min.)	(min.)	( )	(min.m^2/MJ)	(min.m^2/MJ)	( )	( )
2.00	315.0	89	0.28	0.40	0.18	0.44	1.56
8.00	87.0	89	1.02	0.10	0.10	0.99	0.97
12.00	66.0	89	1.35	0.05	0.07	1.31	0.97
20.00	54.6	89	1.63	0.03	0.05	1.93	1.18

Again the correlation is good. The times to failure are very long, hence egress time may not be an issue unless, the compartment is located under a large residential or crowd occupancy with long escape times.

The third compartment used is 30m by 30 m with a ceiling height of 6.0 m. It was assumed to have light timber frame boundaries and the structural element being considered is the 360UBH fire rated with 16 mm GIB fyreline described previously.

Table 5. Results for Fire Rated Steel Beam in GIB Lined 30.0m by 30.0m by 6.0m high Compartment

WINDOW Area	Actual Time to Failure	FRR	FRR/Actual Fail. Time	Calc. Burn Time/ Fuel Load	Calc. Time Equivalent/ Fuel Load	Calc. Time Equiv./Calc Burn Time	FoS Calc./Actual Ratios
(m^2)	(min.)	(min.)	( )	(min.m^2/MJ)	(min.m^2/MJ)	( )	( )
22.50	33.0	84	2.55	0.57	0.22	0.38	0.15
55.00	33.0	84	2.55	0.23	0.16	0.70	0.28
110.00	28.5	84	2.95	0.08	0.10	1.27	0.43
220.00	25.5	84	3.29	0.03	0.06	2.09	0.64

In this very large compartment the results are poor with the factor of safety ranging from 0.15 to 0.64. This is not surprising as the size of the compartment is such that it is outside the range of both the BIA time equivalent formula and the assumption of a well-mixed compartment in COMPF2. This method should not be used for large compartments with a cut-off point in the region of a compartment volume of 1000 m^3.

DISCUSSION

The analysis carried out to date suggest that this method is reasonably accurate, normally conservative and when unconservative, not significantly so. Further analysis is required to determine its adequacy when unprotected steel structures are used. The method should be analysed using structural modelling rather than the simple thermal criteria used here. Testing against other compartment fire models and real fire time-temperatures curves is necessary.

This method has been used to calculate actual factors of safety for egress for two room sizes and various window geometries. The analysis in Appendix 2 assumes a nominal factor of

safety (FRR/RSET) of 2.0 and then calculates an actual factor of safety using this burn time/time equivalent method. A sensitivity study is carried out varying the compartment height, compartment area, window height and window width for the two smaller compartments described previously. Varying the size (height or width) of vents has far more effect than varying the compartment height or area. Values of the actual factor of safety for both compartments for reasonable values of the various parameters were about 0.8 compared with a nominal value of 2.0.

CONCLUSION

The method described is suitable for use in fire engineering design for compartments up to about 1000 m^3 in volume. It is simple to use and utilises simple calculations that practicing fire engineers are already familiar with. It appears to be slightly unconservative in some cases, but is far more conservative than using a fire resistance rating as the available safe egress time. The fire resistance rating is typically between one and two times the actual failure time but can be as much three times the actual failure time of a structural element.

REFERENCES

1. Babrauskas, V. COMPF2, A Program for Calculating Post-Flashover Fire Temperatures. U.S. Department of Commerce/National Bureau of Standards. NBS Technical Note 991. Gaithersburg. United States. 1979.
2. Buchanan A H (Editor) Fire Engineering Design Guide. 2nd Ed. Centre for Advanced Engineering. Christchurch. 2000.
3. Building Industry Authority. Approved Document for New Zealand Building Code Fire Safety Clauses. Wellington. 2000.
4. ISO-834. Fire Resistance Tests - Elements of Construction. (International Standards Organisation). 1975.
5. Jones, W. W.; Forney, G. P.; Peacock, R. D.; Reneke, P. A. Technical Reference for CFAST: An Engineering Tool for Estimating Fire and Smoke Transport. National Institute of Standards and Technology, Gaithersburg, MD. NIST TN 1431; 2000.
6. Sterner, E. & Wickstrom, U. 1990. TASEF - Temperature Analysis of Structures Exposed to Fire. Fire Technology SP Report 1990:05. Swedish National Testing Institute.
7. Thomas GC. Fire Resistance of Light Timber Framed Walls and Floors. University of Canterbury. Christchurch. New Zealand. Fire Engineering Research Report 97/7. 1997.
8. Thomas GC. Fire Resistance of Light Timber Framed Walls and Floors. University of Canterbury. Christchurch. New Zealand. Fire Engineering Research Report 97/7. Section 5.3.1, pp119-121. 1997.
9. Thomas GC. Fire Resistance of Light Timber Framed Walls and Floors. University of Canterbury. Christchurch. New Zealand. Fire Engineering Research Report 97/7. Section 7.5.3, pp167-8. 1997.
10. Thomas GC. Fire Resistance of Light Timber Framed Walls and Floors. University of Canterbury. Christchurch. New Zealand. Fire Engineering Research Report 97/7. Section 15.4, pp295-7. 1997.
11. Winstones. Gib Fire Rated Systems. Winstone Wallboards Limited. Wellington. New Zealand. 2001.

Appendix 2

Sample COMPF2 Input File

```
PESSIMIZED PYROLYSIS FIRE FOR CONCRETE WALL V=.025,FLOAD=100
 ADIA=.FALSE.    pv
AFLOOR=25.0      pv
 AWALL=85.0      pv
 AWDOW=2.2       pv
  BPF=0.9      pv
   CD=0.68      0.68
 CFLPC=44.4      44.4
CPPYR1=.1127     pv
CPPYR2=1010.0    pv
CVGROS=18.7E6    pv
 DENSW=2400.     pv
  DHP=0.0      pv
 DTIME=10.0      pv
   EF=1.0      pv
EISCAN=.FALSE.    FALSE
 EITA=1.00      pv
 FLOAD=3.333333   pv
FLSPEC=.FALSE.    FALSE
 HFLPC=5.40      pv
 HWDOW=1.0      pv
 IRUN=1        sequential
   IX=10      pv
KTRACE=0       0
 MTIME=14400.0    pv
 MWPYR=28.97     pv
NEWPRP=.TRUE.    FALSE
 NFLPC=0.      pv
 OFLPC=38.2      pv
PLFUEL=.FALSE    FALSE
 PRNT= 10.0     pv
REGRES=1.0E-05    pv
RPSPEC=.FALSE.    FALSE
   SH=0      pv
 SHAPE=2.      pv
 SIZE=4.00E-02   pv
STEADY=.FALSE.    FALSE
STOICH=.FALSE.    FALSE
TBOLIC=390.0     pv
THICKW=0.115     pv
 TINPT=0.0      0.0
VTSPEC=.TRUE.    FALSE
 WFLPC=12.0      0.0
 5,10,1,0,0
0.  1.8  25.  1.8  388.  1.28  107.3  0.8  1473.  0.52
0.  909.09 373.  909.09 373.01 3878.79 388.  3878.79 388.01 737.97
393. 737.97 413.  737.97 453.  737.97 473.  1030. 4273.  1030.
 0.0  0.9000
```

Appendix 2

Compartment #1: Hotel Room

$L_f = 5m$
$W_f = 5m$
$H_f = 3m$
$h = 2m$
$w = 3m$
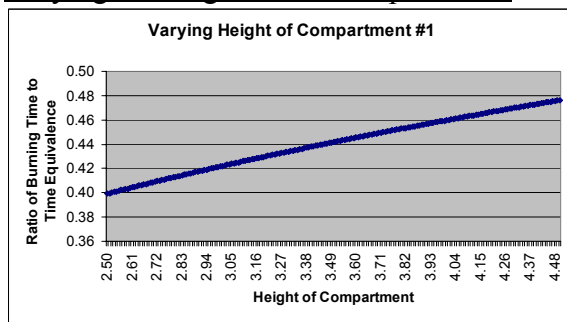$k_b = 0.065$
$FLED = 300 \ MJ/m^2$

Varying the height of the compartment:

The range of height was taken as the reasonable height for a hotel room, from 2.5m to 4.5m.

This shows a fairly proportional relationship between the ratio of burning time and time equivalence to the height of this compartment.

Using a typical height of 3m gives a ratio of 0.42. This leads to a Factor of Safety for a room of this size of only 0.84. This is below the recommended safety factor of 2. The graph shows that for the entire range of height a factor of safety of 2 is not reached.

Varying the floor area of the compartment:
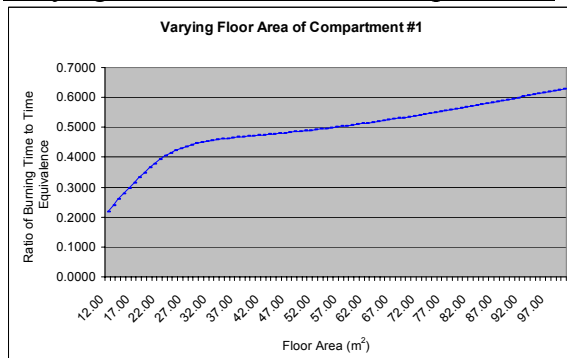
The range of floor area was taken as the reasonable range for this compartment, from $12m^2$ to $100m^2$.

If a typical hotel room has a floor area of approximately 25 -35m^2, it gives a ratio of burning time to time equivalence of 0.42-0.46. This gives a Factor of Safety of 0.84-0.92. A factor of safety of 2 is not reached by this range of floor area.

Varying the height of vents:
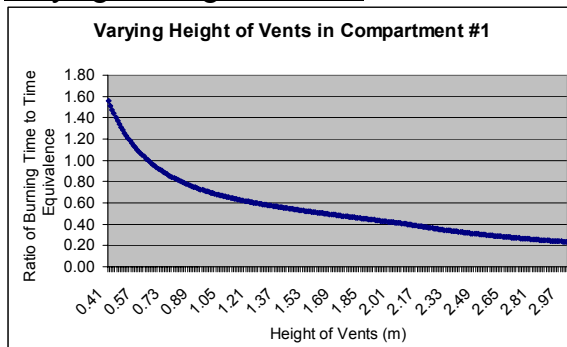
The range of vent height was taken from when flashover is likely to first occur (0.41m) to the limit of floor height (3m).

This shows that when the vents are smaller, changing the height has a greater effect on the ratio. The decreasing ratio shows that time equivalence is lessening less with each increase in height of vents than burning time.

For the mid-range of vent heights the ratio is 0.5. This gives a Factor of Safety of 1. For any room of this size a factor of safety of 2 is only reached when the vents are less than 0.65m in height.

Varying the width of vents:
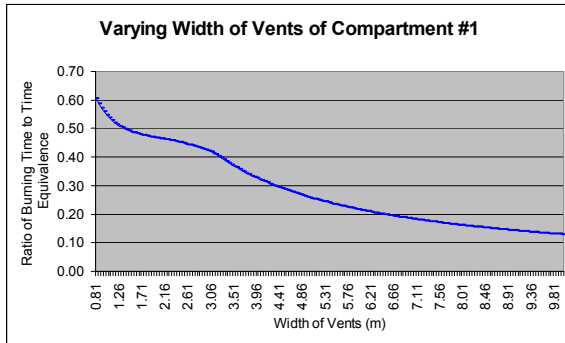
This shows the relationship between time equivalence and the burning time changes as the width of the vents changes.

The mid-range of the widths shows a ratio of approximately 0.3. This gives a Factor of Safety of 0.6.

Compartment #1:
This shows for a compartment of this size with this size vents the factor of safety allowed for in design is well below the recommended level of 2. This suggest for compartments of this size, that the factor of safety currently designed for (FRR/RSET) should be set much higher than only 2, to allow for the difference between burning time and time equivalence. Therefore, fire resistance ratings will need to be higher.
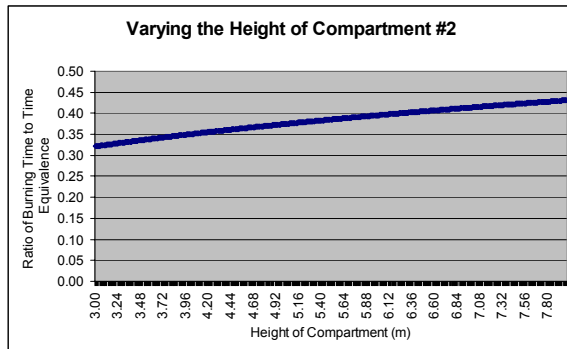
Compartment #2: Retail Store

L_f = 10m
W_f = 8m
H_f = 4m
h = 3m
w = 7m
k_b = 0.065
FLED = 600
Vertical openings = 0m^2

Varying the Height of the compartment:

The range of height was taken from the reasonable range of heights for this compartment, 3m to 8m.

This shows very little change in the burning time and time equivalence when changing the height of this compartment.

Using a typical height of 4m gives a ratio of 0.35. This gives a Factor of Safety of 0.7, well below the recommended level.

Varying the floor area of the compartment:
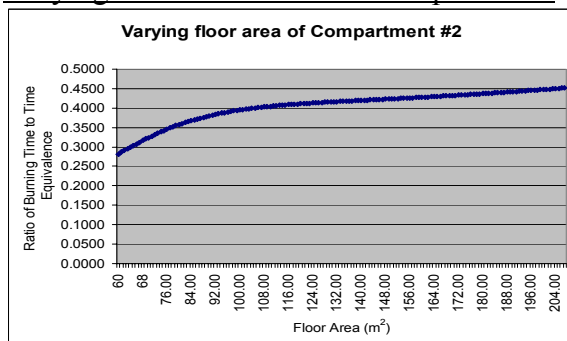
The range of floor areas was taken from the reasonable range for this compartment from 60m^2 – 200m^2.

It shows that burning time increases fairly proportionally to time equivalence when increasing the floor area of the compartment.

The mid-range of the floor area gives a ratio of 0.4. This gives a Factor of Safety of 0.8, which is well below what is recommended.

Varying the height of the vents:
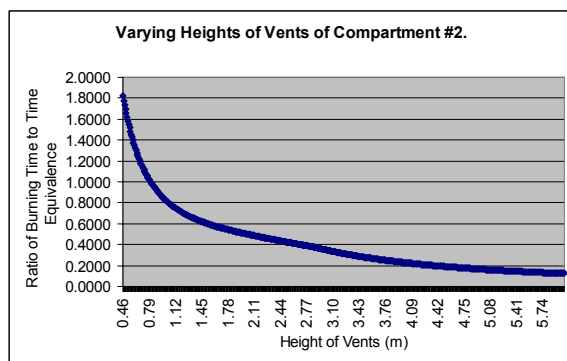
The range of vent heights was taken from the lowest that flashover occurred (0.46m), and the floor height (6m).

When the vents are smaller, the change in size effects the burning time more than the time equivalence, creating the steeply sloped section of the line.

The mid-range of the height of vents gives a ratio of approximately 0.3. This gives a Factor of Safety of 0.6, well below the recommended safety factor of 2.

427

Varying the widths of the vents:

Varying Widths of Vents of Compartment #2
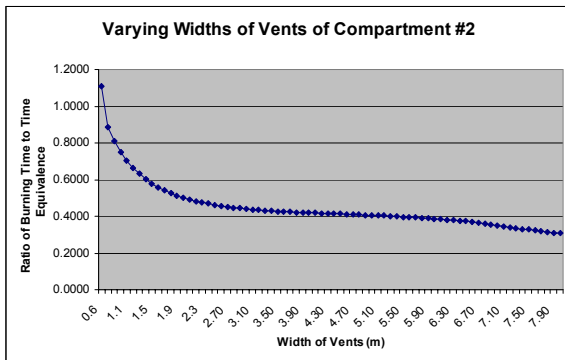
The range of width of the vents of this compartment were taken from where flashover would occur, 0.6m, and the wall length, 8m.

The mid-range of width of vents gives a ratio of approximately 0.4. This gives a Factor of Safety of 0.8.

Compartment #2:
For all variables tested the factor of safety was well below 2. To reach an appropriate level of safety the vents would need to be smaller than 0.8m by 0.6m. This is unsatisfactory for a retail store which uses its windows to sell products. This shows that the design factor of safety (FRR/RSET) should be set higher than 2 to allow for safe egress of the compartment. This can be done by increasing fire resistance ratings to protect means of escape.